

Sheffield Hallam University

Organic complexes of unrefined and milled kaolin: An infrared spectroscopic study.

ILLES, Jane.

Available from the Sheffield Hallam University Research Archive (SHURA) at:

<http://shura.shu.ac.uk/19856/>

A Sheffield Hallam University thesis

This thesis is protected by copyright which belongs to the author.

The content must not be changed in any way or sold commercially in any format or medium without the formal permission of the author.

When referring to this work, full bibliographic details including the author, title, awarding institution and date of the thesis must be given.

Please visit <http://shura.shu.ac.uk/19856/> and <http://shura.shu.ac.uk/information.html> for further details about copyright and re-use permissions.

LEARNING CENTRE
CITY CAMPUS, POND STREET,
SHEFFIELD, S1 1WB.

101 657 573 4



REFERENCE

ProQuest Number: 10697162

All rights reserved

INFORMATION TO ALL USERS

The quality of this reproduction is dependent upon the quality of the copy submitted.

In the unlikely event that the author did not send a complete manuscript and there are missing pages, these will be noted. Also, if material had to be removed, a note will indicate the deletion.



ProQuest 10697162

Published by ProQuest LLC (2017). Copyright of the Dissertation is held by the Author.

All rights reserved.

This work is protected against unauthorized copying under Title 17, United States Code
Microform Edition © ProQuest LLC.

ProQuest LLC.
789 East Eisenhower Parkway
P.O. Box 1346
Ann Arbor, MI 48106 – 1346

Organic Complexes of Unrefined and Milled Kaolin-
An Infrared Spectroscopic Study

Jane Illés

A thesis submitted in partial fulfilment of the requirements of
Sheffield Hallam University
for the degree of Doctor of Philosophy

July 2000

Collaborating Organisation:

English China Clays Limited

Declaration

The material described in this thesis was carried out by the author in the Materials Research Institute at Sheffield Hallam University. It has not been submitted for any other degree. The work is original, except where acknowledged by reference.

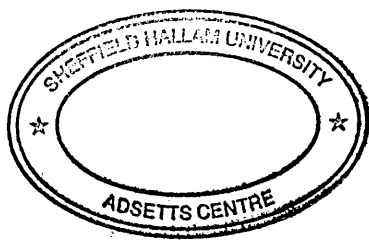
Signed

(candidate)

.....

(Director of Studies)

Date



Acknowledgements

My sincere thanks go to my Director of Studies, Dr Chris Breen and my Supervisor, Prof. Jack Yarwood for their constant advice and support, and for their encouragement, enthusiasm and dedication to my project throughout. Also, thanks for the long debates on trains.

Thank you to my Industrial Advisor, Dr David Skuse for many fruitful discussions. My gratitude also goes to Dave Mogridge, Jeremy Hooper, Dave Greenhill, Jonathan Phipps and many more at ECC, Cornwall for their help over the last 3 years.

I am grateful to Dr Stehen Hillier and Mariane Centino for collecting certain XRD and VT DRIFTS data.

Special thanks to the very lovely Pierre (thanks for the scanning!) and Frannie Clegg for getting me started.

For their various work related and extra curricular contributions, merci beaucoup to the 610 mob, official and honorary (in no particular order), Carine, Peta, Favourite, JP, Delphine, the future Lord Mayor of Sheffield-Chris Constable (like the English landscape artist), Christophe, P Star, Paul, Scott, Nigel, Mr Jeffery Forsyth, Suzanne, Javier, Alex, Gary, Thierry and Tom.

For their financial support, my thanks go to EPSRC.

This work is dedicated to my parents,

Tibor and Jill Illés.

Abstract

Aim: to characterise the surface sites present on unrefined and ball milled Cornish kaolin, with a view to ultimately determining the mode of interaction between the mineral and industrially significant organic molecules. Milling and temperature were found to affect the structure of kaolin and types of surface sites present. These changes were monitored primarily by variable temperature diffuse reflectance infrared Fourier transform spectroscopy (VT DRIFTS) and other complementary techniques including XRD and TGA. Curve fitting of the VT DRIFT spectra was used to aid characterisation of the types of water present on the mineral surface. The diagnostic probe molecule pyridine was used to identify the changes in reactive acid sites present as temperature increased both before and after milling, and oleic acid was used as a representative adsorbate to analyse the effects of carboxylic acid treatment.

As ball milling time increased, so did the kaolin agglomerate size and the amount of surface sorbed water. The types of water present on the surface of unrefined and ball milled Cornish kaolin have been characterised, and grouped into four main types - strongly hydrogen bonded, moderately strongly hydrogen bonded, weakly hydrogen bonded and very weakly hydrogen bonded. The different water environments were observed using DRIFTS in the bending and stretching regions of the spectrum. Changes in the stretching region were generally less distinct, since the bands were broader than in the bending region. However, changes in both regions were elucidated by curve fitting of the VT DRIFT spectra, and certain bands appeared to have similar thermal behaviour.

Freshly milled samples had a greater proportion of strongly hydrogen bonded water compared with the other, more weakly bonded types. Aged samples had less total surface sorbed water, and relatively less strongly hydrogen bonded water compared with the more weakly bonded species.

Pyridine displaced the more strongly hydrogen bonded water (an effect similar to ageing). A dehydrated halloysite impurity was found which intercalated pyridine. VT XRD showed that deintercalation occurred at c 100 °C. The hydrogen bonding nature of the halloysite-pyridine interactions became less pronounced as milling increased. Pyridine adsorption to kaolin was via Brønsted sites in the unmilled kaolin. As milling time increased the mineral surface took on Lewis acid character and less hydrogen bonding occurred. Brønsted associations were present in all the milled (and unmilled) samples and became more significant as milling time increased (as more surface water was present). In addition to the intercalation reaction between halloysite and pyridine, this probe molecule is likely to bind to exposed (broken) edge sites on kaolin and/or halloysite, or to sorb between the slightly expanded mineral layers at the edges of the mineral stacks.

Oleic acid adsorption onto kaolin at pH 3, was via surface adsorption of monodentate. Acid precipitate was loosely associated with the surface via hydrocarbon chain interactions with the adsorbed salt. At pH 9, total surface adsorption was low. Adsorbed species were monodentate in character. Mono- and dioleate were present as loosely bound surface precipitates. At pH 12 the salt was associated with the surface in the bridged bidentate form. Adsorption was high due to hydrocarbon chain associations with micelles, containing some trapped acid species. The precipitate at pH 12 was strongly held, and there was no significant reduction in intensity after washing.

Contents

Chapter 1	Introduction	1
Chapter 2	The effects of ball milling	43
Chapter 3	The interactions of pyridine with kaolin	166
Chapter 4	Kaolin-organic acid interactions	249
Chapter 5	Summary	299

1. Introduction.

1.1 AIMS.....	3
1.2 THE STRUCTURE, COMPOSITION AND PROPERTIES OF KAOLIN.....	4
1.2.1 <i>Classification of minerals</i>	5
1.2.2 <i>Isomorphous substitution</i>	7
1.2.3 <i>Determination of the composition of kaolin using XRF</i>	14
1.2.4 <i>Hydrogen bonding in the kaolin lattice</i>	15
1.3 MATERIALS.....	18
1.3.1 <i>Kaolin sample</i>	18
1.4 METHODS USED TO STUDY CLAY MINERALS.....	18
1.4.1 <i>Infrared spectroscopy</i>	18
1.4.1.1 History of spectroscopy in minerals science.....	18
1.4.1.2 Theory of infrared spectroscopy.....	20
1.4.1.2.1 The vibrational modes of polyatomic molecules.....	22
1.4.1.2.2 Factors affecting the intensity of infrared bands.....	23
1.4.1.2.3 Fourier transform spectroscopy.....	23
1.4.1.2.3.1 Fourier transform.....	24
1.4.1.2.4 Diffuse reflectance.....	25
1.4.1.3 VT and RT DRIFTS experimental parameters.....	32
1.4.1.4 Curve fitting of DRIFT spectra.....	33
1.4.2 <i>XRD</i>	34
1.4.2.1 Theory of XRD.....	34
1.4.2.2 Experimental parameters.....	35
1.4.3 <i>Thermal analyses (TGA, DTA and DCS)</i>	36
1.4.3.1 Experimental parameters.....	36
1.4.4 <i>Ball milling</i>	37
1.4.4.1 Experimental parameters.....	37
1.4.5 <i>XRF</i>	37
1.4.5.1 Experimental parameters.....	37
1.4.6 <i>SEM</i>	37
1.4.6.1 Experimental parameters.....	38
1.5 REFERENCES.....	39

FIGURE 1.1 SEM OF KAOLIN.....	5
FIGURE 1.2 SILICATE MINERALS CLASSIFICATION.....	6
FIGURE 1.3 SCHEMATIC REPRESENTATION OF SILICA TETRAHEDRA.....	6
FIGURE 1.4 SCHEMATIC REPRESENTATION OF TETRAHEDRA.....	7
FIGURE 1.5 SCHEMATIC REPRESENTATION OF KAOLIN.....	9
FIGURE 1.6 SCHEMATIC OF THE THREE SURFACE LAYER TYPES OF KAOLINITE.....	11
FIGURE 1.7 SCHEMATIC OF THE THREE TYPES OF STRUCTURAL DEFECTS OF KAOLINITE.....	12
FIGURE 1.8 POTENTIAL BINDING SITES ON KAOLIN STACKS.....	12
FIGURE 1.9 PROPOSED STRUCTURE FOR HYDROGEN BONDING BETWEEN KAOLIN LAYERS.....	17
FIGURE 1.10 VIBRATIONAL MOTIONS IN A POLYATOMIC MOLECULE(E.G. WATER).....	22
FIGURE 1.11 SCHEMATIC REPRESENTATION OF DIFFUSE REFLECTANCE.....	25
FIGURE 1.12 SCHEMATIC DIAGRAM OF THE DRIFTS SAMPLING ARRANGEMENT.....	28
FIGURE 1.13 A TYPICAL WATER VAPOUR SPECTRUM (THE WATER BENDING REGION).....	31
FIGURE 1.14 A TYPICAL DRIFT SPECTRUM OF KAOLIN.....	33
FIGURE 1.15 SCHEMATIC REPRESENTATION OF AN X RAY DIFFRACTOMETER.....	35
TABLE 1.1 ANALYSIS OF KAOLIN PREPARED FROM A CORNISH MATRIX.....	14
TABLE 1.2 THE ELEMENTAL ANALYSIS OF KAOLIN SAMPLES EXPRESSED AS % OXIDE.....	15
TABLE 1.3 THE SIZE OF SPS GRADE KAOLIN PRODUCED BY ECCI.....	18
TABLE 1.4 PARAMETERS USED IN THE COLLECTION OF IR SPECTRA.....	32

1.1 Aims.

The aim of the work presented herein was to characterise the surface sites present on unrefined and ball milled Cornish kaolin, with a view to ultimately determining the mode of interaction between the mineral and industrially significant organic molecules used in the purification and processing procedures. Milling and temperature were found to affect the structure of kaolin and types of surface sites present. These changes were monitored primarily by variable temperature diffuse reflectance infrared Fourier transform spectroscopy (VT DRIFTS) and other complementary techniques including x ray diffraction (XRD) and thermogravimetric analysis (TGA). Initially, curve fitting of the VT DRIFT spectra was used to characterise the types of water present on the mineral surface. The diagnostic probe molecule pyridine was used to identify the changes in reactive acid sites present as temperature increased both before and after milling, and oleic acid was used as a representative adsorbate to analyse the effects of carboxylic acid treatment.

1.2 The structure, composition and properties of kaolin.

Kaolin, or in its absolutely pure and single layer form, kaolinite, is probably best known as China clay. It is a whitish-opaque powdery mineral which was formed by the metamorphosis of granite under extreme conditions of temperature and pressure in geological time. Kaolin is a phyllosilicate, and the general chemical formula of the kaolin minerals is $\text{Al}_2\text{Si}_2\text{O}_5(\text{OH})_4$. Although there are slight variations in the chemical composition of the kaolin minerals (particularly regarding the number of associated water molecules), the accepted chemistry for the minerals is 46.54 wt % SiO_2 , 39.50 wt % Al_2O_3 and 13.96 wt % H_2O ¹. It is comprised of individual crystals which form booklets from stacks of crystal sheets. Deposits of kaolin comprise pseudo-hexagonal particles with a variety of sizes, varying between micron and sub-micron in diameter^{2,3}. It is ubiquitous throughout the world and is mined extensively throughout Europe and the USA. Primary deposits (kaolin found in the location at which it was created) may be moved over time, for example, by water flow, and transported to another site (secondary deposit). Depending on the location of the deposit, and ultimately the means by which the deposit was formed, kaolin can vary widely in terms of crystallinity, size, aggregation and purity.

Kaolin is extensively used in the cosmetic, paint, rubber and adhesive industries as coating pigment or filling material, and of course, it is the base material from which porcelain and bone china are produced. Primarily though, with approximately 85% going to the paper industry, it is here where its significance and market potential lies. Kaolin may require significant processing and purification before it is suitable for use in these industries, and many of the procedures used are not fully understood at a molecular level. Some of the general procedures used in the processing of kaolin have been documented in a work by Skuse³.

Figure 1.1 SEM of kaolin⁴.



This SEM (scanning electron micrograph) shows clearly the pseudo-hexagonal particles and angular booklet structures expected to be present in a highly crystalline kaolin such as Cornish kaolin. Generally, less ordered kaolin presents particles with poorly developed or irregular hexagonal outlines. The kaolin in Figure 1.1 has a remarkably large particle size, since generally, the dimensions of the particle surface of a well ordered kaolin are from 0.3 - 4 μm wide, with a thickness of around 0.05 - 2 μm ¹. These values are substantially reduced for a poorly crystallised kaolin.

Kaolin is non abrasive due to its ability to delaminate easily. It has a large internal surface area of approximately 600m² per gram, and a specific surface area of approx. 10 m² per gram⁵, factors which make it very useful in a number of applications. In particular it is ideal for use as a coating pigment and filling material used in the industrial preparation of paper. Here it provides a smooth, opaque surface with improved aesthetic and functional properties.

1.2.1 Classification of minerals

Minerals may be divided into several classes. The class of silicates is divided into several sub-classes based on the types of linkages between the basic units of their structure (i.e. SiO₄ tetrahedra).

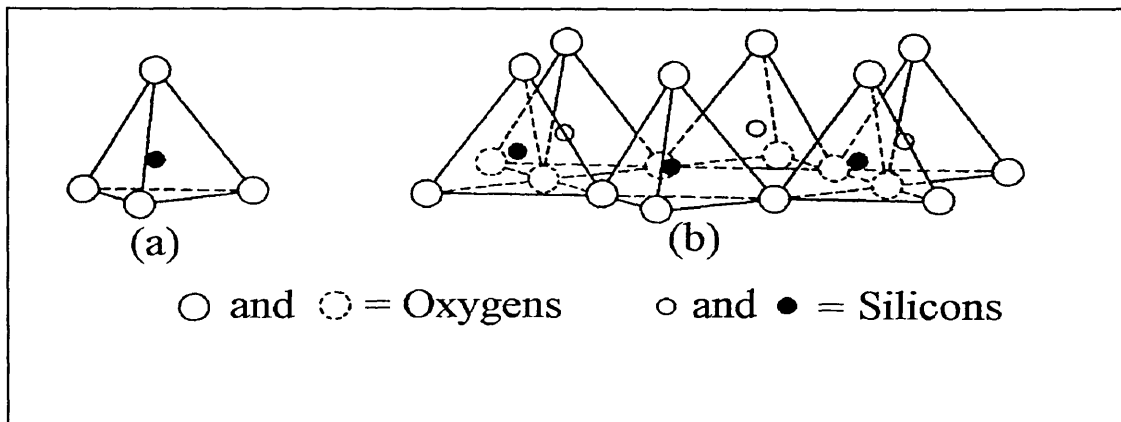
Figure 1.2 Silicate minerals classification.

Class	Subclass	Group	Subgroup
Silicates	Tectosilicates	silica	quartz
		feldspars	alkali series plagioclase series
	Phyllosilicates	smectites	
		kaolinites	
		illites	
		chlorites	

Before describing the minerals of interest in this study, an understanding of clay structure is required.

The feature which distinguishes the subclass phyllosilicates is the presence of SiO_4 tetrahedra which can be linked by sharing three of the four oxygens, and form sheets with a pseudo-hexagonal network (referred to as the silica-tetrahedral layer). Figure 1.3 shows a representation of individual silica tetrahedron and the sheet structure which can be formed.

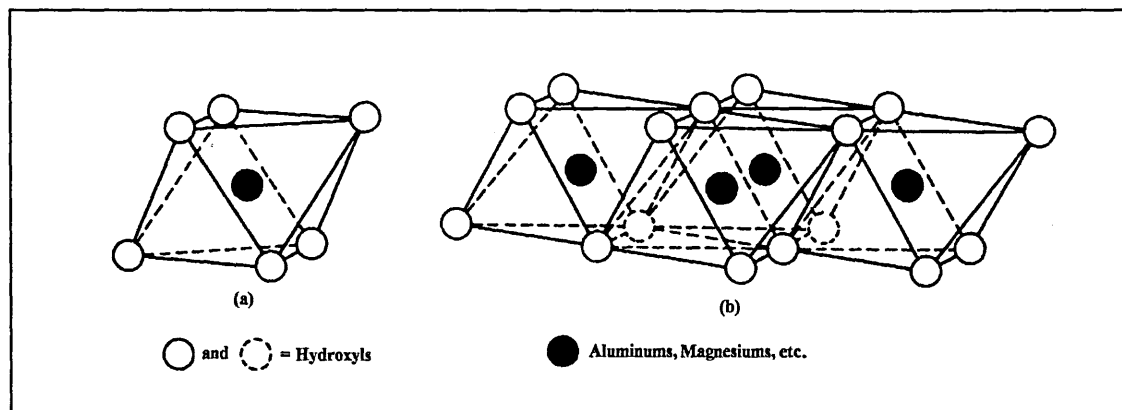
Figure 1.3 Schematic representation of silica tetrahedra.



This tetrahedral layer is combined with another, octahedral sheet. Here, cations in six co-ordination, (mainly Al, Mg and Fe), are surrounded by oxygen and hydroxyl anions in an octahedral pattern. The anions are shared between adjacent octahedra groups and a

planar network results (See Figure 1.4). In kaolin, the anion is almost always Al (see later for isomorphous substitution).

Figure 1.4 Schematic representation of tetrahedra.



The octahedral and tetrahedral sheets may be superimposed upon each other and form layers joined by chemical bonds.

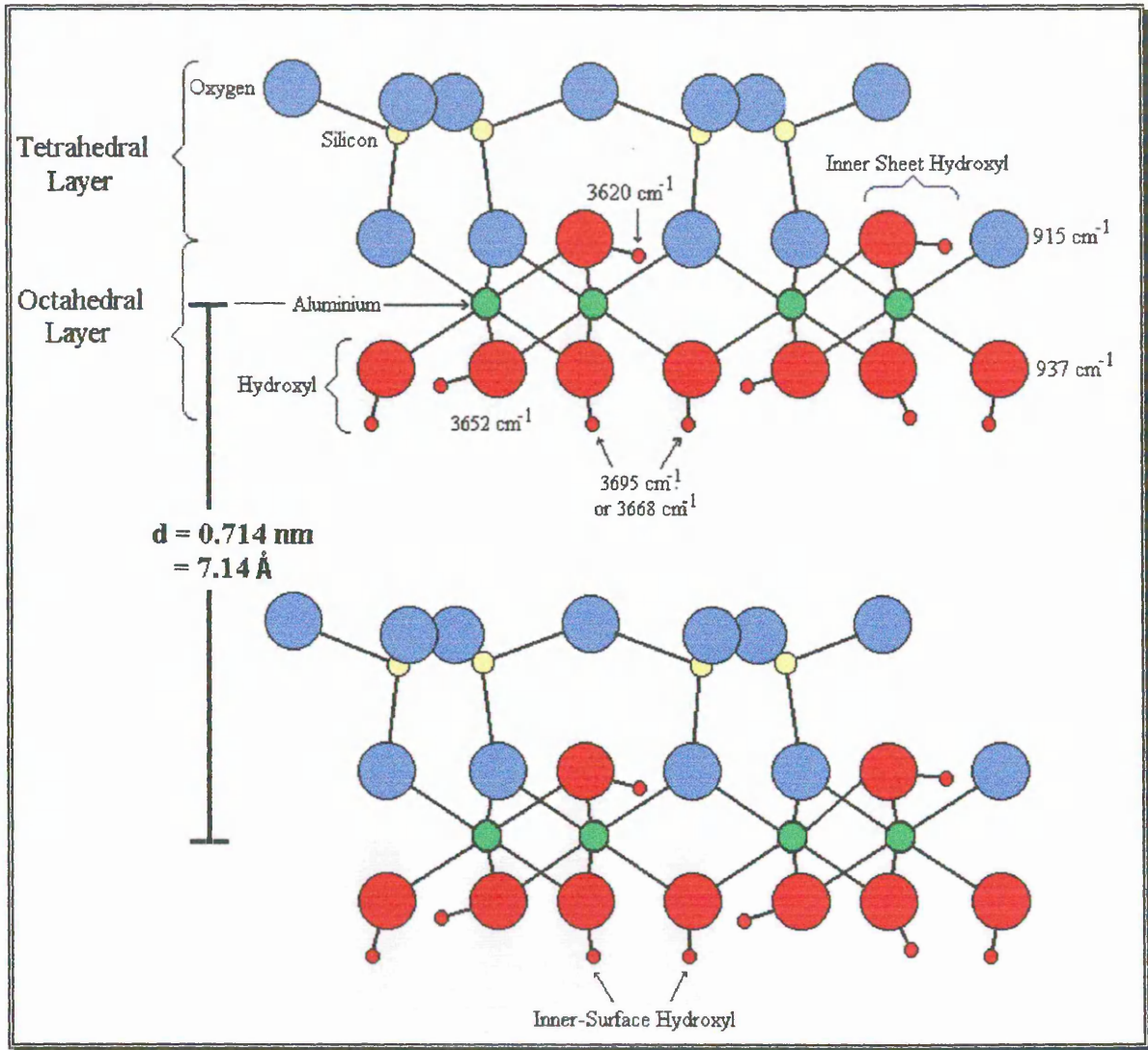
The ratio of tetrahedral (T) to octahedral (O) sheets and the type of cation in the sheets is the basis for the classification system used to assign clays to various groups. For example, if one octahedral sheet and one tetrahedral sheet is shared a 1:1 (TO) layered mineral results (e.g. kaolinite), whereas if two tetrahedral sheets are joined with an octahedral sheet, a 2:1 layered mineral is obtained (TOT) (e.g. montmorillonite, illite and chlorite). 2:1:1 layer silicates, such as the chlorite group of minerals are also formed, and are of the form TOT-O-TOT). The structure of kaolin will be discussed in detail later.

1.2.2 Isomorphous substitution.

In certain clay minerals, isomorphous substitution may occur, where a cation from the tetrahedral or octahedral sheet is replaced by another cation. The exchanged cations usually have the same charge as, but a different valency to (usually lower) the original cations. Isomorphous substitution occurs most commonly in the octahedral sheet. The substitution imparts a negative charge on the structure, and this is satisfied by the sorption of exchangeable cations. The sharing of these exchangeable cations bonds

the clay layers together. These species are thus known as interlayer (exchangeable) cations. The number of cations required to neutralise the lattice is known as the cation exchange capacity (CEC) and is measured in milliequivalents (meq) per 100 grams of clay. Different clays have different CECs. Swelling minerals such as montmorillonite have very large CECs, whilst non swelling minerals such as kaolin have very low CECs. Cation exchange occurs naturally and may also be emulated in the laboratory by placing the clay in a solution of the desired ion, e.g. Na, Ca, Mg and K. Cation exchange is rare in kaolin, since most of the exchangeable cations are associated with the edges of mineral layers, where the ions have unsatisfied valences. These are often referred to as broken edges.

Figure 1.5 Schematic representation of kaolin.

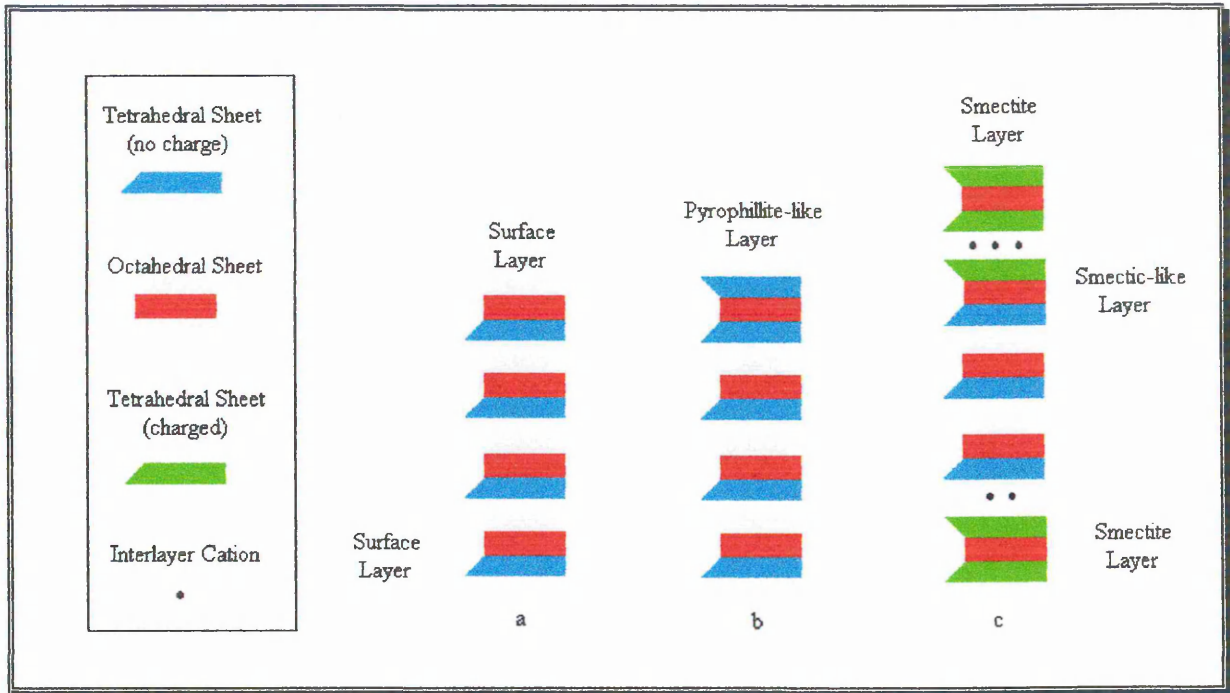


The kaolin structure consists of a single silica tetrahedral sheet condensed with a single alumina, gibbsite-like octahedral sheet combined in a unit so that the apices of the silica tetrahedra and one of the oxygen layers of the octahedral sheet form a common layer. Two thirds of the oxygen atoms are shared by Si and Al atoms, and the remainder are shared by protons and Al atoms. All the apices of the silica tetrahedra point in the same direction and toward the centre of the unit made by the silica and octahedral sheets. The dimensions of the T sheets and O sheets are continuous in their *a* and *b* directions, and stack above one another in the *c* direction. Thus, composite TO layers are formed. The arrangement of the stack determines the specific kaolin mineral type. Several stacked layers are termed “tactoid”. Thus, bulk kaolinite has composite 1:1 TO sheets which are stacked directly above one another, as shown in Figure 1.5. Different types of hydroxyls are present in the kaolin tactoid. The inner sheet hydroxyls belong to the plane of oxygen molecules shared between the tetrahedral and octahedral sheets. Inner surface hydroxyls are internal to the tactoid and belong to the planes which are not involved in the condensation of the sheet. Surface hydroxyls belong to the planes which are external to the tactoid, but are otherwise the same as the inner surface hydroxyls. Because of the multiple stacking in the *c* direction, much of the external surface of the kaolin stack (i.e. tactoid) is dominated by hydroxyl or oxygen species (c 80 %), whilst c15-20 % of the surface area is attributed to edges⁵.

A recent work suggests that the 1:1 type layering of the octahedral and tetrahedral sheets may not always be present at the kaolin surface and that within the bulk layer structure defects may occur⁶. There are three possible types of kaolin surface layers, as shown in Figure 1.6: a) the expected T-O layer, b) a pyrophyllite-like layer (i.e. a 2:1 (TOT) mineral with the chemical formula $Al_2(Si_2O_5)_2(OH)_2$ on one side of the kaolin particle, (i.e. T-O-T....O-T-O-T) which may be found in industrial grade, highly ordered kaolinites, and c) one or more smectite-like layers at one or both ends of the kaolin stack (i.e. (T-O-T)T-O-T.....O-T-O-T(T-O-T), which may be found in some poorly ordered kaolinites. The non-ideal surface layers (types b and c) are not detectable by XRD, and the smectite-like layers of type c are not tightly bound to the kaolin stack, and can be separated from it. This allows the introduction of interlayer cations, thus the smectite-like layer defects can contribute to raised CEC. Typically, the CEC for kaolin is 3-15

milliequivalents/100 g⁷. CEC is affected by the size of the particle and to a lesser extent to the crystallinity of the mineral⁸.

Figure 1.6 Schematic of the three surface layer types of kaolinite.



There are also three types of structural defect in the kaolin stack, as shown in Figure 1.7:

a) a dislocation whereby some of the layers cleave in the *c* direction, b) a lateral layer termination, whereby one or more layers terminate within the stack and other sheets bend to compensate for the “vacant” space, or c) deformation, or bending, of several layers. Types a and b are most common in primary kaolinites and type c are most abundant in secondary (transported) kaolinites.

Figure 1.7 Schematic of the three types of structural defects of kaolinite.

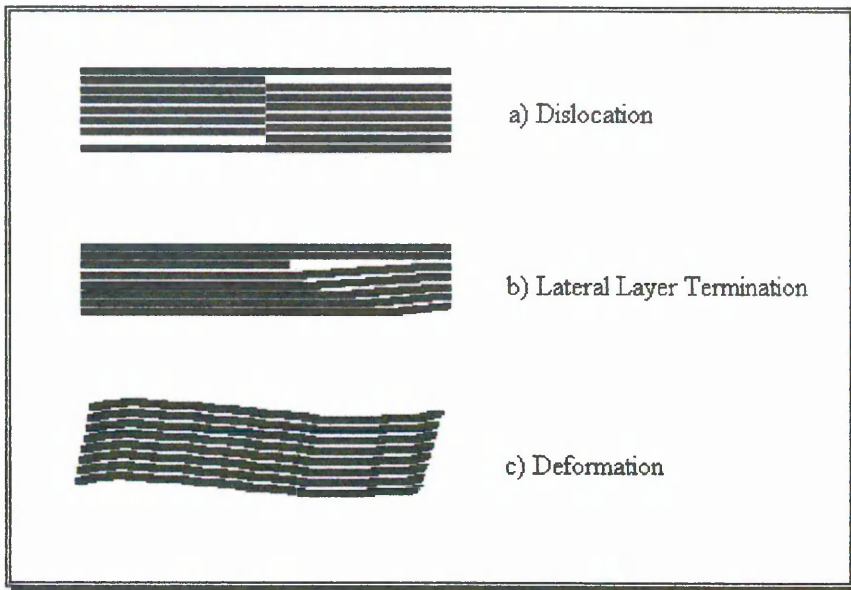
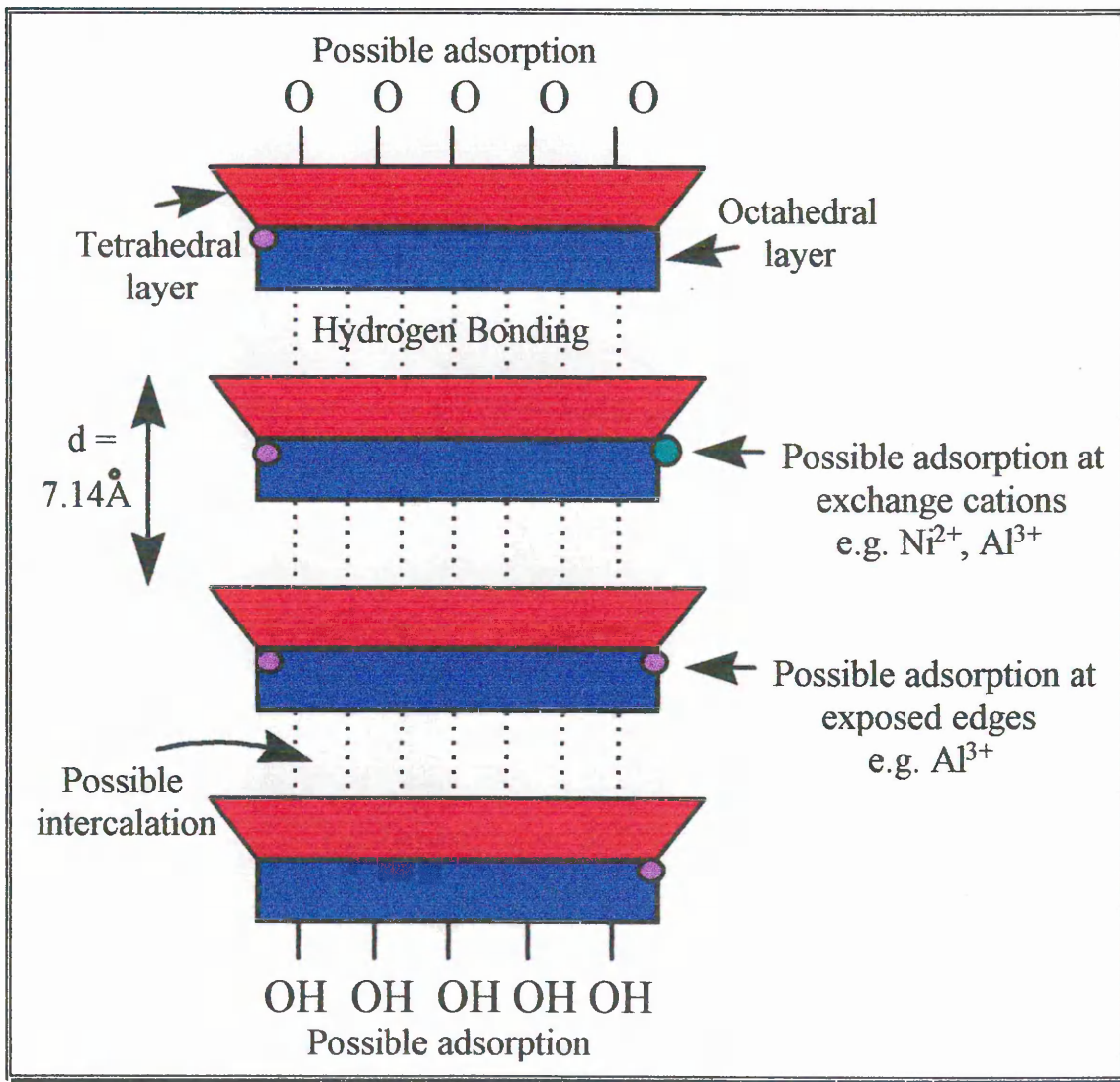


Figure 1.8 Potential binding sites on kaolin stacks.



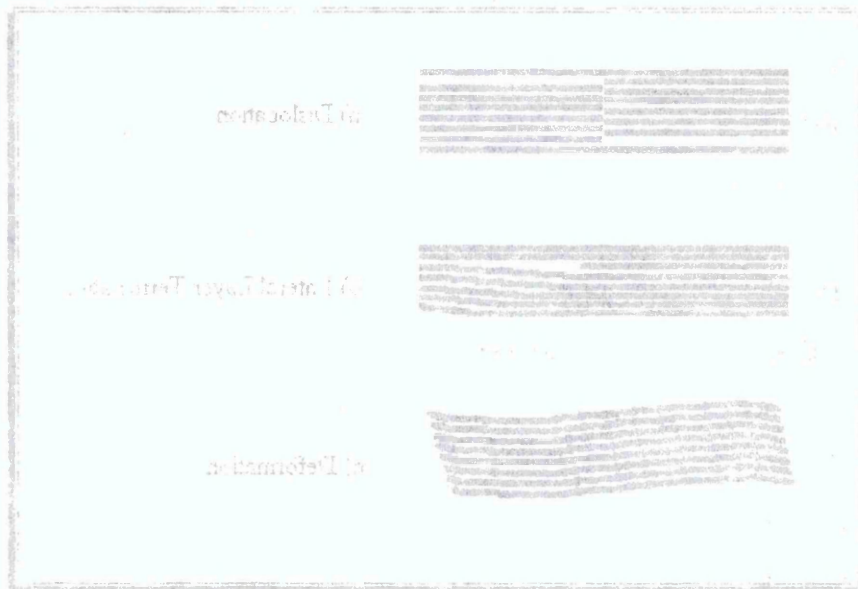
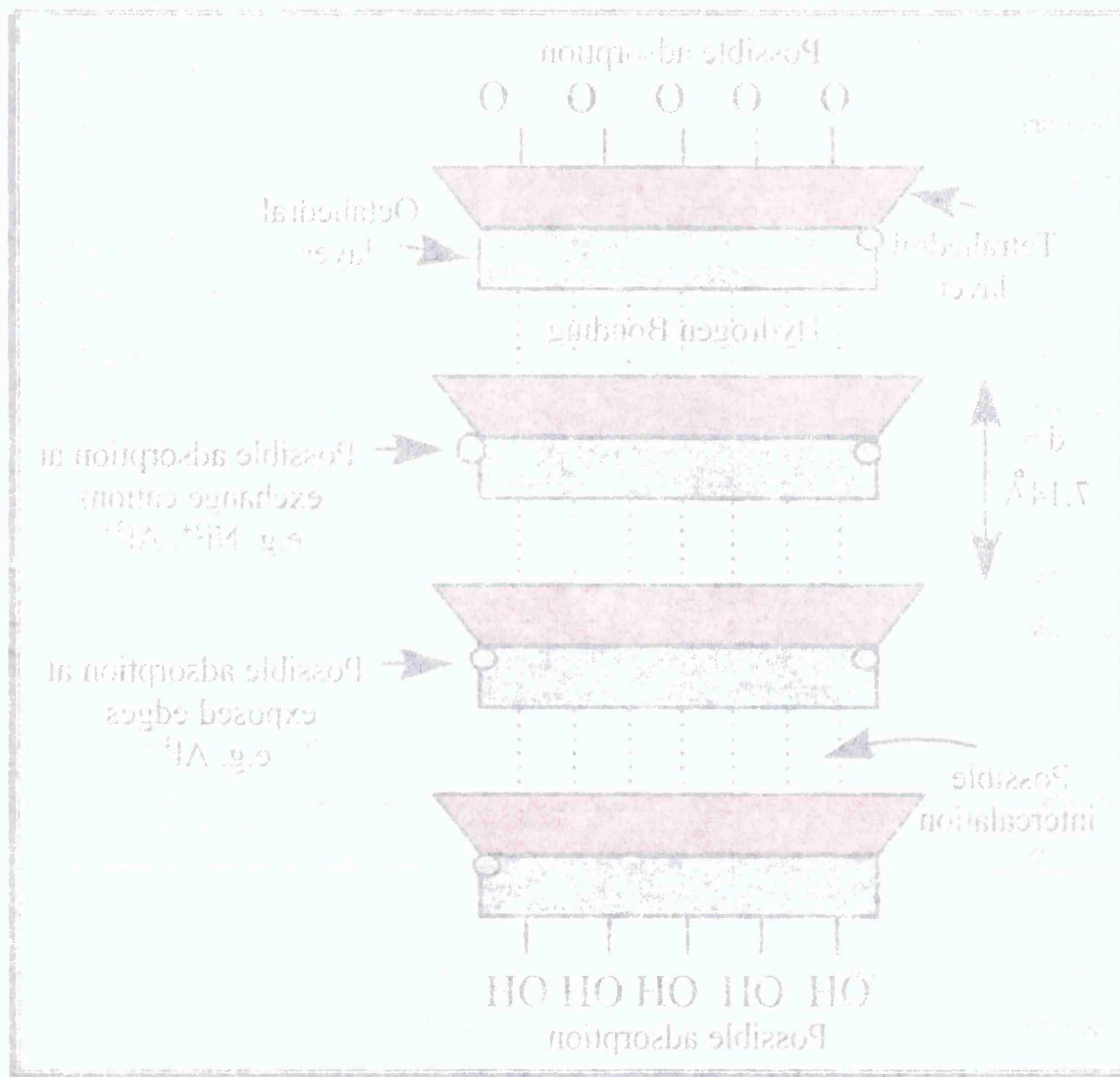


Figure 18. Potential binding sites on kaolin stacks.



The aluminium hydroxyl basal surface carries undissociated aluminols at neutral pH. The small proportion of negative charges on the basal surface arise from isomorphous substitutions in the structure, and are generally believed to be pH independent. (It should be noted that these isomorphous substitutions lead to a small number of cation exchange sites not depicted in Figure 1.8).

The charges on the lateral surfaces arise from protonation or deprotonation of aluminol and silanol groups, and hence are pH dependent. At low pH (5 or below), some aluminol groups are protonated, creating positive charges which may be balanced by the permanent negative charges on the silicate surface and the dissociated silanols on the edge surface⁹ (the effects of these surface/edge charges are discussed more fully in Chapter 4).

Molecules may adsorb to the surface of kaolin at the points shown on the diagram and it is also possible that intercalation of some molecules will occur, whereby the hydrogen bonding network between the kaolin sheets is perturbed due to the ability of the molecules to enter into the hydrogen bonding network. A model for the intercalation of polar organics was proposed by Slonka¹⁰. The formation of intercalates is useful as a tool to distinguish between different types of kaolin, since all will react slightly differently to the presence of an intercalant^{11,12}. Intercalation of certain compounds may be facilitated by the use of an entraining agent- i.e., a molecule which will readily intercalate, but can then be replaced by another molecule. It is also possible to enhance the intercalation of certain compounds by complexing them with another more readily intercalated molecule, e.g. iron (III) chloride intercalation may be enhanced by complexing with DMSO¹³.

Impurities such as mica and feldspar may be found in the kaolin matrix. These are typically very fine grained and therefore it is difficult to completely purify kaolin for academic study, and as such individual samples can exhibit wide variability.

The industrial preparation of kaolin for use in the paper industry is designed to significantly reduce impurities from the end product and typically a Cornish kaolin has

the composition shown in Table 1.1¹⁴. It should be noted that this mineral sample was not used in the current study.

Table 1.1 Analysis of kaolin prepared from a Cornish matrix.

Mineral	% of total mass < 20 μm	% of total mass < 10 μm
Kaolinite	83	90
Mica	14	8
Feldspar	2	1
Fe ₂ O ₃	0.9	0.6
TiO ₂	0.05	0.06
K ₂ O	1.9	1.1

Mica is the least desirable of these impurities, since it will decrease the working life of industrial paper rollers and other equipment due to the abrasive nature of the mineral. However, in the commercial products produced at ECCI, the problem is minimised, since the particle size cut of the final product is such that the slightly larger grained mica is essentially removed by the various sedimentation processes.

1.2.3 Determination of the composition of kaolin using XRF.

An elemental analysis of the Cornish kaolin sample used in the work presented herein was carried out using x-ray fluorescence and the results are shown in Table 1.2 below:

Table 1.2 The elemental analysis of kaolin samples expressed as % oxide.

Oxide	Weight %
SiO ₂	46.43
Al ₂ O ₃	37.28
MgO	0.36
CaO	0.09
TiO ₂	0.03
Na ₂ O	0.29
K ₂ O	0.95
NiO	0.01
Fe ₂ O ₃	0.65

The SiO₂ concentration was higher than expected (compared with the percentage weight of Al₂O₃), and the major contaminants were found to be potassium and iron. These factors are likely to be due to the low concentration of mica impurity identified by XRD (see chapter 2).

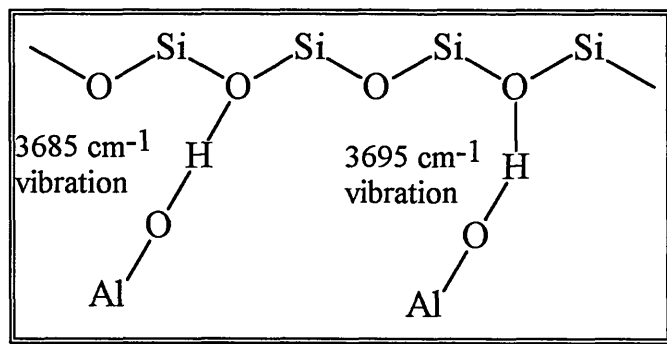
1.2.4 Hydrogen bonding in the kaolin lattice.

A hydrogen bond between a donor covalent pair, H-X (where X is a more electronegative atom than H) and another non-covalently bound electronegative atom with a lone pair of electrons B (in the polar species AB), results from electrostatic attraction. In the direction of the X-H bond, as the electronegativity of X increases, the the positive electric potential of H increases. This gives rise to a dipole with the hydrogen end of the bond being more positive. Coulombic interaction of this dipole with excess electron density at the acceptor atoms forms the hydrogen bond interaction (i.e., $X^{\delta-}-H^{\delta+} \cdots B^{\delta-}-A^{\delta+}$). The hydrogen bond has directional character, which is generally less pronounced than in covalent bonding. The strength of hydrogen bonding varies enormously, with a continuum of strengths between very weak and very strong interaction. If X is exceedingly electronegative, and B has a large excess of electron charge, very strong hydrogen bonds can be formed, which are practically covalent in nature. If, however, X is less electronegative, the hydrogen bond will be weaker, and the

interaction will be primarily electrostatic in nature. The bond length will be greater than that of covalent or strong hydrogen bond association.

A review of the hydrogen bonding interactions between the adjacent tetrahedra and octahedra in the kaolin stack was produced by Yariv⁵. The siloxane group has a low affinity for protons and does not form stable hydrogen bonds. Al-O is a stronger proton acceptor than Si-O, and thus forms stronger hydrogen bonds. As a result of the polarisation of the Si-O and (Al)-OH bonds, the surface oxygen and proton plane obtain a negative and positive charge respectively. Strong electrostatic attraction forces between the planes of parallel layers with opposite charges and van der Waals interactions lead to the stacking of the tetrahedra and octahedra in flat, parallel layers. The hydrogen bonding which results from the interactions between Si-O and Al-OH is thought to be weak (based on bond angle measurements for the inner surface hydroxyls of 168, 146 and 144°). However, bond angle measurements are controversial, and Hess and Saunders¹⁵ suggested that the inner surface hydroxyls are oriented over a range of angles. The positions of the IR spectral bands of the outer sheet hydroxyls (c 3695-3650 cm⁻¹) also indicate that the bonding is weak. Presumably, whatever the angle, the effects of multiple weak hydrogen bonding interactions are synergic, and thus the sum of the interactions between the tetrahedra and octahedra leads to the strong associations observed during intercalation studies (i.e., that intercalation rarely occurs, except with highly polar molecules which are able to penetrate the interlamellar bonding network). Recently, Raman microscopy has been used to study the kaolin structure^{16,17,18,19,20}. Raman microscopy can also discern the 4 major hydroxyl stretching bands of kaolin between c 3695 and 3620 cm⁻¹. Another band at 3685 cm⁻¹ can also be readily distinguished. This band is usually IR inactive. It has been attributed to the in phase analogue of the 3650 cm⁻¹ (out of phase) inner sheet hydroxyl stretch. The 3695 band was said to correspond to the in phase vibration of another inner sheet hydroxyl. This band is coupled with the out of phase vibration of the same hydroxyl at 3670 cm⁻¹. Based on observations of the Raman spectra of various kaolin samples of differing crystallinities and observations of the relative intensity shifts of the 3695 and 3685 cm⁻¹ bands after disordering via intercalation, Frost has proposed a scheme for the hydrogen bonding between adjacent kaolin layers²¹.

Figure 1.9 Proposed structure for hydrogen bonding between kaolin layers.



The hypothesis for differentiating between the Raman active 3685 and 3695 cm^{-1} bands is based on two models for the direction of the Al-OH groups in relation to the Si-O groups of the adjacent layer. If the groups form a linear hydrogen bond, then on the pico second timescale (which is the timescale of measurement by Raman spectroscopy) the hydroxyl proton may form a centre of symmetry between the two oxygens (thus, resulting in a Raman active but IR inactive vibration). If the hydrogen bond is non linear, or covers a range of angles, the hydroxyl mode will be both Raman and IR active. The 3695 cm^{-1} band does not possess a centre of symmetry, and is thus active in both Raman and IR spectroscopy. Intercalation by mechanical and chemical means (i.e. increasing disorder) has resulted in an increased intensity of the 3685 cm^{-1} band compared with the 3695 cm^{-1} band. Thus, it was concluded that the 3685 cm^{-1} band represented a linear hydrogen bond, and that the 3695 cm^{-1} band represented a hydrogen bond which could exist over a range of non linear positions.

Treatments such as grinding^{22,23} temperature²⁴, adsorption²⁵ and intercalation²⁶ can have a considerable effect on not only the physical, but also the chemical properties of kaolin. For example, disaggregation by intercalation of urea was used by Chinese ceramists to increase the dry strength of their “egg-shell” porcelain²⁷. Amongst the most significant changes are the total surface area and the number and type of binding sites which are exposed. The effects of physical or chemical treatments on the structure of kaolin can be studied using a number of techniques, including IR spectroscopy, TGA (thermogravimetric analysis), DTA(differential thermal analysis), XRD and SEM.

1.3 Materials.

1.3.1 Kaolin sample.

Unless otherwise specified, the Cornish kaolin used here was a gift from ECCI, St Austell, Cornwall, England. It was classified as a chemical free, special particle size (SPS) equivalent. Purification was carried out using only gravitation and filtration techniques, which resulted in a particle size cut as shown below in Table 1.3.

Table 1.3 The size of SPS grade kaolin produced by ECCI.

Particle Size (μm)	% of Total
<2	80
<10	100

For infrared spectroscopy, the kaolin was diluted with 99 % pure potassium bromide (KBr), purchased from Sigma Aldrich. Neat KBr was used as a reference material in each case. For variable temperature DRIFTS (see below) the KBr used as background spectra was heated in the same way as the sample.

1.4 Methods used to study clay minerals.

1.4.1 Infrared spectroscopy.

1.4.1.1 History of spectroscopy in minerals science.

IR spectroscopy is particularly suitable to the study of the effects of milling, organic interactions and water adsorption, since it is able to visualise not only interlamellar sites, but also the surface of the mineral, and thus, the base-clay interaction modes (however, it cannot distinguish between these sites, and XRD is thus used as a complementary technique). Bond formation and strength can be estimated from the perturbation of the characteristic infrared adsorption bands of both the organic and mineral species. Hence, the surface sites on the clay, can be distinguished. DRIFTS has been used successfully in a few studies^{28,29,30}, but historically, the most widely used method for the examination of minerals has been the IR transmission of alkali-halide pressed disks³¹. Other techniques have also been used to measure the infrared spectra of powdered samples, in particular, absorption^{32,33,34,35} emission^{36,37} and near IR³⁸. Additionally, the thermal stability of mineral-organic complexes has been well studied by various IR techniques, including

ATR (attenuated total reflection)³⁹, transmission⁴⁰ and emission⁴¹. However, potentially one of the most suitable and informative methods is VT DRIFTS, which has seldom been exploited. It is ideal for use with powdered minerals of small, relatively evenly sized particles. Pandurangi and Seehra⁴² used DRIFTS to quantify the concentration of silica in silica-kaolin mixtures. They established that it was possible to use overtone and combination bands (see later) (e.g. a band at 1875 cm^{-1}) to quantify the silica present and that the relationship between spectral response and concentration remained constant up to 75 mg silica in 300 mg KBr (i.e. 25 %). The work presented herein generally uses concentrations of kaolin well below the expected concentration of non-linearity (between 5 and 10 % in KBr). Pandurangi and Seehra also noted the appearance of Reststrahlen bands in certain areas (e.g., a strongly absorbing band at 1080 cm^{-1}), probably due to the interference of Fresnel reflectance (i.e. Fresnel diffuse reflectance). They noted this effect above 10 % sample in KBr. At higher concentrations, they also noted peak distortions due to (Fresnel) specular reflectance. In a study conducted by the author of the work herein, no spectral distortions were observed in the range 1 to 50 % sample in KBr. The only effect of decreasing sample concentration was the relatively higher contribution of the water vapour spectrum. Due to limitations in the mass of available sample, generally concentrations of 5 or 10 % sample in KBr were used. This technique allows *in situ* FTIR spectrometry of the sample as it is heated. It can be used to assess the effects of heat on the mineral alone or in combination with organic probe molecules.

DRIFTS holds several advantages over pressed disk methods. Perhaps in this work, the most important advantage is that DRIFTS does not require any pressing of the sample. Pressed-halide (usually KBr) disk methods depend upon the powdered sample being exposed to extreme pressures in the sample preparation stage. This can lead to orientation effects and/or degradation of the sample. The KBr disk sample also must be pre-ground, leading to possible decreases in crystallinity and ordering. KBr is frequently used as a diluent in IR spectroscopy of minerals, since it is transparent to IR radiation down to c 250 cm^{-1} and it has a refractive index similar to that of many minerals. However, particular problems arise in the transmission methods, since not only can KBr interact with the mineral during pressing, but also it is hygroscopic. During the pressing of the disc, water adsorption often occurs. Although this adsorption is generally

reversible, its removal is by heating to elevated temperatures (e.g. 100°C) for several hours. Thus the sample may be further altered.

To produce a sample for diffuse reflectance work, the mineral specimen must simply be mixed with KBr for a few seconds, thus ensuring heterogeneity of particle size and thorough distribution of the mineral. The DRIFT spectrum can then be collected immediately.

1.4.1.2 Theory of infrared spectroscopy.

In general terms, spectroscopic techniques measure “the difference between energy levels in a material by measuring the energy of the absorbed or emitted radiation when the material is excited to a higher energy state, or as it decays back to the ground state”⁴³. For IR spectroscopy, the exciting radiation is, naturally, infrared, with a wavelength of between 10^{-3} and 10^{-6} m. A summary of the theory of infrared spectroscopy is presented herein, and for a more detailed account, the reader is directed towards the existing specialised books available^{44,45,46}.

In the simplest, idealised model of an IR active vibrating molecule, 2 atoms of differing mass (m_1 and m_2) are joined by a weightless spring (i.e., a simple harmonic oscillator).

When the atoms are pulled apart, attractive forces pull the atoms back together. Likewise, if the atoms are forced together, repulsive forces may push them apart again. The behaviour of the system is governed by Hooke's Law shown below.

Equation 1

$$f = -k(r-r_e)$$

where f = the restoring force, k = the force constant

r = the internuclear distance, r_e = the internuclear distance

at equilibrium or bond length.

Of course, in a real system, if the atoms are pulled too far apart, the bond (spring) will break, and the atoms become dissociated. The energies associated with the atoms during anharmonic compression and extensions are approximated by the Morse function:

Equation 2

$$V = D_e [1 - \exp\{a(r_e - r)\}]^2$$

Where D_e = dissociation energy a = constant for a particular molecule

r_e = equilibrium distance, or bond length

r = internuclear distance.

This equation can then be used to solve the Schrödinger equation, the permitted energy levels are found to be

Equation 3

$$E_v = (v + \frac{1}{2})\omega_e - (v + \frac{1}{2})^2 \omega_e x_e$$

Where ω_e = oscillation frequency, x_e = anharmonicity constant = $\alpha^2 / 2\mu\omega_e$

$v = 0, 1, 2, \dots$

μ = reduced mass.

Thus, the selection rules for an anharmonic oscillator undergoing vibrational changes are

$$\Delta v = \pm 1, \pm 2, \pm 3, \dots$$

The lowest energy level is when $v = 0$, as is called the ground state. It should be noted that the energy does not equal zero, but it is the “zero point energy” which can be calculated from the approximated equation, Equation 3. A general equation for the energy levels has been derived and is used to fit experimental data and find the dissociation energy of a molecule (Equation 4).

Equation 4

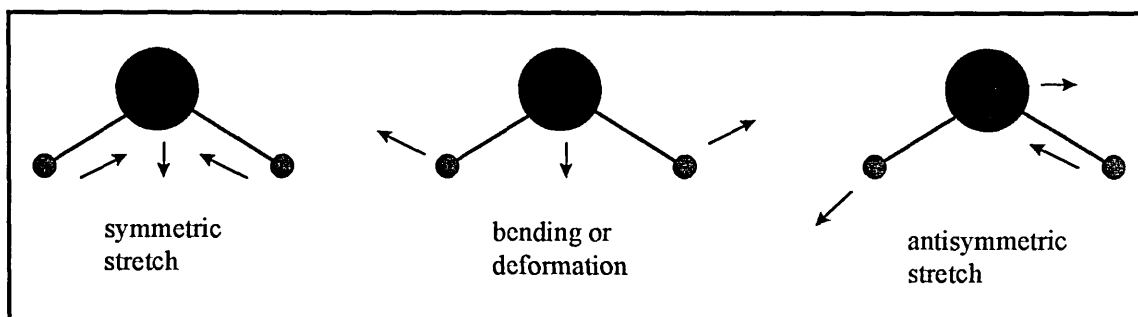
$$E_v = (v + \frac{1}{2})\omega_e - (v + \frac{1}{2})^2 \omega_e x_e + (v + \frac{1}{2})^3 \omega_e y_e \dots$$

If a molecule is to absorb infrared radiation, it must undergo a net change in the dipole moment due to its vibrational motion. The dipole moment is the product of the magnitude of the localised electrical charges within any molecule and the distance separating the positive and negative components of the charges (i.e. the atoms). If the frequency of the incident radiation is the same as that of the molecular vibration, a net transfer of energy can occur. Radiation is absorbed which results in a transition from one vibrational level to a higher vibrational level.

1.4.1.2.1 The vibrational modes of polyatomic molecules.

In a polyatomic molecule, each atom has three degrees of motional freedom, that is, it can move independently in three different directions along the axes of a Cartesian co-ordinate system. If there are n atoms in a molecule, then there are $3n$ degrees of freedom. Three of the degrees are translational (i.e. they involve moving all atoms simultaneously in the same direction parallel to the axes of a Cartesian co-ordinate system). Another three degrees describe rotations about the principle axes. The remaining $3n-6$ degrees are motions which change the bond lengths and angles between atoms. The bonds are elastic, and thus periodic motion occurs. All vibrations of an idealised molecule result from the superposition of $3n-6$ non interacting normal vibrations. The frequency and relative motions of the atoms are governed by force constants of the bonds, the masses of the atoms and the molecular geometry of the local environment. The motions of the vibrating molecule give rise to spectra characteristic of that group of atoms. In a diatomic molecule, if the atoms are alike, no vibrational spectrum is observed. See Figure 1.10 for a schematic representation of the vibrational modes in a polyatomic molecule.

Figure 1.10 Vibrational motions in a polyatomic molecule(e.g. water).



The transitions that are normally observed are

$\nu = 1 \leftarrow 0$, which is a fundamental transition (i.e. the first harmonic) and

$\nu = 2 \leftarrow 0$ or $\nu = 3 \leftarrow 0$, which are overtones, and occur at frequencies of $2\nu_1$ and $3\nu_1$, where ν_1 is the fundamental mode frequency.

Selection rules (see below) permit combination bands and difference bands. The former arise from the addition of two or more fundamental frequencies or overtones, and the latter from the subtraction of two or more overtones or fundamental modes. Combination bands generally have small intensities compared with fundamental vibrations.

1.4.1.2.2 Factors affecting the intensity of infrared bands.

Intensity of the spectrum depends upon three factors:

a, the selection rules for infrared. This determines whether the transition is “forbidden” or “allowed” (see reference⁴⁷ for details).

b, the population of the initial state at thermal equilibrium. For most systems it is found that the ground state is the most heavily populated at thermal equilibrium. The intensities of the transition at thermal equilibrium are proportional to the population of the initial vibrational state. The population is given by the Boltzmann distribution shown in Equation 5

Equation 5

$$N_i/N_0 = g_i/g_0 \exp (-\Delta E/kT)$$

Where N_i = number of molecules in a particular state,

N_0 = number of molecules in the ground state,

ΔE = difference in energy between the states,

k = Boltzman constant, T = temperature,

g_i and g_0 = degeneracies of the particular levels.

c, the number of molecules in the beam. (i.e. sample thickness or concentration).

The relationship connecting the intensity of transmitted and incident radiation to the number of molecules is governed by the Beer-Lambert Law (see Equation 6).

Equation 6

$$\log (I_0/I) = \epsilon cl.$$

Where I_0 = intensity of radiation falling on the sample,

I = transmitted radiation,

c = sample concentration,

l = path length,

ϵ = extinction coefficient at a given wavelength.

1.4.1.2.3 Fourier transform spectroscopy.

Fourier transform (FT) instruments in spectroscopy are now commonplace and hold many advantages over dispersive instruments, where a grating or prism is used in order to resolve the radiation into separate components. FT infrared spectrometers combine a

radiation source, a sampling arrangement (discussed later), a device for spectral dispersion or selection of radiation, and a radiation detector connected to the appropriate recording device. The spectrometer used in the current work employs a Michelson interferometer. A Michelson interferometer allows all the infrared frequencies of the source to be recorded in the time domain as an interferogram, thus reducing the measuring time of the instrument in proportion to the number of spectral elements (the ‘Fellgett advantage’⁴⁴). This is a dramatic improvement compared with traditional dispersive instruments. A Fourier transform is then used to convert this to the frequency domain (see below). During the mathematical conversion an apodisation function is used to smoothly truncate the interferogram thus removing spurious oscillations. The choice of apodisation function can influence the resolution and signal to noise ratio of the spectrum. There is no perfect apodisation function, and the optimum function for any given system should be used.

1.4.1.2.3.1 Fourier transform.

This is a mathematical procedure which converts the signal as a function of time (retardation) to a signal as a function of frequency. The intensity of the radiation at the detector can be described by Equation 7 below.

Equation 7

$$I(x) = 2 \int_0^{\infty} S(\bar{\nu}) \cos(2\pi x \bar{\nu}) d\bar{\nu}$$

Where $S(\bar{\nu}) =$ spectral density as a function of the wavenumber $\bar{\nu}$
 and $x =$ retardation.

In practice, the mirror does not travel an infinite distance, but has a maximum (x_{\max}), which means there is a maximum permitted frequency, known as the aliasing frequency (shown in Equation 8 below).

Equation 8

$$\nu_{\max} = 1/2x_{\max}$$

Thus, a more practical transform is given by Equation 9.

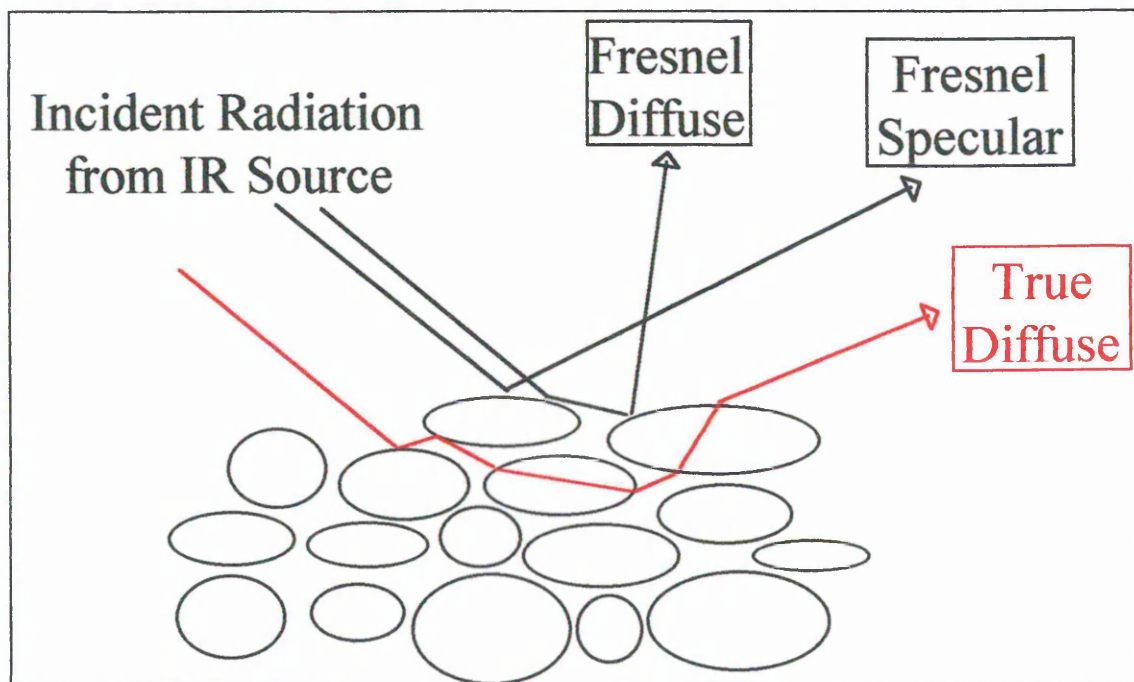
Equation 9

$$I(x) = 2 \int_0^{x_{\max}} S(\bar{\nu}) \cos(2\pi\bar{\nu}x) d\bar{\nu}$$

1.4.1.2.4 Diffuse reflectance.

Specifically, diffuse reflectance infrared spectroscopy is dependent upon the reflection, refraction and diffraction of an infrared beam caused by interactions with a powdered sample. Scattering of the incident beam within the sample is vital to the success of the experiment and this radiation must be collected with the exclusion of the specularly reflected radiation. With a strongly scattering sample, radiation is scattered in all directions above the sample (see Figure 1.11 below)

Figure 1.11 Schematic representation of diffuse reflectance.

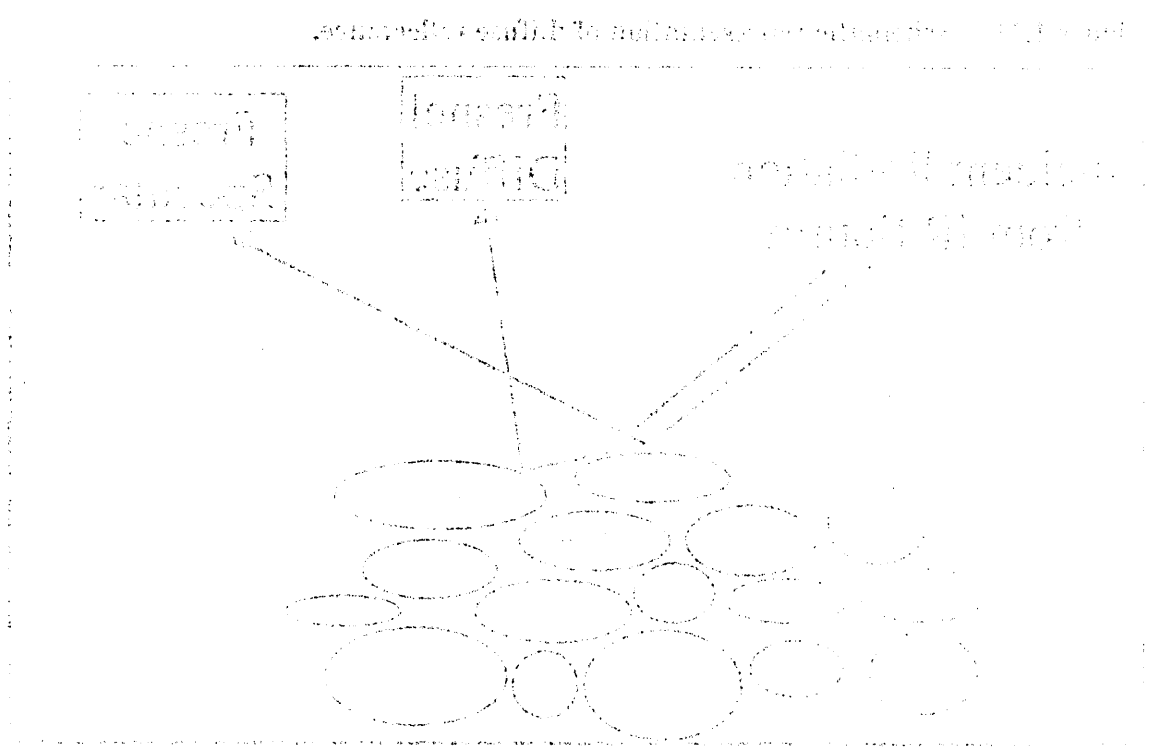


Fresnel specular reflectance occurs when the angles of incidence and reflectance are equal (as if reflected in a mirror). This type of reflectance (sometimes also referred to as specular-, true specular-, front surface- or regular reflectance) is governed by the Fresnel equations^{48,49}.

In the Fresnel diffuse (diffuse specular) type reflectance, the incident beam undergoes multiple reflections off particle surfaces without actually penetrating the particle. The reflected beam emerges from the sample in all directions.

...with the... of... and...
 ...the... of... and...
 ...the... of... and...
 ...the... of... and...

Figure 1: A conceptual model of the research design.



...the... of... and...
 ...the... of... and...
 ...the... of... and...
 ...the... of... and...

...the... of... and...
 ...the... of... and...
 ...the... of... and...
 ...the... of... and...

In the third type of reflectance (true diffuse), before emerging from the sample, the beam passes into the particles and undergoes absorption, reflection, refraction and scattering. This type of reflectance also emerges in all directions.

The possible interference of specular reflectance is one of the major factors affecting DRIFT spectra. The amount of specular component in the spectrum is governed by the refractive index of the sample, (n'), which is the complex sum of the index of refraction (n) (called the real component) and the absorption index (k') (called the imaginary component):

$$n' = n + ik' \quad (\text{for non-absorbing materials, } k'=0)$$

Specularly reflected light may be described by Fresnel's equations (see reference ⁴⁴) which express the reflection of radiation at an interface as a function of the refractive indices of the two media that form the interface. The difference in the refractive indices leads to reflection. The differences in refractive index that lead to reflection can be due to the real or imaginary components.

The absorption index, k' , is related to the absorption coefficient, K , i.e.

$$k' = K/4\pi\nu,$$

where ν is the frequency of radiation (cm^{-1}).

The absorption coefficient, K , is related to the absorptivity, a , by:

$$K=2.303ac,$$

where c is the concentration.

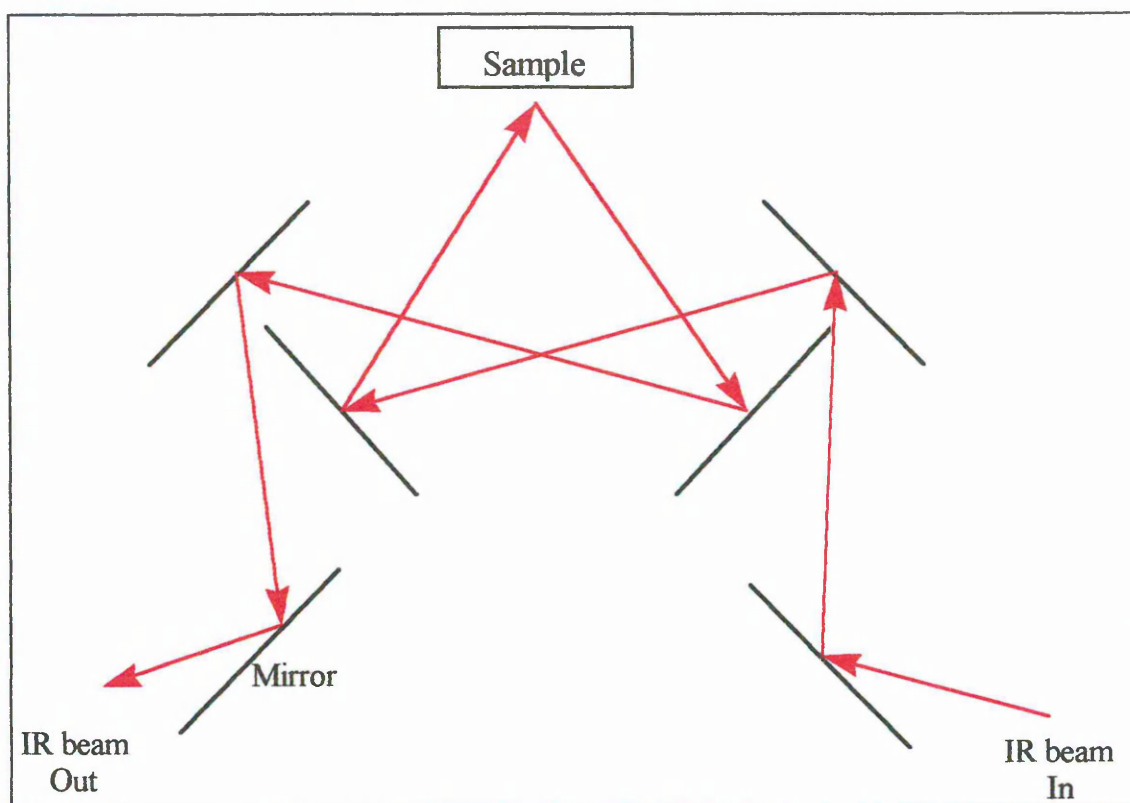
If the sample absorbs, the absorption coefficient, K ($\neq k'$) has an effect on the amount of specular reflectance near the wavelength where absorption occurs. The appearance of the features produced in the infrared spectrum depends on the value of the absorption index and hence the absorptivity.

If the absorptivity is very small, very little if any change in the spectrum results. If the absorptivity is intermediate, as is for most organic compounds, the increased specular reflectance can result in an anomalous dispersion feature. This leads to a derivative shaped feature or a shift in the peak maximum to higher wavenumber of the band in question. If the absorptivity is large, such as the strong bands in some minerals, a large reflectance maximum, called a reststrahlen band results.

In order to collect the spectrally important radiation (i.e. to eliminate as much of the Fresnel diffuse and Fresnel specular components as possible), mirrors covering a large angle are positioned above the sample cup, although efficiency of diffusely reflected radiation may still be low. The collection of specular reflectance radiation by the detector can lead to non-linearity of the DRIFT spectra. Specular reflectance is particularly abundant in compact samples with a smooth surface, and in order to eliminate as much of this as possible, a number of steps can be taken

Firstly, the mirrors are positioned such that the angle of specular reflection is avoided. Early diffuse reflectance cells used a “blocker” in order to further reduce the collection of specular reflectance. The Graseby Specac DRIFTS Accessory used in the current work had a complex mirror arrangement, as shown in Figure 1.12 below. Specular reflectance can also be greatly reduced by mixing the sample with a non absorbing diluent, such as KBr. For a more detailed review of the theory of DRIFTS, the reader is referred to two of the more recent and detailed reviews ^{44,50}.

Figure 1.12 Schematic diagram of the DRIFTS sampling arrangement.



The alignment of the mirrors and sample in this arrangement is critical, since typically only 10 to 50% of the energy throughput is available for DRIFTS analysis compared with the transmission mode.

Diffuse reflectance spectra are not easily reproducible, since the technique depends crucially upon many factors⁵¹. However, it is possible to achieve good reproducibility if these parameters are monitored and controlled as far as possible. Some of the more important factors are listed below:

Choice of halide as a diluent (and reference powder). The use of a sample diluent decreases the specular component of the reflected beam, whilst increasing the diffuse reflectance component, thus reducing (or removing) reststrahlen bands and other anomalous dispersion effects. Alkali-halides are used most frequently in this capacity, since they are highly scattering, good diffuse reflectors, and infrared transparent. KBr was selected as the diluent of choice for the work presented herein, since it has been used historically in minerals analysis by IR very successfully. The interactions with the sample are believed to be negligible under the conditions used for DRIFTS analysis. The hygroscopic nature of alkali halides is a potential disadvantage in IR spectroscopy, since

water produces very intense bands in the c 3300 and 1650 cm^{-1} regions. The adsorption of organics is also a potential problem, since bands are produced at c 2950 cm^{-1} . These areas are also of significance in minerals analysis. To overcome this issue, KBr was dried at 400 °C for at least 2 hours prior to use. It was cooled in a moisture and organic free desiccator and removed immediately prior to background spectrum collection or to mixing with the mineral sample.

Particle size of the sample (and diluent) can influence the amount of diffuse reflectance. Generally, particle size needs to be less than 10 μm for optimum collection of diffuse reflectance, and minimal specular reflectance. Particle size should be kept as constant as possible between samples.

Initially, as the **depth of the sample** is increased, there is a subsequent increase in the absorption bands produced. At a certain depth for a particular sample, no further increase will be observed. The sample is said to be of “infinite thickness”. This thickness generally ranges between 2 and 5 mm. In the present work, a crude investigation was carried out to determine the infinite thickness. It was deemed to be no more than approximately 2 mm. The samples from which DRIFT spectra were collected for presentation in this thesis were no less than c 3 mm in depth.

Sample packing affects diffuse reflectance spectra. An advantage of packing the sample under pressure is that it can help to orient the sample. However, closely packed particles are less suited to diffuse reflectance spectroscopy than lightly packed samples. The closer packing leads to a greater proportion of the incident radiation being specularly reflected. In the present study sample packing was not used, since it is known to significantly alter the physical properties of the sample.

Sample homogeneity is important and good mixing is essential for DRIFTS, since sampling is over a relatively small area. Ball milling can be used to achieve adequate mixing (and provide uniform particle size), but milling has a substantial effect on the structure of the mineral (discussed in detail in Chapter 2) and is not suitable for use here. Instead, the 200 mg sample-alkali halide mixture was mixed lightly using a mortar and

pestle for 40 seconds. This mixing achieved good homogeneity and was intended not to alter the sample integrity.

The **height of the sample** in relation to the optics of the system must be optimised to ensure that the point of contact of the IR radiation is at the focal point of the mirror arrangement.

Polarisers can be used to reduce the specular reflectance component if placed prior to and after the points of reflection. However, the specular component is never completely removed and loss of signal intensity is a secondary result.

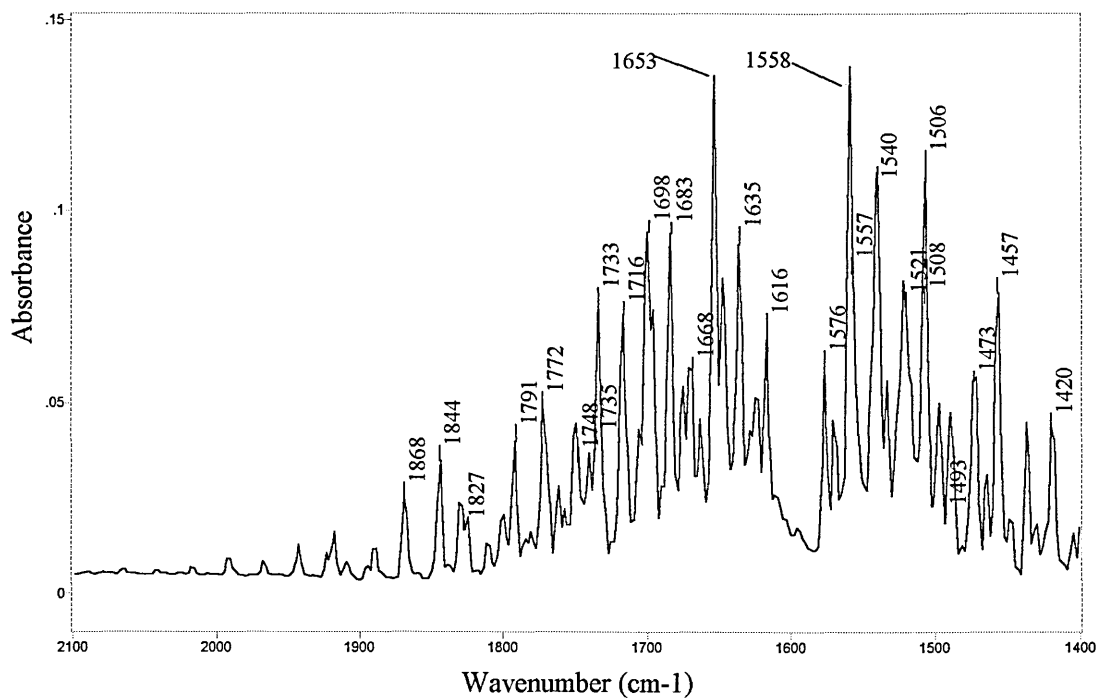
The use of a **blocker** to physically block the specular component from the detector has been used in some DRIFTS systems (often a razor blade placed a few mm above the sample). This is more efficient if the sample is flat and well packed because the angles of specular reflectance are obviously more diverse if the sample contains randomly oriented particles. The use of a blocker results in a loss of intensity of the signal reaching the detector. It is not employed in the DRIFTS accessory used in the present study.

If the physical characteristics of the sample are kept constant, as the sample concentration increases, so does the amount of specularly reflected radiation, thus the diffuse reflectance observed decreases. For this reason it is advantageous to dilute the sample with a non absorbing compound such as KBr.

VT DRIFT spectra are susceptible to baseline artefacts, typically broad features superimposed on the spectra, which can result from instrumental fluctuations occurring between the collection of the reference and the sample spectra, such as interferometer stability. Heating the sample holder also changes the baseline, since the thermal expansion results in changes in the sample-incident beam interface. This effect is minimised by heating the KBr used as a reference to the same temperature as the sample. However, the collection of the sample interferogram and that of the reference interferogram may be days apart, and thus changes in atmospheric water vapour spectra are inevitable. The resulting sample spectrum may have a water vapour spectrum superimposed on it, and as a result the bands of interest in the sample spectrum may

become obscured. This problem is minimised during the practical procedure by purging the instrument with dry air and purging the sample holder with nitrogen. Subsequently, water vapour subtractions can be made using the software package. Here, a ratio is taken of interferograms at two consecutive temperatures in the “stepping” scheme, e.g. 100 and 125 °C. The spectrum of water vapour alone is thus obtained (see Figure 1.13 for an example of a typical water vapour spectrum). The result may then be subtracted from the sample spectrum (at 125 °C). Complete water vapour spectral subtraction is not always possible, but the effect can be minimised this way. The Kramers-Kronig transformation can be used to mathematically overcome spectral distortions caused by the refractive index effect, by separating the real and imaginary components of the spectrum. A spectrum which consists primarily of specular reflectance can be converted into one which displays absorption information. This type of spectral manipulation was not required in the work presented herein.

Figure 1.13 A typical water vapour spectrum (the water bending region).



VT (variable temperature) DRIFTS allows the collection of diffuse reflectance spectra as a sample is heated and can be thought of as an *in situ* method of gaining information regarding the changes occurring during thermal treatment. The information obtained can

be correlated with VT XRD, TGA and DTA. Furthermore, quantitative analysis is feasible using this method of study⁴².

1.4.1.3 VT and RT DRIFTS experimental parameters.

Samples were diluted to 5 or 10 % in KBr. The KBr had previously been dried for at least 2 hours at 400°C in order to drive off excess moisture and inorganic impurities, and stored in an airtight container. Following light mixing using a pestle and mortar, the samples were placed immediately into the VT DRIFTS cell and a spectrum and time = 0 was recorded.

All spectra in the following study were produced using a Mattson Polaris FT-IR spectrometer equipped with a temperature controller with a range of 0 to 500 °C and an MCT detector. The sealed instrument, incorporating a Graseby Specac Ltd “Selector™” DRIFT accessory, was purged with dry air over night to ensure the contribution from water vapour was minimised. N₂ flow was resumed the next morning and spectra were collected at intervals of 25°C up to 200°C and of 50°C thereafter. Temperature within the environmental chamber was controlled by a Graseby Specac P/N 20130 series automatic temperature controller, which has a range of 0-500°C. The selectable parameters were as follows:

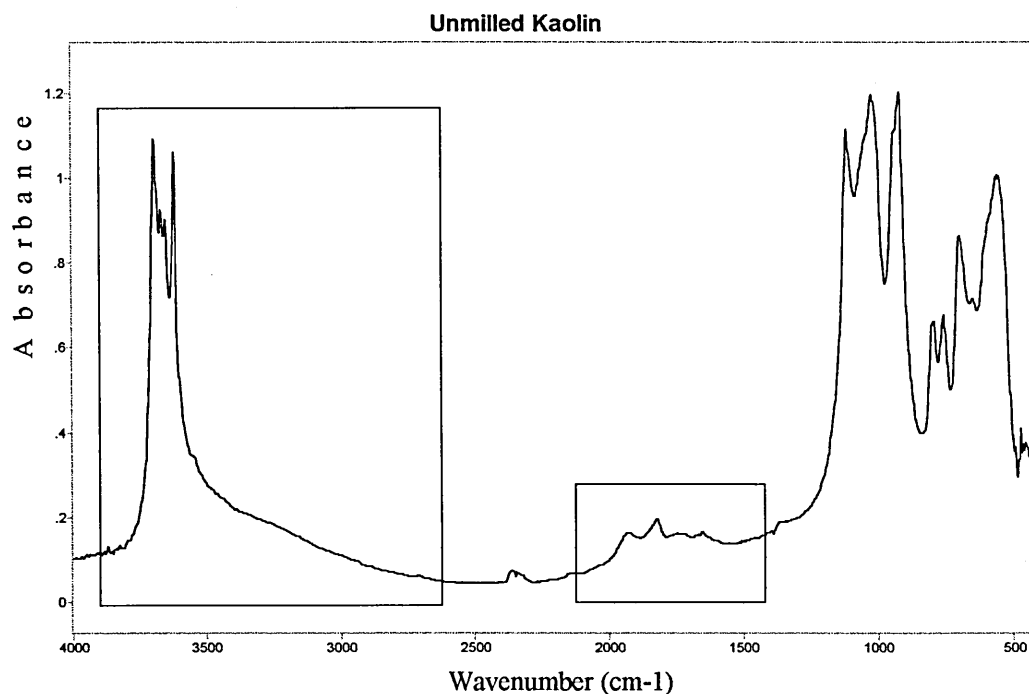
Table 1.4 Parameters used in the collection of IR spectra.

Parameter	Setting
Resolution	4.0 cm ⁻¹
Sample Scans	276
Background Scans	276
Start Wavenumber	400 cm ⁻¹
End Wavenumber	4000 cm ⁻¹
Iris	85%
Signal Gain	1
Apodization function	Triangular

The single beam spectra obtained were ratioed against a neat KBr background which was recorded in a separate experiment under the same conditions. Water vapour was subtracted where appropriate, and multipoint baselines were used to level and zero the data over the regions of interest. Spectral manipulations such as baseline adjustment, curve fitting (band component analysis) and water vapour subtraction were performed using the Spectracalc software package GRAMS (Galactic Industries Corporation, NH, USA.).

1.4.1.4 Curve fitting of DRIFT spectra.

Figure 1.14 A typical DRIFT spectrum of kaolin.



Most of the work in this thesis investigates the influence of various treatments upon the areas of the spectrum highlighted above. A number of bands are present in these regions, but are not all discernible by eye. In order to elucidate information regarding the changes in intensity and frequency of bands in these regions, curve fitting was employed. As far as possible, band positions were used which had previously been discussed in the literature. The shapes of the fitted bands applied are discussed in the relevant chapters. Reliability of fit was achieved by a critical evaluation of the Chi^2 results for a set of, rather than individual spectra. An acceptable set of fits provided Chi^2 values which varied no more than $\pm 5\%$ around the mean value.

1.4.2 XRD.

XRD has historically been very important in the study of the crystalline phases present in clay minerals. Although quantitative analysis is possible, reproducibility is dependant upon many factors including sample length, thickness, position, alignment (pressing), sample homogeneity and the quality of the standards used⁵². Hence, sample preparation is very important in XRD analysis. XRD can be particularly useful in the study of intercalated clays. Identification of clays by XRD is based in the most part on the basal (or d) spacing of the crystallographic planes parallel to the sheet structure. If the d spacing of the untreated mineral is known (7.12 Å in the case of kaolin), an increase in value can be attributed to successful intercalation (e.g. to 8.4 Å for artificially hydrated kaolin⁵³). VT XRD (i.e. variable temperature XRD) can be used to monitor thermal decomposition, i.e., the loss of the intercalated species and the subsequent collapse of the mineral layers with increasing temperature. The extent of expansion of the mineral layers can be calculated using Bragg's Law (see below).

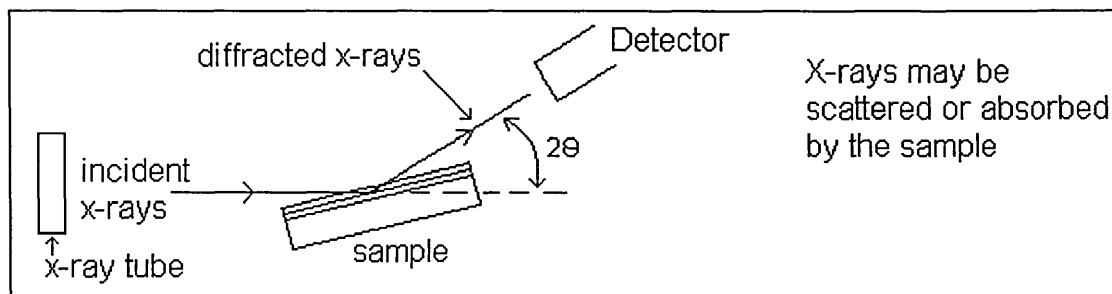
The crystallinity of kaolin may be assessed according to the Hinkley index. However, the index can be greatly influenced by the presence of impurities²¹ and therefore was not utilised in the present work.

1.4.2.1 Theory of XRD.

In modern XRD instruments, an evacuated chamber contains a metal target (Cu in the instrument used for this work) which is struck by incident high speed electrons from a heated filament. X rays are thus produced. The x rays are directed at the sample over a range of angles. X rays are electromagnetic waves characterised by an electric field, the strength of which varies sinusoidally with time at any one point in the beam. This oscillating electric field exerts a force on the electrons of an atom causing any electron it encounters to oscillate about its mean position. This accelerating and decelerating electron emits an electromagnetic radiation, and it is in this sense that the electron is said to scatter x rays. The scattered beam is simply the beam radiated by the electron under the action of the incident beam, and has the same frequency as the incident beam. Thus, the scattering of x rays by matter occurs. Scattering of x rays is proportional to the size of the atom, providing that the dimensions of that atom are less than the x ray

wavelength. See Figure 1.15 for a schematic representation of a typical x ray diffractometer.)

Figure 1.15 Schematic representation of an x ray diffractometer.



(Taken from reference⁵¹)

If Bragg's Law is obeyed, diffraction will occur at an angle θ , if a beam of x rays falls on a series of atom bearing planes within the sample, each a distance, d , apart. Bragg's Law states that $n\lambda = 2d \sin\theta$, where λ = wavelength and n is an integer. During an experiment, both the detector and the sample are rotated in order to reach the required angle. The intensity of the scattered x rays obeying Bragg's Law is measured as a function of the diffraction angle (2θ) and the orientation of the sample. XRD cannot distinguish bulk from surface mineralogy. Thus, by rearranging Bragg's equation, the d -spacing of a mineral can be obtained: $d = n\lambda / 2 \sin \theta$.

1.4.2.2 Experimental parameters.

For room temperature XRD, samples were presented to the Philips PW1830 x ray diffractometer operating at 35kV and 45mA, as pressed powders. A Cu K α radiation source was used, with a wavelength of 1.5418Å. The diffraction patterns were recorded, with an angle range of 5-65 ° 2θ at a scan rate of 2 ° 2θ per minute. VT XRD traces were collected using the same instrumental parameters, but the sample was mounted onto a glass slide as a film. The liquid pyridine treated sample was pasted onto the slide and allowed to dry *in situ*. Drying was complete after approximately 30 minutes. This was placed on a heating plate, and temperatures were ramped in a manner similar to that used in the VT DRIFTS experiments.

1.4.3 Thermal analyses (TGA, DTA and DCS).

It is possible to investigate the thermal stability of mineral complexes using a number of thermal techniques, including TGA (thermogravimetric analysis), DTA (differential thermal analysis) and DCS (differential scanning calorimetry). These techniques are frequently used to assess energy changes and weight loss (or gain) from minerals and mineral-organic complexes upon heating. Sidheswaran *et al.*,⁵⁴ used the techniques to study the thermal decomposition of kaolin-potassium acetate salt intercalates. Although this work was able to discern changes in decomposition between the intercalated and untreated mineral, it was not able to assign the weight losses without other corroborative evidence. Methods of qualifying these weight changes include on line mass spectrometry, or more usually, FTIR.

Most of the thermal analysis in the work presented herein has been carried out using TGA. A few milligrams of sample are suspended from a sensitive recording balance in a refractory crucible. Mass loss from the sample may be recorded as temperature increases. The mass loss curve may be presented as the negative derivative ($-dw/dt$), thus showing rate of change of mass over temperature. Weight losses may thus be observed as maxima. Particle size, initial mass and packing density should vary as little as possible between samples in order to optimise reproducibility. An inert atmosphere was used to suppress the oxidation of organic materials in the clay sample, and also to remove any evolved gaseous by-product of the heating process. The heating strategy was kept constant throughout the course of the study.

DTA depends upon the detection of the exo-or endothermic reactions occurring when a substance is heated. It may be used to examine structural changes such as dehydroxylation (the conversion from kaolin to metakaolin) at c 550 °C, and also events which do not involve weight loss, such as the conversion at c 990 °C of metakaolin to mullite.

1.4.3.1 Experimental parameters.

For TGA and DSC measurements, a Mettler-Toledo TA8000 thermoanalyser was used to analyse samples of between 7 and 10 mg. They were heated from 35 to 800°C at 20

°C per minute under a flow of N₂ carrier gas at 20 ml per minute, after an initial acclimatisation period of 15 minutes at room temperature.

For DTA measurements, samples of approx. 6mg were presented to a Polymer Labs simultaneous thermal analyser (STA 409EP). Samples were heated from 20-1200°C at 10°C per minute under a flow of N₂ carrier gas. Al₂O₃ was used as a reference.

1.4.4 Ball milling.

1.4.4.1 Experimental parameters.

Ball milling of the samples was carried out at Schlumberger, Cambridge, England, using a Retsch MM2 ball mill grinder equipped with 2 tungsten carbide grinding pots (internal volume of 10 ml) and 2 tungsten carbide grinding balls (diameter 12 mm) per pot. 2g of kaolin were ground at a frequency of 45 Hz, for 3, 10 or 30 minutes. Samples were stored in sealed vessels until use

1.4.5 XRF.

XRF is used to quantify the elemental oxides present in a sample. X rays are directed towards the sample, and x ray fluorescence occurs at characteristic “finger print” wavelengths specific to the elements present. The concentration of the element is proportional to the intensity of the fluorescence at that wavelength.

1.4.5.1 Experimental parameters.

1g samples were fused with 10g of Li₂B₄O₇. The beads formed were presented to a Philips PW2400 sequential XRF spectrometer. A wide range oxide analysis was performed using certified synthetic reference standards.

1.4.6 SEM.

Electron microscopy is a long established method for characterising clay minerals (see Shaw⁵⁵ and references therein). The advent of scanning SEM in the late 1940s has facilitated the three dimensional visualisation of clay particles. A disadvantage of SEM is that it is not been possible to examine the mineral sample in its natural state, since multiple and sometimes harsh preparation steps are required before micrographs can be

obtained. Sample preparation was kept to a minimum in the work presented herein, but it is acknowledged that some alterations will have occurred.

1.4.6.1 Experimental parameters.

Lightly ground samples were spotted by blowing, with compressed gas, dry powder onto carbon coated aluminium stubs. Samples were then gold coated, using a sputter coater, to reduce charging problems, and presented to the Philips XL40 scanning electron microscope equipped with an Oxford Instruments LINK energy dispersive x-ray analyser (EDX). Micrographs were produced using a 20 kV electron beam.

Note

Kubelka-Munk (K-M) conversions are sometimes used in the literature to present DRIFT spectra, since the conversion is said to create a result similar to that produced by transmittance spectroscopy. Work by the author (not presented) showed that “absorbance” spectra were almost identical to true transmittance spectra (produced by the pressed pellet method), whereas K-M spectra showed marked differences to the transmittance spectra. For this reason DRIFT spectra presented in the work herein have been converted to “absorbance” spectra.

1.5 References.

- ¹ Grim RE (1964) Clay Mineralogy 2nd Edition. McGraw-Hill Book Company.
- ² Jepson WB (1984). Kaolins: their properties and uses. Phil. Trans. R. Soc. Lond. A 311 411-432.
- ³ Skuse DR & Mogridge DJ ECC Plc (1996). Chemical treatment technology in industrial mineral mining and processing operations. Presented at Flocculants, Coagulants and Precipitants for Water Treatment Conference. Dallas.
- ⁴ www.mindepos.bg.tu-berlin.de/lager/wipki/5bild.htm.
- ⁵ Yariv S (1992). The effect of tetrahedral substitution of Si by Al on the surface acidity of the oxygen plane of clay minerals. International Reviews in Physical Chemistry 11, 2, 345-375.
- ⁶ Ma C & Eggleton RA (1999). Surface layer types of kaolinite: a high - resolution transmission electron microscope study. Clays and Clay Minerals 47, 2, 181-191.
- ⁷ Kirsch H, (1968) "Applied mineralogy", Chapman and Hall (London).
- ⁸ Ma C & Eggleton RA (1999). Cation exchange capacity of kaolinite. Clays and Clay Minerals 47, 2, 174-180.
- ⁹ Lee LT, Rahbari R, Lecourtier J & Chauveteau G (1991). Adsorption of polyacrylamides on different faces of kaolinites. Journal of Colloid and Interface Science 2 147 351-357.
- ¹⁰ Slonka T (1992). Simple model of intercalation reaction of polar organic molecules into kaolinite. Materials Science Forum 91-93, 231-238.
- ¹¹ Churchman GJ (1990). Relevance of different intercalation tests for distinguishing halloysite from kaolinite in soils. Clays and Clay Minerals 38, 6 591-599.
- ¹² Churchman GJ, Whitton JS, Claridge GGC & Theng BKG (1984). Intercalation method using formamide for differentiating halloysite from kaolinite. Clays and Clay Minerals 32, 4 241-248.
- ¹³ Koshevar VD & Lukavykh OV (1992). (Translated from) Zhurnal Prikladnoi Khimii 65, 7 1614-1618.
- ¹⁴ Jepson WB (1984). Kaolins: their properties and uses. Phil. Trans. R. Soc. Lond. A 311 411-432.
- ¹⁵ Hess AC & Saunders VR (1992). Periodic ab initio Hartree-Fock calculations on the low symmetry mineral kaolinite. Journal of Physical Chemistry 96, 4367-4374.
- ¹⁶ Frost RL, Kristof J, Horvath E & Klopogge JT (2000). Kaolinite hydroxyls in dimethylsulphoxide-intercalated kaolinites at 77K-a Raman spectroscopic study. Clay Minerals 35, 443-454.
- ¹⁷ Frost RL (1998). Hydroxyl deformation in kaolins. Clays and Clay Minerals 46, 3, 280-289.
- ¹⁸ Frost RL & Van Der Gaast SJ (1997). Kaolinite hydroxyls-a Raman microscopy study. Clays and Clay Minerals 32, 471-484.
- ¹⁹ Frost RL, Tran THT & Kristof J (1999). The structure of intercalated kaolinite: A Raman and infrared spectroscopic study. 398-401 in Kodama H, Mermut AR & Torrance JK (Eds). Clays for our

- future. Proceedings of the 11th Clay Conference, Ottawa, Canada, 1997. Published by ICC97 Organising Committee, Ottawa, Canada.
- ²⁰ Frost RL (1995). Fourier transform Raman spectroscopy of kaolinite, dickite and halloysite. *Clays and Clay Minerals* **43**, 191-195.
- ²¹ Frost RL, Paroz GN & Van Der Gaast SJ (1999). Hydrogen bonding in kaolinite. 393-396 in Kodama H, Mermut AR & Torrance JK (Eds). *Clays for our future. Proceedings of the 11th Clay Conference, Ottawa, Canada, 1997. Published by ICC97 Organising Committee, Ottawa, Canada.*
- ²² Gonzalez Garcia F *et al* (1991). Effects of dry grinding on two kaolins of different degrees of crystallinity. *Clay Minerals* **26** 549-565.
- ²³ Nakano T, Kamitani M & Senna M (1996). A new inorganic bonding agent from mechanically activated kaolin. *Materials Science Forum* **225-227**, 587-592.
- ²⁴ Kristof E, Juhaz AZ & Vassanyi I (1993). The effect of mechanical treatment on the crystal structure and thermal behaviour of kaolinite. *Clays and Clay Minerals* **41**, 5, 608-612.
- ²⁵ Diner VA, Polushkin VA & Frolov MV (1984). Hydrophobic -hydrophilic properties of kaolin modified by polymerization of adsorbed styrene and isopropene. *Polymer Science USSR* **26**, 10, 2339-2344.
- ²⁶ Ovramenko NA, Kalenchuk VG, Zakharchenko OF & Ovcharenko FD (1994). Effect of the intercalation of (HBO₂) and mechanochemical treatment on the acid-base properties of kaolinite. *Colloid Journal* **56**, 3, 345-347.
- ²⁷ Kristóf J, Mink J, Horváth E & Gábor M (1993). Interaction study of clay minerals by Fourier transform infrared spectrometry. *Vibrational Spectroscopy* **5**, 61-67.
- ²⁸ Michaelian KH, Friesen WI, Yariv S & Nasser A (1991). Diffuse reflectance infrared spectra of kaolinite and kaolinite/alkali halide mixtures. Curve fitting of the hydroxyl stretching region. *Canadian Journal of Chemistry* **69**, 1786-1790.
- ²⁹ Johansson U, Holmgren A, Forsling W and Frost R (1998). Isotopic exchange of kaolinite hydroxyl protons: a diffuse reflectance infrared Fourier transform spectroscopy study. *Analyst* **123**, 641-645.
- ³⁰ Frost RL, Kristof J, Horvath E & Klopogge JT (1999). Modification of the kaolinite hydroxyl surfaces through the application of pressure and temperature, Part III. *Journal of Colloid and Interface Science* **214**, 380-388.
- ³¹ Farmer VC (Ed) (1974). *The infrared spectra of minerals.* Mineralogical Society. London.
- ³² Millar GJ, Rochester CH & Waugh KC (1991). Infrared study of the adsorption of formic acid on silica-supported copper and oxidised copper catalysts. *Journal of the Chemical Society Faraday Transactions* **87(9)**, 1491-1496.
- ³³ Millar GJ, Rochester CH & Waugh KC (1991). Infrared study of methyl formate and formaldehyde adsorption on reduced and oxidised silica-supported copper catalysts. *Journal of the Chemical Society Faraday Transactions* **87(17)**, 2785-2793.

- ³⁴ Constanzo PM, Gieste RF Jr & Lipsicas M (1984). Static and dynamic structure of water in hydrated kaolinites. I. The static structure. *Clays and Clay Minerals* **32**, 5, 419-428.
- ³⁵ Rouxhet PG, Samudacheata N Jacobs H & Anton O (1977). Attribution of the OH stretching bands of kaolinite. *Clay Minerals* **12**, 171-178.
- ³⁶ Frost RL & Paroz GN (1999). The dehydroxylation of urea intercalated kaolinite: an infrared emission spectroscopic study. 403-408 in Kodama H, Mermut AR & Torrance JK (Eds). *Clays for our future. Proceedings of the 11th Clay Conference, Ottawa, Canada, 1997.* Published by ICC97 Organising Committee, Ottawa, Canada.
- ³⁷ Bantignies J_Lewis, Cartier dit Moulin C & Dexpert H (1997). Wettability contrasts in kaolinite and illite clays: Characterisation by infrared and x ray absorption spectroscopies. *Clays and Clay Minerals* **45**, 2, 184-193.
- ³⁸ Petite S, Madejova J, Decarreau A & Martin F (1999). Characterisation of octahedral substitutions in kaolinites using near infrared spectroscopy. *Clays and Clay Minerals* **47**, 1, 103-108.
- ³⁹ Billingham J, Breen C & Yarwood J (1996). *In situ* determination of Brønsted/Lewis acidity on cation-exchanged clay mineral surfaces by ATR-IR. *Clay minerals* **31**, 513-522.
- ⁴⁰ Breen C (1991b). Thermogravimetric and infrared study of the desorption of butylamine, cyclohexylamine and pyridine from Ni- and Co- exchanged montmorillonite. *Clay Minerals* **26**, 487-496.
- ⁴¹ Frost RL & Vassallo AM (1996). The dehydroxylation of the kaolinite clay minerals using infrared emission spectroscopy. *Clays and Clay Minerals* **44**, 5 635-651
- ⁴² Pandurangi RS & Seehra MS (1992) Quantitative analysis of silica in silica-kaolin mixtures by photoacoustic and diffuse reflectance spectroscopies. *Applied Spectroscopy* **46**, 11, 1719-1723.
- ⁴³ Putnis A (1992). *Introduction to minerals science.* Cambridge University Press, Cambridge.
- ⁴⁴ Schrader B (1995). *Infrared and Raman Spectroscopy. Methods and applications.* (Schrader B ed.) VCH, Weinheim, Germany.
- ⁴⁵ Clark RJH & Hester RE. (Ed). (1982). *Advances in infrared and Raman spectroscopy* Vol 9. Heyden and Son LTD. London.
- ⁴⁶ Hollas JM. (1992). *Modern Spectroscopy* 2nd Edition John Willey and Sons. New York.
- ⁴⁷ Sonnessa AJ (1966). *Introduction to molecular spectroscopy.* Reinhold Publishing Corporation, New York.
- ⁴⁸ Wendlandt WWM & Hecht GH (1966). *Reflectance spectroscopy.* Interscience. London.
- ⁴⁹ Kortum G (1969). *Reflectance spectroscopy.* Springer-Verlag. Heidelberg.
- ⁵⁰ Painter PC & Coleman MM (Ed) (1997). *Fundamentals of polymer science.* Technomic. Lancaster.
- ⁵¹ Clegg F (1998) *Thermoanalytical and spectroscopic characterisation of pore lining minerals in reservoir rocks.* Thesis. Sheffield Hallam University.
- ⁵² Moore DM & Reynolds RC (1997). *XRD and the identification and analysis of clay minerals.* Oxford University Press.

⁵³ Tunney J & Detellier C (1994). Preparation and characterisation of an 8.4Å hydrate of kaolinite. *Clays and Clay Minerals* **42**, 4, 473-476.

⁵⁴ Sidheswaran P, Ganguli P & Bhat AN (1987). Thermal behaviour of intercalated kaolinite. *Thermochimica Acta*. **118** 295-303.

⁵⁵ Shaw BT (1942). The nature of colloidal clay as revealed by the electron microscope. Paper presented at the 19th Colloid Symposium, University of Colorado, Colorado, USA.

2. The Effects of Ball Milling

2.1 INTRODUCTION.....	47
2.1.1 Curve fitting.....	60
2.2 RESULTS. THE EFFECTS OF BALL MILLING.....	60
2.2.1 Scanning electron microscopy (SEM).....	60
2.2.2 Thermal Analysis.....	66
2.2.3 XRD.....	73
2.2.4 Infrared of ball milled kaolins. The 3800-2600 cm^{-1} region.....	76
2.2.4.1 The effect of temperature on milled kaolin. The 3800-2600 cm^{-1} region.....	79
2.2.4.1.1 Unmilled (0 minute) kaolin.....	79
2.2.4.1.2 3 minute kaolin (freshly milled).....	90
2.2.4.1.3 10 minute kaolin (freshly milled).....	100
2.2.4.1.4 30 minute kaolin (freshly milled).....	109
2.2.5 Infrared of ball milled kaolins. The 2100-1400 cm^{-1} region.....	110
2.2.5.1 The effect of temperature on milled kaolin. The 2100-1400 cm^{-1} region.....	112
2.2.5.1.1 Unmilled (0 minute) kaolin.....	112
2.2.5.1.2 3 minute kaolin (freshly milled).....	118
2.2.5.1.3 10 minute kaolin(freshly milled).....	125
2.2.5.1.4 30 minute kaolin(freshly milled).....	131
2.2.5.2 The effect of milling on kaolin. The 1300-700 cm^{-1} region.....	132
2.3 RESULTS. THE EFFECTS OF AGEING ON BALL MILLED KAOLINS.....	133
2.3.1 Infrared of ball milled kaolins. The 3800-2600 cm^{-1} region.....	134
2.3.1.1 3 minute milled kaolins. The 3800-2600 cm^{-1} region.....	134
2.3.1.2 10 minute milled kaolins. The 3800-2600 cm^{-1} region.....	140
2.3.1.3 30 minute milled kaolins. The 3800-2600 cm^{-1} region.....	146
2.3.2 Infrared of ball milled kaolins. The 2100-1400 cm^{-1} region.....	147
2.3.2.1 3 minute milled kaolins. The 2100-1400 cm^{-1} region.....	147
2.3.2.2 10 minute milled kaolins. The 2100-1400 cm^{-1} region.....	152
2.3.2.3 30 minute milled kaolins. The 2100-1400 cm^{-1} region.....	157
2.4 CONCLUSIONS.....	158
2.4.1 References.....	163

FIGURE 2.1 ILLUSTRATION OF THE INTERCALATION OF CsCl INTO KAOLIN. 52

FIGURE 2.2 ILLUSTRATION OF THE PROPOSED METHOD OF INTERACTION OF ALKALI CATIONS AND WATER ON THE SURFACE OF KAOLINITE. 53

FIGURE 2.3 SCHEMATIC OF THE POSSIBLE LOCATION OF WATER MOLECULES ON THE KAOLIN SURFACE. 58

FIGURE 2.4 SEM OF UNMILLED KAOLIN. 61

FIGURE 2.5 SEM OF KAOLIN MILLED FOR 3 MINUTES. 62

FIGURE 2.6 SEM OF KAOLIN MILLED FOR 10 MINUTES. 63

FIGURE 2.7 SEM OF KAOLIN MILLED FOR 30 MINUTES. 64

FIGURE 2.8 TGA OF UNMILLED KAOLIN. 66

FIGURE 2.9 TGA OF 3 MINUTE MILLED KAOLIN. 67

FIGURE 2.10 TGA OF 10 MINUTE MILLED KAOLIN. 68

FIGURE 2.11 TGA OF 30 MINUTE MILLED KAOLIN. 69

FIGURE 2.12 COMBINED TGA / DTA OF 0, 3, 10 AND 30 MINUTE BALL MILLED KAOLIN. 70

FIGURE 2.13 XRD OF UNMILLED KAOLIN. 73

FIGURE 2.14 XRD OF 3 MINUTE MILLED KAOLIN. 73

FIGURE 2.15 XRD OF 10 MINUTE MILLED KAOLIN. 74

FIGURE 2.16 XRD OF 30 MINUTE MILLED KAOLIN. 74

FIGURE 2.17 RT (ROOM TEMPERATURE) DRIFTS OF BALL MILLED KAOLINS. 76

FIGURE 2.18 BALL MILLED KAOLINS. THE 3800-3475 cm^{-1} REGION. 77

FIGURE 2.19 UNMILLED (0 MINUTE) KAOLIN. THE 3800-2600 cm^{-1} REGION. 79

FIGURE 2.20 UNMILLED KAOLIN. THE 3800-2600 cm^{-1} REGION. ROOM TEMPERATURE CURVE FIT. . 80

FIGURE 2.21 UNMILLED KAOLIN. THE 3800-2600 cm^{-1} REGION. 200 °C CURVE FIT. 80

FIGURE 2.22 UNMILLED KAOLIN. THE 3800-2600 cm^{-1} REGION. 350 °C CURVE FIT. 81

FIGURE 2.23 UNMILLED KAOLIN. THE 3800-2600 cm^{-1} REGION. THE CHANGE IN INTENSITY OF BANDS A, B, C, D AND E. 82

FIGURE 2.24 UNMILLED KAOLIN. THE CHANGE IN INTENSITY OF BAND E. 83

FIGURE 2.25 UNMILLED KAOLIN. THE CHANGE IN INTENSITY OF BANDS F, G & H. 84

FIGURE 2.26 THE CHANGE IN POSITION OF BANDS IN THE 3800-2600 cm^{-1} REGION AS A FUNCTION OF TEMPERATURE. 86

FIGURE 2.27 UNMILLED KAOLIN PEAK POSITIONS - BANDS F, G & H. 87

FIGURE 2.28 3 MINUTE KAOLIN(FM). THE 3800-2600 cm^{-1} REGION. 91

FIGURE 2.29 3 MINUTE KAOLIN(FM). THE 3800-2600 cm^{-1} REGION. ROOM TEMPERATURE CURVE FIT. 91

FIGURE 2.30 3 MINUTE KAOLIN(FM). THE 3800-2600 cm^{-1} REGION. 150 °C CURVE FIT. 92

FIGURE 2.31 3 MINUTE KAOLIN(FM). THE 3800-2600 cm^{-1} REGION. 350 °C CURVE FIT. 92

FIGURE 2.32 3 MINUTE KAOLIN (FM). THE 3800-2600 cm^{-1} REGION. THE CHANGE IN INTENSITY OF BANDS A, B, C, D AND E. 95

FIGURE 2.33 3 MINUTE KAOLIN (FM). THE CHANGE IN INTENSITY OF BANDS F, G AND H. 96

FIGURE 2.34 THE CHANGE IN POSITION OF BANDS IN THE 3800-2600 cm^{-1} REGION AS A FUNCTION OF TEMPERATURE. 97

FIGURE 2.35 10 MINUTE KAOLIN(FM). THE 3800-2600 cm^{-1} REGION. 101

FIGURE 2.36 10 MINUTE KAOLIN(FM). THE 3800-2600 cm^{-1} REGION. ROOM TEMP CURVE FIT. 101

FIGURE 2.37 10 MINUTE KAOLIN (FM). THE 3800-2600 cm^{-1} REGION. 150 °C CURVE FIT..... 102

FIGURE 2.38 10 MINUTE KAOLIN(FM). THE 3800-2600 cm^{-1} REGION. 350 °C CURVE FIT. 102

FIGURE 2.39 10 MINUTE KAOLIN (FM). THE 3800-2600 cm^{-1} REGION. THE CHANGE IN INTENSITY OF BANDS A, B, C, D AND E..... 105

FIGURE 2.40 10 MINUTE KAOLIN (FM). THE CHANGE IN INTENSITY OF BANDS F, G & H. 106

FIGURE 2.41 10 MINUTE KAOLIN(FM). THE CHANGE IN POSITION OF BANDS IN THE 3800-2600 cm^{-1} REGION AS A FUNCTION OF TEMPERATURE..... 107

FIGURE 2.42 10 MINUTE KAOLIN(FM). THE CHANGE IN POSITION OF BANDS IN THE 3800-2600 cm^{-1} REGION AS A FUNCTION OF TEMPERATURE..... 108

FIGURE 2.43 30 MINUTE KAOLIN(FM). THE 3800-2600 cm^{-1} REGION. 110

FIGURE 2.44 RT DRIFTS OF BALL MILLED KAOLINS..... 111

FIGURE 2.45 UNMILLED (0 MINUTE) KAOLIN. THE 2100-1400 cm^{-1} REGION..... 112

FIGURE 2.46 UNMILLED (0 MINUTE) BALL MILLED KAOLIN. THE 2100-1400 cm^{-1} REGION. ROOM TEMPERATURE CURVE FIT. 113

FIGURE 2.47 UNMILLED (0 MINUTE) BALL MILLED KAOLIN. THE 2100-1400 cm^{-1} REGION. 200 °C CURVE FIT..... 113

FIGURE 2.48 UNMILLED (0 MINUTE) BALL MILLED KAOLIN. THE 2100-1400 cm^{-1} REGION. 350 °C CURVE FIT..... 114

FIGURE 2.49 UNMILLED KAOLIN - THE CHANGE IN INTENSITY OF BANDS S, T, U AND V..... 115

FIGURE 2.50 UNMILLED KAOLIN. THE CHANGE IN INTENSITY OF BAND V..... 116

FIGURE 2.51 THE CHANGE IN POSITION OF BANDS IN THE 2100-1400 cm^{-1} AS A FUNCTION OF TEMPERATURE. 117

FIGURE 2.52 3 MINUTE KAOLIN (FM). THE 2100-1400 cm^{-1} REGION..... 118

FIGURE 2.53 3 MINUTE KAOLIN (FM)..THE 2100-1400 cm^{-1} REGION. ROOM TEMPERATURE CURVE FIT..... 120

FIGURE 2.54 3 MINUTE KAOLIN (FM)..THE 2100-1400 cm^{-1} REGION. 150° C CURVE FIT..... 120

FIGURE 2.55 3 MINUTE KAOLIN (FM).THE 2100-1400 cm^{-1} REGION. 350° C CURVE FIT..... 121

FIGURE 2.56 CHANGE IN INTENSITY OF BANDS W & R. 122

FIGURE 2.57 3 MINUTE KAOLIN. FREQUENCIES OF BANDS IN 2100-1400 cm^{-1} REGION. 124

FIGURE 2.58 10 MINUTE KAOLIN(FM). THE 2100-1400 cm^{-1} REGION. 125

FIGURE 2.59 10 MINUTE KAOLIN(FM). THE 2100-1400 cm^{-1} REGION. ROOM TEMP CURVE FIT. 126

FIGURE 2.60 10 MINUTE KAOLIN(FM). THE 2100-1400 cm^{-1} REGION. 150 °C CURVE FIT. 126

FIGURE 2.61 10 MINUTE KAOLIN(FM). THE 2100-1400 cm^{-1} REGION. 350 °C CURVE FIT. 127

FIGURE 2.62 10 MINUTE KAOLIN(FM). THE 2100-1400 cm^{-1} REGION. 450 °C CURVE FIT. 127

FIGURE 2.63 10 MINUTE KAOLIN(FM). THE CHANGE IN INTENSITY OF BANDS W & X. 129

FIGURE 2.64 10 MINUTE KAOLIN(FM) THE CHANGE IN POSITION OF BANDS IN THE 2100-1400 cm^{-1} REGION..... 130

FIGURE 2.65 30 MINUTE KAOLIN(FM). THE 2100-1400 cm^{-1} REGION. 131

FIGURE 2.66 BALL MILLED KAOLINS. THE 1300-700 cm^{-1} REGION. 132

FIGURE 2.67 3 MINUTE FRESHLY MILLED AND AGED KAOLINS THE 3800-2600 cm^{-1} REGION. 134

FIGURE 2.68 3 MINUTE AGED KAOLIN. THE 3800-2600 cm^{-1} REGION. ROOM TEMP. CURVE FIT. 135

FIGURE 2.69 3 MINUTE AGED KAOLIN. THE 3800-2600 cm^{-1} REGION. 150°C CURVE FIT. 135

FIGURE 2.70 3 MINUTE AGED KAOLIN. THE 3800-2600 cm^{-1} REGION. 350°C CURVE FIT. 136

FIGURE 2.71 3 MINUTE AGED KAOLIN. THE CHANGE IN INTENSITY OF BANDS F, F*, G & H. 138

FIGURE 2.72 3 MINUTE AGED KAOLIN. CHANGE IN POSITION OF BANDS F, F*, G AND H. 139

FIGURE 2.73 10 MINUTE FRESHLY MILLED AND AGED KAOLINS. 140

FIGURE 2.74 10 MINUTE AGED KAOLIN. THE 3800-2600 cm^{-1} REGION. ROOM TEMP. CURVE FIT. 141

FIGURE 2.75 10 MINUTE AGED KAOLIN. THE 3800-2600 cm^{-1} REGION. 150°C CURVE FIT. 141

FIGURE 2.76 10 MINUTE AGED KAOLIN. THE 3800-2600 cm^{-1} REGION. 350°C CURVE FIT. 142

FIGURE 2.77 10 MINUTE AGED KAOLIN. CHANGE IN INTENSITY OF BANDS F, F*, G & H. 144

FIGURE 2.78 10 MINUTE AGED KAOLIN. CHANGE IN POSITION OF BANDS F, F*, G AND H. 145

FIGURE 2.79 30 MINUTE FRESHLY MILLED AND AGED KAOLINS. 146

FIGURE 2.80 3 MINUTE FRESHLY MILLED AND AGED KAOLINS THE 2100-1400 cm^{-1} REGION. 147

FIGURE 2.81 3 MINUTE KAOLIN (AGED). THE 2100-1400 cm^{-1} REGION. ROOM TEMP. CURVE FIT. . 148

FIGURE 2.82 3 MINUTE KAOLIN (AGED). THE 2100-1400 cm^{-1} REGION. 150 °C CURVE FIT. 148

FIGURE 2.83 3 MINUTE KAOLIN (AGED). THE 2100-1400 cm^{-1} REGION. 350°C CURVE FIT. 149

FIGURE 2.84 3 MINUTE KAOLIN (AGED) THE CHANGE IN INTENSITY OF BANDS W AND X. 150

FIGURE 2.85 3 MINUTE KAOLIN (AGED) THE CHANGE IN POSITION OF BANDS W AND X. 151

FIGURE 2.86 10 MINUTE FRESHLY MILLED AND AGED KAOLINS. 152

FIGURE 2.87 10 MINUTE KAOLIN (AGED). THE 2100-1400 cm^{-1} REGION. ROOM TEMP. CURVE FIT. 153

FIGURE 2.88 10 MINUTE KAOLIN (AGED). THE 2100-1400 cm^{-1} REGION. 150 °C CURVE FIT. 153

FIGURE 2.89 10 MINUTE KAOLIN (AGED). THE 2100-1400 cm^{-1} REGION. 350 °C CURVE FIT. 154

FIGURE 2.90 10 MINUTE KAOLIN (AGED). THE CHANGE IN INTENSITY OF BANDS W & X. 155

FIGURE 2.91 10 MINUTE KAOLIN (AGED). THE CHANGE IN POSITION OF BANDS W & X. 156

FIGURE 2.92 30 MINUTE FRESHLY MILLED AND AGED KAOLINS. 157

FIGURE 2.93 SCHEMATIC OF THE EFFECTS OF MILLING AND AGEING. 158

FIGURE 2.94 SCHEMATIC OF WATER BONDING WITH THE CHARACTERISTIC IR FREQUENCIES. 159

TABLE 2.1 IR FREQUENCIES OF BANDS IN WATER STRETCHING REGION OF KAOLIN SPECTRUM. 54

TABLE 2.2 IR FREQUENCIES OF BANDS IN WATER BENDING REGION OF KAOLIN SPECTRUM. 55

TABLE 2.3 IR FREQUENCIES OF LATTICE MODES OF THE KAOLIN SPECTRUM. 56

TABLE 2.4 WEIGHT LOSSES FROM KAOLIN DURING THERMAL ANALYSIS. 71

2.1 Introduction.

The aim of this work was to characterise the water sorbed by kaolin before and after dry ball milling, and to study its thermal stability between ambient temperature and 500°C using variable temperature diffuse reflectance infrared Fourier transform spectroscopy (VT DRIFTS). The effects of ageing were also investigated.

Studies on the effects of milling (or grinding) kaolin have been carried out for several decades by various investigators, and the effects of micronization have been examined using many techniques including thermal analysis¹ SEM, TEM², XRD³, NMR⁴ surface area measurements^{1,33}, photoacoustic IR⁵ and IR absorption¹⁹ spectroscopy. Molecular modelling has also been attempted⁶. (Note: some of the more recent literature has been referenced herein, and many contain information gathered using more than one technique.)

The effects of grinding on other clays have also been studied. Sondi *et al*⁷, examined the changes in the surface properties of (non swelling layered silicate) ripidolite and (swelling aluminosilicate smectite) beidellite clays after milling. The first stages of milling caused cleavage along the (001) basal plane (i.e. delamination) and subsequent milling induced cleaving normal to the basal plane (i.e. fracture). Changes in surface area (due to the break up of clay stacks), cation exchange capacity (due to the exposure of new edge sites) and electrophoretic mobilities (zeta potential) resulted. The alteration in zeta potential was particularly significant, since in their natural state these clays do not have an isoelectric point. The charge in unmilled ripidolite and beidellite is carried by basal surfaces with a constant negative charge. This is pH independent and is due to the isomorphous substitution of Si⁴⁺ by Al³⁺. After milling, the mineral edges are fractured, resulting in broken bonds and pH dependant charge. The changes occurred rapidly (after approximately 6-10 minutes) and subsequent milling for up to 300 minutes did not significantly alter the properties examined.

Drief and Nieto⁸ used several techniques including XRD, thermal analyses and IR spectroscopy to examine the effects of milling of the serpentine mineral, antigorite. They suggest that in the early stages of grinding the octahedral sheets are preferentially

destroyed. Further grinding results in the destruction of both sheets, resulting in a mixture similar in composition to the starting material, but having only weak associations between the tetrahedral and octahedral layers.

The effects of milling upon kaolin will be discussed in detail later in this chapter, but in crude terms, the most obvious changes are similar to those observed with the milling of other minerals: initially, the kaolin sheets are cleaved along the basal plane, resulting in delamination, followed by the fracture of particles normal to the basal plane after prolonged milling. Thus, an increased number of edge sites are exposed. The amount of surface-sorbed water species increases.

Water adsorption and desorption on swelling clays has been well studied by IR spectroscopy and other standard techniques such as TGA^{9,10,11,12}. More unusual techniques have also been used to monitor the thermal desorption of water, for example, using a vacuum microbalance apparatus¹³. The milling study carried out by Drief and Nieto⁸ on antigorite highlighted a water stretching mode in the IR spectra at 3436 cm⁻¹ which increased as milling progressed, and was attributed to randomly attached OH ions and adsorbed water. Bands in the water bending region at approximately 1630 and 1650 cm⁻¹ were also obvious from the spectra presented, but were not commented upon in the text.

Certain aspects of the infrared spectrum of water and hydroxyls on kaolin have been well studied. The intensity in the bending and stretching regions of the IR spectrum are dependent upon both the degree of hydration and ball-milling time. Some work has examined the adsorption / desorption of water and the observed intensity increase or decrease in certain regions of the spectrum after milling^{16,43}. In a comprehensive study of the effects of dry and wet milling on kaolin (using IR spectroscopy, XRD, TGA, DTA, SEM, surface analysis, particle size analysis and pore volume measurements), it was postulated by Suraj and co-workers¹⁴ that initially the dry grinding process exposed directed hydroxyl bonds between the octahedral and tetrahedral layers (amorphization), and that these OH groups became less stable as grinding progressed. They found that dry grinding had a greater micronization effect compared with wet grinding, probably due the water (involved in wet grinding) damping down the effect of the zirconia balls

used in both milling techniques. They suggested that “the newly formed vacant sites... accommodate extra structural water” and therefore that the OH bands at 3708 and 3620 cm^{-1} and the Al-OH bending bands at 938 and 918 cm^{-1} broadened. They reported that dry grinding caused amorphization, i.e. it exposed the directed hydroxyls between the tetrahedral and octahedral layers. Prolonged grinding led to the hydroxyl groups becoming unstable. Vacant sites on the outer surfaces were formed, and these were able to accommodate extra structural water. This had the effect of broadening the hydroxyl bands in the spectrum. The continued availability of the structural hydroxyl groups was visualised by the persistence of the 938 and 918 cm^{-1} Al-OH bands (not shown). These factors and variations in the relative intensity of the inner surface and inner hydroxyl stretching modes (in the present work designated a and d, with frequencies of around 3695 and 3620 cm^{-1} respectively) confirm the structural deterioration of the mineral.

Although not discussed in detail in their work, there was also a very obvious broadening of the c 3000 - 2600 cm^{-1} region after grinding and the appearance of a new band at 1620 cm^{-1} (this band was partially obscured by intense water vapour bands). A broadening of the 3695 (c.f. 3708 cm^{-1}) and 3620 cm^{-1} bands was not quantifiable in the current work, it is clear from the data presented herein that as milling time increased more loosely bound water (in various forms) was present on the surface of the kaolin (although as milling time increased, there was an overall decrease in the total amount of water present). Although the possible broadening in the present work was not quantified, there was at times a detectable change in the width of the OH bands. It is not certain if this change was a result of inaccurate curve fitting due to software difficulties in distinguishing between bands, or if it was a real change. Although it is not possible to rule out this phenomenon, it is postulated that the water in the current study was adsorbed mainly to broken edge sites, rather than to the upper or lower surfaces. The “extra” water is likely to originate both from atmospheric moisture and from prototropy, i.e. the migration of protons to hydroxyl groups, thus forming “new” water molecules. It is the opinion of the author of the work herein that the interpretation of the IR work by Suraj *et al.*, is a little simplistic. It is postulated that the bands at 3708 and 3620 cm^{-1} (and those in between) were indeed losing their integrity after milling, but that this effect

was not merely due to the broadening of these bands. More realistically, they were being swamped by water bands at lower frequency which increase in intensity as milling increased.

Another detailed study of the effects of milling of kaolin was carried out by La Iglesia and Aznar². Their work examined the effects upon four different types of kaolin when subjected to milling at different pressures for various times. Using XRD, DTA, TGA, IR and TEM they were able to assess the changes in particle morphology, structure and crystallinity after milling. In the range of pressure (0.1-2 GPa) and grinding studied (1-12 hours) it was found that grinding was more destructive to the integrity of the mineral than pressure. Grinding was found to alter the morphology, resulting in small particles, periodicity disorder and short range disorder, whereas pressure resulted in limited changes. Short range disorder resulted in the formation of an amorphous phase. Grinding decreased the temperature and intensity of the endothermic processes at approximately 550 °C (i.e. dehydroxylation) and marginally increased the temperature of the exothermic processes at approximately 980 °C (i.e. metakaolin-mullite transformation). Dehydroxylation temperature decreased in both pressure treated and ground samples because both treatments produced changes in the crystal structure which facilitated the elimination of hydroxyls (i.e. water).

Interestingly, a large increase in the overall % weight loss was also observed. This effect is not mimicked in the work presented herein. For samples that were ground for over 4 hours (in the referenced study), a new endotherm was observed at approximately 200 °C. Although the cause of this effect is not explained in the study by La Iglesia and Aznar, it is likely that it is the result of low temperature loss of relatively weakly bound surface water.

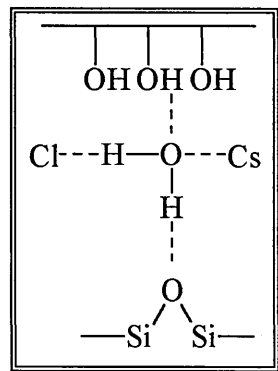
Only very recently has DRIFT spectroscopy been introduced into the study of clay minerals^{15,16,29,5}. To date DRIFTS has not been widely exploited in variable temperature work. Michaelian *et al*⁵, studied the effects of the wet and dry grinding of kaolinite in the presence and absence of CsBr, CsCl and CsI. They determined that upon ageing, a mixture of kaolin and CsCl sorbed water and formed an intercalation complex. If the mixture was dry ground, the intercalation process was more rapid. If the mixture was

wet ground, the intercalation complex was formed during the grinding process. They showed that the dry grinding of kaolin with CsBr and CsI did not lead to intercalation formation. They suggest that this phenomenon indicates that environmental (atmospheric) salt or water molecules do not react with the mineral to form an intercalation complex. CsBr and water formed an intercalation complex upon wet grinding (although this effect was not mimicked by the CsI and water system). It was concluded in that study that the degree of intercalation of kaolin with a caesium halide salt was governed in some way by the size of the halide ion- the larger the ion, the lower the degree of intercalation. There are two possible causes of the observed phenomena. Firstly, the intercalation into the interlamellar network may be restricted by the physical size of the halide ion, (Cl⁻ being small enough to fit easily into the interlayer space, Br⁻ penetrating when forced to do so, and I⁻ being too large). The other possible explanation is that hydrogen bonding between sorbed water molecules and the ions are essential for the intercalation process, (Cl⁻ forming weak associations, Br⁻ forming very weak associations, and I⁻ forming few (if any) associations). The second explanation appears to be more plausible, since there were observed shifts in the IR frequencies of the water modes between the CsBr and CsCl systems. After delamination induced by milling, intercalation complexes between CsCl, (and to a lesser extent with CsBr), water and kaolinite were formed, whereby hydrogen bonds formed between hydroxyl groups of the octahedral sheet and the oxygen of water, and between protons of the water and the siloxane oxygens of the tetrahedral sheet (see Figure 2.1). It was found in another study¹⁶ that intercalation was most likely in wet ground samples, least likely in lightly mixed samples, and moderately likely in air ground samples.

It was determined that the intercalation of water and CsCl was a two step process, with the delamination occurring during grinding and the subsequent intercalation taking sometimes over a month to complete. They apparently observed no spectral changes when the kaolin was dry ground with CsBr and CsI at ambient atmosphere, and that this led to the conclusion that water molecules from the atmosphere do not react to form intercalation complexes with these molecules. However, water molecules from the atmosphere were involved in the intercalation of CsCl, and adding extra water increased the rate of intercalation with CsCl. CsBr intercalation only occurred when a few drops of water were added during the grinding process. The spectra recorded by Michaelian *et*

al.,⁵ were produced a minimum of 3 months after the initial treatment. During this time it is likely that significant changes would occur, particularly in the water bending region of the spectrum (see section 2.3). The possible changes after this 3 month period were discussed in the reference, but there was no evidence of investigations carried out prior to this period. It is the author's opinion that an investigation of this kind should include spectra taken immediately after treatment of the mineral, since, as discussed later in this chapter, ageing has a considerable effect on the IR spectra of ground kaolin.

Figure 2.1 Illustration of the intercalation of CsCl into kaolin.



5

It was suggested by Michaelian *et al.*,⁵ that a water molecule co-ordinated to the Cs cation donates one proton to a siloxane oxygen and the other to a halide, while accepting a proton from an inner surface hydroxyl. The CsCl -kaolin complex was able to sorb atmospheric water for use in this process, whereas the CsBr-kaolin system was not, and therefore water had to be incorporated during the milling process.

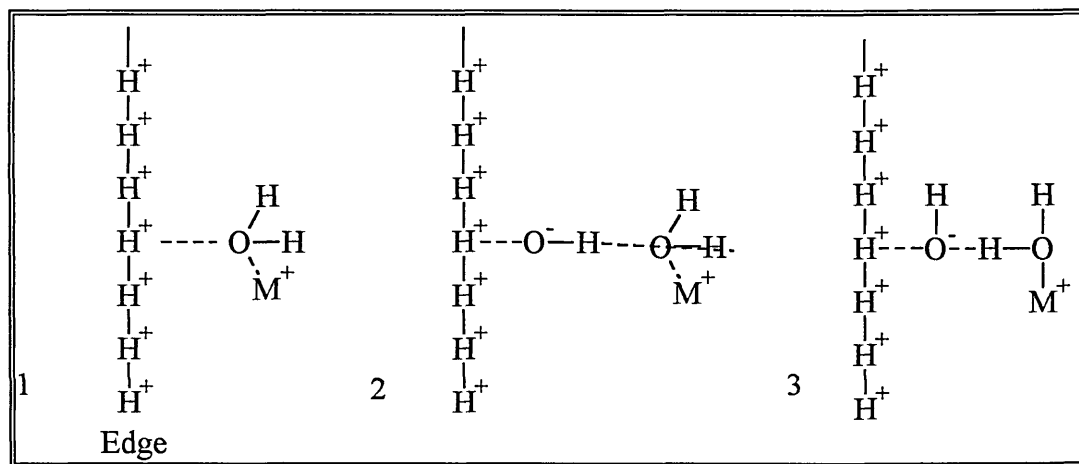
Yariv⁴³ also studied the grinding of kaolinite in the presence and absence of alkali chlorides. The adsorption of water was examined in some detail in this work. After delamination, Yariv noted that the layer became hydrated, and concluded that this water was sorbed from the atmosphere. The reaction with water was divided into 3 stages:

- a) during grinding, the layer was disintegrated and kaolin structural atoms became exposed. Protons were attracted to exposed hydroxyls, and hydroxyls were attracted to exposed silicon and aluminium.
- b) enhanced by the lattice defects caused during grinding, excess protons were sorbed by the kaolin, causing the surface to become positively charged.

c) Free water molecules were sorbed by the positively charged kaolinite surface.

This sample was ground with alkali chlorides, and Yariv went on to say that the water molecules were polarised by the alkali cation, and thus their adsorption occurred. Figure 2.2 shows the mechanism proposed by Yariv. Presumably, the absence of the alkali chloride when grinding (as in the current work) does not inhibit the sorption of water.

Figure 2.2 Illustration of the proposed method of interaction of alkali cations and water on the surface of kaolinite.



43

Other work carried out by the author (see chapter “The adsorption of pyridine to kaolin”) has discovered that the predominant surface sites present on the surface of unmilled kaolin at room temperature are of the Lewis type. However, after 10 minutes of ball milling, Brønsted sites are more prevalent, i.e., the probe molecule used in the work was increasingly likely to be bound (to an edge site) via a water molecule, rather than directly to the kaolin surface as milling time increased. These results suggest that the theory of Yariv, whereby water sorbs to edge sites is the more likely.

Perhaps the most widely examined characteristic of the spectrum is the group of 4 distinct peaks in the $3700\text{-}3600\text{ cm}^{-1}$ region. Although several papers have addressed this area, the assignments of these bands is still the subject of some controversy^{17,18}.

Generally, the agreed assignments for the more commonly detected bands are as follows:

Table 2.1 IR frequencies of bands in water stretching region of kaolin spectrum.

Frequency (cm ⁻¹)	Assignment
3695 (a)	Free outer OH / inner surface OH stretch
3669 (b)	Inner surface OH stretch
3650 (c)	Inner surface OH stretch
3620 (d)	Inner OH stretch
3627	inner stretch halloysite (different because of the rolling of the layers) ³⁸
3590 (e)	Interlayer or intercalated water (especially in disordered kaolins and halloysites) ³⁸
2600-3600 (f-h)	Stretching modes of water adsorbed to kaolin surface.

Note ⁽ⁱ⁾

In the DRIFT spectrum of kaolin there is also a broad absorbance between approximately 3600 and 2600 cm⁻¹ which has variable intensity and incorporates several overlapping bands. Several workers using IR techniques have noted variations in this area, which have been generally been loosely assigned to “water stretching” vibrations of adsorbed water ^{19,38,42}.

There has been less interest in the mid-frequency range of the spectrum and with the exception of a water band near to 1640 cm⁻¹, ^{19,5} assignments have seldom been made. Mendelovici¹⁹ noted changes in the 1640 cm⁻¹ region and conceded that water molecules of different bonding characteristics contributed to the band, but did not explain what the bonding environments may be, and did not interpret the changes observed with grinding or increasing temperature. Three bands at 1637, 1823 and 1933 cm⁻¹ were observed by Michaelian *et al*⁵, who assigned the 1637 cm⁻¹ band to water and the latter bands to combination transitions involving strong bands at low frequency. Other workers have tentatively assigned more IR bands, and the merits of these assignments will be discussed in more detail in the bulk text. Some of the more established assignments are included in the table below.

⁽ⁱ⁾ Specific references have not been given where the assignments are commonly accepted.

Table 2.2 IR frequencies of bands in water bending region of kaolin spectrum.

Frequency (cm ⁻¹)	Assignment
1930 (s)	Kaolin combination band of Si-O stretching mode @ 1020 cm ⁻¹ and OH deformation at 915 cm ⁻¹ ¹⁵ .
1830 (t)	Kaolin overtone band from doubling of the 915 cm ⁻¹ OH deformation mode ¹⁵ .
1730 (u)	Kaolin combination band (precise assignment currently unknown*).
1679 (w)	HOH bending of water very strongly H-bonded to kaolinite (siloxane) surface ⁴¹ .
1651 (v)	HOH bending of water very strongly H-bonded to kaolinite (siloxane) surface ⁴¹ .
1627 (x)	HOH bending of water adsorbed to kaolin surface ⁴¹ .
1578 (r)	HOH bending of water molecules in the second sphere of hydration and weakly hydrogen bonded to kaolin surface ⁴¹ .

*Bands at 1740 and 1710 cm⁻¹ have previously been observed in the DRIFT spectrum of kaolin, but not assigned²⁰. They are not usually present in pressed disk spectra. In the spectra of the Cornish kaolin studied in the present work, only one band centring at c 1730 cm⁻¹ was resolved. The intensities of the 1910, 1810, 1740 and 1710 cm⁻¹ bands are said to reduce with lattice disorder.

Assignments of the bands in the kaolin IR spectrum in the c 1100 - 400 cm⁻¹ region are given below for completeness, but the changes in these bands will not be discussed in detail in the work herein.

Table 2.3 IR frequencies of lattice modes of the kaolin spectrum.

Frequency (cm ⁻¹)	Assignment
1115	vibration of in plane Si-O
1031	vibration of in plane Si-O
1009	vibration of in plane Si-O
939	inner surface OH deformation
912	inner OH deformation
797	vibration of gibbsite-like sheets
789	vibration of gibbsite-like sheets
751	vibration of gibbsite-like sheets
693	vibration of gibbsite-like sheets
542	Si-O-Al skeletal vibrations
476	Si-O-Al skeletal vibrations

(taken from Farmer & Russell²¹)

Like the broad area between 3600 and 2600 cm⁻¹, the water bending modes between 1670 and 1630 cm⁻¹ are affected by hydration and ball-milling.

A detailed study of the 3700-2600 and the 2100-1400 cm⁻¹ regions, with specific reference to the relative intensities and shifts in the frequency of the water modes, as a function of milling and temperature has not previously been made. Curve fitting of the OH stretching region of unmilled kaolin and kaolin ground with CsCl and KBr was carried out by Michaelian and co-workers¹⁶ although they attempted only to fit down to 3200 cm⁻¹, and their work concentrated mainly on the changes in the 4 peaks between 3695 and 3620 cm⁻¹. Frost²² also carried out curve fitting, but using Raman spectra. This work examined the hydroxyl deformation modes in the region between c 800 and 1000 cm⁻¹ of unmilled kaolinite, dickite and halloysite from different locations. Shoval *et al*²³, carried out a curve fitting study of selected bands in the c 3750-3550 cm⁻¹ region of the IR and Raman spectrum. Although the work gives a detailed comparison of the two spectral techniques, “multiple points on either side of the region of interest were selected for linear baseline correction,” and as a result, no attempt has been made to account for

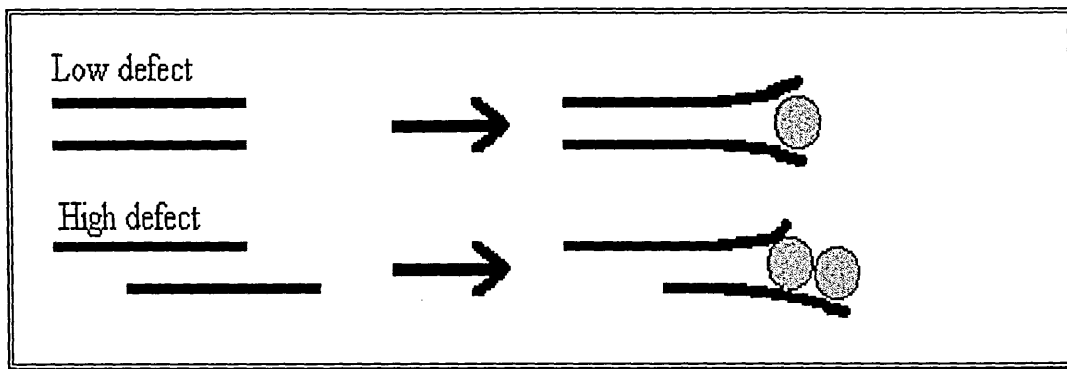
the intensity of any other bands (worthy of particular note is the apparent absence of any contribution of surface-sorbed water in the lower frequency region).

The effects of increasing temperature have also been studied in isolation (i.e. in the absence of grinding). Various methods have been employed to monitor the effects upon kaolin including IR techniques^{24, 25, 26, 27}, XRD¹⁹ and DTA²⁸ (also included XRD data). Perhaps the most detailed study of its kind was by Frost and Vassallo²⁶. The work concentrated on monitoring the dehydroxylation process of kaolin (and other minerals) by examining the changes in the stretching and lattice vibration regions at 3750-3550 cm⁻¹ and 1400-400 cm⁻¹ respectively. However, curve fitting technology was not used, and for this reason, the effects were based upon general trends, rather than more specific data.

Kristof *et al*³³, used IR, XRD, DTA and surface area analysis to conduct an experiment examining the change in thermal effects and the structural alterations occurring after the milling of kaolin. This work concentrated on the 1640 cm⁻¹ water bending mode. Although an interesting article, it is lacking in detail. For example, in the spectra presented, the 1640 cm⁻¹ band is broad and there is clear asymmetry, but only one band has been assigned. It appears that upon heating, the asymmetry is reduced, thus it appears that one (or more) type(s) of water is less resistant to heating than the other(s).

Frost *et al*³⁸, studied the effects on the water stretching, bending and librational regions of the kaolinite IR spectrum after pressure and heat treatment using DRIFTS. Of particular interest were the conclusions drawn regarding the partial intercalation of water molecules at exposed edge sites when water was forced into the kaolin under high pressure (approximately 20 bars). The workers observed differences in the IR spectra in the water bending and stretching regions of low and high defect kaolins when exposed to these treatments.

Figure 2.3 Schematic of the possible location of water molecules on the kaolin surface.



It was proposed by Frost *et al*³⁸, that the high and low defect kaolins had different mechanisms of water adsorption, shown in Figure 2.3 above. The low defect mineral has regular stacks of layers, whilst the high defect kaolin has layers with disordered stacking (a halloysite with broken tubes). When the low defect kaolin edges were expanded (as a result of temperature and pressure treatment) the two layers are thought to expand congruently, and thus allow a water molecule to fit in between. In contrast, when the high defect kaolin edges are expanded, the curved edges leave more space for an increased number of water molecules to fit into (or adsorb onto). In the stretching region, the untreated high defect kaolin gave rise to bands at c 3600 cm^{-1} and 3564 cm^{-1} , corresponding to intercalated water and adsorbed water respectively. The intercalated water band at 3600 cm^{-1} was observed since the mineral is a halloysite, with interlayer water. After heating to $120\text{ }^{\circ}\text{C}$ and pressure treatment of 2 bars, additional bands at 3585 and 3555 cm^{-1} appeared, which were assigned to edge intercalated water. The overall contribution of the water increased by 10% compared with the untreated sample. XRD showed that there had been expansion of the d-spacing from 7.35 to 7.6 \AA , and it was determined that the additional water was filling the voids between the edges of the sheets. Heating the sample to $220\text{ }^{\circ}\text{C}$ at a pressure of 20 bars decreased the intensity of the water bands compared with the lower temperature and pressure treatments. However, these findings were thought to be due to experimental error or to problems associated with overlapping bands.

The untreated low defect kaolin had one water band at 3590 cm^{-1} , which was assigned to interlayer water. This assignment was surprising, since interlayer water would not be

expected in an untreated, low defect kaolin. After heat and pressure treatments (120 °C and 2 bars) a new and intense band at 3610 cm⁻¹ appeared, corresponding to “non hydrogen bonded water” between the layers. It is thought unlikely by the author of the work herein that this assignment is incorrect. It is more likely that the water molecules represented by the 3610 cm⁻¹ band are extremely weakly hydrogen bonded between the expanded layer of the kaolin. After heating to 220°C and a pressure of 20 bars water bands were present at 3593 and 3450 cm⁻¹ corresponding to edge intercalated and strongly hydrogen bonded water respectively. Although shifted in frequency, the bands were of similar significance to that in the lower temperature and pressure treated sample. Again, XRD confirmed that expansion of the layers had occurred.

In the bending region, the high defect kaolin examined presented a water mode at 1630 cm⁻¹ in the untreated sample. After heat and pressure treatments, the band split and shifted to 1650 and 1623 cm⁻¹. The 1650 cm⁻¹ was attributed to water hydrogen bonded to the kaolin surface, and the 1623 cm⁻¹ band to adsorbed water fitting into the spacers between expanded layers. In contrast, the untreated low defect kaolin produced no water bending mode in the IR spectrum. However, after heat and pressure treatments, two new bands appeared at 1682 and 1605 cm⁻¹. The high frequency 1682 cm⁻¹ band was attributed to strongly hydrogen bonded water co-ordinated to the kaolin surface, and the 1605 cm⁻¹ band to edge intercalated, weakly hydrogen bonded water. The 1682 cm⁻¹ was associated with the 3450 cm⁻¹ band in the stretching region, whilst the 1605 cm⁻¹ band was associated with the 3595 cm⁻¹ band.

The work presented herein is unique in that it uses VT DRIFTS to correlate, in a systematic manner, curve fit findings in the water bending (2100-1400 cm⁻¹) and water stretching (3800-3600 cm⁻¹) regions, as both milling time and temperature increase. VT DRIFTS was chosen over other infrared methods (e.g. VT transmission) since it facilitates the *in situ*, dynamic study of the effects of temperature on a powdered sample. It has high sensitivity and a high signal to noise ratio. Sample preparation is also much more simple than for other IR techniques. Bell *et al.*,²⁹ showed that the sample preparation involved in collecting a DRIFT spectrum of kaolinite removed the spurious

effects which can be produced by harsh pressing or grinding used in the more traditional transmission methods^{29,30}.

The changes occurring in each region are related to each other and to the types of structural water present on the surface. The intensities of the bands associated with various water types have been semi-quantified using curve fitting procedures carried out using the Grams software (See Chapter 1)

2.1.1 Curve fitting.

Curve fit parameters were kept constant throughout the work. Bands a-f, r and u-x were all fitted using Lorentzian functions, but for bands g, h, s and t, a reliable fit could not be produced with this function. Therefore, bands g, h and s were fitted using a Gaussian function, whilst band t was fitted most appropriately with a 50 : 50 Gaussian : Lorentzian combination (see Table 2.1 and Table 2.2 for details of bands).

Curve fits of the 30 minute ball milled sample have not been included in this chapter, since due to the very broad nature of the bands, reproducible fits were not achievable.

2.2 Results. The effects of ball milling

2.2.1 Scanning electron microscopy (SEM).

Representative micrographs of unrefined and ball milled kaolin are presented on the following pages.

Figure 2.4 SEM of unmilled kaolin.

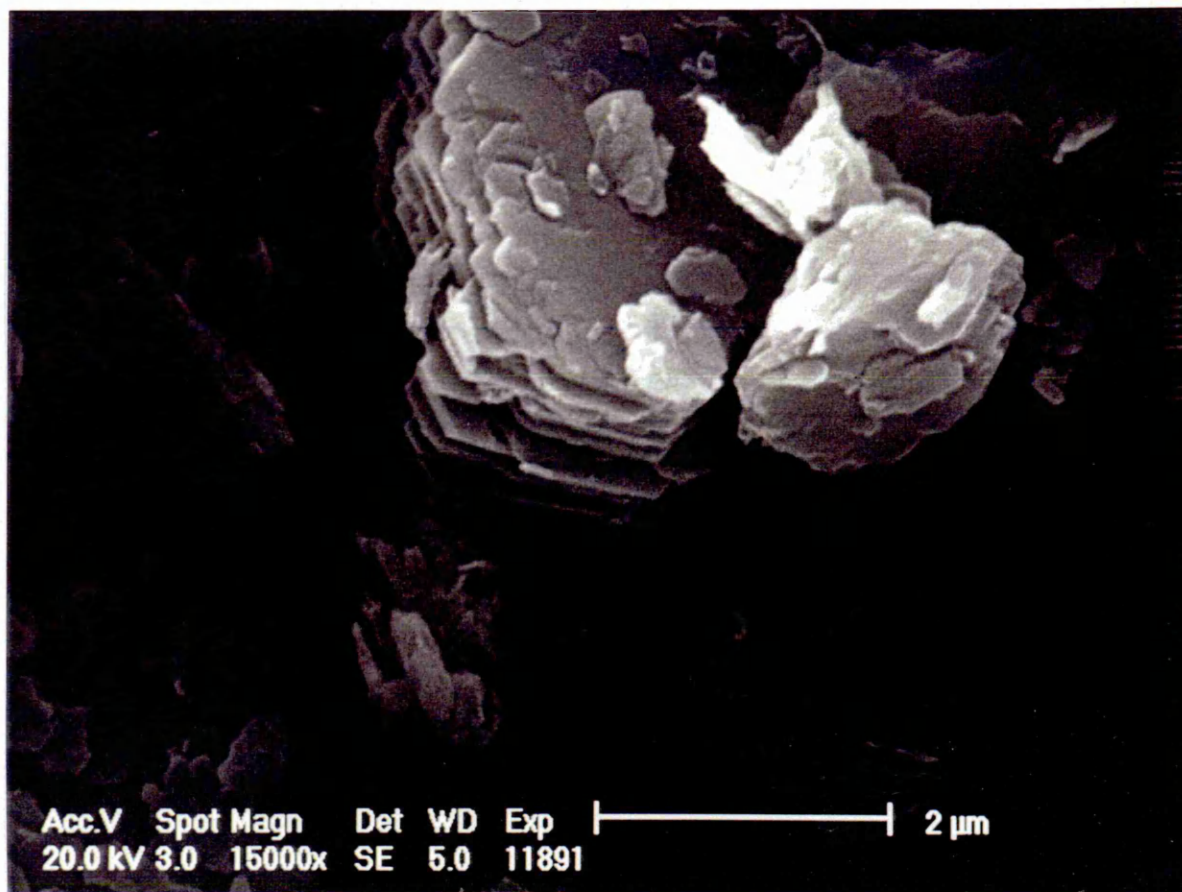


Figure 2.5 SEM of kaolin milled for 3 minutes.

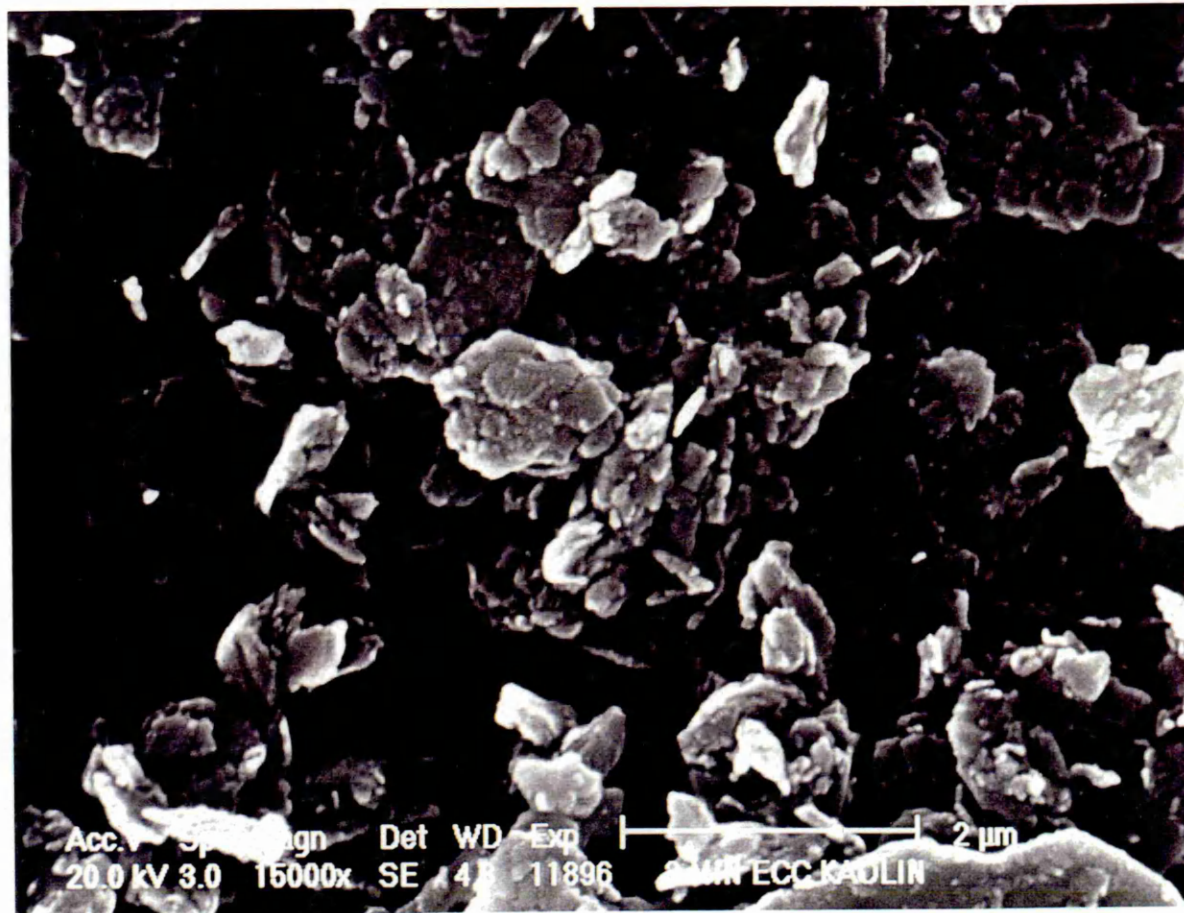


Figure 2.6 SEM of kaolin milled for 10 minutes.

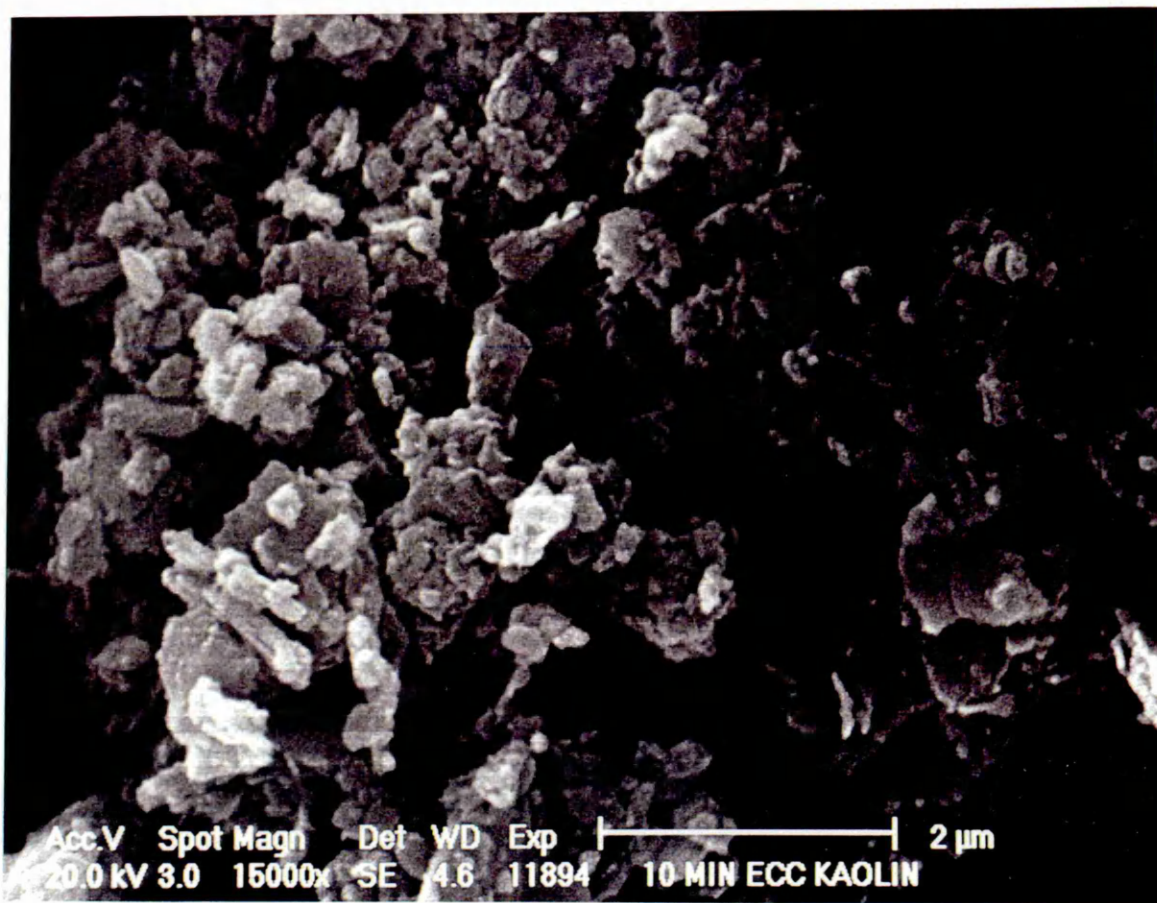
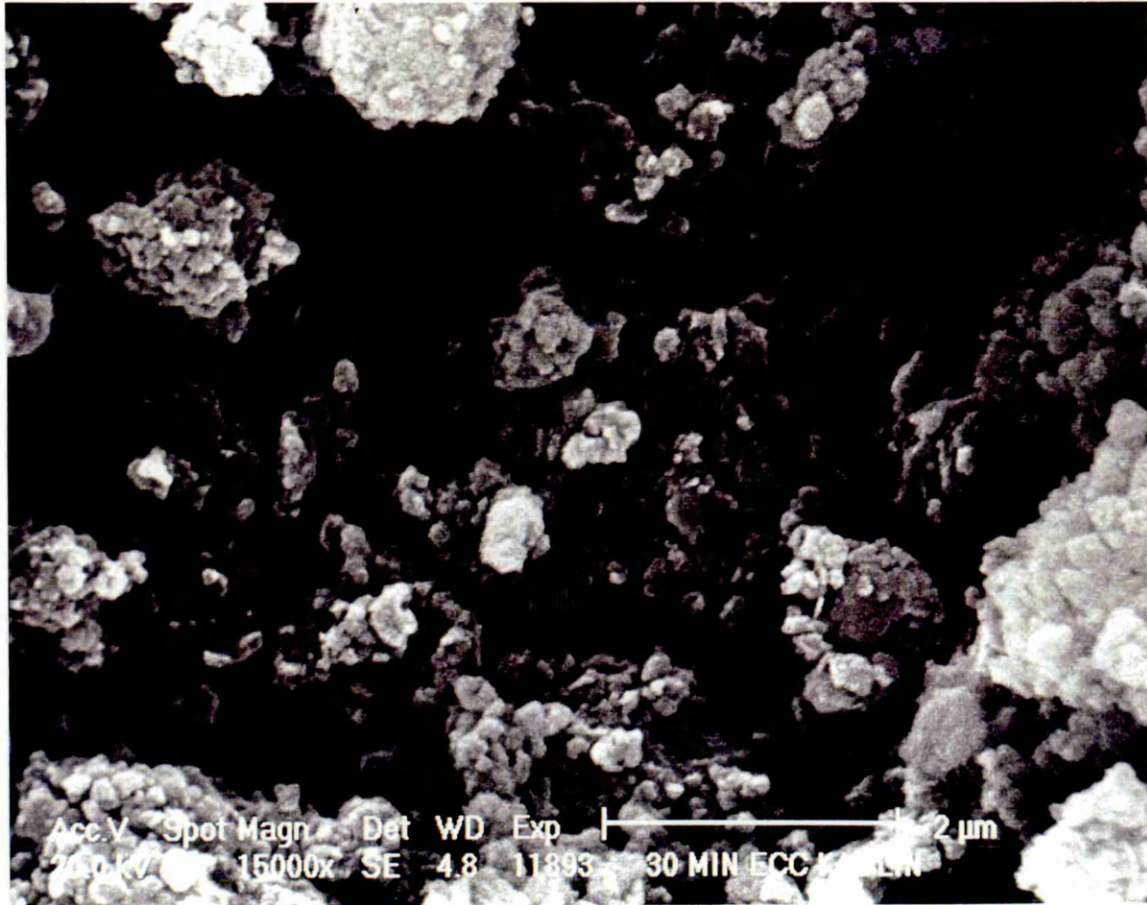


Figure 2.7 SEM of kaolin milled for 30 minutes.



Using electron microscopy it was possible to elucidate some information about the structural changes occurring after milling. The unmilled kaolin consisted of angular leaves with some evidence of stacking. Larger leaves had a diameter of up to 10 μm .

Using a wet sedimentation technique carried out at English China Clays International, Cornwall, UK, the initial particle size of the unmilled kaolin was determined to be 100% < 10 μm , 80% < 2 μm .

After 3 minutes ball milling, little evidence of stacking remained and individual particles lost their shape and decreased in size. After 10 minutes the individual particles were again much smaller, but evidence of the formation of larger aggregates was apparent.

Figure 2.7 shows that after 30 minutes milling, large agglomerates were formed. No booklets remained and individual particle fragments were very small. It is likely that the aggregate formation is a result of smaller particles adhering to each other due to the increased surface energy and the action of the amorphous surface layers during prolonged grinding^{7,31}.

Similar patterns have been observed in work carried out by others,³² however, the timescale over which this process occurs can be very different. Under the conditions of Gonzalez Garcia³², Burela kaolin aggregate formation began “incipiently” after 8 hours, and only after 36 and 65 hours did it become obvious. The less crystalline Alcaniz kaolin showed signs of aggregate formation after 4 hours of grinding. The mass of kaolin used in the Gonzalez Garcia work was much greater than that in the present study, and the force with which the kaolins were ground is not known. It is postulated that these factors may explain some of the discrepancies between the two sets of data, although it would be unreasonable to assume that the Cornish kaolin would aggregate at precisely the same rate under the conditions used in the Gonzalez Garcia work.

2.2.2 Thermal Analysis.

Figure 2.8 TGA of unmilled kaolin.

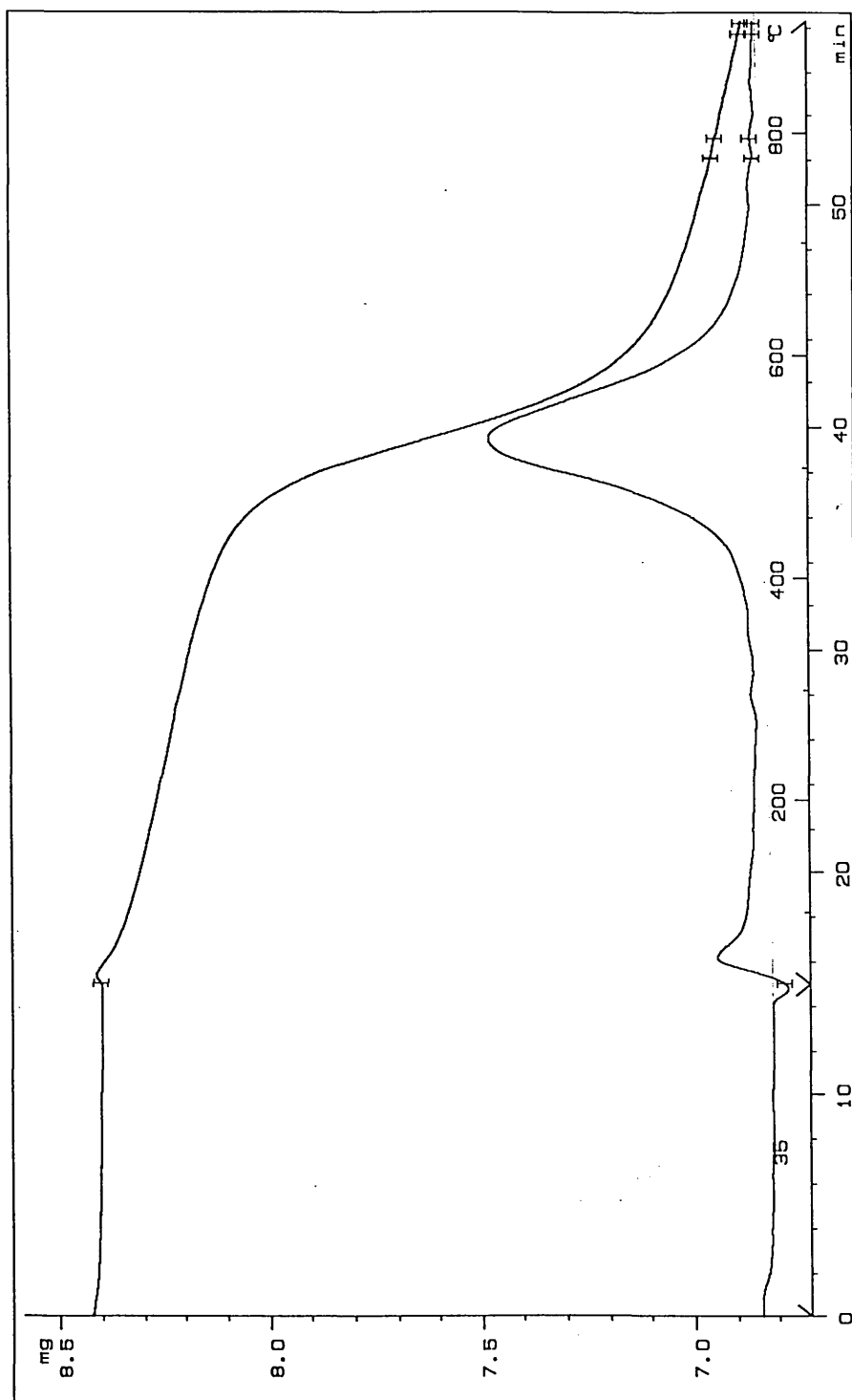


Figure 2.9 TGA of 3 minute milled kaolin.

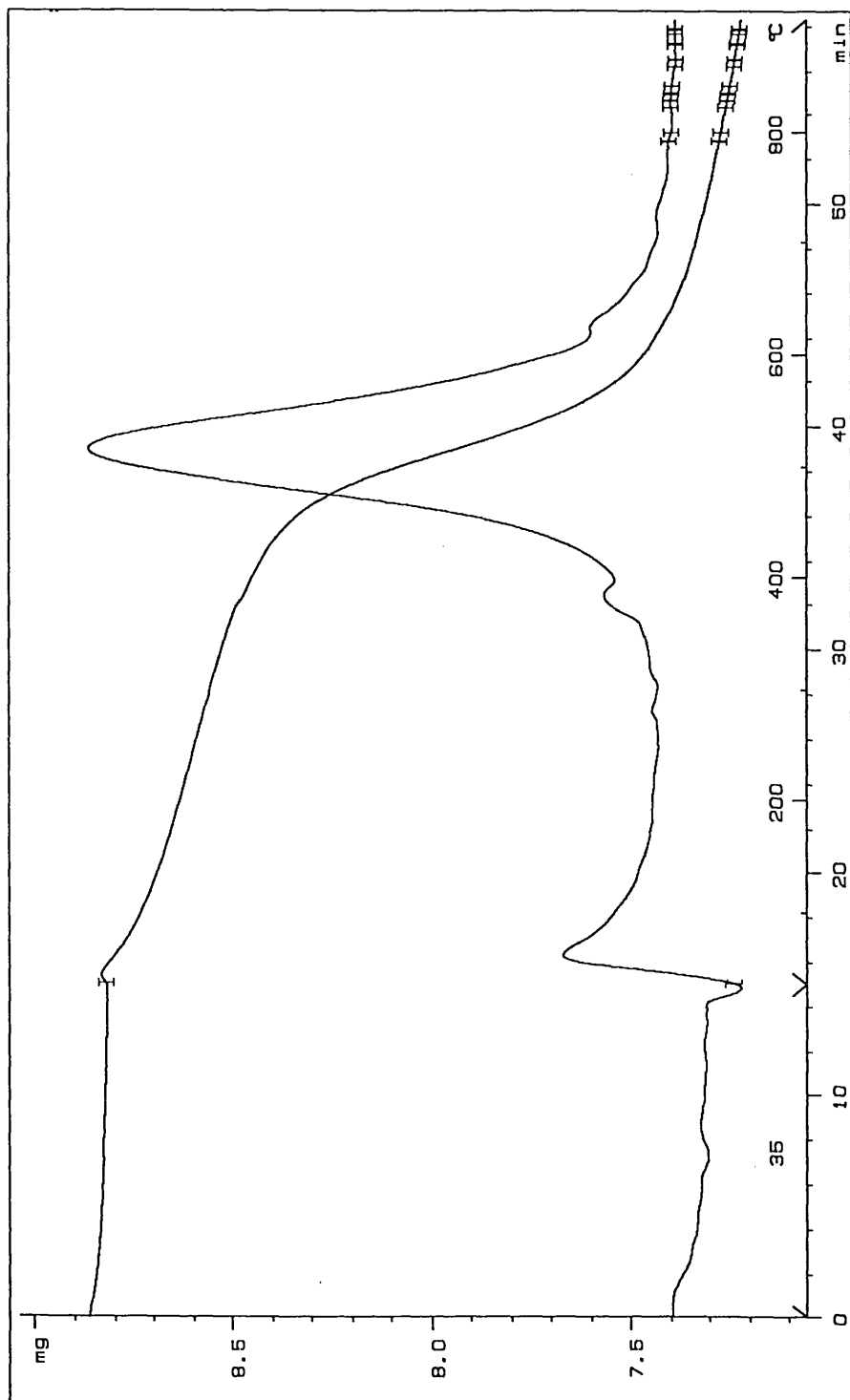


Figure 2.10 TGA of 10 minute milled kaolin.

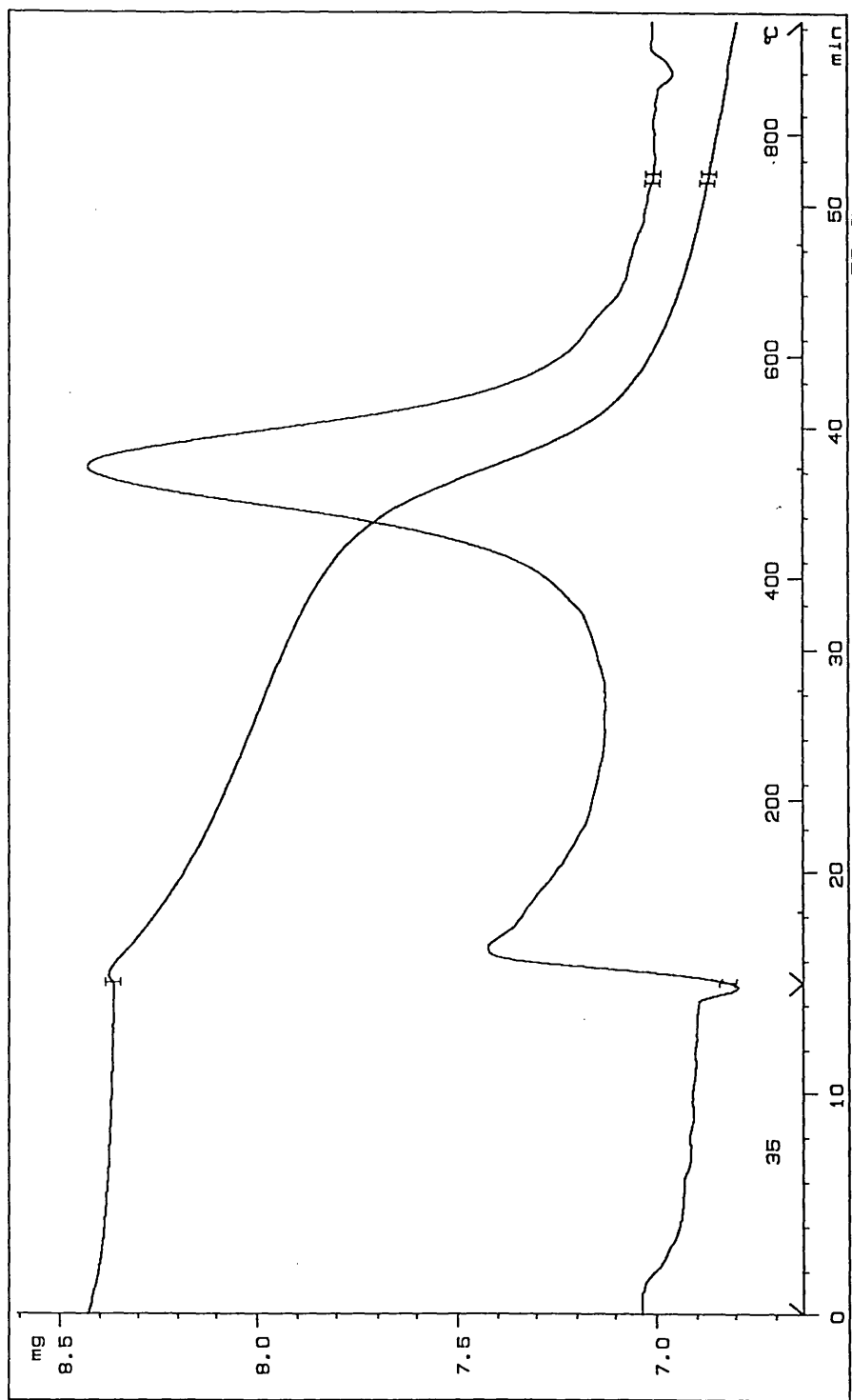


Figure 2.11 TGA of 30 minute milled kaolin.

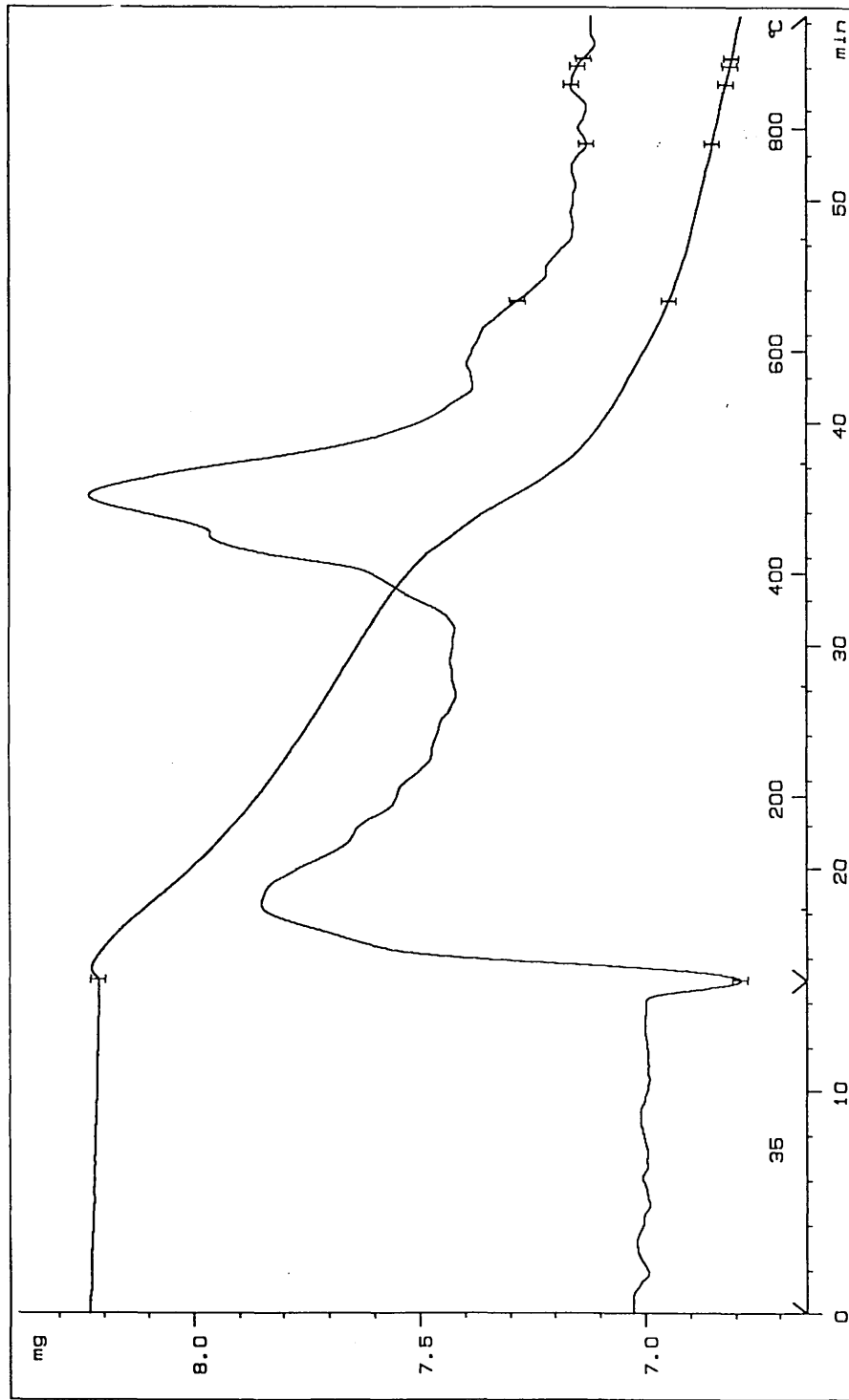
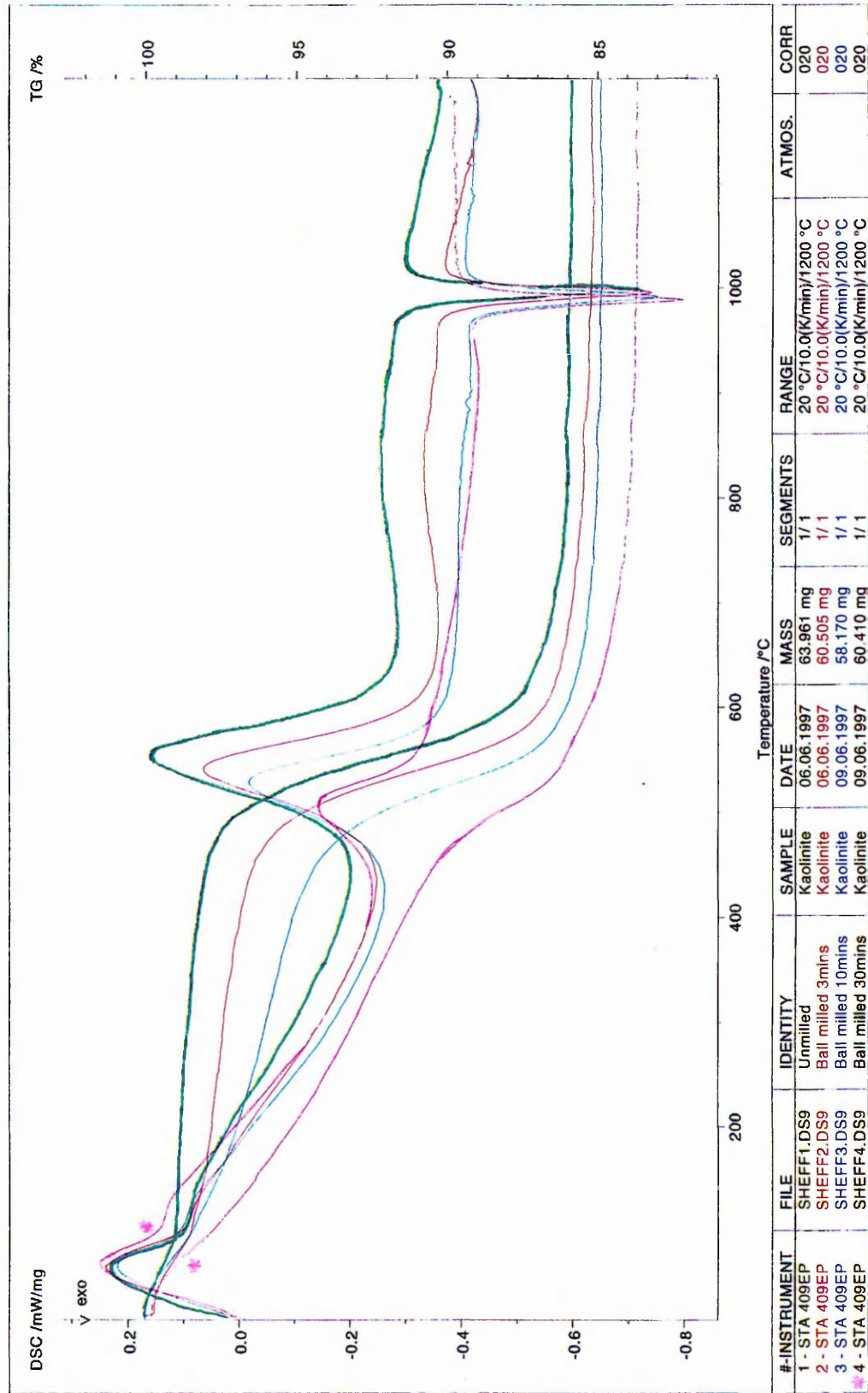


Figure 2.12 Combined TGA / DTA of 0, 3, 10 and 30 Minute Ball Milled Kaolin.



As shown by TGA and DTG data (Figure 2.8 to Figure 2.11), ball milling induced a change in the dehydroxylation (deOH) temperature. In unmilled kaolin, physisorbed water is reversibly lost up to c 450°C. There is then a major, irreversible weight loss at around 550°C, which is indicative of structural dehydroxylation. This temperature decreased significantly after milling. The weight loss curves of the milled kaolin show that a greater proportion of water loss occurred at lower temperature (indicated by increased weight loss below 400°C). One reason for this increase at reduced temperatures is that there is an increased amount of adsorbed water on the clay surface as milling increases. Although weight loss increased at low temperatures, there is no evidence to suggest that total weight loss before dehydroxylation at around 600°C increased. To the contrary, there was a very slight decrease in the total weight loss as milling time increased which may have been within the limits of calculation error (see Table 2.4 below).

Table 2.4 Weight losses from kaolin during thermal analysis.

Milling time (mins)	Weight loss under 400°C (%)	Total weight loss (%)
0	3.0	16.8
3	3.6	16.2
10	5.7	16.1
30	8.7	16.0

The shift in the DTA peak (initially at 550°C for unmilled kaolin) to lower temperature was mimicked by the shift in, and intensity reduction of the deOH endotherm with increased milling time (see Figure 2.12).

In the present work, milling even for 30 minutes exerted little influence on the irreversible metakaolin to mullite transformation temperature, indicated by the sharp exothermic peak at around 990°C.

In work by Kristóf and co-workers³³ crystallographic changes in the formation of mullite from a milled Sedac kaolin were noted. The metakaolin-mullite transformation is influenced by the structural state of the metakaolin, but after very extensive structural

perturbation. After milling the Sedac kaolin for 10 hours the exothermic peak representing this transformation occurred at 920°C rather than 1000°C. It is clear that the Cornish kaolin in this work was not milled extensively enough to cause significant changes in the transformation temperature.

2.2.3 XRD.

Figure 2.13 XRD of unmilled kaolin.

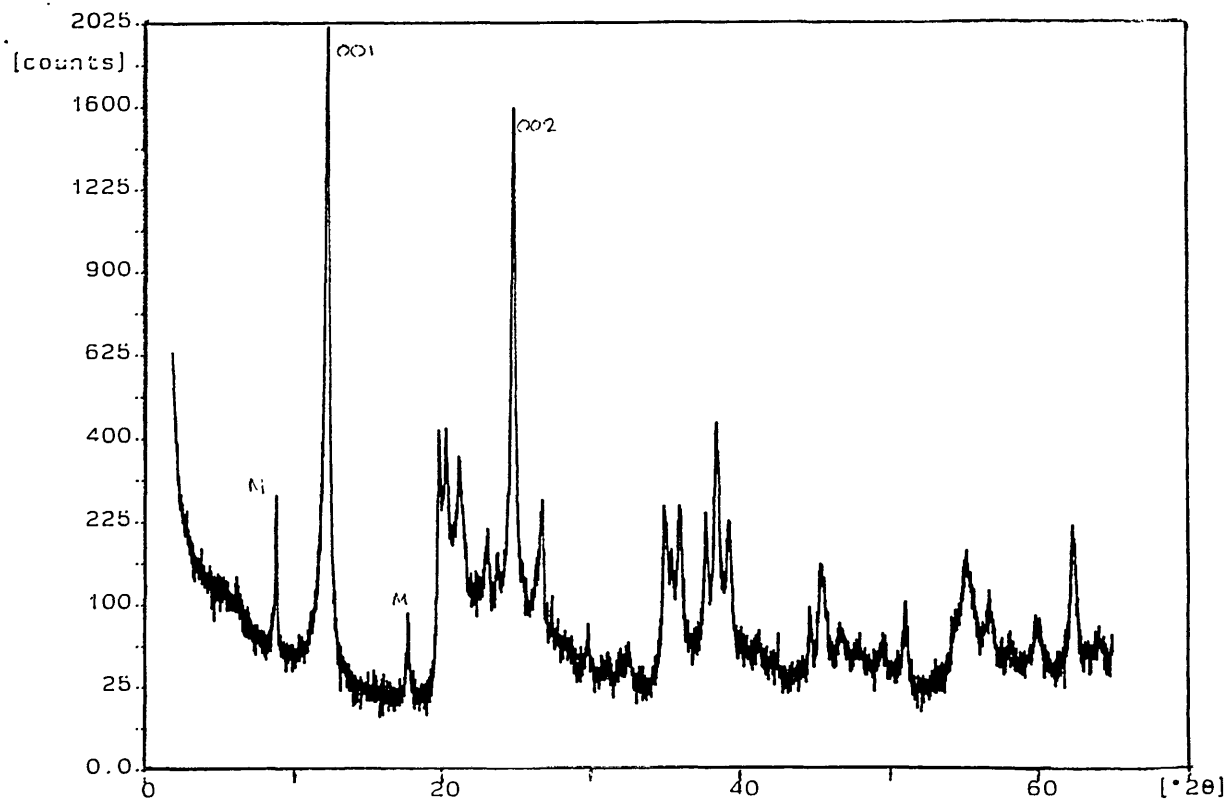


Figure 2.14 XRD of 3 minute milled kaolin.

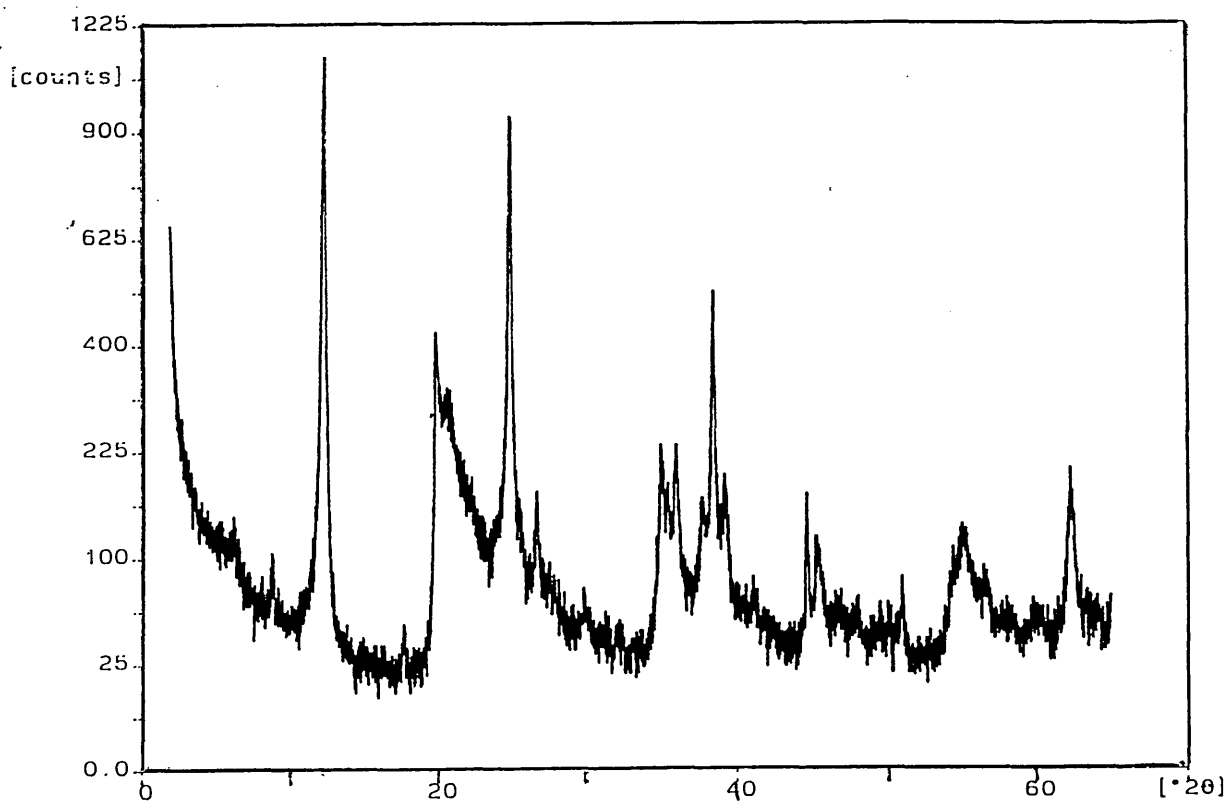


Figure 2.15 XRD of 10 minute milled kaolin.

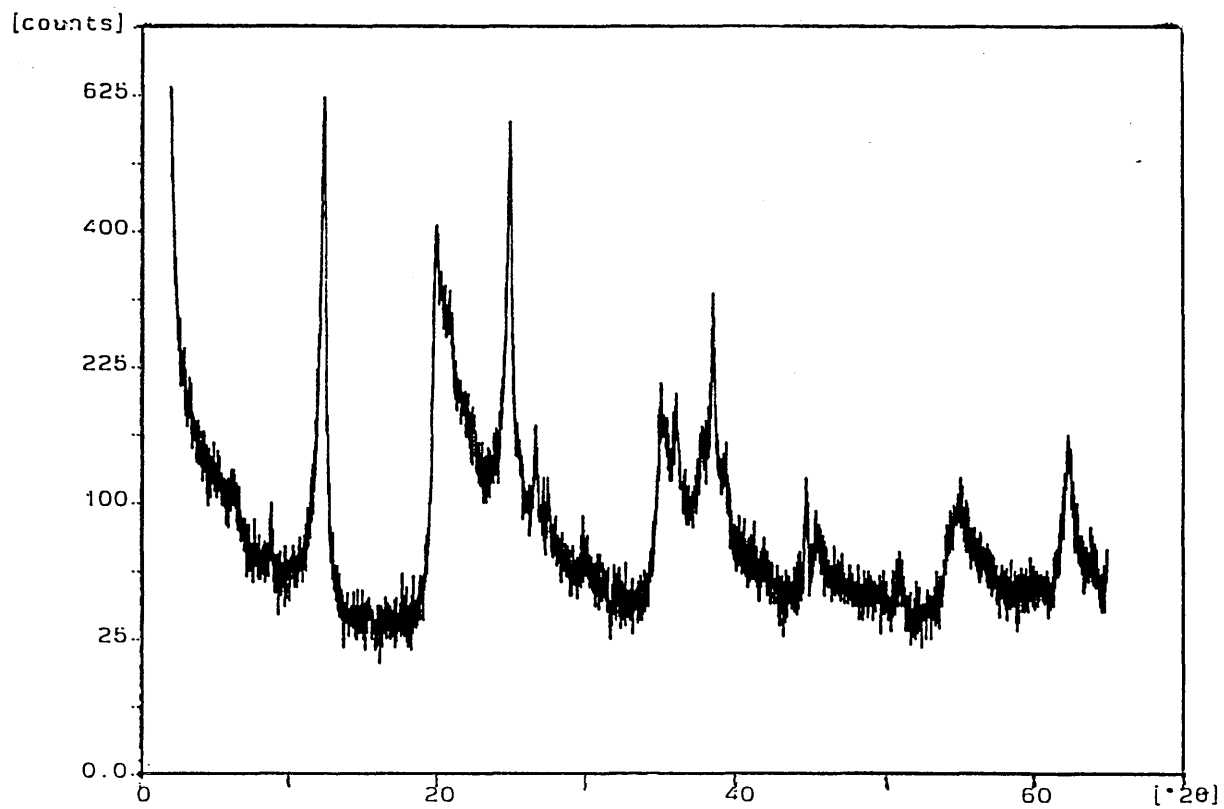
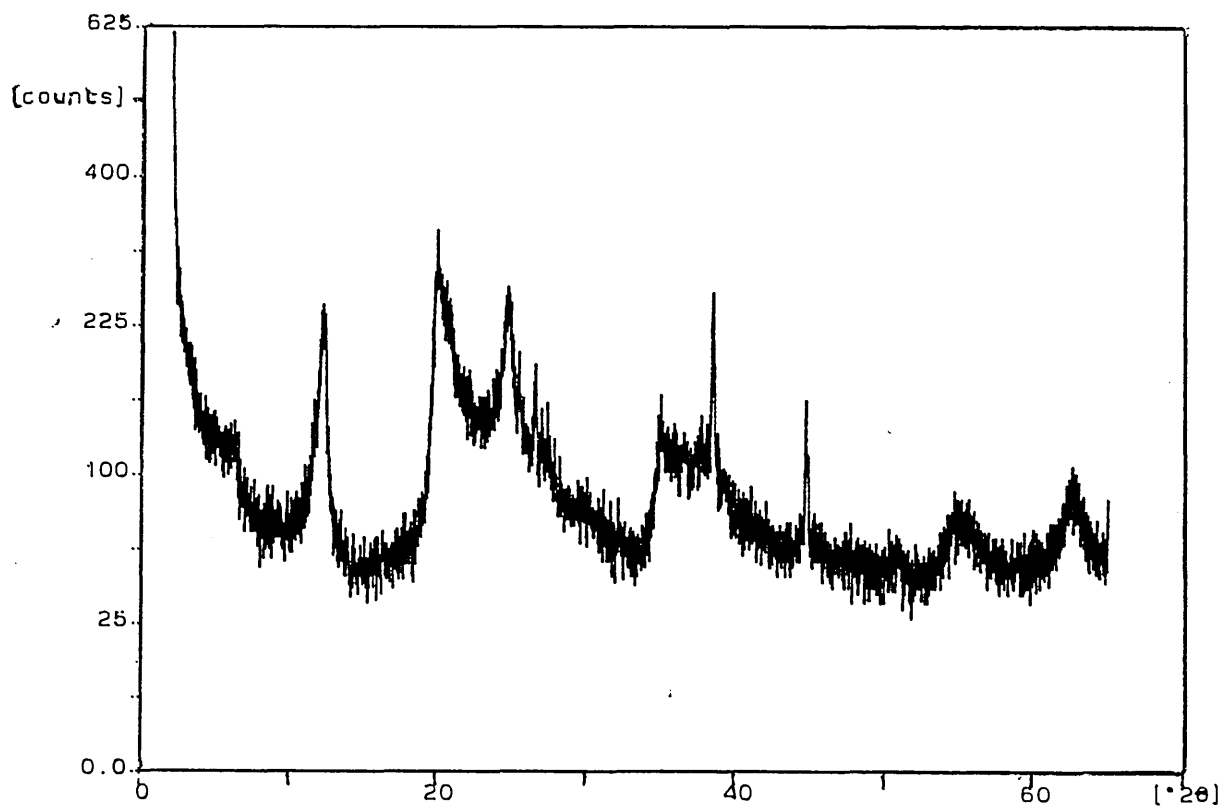


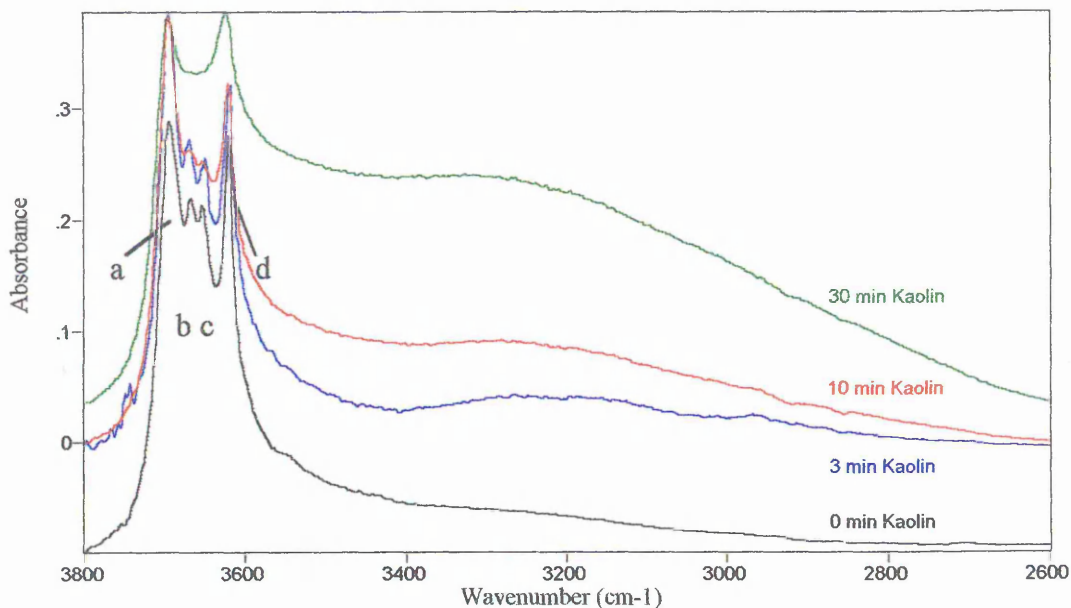
Figure 2.16 XRD of 30 minute milled kaolin.



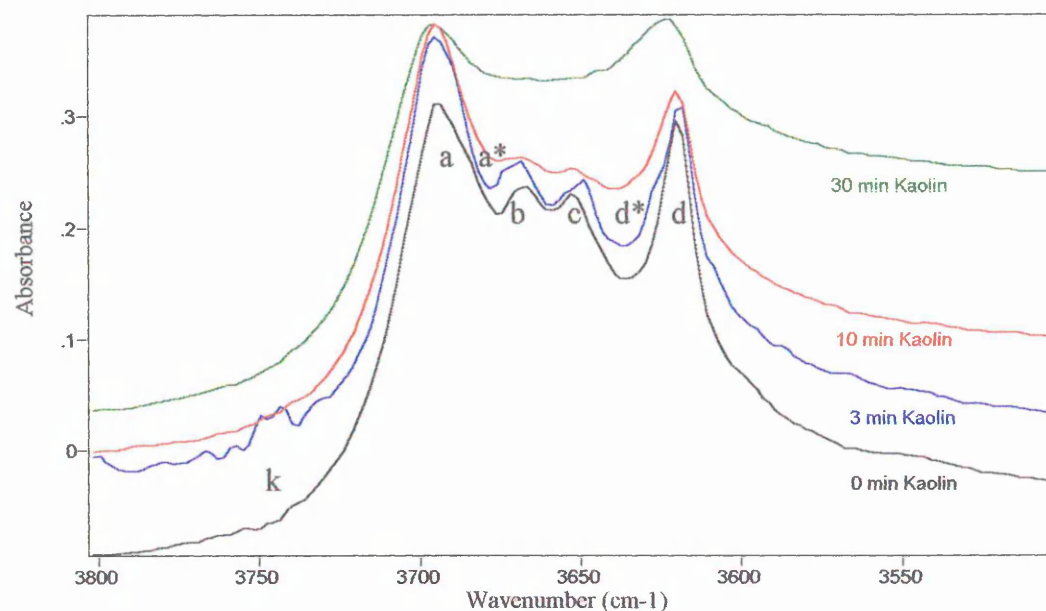
XRD traces are shown in Figure 2.13 to Figure 2.16. In these kaolin samples, it is possible that mixed layer minerals are present but it is very difficult to distinguish these in a bulk analysis. For example, halloysite has a 10 Å d spacing in its usual state (i.e. hydrated) at room temperature. When it is dehydrated the spacing becomes 7 Å and is indistinguishable by XRD from kaolin. It is possible to distinguish the two minerals by their morphology, but in the SEM work carried out herein, no halloysite component was found. The XRD study was not intended to form a detailed investigation, but more to confirm gross changes present after milling. Figure 2.13 is typical of the trace of a well crystallised kaolin. It contains well defined, sharp and intense reflection bands. There is evidence of a mica impurity (designated "M"), and also a small amount of what is likely to be smectite at approximately $6^{\circ}2\theta$. After milling for 3 minutes, (Figure 2.14) the intensity of the kaolin bands has reduced and fewer bands are recognisable. The amorphous hump between 20 and 30 $^{\circ}2\theta$ is a more prominent spectral feature (due to the relative decrease in intensity of the other kaolin peaks). The mica impurity is still evident. The 10 minute milled trace (Figure 2.15) shows a further reduction in the intensity of the kaolin peaks. The kaolin peaks continue to become less well resolved. There is still clear evidence of the mica impurity. This is unsurprising, since mica is harder than, and therefore more resistant to milling than kaolin. After 30 minutes ball milling, (Figure 2.16), a trace is obtained which is characteristic of a very poorly ordered kaolin. The characteristic kaolin peaks have been very greatly reduced in intensity. There is still some evidence of a mica band at approximately 8 $^{\circ}2\theta$, although it is now less obvious due to structural degradation. This trace suggests the structure of the kaolin has been significantly damaged. The trend in these findings is also confirmed in the literature of the milling of kaolin^{3,14,33} and other minerals⁷.

2.2.4 Infrared of ball milled kaolins. The 3800-2600 cm^{-1} region.

Figure 2.17 RT (Room Temperature) DRIFTS of ball milled kaolins.



As milling time increased, there was a dramatic increase in the intensity in the c 3400-2800 cm^{-1} region. Also, bands a-d began to converge after only 3 minutes milling. The relative intensities of bands a and d alter. Initially, after 3 minutes milling, the intensity of band a increases with respect to band d. After prolonged milling (30 minutes) band d becomes more intense than band a. This region of the spectrum has been enlarged, and is shown in the figure below.

Figure 2.18 Ball milled kaolins. The 3800-3475 cm^{-1} region.

The RT DRIFTS show that the bands a-d alter in frequency and relative intensity according to milling time. These phenomena have been observed and studied to varying degrees of detail by many workers using IR spectroscopy techniques^{3,7,19,29,33,43}.

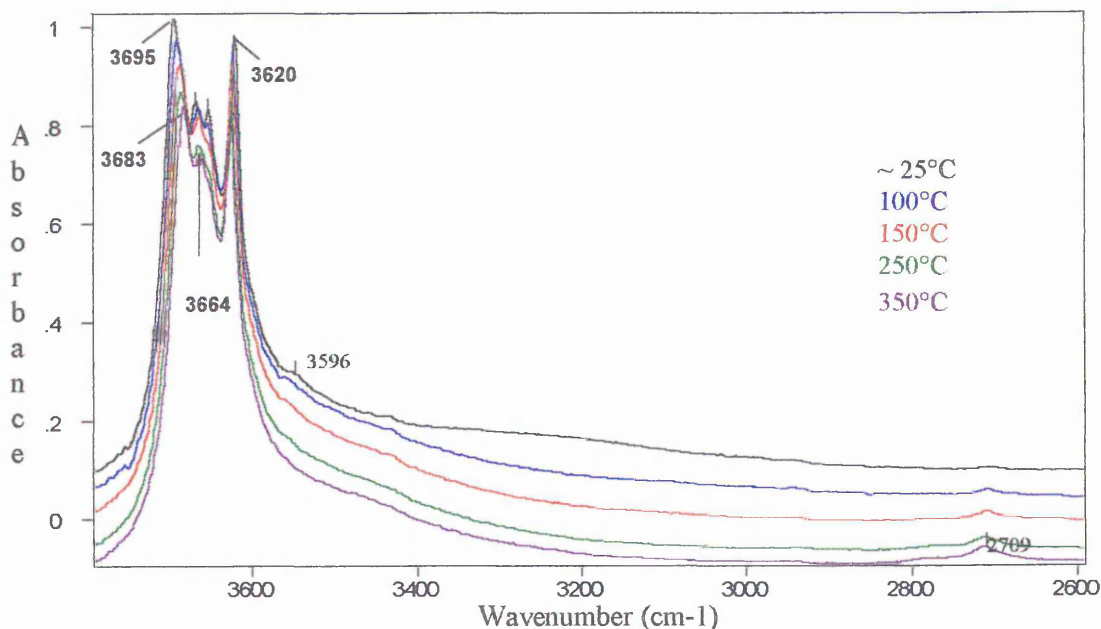
As well as the 4 obvious bands above, there is some controversy over the existence in the IR spectrum of other bands (usually present as shoulders). One such shoulder is present at around 3684 cm^{-1} . The spectra above are inconclusive with regard to the presence of overlapping bands, but, particularly in the unmilled kaolin spectrum, there is a clear asymmetry of band a, which suggests the presence of another band (designated a*). This band has been assigned to the uncoupled inner surface OD or OH stretching vibration in weakly deuterated kaolinite³⁴. However, the Cornish kaolin used here is not deuterated and the band is instead tentatively assigned to halloysite²⁶. At this point it should be noted that the concentration of the 3 minute milled kaolin is lower than that of the other spectra presented. The possible effects upon the collected spectrum will be discussed in more detail later, but one of the gross effects is to make the complete subtraction of water vapour more difficult, due to the relative increase in water vapour intensity with respect to the collected spectrum of interest. One interesting feature seen here is the weak band, kaolin, at 3750 cm^{-1} in the 3 minute milled sample, which appears as a doublet due to incomplete water vapour subtraction. According to Frost et al.³⁵, it

represents vapour-like monomeric non hydrogen bonded water. It is not reasonable to expect non hydrogen bonded water in this system, and therefore, an assignment is based on another work by Frost⁴¹ which offered an alternative assignment for a band at this frequency and identified a corresponding band in the bending region at c 1580 cm⁻¹ (see Figure 2.52). The band was attributed to very weakly hydrogen bonded water in the second sphere of hydration. This is a much more likely assignment, since it is reasonable to expect “multilayers” of hydration within this system. There also appears to be a shoulder on band d (d*) in the 3 minute milled sample. This could correspond to a halloysite hydroxyl stretching mode²⁶.

2.2.4.1 The effect of temperature on milled kaolin. The 3800-2600 cm^{-1} region.

2.2.4.1.1 Unmilled (0 minute) kaolin.

Figure 2.19 Unmilled (0 minute) kaolin. The 3800-2600 cm^{-1} region.



In all samples, (0 to 30 minutes milled) peaks a and d in the 3700-3600 cm^{-1} region were distinguishable at room temperature, although peaks b and c were at times inseparable by eye. The curve fit programme allowed these peaks to be identified by position, although it was not able to reliably distinguish between the relative intensities of peaks b and c, since often the areas were readily interchangeable. However, since these are generally assigned to inner surface hydroxyls, precise information regarding the absolute peak intensities was, for the purpose of this work, not necessary. There are many possible ways in which curve fitting can be carried out. The results presented here represent one of a number of possibilities. However, they are believed by the author to be a true representation of the effects of the physical processes occurring during milling. Presented below are 3 representative curve fits of the unmilled kaolin. A detailed description of the changes occurring after heating follows.

Figure 2.20 Unmilled kaolin. The 3800-2600 cm^{-1} region. Room temperature curve fit.

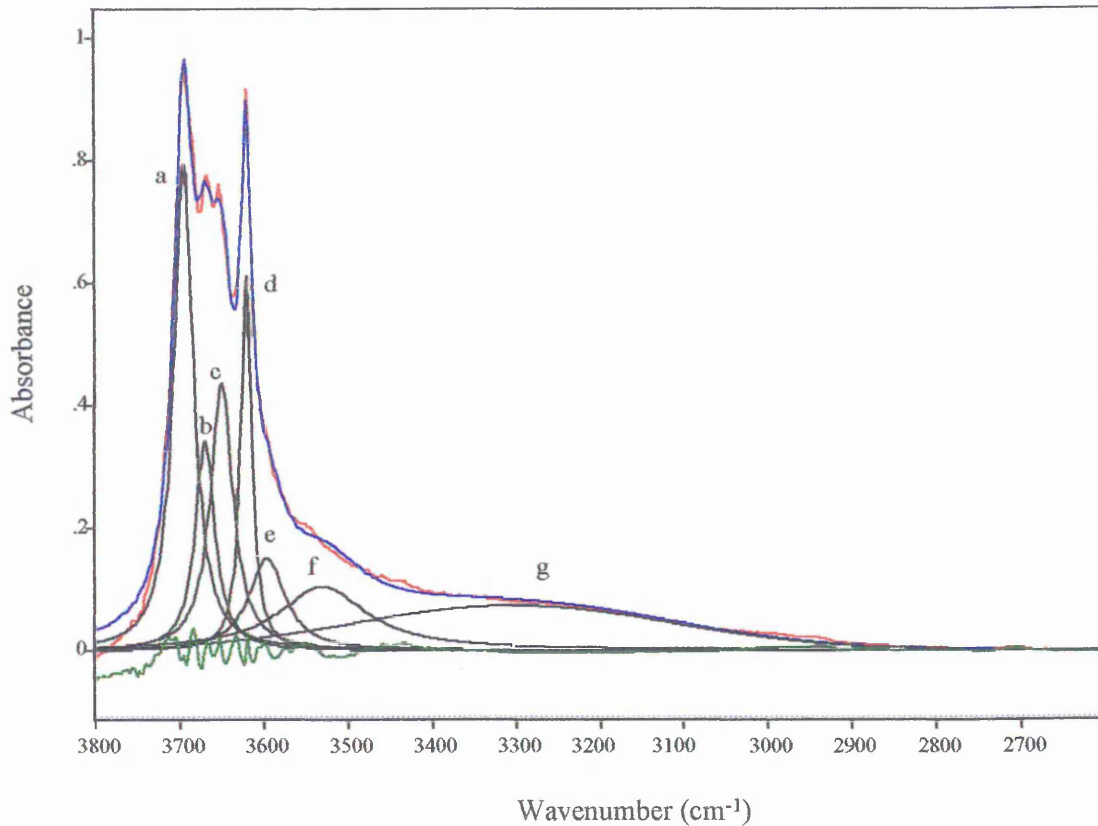


Figure 2.21 Unmilled kaolin. The 3800-2600 cm^{-1} region. 200 $^{\circ}\text{C}$ curve fit.

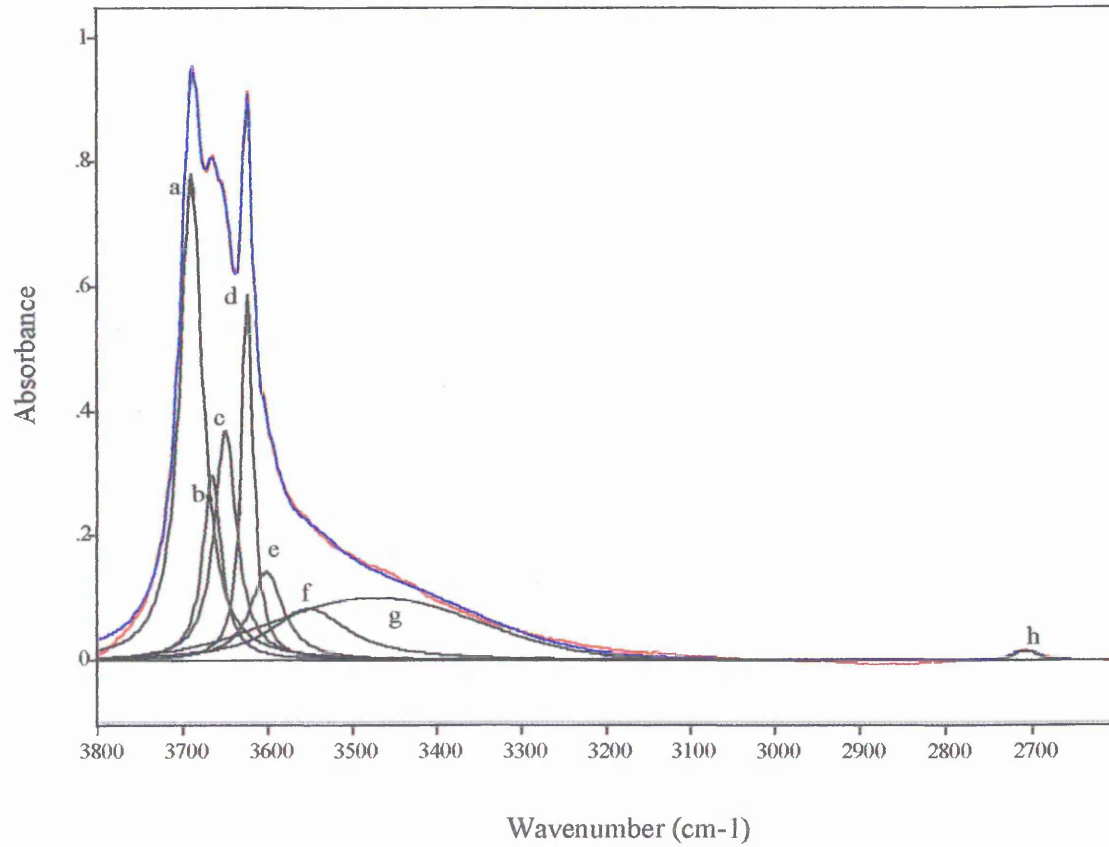
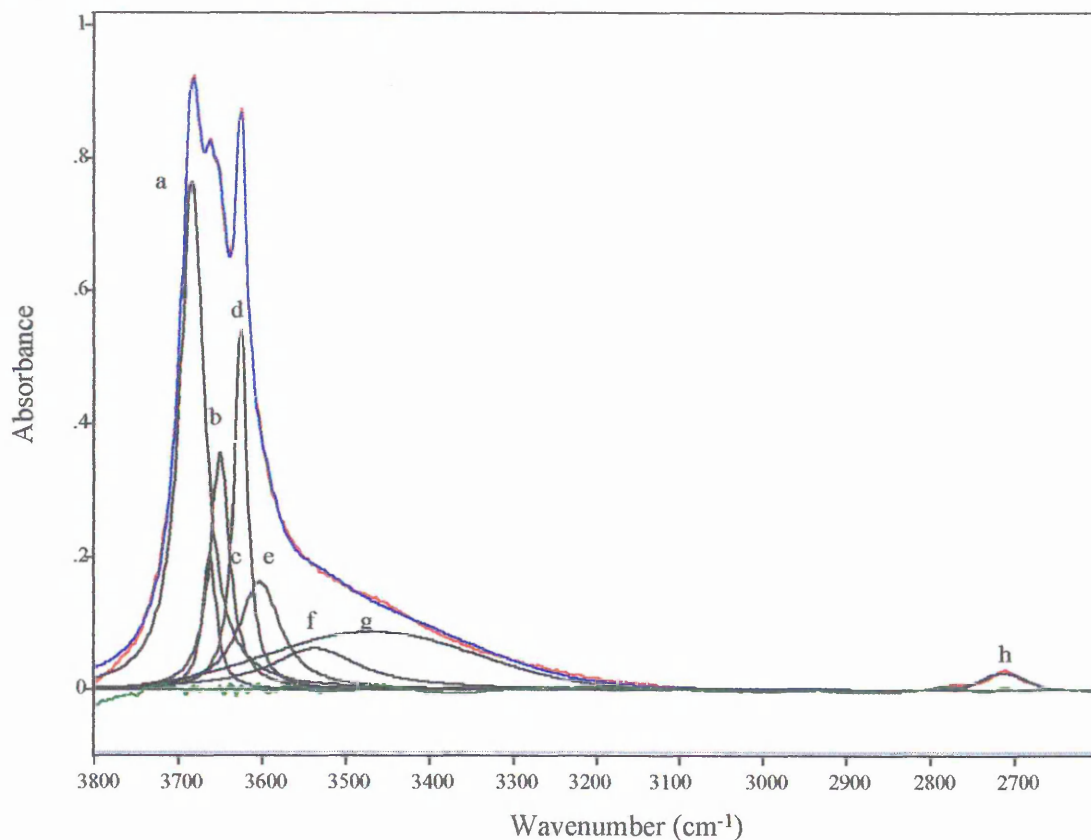


Figure 2.22 Unmilled kaolin. The 3800-2600 cm^{-1} region. 350 $^{\circ}\text{C}$ curve fit.



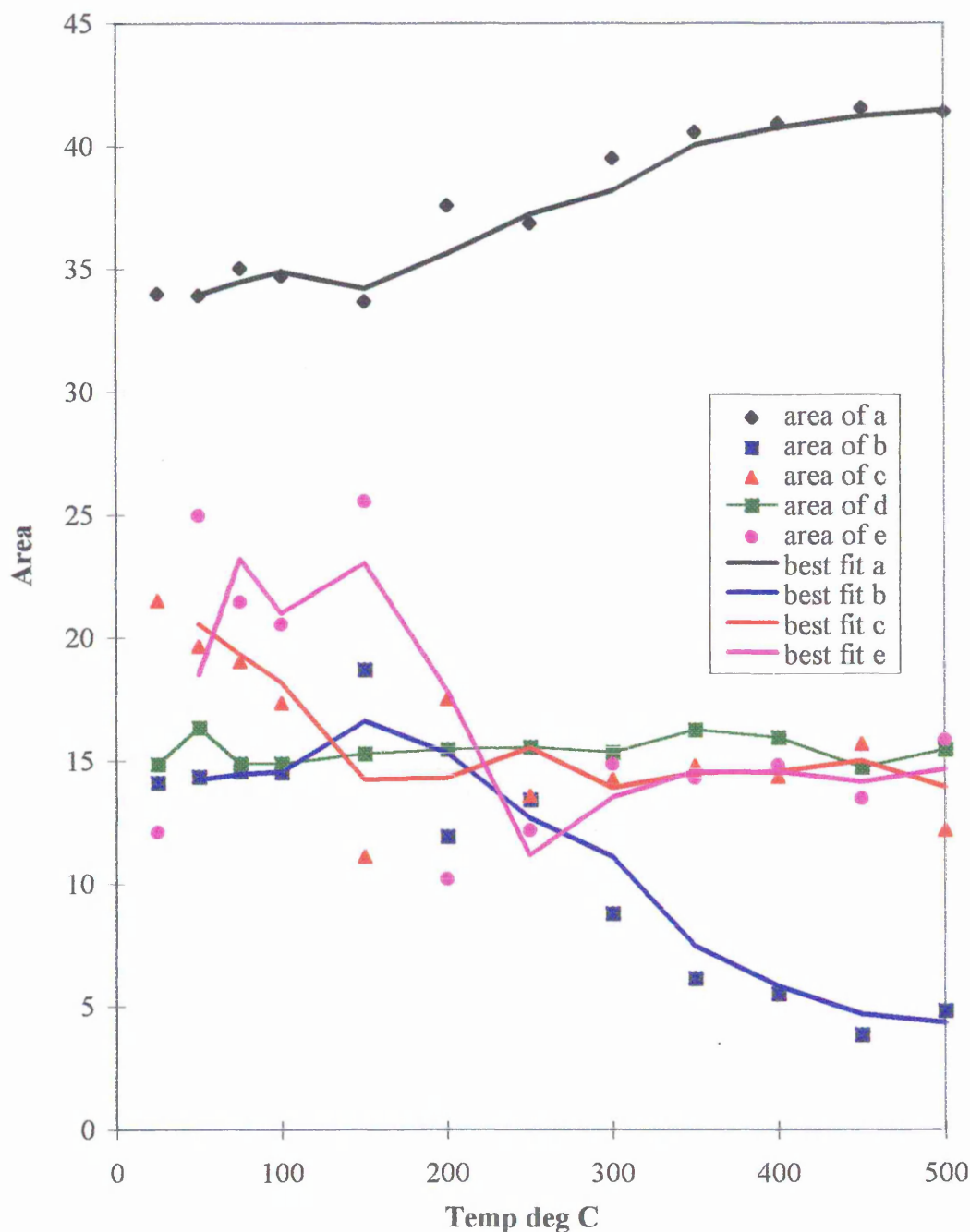
At room temperature bands a to d were well defined. There was a small amount of surface-sorbed water with a band (g) centring at around 3300 cm^{-1} . Bands e and f were present at approximately 3600 and 3550 cm^{-1} respectively.

At 200 $^{\circ}\text{C}$, bands a and d remained distinct, but bands b and c began to converge. A peak was still evident in the position of band b, but c was distinguishable only by curve fitting. Band e has remained almost constant in position. Bands f and g shifted to higher frequency and g in particular decreased in relative intensity. Band h at approximately 2700 cm^{-1} became more obvious.

After heating to 350 $^{\circ}\text{C}$, the relative intensity of band a increased (largely due to the decrease in intensity of the water components g and f), but also because of the inability of the curve fit package to distinguish between not only bands b and c, but also between bands a, b and c. Band e decreased in relative intensity up to around 200 $^{\circ}\text{C}$, but remained fairly constant thereafter. There was a slight shift to higher frequency. Band f decreased in relative intensity and shifted approximately 50 cm^{-1} in frequency from around 3500 cm^{-1} at 150 $^{\circ}\text{C}$ to around 3550 cm^{-1} at 350 $^{\circ}\text{C}$. Band g appeared to shift

dramatically over this temperature range. This phenomenon will be discussed in more detail later. Band h became more distinct.

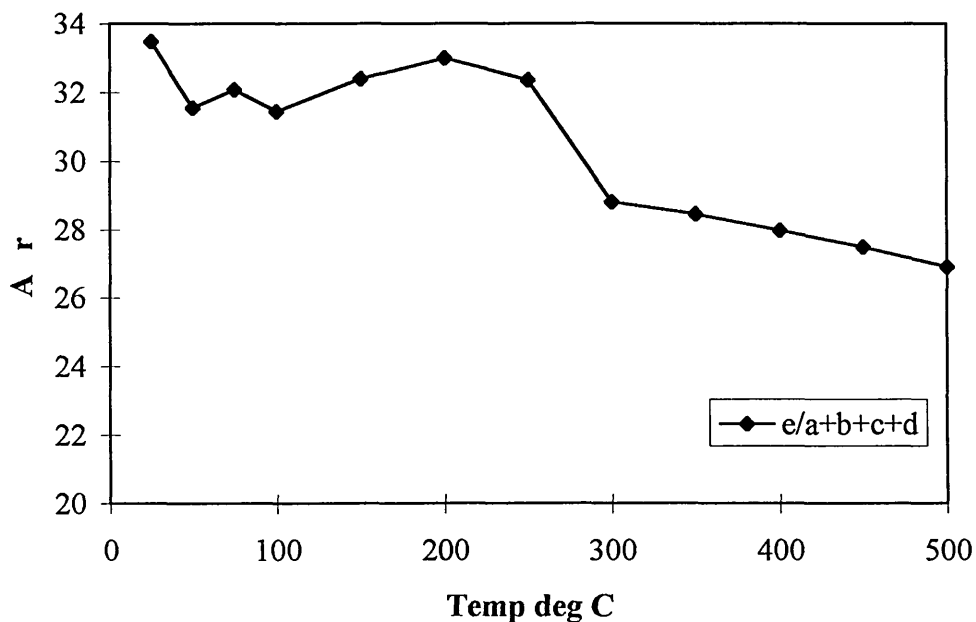
Figure 2.23 Unmilled kaolin. The 3800-2600 cm^{-1} region. The change in intensity of bands a, b, c, d and e.



The relative intensity of band a appeared to increase as temperature increased. However, this is probably an effect of the curve fitting procedure used. The intensity of the band was not restricted, and therefore, as bands b and c became less well defined as temperature increased, the relatively stable and intense band a effectively “stole” intensity

from the weaker bands. The intensities of bands b and c were generally interchangeable up to around 250 °C. Thereafter, band b appeared to lose intensity very quickly. However, this is due to “swamping” by band a. It is, probable that there was an overall decrease in the intensity of band a compared with band d, although this is not shown in Figure 2.23 for reasons given above. An interesting feature is that the intensity of band d remained constant over the entire temperature range. This is as expected, since band d represents the inner hydroxyl which is least exposed to external factors, since it is well protected within the kaolin structure. At low temperatures, band e had a high intensity, which decreased by 4 % (absolute) or 12.5 % (relative) at around 200 - 250 °C.

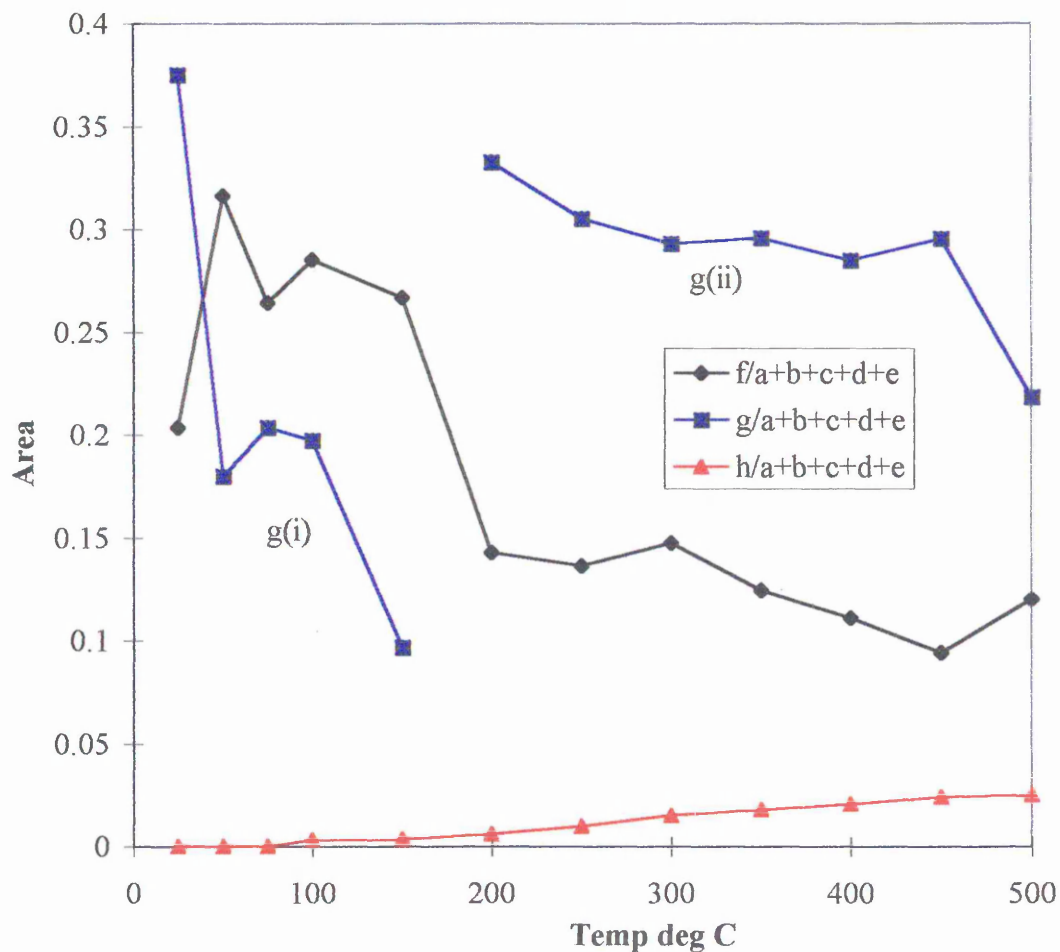
Figure 2.24 Unmilled kaolin. The change in intensity of band e.



The plot above further illustrates the 2 distinct phases of band e. This band at room temperature was at a frequency of 3596 cm^{-1} and was necessary for a sensible fit. The intensity of this band remained uniform and high between 25 and 250 °C, probably indicating that this is a structural band. At 300 °C, there was a marked decrease in intensity (of approximately 12 % of the initial intensity), which is likely to represent the partial break down of structure (reversible dehydroxylation) or the loss of a small amount of surface bound water. Band e in the most part is not considered to represent water, since it undergoes very little intensity loss at low temperature. It is possible, however, that this band represents a mineral other than kaolin. It could be due to the impurity mica, or another kaolinite mineral such as halloysite. Frost *et al.*,³⁸ noted a band at 3590

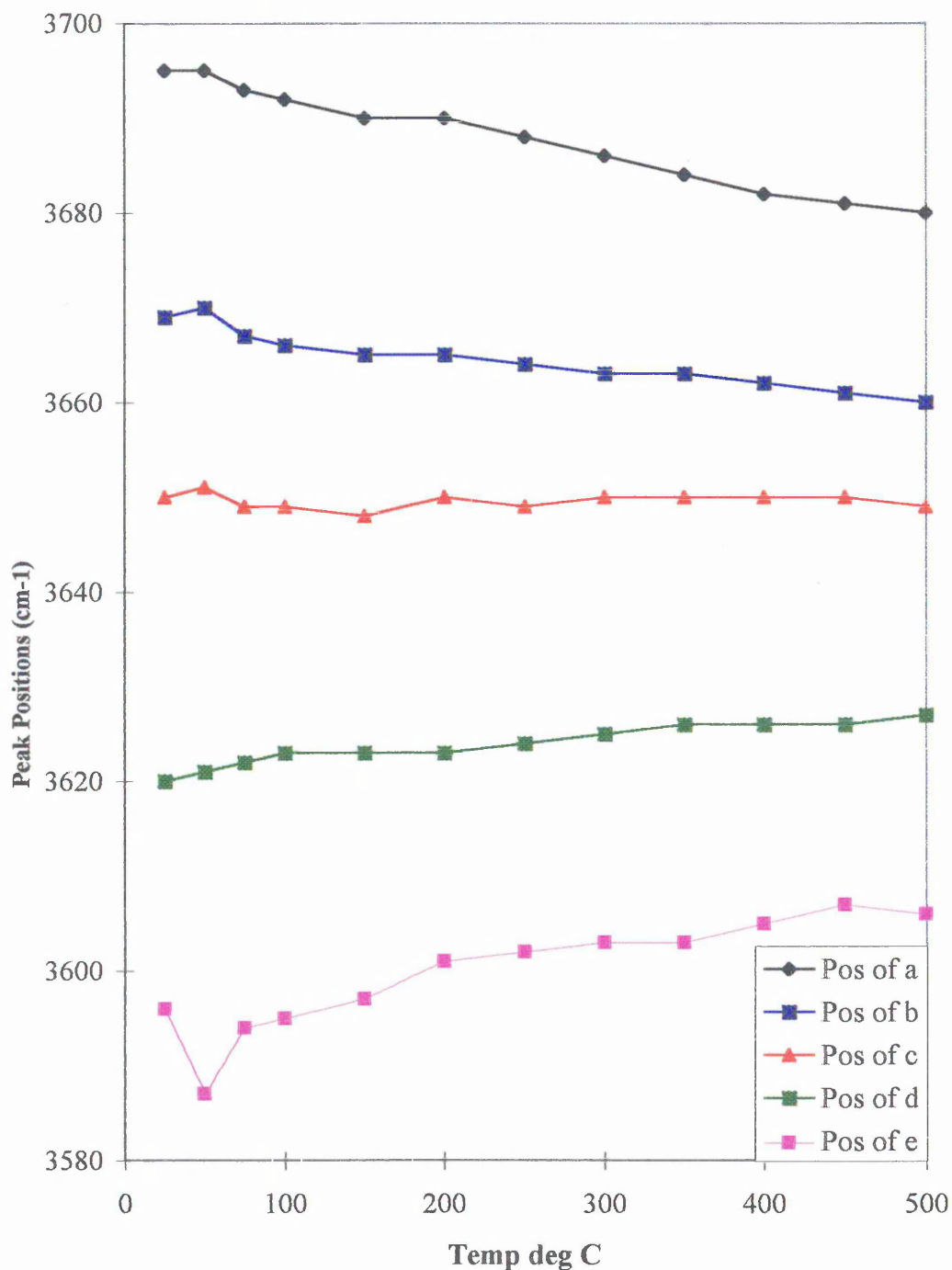
cm⁻¹ and attributed it to interlayer or intercalated water. It was stated in that work that bands at that frequency are often seen in disordered kaolinites and halloysites. Mendelovici *et al.*,³⁶ observed this band (at 3596 cm⁻¹) also, but only in kaolins containing iron. It is also a possibility that this band is exhibited by the mica impurity contained within the sample. Besson and Drits³⁷ noted many mica bands in this region. It is not possible to elucidate which of these assignments is correct at this time, so for the purpose of this report and therefore for subsequent plots, band e is considered to be structural, and is included as a reference band along with bands a-d. The sum of the areas of bands a - e are considered to be constant, and the use of these bands as references allows the comparison of relative, rather than absolute intensities of the remaining water bands of interest. Area values quoted within this work are relative values unless otherwise stated.

Figure 2.25 Unmilled kaolin. The change in intensity of bands f, g & h.



Between 50 and 200 °C band f lost intensity until by 200 °C it was around half of the maximum value ($t^{1/2}$). Thereafter it remained relatively stable, with a very slight decrease. Band g appeared to decrease initially up to 150 °C, and then increase again by 200 °C to an intensity almost equal to that at room temperature. This was not a real phenomenon, and was actually an artefact created by the fitting regime. In fact, 2 bands were being observed- band g(i) present between 25 and 150 °C, and band g(ii) which was present at all temperatures, but which became obvious only after the intensity at position g(i) was reduced. In reality, band g(ii) is probably not distinguishable from band f at elevated temperatures. Both bands have similar frequencies and with such broad features it is difficult to reliably comment on their resolution. When band g(ii) “appears” there is a concurrent fall in the intensity of band f. The hypothesis that the band originally designated “g” is in fact two bands is corroborated by Figure 2.26. The position of g(i) between 25 and 150 °C was stable up to 150 °C, and thereafter, it shifted by over 150 cm^{-1} to higher frequency - the position of band g(ii) -which is also close to the position of f. Band h became more obvious as temperature increased.

Figure 2.26 The change in position of bands in the 3800-2600 cm^{-1} region as a function of temperature.

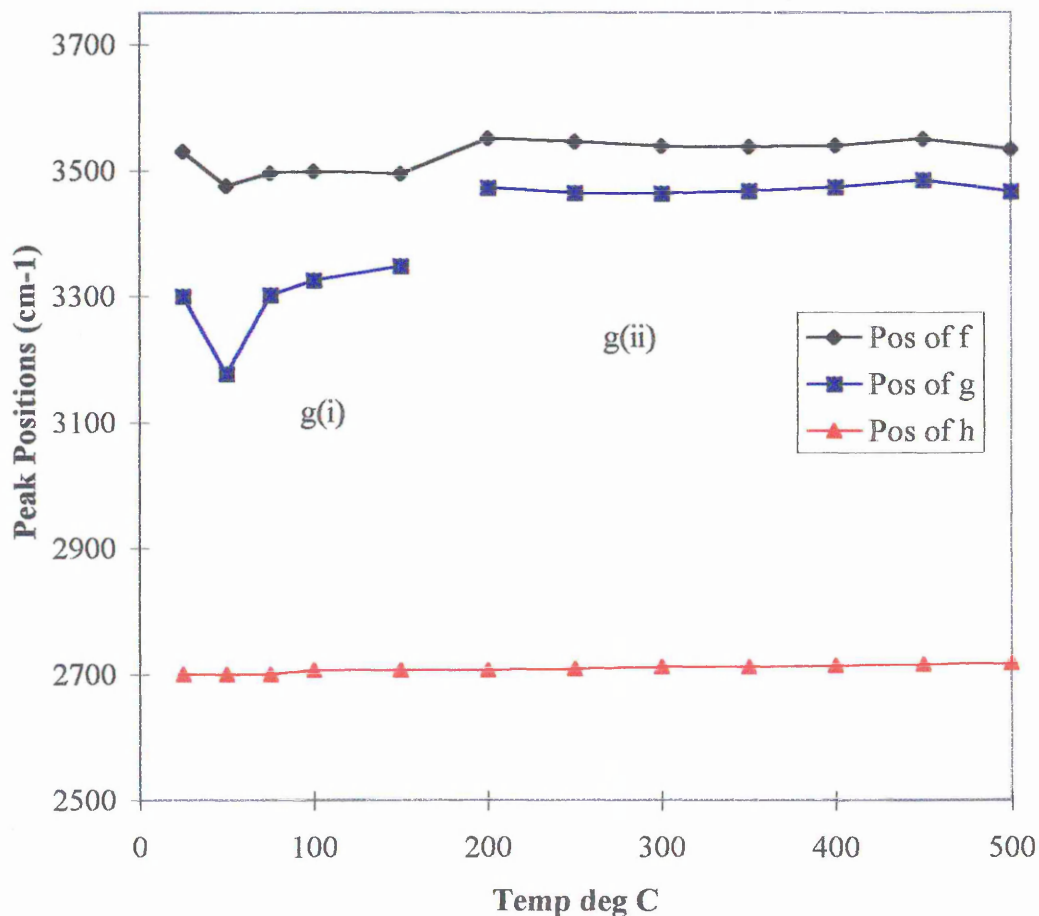


As the literature suggests in an unmilled, well crystallised kaolin at room temperature, peaks a-d in this sample were readily distinguishable^{3,7,19,29,33,43}. As temperature increased peaks a and d began to converge, with peak a shifting from 3695 to 3680 cm^{-1} and peak d from 3620 to 3627 cm^{-1} by 500 °C. A change in relative intensity was noted, whereby band a became smaller with respect to band d. This temperature related effect

has been observed by Frost & Vassallo using the IR emission technique ²⁶, and the shifts are similar to those caused by light milling.

Bands b and c merged gradually, and were almost indistinguishable by 250°C. The frequency of band e increased by 10 cm⁻¹ after heating. This is similar to the shift observed for band d.

Figure 2.27 0 Min Kaolin Peak Positions - Bands f, g & h.



A wide band centred at 3300-3400 cm⁻¹ was noted by several groups ^{3,19,40,43}. In 1975, Yariv ⁴³ attributed a broad feature between 3370 and 3600 cm⁻¹ to “hydroxyls of widely varying nature”. In later years, interpretations have generally not become any more specific. This region is usually referred to as the hydroxyl stretching region of surface sorbed water.

In this work, 2 broad bands (f and g) centred at 3530 and 3300 cm⁻¹ were fitted, and these were assigned to weakly and more strongly surface -sorbed water respectively.

Band g has also been subdivided into bands g(i) and g(ii) (see above). However, since bands e, f and g are present to such high temperatures, if they represent water, it must be concluded that this water is extremely resistant to heat treatment. It may be that a certain proportion of the intensity at these frequencies is due to kaolin structural components which are masked at lower temperatures by adsorbed water. With regard to water species present in this large feature and with such a large range of possible environments in which water may be present on the surface of kaolin, it is unlikely that they are represented by these bands alone. However, in fitting two representative bands, it was possible to identify trends in the general behaviour of the sorbed water. According to Frost *et al.*,³⁸ (after treating at elevated temperature and/or pressure) adsorbed water displays an infrared band at c3550 cm⁻¹. Band f is at 3530 cm⁻¹ at room temperature, but there is an apparent shift to 3475 cm⁻¹ by 50°C. The latter position is more likely to be representative of the true value, since room temperature spectra are often affected by increased water vapour which leads to spurious shifts in position and increases in intensity. A broad band at 3370-3600 cm⁻¹ was assigned partly to water formed by prototropy³⁹. Protons migrate from their original position and travel towards the inner oxygens (hydroxyls). These water molecules can be removed at low temperatures.

Band f remained relatively constant in position, with a fluctuation at mid range temperatures between 3475 and 3550 cm⁻¹. However, after 300°C, the position remained at 3540 cm⁻¹ +/- 9 cm⁻¹. A band at 3560 cm⁻¹ was reported by Michaelian *et al.*⁶, where kaolinite was ground with alkali halide, but it was assigned to either FeO-H stretching or an intercalated water molecule, possibly located within the kaolin-alkali halide interface. The latter assignment is not feasible in the present work since the samples which were milled were treated in the absence of alkali halide, and indeed, the peak also appears in the unmilled sample (although the samples in the present work were mixed very lightly with KBr minutes prior to spectrum collection, it is thought highly unlikely that reaction between the mineral and halide would occur).

The relative intensity of band f decreased between 50 and 200 °C, indicating a loss of less strongly bound water. This phenomenon was corroborated by thermal analyses (Figure 2.8), which showed a gradual decrease in mass between c 50 and 400°C. Above

this temperature the relative intensity remained virtually constant, indicating a contribution either from a structural component at this frequency or a strongly held water species.

The position of band g appeared to shift dramatically from 3300 cm^{-1} at 25°C to 3466 cm^{-1} at 500°C . There was a sudden shift in position of this band at 200°C . It is postulated that there are in fact 2 distinct bands present in this area - one at 3300 cm^{-1} and the other at c 3470 cm^{-1} . At temperatures below 200°C the 3300 cm^{-1} was very intense, but as this water was removed by heating, the more strongly bound 3470 cm^{-1} water became more prominent, thus creating the illusion of a shift of band g of c 170 cm^{-1} .

Therefore, the more weakly bound g(i) water at higher frequency was lost at lower temperatures, and the structural combination band (g(ii)), at lower frequency, was present at all temperatures, but only became evident when the sorbed water at g(i) was removed.

Band h was visible in all spectra, but only became quantifiable at 75°C . It remained almost constant in position and increased in intensity as temperature increased. It is postulated that band h represents a structural feature of kaolin which at lower temperatures was masked by the water band(s) at lower frequencies. When this water was driven off band h became more obvious.

A band at this frequency has been observed by several experimenters. Rouxhet *et al.*,⁴⁰ observed a band at 2723 cm^{-1} as well as a band at 2708 cm^{-1} (with others at 2679 and 2672 cm^{-1}) in strongly deuterated kaolinite. When deuteration was below 20%, the 2 bands were replaced by a single band at 2714 cm^{-1} . They postulated that the 2723 and 2708 cm^{-1} bands were due to the symmetric and antisymmetric modes of similar OD groups, and that the 2714 cm^{-1} band represented isolated, uncoupled OD groups diluted amongst OH groups.

The band at 2708 cm^{-1} in the current work is very low intensity, and other bands assigned to OD in this region are not present at room temperature (for example, the 2723 cm^{-1} band). However, an interesting feature of the unmilled kaolin VT DRIFT spectra is that

the position of band h shifts from 2707 cm^{-1} at 100°C to 2718 cm^{-1} at 500°C . This might indicate the presence of a small concentration of OD, although for this kaolin sample, deuteration is highly unlikely.

An alternative assignment made by Frost and Johansson¹⁵ proposed that the 2708 cm^{-1} band is due to the coupling of the 3620 and 915 cm^{-1} (the inner hydroxyl deformation mode) bands. The difference is 2705 cm^{-1} , which is very close to the observed frequency. Although they concur with Rouxhet *et al.*, that deuterol bands are also present at this frequency, Frost and Johansson say that OD bands are approximately 3 times more intense than the OH band. In the present work, the spectra do not contain all the characteristic bands of a deuterated sample. Therefore, it is likely that band h in this case was due to OH, rather than OD vibrations, since it was present in isolation, was of relatively low intensity, and there was no other conclusive evidence of deuteration.

The intensity of band h increased because it represents uncoupled hydroxyl vibrations of free hydroxyls. These vibrations became more abundant as temperature increased. Also, the water bands at higher frequency were reduced, thus “revealing” this area of the spectrum.

2.2.4.1.2 3 minute kaolin (freshly milled).

Spectra of kaolin dry ball milled for 3 minutes follow. They have been described as “freshly milled” (“FM”) This nomenclature refers to the length of time between sample milling and spectra collection. In all cases (for 3, 10 and 30 minute FM samples) the spectra were collected less than a month after milling. (See later for a comparison of FM and “Aged” samples (where spectra were taken approximately 6 months after the milling process).

These spectra were collected from a 99% dilution (i.e. 99% KBr:1% kaolin) rather than the standard 90 or 95% dilution due to limited sample availability. This resulted in lower absorbance and therefore, water vapour was more influential on the spectra. It is not thought to alter the data collected in any other way.

Figure 2.28 3 minute kaolin(FM). The 3800-2600 cm^{-1} region.

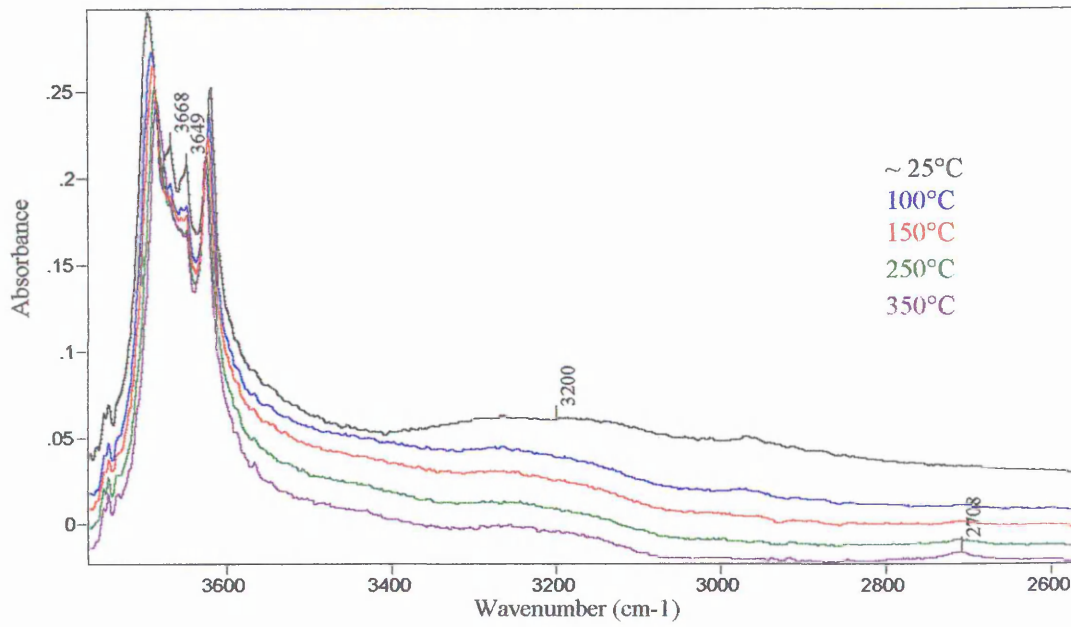


Figure 2.29 3 minute kaolin(FM). The 3800-2600 cm^{-1} region. Room temperature curve fit.

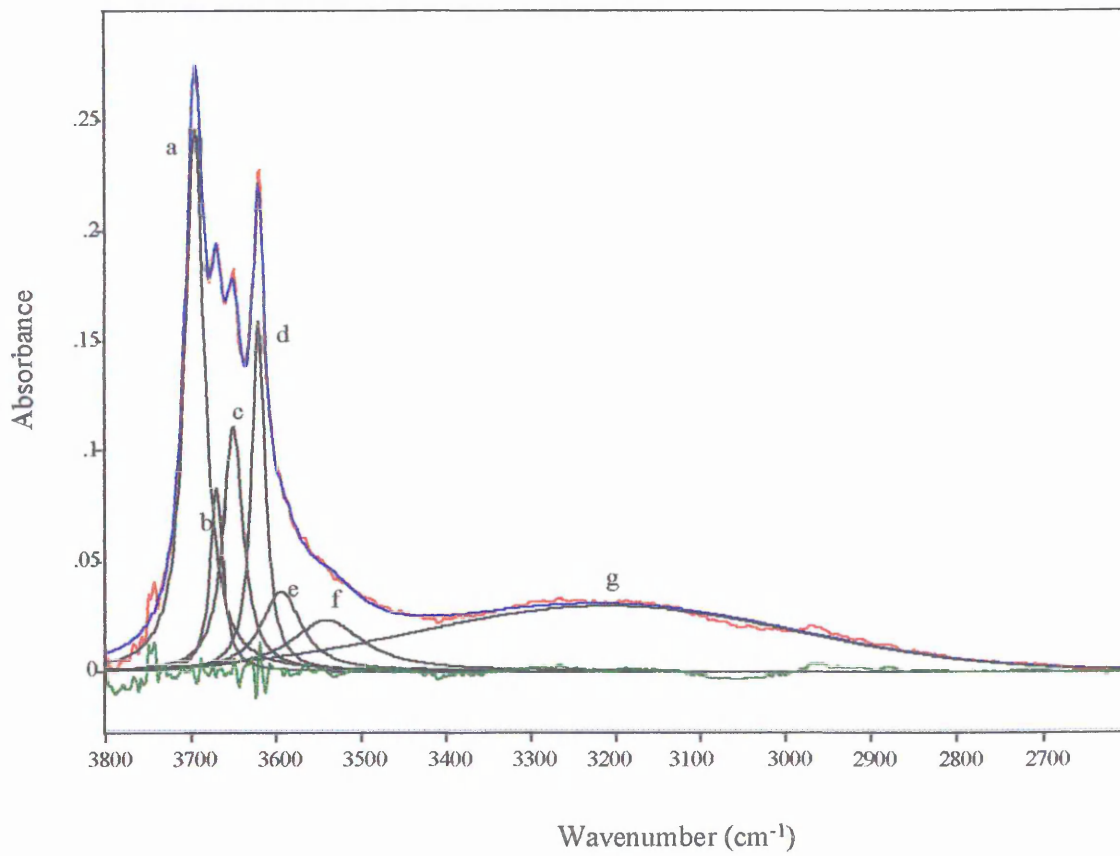


Figure 2.30 3 minute kaolin(FM). The 3800-2600 cm^{-1} region. 150 °C curve fit.

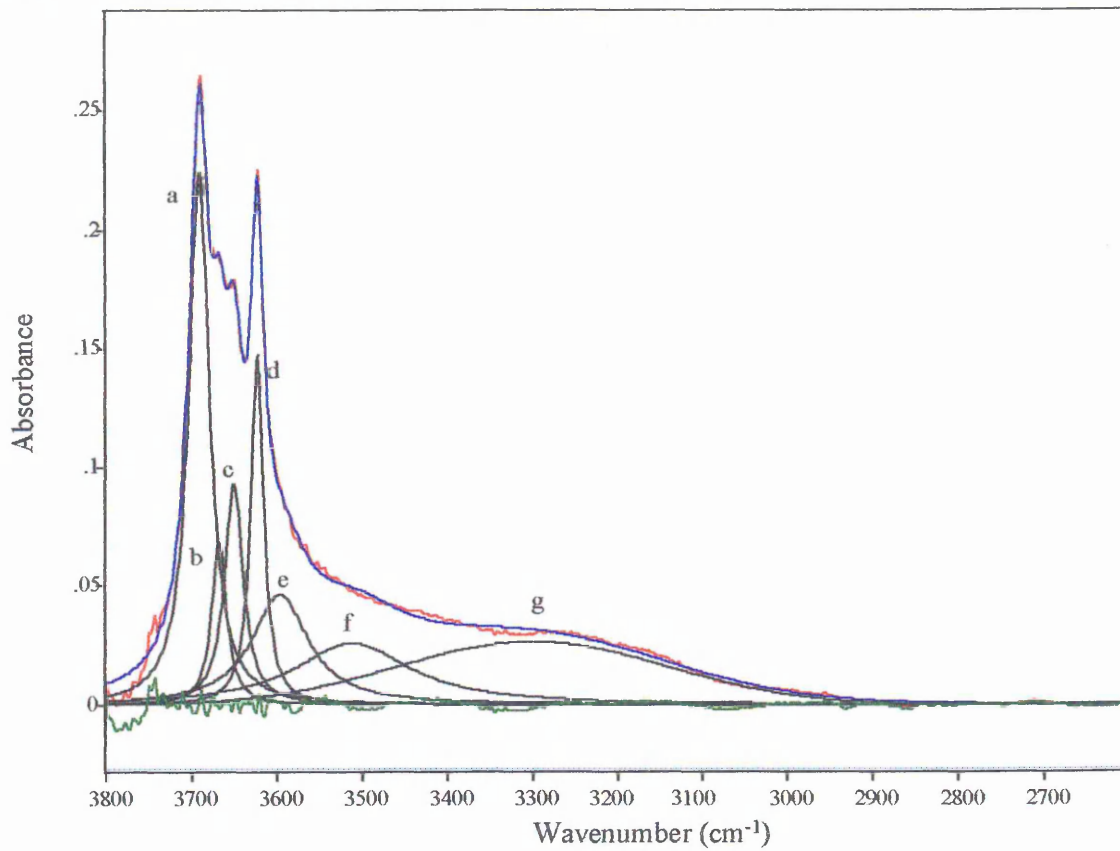
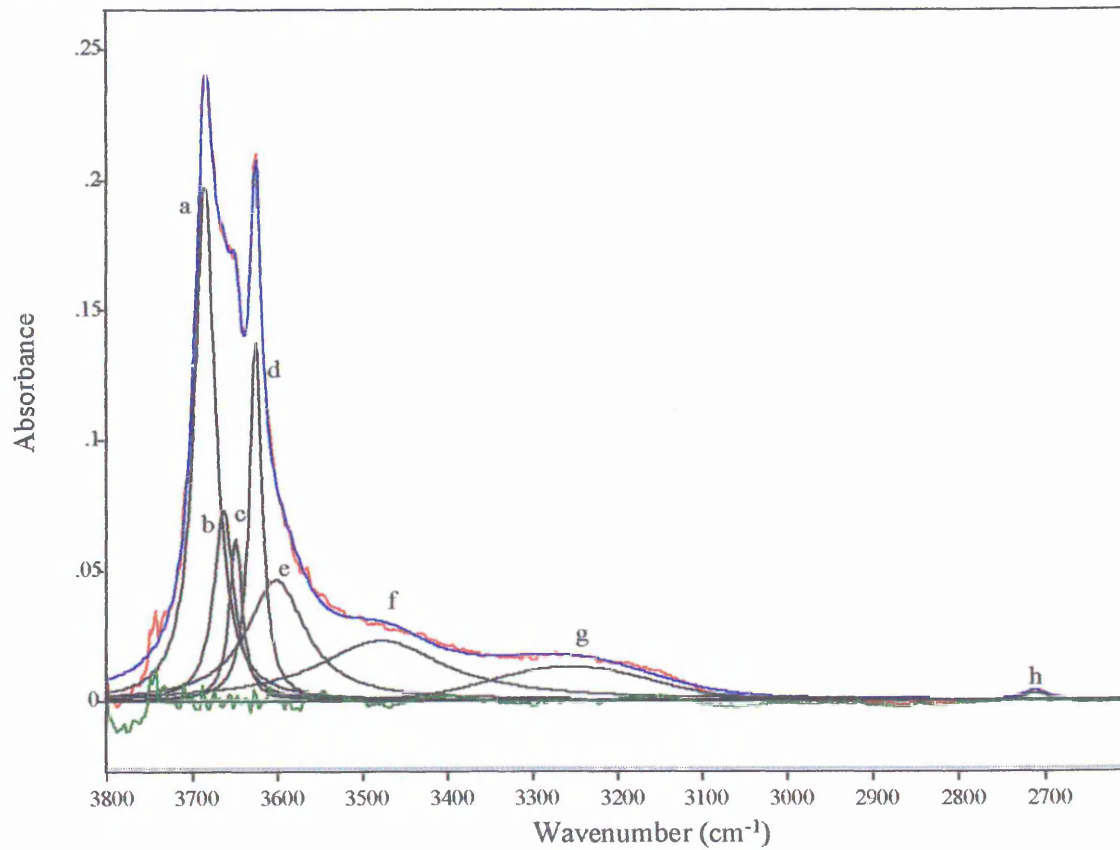


Figure 2.31 3 minute kaolin(FM). The 3800-2600 cm^{-1} region. 350 °C curve fit.



Probably the most striking feature of Figure 2.28 is the increase in the intensity of the broad feature between 3600 and 2600 cm^{-1} (with respect to bands a - d) compared with that of the unmilled sample (see Figure 2.19). After 3 minutes milling, at room temperature bands a to d were resolved (Figure 2.29). The relative intensity of a with respect to d altered compared with the unmilled sample, with a now being of relatively much greater intensity.

The water band, g, is also of greater intensity than before milling, with the centre having shifted slightly from 3300 cm^{-1} in unmilled room temperature spectrum to 3275 cm^{-1} in the 3 minute sample, thus indicating an overall increase in the amount of sorbed hydroxyl species, with stronger hydrogen bonding on average.

Figure 2.30 shows that bands a to d have begun to converge and it has become more difficult to distinguish between bands b and c. Bands e and f changed little, with a slight shift to lower frequency of the latter band. There was an intensity loss of band g and a shift from 3200 cm^{-1} at room temperature to 3300 cm^{-1} at 150 °C. Interestingly, the water features, f and g, in this spectrum resemble those in the room temperature unmilled kaolin spectrum.

Interestingly, after heating to 350 °C (Figure 2.31), band g was still an obvious feature. The centre of the band now presented at around 3230 cm^{-1} - lower frequency than in the unmilled kaolin spectrum. This represents more strongly hydrogen bonded water. The increased intensity of band g (compared with Figure 2.22) indicated that water was more thermally stable after this short period of milling. The relative intensity of bands a and d appeared to have altered little and bands b and c became indistinguishable by eye. Band e, as expected, altered only marginally in both position and relative intensity. Band f was still relatively intense and a further decrease in position was observed.

Figure 2.32 below shows that again, the intensities of bands b and c were interchangeable, with an apparent decrease in one leading to an apparent increase in the other. This was not a real effect, but one created by the curve fitting procedure. The area of band d remained almost constant throughout the experiment, but the decrease in the intensity of band a is clearly illustrated here. Curiously, the relative intensity of band e actually appeared to increase with respect to the other bands. One explanation is that the “extra” intensity came from the water bands at lower wavenumbers, and that it does not represent an increase in structural components. Another consideration is that band e represented a mica impurity, which, according to XRD traces shows a slight decrease after milling. It is postulated that a similar effect (i.e. structural degradation) is caused by milling. Therefore, the intensity would decrease.

Figure 2.32 3 Minute Kaolin (FM). The 3800-2600 cm^{-1} region. The change in intensity of bands a, b, c, d and e.

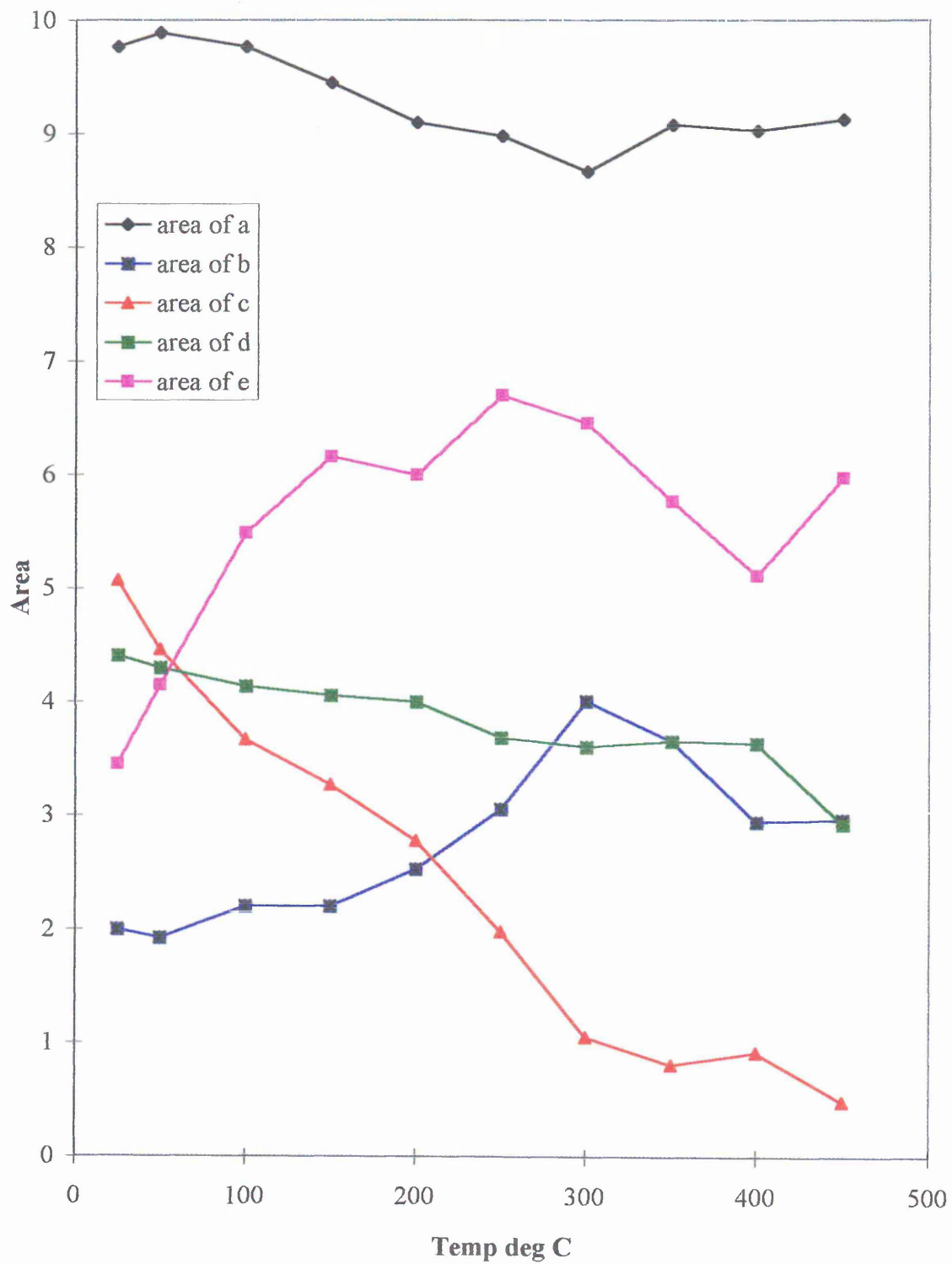
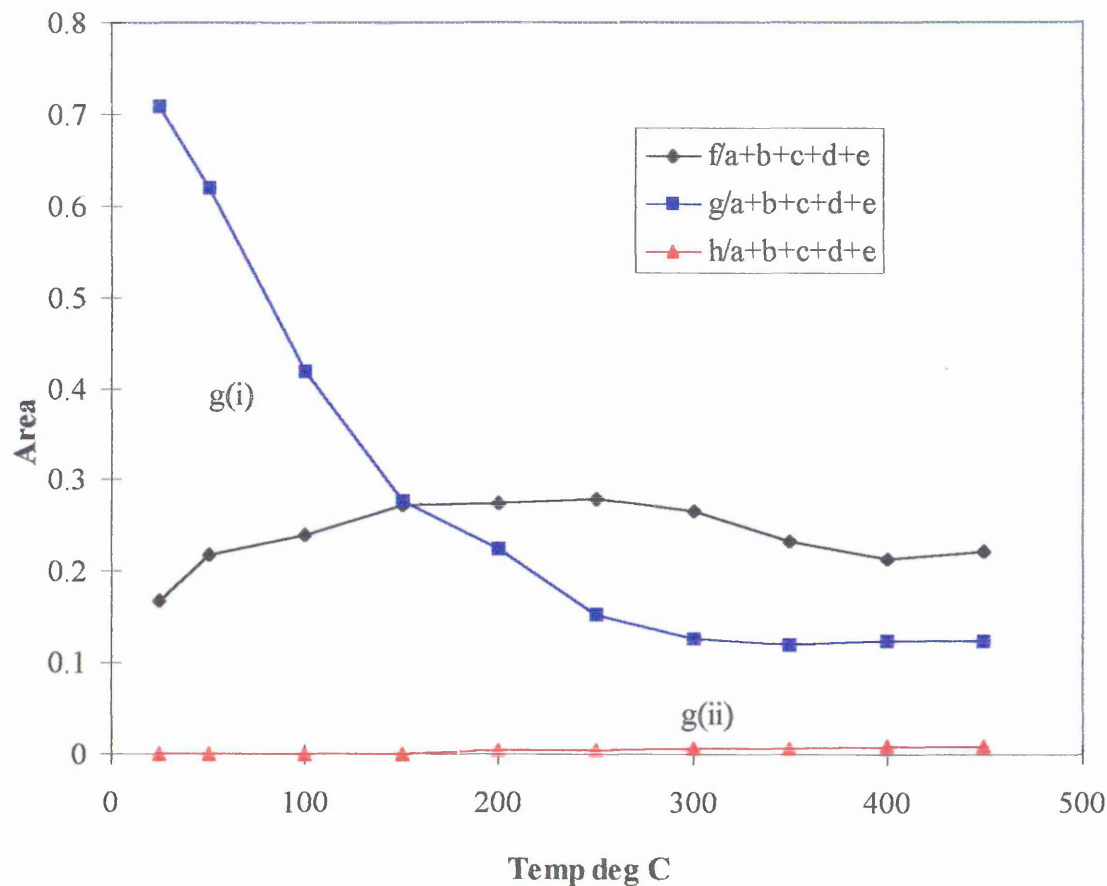


Figure 2.33 3 Minute Kaolin (FM). The change in intensity of bands f, g and h.



The sum of the areas of the structural bands a to e were again constant over the entire temperature range and were used as a means by which to normalise the other spectral features. Once again, band g has been subdivided into 2 bands- g(i) which was present between 25 and 300 °C, and band g(ii) which was present at all temperatures, but only became quantifiable at temperatures above 300 °C. Band g(i) represented physisorbed water which was removed at lower temperatures. Interestingly, this water was more thermally stable than the corresponding band in the unmilled kaolin data. Band g(ii) (which was at lower frequency than g(i) and thus more strongly hydrogen bonded) was present throughout the temperature range, and thus was highly resistant to heat.

Figure 2.34 The change in position of bands in the 3800-2600 cm^{-1} region as a function of temperature.

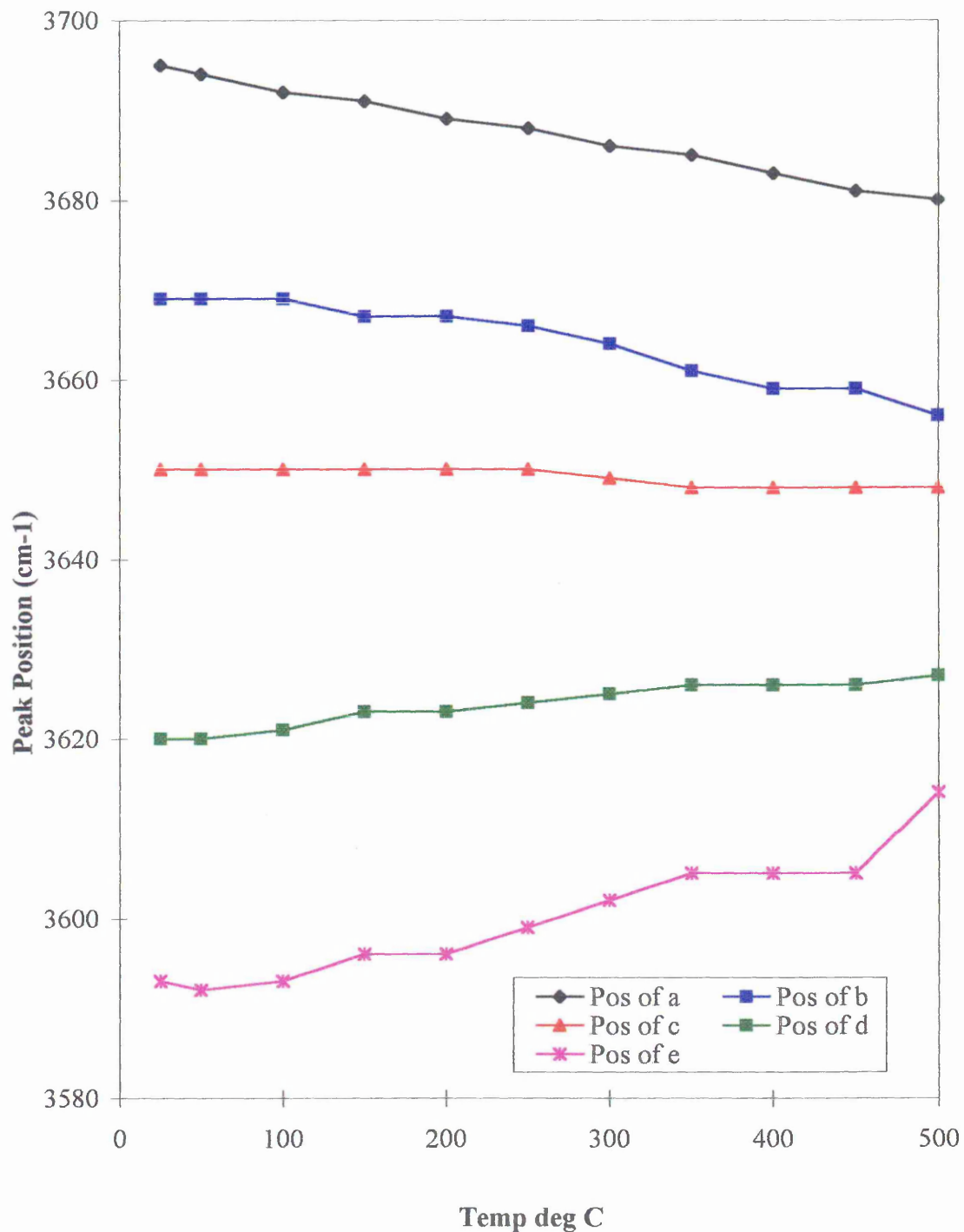


Figure 2.34 shows that at room temperature, peaks a-d were resolved. As temperature increased peaks a and d started to converge, with peak a shifting from 3694 to 3680 cm^{-1}

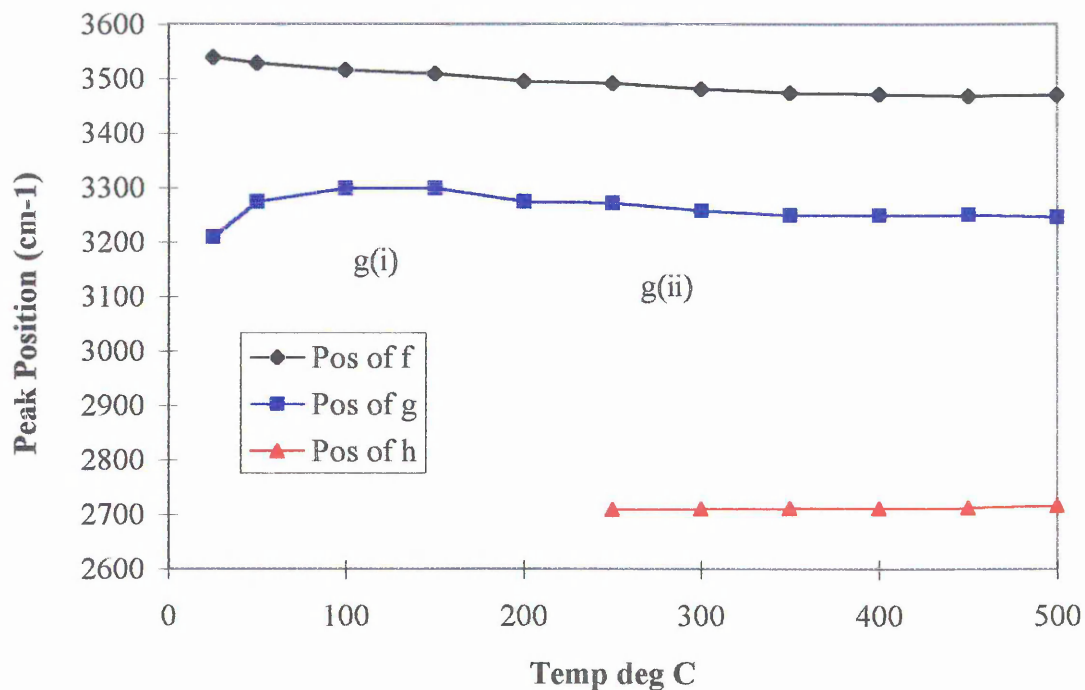
and peak d from 3620 to 3627 cm^{-1} at 50 and 500°C respectively. The relative intensity of band a became smaller with respect to band d.

Bands b and c again merged gradually, and were indistinguishable by eye at 300°C- 50°C higher than for the unmilled sample.

The position of band e (at 3596 cm^{-1} at room temperature in unmilled kaolin) showed an increase in frequency from 3592 at room temperature to 3614 cm^{-1} at 500°C. The shift here was larger than that in the unmilled kaolin sample, indicating a reduction in the strength of hydrogen bonding as temperature increased.

The sum of the areas of the structural bands a to e were again constant over the entire temperature range and were used as a means by which to normalise the other spectral features. Once again, band g has been subdivided into 2 bands- g(i) which was present between 25 and 300 °C, and band g(ii) which was present at all temperatures, but only became quantifiable at temperatures above 300 °C. Band g(i) represented physisorbed water which was removed at lower temperatures. Interestingly, this water was more thermally stable than the corresponding band in the unmilled kaolin data. Band g(ii) (which was at lower frequency than g(i) and thus more strongly hydrogen bonded) was present throughout the temperature range, and thus was highly resistant to heat.

Figure 2.34 The change in position of bands in the 3800-2600 cm^{-1} region as a function of temperature.



Band f (at 3530 cm^{-1}) was in a similar position as in the unmilled kaolin data, but band g in the 3 minute milled sample centred slightly lower at 3274 cm^{-1} . Initially there was an increase in frequency to 3300 cm^{-1} , with the centre returning to 3272 cm^{-1} by 200°C . Subsequently the position shifted to around 3250 cm^{-1} at 300°C where it remained for the duration of the experiment. The band position of g(i) in the room temperature unmilled data was also 3250 cm^{-1} (see Figure 2.20), thus it is implied that these water environments are similar. The overall decrease in frequency suggested that higher frequency (loosely bound) OH were being removed at lower temperatures, and at temperatures of 250°C and over, more strongly bound (lower frequency) OH remained. Although the nomenclature of the bands in the unmilled sample was the same as that used here, it should be noted that bands g(i) and g(ii) do not represent the same species in the two samples. It should also be recognised that the prefix “g” is not intended to lead to the belief that the bands are associated with each other.

Band h became apparent at around 150°C (compared with 75°C in the unmilled sample). The position shifted only slightly from 2710 to 2716 cm^{-1} and the relative intensity more than doubled. The intensity of this band increased because it represents uncoupled OH

vibrations of “free OHs”, so when temperature increased, so did the number of these vibrations.

In summary, the 3 minute milled sample showed evidence of an increased amount of sorbed hydroxyl species. They were generally more heat stable and were at lower frequency, indicating stronger hydrogen bonding compared with the unmilled kaolin sample.

2.2.4.1.3 10 minute kaolin (freshly milled).

The figure below shows that after 10 minutes milling, there was a very large increase in the total amount of sorbed water species (indicated by the high intensity of the 3600 - 2600 cm^{-1} feature). Bands a to d converged more than in both the unmilled and 3 minute milled samples. It was difficult to distinguish bands b and c by eye.

Figure 2.35 10 minute kaolin(FM). The 3800-2600 cm^{-1} region.

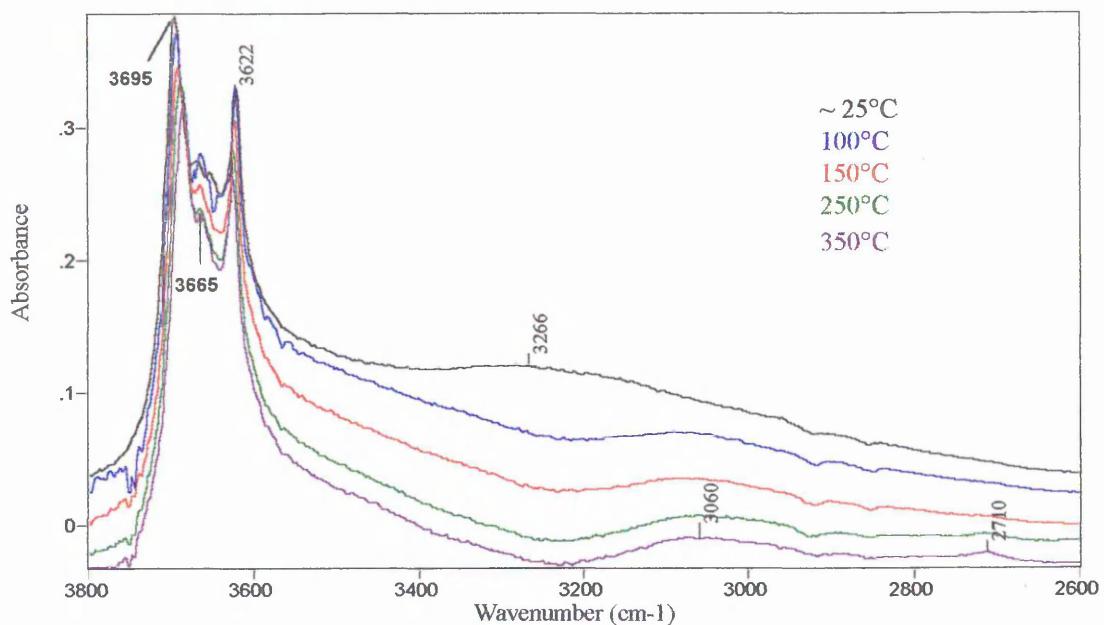


Figure 2.36 10 minute kaolin(FM). The 3800-2600 cm^{-1} region. Room temp curve fit.

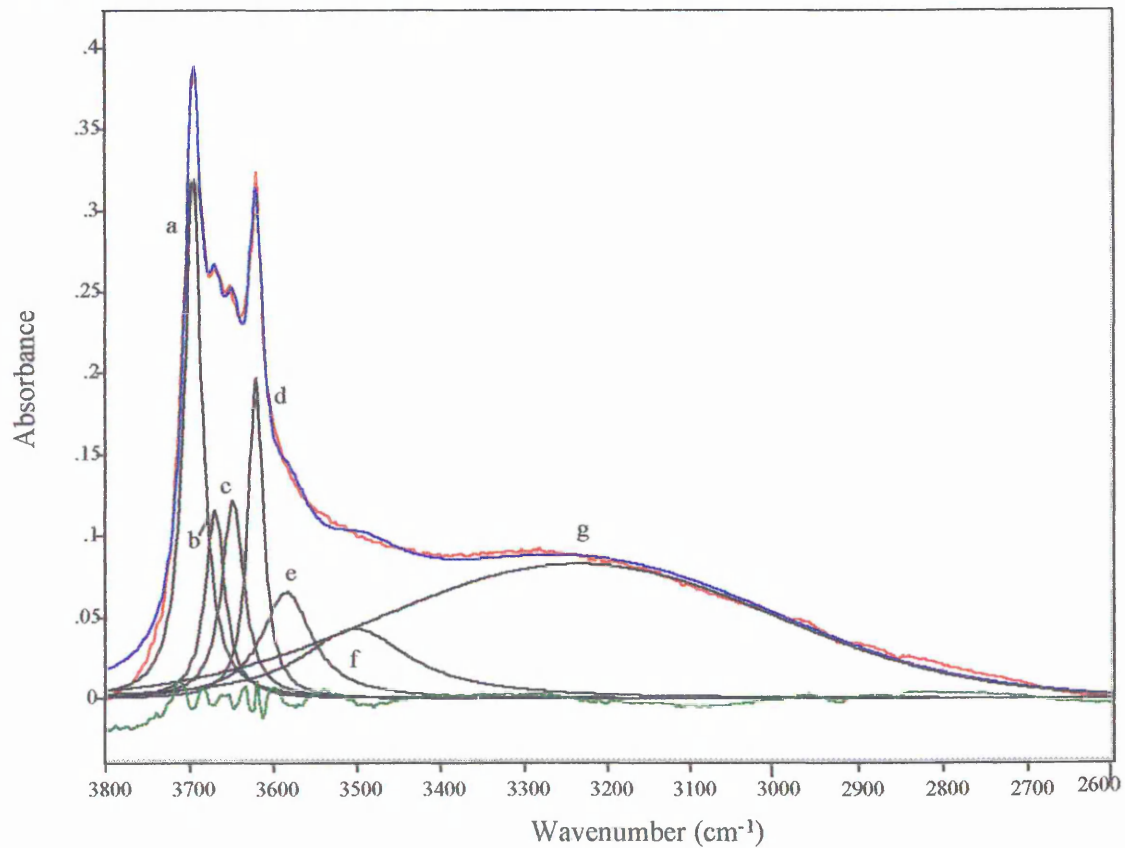


Figure 2.37 10 minute kaolin (FM). The 3800-2600 cm^{-1} region. 150 $^{\circ}\text{C}$ curve fit.

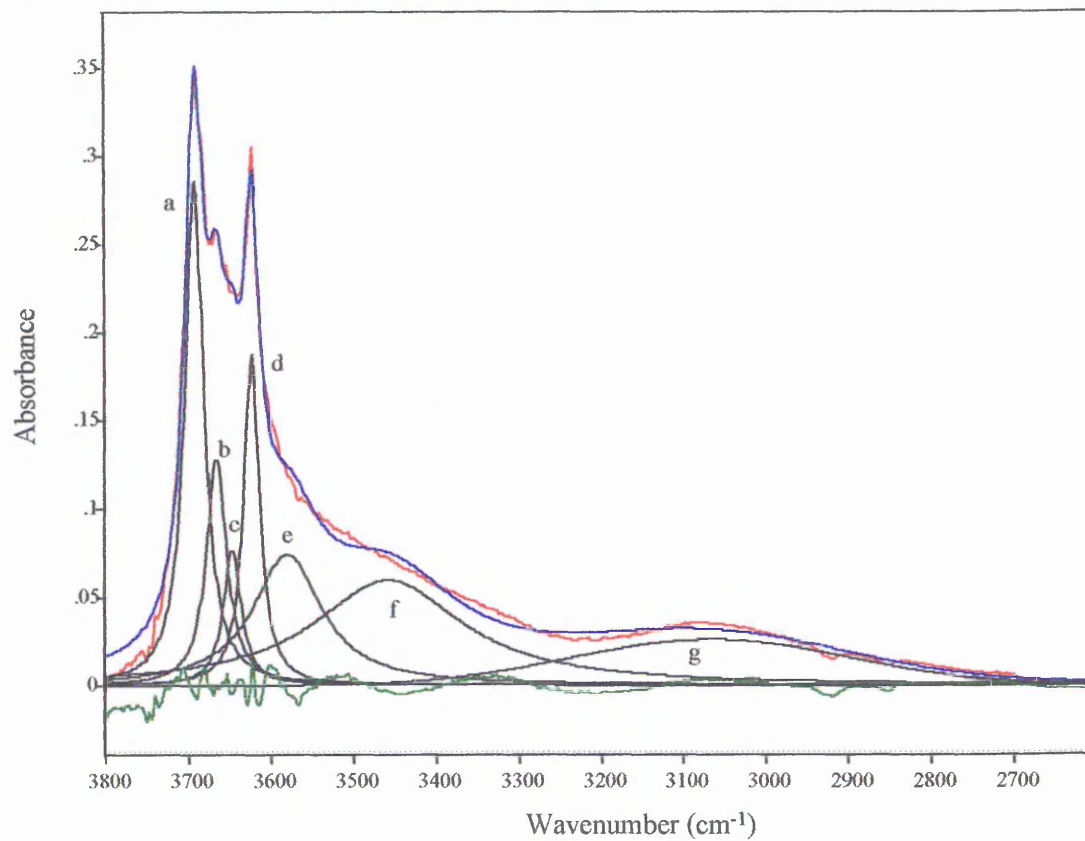
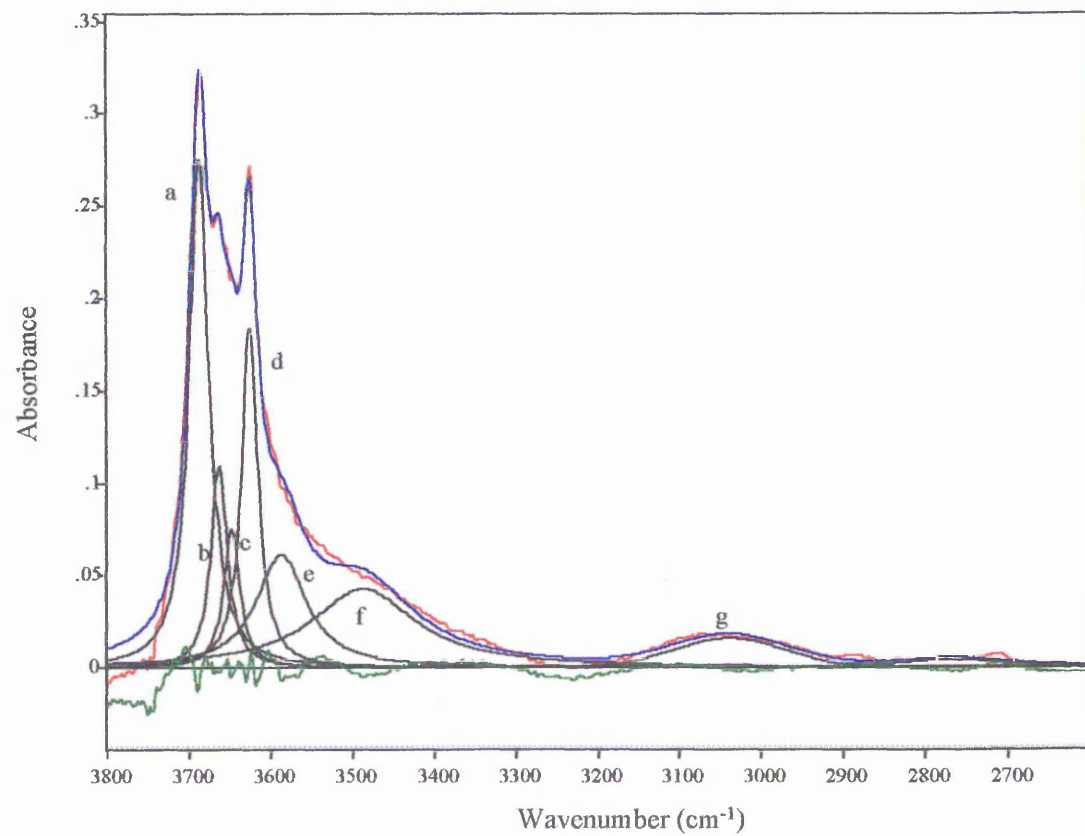


Figure 2.38 10 minute kaolin(FM). The 3800-2600 cm^{-1} region. 350 $^{\circ}\text{C}$ curve fit.



The most noticeable feature of the room temperature curve fit, (Figure 2.36) was the very extensive area of band g at 3230 cm^{-1} . It increased greatly compared with the 3 minute milled sample. Bands a - d were distinguishable by eye at room temperature. Bands e and f were still necessary for a reliable fit. Band f was present at around 3500 cm^{-1} , approximately 50 cm^{-1} lower than the corresponding band in the unmilled and 3 minute samples. An additional small water band between bands f and g in this sample would compensate for the shift. However, another band was not fitted because it would be impossible to determine the exact position of the additional water species present in this sample (although a band at c 3400 cm^{-1} is the most likely position).

Figure 2.37 shows that band g has undergone an apparent shift from 3230 to 3050 cm^{-1} (see later for details). Band f shifted to lower frequency, with an apparent increase in relative intensity. It is likely that extra intensity was originating from the additional water mode discussed above (but not included in the fit). Band g decreased in frequency dramatically and it was no longer able to contain the intensity of the “missing” band at around 3400 cm^{-1} . Bands b and c were no longer distinguishable by eye.

After heating to $350\text{ }^{\circ}\text{C}$, (Figure 2.38) the position of band f returned to around 3500 cm^{-1} . This implies that the surface sorbed water at around 3400 cm^{-1} was removed, and no longer influenced band f. The peak heights of bands a to d reduced absolutely, but their relative intensities remained quite constant compared with lower temperature data. Bands b and c merged.

Band g was still clearly present, but the frequency was at approximately 3050 cm^{-1} , (compared with 3250 cm^{-1} in the 3 minute milled sample). This implies that the water at 3050 cm^{-1} in the 10 minute sample was in a more strongly hydrogen bonded environment than in either the unmilled or the 3 minute samples. This could mean that the water is being trapped inside the kaolin agglomerates which were formed as milling progressed.

The water species at this frequency were very resistant to heating, which again suggested that they were being protected.

Figure 2.39 below shows the absolute changes in intensity of the bands a to e. It is worthy of note that the area of band d once again remained virtually constant throughout the entire experiment- a situation which was expected since this band represents the virtually inaccessible 3620 cm^{-1} inner hydroxyl species. The sum of the areas of these bands remained virtually constant up to $300\text{ }^{\circ}\text{C}$, with a marginal decrease thereafter.

Chapter 2 The Effects of Dehydration
Figure 2.39 10 Minute Kaolin (FM). The 3800-2600 cm^{-1} region. The change in intensity of bands a, b, c, d and e.

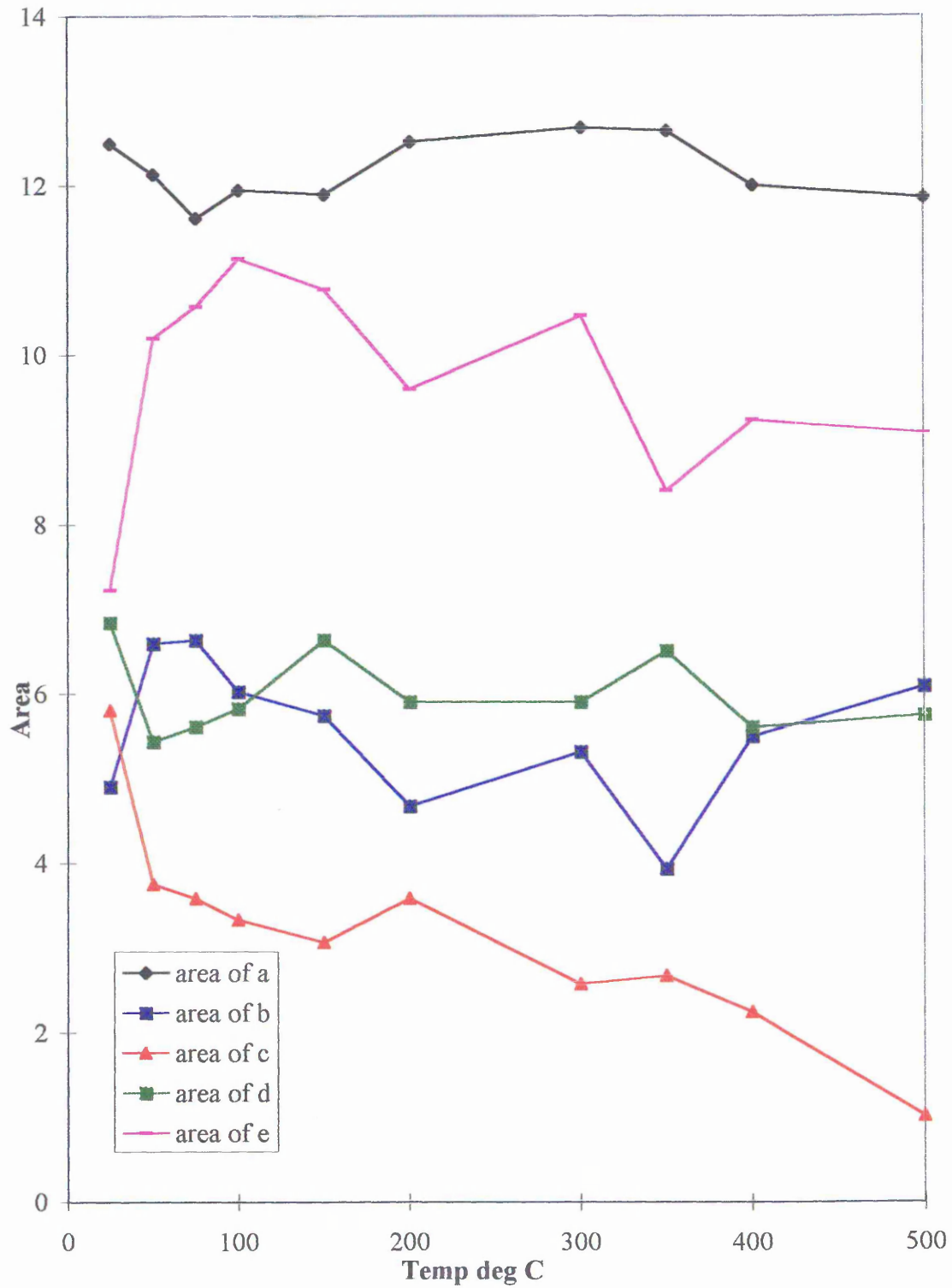
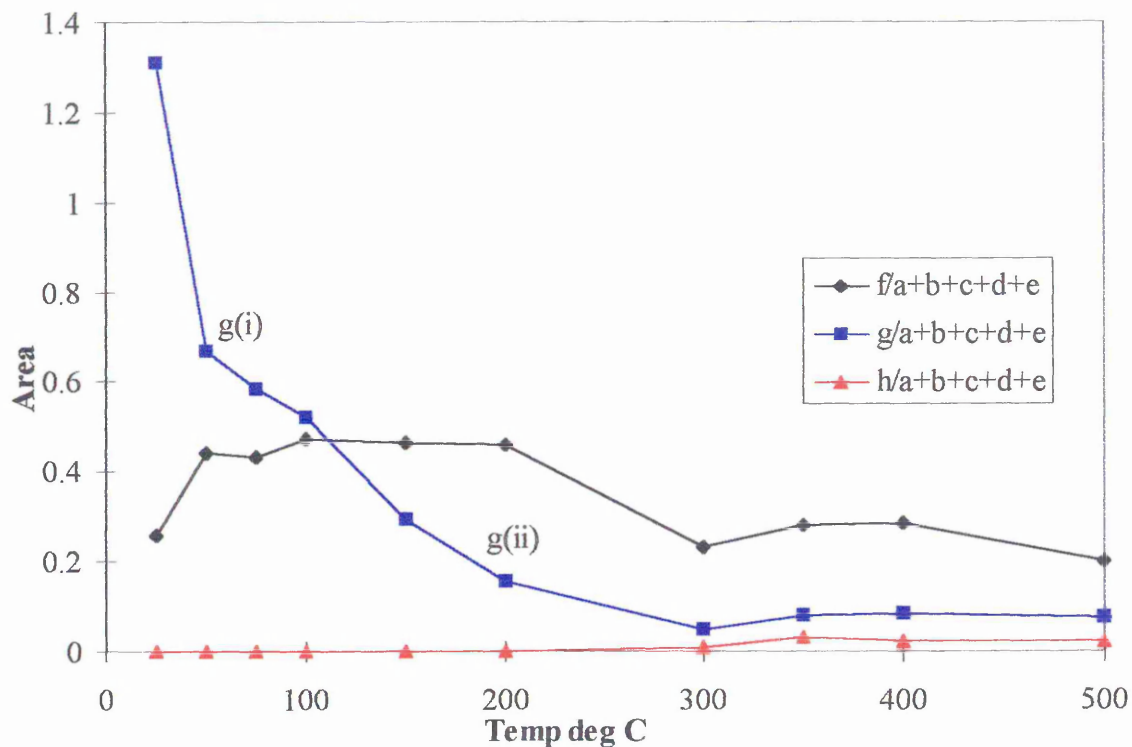
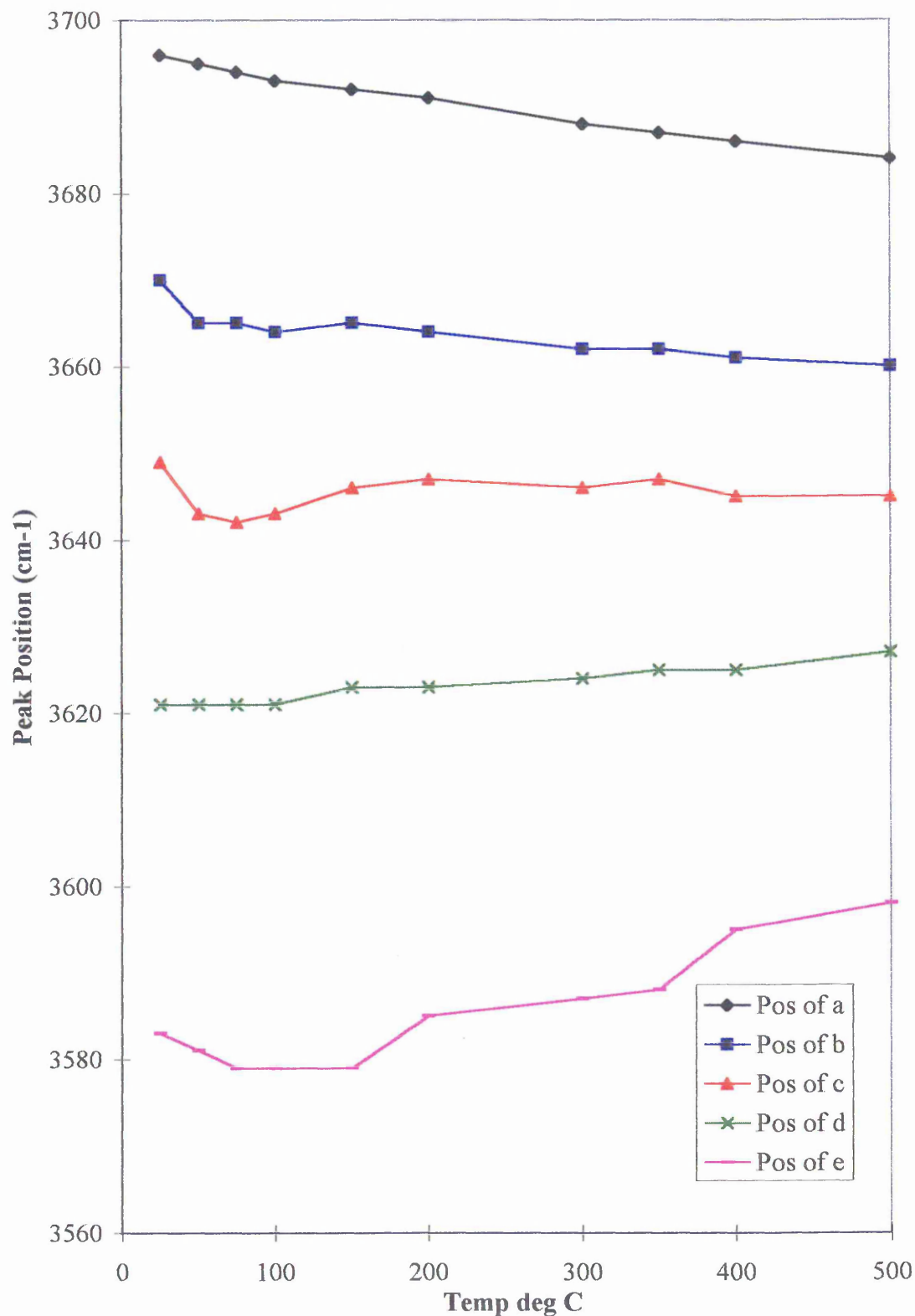


Figure 2.40 10 Minute Kaolin (FM). The change in intensity of bands f, g & h.



It is postulated that below 150-200 °C, most of the large concentration of hydroxyls present at c 3150 cm⁻¹ (band g(i)) were mainly present as loosely bound water which was removed easily by relatively gentle heating. The more strongly bound hydroxyls at around 3030 cm⁻¹ (band g(ii)) were present at all temperatures but became evident only at elevated temperatures when the intense feature, g(i), was removed. This very strong hydrogen bonding environment was not present in the less extensively milled (or unmilled) samples. Band h was sufficiently large only to be quantifiable above 300°C (compared with 150°C for the 3 minute sample), because it was being masked by the very intense water bands.

Figure 2.41 10 Minute Kaolin(FM). The change in position of bands in the 3800-2600 cm^{-1} region as a function of temperature.

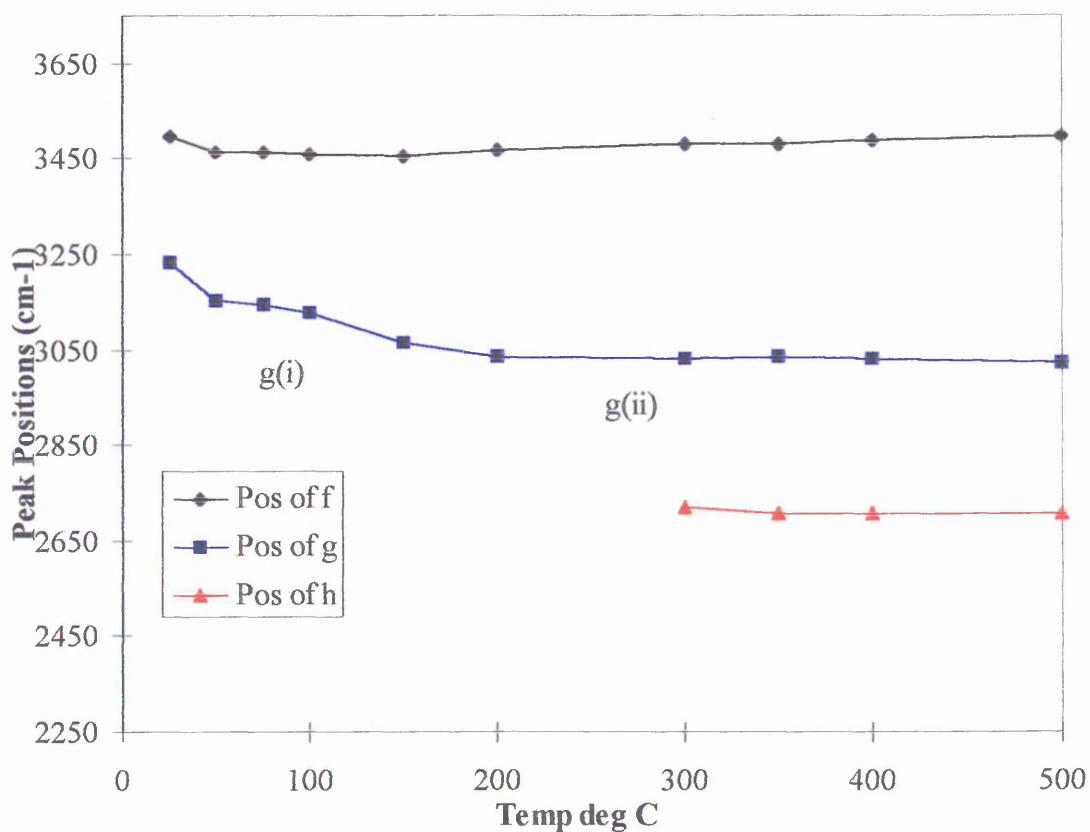


At room temperature peaks a-d were resolved. As temperature increased peaks a and d started to converge, with peak a shifting from 3695 to 3684 cm^{-1} and peak d from 3621

to 3627 cm^{-1} at 50 and 500°C respectively, although the peak height of band a with respect to band d remained fairly constant throughout. Peaks b and c became indistinguishable at around 300°C , similar to the temperature at which the peaks merged in the spectra of the 3 minute sample.

There was a small shift in position of band e of 14 cm^{-1} , from 3584 cm^{-1} at 25°C to 3598 cm^{-1} at 500°C . This shift was caused by the influences of fitting the large g(i) band at 25°C and the smaller (dramatically shifted) band g(ii) band at 500°C .

Figure 2.42 10 Minute Kaolin(FM). The change in position of bands in the $3800\text{-}2600\text{ cm}^{-1}$ region as a function of temperature.



Band f initially had a slightly lower frequency (3500 cm^{-1}) compared to the unmilled and 3 minute samples.

Band g at room temperature had a lower frequency than for either of the other two (unmilled and 3 minute) samples. It decreased rapidly from 3234 cm^{-1} to c 3150 cm^{-1} by 75°C . The frequency decreased by around 100 cm^{-1} over the first 100°C and then stabilised near 3030 cm^{-1} between 200 and 500°C . This is a much lower frequency than

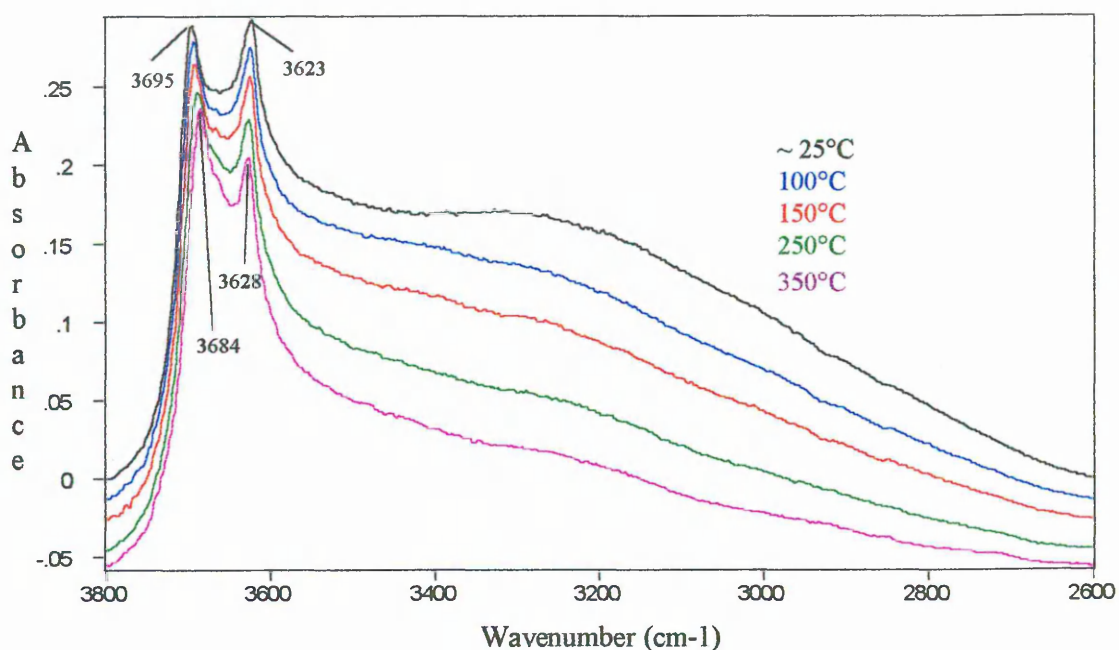
OH in either of the other two samples. Therefore, as with the 3 minute milled kaolin, it is proposed that band g represents 2 distinct bands. Weakly bound water present between room temperature and 150-200 °C is represented by band g(i) and very strongly hydrogen bonded water is represented by g(ii) at a frequency of 3030 cm⁻¹.

In summary, after 10 minutes of milling, the total amount of sorbed water species increased compared with unmilled and 3 minute milled kaolins. There was an overall increase in the amount of relatively loosely bound water, represented by band g(i), which was removed by heating to 150-200°C. There was an increase in the thermal stability of the more strongly hydrogen bonded water, g(ii). This new water environment may be inside kaolin agglomerates formed during the milling process.

2.2.4.1.4 30 minute kaolin (freshly milled).

Although reliable curve fits of these data were not possible, the VT DRIFT spectra of the 30 minute freshly milled kaolin sample are presented below. The stretching region (Figure 2.43) shows that there was huge intensity in the 3600-2600 cm⁻¹ region. The vast array of bands which were encompassed under this area were of extremely high intensity and had significantly more area than the structural bands a and d. Bands b and c were not distinguishable by eye or curve fitting procedures. The peak heights of bands a and d were almost the same, indicating structural degradation. As temperature increased, water was lost from the 3600-2600 cm⁻¹ region, but even at 500 °C, a very intense band remained. These spectra indicated that after 30 minutes milling, the structure of kaolin has become more damaged, allowing the adsorption of very high concentrations of water species which are retained to very high temperatures. It is postulated that the very highly heat stable waters were trapped within the large kaolin agglomerates which increased in size as milling progressed.

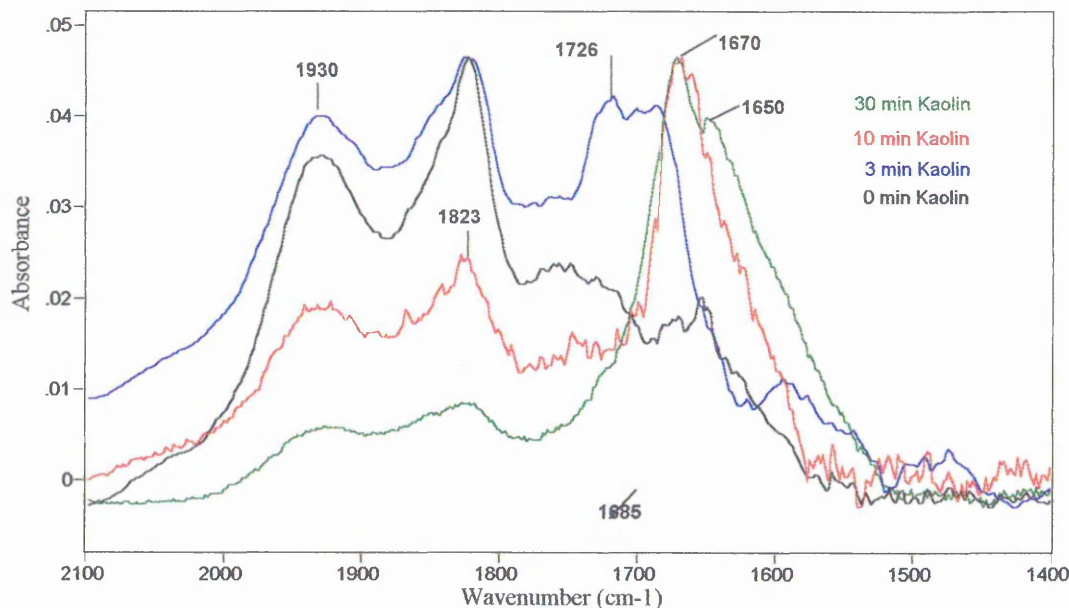
Figure 2.43 30 minute kaolin(FM). The 3800-2600 cm^{-1} region.



2.2.5 Infrared of ball milled kaolins. The 2100-1400 cm^{-1} region.

Historically, bands in this region have not been extensively studied. Frost *et al*⁸⁸, conducted some work examining this region, but the presentation of spectra in that study was limited. Another report by Frost *et al*⁴¹, studied the region more closely, but this time in the context of the intercalation of kaolinite with hydrazine. Thus, the work in the reference and the work presented herein are not readily comparable. Other studies have also shown this region^{14,15,19,26,42}, but generally, the spectra have been few, small or of substandard quality, and the interpretation (if attempted) has been limited. As a consequence, the results have not generally been well discussed. An exception is the work by Mendelovici *et al*¹⁹, which shows in some detail the water bending region of unground and mortar ground kaolinites before and after heating. Only one band is assigned in the region - a water bending mode ascribed to "molecular water". The spectra have been simplistically explained and detail is lacking. One reason for the lack of literature is that this region does not lend itself readily to study by conventional IR methods. With the advent of DRIFTS the study of the bending region has become plausible.

Figure 2.44 RT DRIFTS of ball milled kaolins.



In order to compare relative intensities of bands between spectra, most have been normalised to bands s, t and u. However, due to software limitations, this has not been possible in Figure 2.44 above.

After milling there were very obvious changes in this region. Although it is not clear from Figure 2.44, the intensities of the bands at 1930, 1830 and 1730 cm⁻¹ (s, t and u) which are assigned to kaolin combination bands, show little change in either position or relative intensity, and for this reason, they can be used as a means by which to compare the changes in intensity of the water bands at lower frequency. The water bending modes at c 1670-1630 cm⁻¹ increase dramatically in intensity until after 30 minutes of ball milling they dwarf the kaolin combination bands. This corroborates evidence in the 3800-2600 cm⁻¹ region that as milling time increases so does water adsorption. It is likely that as well as atmospheric water adsorption, some hydroxyls migrate through prototropy from elsewhere in the kaolin structure.

2.2.5.1 The effect of temperature on milled kaolin. The 2100-1400 cm^{-1} region.

2.2.5.1.1 Unmilled (0 minute) kaolin.

Figure 2.45 Unmilled (0 minute) kaolin. The 2100-1400 cm^{-1} region.

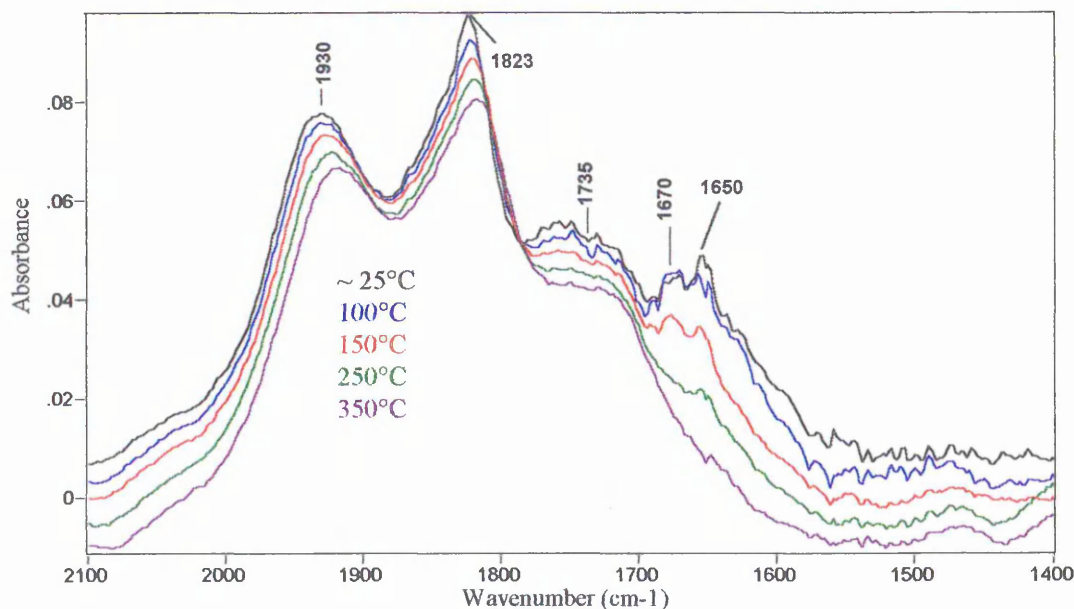


Figure 2.45 shows that at room temperature, the water band in unground kaolin was at 1650 cm^{-1} (ν) and was relatively small when compared to the intensity of bands s and t. Incomplete water vapour subtraction resulted in the lower temperature spectra appearing to have a doublet at 1670 and 1650 cm^{-1} . The curve fitting data below show that in fact only one band was present at 1650 cm^{-1} . As temperature increased, there was very little change in either the position or intensities of bands s, t and u. The water band decreased as temperature increased, and by $350 \text{ }^\circ\text{C}$, very little water was detectable.

Figure 2.46 Unmilled (0 minute) ball milled kaolin. The 2100-1400 cm^{-1} region. Room temperature curve fit.

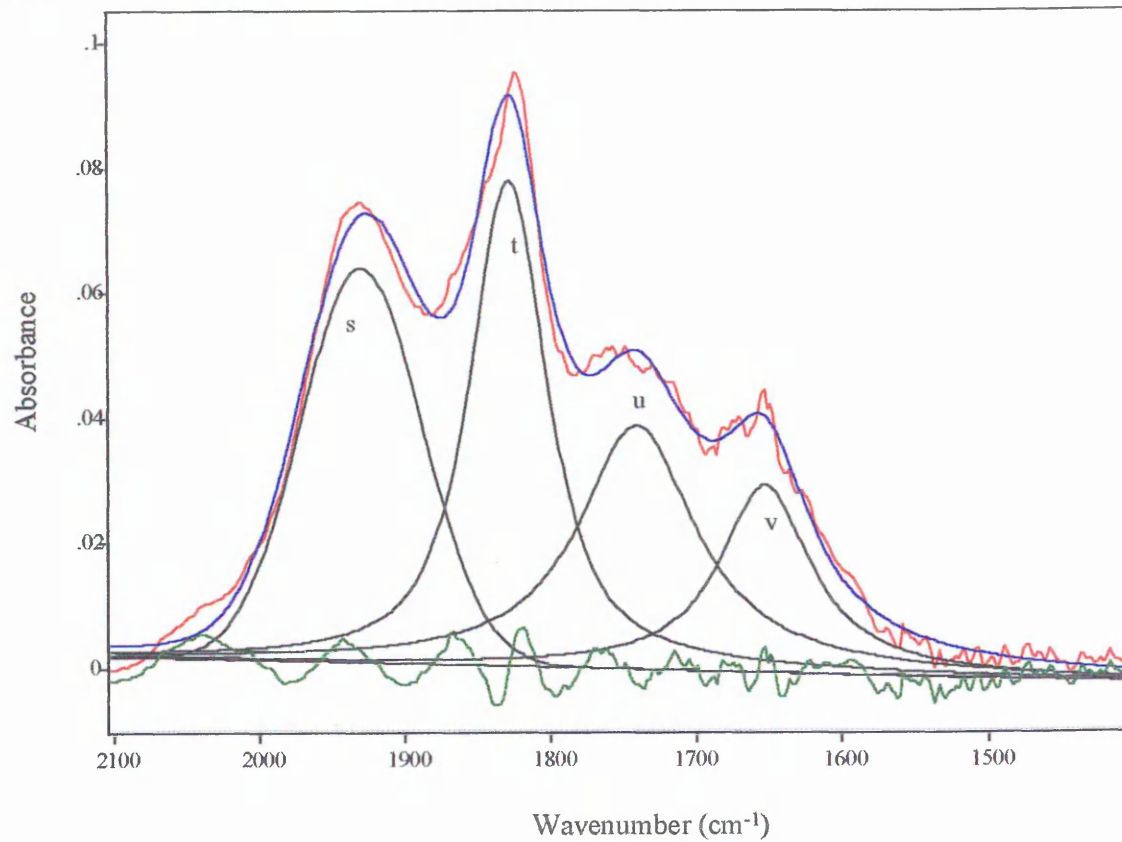


Figure 2.47 Unmilled (0 minute) ball milled kaolin. The 2100-1400 cm^{-1} region. 200 °C curve fit.

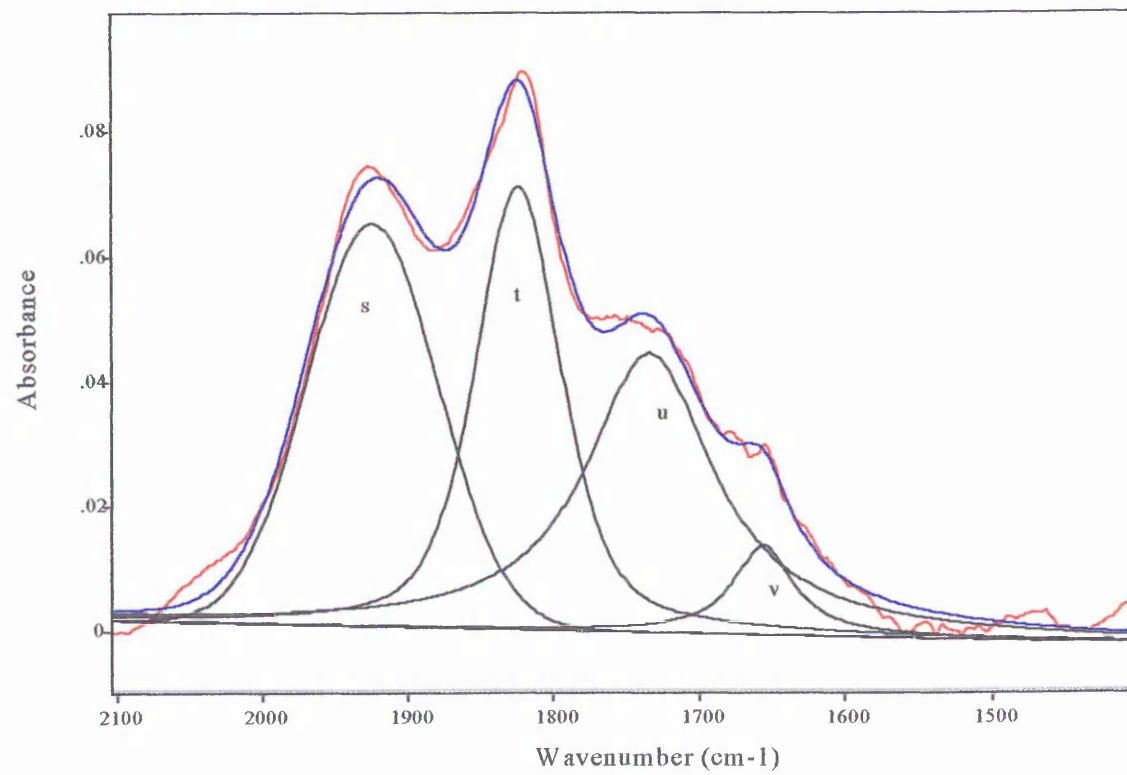
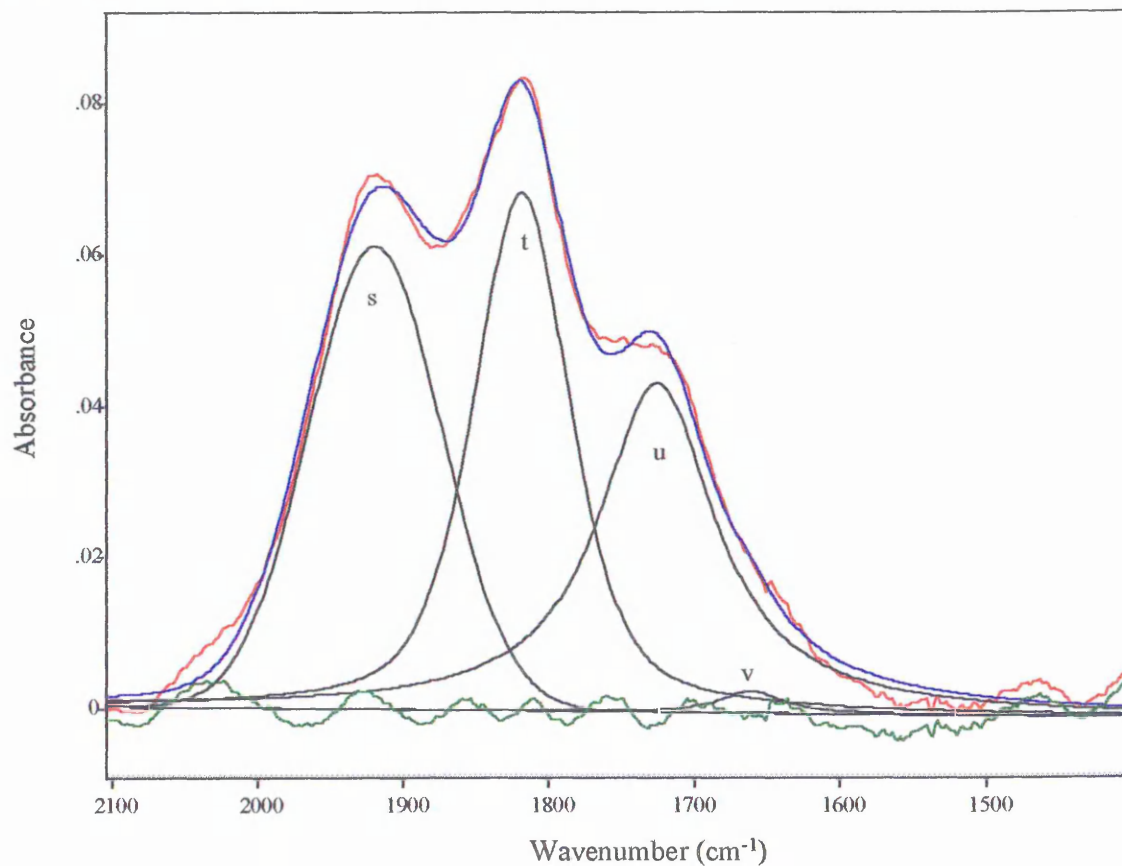
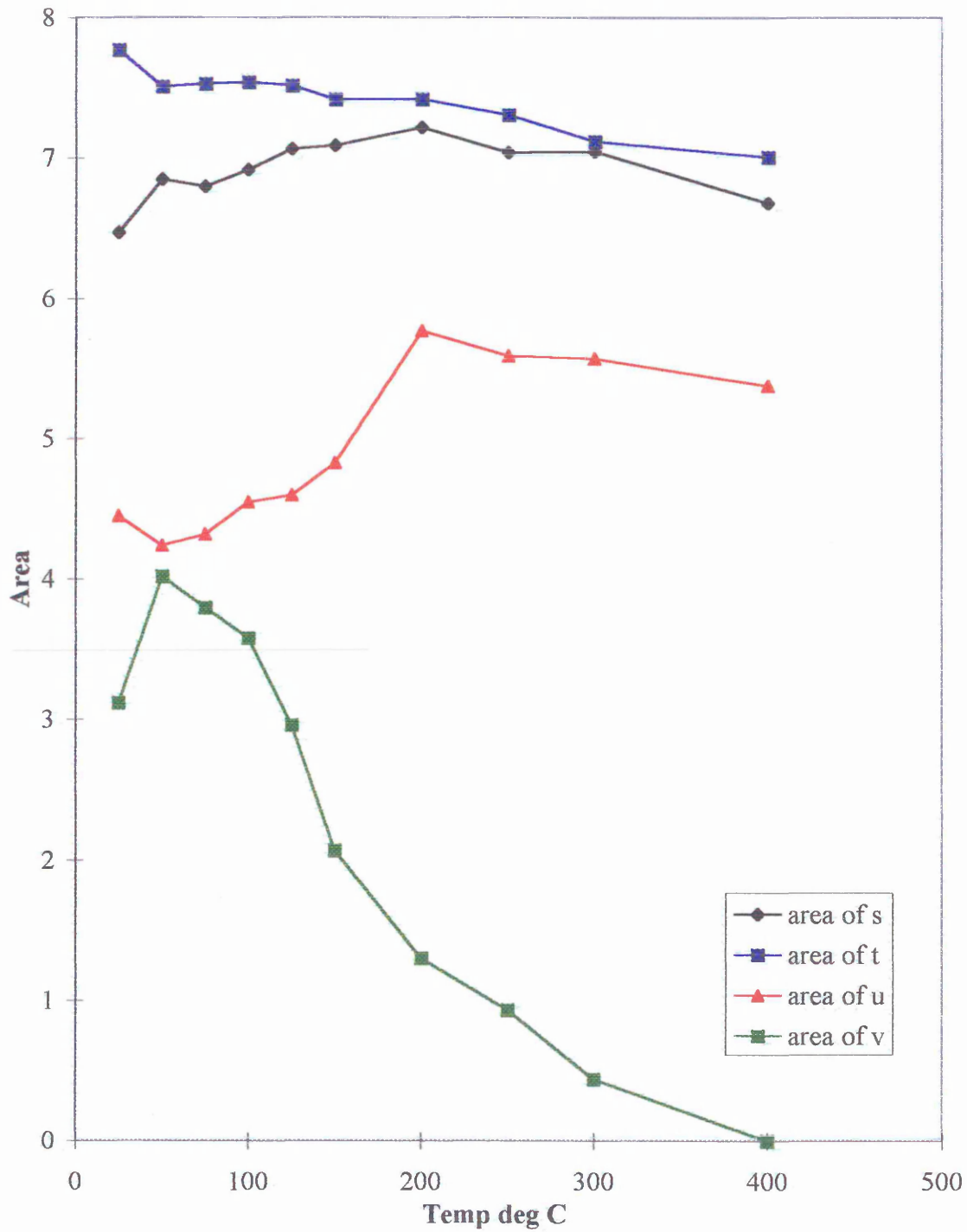


Figure 2.48 Unmilled (0 minute) ball milled kaolin. The 2100-1400 cm^{-1} region. 350 °C curve fit.



Bands s, t and u were apparent in all spectra and they have been attributed to structural combination bands (see Table 2.2 for assignments). Band v initially had an area approximately three quarters that of band u. After heating to 200 °C, band v decreased in intensity to approximately a quarter that of band u, and by 350 °C it was virtually indistinguishable.

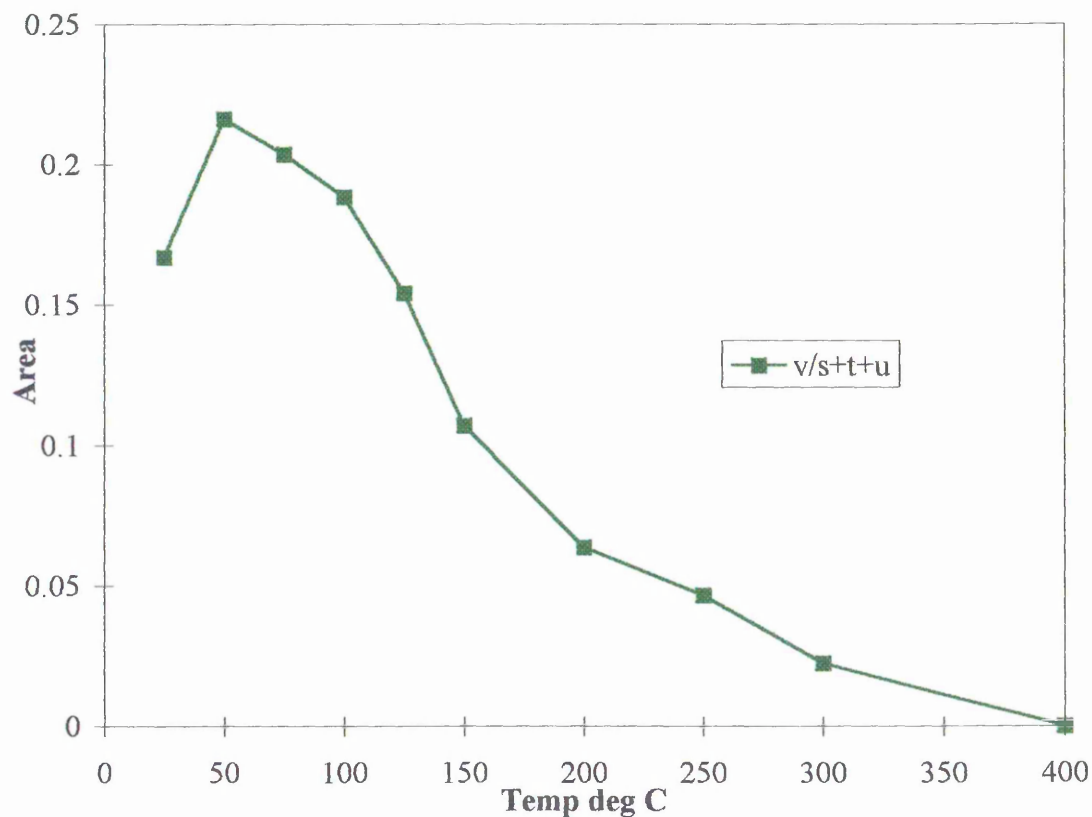
Figure 2.49 Unmilled kaolin - The change in intensity of bands s, t, u and v.



The sum of the relative intensities of bands s, t and u remained quite constant throughout the heating process, and for this reason they have been assigned to combination bands. The marginal decrease in the intensities of bands s and t, and the increase in intensity of band u beginning between 150 and 200 °C, are probably aberrations caused by the fitting

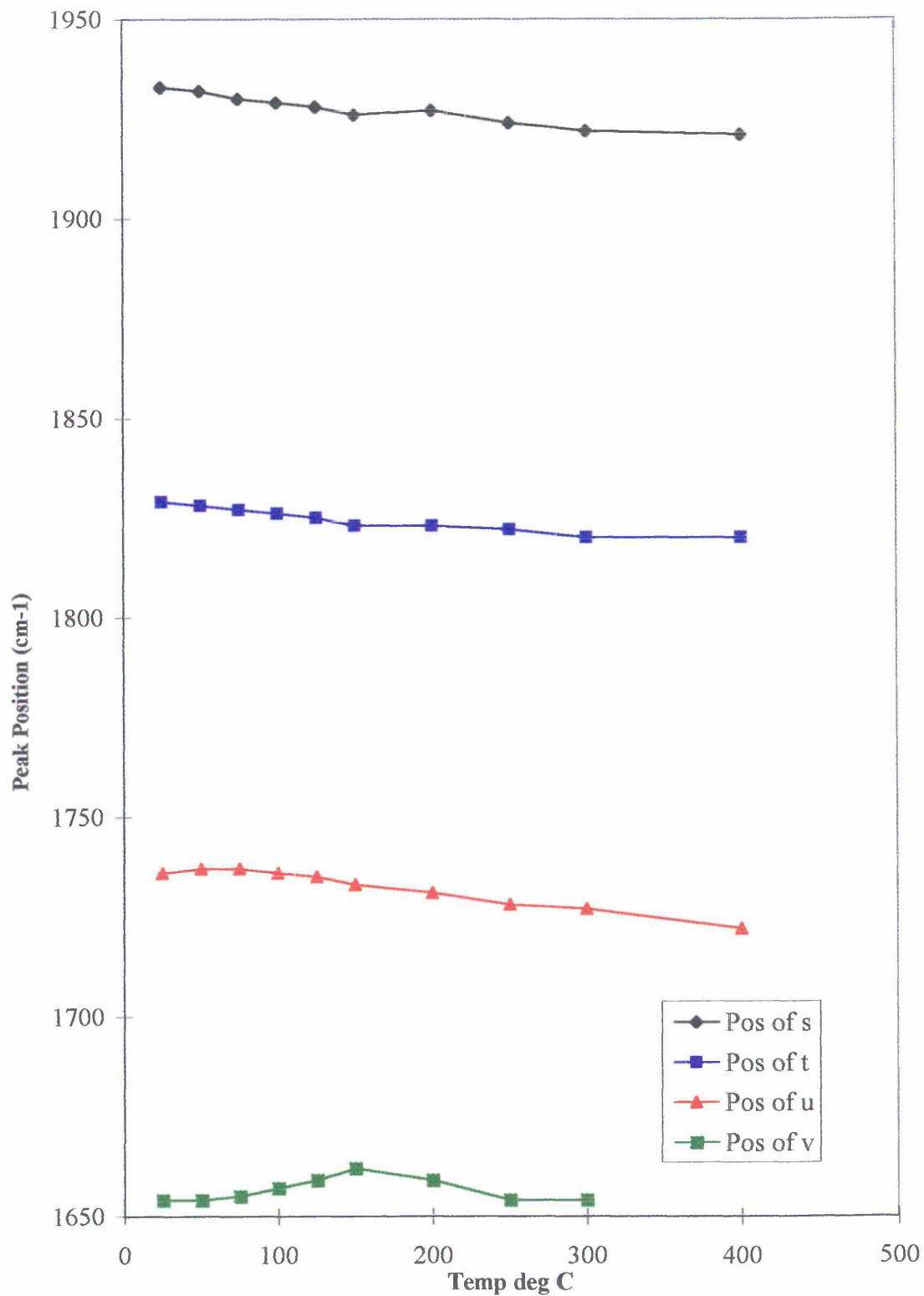
Chapter 2 The Effects of ...
procedure, since the intensities of these bands are not restricted. Therefore, certain proportions of intensity can be transferred from one band to the other. However, the intensity of band v alters dramatically at temperatures above c 100°C. The intensity of this band has been ratioed against the sum of bands s to u, and this plot can be seen in Figure 2.50.

Figure 2.50 Unmilled kaolin. The change in intensity of band v.



It can be clearly seen from the figure above that the intensity of band v fell markedly when the temperature was increased above 50°C. Between 25 and 150 °C there was a loss of intensity which accounted for 50% of the total initial area. The $t_{1/2}$ (i.e. the temperature at which 50% of the initial intensity of a band has been removed) was therefore c 150°C. The diminution continued throughout the temperature range of the study, but the incremental decrease was less between 200 and 400 °C. At 400 °C, no water was detectable by curve fitting methods in position v. The apparent increase in intensity between 25 and 50 °C is a spurious effect of the curve fitting procedure.

Figure 2.51 The change in position of bands in the 2100-1400 cm^{-1} as a function of temperature.



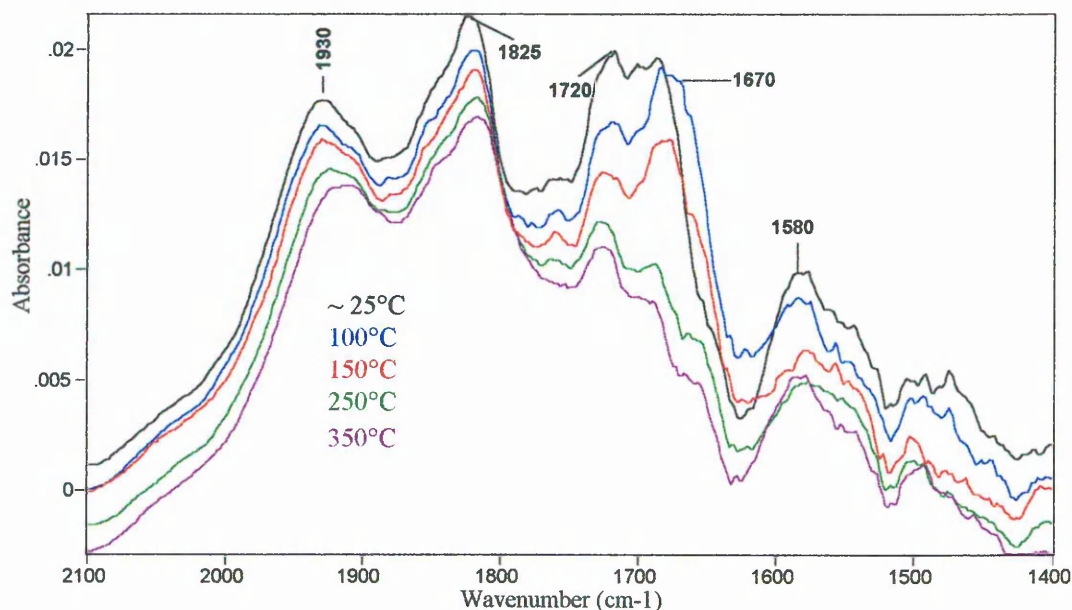
As temperature increased band v shifted marginally to increased frequency (by 10 cm^{-1} to 1660 cm^{-1} at $175 \text{ }^\circ\text{C}$) and decreased in intensity. This corresponds to the more loosely bound (physisorbed) water being driven from the surface, and is confirmed by low

temperature mass loss in thermal analysis. Subsequently there was a only a minor and gradual shift towards lower wavenumber for all of the bands. By 300°C, most of the 1650 cm⁻¹ water was lost. Band y at approx. 1490 cm⁻¹ was clearly visible.

The unmilled kaolin data shows the presence of a small amount of surface-sorbed water. The water is relatively heat sensitive, and is removed completely by heating to 300 °C

2.2.5.1.2 3 minute kaolin (freshly milled).

Figure 2.52 3 minute kaolin (FM). The 2100-1400 cm⁻¹ region .



In the above spectra, there can clearly be seen a band at 1580 cm⁻¹ (band r). Frost *et al*³⁵, attributed this band to monomeric non hydrogen bonded water (the corresponding stretching band (f) can be seen at c 3550 cm⁻¹ in Figure 2.29). It is possible that band r (at 1580 cm⁻¹) and band k in the stretching region are spectral aberrations brought about by the low sample concentration used in this particular experiment. As discussed previously, here, the dilution of sample was 99 % - more dilute than the other samples. However, since both bands are clearly visible, and in the absence of any other “aberrations”, it would not be wise to discount them entirely. There was a shift in the frequency of the water bending mode to 1670 cm⁻¹ (w) at room temperature. The relative intensity of the water band was much greater after 3 minutes milling than the

water band, ν , (at 1650 cm^{-1}) in the unmilled kaolin spectrum. Frost *et al.*,³⁸ attribute the 1650 cm^{-1} band to water hydrogen bonded to the kaolin surface and the 1623 cm^{-1} band to water fitting into the spaces between slightly expanded edges of the kaolin (see Figure 2.3) They propose that water treatment of kaolin at elevated temperatures and pressures induced the layers of kaolin to expand at the edges. In the present work, pressure treatments were not used. However, it is postulated that the milling procedure induced effects similar to those of pressure, and thus the layers became partially expanded.

Frost and co-workers compared low and high defect kaolins (c.f. unmilled and ball milled kaolins) and they observed bands corresponding to water adsorption at different frequencies according to whether the kaolin was low or high in defect.

Figure 2.53 3 minute kaolin (FM). The 2100-1400 cm^{-1} region. Room temperature curve fit.

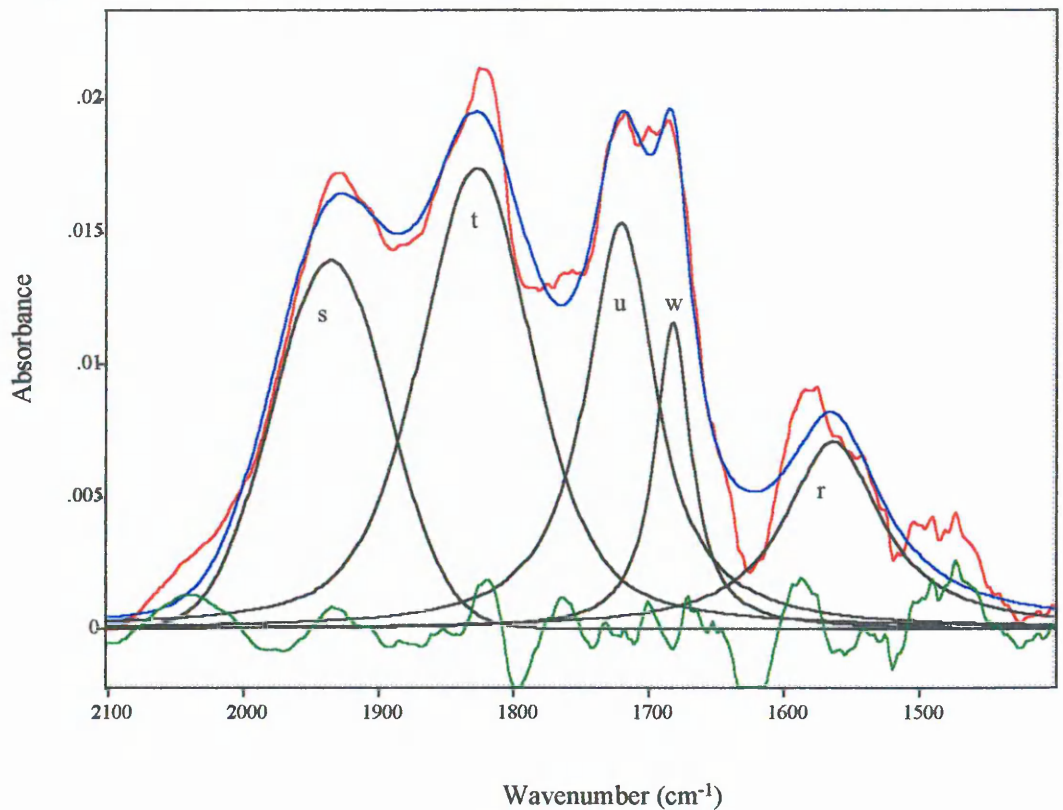


Figure 2.54 3 minute kaolin (FM). The 2100-1400 cm^{-1} region. 150° C curve fit.

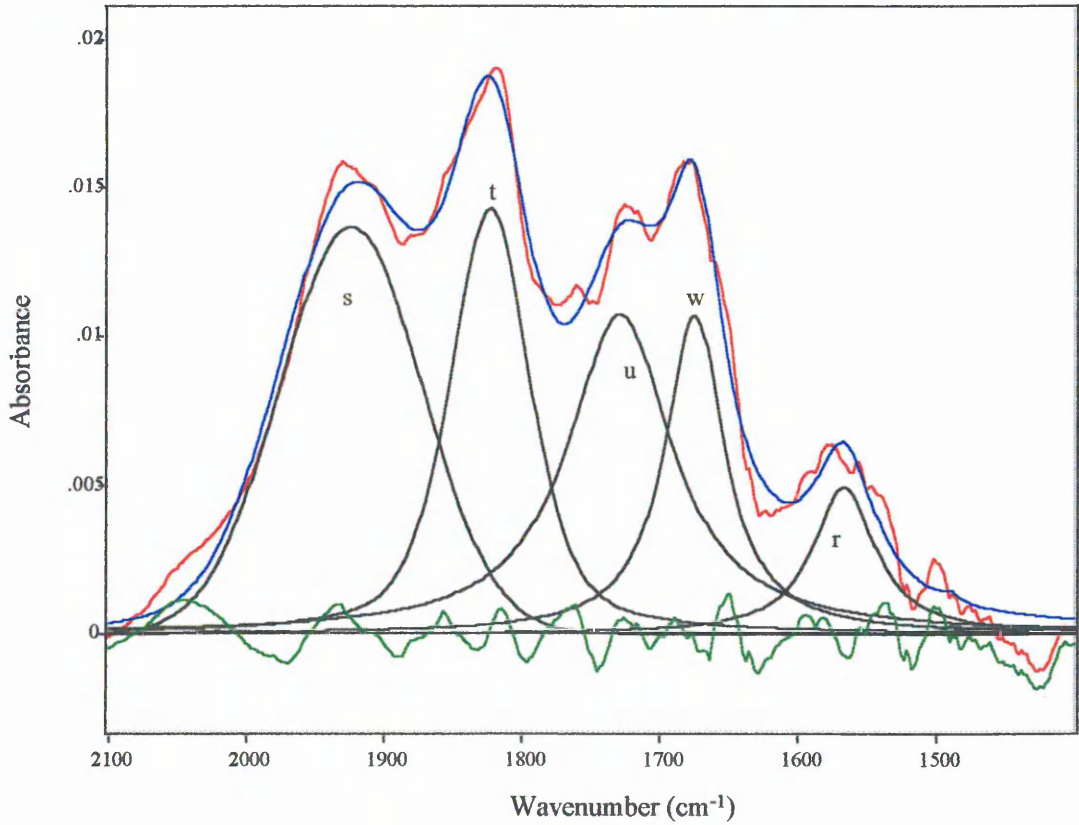


Figure 2.55 3 minute kaolin (FM). The 2100-1400 cm^{-1} region. 350° C curve fit.

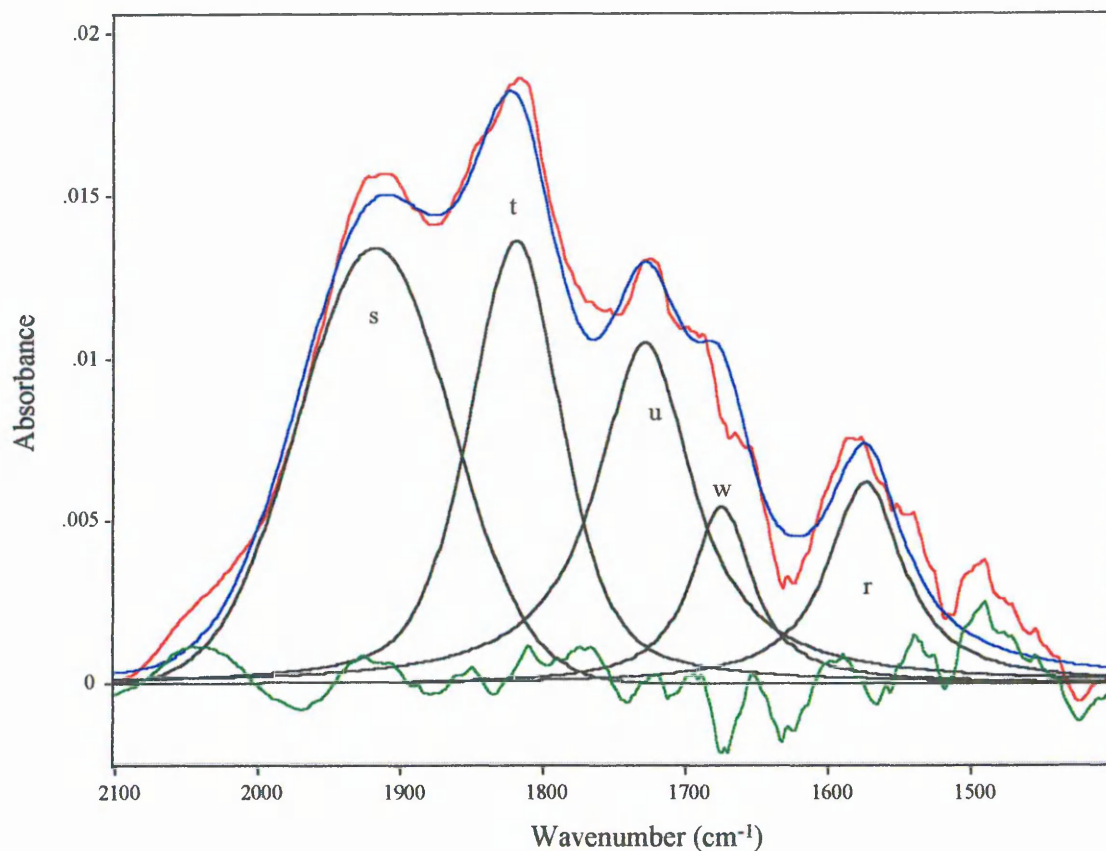
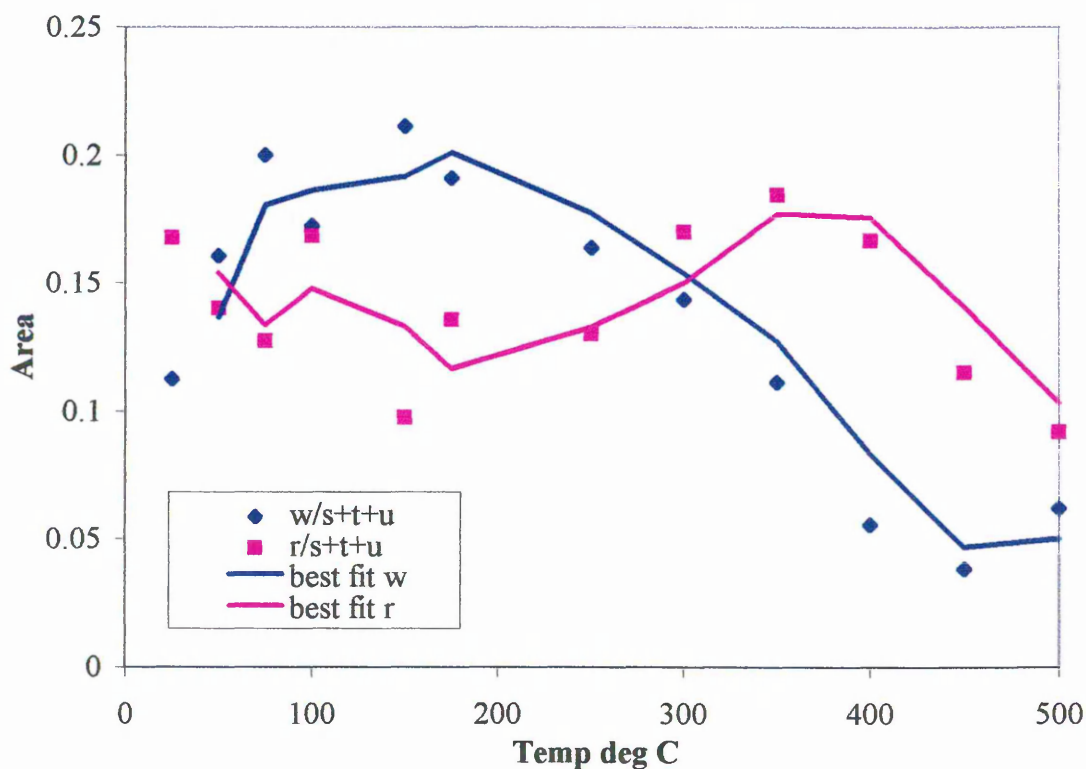


Figure 2.53 shows that at room temperature, although only 4 bands were obvious by eye, 2 bands were present in the 1650-1670 cm^{-1} region, rather than one. The three combinations bands, s, t and u were present (as predicted). Interestingly, the water band present at 1650 cm^{-1} in the unmilled sample shifted to higher frequency, indicating the presence of more strongly hydrogen bonded water. Band r was obvious at 1590 cm^{-1} . This may be due to very loosely hydrogen bonded trapped water, for example, a bridging water species. A band at 1578 cm^{-1} was seen by Frost *et al*⁴¹. They attributed it to water molecules in the second sphere of hydration which are therefore only weakly hydrogen bonded. This band probably represents a very small concentration of this type of water, since it is likely to have a high extinction coefficient. Overall, the concentration of water present increased compared with the unmilled data. The peak intensity of band w compared with that of band u is much greater than the corresponding water band in the unmilled data.

At 150 °C, (Figure 2.54) the intensity of band w appeared to increase. This is because of the difficulty in distinguishing between band w and band u. It is likely that the band reduced overall, and the fits up to 100 °C attributed too little intensity to band w and instead it was being attributed to band u. However, both bands w and r were very obvious.

Figure 2.55 shows that even at this high temperature there is clear evidence of bound water in both regions. The unmilled kaolin lost all surface water by this temperature, and this observation further substantiates the theory that as milling time increases so does the strength of binding of water.

Figure 2.56 Change in intensity of bands w & r.

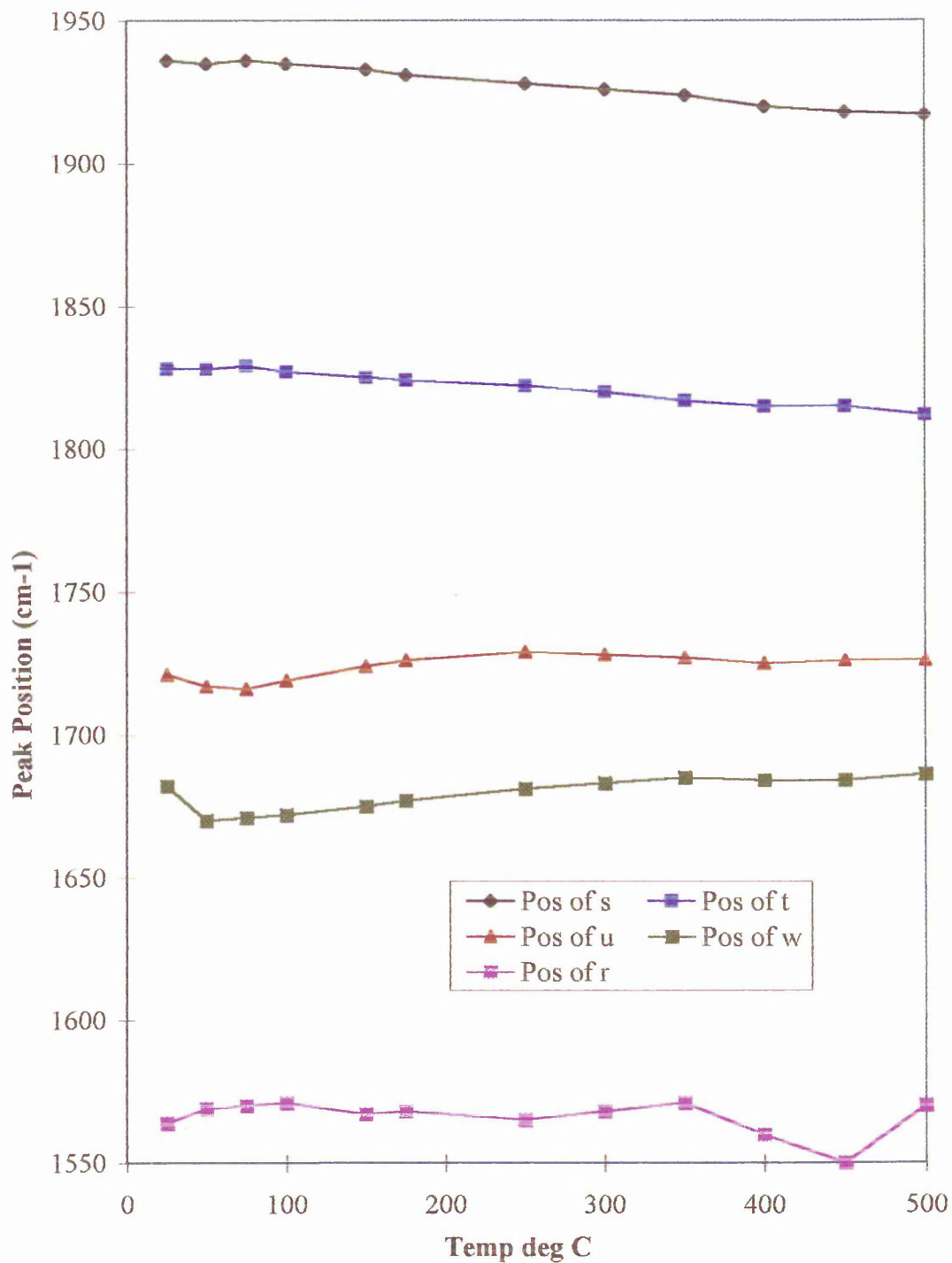


The fact that water remained obvious in the spectrum until remarkably high temperatures substantiates the work carried out by Yariv⁴³, where it was hypothesised that the longer the grinding process, the more tightly held is the sorbed water. Here, although some water was lost at lower temperatures, at 350 °C a band at 1670 cm⁻¹ was still evident. Degassing studies by Conley and Althoff⁴⁴ indicated that monolayer water on the surface of kaolin was removed completely only after heating to over 250 °C. They also saw

thermally resistant molecular water which was retained after heating to 280 °C. They attribute these highly stable water molecules to those which have undergone prototropy (i.e., the migration of protons to exposed oxygens or hydroxyl sites on the surface of the mineral). This follows, since increased grinding gives more prototropic effects, and therefore, more new OH associations (which are more thermally stable). So, as milling time increases, water in certain environments is present at ever increasing temperatures. It is believed by the author that band r was a real spectral feature and it may be attributed to very weakly hydrogen bonded water trapped inside the mineral agglomerates (see section 2.4 for a more detailed account of this band and its correlation with the stretching region).

It can be seen from Figure 2.56 that the rate of decrease of the intensity of the water band, w, is slower than that of the water band, v, in the unmilled kaolin data. In the 3 minute milled sample, more water is retained until higher temperatures.

Figure 2.57 3 Minute Kaolin. Frequencies of bands in 2100-1400 cm^{-1} region.



The positions of bands s, t and u shifted slightly during the course of the experiment, probably indicating partial breakdown of the kaolin structure. The shifts are comparable to those of bands a - e in the stretching region. Band w shifted slightly to higher frequency, indicating, as expected, the less strongly bonded water was removed at lower

temperatures. The centre of band r shifted slightly from 1565 to 1570 cm^{-1} at 25 and 500 $^{\circ}\text{C}$ respectively.

2.2.5.1.3 10 minute kaolin(freshly milled).

Figure 2.58 10 minute kaolin(FM). The 2100-1400 cm^{-1} region.

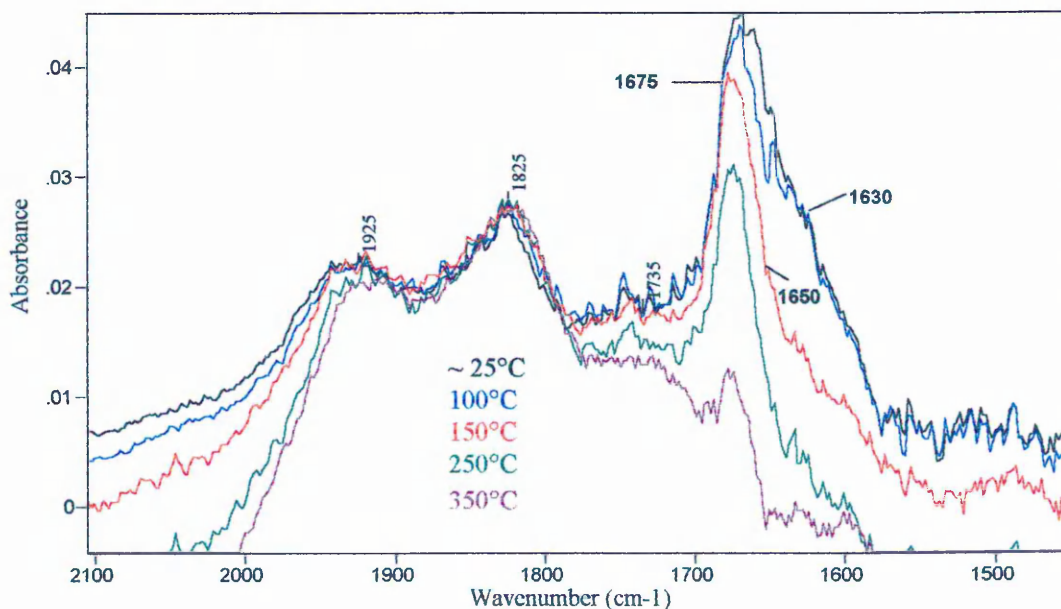


Figure 2.58 above has not been normalised to bands s, t and u due to the limitations of the software package. The overall intensity of the HOH bending region was approximately twice as large as that of band t - again indicating that milling further increased the amount of surface-sorbed water. In this sample, however, there was a very intense band at around 1670 cm^{-1} and a relatively weak (although still quite intense in absolute terms) band at 1628 cm^{-1} (x). There was no obvious 1650 cm^{-1} band, although it is possible to fit a band there. However, it is not readily distinguished from the 1670 and 1628 cm^{-1} bands and has therefore been omitted from this fitting strategy. It is, however, likely that water in this environment does exist. Neither has the 1580 band r been fitted in this scheme, but it too is likely to be present, but is hidden beneath the very intense bending modes at 1670 and 1630 cm^{-1} (and is thus not easily distinguished from them).

Figure 2.59 10 minute kaolin(FM). The 2100-1400 cm^{-1} region. Room temp curve fit.

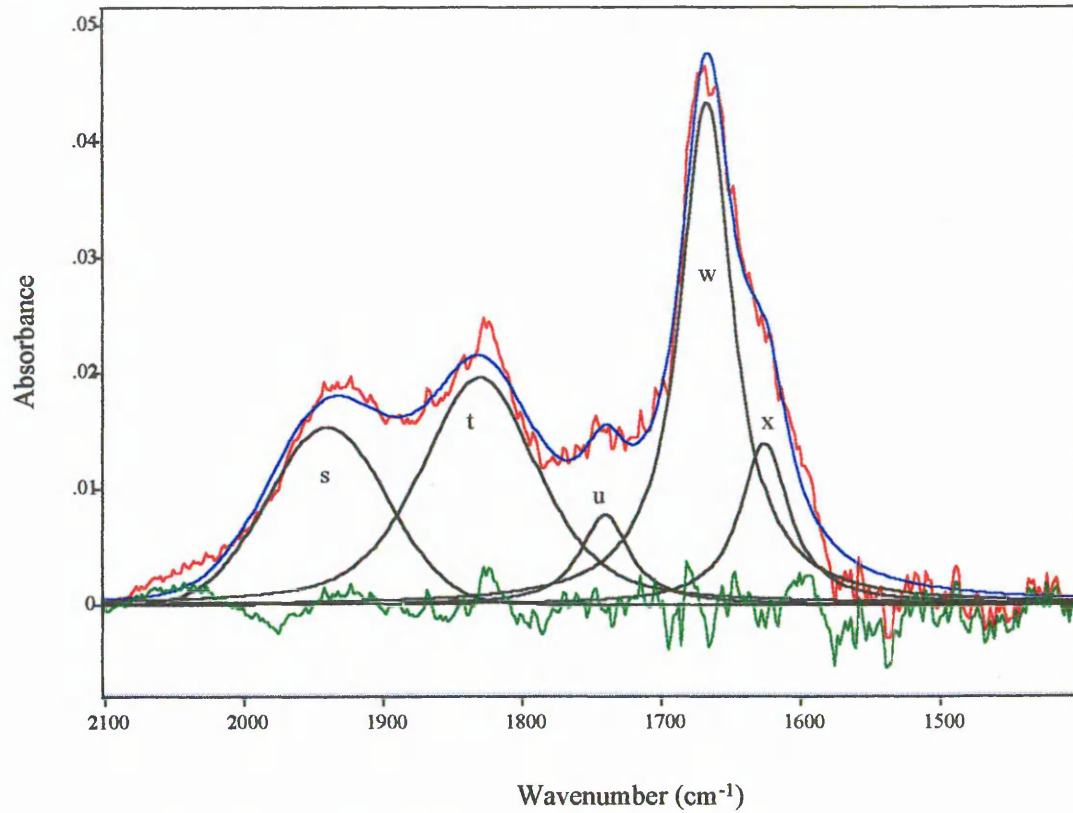


Figure 2.60 10 minute kaolin(FM). The 2100-1400 cm^{-1} region. 150 $^{\circ}\text{C}$ curve fit.

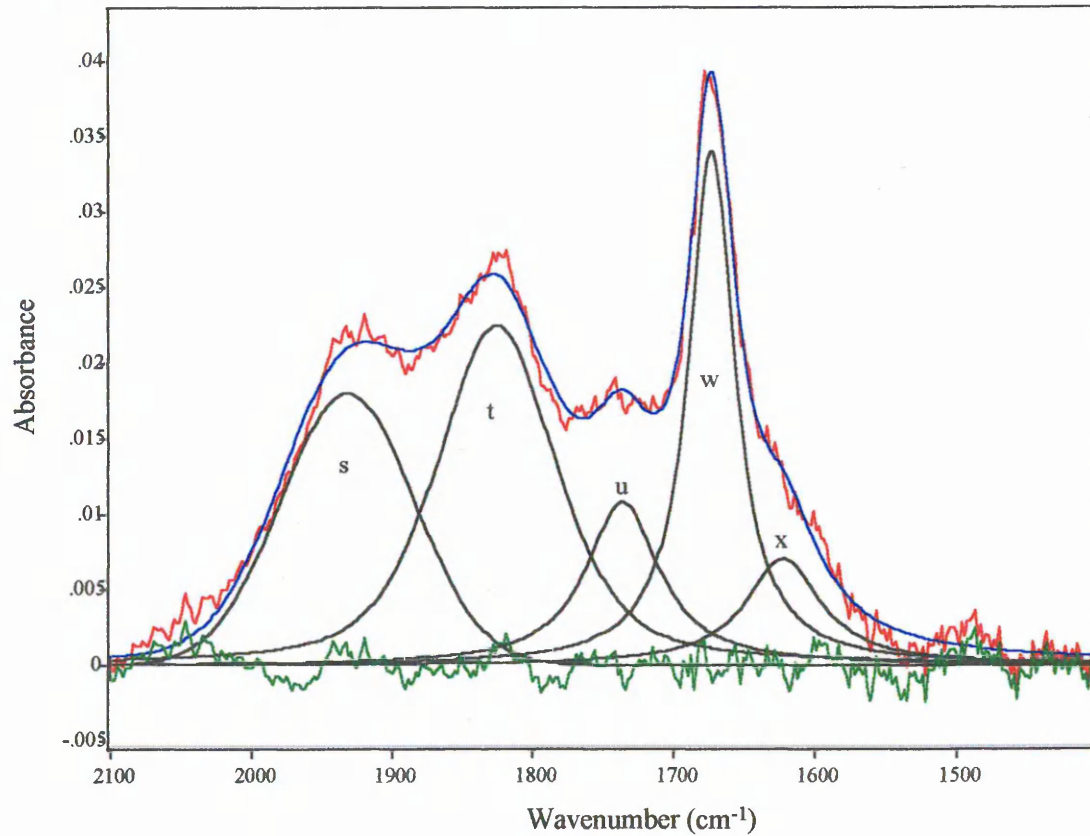


Figure 2.61 10 minute kaolin(FM). The 2100-1400 cm^{-1} region. 350 °C curve fit.

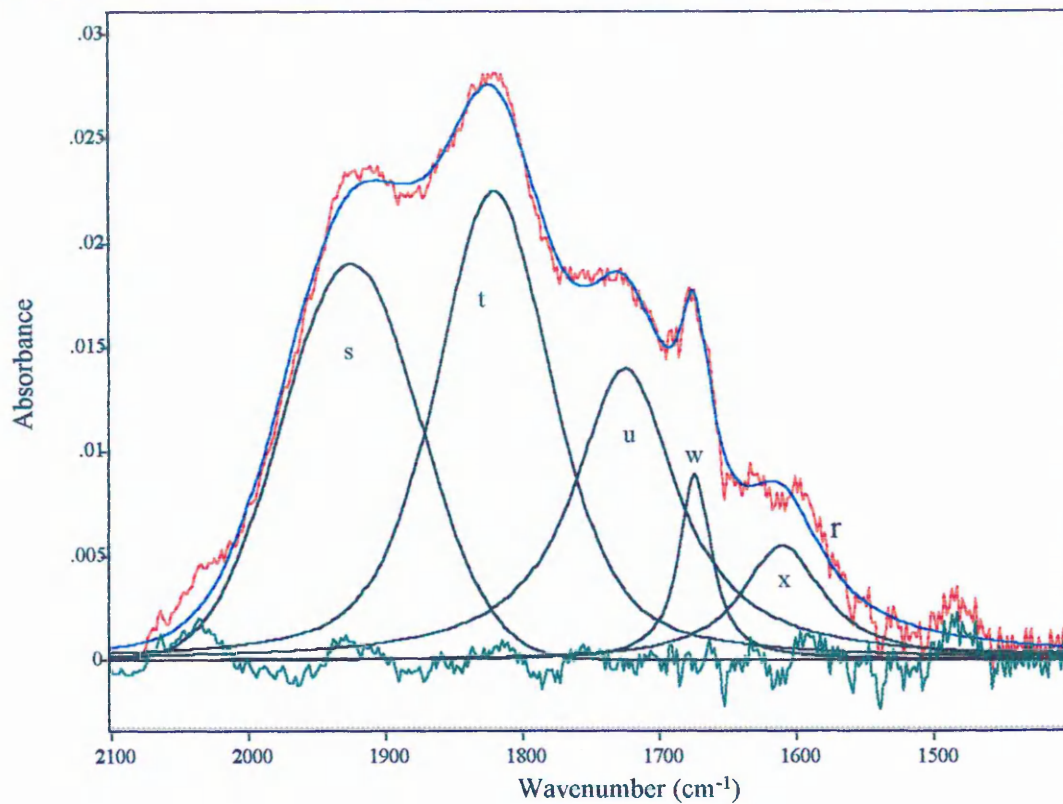
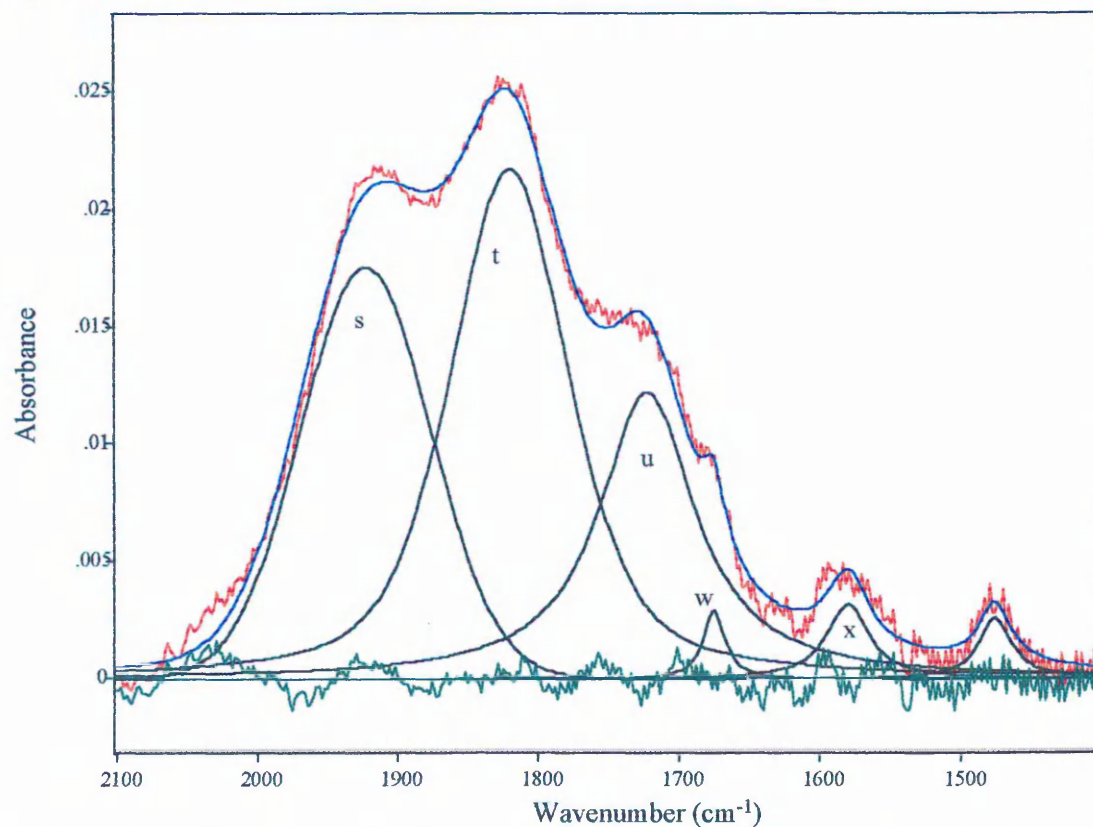


Figure 2.62 10 minute kaolin(FM). The 2100-1400 cm^{-1} region. 450 °C curve fit.



At room temperature, (Figure 2.59), the combination bands were dwarfed by the huge water bands w and x. There was a very large overall increase in the amount of sorbed

water compared with both the unmilled and 3 minute milled data. The major water mode was w at 1670 cm^{-1} , but there was also a significant contribution from band x at 1630 cm^{-1} . Band u is of peculiarly low intensity. This is due to the inability of the fitting parameters to distinguish exactly where the boundaries of bands u and w lie. Thus, it follows that band w appears to be slightly more intense than in actually is.

When heated to $150\text{ }^{\circ}\text{C}$ (Figure 2.60) although the intensities of both water features reduced, the spectrum was still dominated by these very intense bands, and at $350\text{ }^{\circ}\text{C}$ (Figure 2.61) the bands were still identifiable by eye. The $450\text{ }^{\circ}\text{C}$ spectrum of this sample has been included to illustrate the ever increasing thermal stability of adsorbed water after ball milling. Figure 2.62 shows that both bands w and x were present at this very high temperature. However, x appeared to shift to c 1590 cm^{-1} . This corresponds to the position of band r in the 3 minute sample. This band was masked at lower temperatures by the very intense 1630 cm^{-1} band.

Figure 2.63 shows that both w and x decreased in intensity steadily over the course of the experiment. There was a large decrease in the first $200\text{ }^{\circ}\text{C}$ (approximately half of the total intensity ($t^{1/2}$)), which represented the removal of the less heat stable surface sorbed water- i.e. loosely bound water. Band w in the 3 minute milled sample may be more thermally stable than in the 10 minute sample, since in the former the intensity does not begin until above $200\text{ }^{\circ}\text{C}$. However, the intensity change of band w is accentuated here because at lower temperatures, the very large band w (compared with the 3 minute sample) also encompasses some of the area which should belong to band u. Bands w in the 10 minute sample was still present at $500\text{ }^{\circ}\text{C}$. The position shift of band x indicates that in fact this band is removed by approximately $250\text{ }^{\circ}\text{C}$ and allows the emergence of band r at 1580 cm^{-1} .

Figure 2.63 10 minute kaolin(FM). The change in intensity of bands w & x.

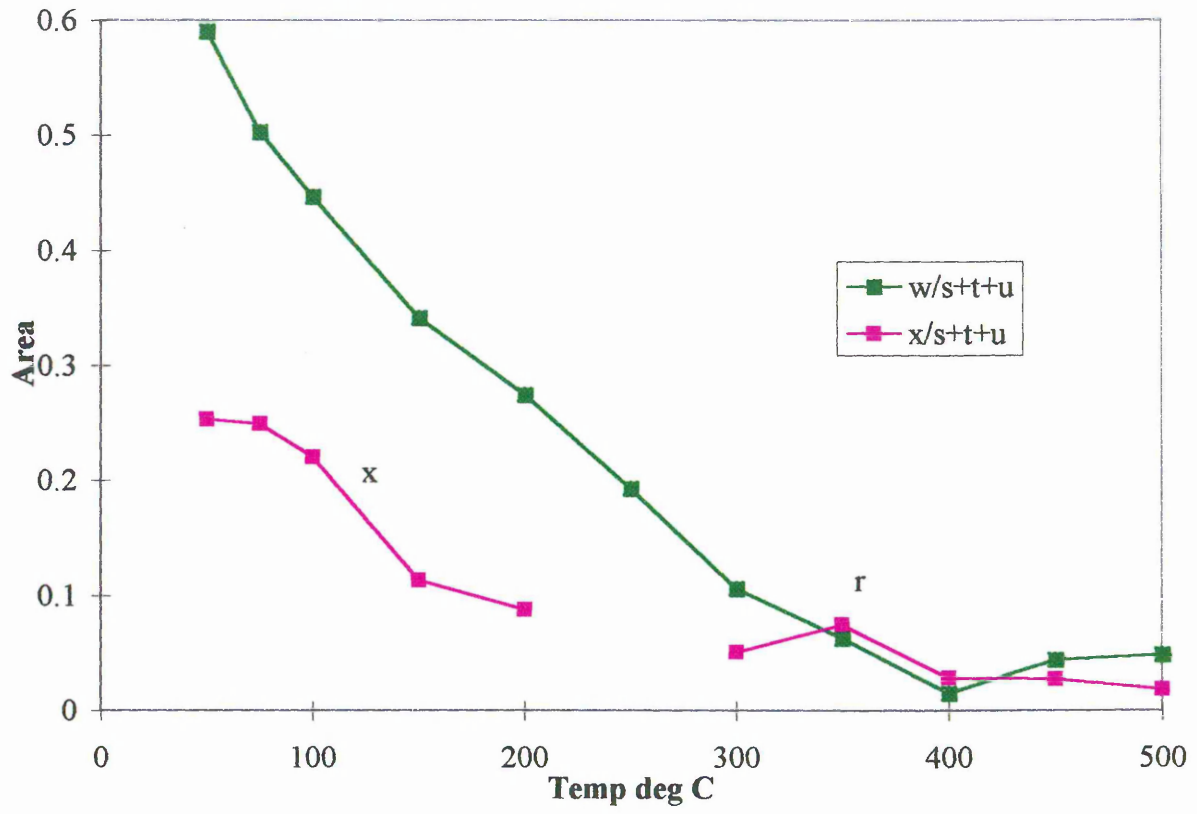
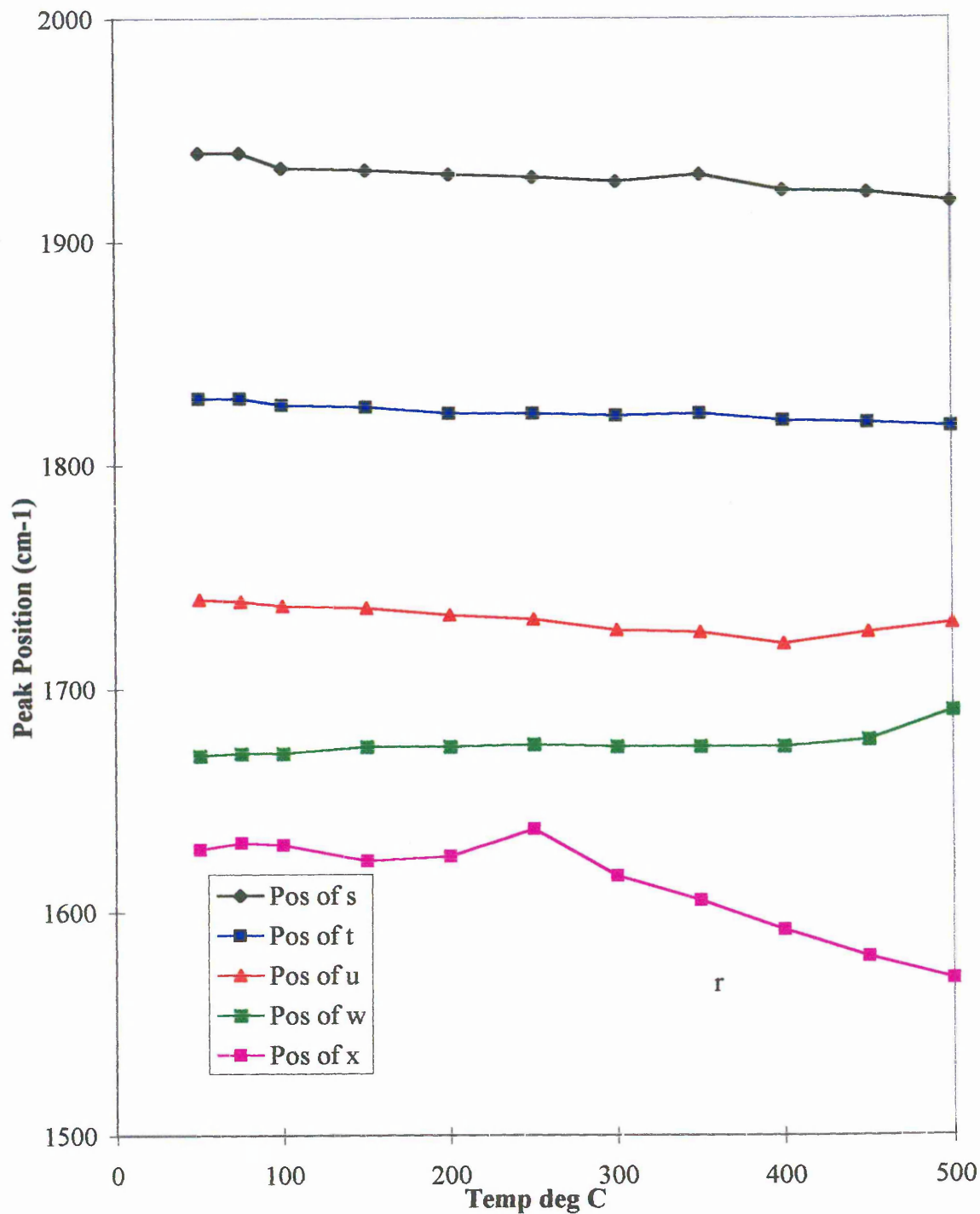


Figure 2.64 10 minute kaolin(FM) The change in position of bands in the 2100-1400 cm^{-1} region.

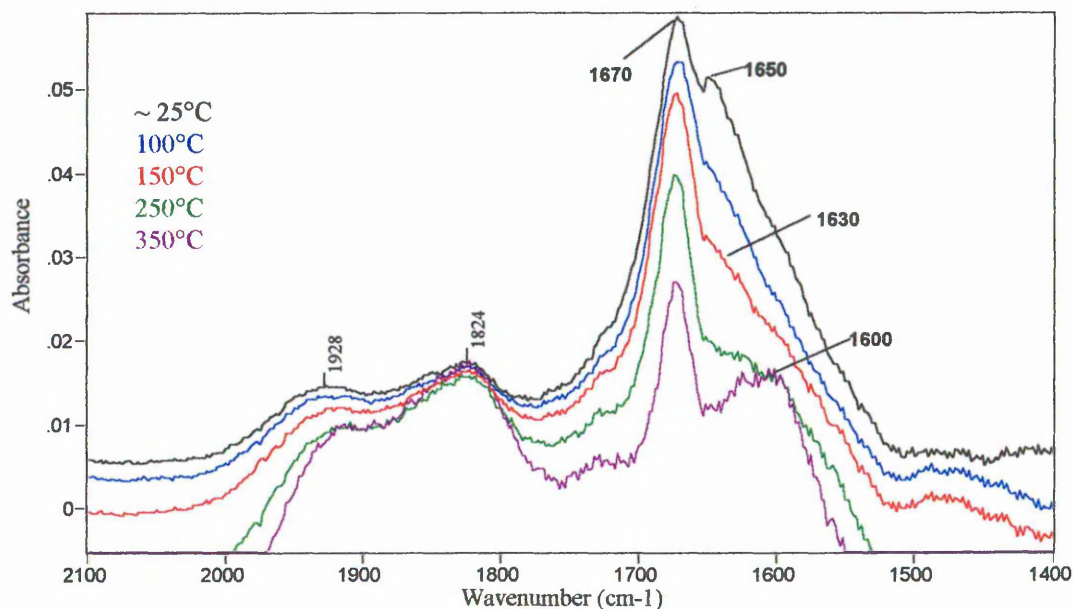


Water loss was gradual, with a significant amount of both w and x still evident at 250°C. Even at 450°C, there remained some evidence of band w at 1677 cm^{-1} . This indicated the presence of bound water more tightly held than in the 3 minute milled (or unmilled)

kaolins. Band x was now at a position similar to that of band r in the 3 minute sample, indicating the persistence of the trapped water. The increased intensity of the 1670 cm^{-1} band compared with the 3 minute milled sample indicated that a higher proportion of the adsorbed water species were more strongly hydrogen bonded to the surface.

2.2.5.1.4 30 minute kaolin(freshly milled).

Figure 2.65 30 minute kaolin(FM). The $2100\text{-}1400\text{ cm}^{-1}$ region.

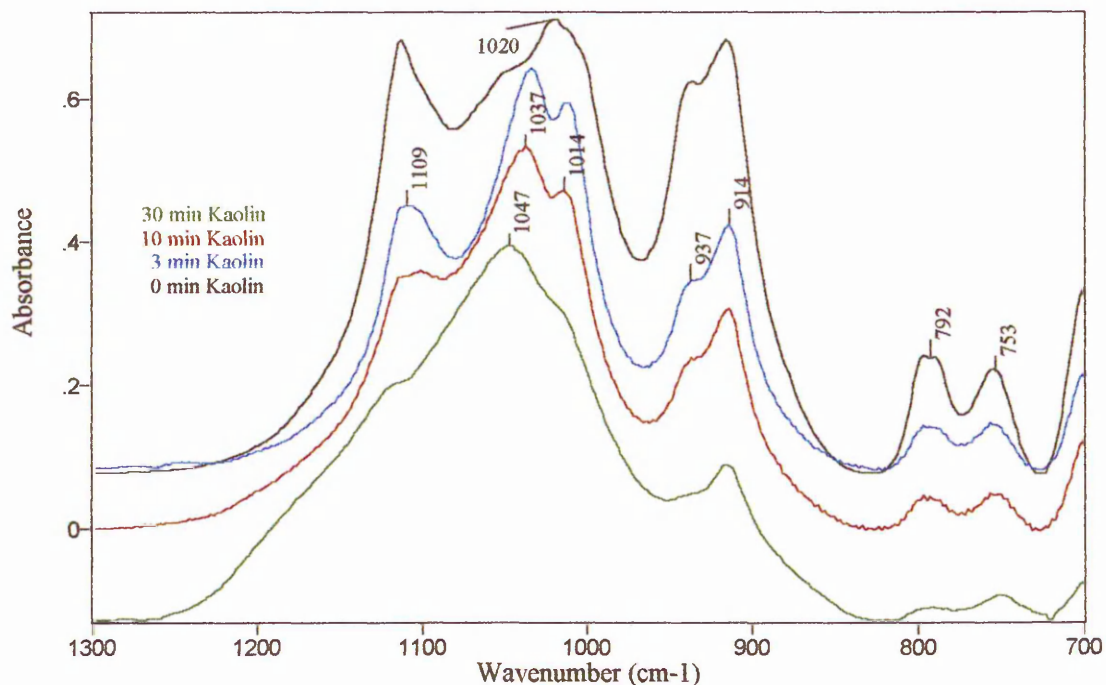


Due to the huge intensity of the water bands it was not possible to normalise these spectra. However, clearly visible were bending modes at 1670 , 1650 and 1630 cm^{-1} . As in the stretching region of the 30 minute milled kaolin spectra, curve fit results were not considered reliable, due to the very large area covered by the water bands at $c\ 1700\text{ cm}^{-1}$ to 1550 cm^{-1} . Nevertheless, Figure 2.65 shows a selection of the VT DRIFTS spectra. The water bands were relatively intense until very high temperatures. More water appeared to be present at $350\text{ }^\circ\text{C}$ than in the 10 minute milled data, thus suggesting even more tightly bound hydroxyl species. Indeed, there is clear evidence of a sharp band at 1670 cm^{-1} even at $350\text{ }^\circ\text{C}$. It is unlikely that this phenomenon is due to surface water. It is thought to be brought about by hydrogen bonded water trapped inside the large agglomerates formed after extensive milling. It seems that the 1650 cm^{-1} is being desorbed preferentially (which would be expected since the more strongly bound

hydroxyl species are present at lower wavenumber). Another feature worthy of note is the apparent increase in the intensity of the r band at 1595 cm^{-1} which further indicates the presence of an increased concentration of “trapped” water.

2.2.5.2 The effect of milling on kaolin. The $1300\text{-}700\text{ cm}^{-1}$ region.

Figure 2.66 Ball milled kaolins. The $1300\text{-}700\text{ cm}^{-1}$ region.



Changes can also be seen in this region of the spectrum after milling. The shape and intensity of the broad band at $c\ 1100\text{ cm}^{-1}$ altered during the milling process. There was a successive decrease in intensity, and the spectral band produced by the sample milled for 30 minutes was less well defined than the same band in all other samples.

Although not a fundamental part of this study, it is worthy of note that a detailed IR adsorption study investigating the effects of grinding kaolinite in the presence and absence of alkali chlorides was carried out by Yariv⁴³. Perhaps the most interesting feature noted by Yariv was that the Si-O stretching band at $c\ 1080\text{ cm}^{-1}$ is very sensitive to grinding. He noted that in both the presence and absence of salts, when the kaolin was ground there were 2 distinct stages in the alteration of this band (designated “band P” in the referenced work). Firstly band P became sharp and shifted to higher frequency,

and secondly it became broad and shifted to lower frequency. The first stage was said to represent delamination of the mineral and this process was faster in the absence of salt. The second stage was likely to represent prototropy, where protons migrate from their original position within the structure towards the inner oxygens. This process can also be monitored in the OH stretching region (bands a, b, c and d in particular). Shifts in the positions of bands a, b and c are said to represent interactions between the inner sheet hydroxyl groups with adsorbed water. Decreases in the intensity of these bands have also been said to represent prototropy which is facilitated by the grinding process. The 1080 cm^{-1} in the work presented herein is not fully resolved from the 1100 cm^{-1} band. However, it appears that the initial trend observed by Yariv is also being followed here. It seems likely that delamination occurs after milling for 30 minutes.

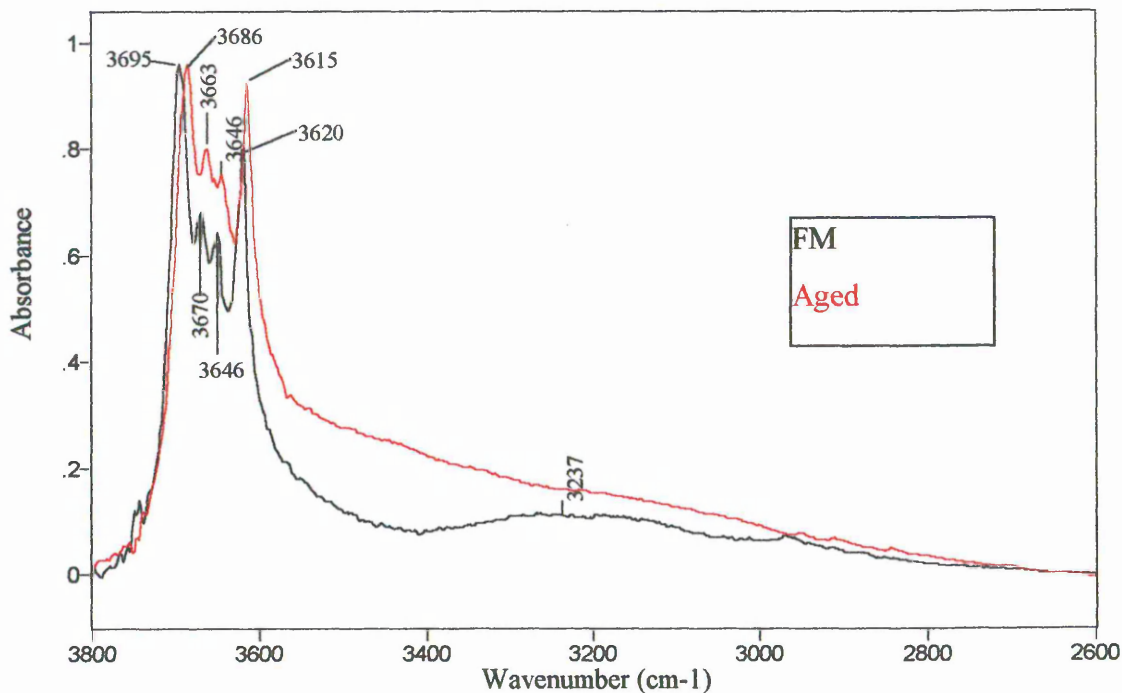
2.3 Results. The effects of ageing on ball milled kaolins.

After the initial spectra (FM) were collected, the samples were stored in sealed vessels at ambient temperature and pressure. After ageing for between 4 and 6 months, dramatic spectral changes were noted in the water bending and stretching regions of all milled samples. Some representative spectra are presented in the following section.

2.3.1 Infrared of ball milled kaolins. The 3800-2600 cm^{-1} region.

2.3.1.1 3 minute milled kaolins. The 3800-2600 cm^{-1} region.

Figure 2.67 3 minute freshly milled and aged kaolins The 3800-2600 cm^{-1} region.



There was an overall increase in the amount of adsorbed water after ageing (at room temperature, as shown above). There was a particularly large increase in the 3700-3350 cm^{-1} , region corresponding to an increase in weakly hydrogen bonded water species. The spectra below show curve fits at representative temperatures.

Figure 2.68 3 minute aged kaolin. The 3800-2600 cm^{-1} region. Room temp. curve fit.

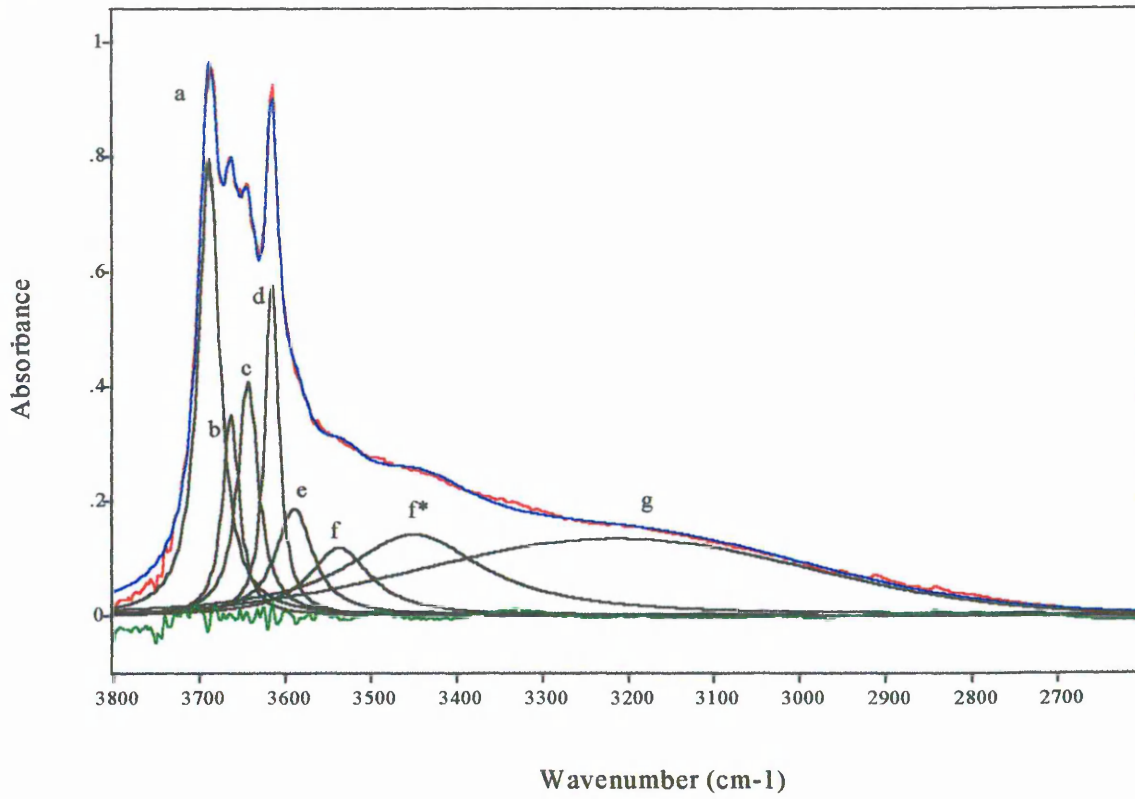


Figure 2.69 3 minute aged kaolin. The 3800-2600 cm^{-1} region. 150°C curve fit.

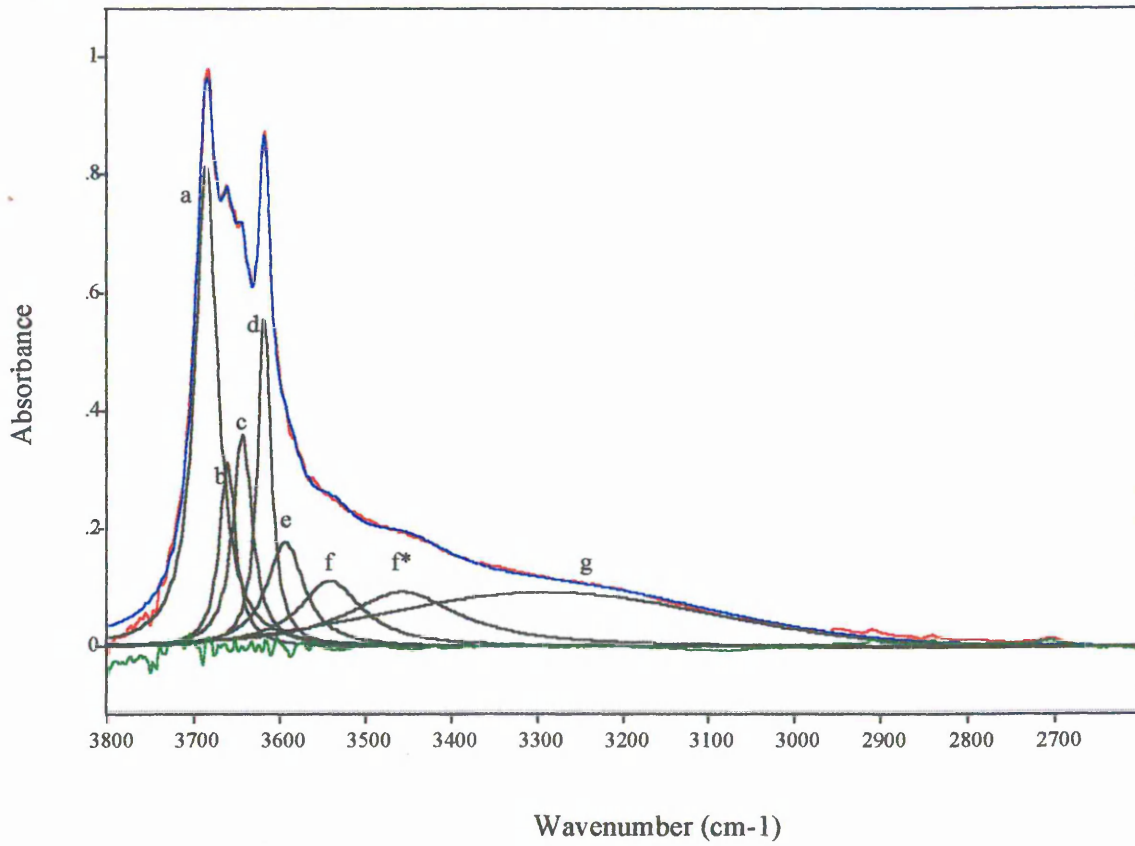


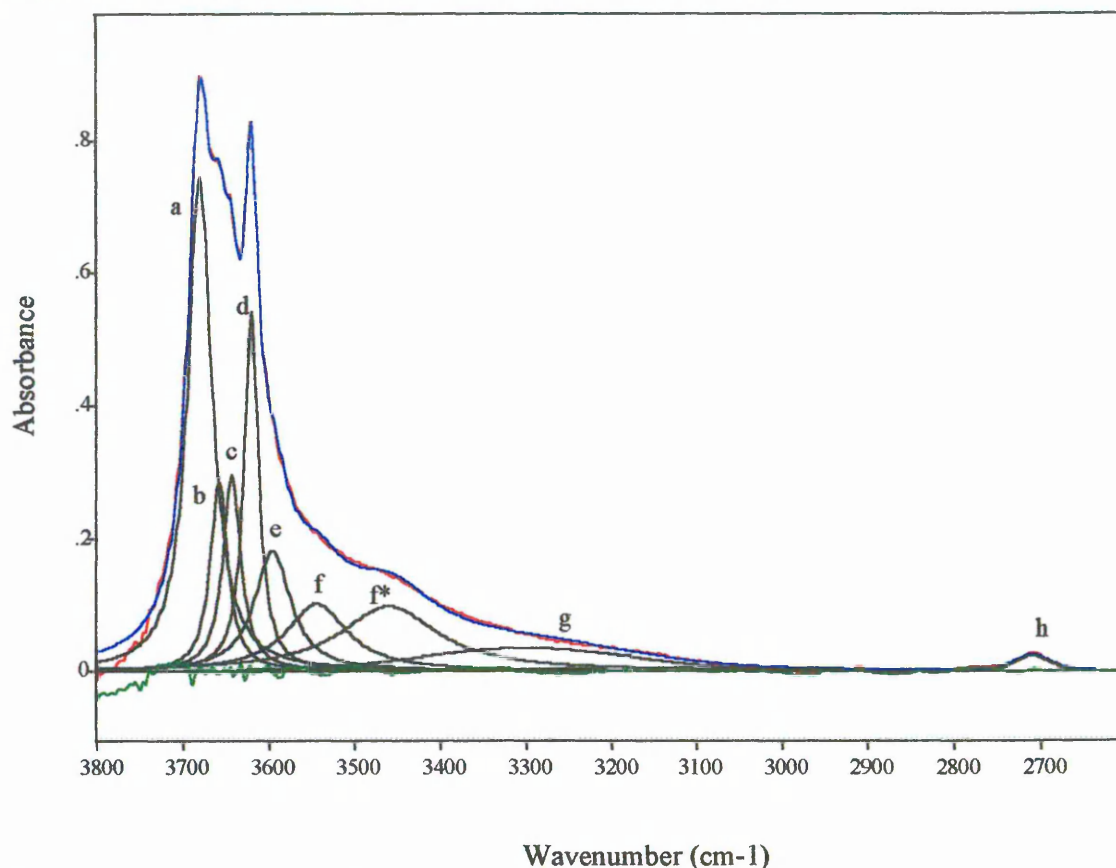
Figure 2.70 3 minute aged kaolin. The 3800-2600 cm^{-1} region. 350°C curve fit.

Figure 2.68 (room temperature) shows that after ageing another water environment has appeared (band f^*). This species may have been present in the FM sample, but it was in much lower concentration, therefore it was omitted from the fitting regime. After ageing, there is an increase in this type of water. It represents an increase in the amount of weakly hydrogen bonded water compared with the FM sample (Figure 2.29). At 150 °C bands e (c 3590 cm^{-1}) and f (c 3550 cm^{-1}) changed little in intensity or frequency compared with the room temperature spectrum. Band f^* remained at the same frequency (compared with room temperature), but the intensity decreased by approximately a half. Band g shifted by 70 cm^{-1} to higher frequency and decreased in intensity. Figure 2.70 shows that at 350 °C the spectrum of the aged sample resembles that of the FM kaolin (Figure 2.31). Bands e and f were very similar to those in the 150 °C spectrum. Band g dramatically decreased in intensity, and increased slightly in frequency. Band f^* changed little in frequency, and a small decrease in intensity was observed compared with the 150 °C spectrum. Although not fitted in the FM sample, band f^* is likely to be represented by intensity encompassed by band f. In the spectral fit of the aged sample at 350 °C,

(Figure 2.31), band f* is a more prominent feature, indicating that the surface water was more thermally stable than the corresponding band in the FM sample.

Figure 2.70 below shows that, as expected, the intensity of band f remained virtually constant over the temperature range studied. Band f* lost intensity rapidly, with a decrease of c 50 % over the first 150 °C. Thereafter the intensity remained constant, even up to 350 °C. Band g was initially very intense, but it too lost 50 % of the intensity by 150 °C. It continued to decrease at a similar rate over the entire temperature range. It was approximately 1/8 of the initial intensity at 350 °C. Band h at c 2708 cm⁻¹ became more apparent as temperature increased.

Figure 2.71 3 minute aged kaolin. The change in intensity of bands f, f*, g & h.

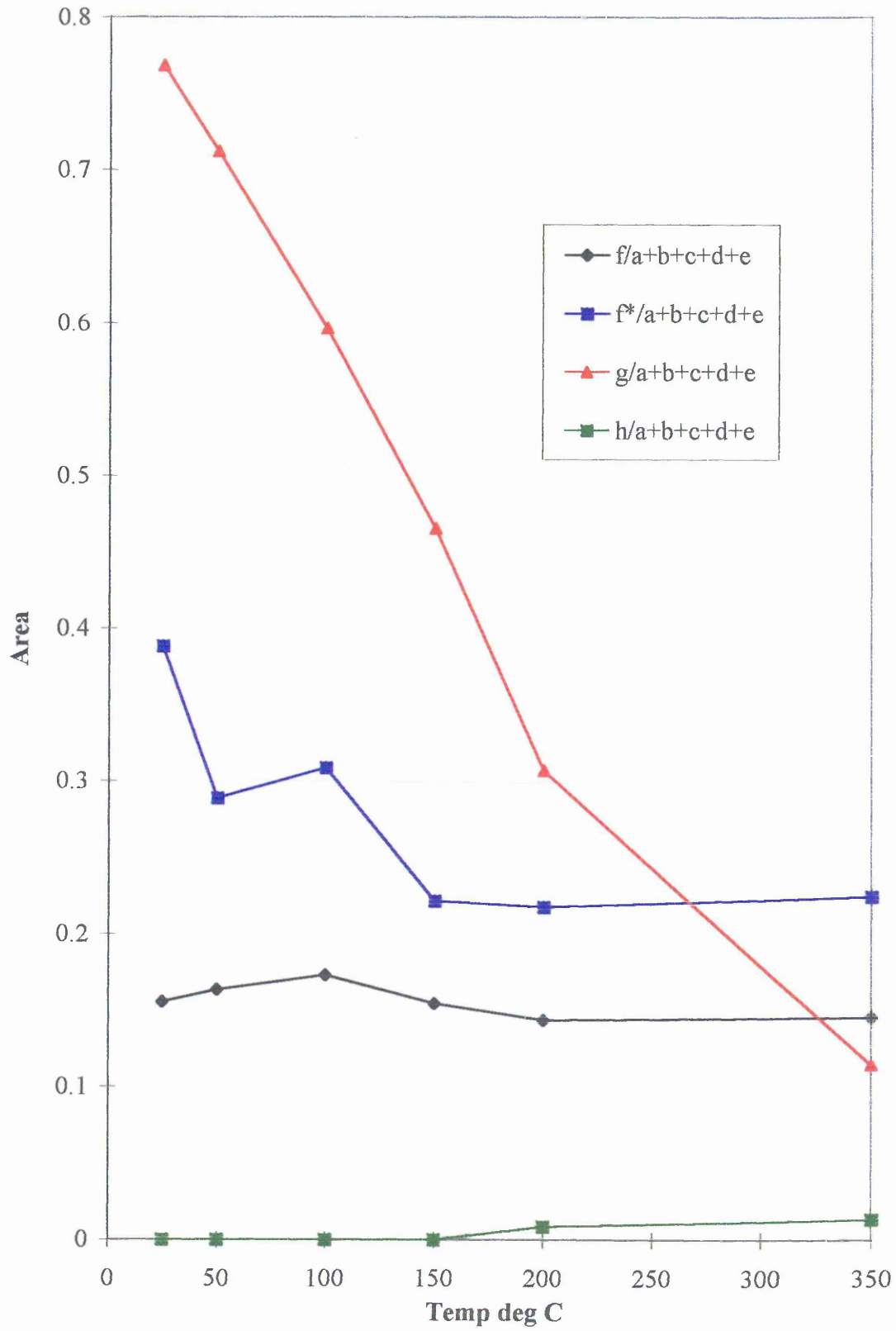


Figure 2.72 3 minute aged kaolin. Change in position of bands f, f*, g and h.

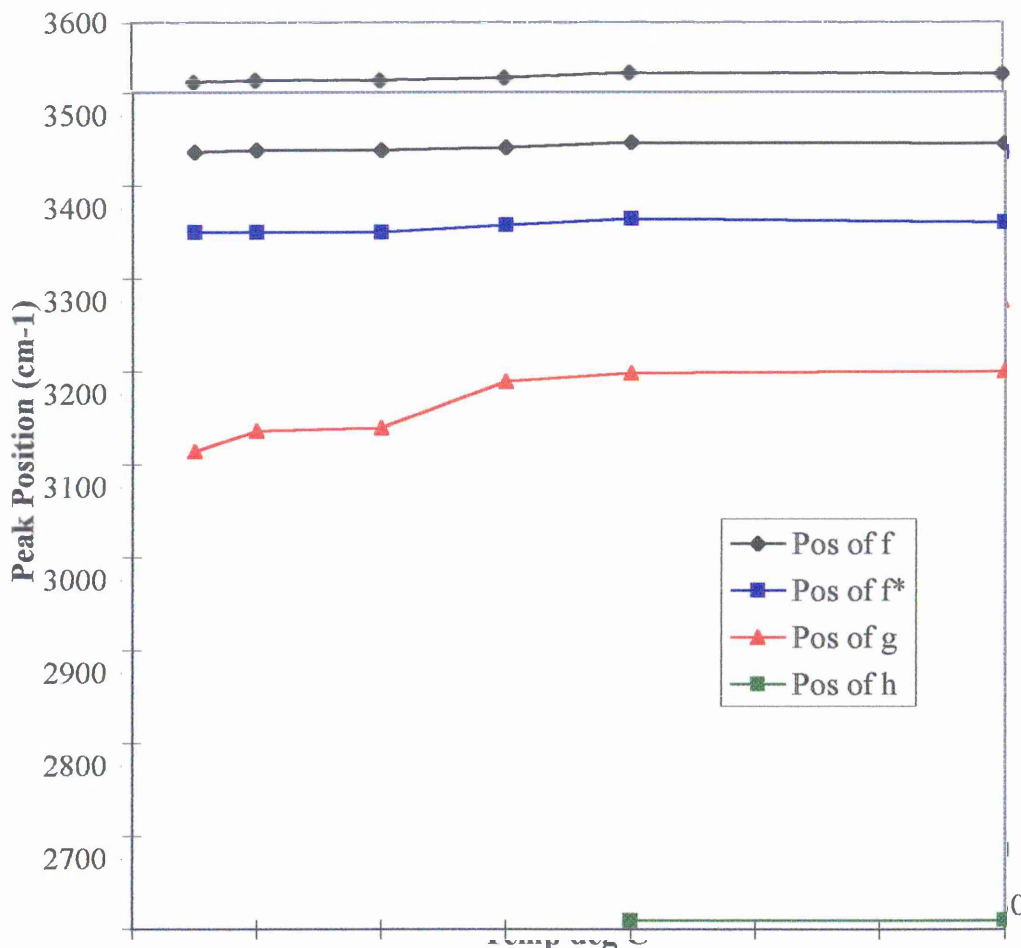
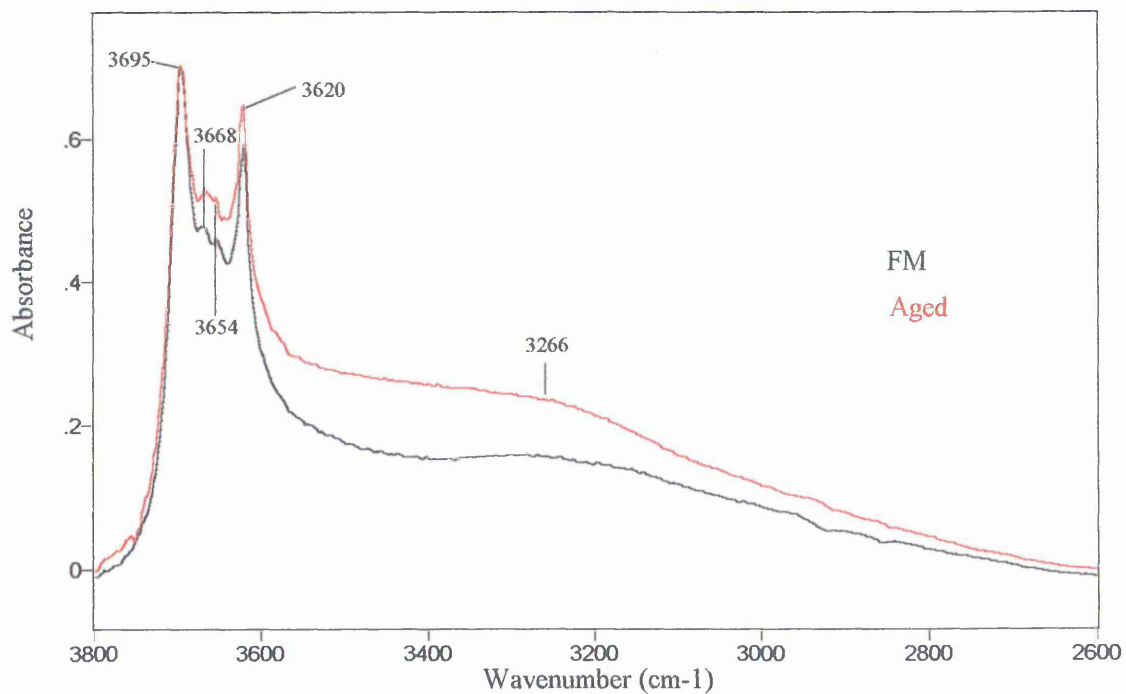


Figure 2.72 shows that the positions of f, f* and h remained constant throughout the temperature range of study. The frequency shift (of approximately 40 cm^{-1}) of band g may suggest the existence of two bands (as for the FM sample). However, the thermal behaviour of this band does not give conclusive evidence of the existence of two readily distinguishable, discrete bands. The shift is due to the “weakening” of the more strongly held water species as temperature increased. Thus, the band shifted from lower to higher frequency. As expected, the frequency of band h did not alter significantly after heating.

2.3.1.2 10 minute milled kaolins. The 3800-2600 cm^{-1} region.

Figure 2.73 10 minute freshly milled and aged kaolins.



As for the 3 minute milled kaolin sample, there was an overall increase in the amount of surface water present after ageing of the 10 minute sample. Again, there seems to be a more dramatic increase in the amount of less strongly hydrogen bonded hydroxyl species.

Figure 2.74 10 minute aged kaolin. The 3800-2600 cm^{-1} region. Room temp. curve fit.

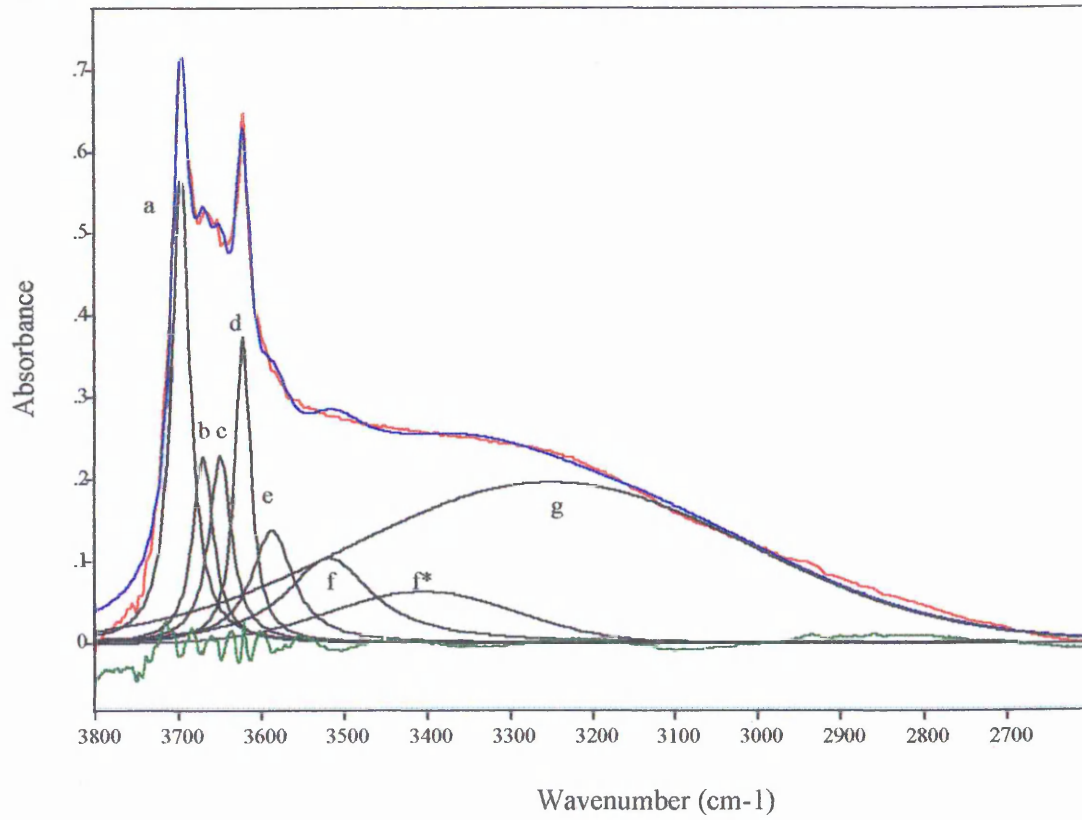


Figure 2.75 10 minute aged kaolin. The 3800-2600 cm^{-1} region. 150°C curve fit.

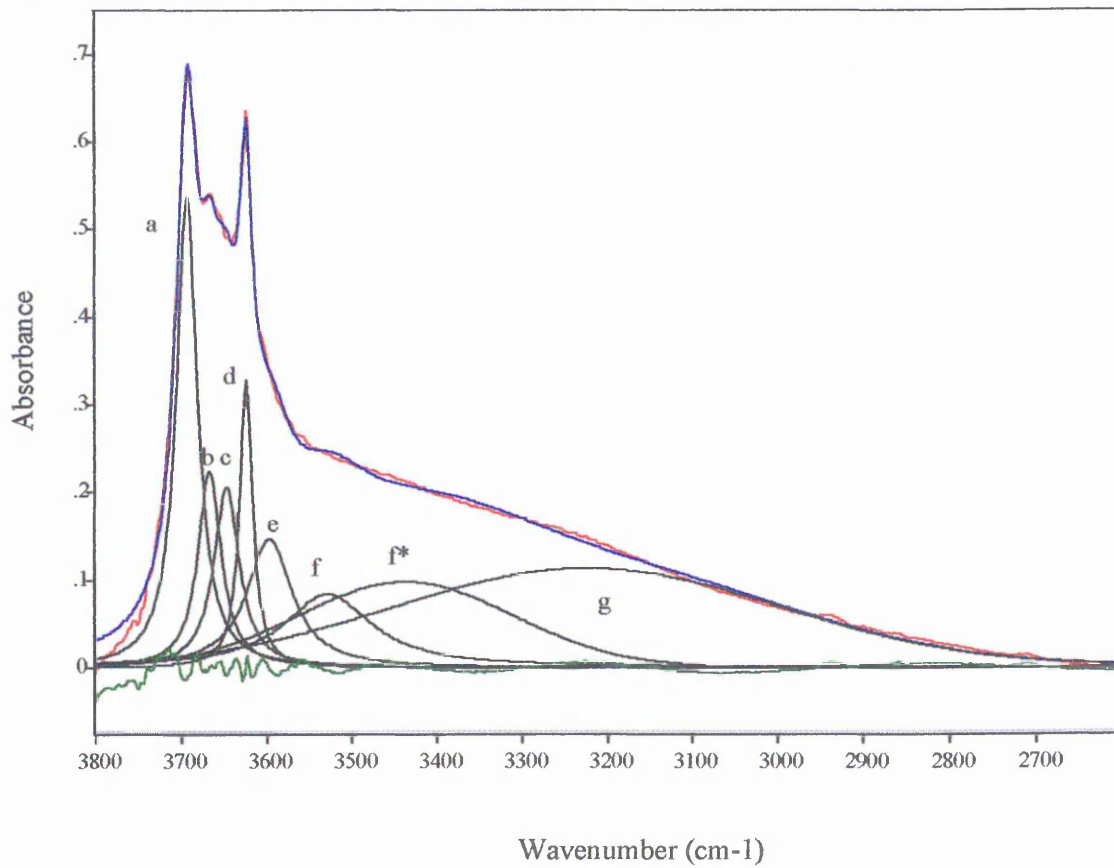
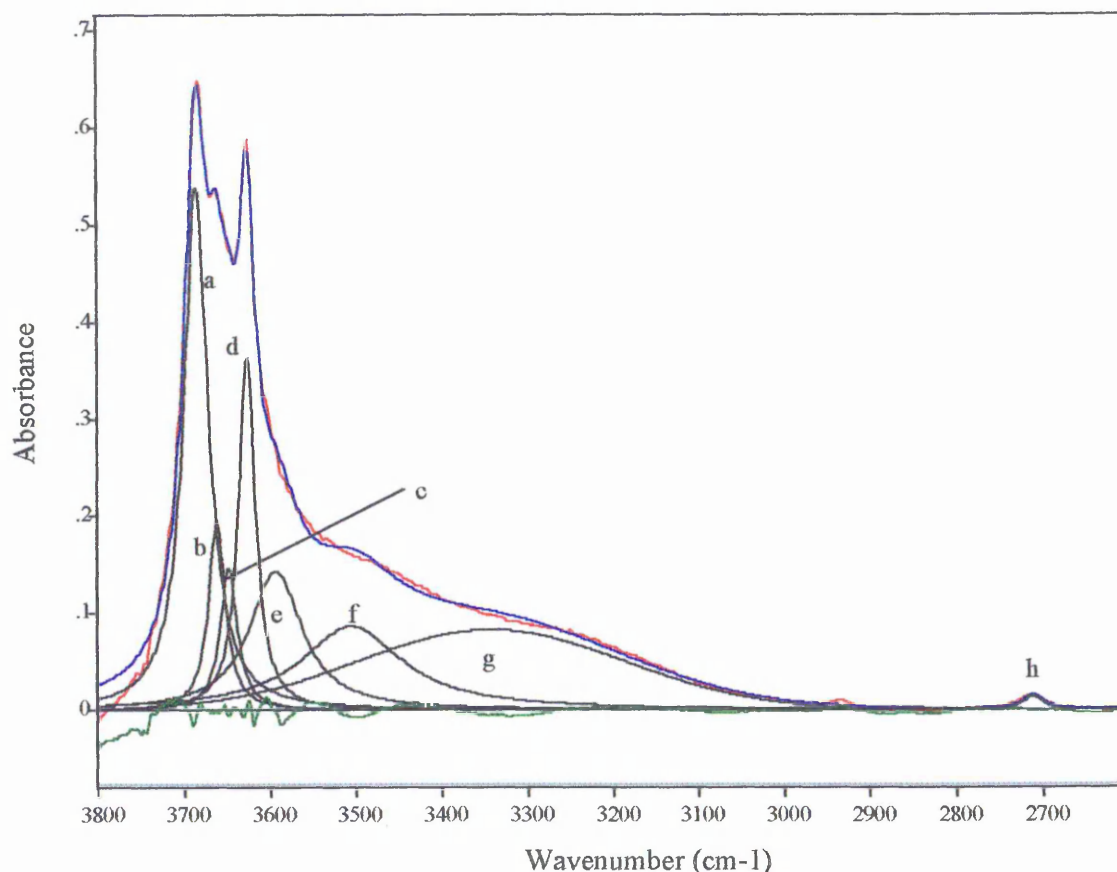


Figure 2.76 10 minute aged kaolin. The 3800-2600 cm^{-1} region. 350°C curve fit.



The figure above shows that there was an overall increase in the amount of surface water at room temperature compared with the FM sample (Figure 2.36). Interestingly, here too (as for the 3 minute milled aged sample) an additional band (f^*) has become necessary for a good mathematical fit. This band is at a similar frequency to the additional band in the aged 3 minute milled sample, and in the present case it is also attributed to less strongly hydrogen bonded water. It appears to be less intense than band f^* in the 3 minute aged sample. However, this is very unlikely, since the shape of the room temperature spectrum suggests a very intense band at this frequency. The apparently low intensity can be accounted for, since much of the actual area of band f^* has been masked by the “wings” of the very intense band g. Band g has become more intense compared with the same band in the FM sample.

Figure 2.75 (150 °C) shows that the aged 10 minute milled spectrum differs significantly from the FM sample (Figure 2.37). The water modes are still very significant, but band g has apparently shifted towards higher wavenumber in the aged sample (whereas in the FM sample, band g(i) at around 3200 cm^{-1} had all but disappeared). The persistence of

band g (comparable with band g(i) in the FM sample) corroborates the room temperature evidence that after ageing there is a greater concentration of more weakly hydrogen bonded water (i.e. higher wavenumber) than in the FM sample. Band f* appeared to increase in intensity. The absolute intensity of this band is more likely to be accurate than the room temperature fit, because the intensity of the water band g has decreased, therefore the interference of this large band present at room temperature has been significantly reduced.

In the 350 °C spectrum (Figure 2.75), there is still some intensity due to the component f* present, but it was not possible to distinguish between it and f therefore, only band f was fitted. For this reason, band f appears to be of greater intensity than expected in Figure 2.76. A very interesting feature of this spectrum is the absence of a band at approximately 3040 cm⁻¹ (i.e. the frequency of band g(ii) in the 10 minute FM sample (Figure 2.38)). This suggests that the previously very strongly hydrogen bonded water in the FM sample has been removed by ageing - or more likely the bonding has become weakened over time. This less strongly hydrogen bonded water (compared with the FM sample) still persists at 350 °C and is represented spectrally by band g , centring at approximately 3320 cm⁻¹.

Figure 2.77 10 minute aged kaolin. Change in intensity of bands f, f*, g & h.

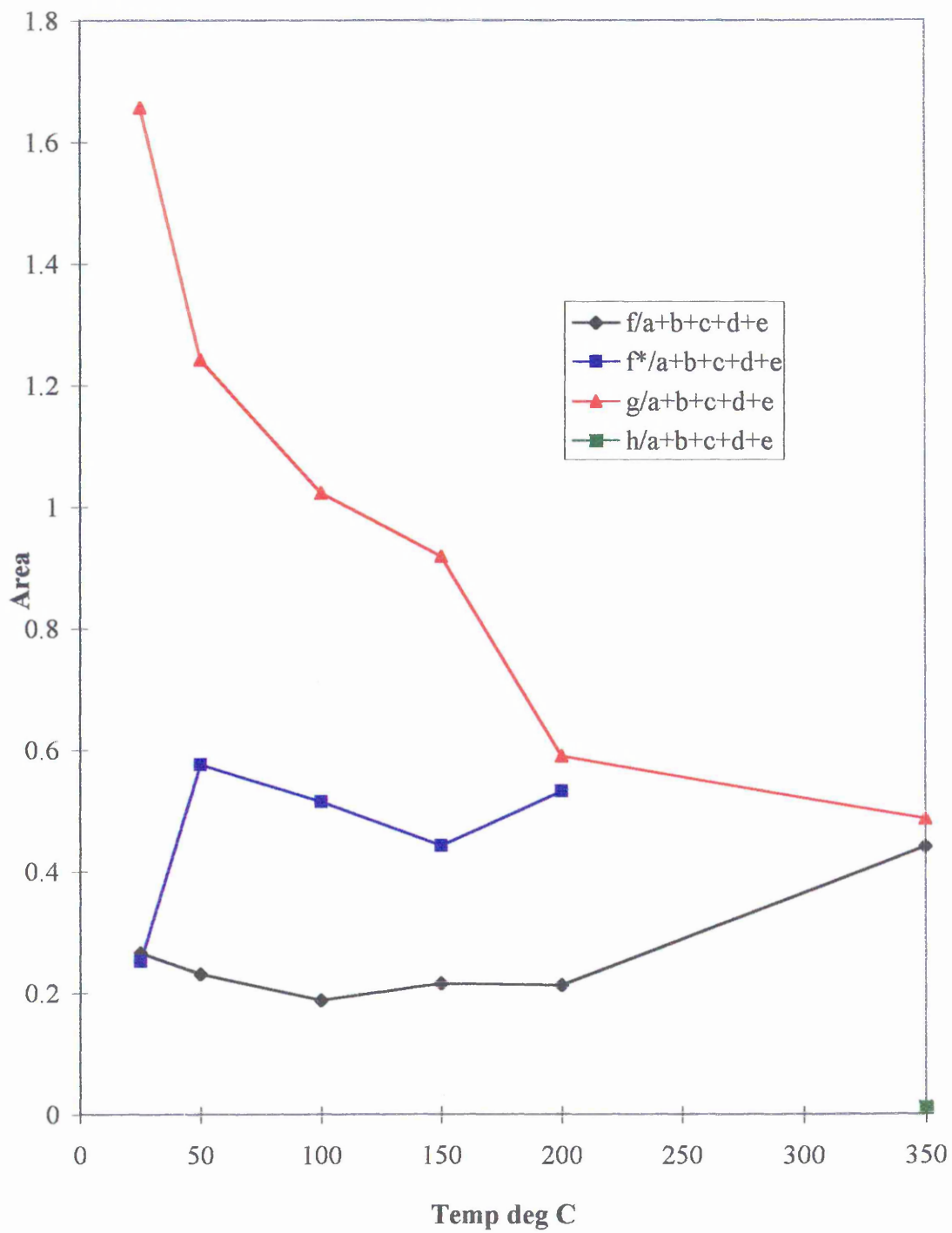


Figure 2.78 10 minute aged kaolin. Change in position of bands f, f*, g and h.

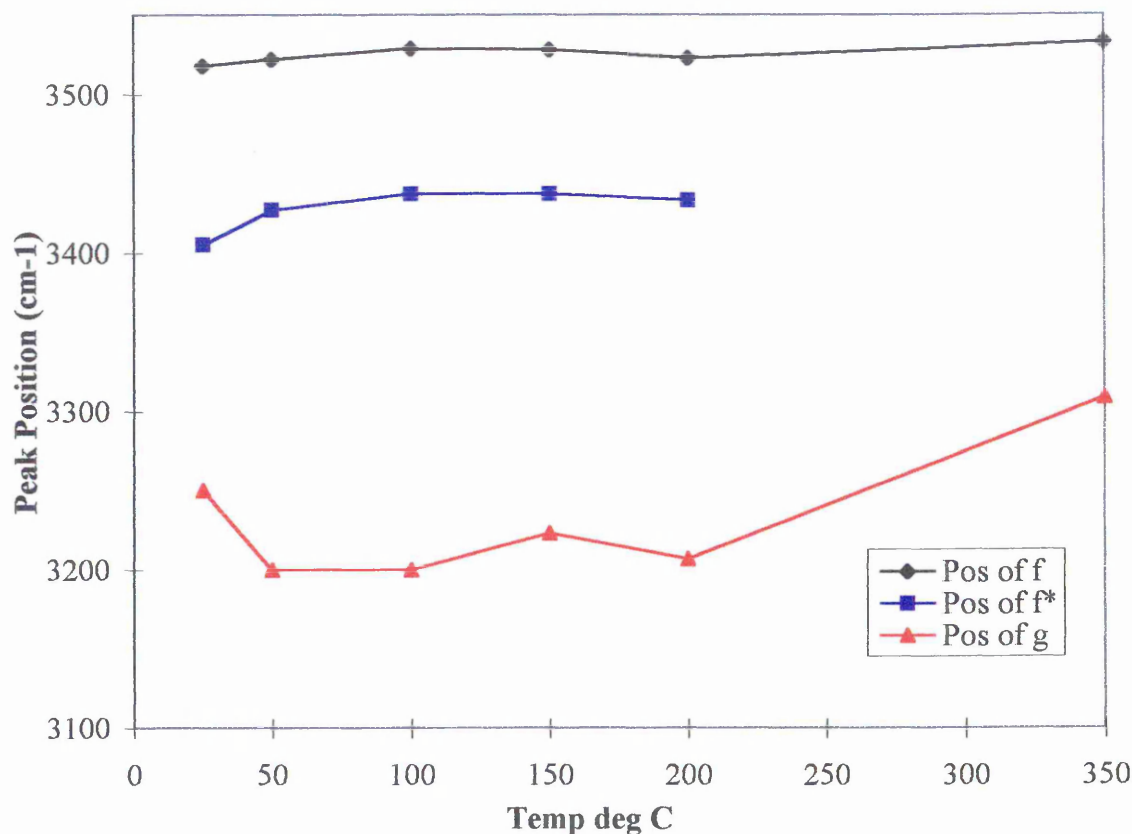


Figure 2.77 shows that the intensity of band f remains constant throughout. The apparent increase in intensity between 200 and 350 °C is due to the overlap of bands f and f*- as described earlier, bands f and f* are represented at 350 °C by band f alone.

At 150 °C, half the initial intensity of band g was removed. The rate of decrease lessened thereafter, with approximately ¼ of the initial intensity still present at 350 °C. Band h was not distinguishable until 350 °C, due to the interference from the larger water bands.

Figure 2.78 indicates that the position of band g remained constant between 50 and 200 °C. The apparent increase at 25 °C is mimicked by the apparent decrease in frequency of band f *at room temperature compared with the 50 °C spectrum. This is because the fitting programme was unable to distinguish between these two bands. Between 200 and 350 °C, band g appears to increase in intensity. This is also a spurious effect, and is due to the fitting programme compensating for the loss of band f*. Indeed, this shift in the

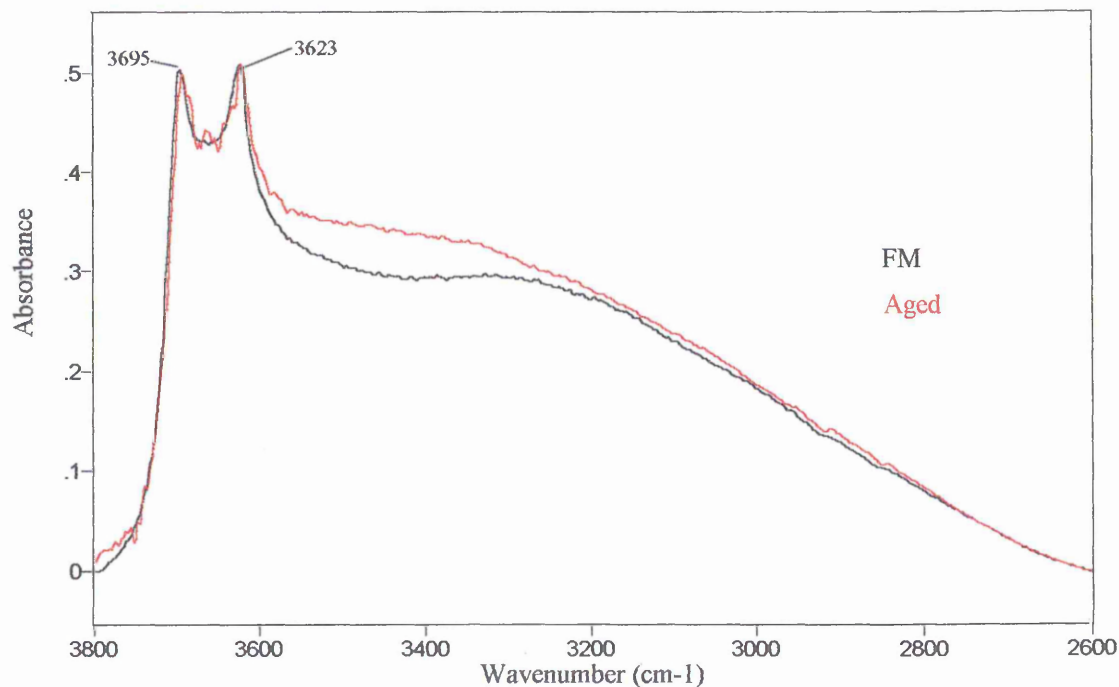
position of band g is another indication that band f* does still have intensity at 350 °C, although it is not discernible by the fitting procedure.

Band h has been omitted from this plot, since it became quantifiable only at 350 °C. Its position was 2713 cm⁻¹.

2.3.1.3 30 minute milled kaolins. The 3800-2600 cm⁻¹ region.

Fits of this sample were not made, but the room temperature spectra are included for completeness. Compared with the 3 and 10 minute milled kaolins, there was comparatively little change in the 30 minute milled spectra before and after ageing. However, there was an increase of intensity between approximately 3300 and 3600 cm⁻¹. Again, this represents an absolute increase in the concentration of more weakly hydrogen bonded water after ageing. The IR data suggests that overall there was a slight increase in the intensity of the water bands after ageing.

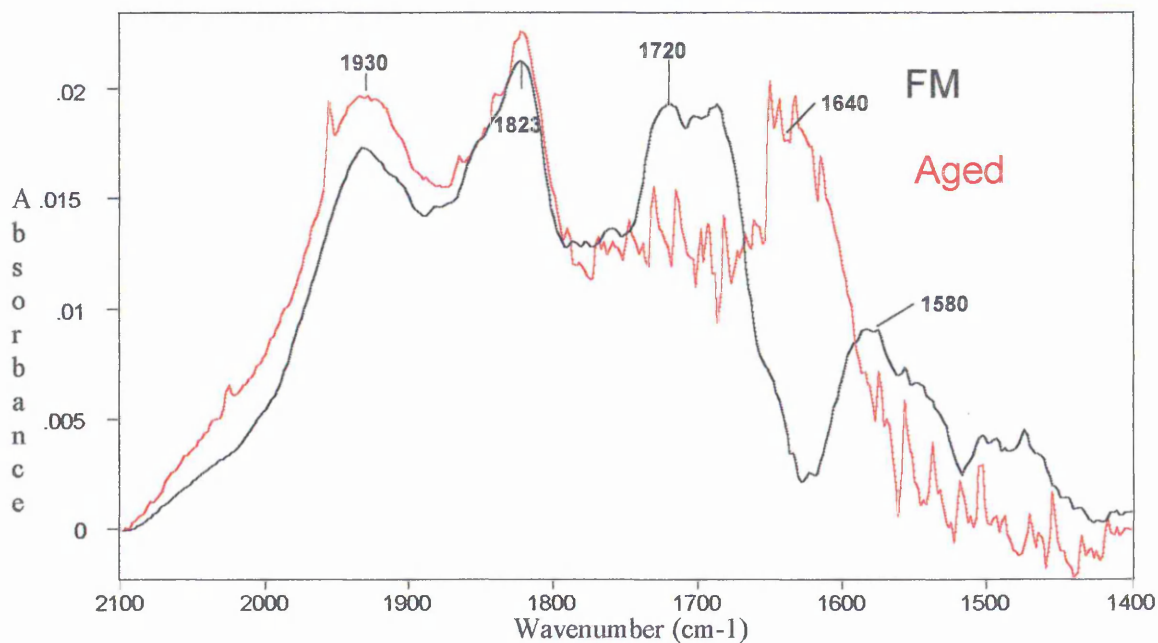
Figure 2.79 30 minute freshly milled and aged kaolins.



2.3.2 Infrared of ball milled kaolins. The 2100-1400 cm^{-1} region.

2.3.2.1 3 minute milled kaolins. The 2100-1400 cm^{-1} region.

Figure 2.80 3 minute freshly milled and aged kaolins The 2100-1400 cm^{-1} region.



Note ⁽ⁱ⁾

Overall, these spectra show a marked change after ageing. There was a shift in the water bending mode from 1670 cm^{-1} to 1640 cm^{-1} (i.e. the adhesive water became less strongly hydrogen bonded). The increased intensity at 1720 / 1670 cm^{-1} present in the FM sample has reduced to baseline level (i.e. the intensity expected of an unmilled sample). The band at 1580 cm^{-1} has also reduced to baseline level, illustrating the removal of the edge intercalated water species.

⁽ⁱ⁾ The aged sample spectra were produced using a sample diluted to 2% in KBr. This decreased concentration resulted in the increased water vapour component seen in the Figure 2.80 above.

Figure 2.81 3 minute kaolin (aged). The 2100-1400 cm^{-1} region. Room temp. curve fit.

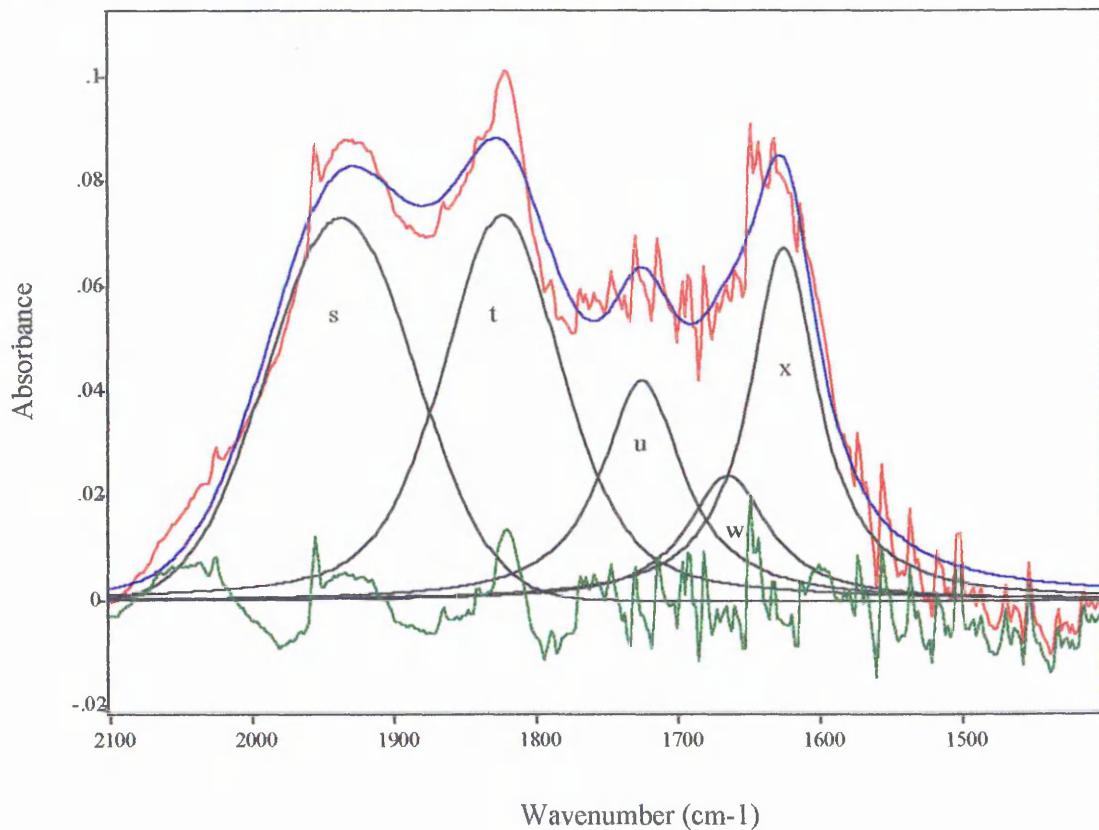


Figure 2.82 3 minute kaolin (aged). The 2100-1400 cm^{-1} region. 150 °C curve fit.

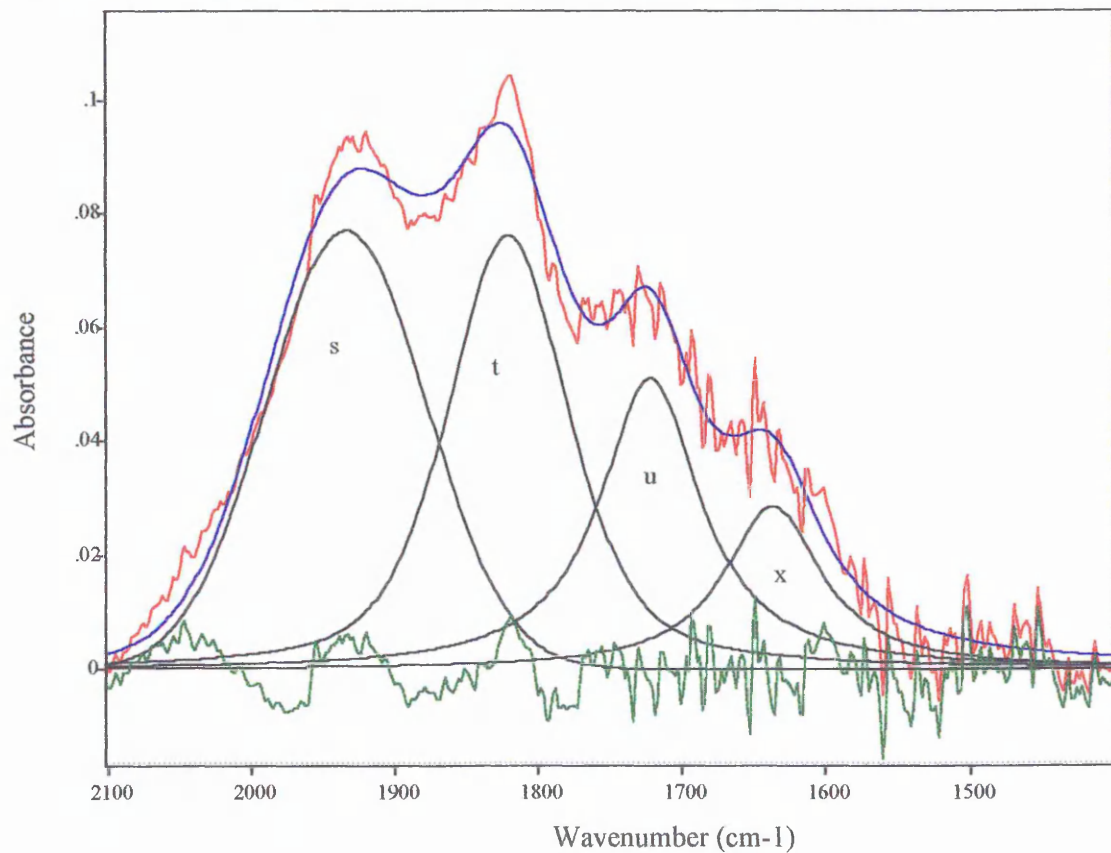
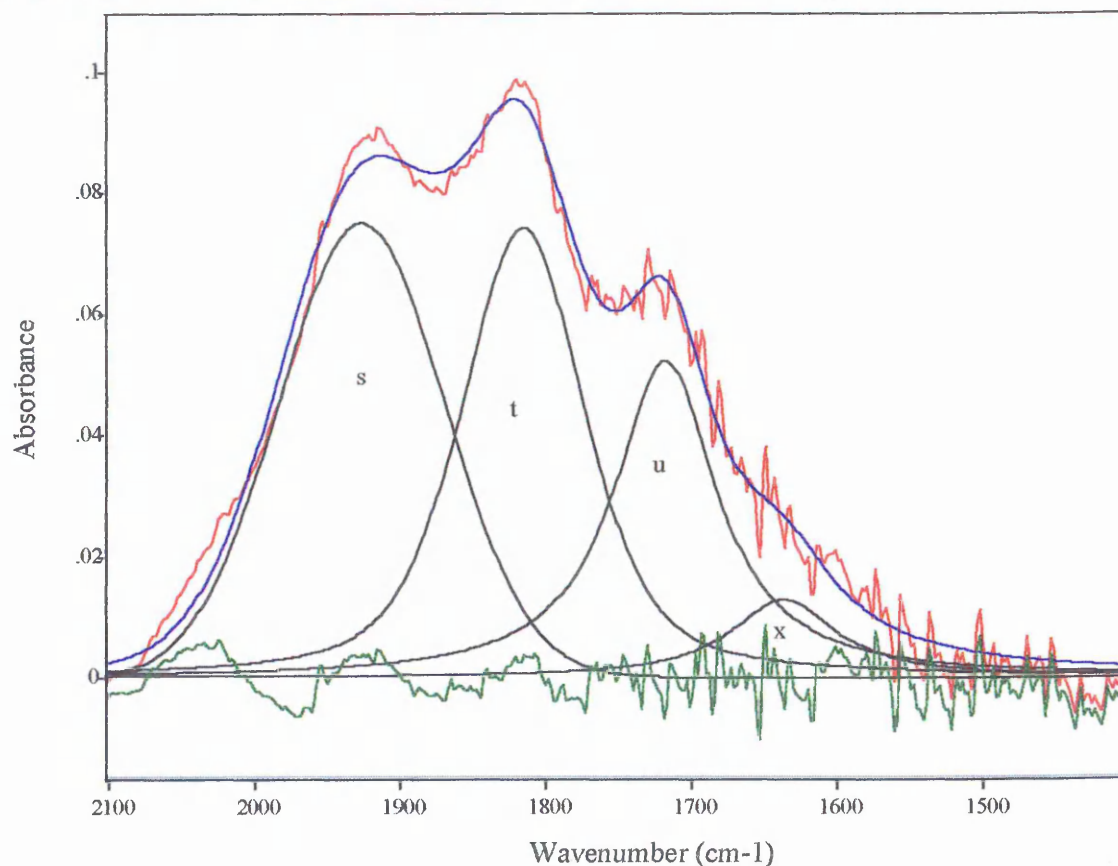


Figure 2.83 3 minute kaolin (aged). The 2100-1400 cm^{-1} region. 350°C curve fit.



At room temperature, (Figure 2.80), band w decreased considerably compared with the FM sample. In the aged sample band x (at 1630 cm^{-1}) was present, whereas it was absent in the FM sample. Band r (at 1580 cm^{-1}) in the FM sample was clearly present at room temperature, however, after ageing it was reduced to baseline levels. It was still present after ageing, but was masked by the very intense feature x.

The fit of the $150 \text{ }^\circ\text{C}$ spectrum shows that band w was completely removed. However, it is probable that there was a small contribution from this band which has become incorporated into band x. The intensity of band x also decreased compared with the room temperature fit.

By $350 \text{ }^\circ\text{C}$ band x decreased further, but was still clearly present. The intensity of this band is considerably lower than the water bands present in the FM sample at $350 \text{ }^\circ\text{C}$.

Figure 2.84 3 minute kaolin (aged) The change in intensity of bands w and x.

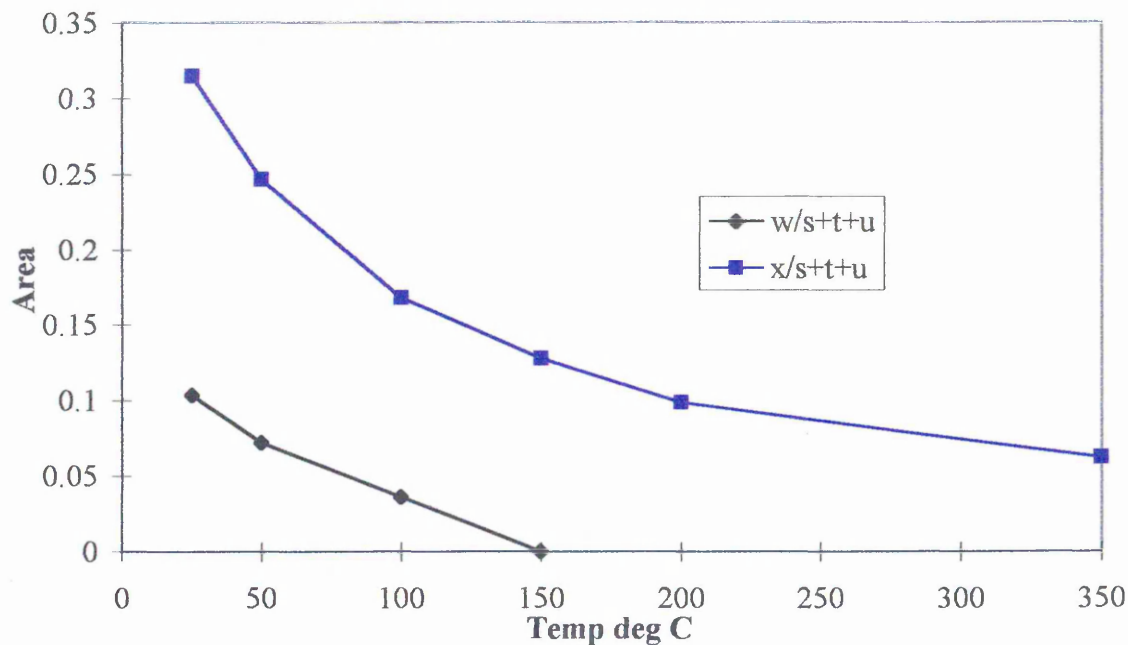
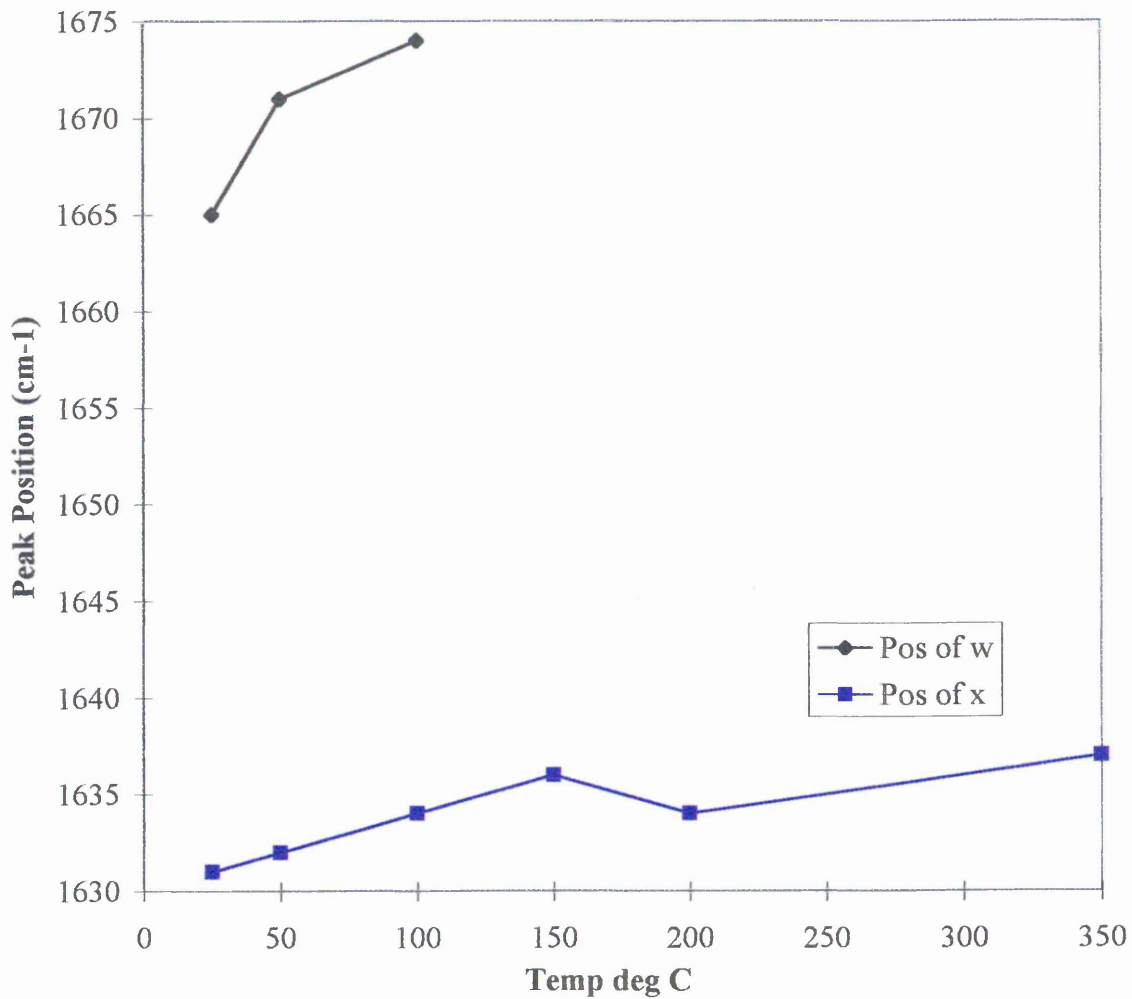


Figure 2.84 shows that band x decrease in intensity rapidly initially, with $\frac{1}{2}$ of the initial intensity being removed by c 100 °C. Thereafter, the rate decreased. There was still considerable intensity present at this frequency at 350 °C. Band w (of relatively stronger hydrogen bonding compared with band x) diminished in intensity rapidly, with a decrease of 50 % after heating to 50 °C. It was no longer distinguishable by 150 °C. It appears that the more strongly hydrogen bonded species “converted” to more weakly bonded species as heating progressed.

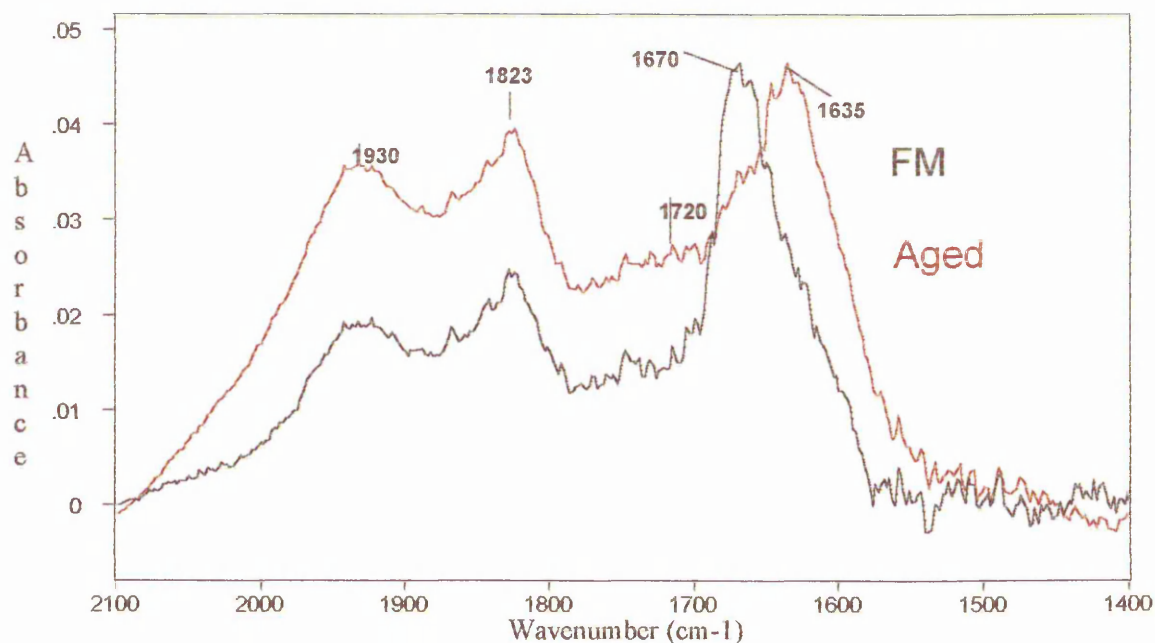
Figure 2.85 3 minute kaolin (aged) The change in position of bands w and x.



Both water bending modes varied marginally in frequency by approximately $\pm 5 \text{ cm}^{-1}$. The mean position of band w was 1670 cm^{-1} , and the mean of the position of band x was 1635 cm^{-1} .

2.3.2.2 10 minute milled kaolins. The 2100-1400 cm^{-1} region.

Figure 2.86 10 minute freshly milled and aged kaolins.



It was not possible to normalise these spectra in the usual way. The 1930, 1823 and 1720 cm^{-1} bands are in fact the same intensity. There is, however, a vast difference in the overall intensity of the water bending modes- the aged sample having vastly reduced more strongly hydrogen bonded surface water. This could be an effect of the breakdown of the agglomerates produced by milling, thus allowing the water trapped therein to be released. There is also a shift in the water bands towards lower wavenumber. The initially strong 1670 cm^{-1} (FM) band has significantly reduced and become smaller than the intense 1635 cm^{-1} (aged) band.

Figure 2.87 10 minute kaolin (aged). The 2100-1400 cm^{-1} region. Room temp. curve fit.

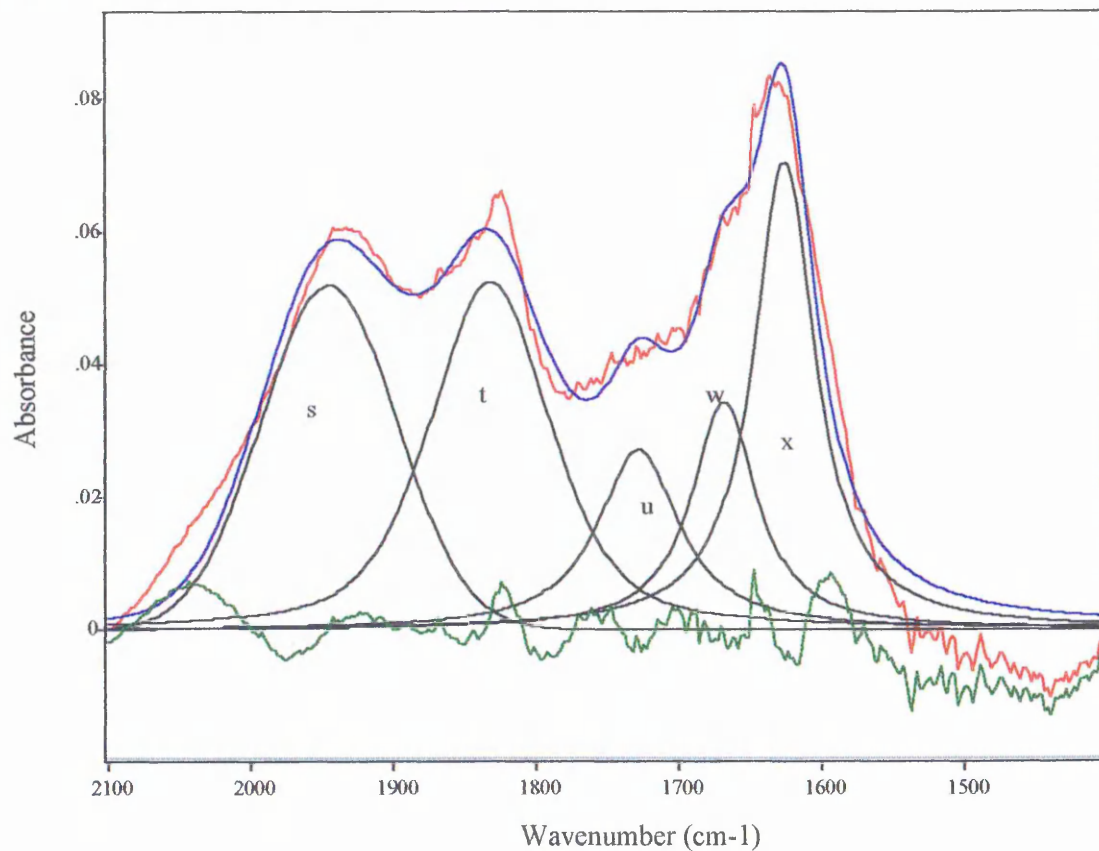


Figure 2.88 10 minute kaolin (aged). The 2100-1400 cm^{-1} region. 150 $^{\circ}\text{C}$ curve fit.

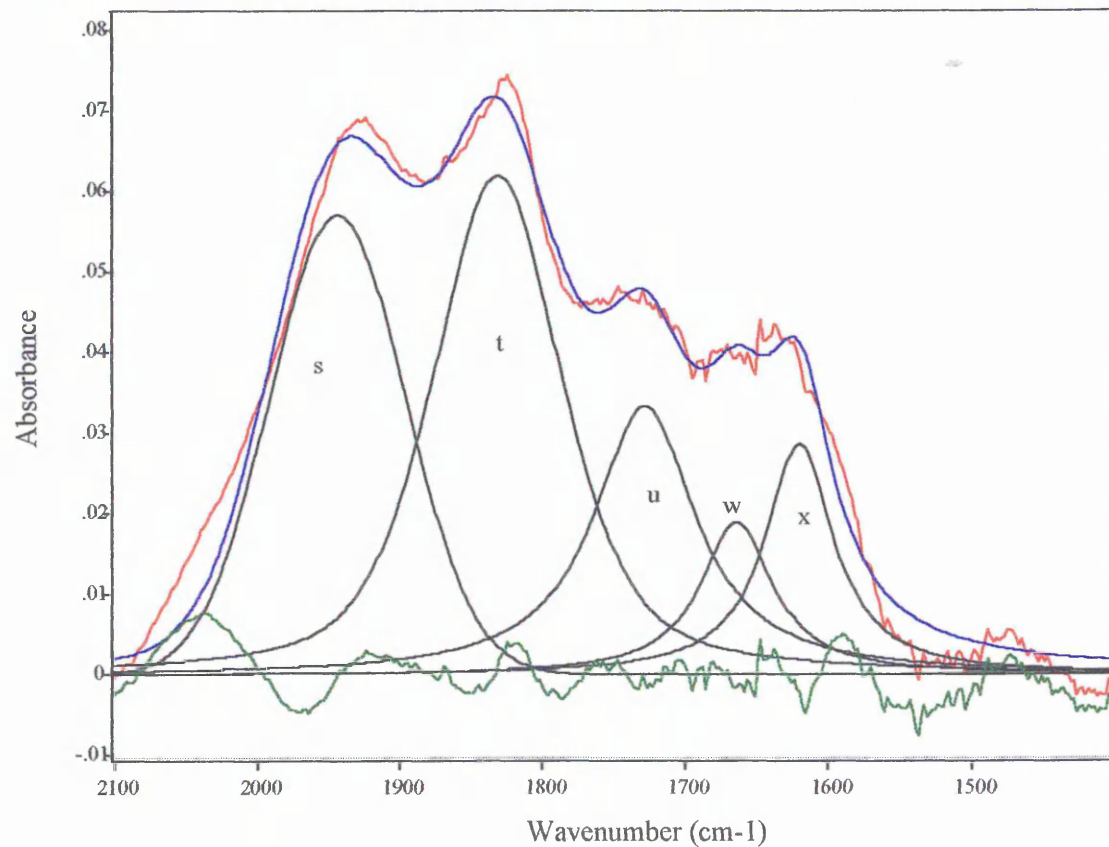


Figure 2.89 10 minute kaolin (aged). The 2100-1400 cm^{-1} region. 350 °C curve fit.

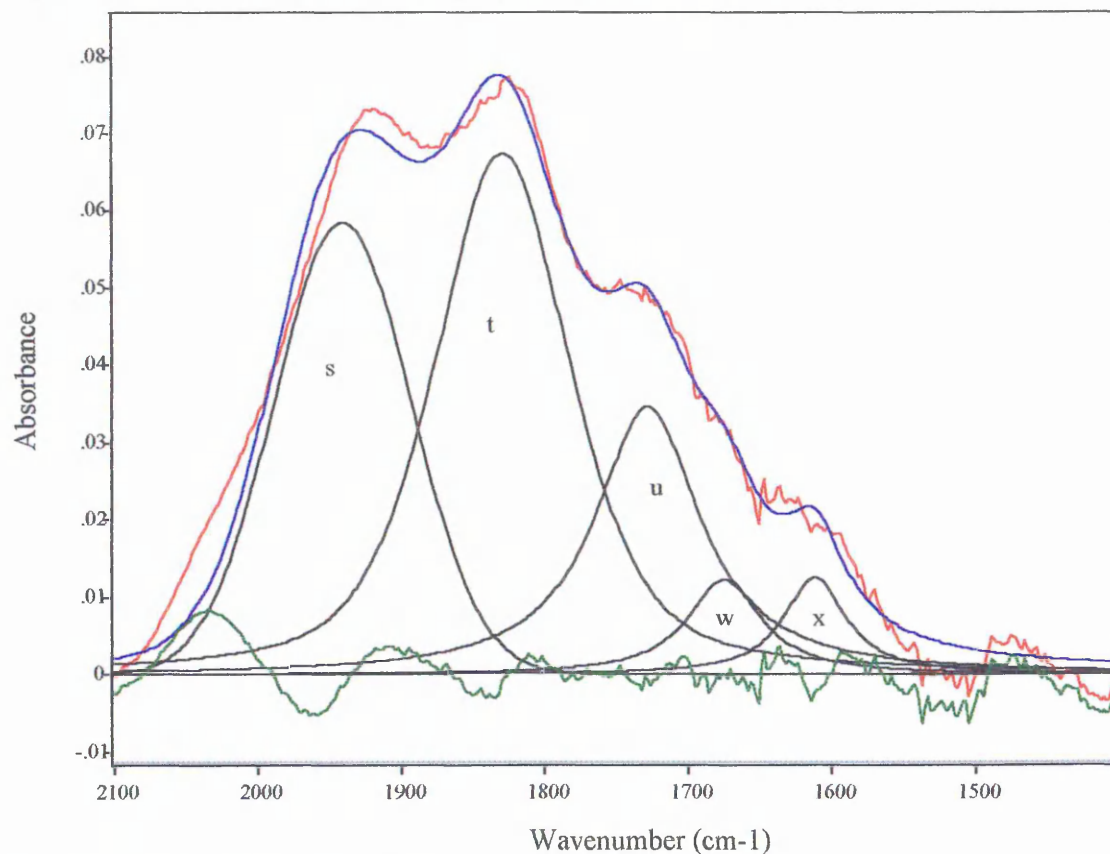


Figure 2.87 illustrates that after ageing, band x has much greater intensity than band w. In the FM sample, the converse was true (see Figure 2.59), with band w having significantly greater intensity than the lower frequency band x.

At 150 °C, (Figure 2.88) the intensity of both water modes w and x have reduced significantly. However, band x has been removed preferentially. This is predicted by theory, since in the bending region more loosely hydrogen bonded water presents at lower frequency (indeed, in the aged 3 minute milled sample, $\frac{1}{2}$ of the initial intensity was removed by 100 °C). Subsequent heating to 350 °C (Figure 2.89) leads to the further reduction in intensity of both water bands. Compared with the FM sample at the same temperature (Figure 2.61), band w (in the aged sample) is of lower relative intensity. Band x is of similar intensity in both the aged and FM samples.

Figure 2.90 10 minute kaolin (aged). The change in intensity of bands w & x.

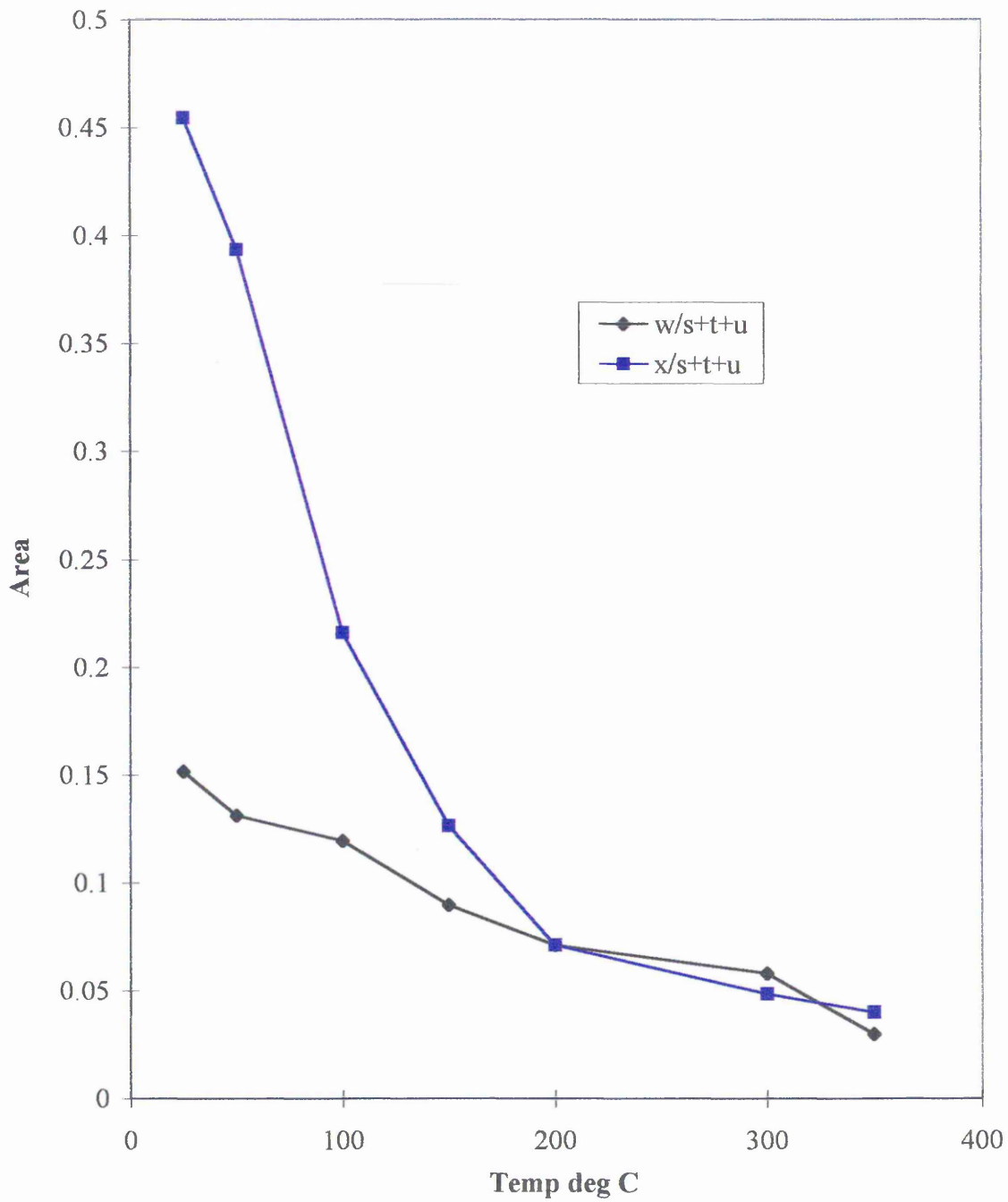


Figure 2.91 10 minute kaolin (aged). The change in position of bands w & x.

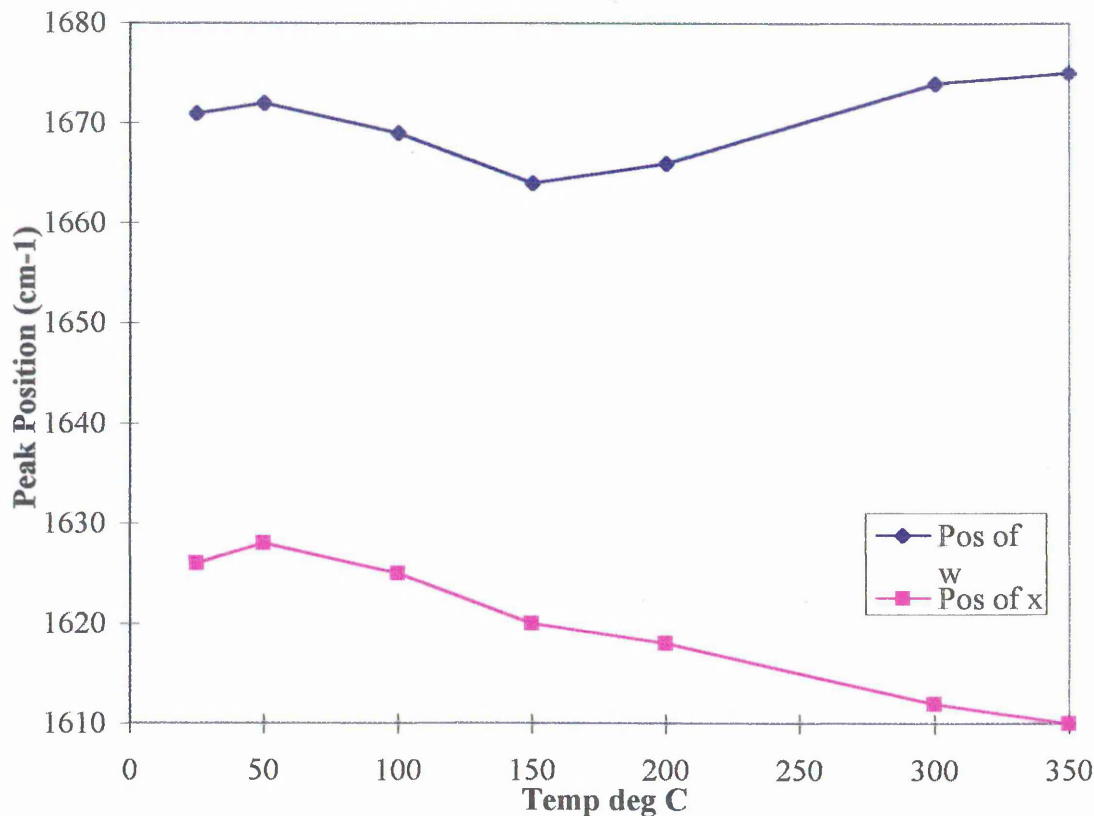
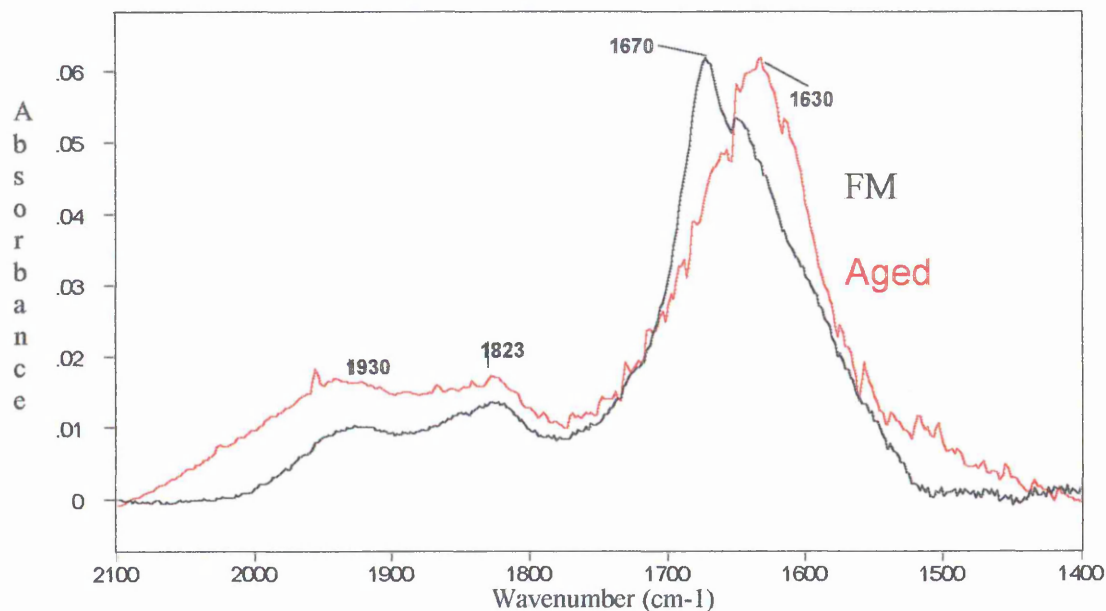


Figure 2.90 shows that band x decreased in intensity by 50 % over the first 100 °C (as was the case in the aged 3 minute milled sample). The intensity of band w decreased less rapidly, with 50 % being removed at approximately 200 °C. This is expected, since band w represents more strongly hydrogen bonded water than band x. Both bands retain quantifiable intensity up to 350 °C.

Figure 2.91 shows that there was an apparent variation in the positions of both bands w and x. It is likely that the apparent fluctuations in the most part are due to the inability of the fitting package to distinguish between the frequencies of the two bands at similar frequencies.

2.3.2.3 30 minute milled kaolins. The 2100-1400 cm^{-1} region.

Figure 2.92 30 minute freshly milled and aged kaolins.

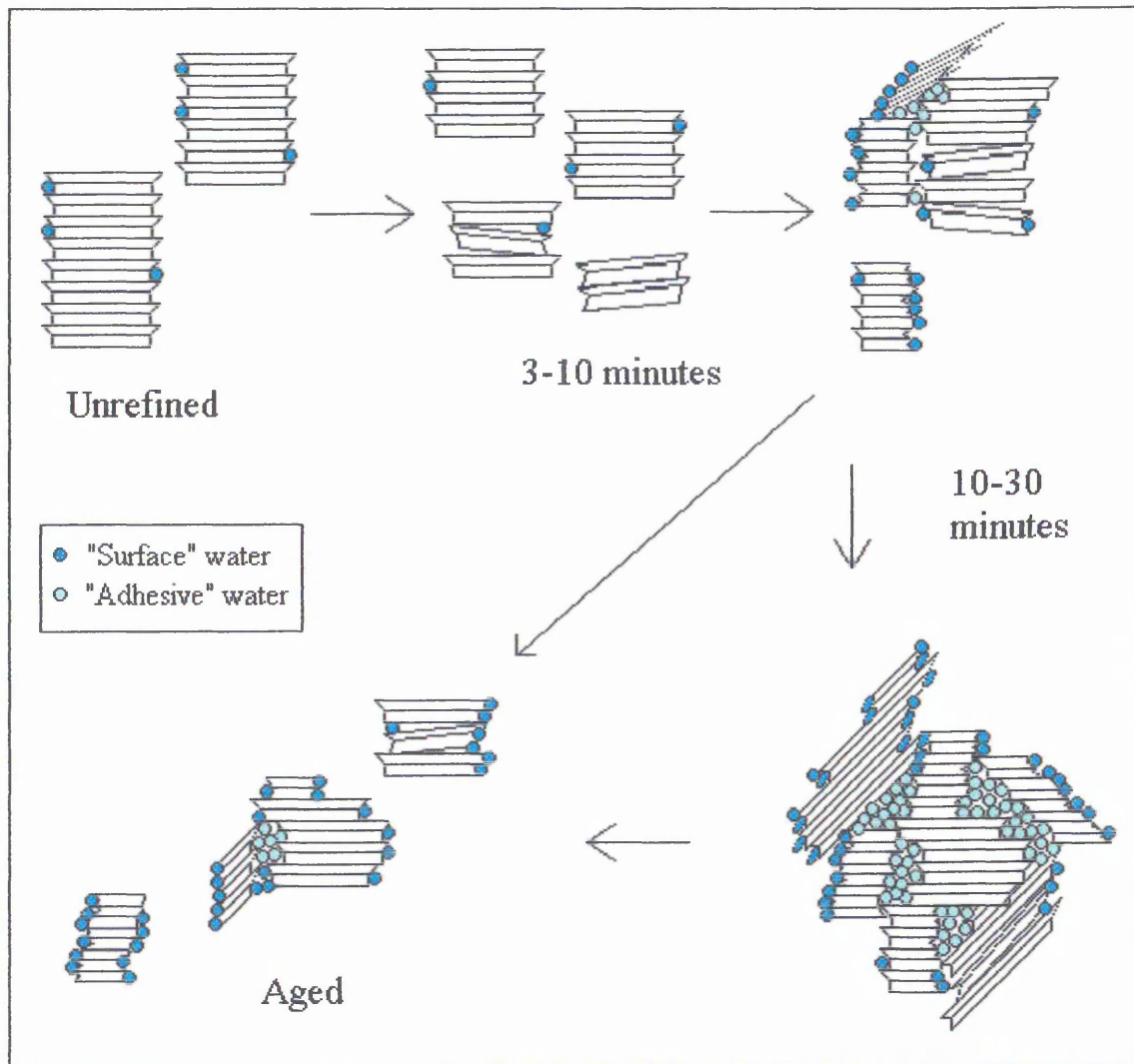


Although curve fitting could not be carried out on this data, the spectra above show marked differences before and after ageing. It was not possible to normalise the spectra above, but the reader is reminded that the 1930 and 1823 cm^{-1} bands are in fact of equal intensity in both aged and freshly milled spectra. Like the 10 minute milled sample, there is a shift to lower wavenumber. The aged sample now presents a strong 1630 cm^{-1} band and a relatively weak 1670 cm^{-1} mode. The converse was true for the FM sample. There was an overall loss in the intensity of water bands after ageing .

2.4 Conclusions.

As milling time increased, so did the amount of surface-sorbed water. It is possible to characterise this water in both the OH stretching and bending regions as strongly hydrogen bonded, moderately strongly hydrogen bonded and weakly hydrogen bonded.

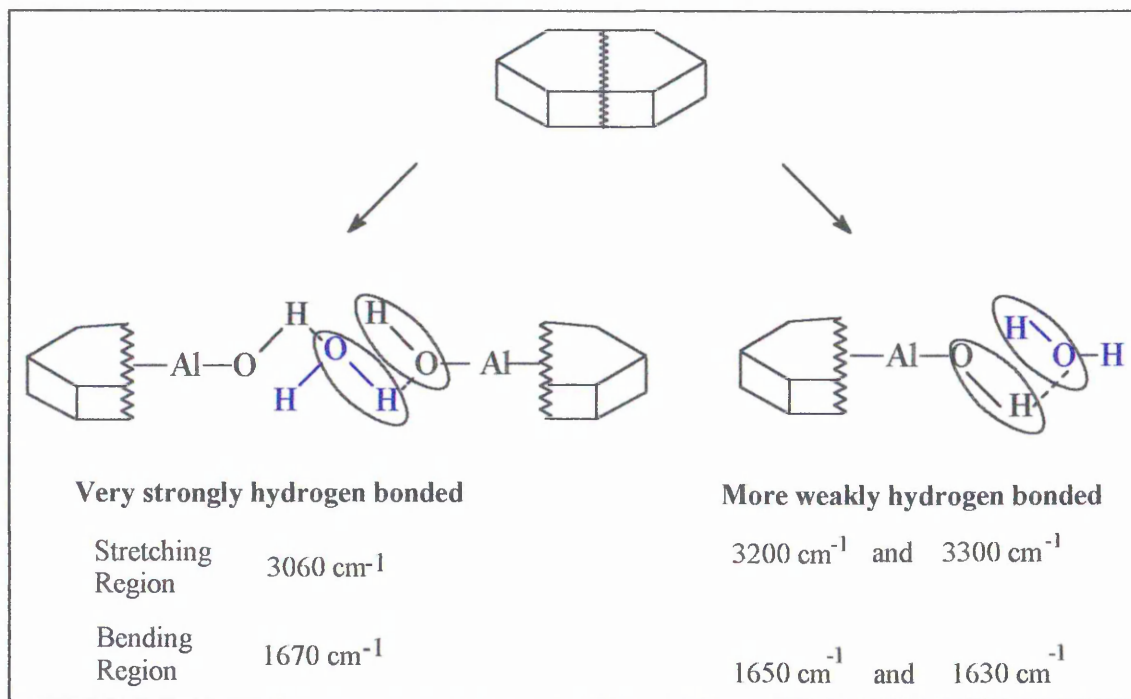
Figure 2.93 Schematic of the effects of milling and ageing.



The simplified figure above illustrates the overall effects of the milling and ageing processes. SEM studies have shown that at all times there is a mixture of damaged and undamaged kaolin particles. Therefore, it is not possible to draw a distinct line between the condition of the mineral at any specific milling time, since all data collected are a composite response of a number of different phases. However, the overall effects of

milling are discussed below (in conjunction with Figure 2.93 and Figure 2.94), according to the condition of the majority of the particles.

Figure 2.94 Schematic of water bonding with the characteristic IR frequencies.



In the stretching region at room temperature, the most obvious effect of milling is an increase in the area of the broad water bands in the 3600-2600 cm^{-1} region. Band fitting has allowed the identification of types of water of differing hydrogen bonding characteristics. At room temperature, there is an overall increase in the intensity of the band representing the more strongly hydrogen bonded water at 3200-3300 cm^{-1} (band g(i)). The water bands in this region are very broad, and it is difficult to draw conclusions from this spectral region alone. For this reason, the data must be considered in conjunction with those in the bending region.

In the bending region at room temperature, there is, perhaps a more obvious alteration in the relative concentrations of the different types of water present, with unmilled kaolin water frequency approximately 1650 cm^{-1} , (band v) the 3 minute milled kaolin water bending mode at 1670 cm^{-1} (w), 10 minute milled kaolin modes at 1670 cm^{-1} and 1630 cm^{-1} (x) and the 30 minute milled kaolin water bending frequencies at 1630, 1650 and 1670 cm^{-1} .

The unmilled (i.e. unrefined) mineral has a large number of kaolin stacks. There is a very small amount of water adsorbed to the outer surfaces (illustrated most clearly by the bending mode at c 1660 cm^{-1} (v)). However, there are very few exposed broken edge sites, and this results in a low concentration of sorbed water.

The shift in frequency of the water bending modes in this work from 1650 to 1670 or 1630 cm^{-1} and the corresponding shifts in the water modes in the $3500\text{-}2600\text{ cm}^{-1}$ region may be indicative of prototropy, whereby upon grinding, protons migrate from their original positions and may approach the oxygens shared between the tetrahedral and octahedral sheets or begin to interact with other hydroxyls to, thus forming new associations.

After moderate milling, (i.e. 3-10 minutes), the mineral stacks begin to delaminate. Some of the stacks fracture along the vertical axis, thus exposing an increased number of broken edge sites. This leads to an increase in the total amount of surface sorbed water, specifically an increase in the more weakly hydrogen bonded (surface sorbed) water at 1630 cm^{-1} . Aggregate formation and slight expansion of the kaolin layers begins and this leads to sites between the mineral stacks (either broken or complete) where water becomes trapped (“adhesive water”) or partially intercalated. It is thought that the water trapped between the agglomerates is in some way responsible for binding the mineral aggregates together. It is represented spectrally by a bending mode at 1670 cm^{-1} corresponding to relatively strongly hydrogen bonded water. It is also likely that band r (at 1580 cm^{-1}) represents a small amount of very loosely hydrogen bonded water trapped within the aggregates or between the slightly expanded edges of the mineral during the primary stages of milling. Extended milling (10-30 minutes) leads to further breakdown of the kaolin stacks and an increase in the size of the agglomerates. There is therefore an overall increase in the total adsorbed water species - both on the outer surfaces at exposed broken edge sites and the species trapped within the agglomerate network.

As milling time increases, the overall strength of hydrogen bonding increases, with all types of water being held until higher temperatures. Upon increasing the temperature of the samples, the water types are lost at different rates. In the bending region, weakly

hydrogen bonded water is lost at lower temperatures, followed by moderately strongly hydrogen bonded water, and finally strongly hydrogen bonded water.

For the 3 minute milled kaolin it can be postulated that band g(i) (OH stretching region at approximately 3200 cm^{-1}) and band w (OH bending region at approximately 1670 cm^{-1}) both represent very strongly hydrogen bonded water species (relative to the water species present in the unmilled sample), since they exhibit very similar thermal characteristics and are at comparable extremes of the water bending and stretching regions. (See the plots showing the change in intensity of bands with temperature in Figure 2.33 (band g(i)) and Figure 2.56 (band w).

In the 10 minute milled kaolin sample, bands g(i) at 3150 cm^{-1} and x (1630 cm^{-1}) both represent similar types of more loosely hydrogen bonded water, which are lost at relatively low temperature.

Band g(ii) at 3050 cm^{-1} and band w, at 1670 cm^{-1} are both thought to represent similar species of very strongly hydrogen bonded (adhesive) waters. Although not discussed with reference to spectroscopy, Kirsh⁴⁵ commented that clay particles could be strongly bonded together by oriented layers of water. It is not known if the waters in the kaolin system in the present work are oriented. However, they are present throughout the temperature range of study and remain very intense until greatly elevated temperature.

It can be further deduced that band f in the stretching region (c 3550 cm^{-1}) and band r in the bending region (c 1580 cm^{-1}) both represent very weakly hydrogen bonded water, since their thermal behaviour in the 3 and 10 minute milled samples are very similar (for example, see the plots of the change in intensity of bands with temperature in Figure 2.56 (band r) and Figure 2.33 (band f). This hypothesis is, however, not supported by the unmilled sample data, where band r is not obvious, whilst band f is of similar significance to that in the milled samples. At this time a suitable explanation for this anomaly has not been deduced. It should once again be noted that it would not be correct to assume that only one type of water is monitored by the behaviour of any one band. There is a great deal of overlap between the intensities and frequencies of adjacent bands, and as a result, only semi quantitative trends can be described.

After ageing, DRIFT spectroscopy indicates that there is an increase in the intensity of the more weakly hydrogen bonded water species. In the OH stretching region the precise discrepancies are difficult to distinguish. However, there is generally an obvious increase in the intensity of the more weakly hydrogen bonded water in the OH bending region. From the bending region spectra it can be seen that there is a decrease in the relative intensity of the “adhesive” water bands at 1670 cm^{-1} with respect to the surface water bands at 1630 cm^{-1} (for example, compare the 10 minute FM and aged room temperature sample spectra in Figure 2.59 and Figure 2.87 respectively. There is now relatively more of the weakly hydrogen bonded surface bound water at 1630 cm^{-1} compared with the more strongly hydrogen bonded water at 1670 cm^{-1} . This implies that the agglomerates may be breaking down, with a concurrent release of the “trapped”, adhesive water. Although not carried out in the present work, this hypothesis may be confirmed by SEM studies. These events may have wide ranging implications in the minerals processing industry, where samples are often milled and stored for weeks, months or even years before use.

2.4.1 References

- ¹ Aglietti EF, Porto Lopez JM & Pereira E (1986). Mechanochemical effects in kaolinite grinding. I. Textural and physicochemical aspects. *International Journal of Mineral Processing* **16**, 125-133.
- ² La Iglesia A & Aznar AJ (1996). Crystallinity variations in kaolinite induced by grinding and pressure treatments. *Journal of Materials Science* **31**, 4671-4677.
- ³ Aglietti EF, Porto Lopez JM & Pereira E (1986). Mechanochemical effects in kaolinite grinding. II. Structural aspects. *International Journal of Mineral Processing* **16**, 135-146.
- ⁴ Kodama H, Kotlyar LS & Ripmeester JA (1989). Quantification of crystalline and nonsystalline material in ground kaolinite by x-ray powder diffraction, infrared, solid state nuclear magnetic resonance, and chemical-dissolution analyses. *Clays and Clay Minerals* **37**, 4, 364-370.
- ⁵ Michaelian KH, Yariv S & Nasser A (1991). Study of the interactions between caesium bromide and kaolinite by photoacoustic and diffuse reflectance infrared spectroscopy. *Canadian Journal of Chemistry* **69**, 749-754.
- ⁶ Kheifets AS & Lin IJ (1998). Energetic approach to kinetics of batch ball milling. *International Journal of Mineral Processing* **54**, 81-97.
- ⁷ Sondi I, Stubicar M & Pravdic V (1997). Surface properties of ripidolite and beidellite clays modified by high- energy ball milling *Colloids and Surfaces A* **127**, 141-149.
- ⁸ Drief A & Nieto F (1999). The effect of dry grinding on antigorite from Mulhacen, Spain. *Clays and Clay Minerals* **47**, 4, 417-424.
- ⁹ Sposito G, Prost R & Gaultier JP (1983). Infrared spectroscopic study of adsorbed water on reduced - charge Na/Li- montmorillonites. *Clays and Clay Minerals* **31**, 1, 9-16.
- ¹⁰ Johnston CT, Sposito G & Erickson C (1992). Vibrational probe studies of water interactions with montmorillonite. *Clays and Clay Minerals* **40**, 6, 722-730.
- ¹¹ Fu MH, Zhang ZZ & Low PF (1990). Changes in the properties of a montmorillonite-water system during adsorption and desorption of water. *Clays and Clay Minerals* **38**, 5, 485-492.
- ¹² Prost R, Koutit T, Benchara A & Huard E (1998). State and location of water adsorbed on clay minerals:consequences of the hydration and swelling-shrinkage phenomena. *Clays and Clay Minerals* **46**, 2, 117-131.
- ¹³ Hall PL & Astill DM (1989). Adsorption of water by homoionic exchange forms of Wyoming montmorillonite (Swy-1). *Clays and Clay Minerals* **37**, 4, 355-363.
- ¹⁴ Suraj G, Iyer CSP, Rugmini S & Lalithambika M (1997). The effect of micronization on kaolinites and their sorption behaviour. *Applied Clay Science* **12**, 111-130.
- ¹⁵ Frost RL & Johansson U (1998). Combination bands in the infrared spectroscopy of kaolins-a DRIFT spectroscopic study. *Clays and Clay Minerals* **46**, 4, 466-477.

- ¹⁶ Michaelian KH, Friesen W, Yariv S & Nasser A *et al.* (1991). Diffuse reflectance infrared spectra of kaolinite /alkali halide mixtures. Curve fitting in the OH stretching region. *Canadian Journal of Chemistry* **69**, 1786-1790.
- ¹⁷ Johansson U, Holmgren A, Forsling W & Frost R (1998). Isotopic exchange of kaolinite hydroxyl protons: a diffuse reflectance infrared Fourier transform spectroscopy study. *Analyst* **123**, 641-645
- ¹⁸ Conley RF & Althoff AC (1971). *Journal of Colloid and Interface Science* **37**, 1, 186-195.
- ¹⁹ Mendelovici E, Villalbi R, Sagarzazu S & Carias O (1995). The 1640 cm⁻¹ band monitor for the gain and thermal stability of water produced in ground kaolinites. *Clays and Clay Minerals* **30**, 307-313.
- ²⁰ Nguyen TT, Janik Lewis & Raupach M (1991). Diffuse reflectance infrared Fourier transform (DRIFT) spectroscopy in soil studies. *Australian Journal of Soil Research* **29**, 49-67.
- ²¹ Farmer VC & Russell JD (1964). The infrared spectra of layer silicates. *Spectrochimica Acta* **20**, 1149-1173.
- ²² Frost RL (1998). Hydroxyl deformation in kaolins. *Clays and Clay Minerals* **46**, 3, 280-289.
- ²³ Shoval S, Yariv S, Michaelian KH, Boudeulle M & Panczer G (1999). Hydroxyl-stretching bands "A" and "Z" in the Raman and infrared spectra of kaolinites. *Clay Minerals* **34**, 551-563.
- ²⁴ Prost R, Dameme A, Huard E, Driard J & Leydecker JP (1989). Infrared study of structural OH in kaolinite, dickite, nacrite, and poorly crystalline kaolinite at 5 to 600 K. *Clays and Clay Minerals Vol 37* 5 464-468.
- ²⁵ Gábor M, Tóth M, Kristóf & Komáromi-Hiller G (1995). Thermal behaviour and decomposition of intercalated kaolinite. *Clays and Clay Minerals* **43**, 2, 223-228.
- ²⁶ Frost RL & Paroz GN (1999). The dehydroxylation of urea intercalated kaolinite: an infrared emission spectroscopic study. P403-408 in Kodama H, Mermut AR & Torrance JK (Eds.) *Clays for our future. Proc. 11th International Clay Conference, Ottawa, Canada, 1997. Published by ICC97 Organising Committee, Ottawa, Canada.*
- ²⁷ Frost RL, Vassallo AM (1996). The dehydroxylation of the kaolinite clay minerals using infrared emission spectroscopy. *Clay and Clay Minerals* **44**, 5, 635-651.
- ²⁸ Van der Gaast SJ, Frankema W, Tran THT & Frost RL (1996). Dehydroxylation steps of kaolinite & dickite: An XRD & DTA study. *International Laboratory News (August)* 8.
- ²⁹ Bell VA, Citro VR & Hodge GD (1991). Effect of pellet pressing on the infrared spectrum of kaolinite. *Clays and Clay Minerals* **39**, 3, 290-292.
- ³⁰ Farmer VC (1958). Effects of grinding during the preparation of alkali-halide disks on the infrared spectra of hydroxylic compounds. *Spectrochimica Acta.* **8**, 374-389.
- ³¹ Cornejo J & Hermosis MC. (1998). Structural alteration of sepiolite by dry grinding. *Clay Minerals* **23**, 391-398.

- ³² Gonzalez Garcia F *et al.* (1991) Effects of dry grinding on two kaolinites of different crystallinity. *Clay Minerals* **26**, 549-565.
- ³³ Kristóf É, Juhász AZ & Vassányi I (1993) The effect of mechanical treatment on the crystal structure and thermal behaviour of kaolinite. *Clays and Clay Minerals* **41**, 5, 608-612.
- ³⁴ Michaelian KH, Bukka K & Permann DNS (1987) Photoacoustic infrared spectra (250-10 000 cm⁻¹) of partially deuterated kaolinite #9. *Canadian Journal of Chemistry* **65**, 1420-1423.
- ³⁵ Frost RL, Kristof J, Paroz GN & Klopogge JT (1998). Molecular structure of dimethyl sulphoxide intercalated kaolinites. *Journal of Physical Chemistry B* **102**, 8519-8532.
- ³⁶ Mendelovici E, Yariv SH & Villaba R (1979). Iron bearing kaolinite in Venezuelan laterite. I. Infrared spectroscopy study and chemical dissolution evidence. *Clay Minerals* **14**, 323-327.
- ³⁷ Besson G & Drits VA (1997). Refined relationships between chemical composition of dioctahedral fine-grained mica minerals and their infrared spectra within the OH stretching region. Part I: identification of the OH stretching bands. *Clays and Clay Minerals* **45**, 2, 158-169.
- ³⁸ Frost RL, Kristof J, Horvath E & Klopogge JT (1999). Modification of the kaolinite hydroxyl surfaces through the application of pressure and temperature, part III. *Journal of Colloid and Interface Science* **214** 380-388.
- ³⁹ Miller JG & Oulton TD (1970). Prototropy in kaolinite during percussive grinding. *Clays and Clay Minerals* **18**, 313-323.
- ⁴⁰ Rouxhet PG, Samudacheata N, Jacobs H & Anton O (1977). Attribution of the OH stretching bands of kaolinite. *Clay Minerals* **12**, 171-178.
- ⁴¹ Frost RL, Kristof J, Paroz GN & Klopogge JT (1998). Role of water in the intercalation of kaolinite with hydrazine. *Journal of Colloid and Interface Science* **208**, 216-225.
- ⁴² Kristof J, Mink J, Horváth E & Gábor M (1993). Intercalation study of clay minerals by Fourier transform infrared spectrometry. *Vibrational Spectroscopy* **5**, 61-67.
- ⁴³ Yariv S (1975) Infrared study of grinding kaolinite with alkali metal chlorides. *Powder Technology* **12**, 131-138.
- ⁴⁴ Conley RF & Althoff AC (1971). Surface acidity in kaolinites. *Journal of Colloid and Interface Science* **37**, 1, 186-195.
- ⁴⁵ Kirsch H, (1968) "Applied mineralogy", Chapman and Hall (London).

3. The interactions of pyridine with kaolin.

3.1 INTRODUCTION.....	169
3.1.1 <i>The binding mechanisms of pyridine.</i>	170
3.1.1.1 Brønsted bound pyridine or the pyridinium cation.....	172
3.1.1.2 Lewis bound pyridine.....	173
3.1.2 <i>The use of other probe molecules.</i>	181
3.1.3 <i>Distinguishing kaolin from halloysite.</i>	182
3.2 EXPERIMENTAL.....	185
3.2.1 <i>Method development and sample preparation.</i>	185
3.2.2 <i>Stability test of the pyridine treated samples.</i>	186
3.3 RESULTS.....	188
3.3.1 <i>Impurity identification using XRD and DRIFTS.</i>	188
3.3.2 <i>TGA.</i>	200
3.3.3 <i>VT-DRIFTS of halloysite.</i>	205
3.3.4 <i>VT-DRIFTS of pyridine exposed halloysite.</i>	206
3.3.5 <i>VT-DRIFTS of ball-milled (FM) kaolin-pyridine.</i>	209
3.3.5.1 Unmilled kaolin-pyridine. The 3800-2600 cm^{-1} region.....	209
3.3.5.2 3 minute milled kaolin-pyridine. The 3800-2600 cm^{-1} region.....	210
3.3.5.3 10 minute milled kaolin-pyridine. The 3800-2600 cm^{-1} region.....	211
3.3.5.4 30 minute milled kaolin-pyridine. The 3800-2600 cm^{-1} region.....	212
3.3.5.5 Unmilled kaolin-pyridine. The 2100 1400 cm^{-1} region.....	213
3.3.5.6 3 minute milled kaolin-pyridine. The 2100-1400 cm^{-1} region.....	221
3.3.5.7 10 minute milled kaolin-pyridine. The 2100-1400 cm^{-1} region.....	229
3.3.5.8 30 minute milled kaolin-pyridine. The 2100-1400 cm^{-1} region.....	237
3.4 CONCLUSIONS.....	241
3.5 REFERENCES.....	246

FIGURE 3.1 BRØNSTED BINDING.....	172
FIGURE 3.2 CAUSES FOR THE SUPPRESSION OF THE 1540 cm^{-1} BAND.	173
FIGURE 3.3 LEWIS BINDING.....	173
FIGURE 3.4 CHARACTERISTIC BAND INTENSITIES OF BRØNSTED AND LEWIS BOUND PYRIDINE.	175
FIGURE 3.5 CHARACTERISTIC IR FREQUENCIES OF BOUND PYRIDINE.	176
FIGURE 3.6 PROPOSED BINDING IN THE FORMATION OF THE 1440 & 1450 cm^{-1} BANDS.....	178
FIGURE 3.7 SCHEMATIC OF PROPOSED ORIENTATION OF PYRIDINE-INTERCALATED KAOLIN.....	179
FIGURE 3.8 SCHEMATIC REPRESENTATION OF THE STRUCTURE OF HYDRATED HALLOYSITE.....	182
FIGURE 3.9 STABILITY TEST OF PYRIDINE EXPOSED KAOLIN. THE 3800-2600 cm^{-1} REGION.....	187
FIGURE 3.10 STABILITY TEST OF PYRIDINE EXPOSED KAOLIN. THE 2100-1400 cm^{-1} REGION.....	187
FIGURE 3.11 XRD COMPARISON OF UNEXPOSED AND PYRIDINE EXPOSED KAOLIN.....	189
FIGURE 3.12 SCHEMATIC OF THE SWELLING OF HALLOYSITE WITH PYRIDINE.....	190
FIGURE 3.13 SCHEMATIC OF THE SWELLING OF SMECTITE WITH PYRIDINE.....	191
FIGURE 3.14 SCHEMATIC OF REACTIONS OF KAOLIN AND HALLOYSITE WITH FORMAMIDE.	192
FIGURE 3.15 XRD TRACE OF UNMILLED, UNEXPOSED KAOLIN.....	193
FIGURE 3.16 XRD TRACE OF UNMILLED, FORMAMIDE EXPOSED KAOLIN*.....	194
FIGURE 3.17 SCHEMATIC OF THE REACTIONS OF CHLORITE AND SMECTITE WITH ETHYLENE GLYCOL.....	195
FIGURE 3.18 XRD TRACE OF ETHYLENE GLYCOL-EXPOSED UNMILLED KAOLIN.	196
FIGURE 3.19 XRD TRACES OF UNEXPOSED HALLOYSITE AND VT XRD OF PYRIDINE EXPOSED HALLOYSITE.....	198
3.3.3 FIGURE 3.20 TGA OF PYRIDINE EXPOSED UNMILLED KAOLIN.	200
FIGURE 3.21 TGA OF PYRIDINE EXPOSED 3 MINUTE MILLED KAOLIN.....	201
FIGURE 3.22 TGA OF PYRIDINE EXPOSED 3 MINUTE MILLED KAOLIN.....	202
FIGURE 3.23 TGA OF PYRIDINE EXPOSED 3 MINUTE MILLED KAOLIN.....	203
FIGURE 3.24 HALLOYSITE. THE EFFECT OF TEMPERATURE. THE 3800-2400 cm^{-1} REGION.	205
FIGURE 3.25 HALLOYSITE. THE EFFECT OF TEMPERATURE. THE 2100-1400 cm^{-1} REGION*.....	205
FIGURE 3.26 HALLOYSITE-PYRIDINE. THE EFFECT OF TEMPERATURE. THE 3800-2400 cm^{-1} REGION*... ..	206
FIGURE 3.27 HALLOYSITE-PYRIDINE. THE EFFECT OF TEMPERATURE. THE 2100-1400 cm^{-1} REGION.* ...	207
FIGURE 3.28 COMPARISON OF UNEXPOSED AND PYRIDINE EXPOSED KAOLIN (ROOM TEMP.).....	209
FIGURE 3.29 COMPARISON OF UNEXPOSED AND PYRIDINE EXPOSED KAOLIN (250 °C).....	209
FIGURE 3.30 COMPARISON OF UNEXPOSED AND PYRIDINE EXPOSED KAOLIN (ROOM TEMP.).....	210
FIGURE 3.31 COMPARISON OF UNEXPOSED AND PYRIDINE EXPOSED KAOLIN (250 °C).....	210
FIGURE 3.32 COMPARISON OF UNEXPOSED AND PYRIDINE EXPOSED KAOLIN (ROOM TEMP.).....	211
FIGURE 3.33 COMPARISON OF UNEXPOSED AND PYRIDINE EXPOSED KAOLIN (250 °C).....	211
FIGURE 3.34 COMPARISON OF UNEXPOSED AND PYRIDINE EXPOSED KAOLIN (ROOM.....	212
FIGURE 3.35 COMPARISON OF UNEXPOSED AND PYRIDINE EXPOSED KAOLIN (250 °C).....	212
FIGURE 3.36 COMPARISON OF UNEXPOSED AND PYRIDINE EXPOSED KAOLIN (ROOM TEMP.).....	213
FIGURE 3.37 COMPARISON OF UNEXPOSED AND PYRIDINE EXPOSED KAOLIN (250 °C).....	214
FIGURE 3.38 UNMILLED KAOLIN-PYRIDINE. THE EFFECT OF TEMPERATURE. THE 2100-1400 cm^{-1} REGION.....	215
FIGURE 3.39 UNMILLED KAOLIN-PYRIDINE. THE 2100-1400 cm^{-1} REGION. ROOM TEMPERATURE CURVE FIT.....	216
FIGURE 3.40 UNMILLED KAOLIN-PYRIDINE. THE 2100-1400 cm^{-1} REGION. 150 °C CURVE FIT.....	216
FIGURE 3.41 UNMILLED KAOLIN-PYRIDINE. THE 2100-1400 cm^{-1} REGION. 250 °C CURVE FIT.....	217
FIGURE 3.42 UNMILLED KAOLIN-PYRIDINE. THE 2100-1400 cm^{-1} REGION. THE CHANGE IN INTENSITY OF THE WATER BAND (ν) AT 1650 cm^{-1}	218
FIGURE 3.43 UNMILLED KAOLIN-PYRIDINE. THE 2100-1400 cm^{-1} REGION. THE CHANGE IN INTENSITY OF PYRIDINE BANDS.	219
FIGURE 3.44 RATIO OF THE AREA OF THE 1440 : 1490 cm^{-1} PYRIDINE BANDS.....	220
FIGURE 3.45 COMPARISON OF UNEXPOSED AND PYRIDINE EXPOSED KAOLIN (ROOM TEMP.).....	221
FIGURE 3.46 COMPARISON OF UNEXPOSED AND PYRIDINE EXPOSED KAOLIN (250 °C).....	221
FIGURE 3.47 3 MINUTE KAOLIN-PYRIDINE (FM). THE EFFECT OF TEMPERATURE. THE 2100-1400 cm^{-1} REGION.....	223
FIGURE 3.48 3 MINUTE KAOLIN-PYRIDINE (FM). THE 2100-1400 cm^{-1} REGION. ROOM TEMPERATURE CURVE FIT.....	224
FIGURE 3.49 3 MINUTE KAOLIN-PYRIDINE (FM). THE 2100-1400 cm^{-1} REGION. 100 °C CURVE FIT.....	225
FIGURE 3.50 3 MINUTE KAOLIN-PYRIDINE (FM). THE 2100-1400 cm^{-1} REGION. 200 °C CURVE FIT.....	225
FIGURE 3.51 3 MINUTE KAOLIN-PYRIDINE (FM). THE 2100-1400 cm^{-1} REGION. THE CHANGE IN INTENSITY OF WATER BANDS AT 1660 & 1630 cm^{-1}	227

FIGURE 3.52 3 MINUTE KAOLIN-PYRIDINE (FM). THE 2100-1400 cm^{-1} REGION. THE CHANGE IN INTENSITY OF PYRIDINE BANDS.....	228
FIGURE 3.53 RATIO OF THE AREA OF THE 1440 & 1450 : 1490 cm^{-1} PYRIDINE BANDS.	228
FIGURE 3.54 COMPARISON OF UNEXPOSED AND PYRIDINE EXPOSED KAOLIN (ROOM TEMP.).	229
FIGURE 3.55 COMPARISON OF UNEXPOSED AND PYRIDINE EXPOSED KAOLIN (250 $^{\circ}\text{C}$).....	229
FIGURE 3.56 10 MINUTE KAOLIN-PYRIDINE (FM). THE EFFECT OF TEMPERATURE. THE 2100-1400 cm^{-1} REGION.....	230
FIGURE 3.57 10 MINUTE KAOLIN-PYRIDINE (FM). THE 2100-1400 cm^{-1} REGION. ROOM TEMPERATURE CURVE FIT.....	231
FIGURE 3.58 10 MINUTE KAOLIN-PYRIDINE (FM). THE 2100-1400 cm^{-1} REGION. 100 $^{\circ}\text{C}$ CURVE FIT.....	231
FIGURE 3.59 10 MINUTE KAOLIN-PYRIDINE (FM). THE 2100-1400 cm^{-1} REGION. 250 $^{\circ}\text{C}$ CURVE FIT.....	232
FIGURE 3.60 PROPOSED ASSIGNMENT OF THE 1450 cm^{-1} BAND.....	233
FIGURE 3.61 10 MINUTE KAOLIN-PYRIDINE (FM). THE 2100-1400 cm^{-1} REGION. THE CHANGE IN INTENSITY OF WATER BANDS AT 1680 & 1620 cm^{-1}	234
FIGURE 3.62 10 MINUTE KAOLIN-PYRIDINE (FM). THE 2100-1400 cm^{-1} REGION. THE CHANGE IN INTENSITY OF PYRIDINE BANDS.	235
FIGURE 3.63 RATIO OF THE AREA OF THE 1450 : 1490 cm^{-1} PYRIDINE BANDS.....	236
FIGURE 3.64 COMPARISON OF UNEXPOSED AND PYRIDINE EXPOSED KAOLIN (ROOM TEMP.).	237
FIGURE 3.65 COMPARISON OF UNEXPOSED AND PYRIDINE EXPOSED KAOLIN (250 $^{\circ}\text{C}$).....	237
FIGURE 3.66 30 MINUTE KAOLIN-PYRIDINE (FM). THE EFFECT OF TEMPERATURE. THE 2100-1400 cm^{-1} REGION.....	238
FIGURE 3.67 PROPOSED MECHANISM OF PYRIDINE DISPLACEMENT OF WATER IN BRØNSTED TYPE BINDING.....	242
FIGURE 3.68 PROPOSED MECHANISM OF PYRIDINE DISPLACEMENT OF WATER IN LEWIS TYPE BINDING.....	243
FIGURE 3.69 CONVERSION FROM BRØNSTED TYPE BINDING TO LEWIS TYPE BINDING.	244
TABLE 3.1 WEIGHT LOSSES FROM KAOLIN DURING THERMAL ANALYSIS.....	204
TABLE 3.2 POSSIBLE ASSIGNMENTS OF PYRIDINE BANDS AT ROOM TEMPERATURE.	217
TABLE 3.3 THE EFFECTS OF PYRIDINE EXPOSURE ON THE SORBED WATER SPECIES PRESENT ON MILLED AND UNMILLED KAOLIN. THE OH BENDING REGION.	240

3.1 Introduction.

This chapter will describe a method by which the binding sites present on the surface of a Cornish kaolin have been determined, both before and after ball-milling, by the use of the organic probe pyridine and VT-DRIFTS.

Ball milling has many effects upon the surface of kaolin (see Chapter 2). Therefore, it can be predicted that the types of surface sites available for organic interactions alter after the mineral has been milled. The use of pyridine as a probe molecule allows the nature of the exposed sites to be determined before and after milling. Gross changes occurring can also be semi-quantified by using curve fitting.

Molecular probes were defined by Johnston¹ as “a solute or solvent species capable of interacting with a solid surface...sensitive to changes in their local environment through diagnostic properties”. The diagnostic properties referred to were a change in the spectroscopic signal. The interactions of the probe molecule, pyridine with various clay minerals have been well studied in the literature^{2,3,12,16,17,18}. The type of surface site available for binding can greatly affect the physical properties of a mineral. Pyridine has successfully been used for many years to characterise the surface properties of many diverse minerals. For example, it has been used to study the hydroxyls of montmorillonite and Al-pillared montmorillonite^{4,5}, to investigate the surface properties of hydrated and dehydrated cation exchanged hectorites⁶, to analyse the effect of the pillaring species on the types of surface sorption sites exhibited by pillared rectorite, montmorillonite, and synthetic mica-montmorillonite⁷, to determine the nature of the acid sites present on Al-pillared and Na-exchanged saponites used as catalysts⁸, to characterise the surface sites of copper-exchanged zeolites used in the activation of hydrocarbons⁹, to study the surface acidity of metal oxide catalysts and to explain the mechanism by which they decompose 2-propanol¹⁰, and to monitor surface acidity of metal modified aluminas¹¹.

Pyridine was chosen as a probe molecule for the work presented herein in order to elucidate information regarding the types of surface sites which are available on the surface of kaolin during the industrial processing procedure.

It was deemed to be a suitable molecule in this study since it is not easily intercalated into kaolin and it has a well documented and readily interpreted IR spectrum which provides a strong, diagnostic IR signal depending on the sites to which it binds. It adsorbs readily to strong acid sites at the surface¹², and, very importantly, it can act as both a Lewis and Brønsted base. These properties make it particularly useful as a tool for investigating the type of exposed active sites available for binding.

3.1.1 The binding mechanisms of pyridine.

It is well known that the surfaces (and interlayer space in swelling minerals) is populated by Brønsted and Lewis acid sites. The majority of the interactions between clay surfaces and adsorbed organic species are of the acid-base type. Johnston¹ described six main types of active sites on clay minerals. However, only three of these types are present on the surface of kaolin.

a Exchangeable metal cations/structural metal ions and exposed under co-ordinated metal atoms. Here, the probe molecule co-ordinates directly to a metal cation, which functions as a Lewis acid (see Lewis bound pyridine). Two factors affect the Lewis acidity of the mineral: the reduction potential of the cation, and the water content of the surface. Since most of the exposed cations on the surface of kaolin are Al^{3+} , the dominant factor for this mineral is the water content. At high coverage of water, the organic probe has limited ability to compete for co-ordination positions around the hydrated cation. At lower water coverage, the competition for co-ordination positions is reduced, and thus direct co-ordination by electron transfer can progress.

b Polarised water molecules surrounding exchangeable cations. It is suggested that when water is sorbed to exchangeable cation species, there are two environments in which they can be found in a non swelling clay: (i) co-ordinated directly to the metal cation and (ii) water physisorbed to the surface which occupies interstitial pores or polar sites on external surfaces. These water molecules are able to donate protons to adjacent organic probe molecules (more readily than bulk water), and act as Brønsted acid sites

(see “Brønsted bound pyridine or the pyridinium cation” below). However, the water bound to the cation will be more polar, and thus proton donation from this type of water is the more likely. Brønsted acidity depends upon both the nature of the cation and the amount of water present. As the charge on the cation increases, and size decreases, Brønsted acidity increases. Exchangeable cations are rare in kaolin, and are usually found at exposed edges of kaolin. They may also be found on the basal surfaces if isomorphous substitution of aluminium for silica occurs (see Yariv¹³ for a review of the effects of isomorphous substitution on various minerals). The bonding of water rather than hydroxyls distinguishes them (although water may become very polarised, and tend towards OH).

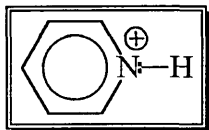
c Broken edge sites (i.e. surface hydroxyl groups located on broken edge surfaces). When the kaolin sheet becomes damaged, under co-ordinated metal ions may become exposed. Water can react with these sites, and the hydroxyl groups bond and attempt to complete the co-ordination sphere of the metal. These water molecules effectively become very reactive, “structural” hydroxyls since there is strong interaction between the hydroxyl and the surface. At low pH values, the sites are positively charged due to the adsorption of protons, and organic acids can interact strongly at these sites (see Chapter 4.). As pH increases, the charge becomes neutral until after the point of zero charge (PZC), the surface charge becomes negative. Kaolin has very few cation exchange sites (unlike swelling clays) and the contribution from type c sites forms the principle type of reactivity. In their hydroxylated form, these sites are Brønsted acid in character. If the hydroxyl species is removed, the under co-ordinated metal ion becomes a Lewis acid site.

A wide ranging investigation of the adsorption of various organics (e.g. fatty acids, phenols, aniline etc.) to swelling clays (e.g. montmorillonite, smectites, vermiculites etc.) was carried out by Yariv¹⁴. The work aimed to elucidate information regarding bond strength and type using IR spectroscopy to monitor the effect of heat. Although swelling clays were not examined in the present study, the mechanisms of Lewis and Brønsted binding which were discussed in the work by Yariv can be extrapolated to the kaolin-pyridine system.

3.1.1.1 Brønsted bound pyridine or the pyridinium cation.

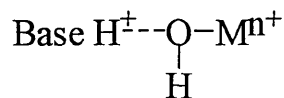
In Brønsted type binding, pyridine binds to an exposed proton on the mineral surface. Where adsorbed water is co-ordinated to exchangeable metal cations (e.g. at broken edge sites in the kaolin system), this water can serve as a proton donor, i.e. a Brønsted acid.

Figure 3.1 Brønsted binding

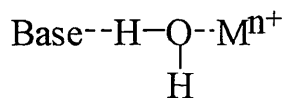


The proton may be directly bonded to a cation, or via one or more water molecules. When Brønsted binding occurs, an IR marker band is present at 1540 cm^{-1} . The associations can be formed in two ways, depending on the polarising power of the metal and the basic strength of the adsorbed organic species (B). The associations may occur simultaneously in the same system.

(i) the organic base may be protonated by accepting a proton from a water molecule, thus gaining a positive charge.



(ii) the organic base may be hydrogen bonded with a polar water molecule.



After thermal (or chemical) dehydration, the metal cations may serve as Lewis acids.

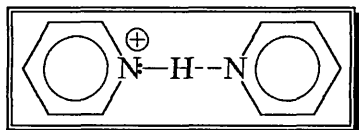
A possible complication can occur in this system, since it is possible that the proton may not be co-ordinated to the surface, and therefore the diagnostic IR band at 1540 cm^{-1} may not be visible at room temperature. The species causing the suppression is generally loosely bound and it may be removed by gentle heating. If Brønsted binding is present,

the 1540 cm^{-1} band may be visualised by elevating the temperature to approximately 50-100 °C, thus removing the other species.

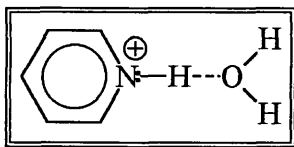
There are two common species which are likely to cause this phenomenon in the work presented herein:

Figure 3.2 Causes for the suppression of the 1540 cm^{-1} band.

a) an excess of pyridine



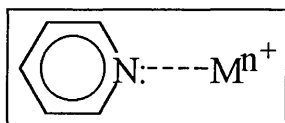
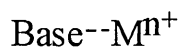
b) water



3.1.1.2 Lewis bound pyridine.

This involves the non hydrated exchangeable metal cations (usually Al for kaolin) present at the broken edges of kaolin which act as Lewis acid centres. The acid strength increases with the charge of the cation, and decreases with increasing cation size¹³. These sites may be masked by water at lower temperatures. In Lewis type binding, the organic base (i.e. pyridine in this case) becomes co-ordinated directly to the cation.

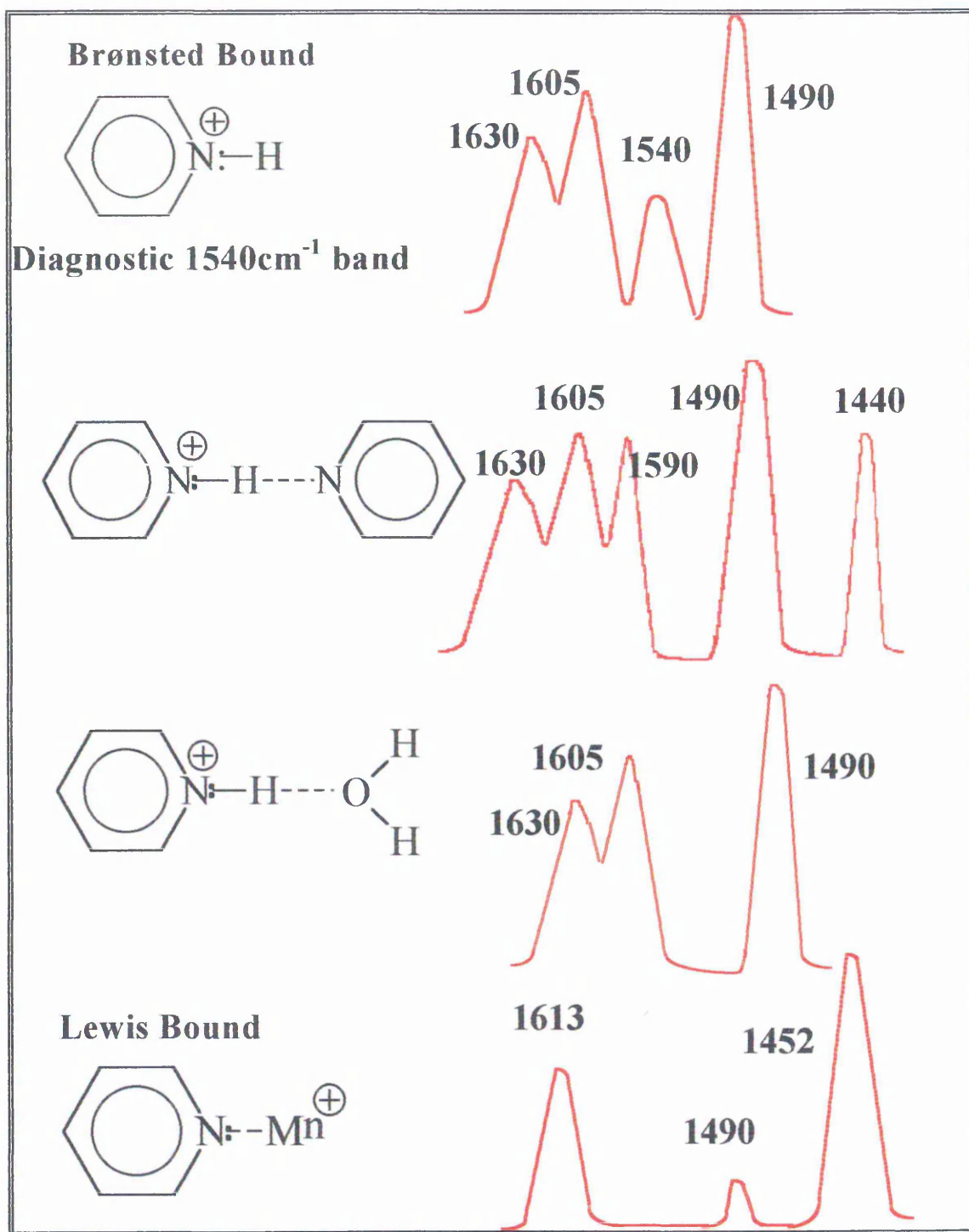
Figure 3.3 Lewis binding



Here, the Brønsted diagnostic IR band at 1540 cm^{-1} is not present. This type of adsorption is characterised by a strong, temperature resistant band in the $1440\text{-}1450\text{ cm}^{-1}$ region. It should again be noted that, due to the diverse nature of mineral surfaces, usually a combination of Brønsted and Lewis associations is present. The relative intensities and thermal stabilities of the bands must then be assessed in order to correctly identify the type of binding.

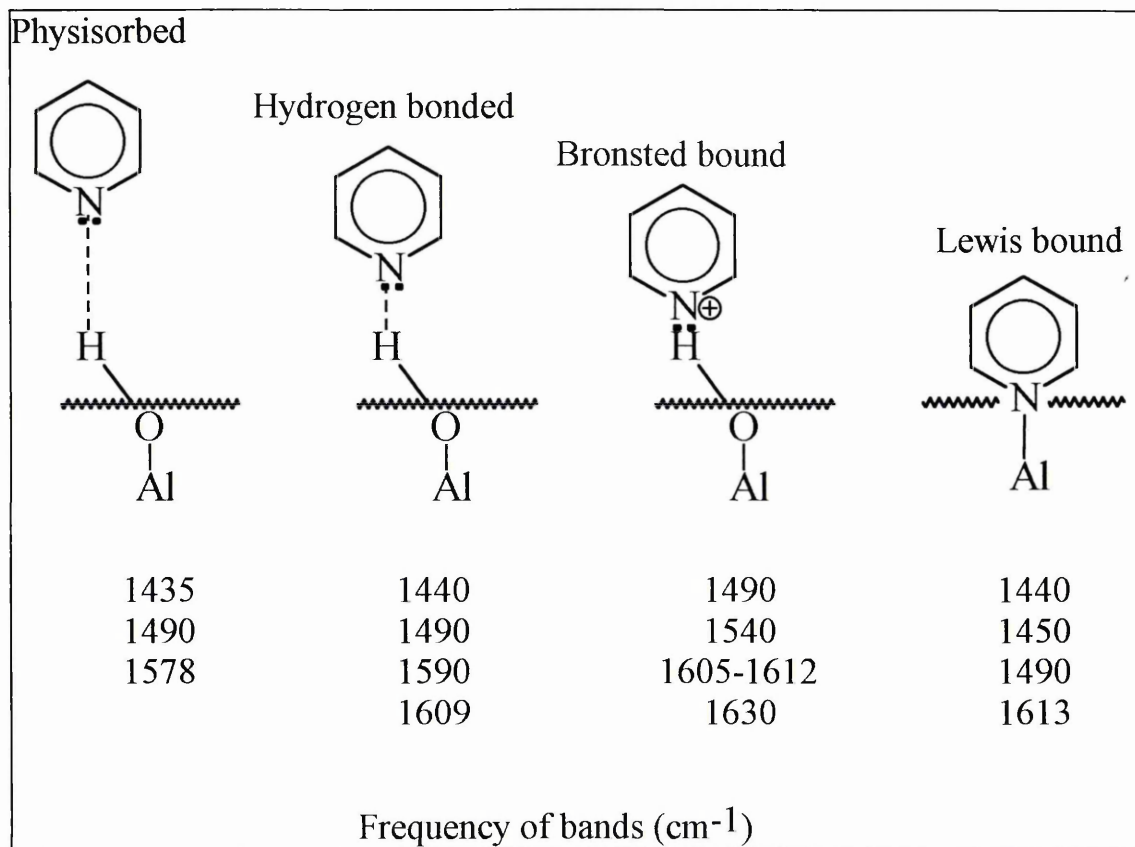
For example, if, at room temperature, two major bands are present, an intense band at 1450 cm^{-1} , and a weaker band at 1490 cm^{-1} , the most obvious assignment is to Lewis type binding. If, however, after moderate elevation of temperature (e.g. to $50\text{ }^{\circ}\text{C}$), the 1440 cm^{-1} band reduces in intensity and the 1490 cm^{-1} does not, the most likely type of binding is Brønsted type. In that case, the 1440 cm^{-1} band at room temperature would represent hydrogen bonded (or physisorbed) pyridine, and the 1490 cm^{-1} band would represent Brønsted type binding. This can be confirmed by the appearance at elevated temperatures of a band at c 1540 cm^{-1} (see Figure 3.4 below for characteristic band intensities).

Figure 3.4 Characteristic band intensities of Brønsted and Lewis bound pyridine.



Adsorption of molecules onto the surface of kaolin is a more common phenomenon than intercalation, since the former does not require penetration into the hydrogen bonding network. Instead, the molecule adheres to the surface of one of the faces or edges of the mineral. The major IR bands of adsorbed pyridine are listed in Figure 3.5 below. It should be noted that rarely do these bands appear in isolation.

Figure 3.5 Characteristic IR frequencies of bound pyridine.



Assignments taken from Billingham *et al*¹⁷. A comprehensive review of the assignments of pyridine in liquid form can be found in a work by Breen¹⁵.

The types of sites available on swelling clays for the binding of organics can be dramatically altered by cation exchange^{11,12,17,18}. In the present work, cation exchange studies on the unmilled kaolin, using aluminium and nickel ions did not yield infrared results significantly different from those discussed in the results section, where no attempt at cation exchange was made (although XRF analysis showed that cation exchange had been successful). It is commonly recognised, however, that non swelling clays do not have a large cation exchange. A typical value is 3-15 milliequivalents/100 g²³. Reis Jr *et al*¹⁶, however, studied the thermodynamic changes involved in the interactions of pyridine exposed, cation exchanged kaolin. Monoionic kaolin samples were prepared by Reis Jr *et al*, by shaking the mineral with an aqueous solution of M(NO₃)_n (where M = Cu²⁺, Ca²⁺, Zn²⁺, Al³⁺ or Fe³⁺) for 7 hours at 40 °C, followed by water washing and vacuum drying at 25 or 250 °C for 4 hours. H- exchanged kaolin was also prepared in the same way. In order to collect IR spectra of pyridine exposed

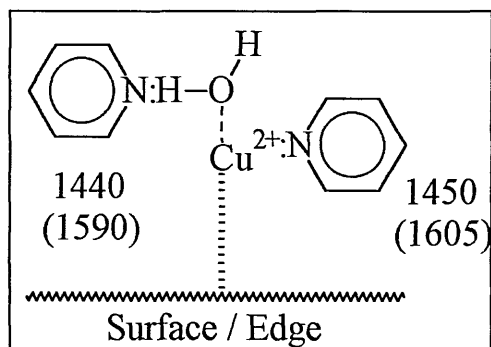
samples, a few drops of pyridine were dropped onto the surface of a pre-pressed pastille of kaolin. In the opinion of the author this practise may give rise to a composite spectrum of kaolin and pyridine, rather than a true reflection of the kaolin-sorbed pyridine complexes. Although the study was flawed and the IR spectra were of questionable quality and scarce, some interesting hypotheses were made regarding the adsorption mechanisms of pyridine. The spectra presented for Al^{3+} , H and Cu^{2+} exchanged kaolins (dried at 25 °C) were said to be very similar to the Fe^{3+} , Ca^{2+} and Zn^{2+} exchanged kaolins respectively (dried under the same conditions).

The Al^{3+} (and Fe^{3+}) exchanged kaolin spectra did not exhibit well defined peaks. However a small band at 1489 cm^{-1} was observed which was attributed to pyridine hydrogen bonding at a Brønsted acid centre, i.e., $\text{X-H} + \text{:P} \rightarrow \text{X}\cdots\text{H}\cdots\text{P}$
Where X represents a surface e.g. SiO, AlO etc, and :P = pyridine.

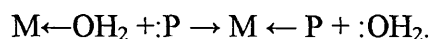
The H (and Ca^{2+}) exchanged kaolin also presented a band at 1489 cm^{-1} which was assigned to hydrogen bonded pyridine. This was the predominant type of binding in the H exchanged system. Overlapping bands at 1440 and 1450 cm^{-1} were evident and these were assigned to Lewis co-ordination. In the calcium exchanged system, the latter type of binding was said to prevail.

In the copper (and Zn^{2+}) exchanged system, (Brønsted) hydrogen bonded pyridine presented at 1490 cm^{-1} . Pyridine was also found to replace the co-ordination water molecules on the copper, resulting in (Lewis) co-ordinated pyridine which gave bands at 1440 and 1450 cm^{-1} . The 1440 cm^{-1} band was attributed to “water co-ordinated to Cu^{2+} ” and the 1450 cm^{-1} band attributed to pyridine co-ordinated directly to Cu^{2+} . Presumably pyridine is also involved in the formation of the former band, although the exact mechanism of the interaction was not described. It is postulated by the author of the work herein that the mechanism is as shown below in Figure 3.6.

Figure 3.6 Proposed binding in the formation of the 1440 & 1450 cm⁻¹ bands.



The Lewis bonding mechanism of the 1450 cm⁻¹ band was described as follows:



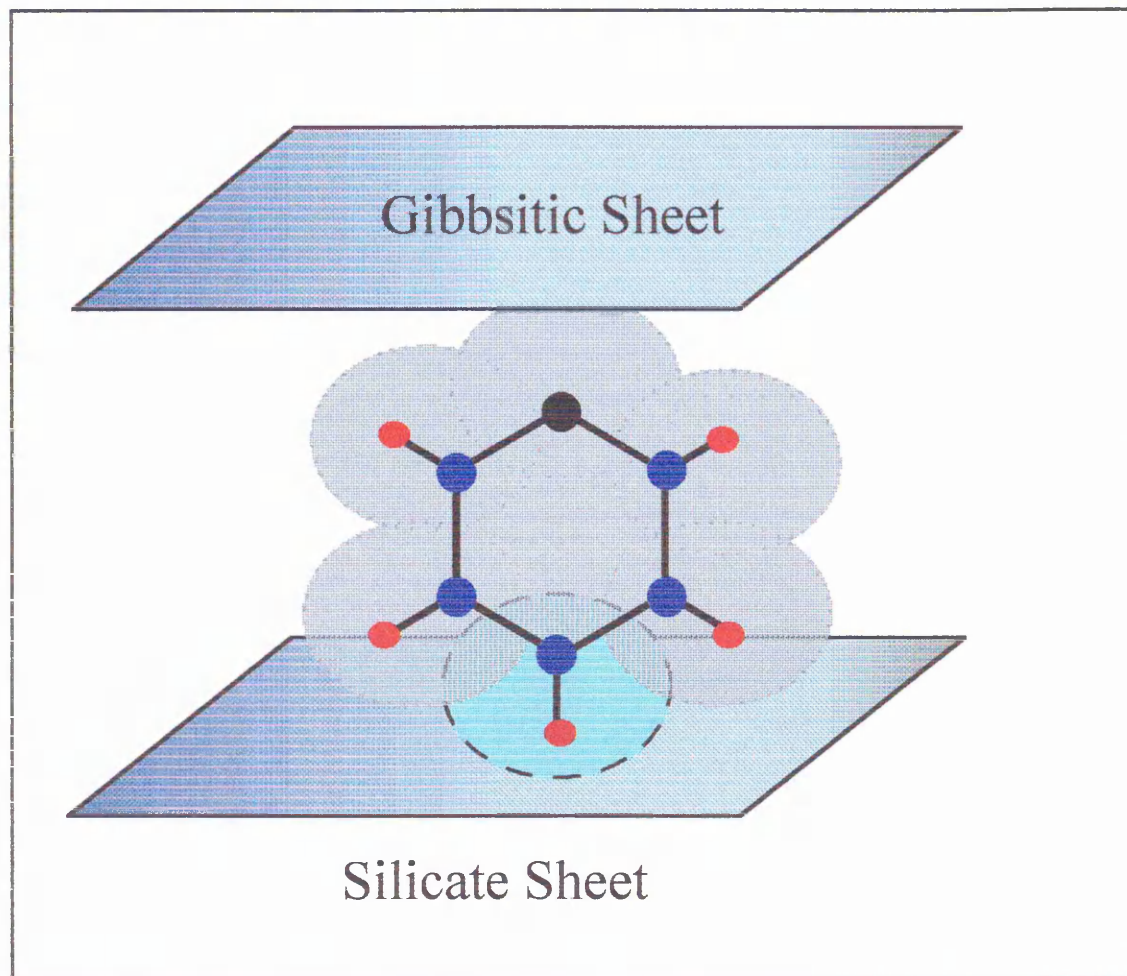
Unfortunately no data regarding the strength of pyridine binding or the thermal stability of the complexes were given.

In a study by Billingham *et al*¹⁷, pyridine was employed to determine the nature of the acid sites present on cation exchanged montmorillonite. It was found that, when the Ni²⁺ exchanged mineral was exposed to liquid pyridine, it presented diagnostic infra red bands indicating Lewis bound pyridine. Therefore, the predominant binding sites on the mineral were Lewis acid (electron pair accepting) sites. However, when the Al³⁺ exchanged montmorillonite was exposed in the same way, the IR spectra showed bands indicative of Brønsted bound pyridine, where the majority of sites present on the mineral were Brønsted acid, or proton donating sites.

A study of the desorption of probe molecules from cation exchanged montmorillonite was carried out by Breen¹⁸ and this investigation has been used as one of the models for the work presented herein. Breen, studied the desorption of pyridine from Ni²⁺ and Co²⁺ exchanged montmorillonite by thermogravimetric and IR techniques and compared it with that of the trivalent ion (Al³⁺) exchanged form. This work discovered (by IR spectroscopy) that, before the point of desorption, (measured by derivative thermal analysis), the Ni²⁺ exchanged montmorillonite contained predominantly Lewis acid sites, as did the other divalent ion (Co²⁺) exchanged mineral. This was in contrast to the predominately Brønsted acid sites exhibited by trivalent-ion exchange forms.

A study by Sugahara *et al.*², showed it was possible to form a well ordered intercalation complex of pyridine with kaolin which had a basal spacing of 12Å. This measurement suggests that the pyridine was in an approximately perpendicular position, with the nitrogen facing the gibbsitic layer. The pyridine complex was stable, with the aromatic ring of pyridine keying into the silicate layer. Attachment was thought to be via hydrogen bonding between the inner surface hydroxyls and the slightly negatively charged nitrogen of the pyridine (see Figure 3.7²).

Figure 3.7 Schematic of proposed orientation of pyridine-intercalated kaolin.



The intercalation theory was supported, since IR spectroscopy visualised hydrogen bonding between structural hydroxyls and water, i.e. there was disruption of the structural hydroxyl bands between c 3695 and 3620 cm^{-1} . Most notably a new band at 3637 cm^{-1} was observed. This band was assigned to the inner surface hydroxyl interactions with pyridine. The relative intensities of the 3621 to 3693 cm^{-1} bands were said to remain similar throughout (possibly indicating that the inner surface and inner

hydroxyls were affected by the same degree). However, in the opinion of the author of the work presented herein, there is a dramatic increase in the intensity of the c 3550-3600 cm^{-1} region after intercalation.. This could be due to the hydrogen bonding of one of the inner surface hydroxyls with pyridine, thus, causing a shift to lower frequency. Similar effects have been observed by Ledoux & White¹⁹ after studying the intercalation of kaolin with hydrazine, formamide and urea, whereby the inner surface hydroxyls interact with the intercalating species, thus causing a decrease in the relative intensities of the corresponding hydroxyl bands, with a concurrent shift to decreased frequency.

Due to the relative intensities of the 1440 and 1593 cm^{-1} bands, the mechanism of binding was determined by Sugahara *et al*², to be by hydrogen bonding. The method used for intercalation was harsh and complex, and firstly involved the use of an entraining agent (i.e. a molecule which will intercalate, but can then be replaced by another molecule. The entraining agent used in this case was di-methyl sulphoxide (DMSO). The formation of a fluorinated kaolinite-DMSO intercalation complex was followed by heat treatment at 110 °C for 4 hours. Subsequent hydration resulted in the formation of a 10Å hydration complex. This complex was unstable in air, and after a few days exposure it collapsed to 7.2Å via an 8.4Å intermediate. If the 10Å hydrated kaolin was exposed immediately to liquid pyridine, intercalation occurred after stirring at room temperature. This successful method of pyridine intercalation was also attempted using NMF-intercalated and raw kaolin samples. However, no changes occurred to suggest that intercalation of pyridine had been successful in these cases.

XRD traces of the pyridine intercalated sample showed that an intense 001 peak at 7.36 °2 θ (12Å) appears, with a concurrent disappearance of the 10Å peak associated with hydrated kaolin. This implied that all the kaolin had been converted to the intercalation complex. The kaolin-pyridine complex was found to be stable to drying in a desiccator. Infrared bands at 1440, 1489, 1593 and 1612 cm^{-1} were observed in the intercalated kaolin-pyridine complex spectra. These bands had shifted from the positions found in the spectrum of pyridine dissolved in CCl_4 , and this was seen as evidence of intercalation. It is believed by the author of the present work that there is also strong evidence for Lewis type co-ordination or hydrogen bonding, since there is a relatively strong 1440 cm^{-1} band, accompanied by a relatively weak 1490 cm^{-1} . This matter was not discussed in the

cited paper. Heating the sample would give more conclusive evidence of the binding mechanism based on relative thermal stabilities.

3.1.2 The use of other probe molecules.

Cyclohexylamine is another frequently used probe molecule which will interact with both weak and strong acid sites¹², due to its highly basic properties. Breen studied the desorption of cyclohexylamine from 2 divalent cation exchanged montmorillonites¹⁸, and this work facilitated the identification and quantification of the number and type of acid sites present on the exchanged mineral. It was concluded that these clays exhibited predominantly Lewis character, which increased with increasing cation loading. These sites were in contrast to those discerned on the surface of trivalent cation exchanged montmorillonite, where Brønsted sites predominated.

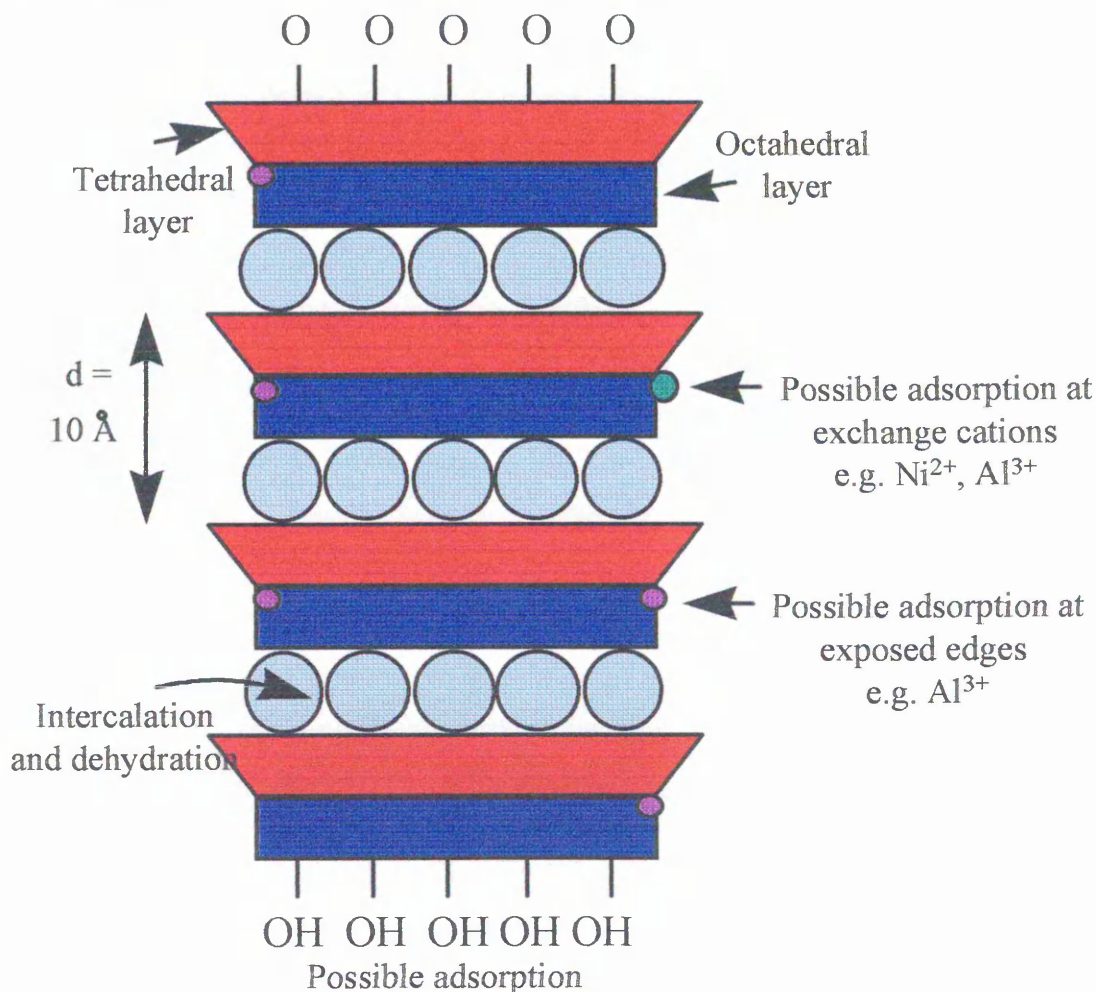
Lipsicas *et al.*,²⁰ assessed the altered properties of a well crystallised kaolin after intercalation with several species including formamide using NMR (nuclear magnetic resonance), IR, EPR (electron paramagnetic resonance spectroscopy) and Cp (specific heat) measurements. IR showed mild perturbations of the inner surface hydroxyls. Formamide induced stacking faults in the kaolin structure, which, upon de-intercalation by heat, were found to be partly permanent and partly temporary. EPR showed the perturbation of kaolin with formamide to be relatively weak in comparison to NMF and DMSO

DMSO is able to intercalate very efficiently due to strong dipole interactions with the silicate layers. It was shown by Breen & Lynch²¹ that 1.5 DMSO molecules were intercalated per unit cell of kaolinite. DMSO was found to greatly distort the kaolin layer due to the very strong interactions. Removal of the DMSO did not return the structure to a state like that of the pre-intercalated material. This was due to the introduction of irreversible severe stacking faults. By IR spectroscopy it was possible to show that the intercalation of the DMSO and its oxygens with their very basic, electron donor characteristics, resulted in strong perturbations of the inner surface hydroxyls²²

3.1.3 Distinguishing kaolin from halloysite.

In the course of the present work, there was reason to suspect an impurity in the Cornish kaolin sample which is likely to be halloysite (discussed in detail in Section 3.3.1). For this reason, a brief review of halloysite and its differentiation from kaolin has been included in this chapter.

Figure 3.8 Schematic representation of the structure of hydrated halloysite.



Halloysite (sometimes also known as endellite) is part of the kaolinite mineral group, along with dickite and nacrite. The structure of hydrated halloysite is very similar to that of kaolin (see Chapter 1). It has the same chemical formula as kaolin ($\text{Al}_2\text{Si}_2\text{O}_5 \cdot 4\text{H}_2\text{O}$), but each unit is associated with 4 water units, compared with 2 in the kaolin structure. In its hydrated form, a d spacing of 10\AA means that it may be distinguished from kaolin. However, when it is dehydrated, the d spacing reverts to c 7\AA , and thus discriminating

between the two minerals becomes more complex. Halloysite also has a 1:1 T:O structure, but the sheets are interspersed at variable intervals with water molecules²³. The negative oxygens of the water molecules are oriented towards the hydroxyl plane and the positive hydrogens are oriented towards the oxygen plane. The intercalation of water is thought to weaken the hydrogen bonds between the sheets and at room temperature the characteristic infrared kaolin inner sheet hydroxyl bands at c 3695, 3669 and 3650 cm^{-1} are not present or are greatly reduced. At elevated temperature (approximately 75-100 °C) these bands begin to appear due to the removal of the interlayer water (See VT DRIFTS data). However, this dehydrated halloysite does not “convert” to kaolin, since the layers are not stacked directly above one another. Bailey²⁴ and Singh²⁵ have recently produced literature explaining the mechanisms by which the tube formation occurs. Although halloysite is commonly found in a tubular form, there have also been many accounts of halloysite in other configurations, for example, spheroidal, platy, and prismatic. Due to the diverse morphologies of halloysite, and its chemical similarities with kaolin, it is often difficult to distinguish halloysite from other minerals.

The morphology of halloysite differs from kaolin in that it forms tubular structures (due to the misalignment of the sheets) rather than stacks. The different forms may sometimes be distinguished by electron microscopy, although this can be a very time consuming process if there are a number of minerals present. A disadvantage to this technique is that, halloysite can sometimes be found in platy shapes (i.e. kaolin-like) and kaolin can be found in tubular shapes (i.e. halloysite-like). This causes much difficulty in identification by this means (see review by Churchman and Carr²⁶). However, kaolin does not readily lend itself to intercalation with organic molecules (notable exceptions being DMSO, formamide, NMF, hydrazine and potassium acetate²⁷), due to the strong hydrogen bonding network between the layers. Halloysite, however, will form intercalation complexes with many organics, and this is the basis for the separation techniques currently used.

In 1961, Wada²⁸ devised a laborious method by which to distinguish kaolin from halloysite by washing with potassium acetate. Different intercalation rates were used to

distinguish the two minerals- halloysite more readily forming an intercalation complex than kaolin.

Hydrazine can be used as an entraining agent, since it interacts strongly with the silicate layers of kaolin forming a stable intercalation complex. Stability of the complex is achieved via hydrogen bonding if the mineral is immersed for 24 hours into a solution containing hydrazine²². Hydrazine penetrates into the structure via the hexagonal hole (or ditrigonal cavity) and perturbs the inner sheet hydroxyl (represented in IR spectroscopy by alterations in the 3620 and 915 cm⁻¹ bands). This is a very efficient process, since XRD data from this study²² showed that the process gave essentially complete intercalation. The differing intercalation abilities of halloysite and kaolin to intercalate hydrazine were exploited by Range *et al.*²⁹, who devised another method for distinguishing kaolin and halloysite, known as the “HWG” method. The treatment involved firstly intercalating the mineral with hydrazine (the entraining agent). Hydrazine intercalation was followed by water, and finally glycerol (hence HWG) intercalation. Kaolin did not expand under these conditions, but halloysite did, and the d spacing of the latter mineral increased from 7 to 11 Å. However, this process was also time consuming and complex.

In 1984, Churchman *et al.*,³⁵ developed a method to distinguish between kaolin and halloysite using formamide intercalation. This method was used in the work presented herein and is discussed more fully in Section 3.3.1. Theng *et al.*,³⁰ compared formamide, potassium acetate and hydrazine methods for distinguishing the two minerals. They concluded that all three methods were able to distinguish one from the other equally well in qualitative terms. However, generally the formamide and potassium acetate methods tended to underestimate the halloysite concentration. Since in the present study, quantitative information was not required, the reliable, yet swift immersion in formamide technique was used.

Historically, XRD has been used to distinguish between minerals in selective intercalation studies. However, more recently, Raman microscopy techniques have been successful in distinguishing kaolin from dickite³¹ after intercalation with potassium acetate. It is

believed that the extent of intercalation into kaolin is dependant upon the molecular weight of the guest compound³².

3.2 Experimental.

3.2.1 Method development and sample preparation.

Initially, kaolin was exposed to vapour phase pyridine at room temperature for 1 week. However, this method yielded poor results, with little, if any, adsorption occurring (results not shown). Therefore, in order to increase adsorption, in all the work presented herein, the samples were immersed in liquid pyridine and prepared as detailed below.

- a) Approx. 50 mg of 0, 3, 10 and 30 minute kaolin samples were immersed in a few drops of pyridine liquid.
- b) Samples were stored in air tight containers for approximately 1 week with regular shaking.
- c) Cold air was used to dry off just enough sample for experimental procedures.
- d) Remaining wet sample was stored in air tight containers until required.
- e) Step c) was repeated when additional sample was required.

For DRIFTS, the sample was diluted to 5% with KBr and the mixture was very lightly ground with a pestle and mortar for 40 seconds to obtain a uniform particle size and to provide adequate particle mixing. Spectra were collected according to the method described in Chapter 1.

3.2.2 Stability test of the pyridine treated samples.

In order to ensure that the potential kaolin-pyridine complex was stable at room temperature, the following investigation was conducted: Initially the DRIFT spectra at room temperature (RT DRIFTS) of the pyridine treated samples (sample 1) were recorded. . The wet sample was stored (as (d) above). Sampling was then repeated (as (e) above), the sample was diluted to 5% in KBr and a spectrum was obtained (sample 2). The remaining 5% mixture was stored in a sealed vessel for 24 hours, after which time, another spectrum was obtained (sample 3). Since it is a requirement of both variable temperature (VT-) DRIFTS and TGA that the sample be purged with N₂ carrier gas, after a further 24 hours storage in a sealed vessel, the mixture was purged for 30 minutes under a nitrogen flow of 10 ml per minute and the RT DRIFT spectra were subsequently recorded (sample 4). No observable changes in the spectra were noted (see Figure 3.9) The spectra were offset for clarity.

Figure 3.9 Stability test of pyridine exposed kaolin. The 3800-2600 cm^{-1} region.

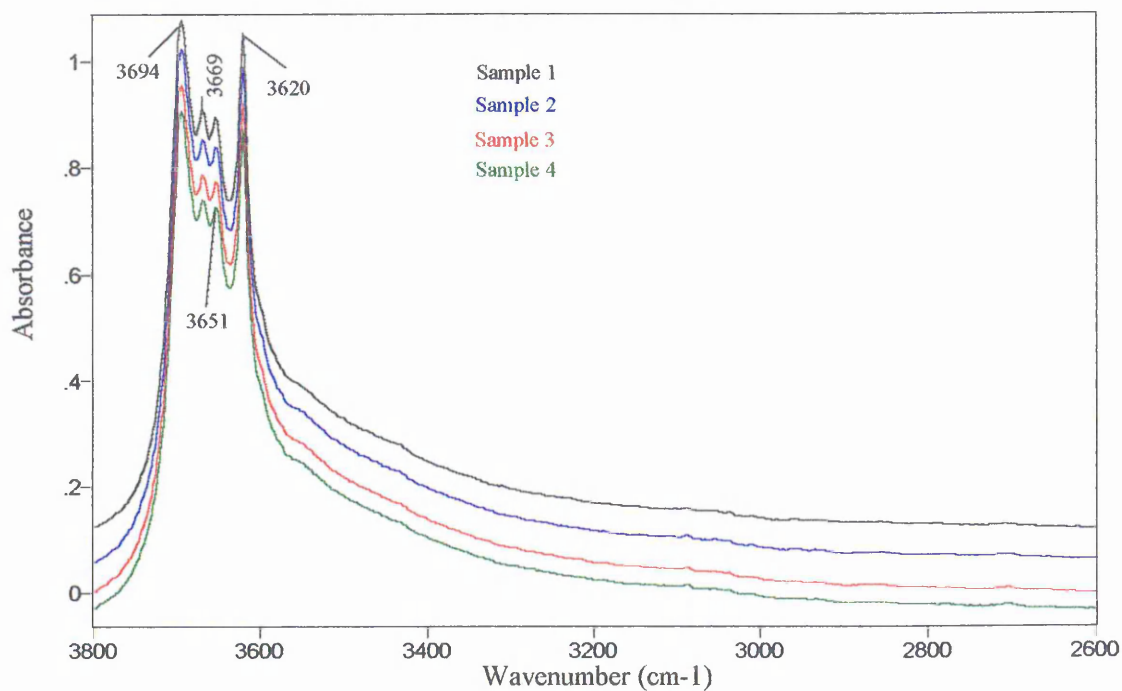
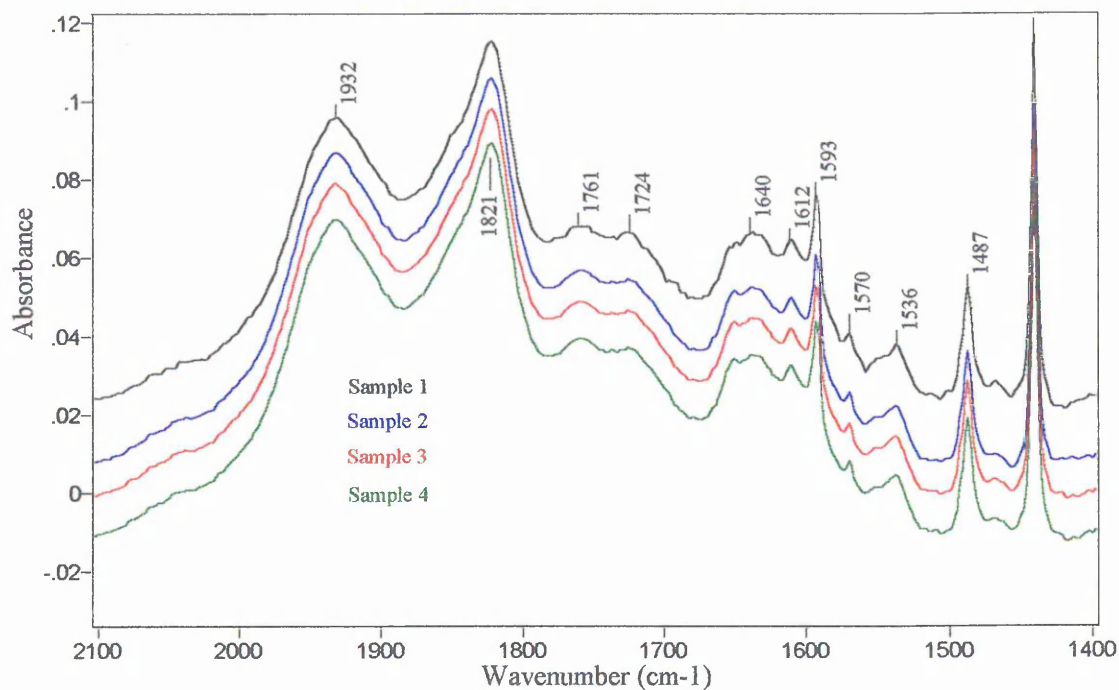


Figure 3.10 Stability test of pyridine exposed kaolin. The 2100-1400 cm^{-1} region.



3.3 Results.

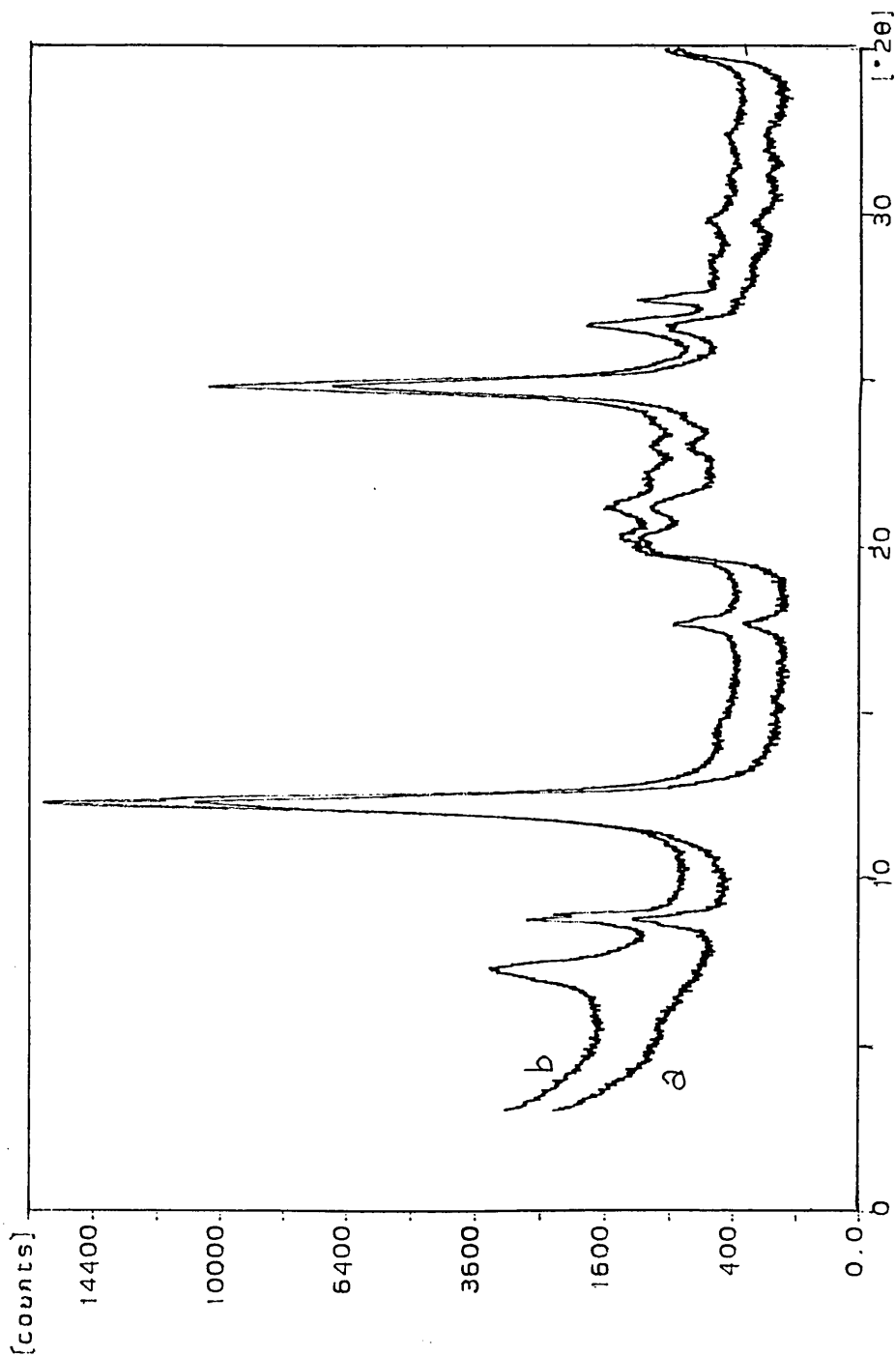
3.3.1 Impurity identification using XRD and DRIFTS.

Although halloysite readily intercalates water to yield a 10\AA phase, hydrated kaolins do not exist naturally. Several mechanisms have been described for preparing hydrated kaolin^{2,33} using entraining agents to facilitate the entry of water into the interlamellar spaces. The intercalation of kaolin with pyridine has not been previously described under the conditions used in the present work. When pyridine forms an intercalation complex with halloysite, the d spacing is 12\AA ³⁴.

The XRD traces yielded interesting results. The gross changes associated with the milling of kaolin were discussed in Chapter 2. The attention of the reader is now drawn to Figure 3.11 below.

Trace b (pyridine exposed sample) shows that there is clear evidence of a swelling component giving a peak at $7.33^\circ 2\theta$ (d spacing of 12.06\AA). Under ambient conditions such as those used for pyridine exposure in the current work, kaolin is not known to swell in the presence of pyridine. The identity of this swelling component was therefore questionable, and an attempt to identify it was made. XRD elucidated a suspected mica impurity, however, mica is not known to swell in the presence of pyridine. Other common impurities in kaolin mineral samples are halloysite, smectite and chlorite. Halloysite does swell in the presence of pyridine, and gives a d spacing of 12.06\AA if the pyridine is perpendicular to the sheets, and 10.1\AA if it is parallel (see Figure 3.12). Note that similar d spacings are expected for pyridine intercalated kaolin, but this reaction is not thought to take place under ambient conditions². Smectite does swell after pyridine exposure, giving a d spacing of 12.5\AA if the organic is parallel with the mineral layers, and 14.8\AA if it is perpendicular (see Figure 3.13).

Figure 3.11 XRD Comparison of unexposed and pyridine exposed kaolin.



Trace a shows unmilled, unexposed kaolin.

Trace b shows the same sample after exposure to pyridine for 3 days*.

* It should be noted that a trace showing kaolin exposed to pyridine for 3 weeks was the same as that for the sample exposed for 3 days.

Figure 3.12 Schematic of the swelling of halloysite with pyridine.

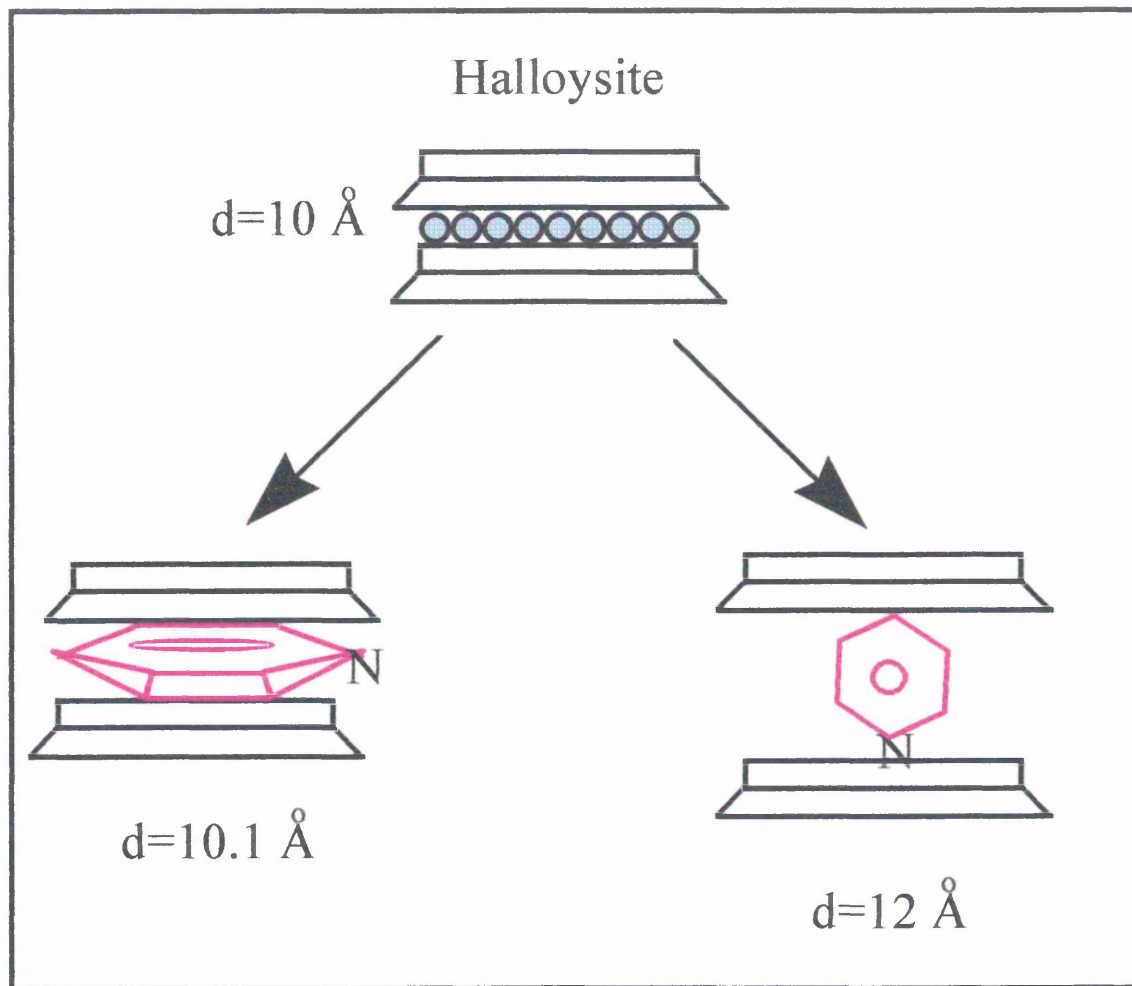
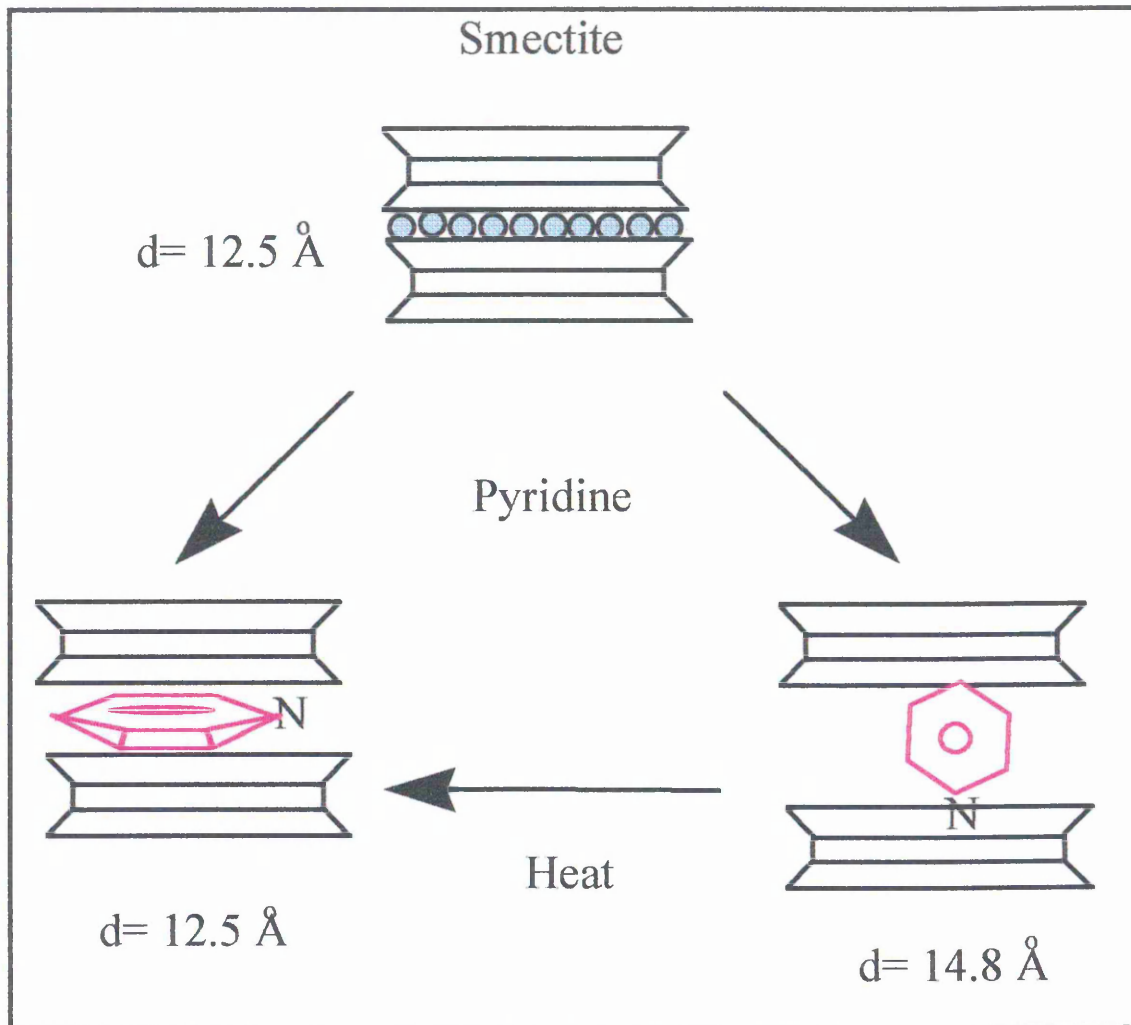


Figure 3.13 Schematic of the swelling of smectite with pyridine.



Another reason for suspecting these minerals as an impurity is the presence of a broad feature centring at $c 5.5^{\circ}2\theta$ in the unexposed kaolin. This could correspond to chlorite or smectite. Halloysite in the dehydrated form would have a d spacing of 7.2 \AA and be hidden under the very intense kaolin 001 peak at the same position. Hydrated halloysite, however would have a d spacing of 10 \AA and be present $c 8.5^{\circ}2\theta$ - the same position as the mica peak.

In order to test for traces of halloysite and smectite, the following studies were carried out.

a) Test for halloysite.

The method was published by Churchman et al³⁵. An XRD trace of the unmilled, unexposed kaolin was collected (Figure 3.15). The same sample was then exposed to

analytical grade formamide for less than one hour. Another XRD trace, this time of the formamide exposed kaolin, was collected under the same conditions (Figure 3.16). Under these conditions, kaolin does not swell. However, hydrated halloysite, or naturally dehydrated halloysite will be expanded by formamide and swell to a d spacing of 10.4 Å (see Figure 3.14).

Figure 3.14 Schematic of reactions of kaolin and halloysite with formamide.

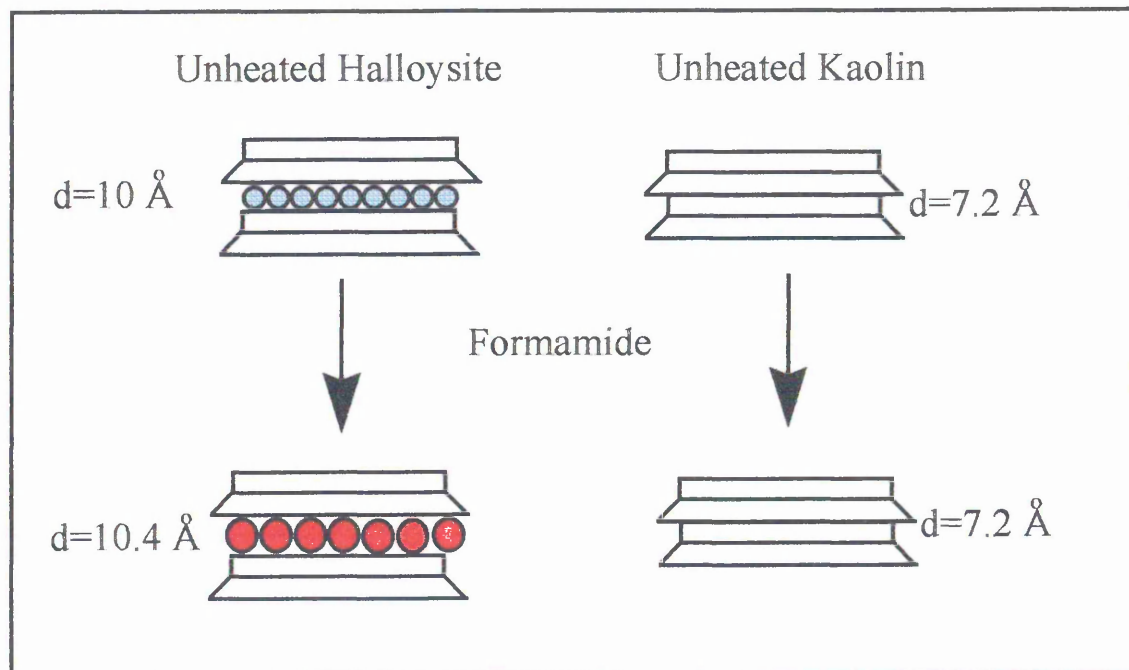
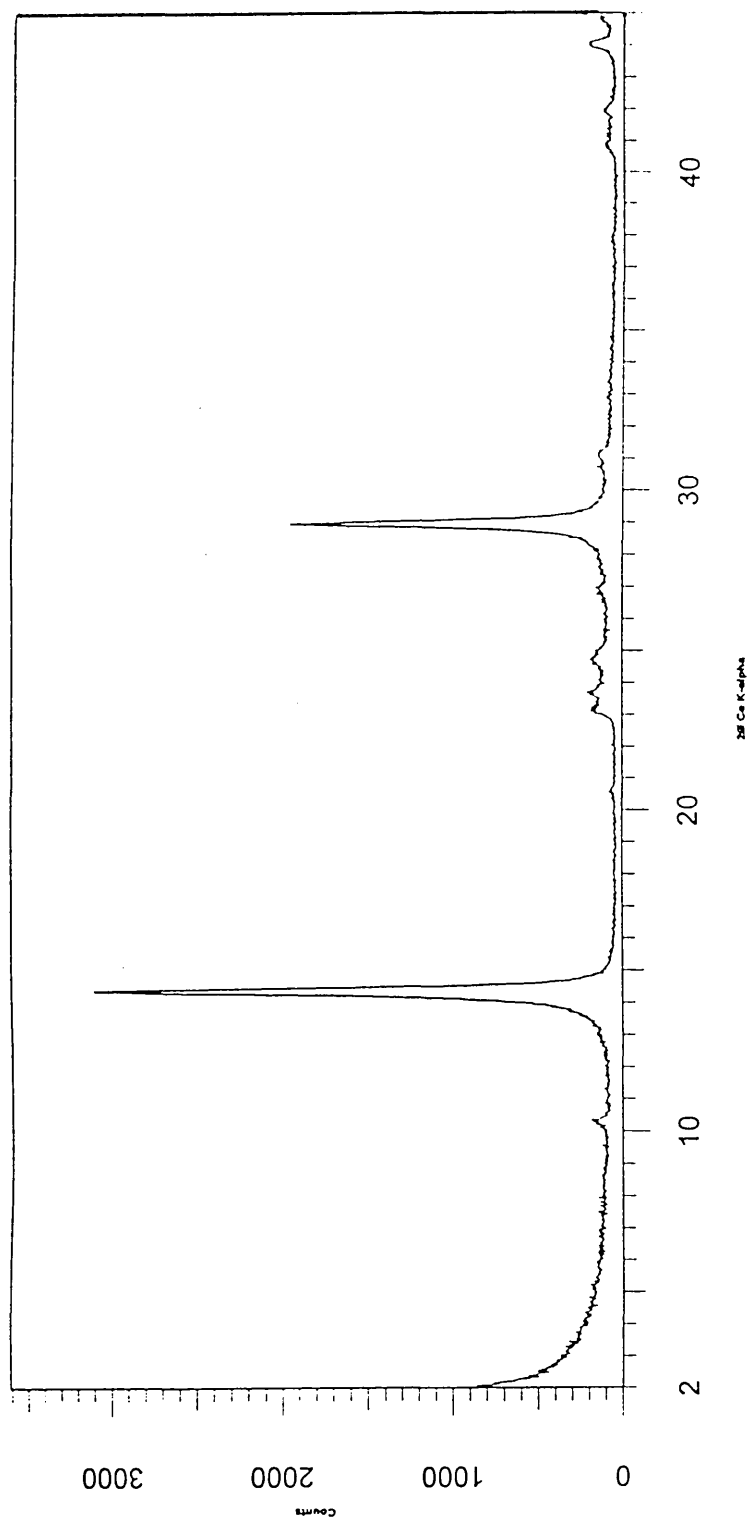


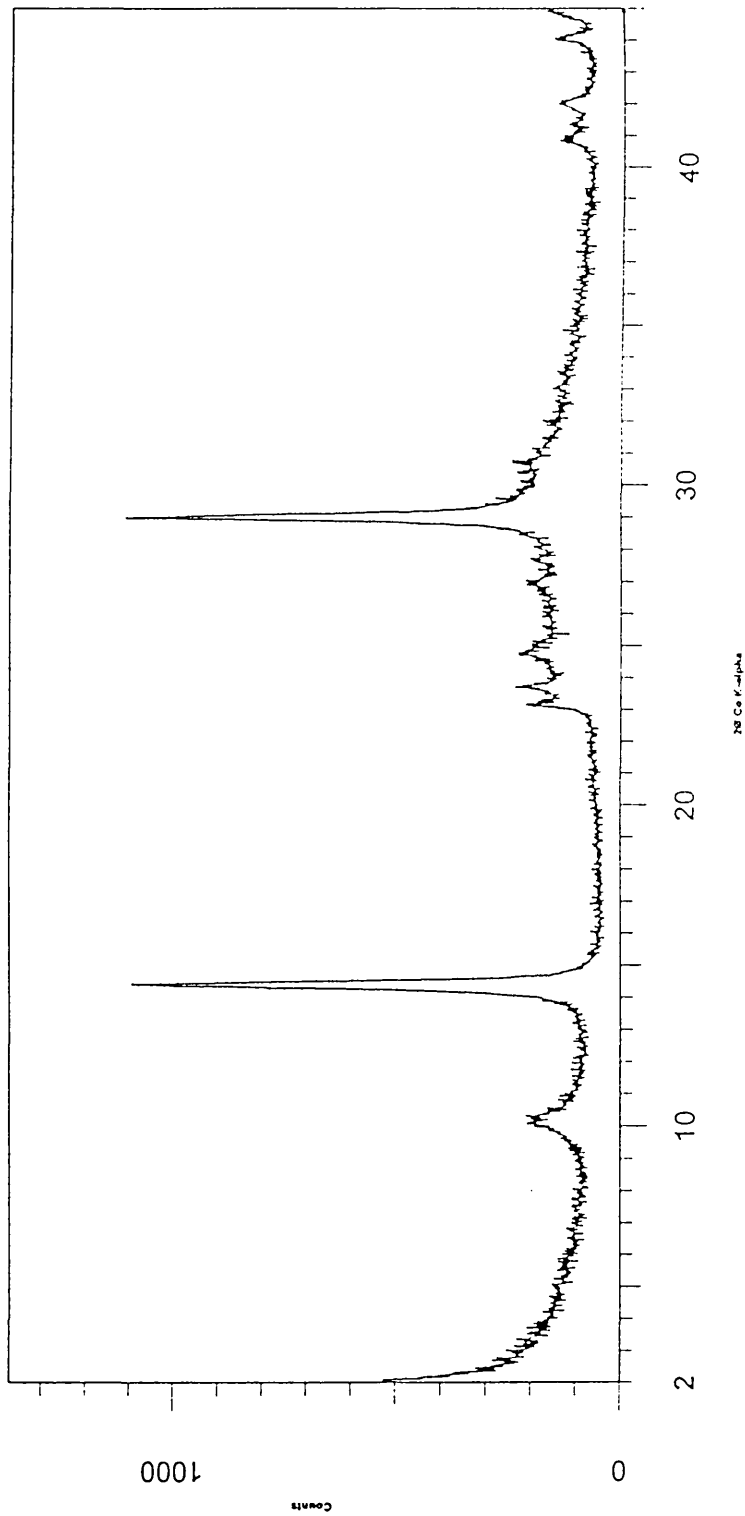
Figure 3.16 shows that there is a feature at c 10 Å in the formamide treated sample, suggesting the presence of formamide- intercalated halloysite. The small band at c 10 Å in the unexposed sample may be due to either water expanded halloysite or mica. However, this band does not change in the pyridine exposed kaolin XRD trace (Figure 3.11), so it is not likely to represent water expanded halloysite, because this would be intercalated with pyridine. Thus, this peak is more likely to represent mica.

Figure 3.15 XRD trace of unmilled, unexposed kaolin*.



* Data collected by Dr Stephen Hillier, Soil Science Group, Macaulay Land Use Research Institute.

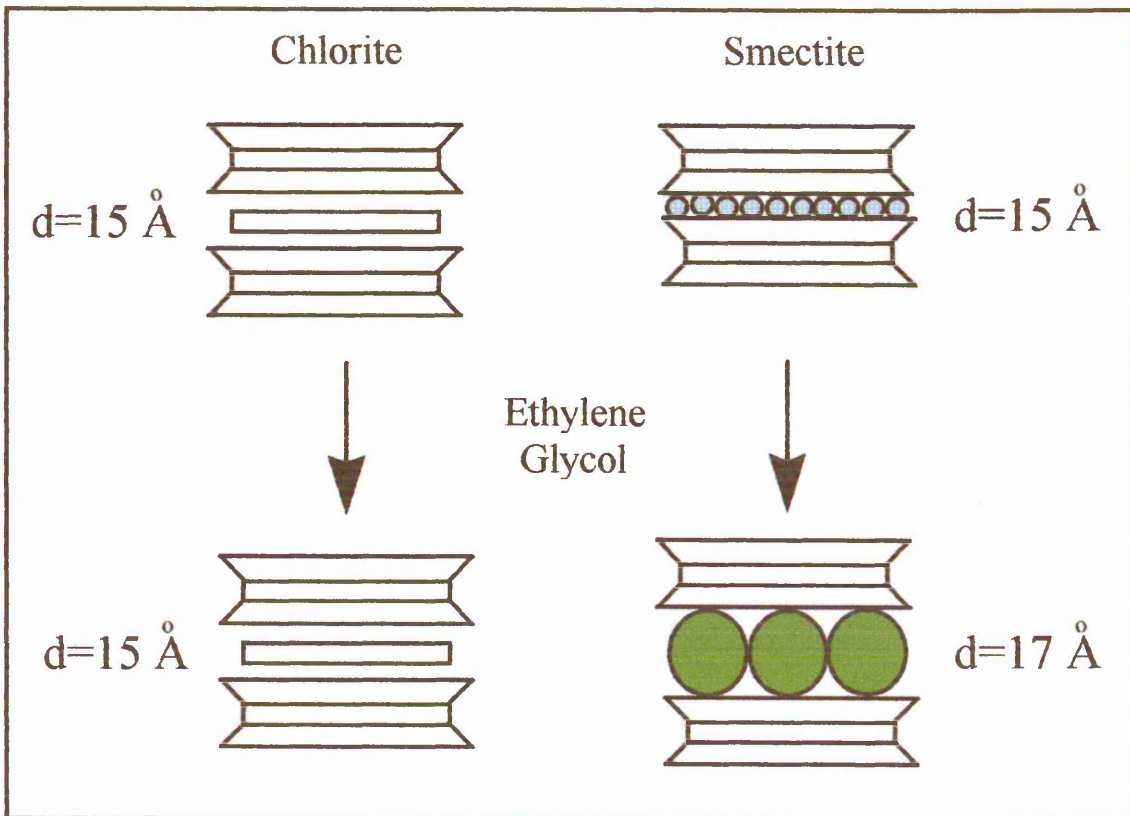
Figure 3.16 XRD trace of unmilled, formamide exposed kaolin.



b) Test for smectite.

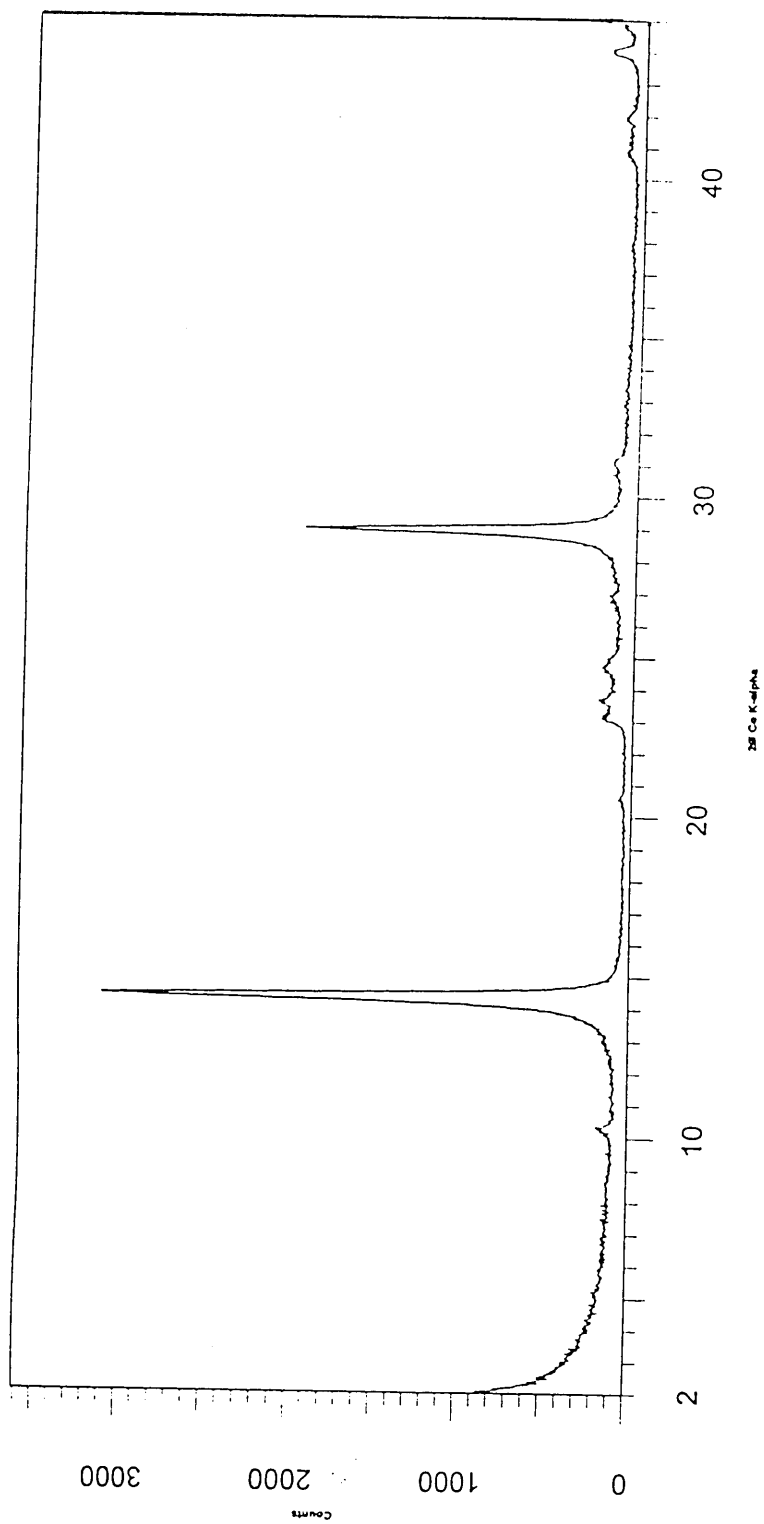
Smectite (with a d spacing of 15 Å in its naturally hydrated state) is known to swell in the presence of ethylene glycol to give a d spacing of 17Å (see Figure 3.17). Glycol does not swell kaolin, nor does it swell the possible contaminant, chlorite.

Figure 3.17 Schematic of the reactions of chlorite and smectite with ethylene glycol.



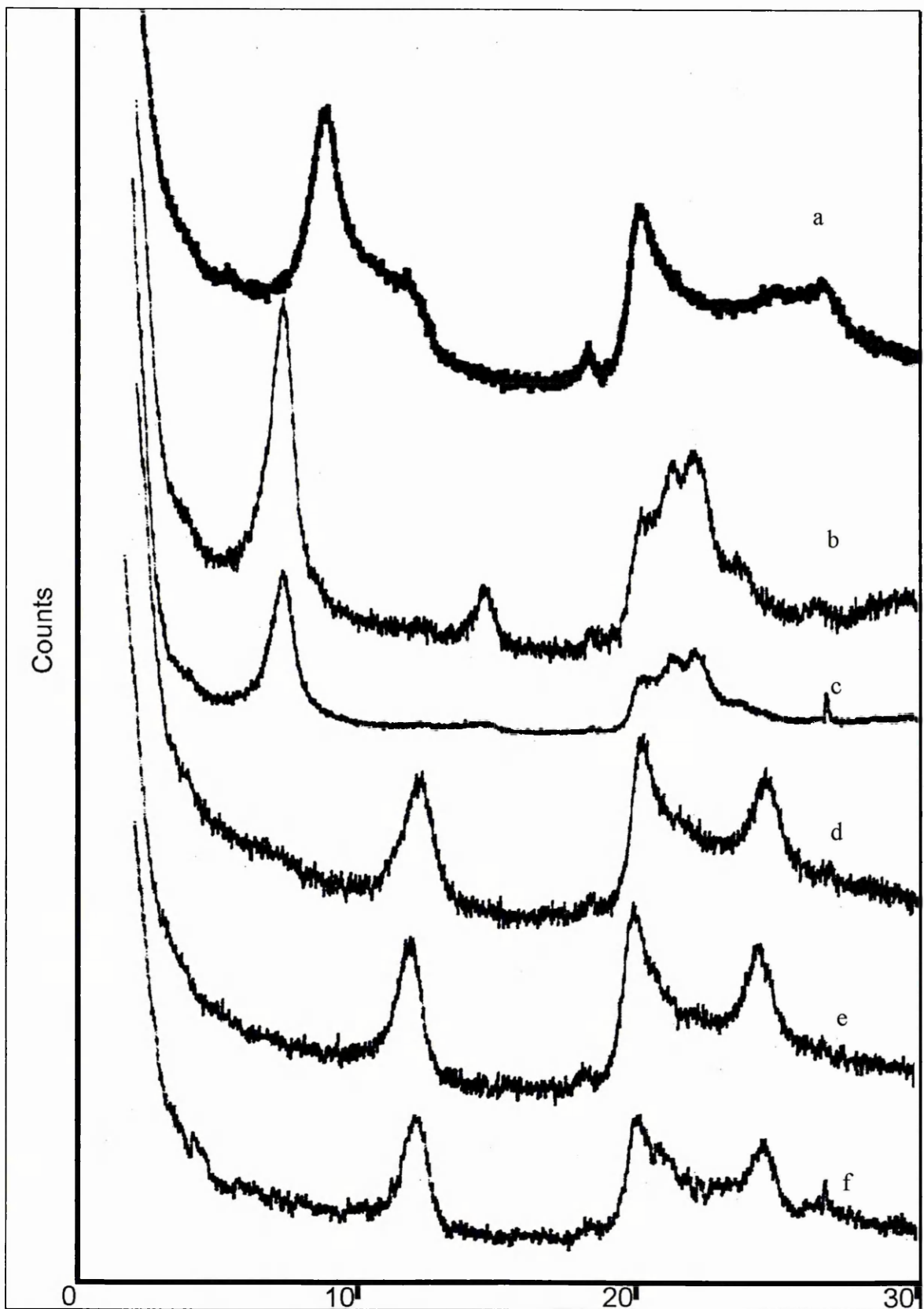
The figure above shows the XRD trace of unmilled kaolin treated with di-ethylene glycol. Clearly, there is no evidence of a 17Å component, therefore the swelling component in the kaolin sample cannot be smectite. The broad feature at approximately 15Å is still visible. It is thought that this band represents a chlorite impurity. Due to the $\text{Mg}(\text{OH})_2$ layer which is between the chlorite sheets, further intercalation is not possible with glycol, and thus, the d spacing remains 15Å.

Figure 3.18 XRD trace of ethylene glycol-exposed unmilled kaolin.



Thus it was concluded that the swelling component present as an impurity in the kaolin sample was naturally dehydrated halloysite. Further evidence for this hypothesis was that the relative intensity of the 001 peak at $7.33^{\circ}2\theta$ in Figure 3.11 was higher than expected compared with the 002 peak³⁶ before pyridine exposure, but the relative intensities became more usual for a well ordered kaolin after pyridine exposure. The 001 band of dehydrated halloysite is also at $12.5^{\circ}2\theta$, and since it reduced in intensity (compared with the 002 peak) after pyridine exposure, this suggests that the previously dehydrated halloysite is becoming swollen by the pyridine, thus giving a new peak at $7.33^{\circ}2\theta$ (12.06\AA). VT XRD studies showed that the pyridine-intercalated structure was shown to collapse at c 100°C , VT DRIFTS studies showed that pyridine was not completely removed from this sample until c 200°C . VT DRIFTS studies of the pyridine exposed Cornish kaolin (see later) show that pyridine can remain visible until very high temperatures (e.g. 300°C). Therefore, initially, the spectra presented between room temperature and 100°C are composites of pyridine adsorbed onto kaolin, and intercalated pyridine-halloysite. Thereafter, the pyridine associations observed are due solely to the interactions of pyridine with kaolin, and pyridine with halloysite via adsorption (although “pockets” of trapped pyridine may form in the collapsed halloysite structure-also see later for full explanation).

Figure 3.19 XRD traces of unexposed halloysite and VT XRD of pyridine exposed halloysite



Trace a shows the low angle reflections for a naturally partially dehydrated (unexposed) halloysite at room temperature. There is an intense 001 band at $c 10^\circ 2\theta$, representing a d spacing of 10 Å. It has a broad and intense shoulder at 7.2 Å, which corresponds to the 001 reflection of dehydrated halloysite. (compare with the room temperature XRD trace of unexposed, unmilled kaolin presented in Chapter 2). Trace b shows that, after exposure to pyridine, there is no evidence of the 10 Å or 7Å bands. There is a strong band at 12 Å, which corresponds to halloysite which has become fully expanded by pyridine. Pyridine is thus being intercalated perpendicular to the mineral sheets, as predicted. After heating to 50 °C, the pyridine exposed halloysite trace (c) shows that there has been a decrease in the intensities of both the 001 and 002 reflections. Trace d shows that at 100 °C, there has been a dramatic change in the expansion of the mineral. The 12 Å pyridine-intercalated halloysite reflection has disappeared, but there is now clear evidence of a 7.2 Å reflection which corresponds to dehydrated halloysite. This trace suggests that all detectable pyridine has been expelled from between the halloysite layers, and that the mineral structure has collapsed. There was very little change in the XRD traces between 100 and 175 °C (traces e and f were collected at 150 and 175 °C respectively).

3.3.2 TGA.

3.3.3 Figure 3.20 TGA of pyridine exposed unmilled kaolin.

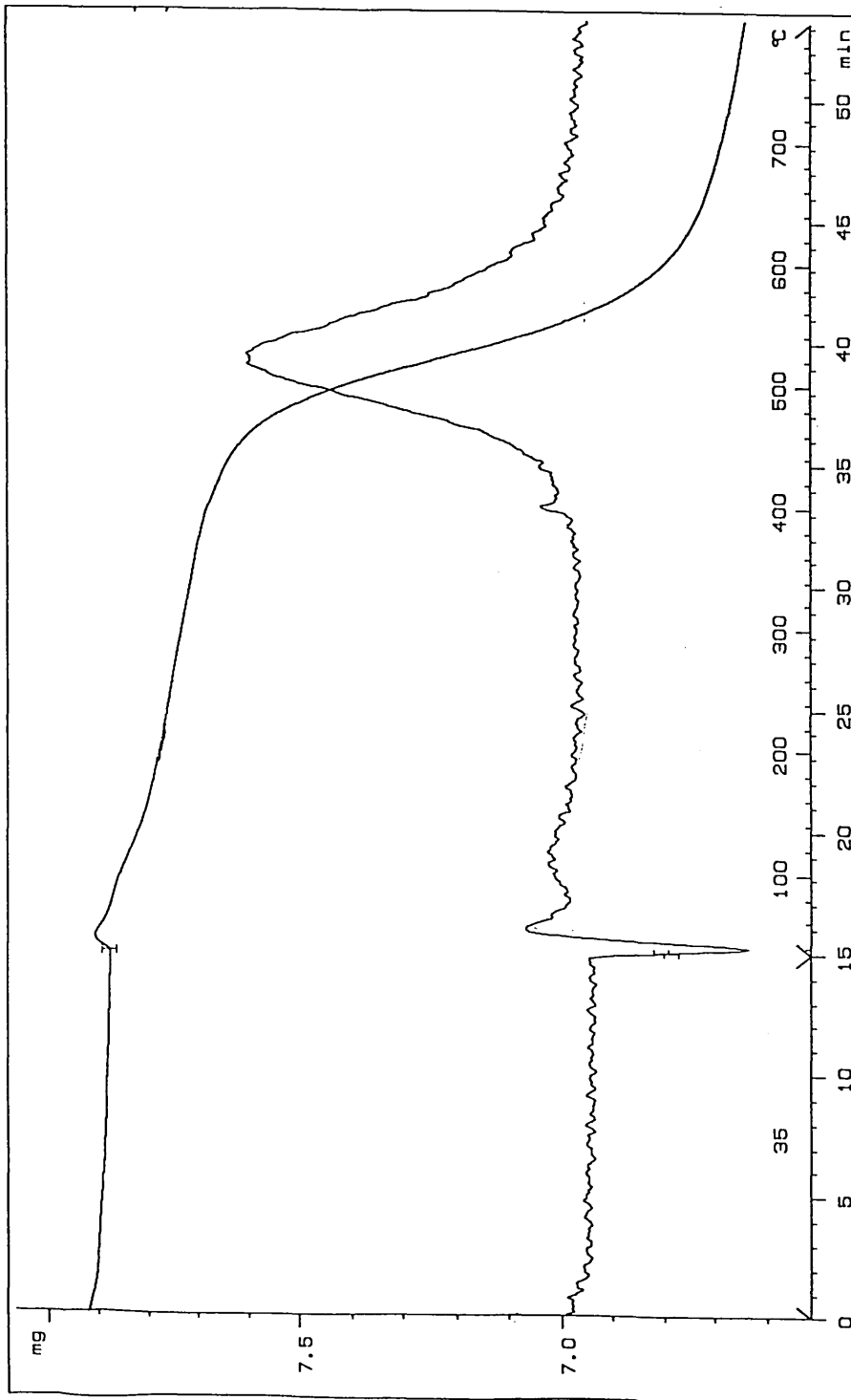


Figure 3.21 TGA of pyridine exposed 3 minute milled kaolin.

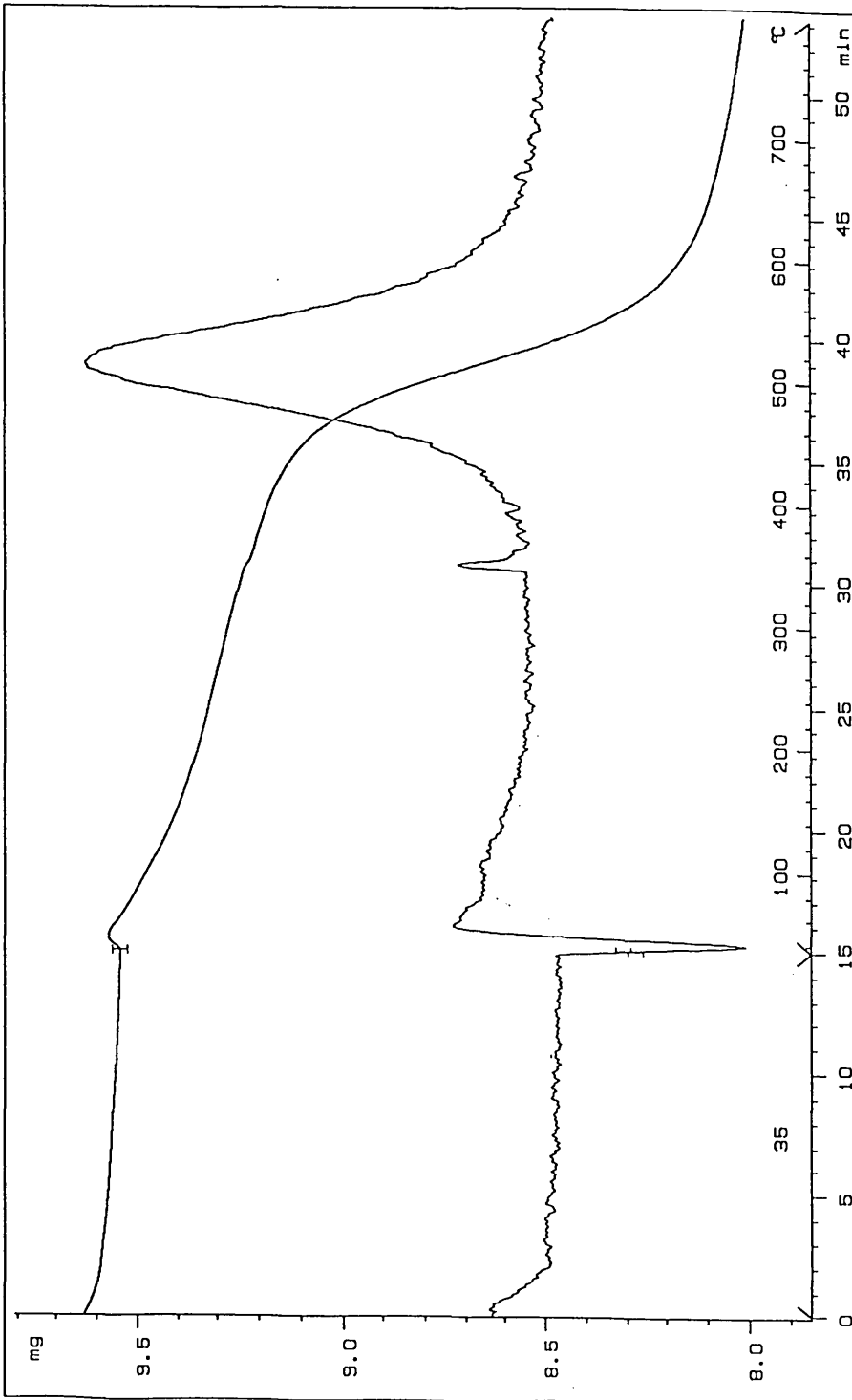


Figure 3.22 TGA of pyridine exposed 10 minute milled kaolin.

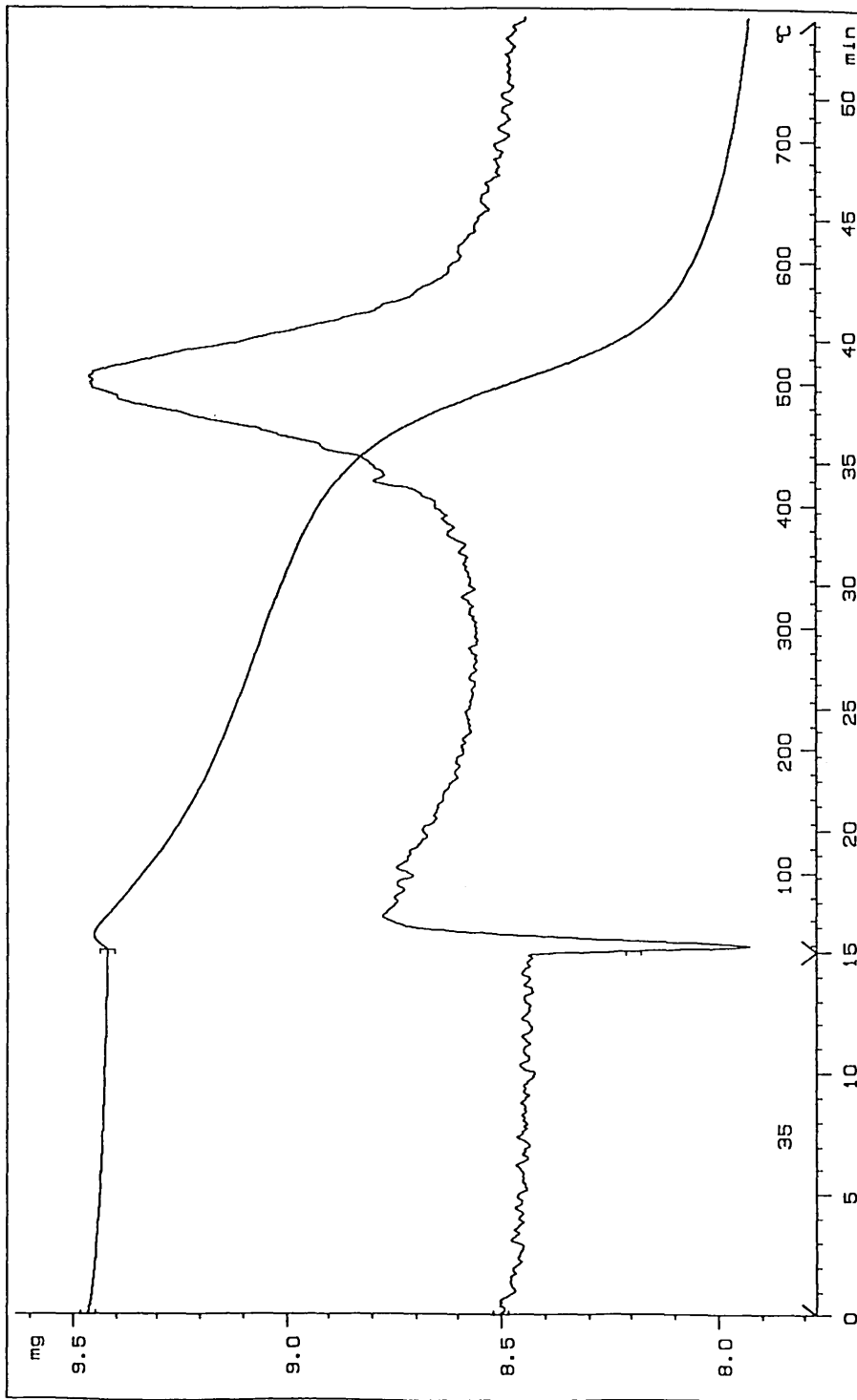


Figure 3.23 TGA of pyridine exposed 30 minute milled kaolin.

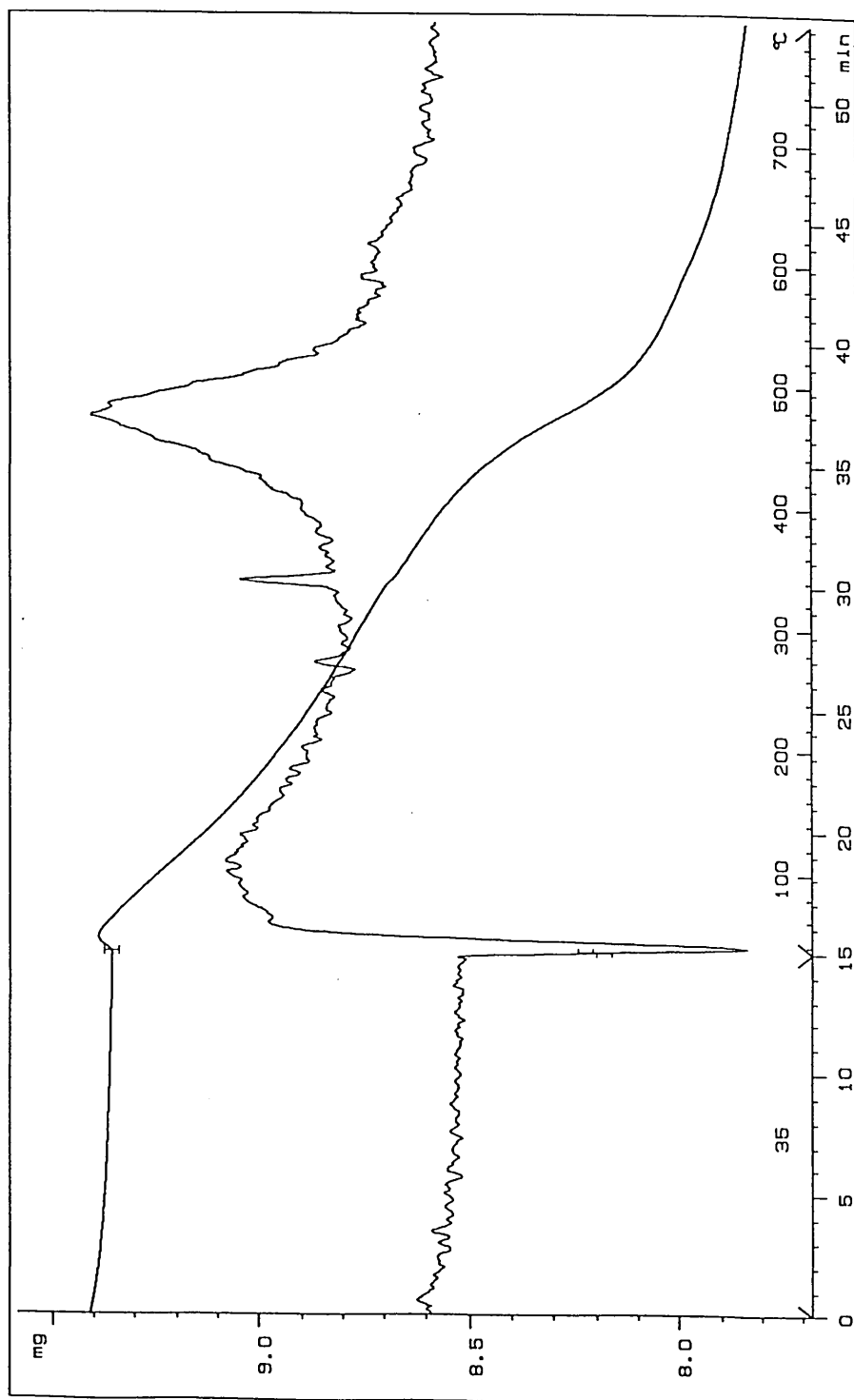


Table 3.1 Weight losses from kaolin during thermal analysis.

Milling time (mins)	Weight loss under 400°C (%)	Total weight loss (%)
0	2.4	15.4
3	3.4	15.4
10	5.0	15.0
30	7.9	15.1

The weight loss under 400 °C is very loosely assigned to the loss of “sorbed water” and pyridine. The weight loss increased as milling time increased. This trend was also observed in the unexposed kaolin TGA data. The values for all the pyridine exposed kaolin samples are lower than for the unexposed equivalent sample. The total weight losses from the pyridine exposed samples was very similar for all ball milling times. The total weight losses were also slightly reduced compared with the unexposed ball milled kaolins. The differences in weight loss between the unexposed and exposed samples is always less than 1 % and may fall within the limits of the error of the method, and therefor may not be significant. However, if the results are significant, they support the theory that water is being replaced by pyridine, and as such, the removal of the lower density pyridine is causing reduced weight loss.

3.3.4 VT-DRIFTS of halloysite.

Figure 3.24 Halloysite. The effect of temperature. The 3800-2400 cm^{-1} region*.

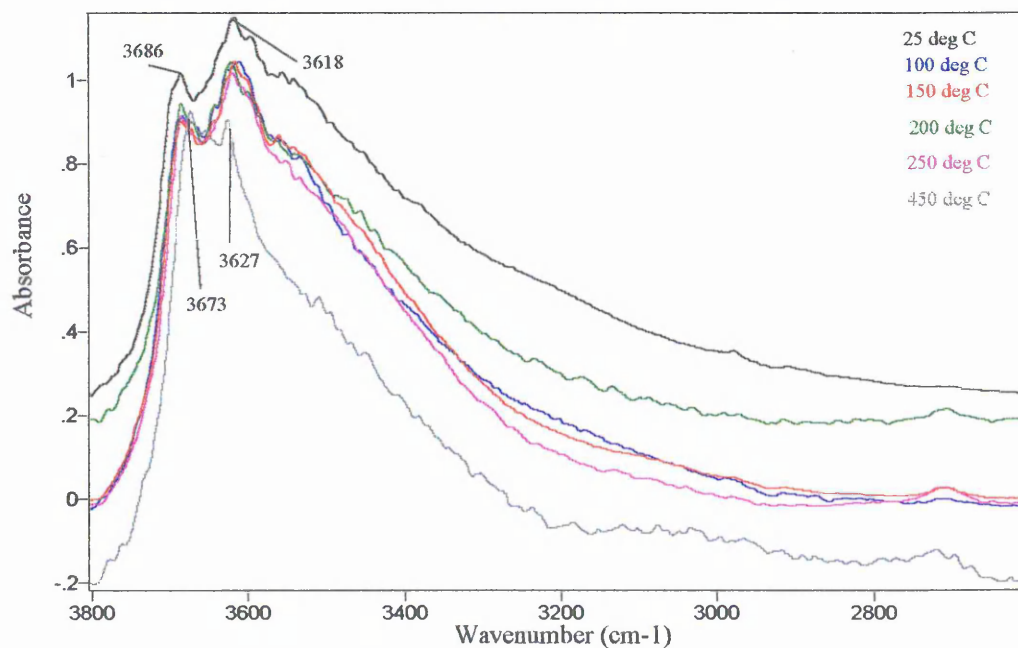
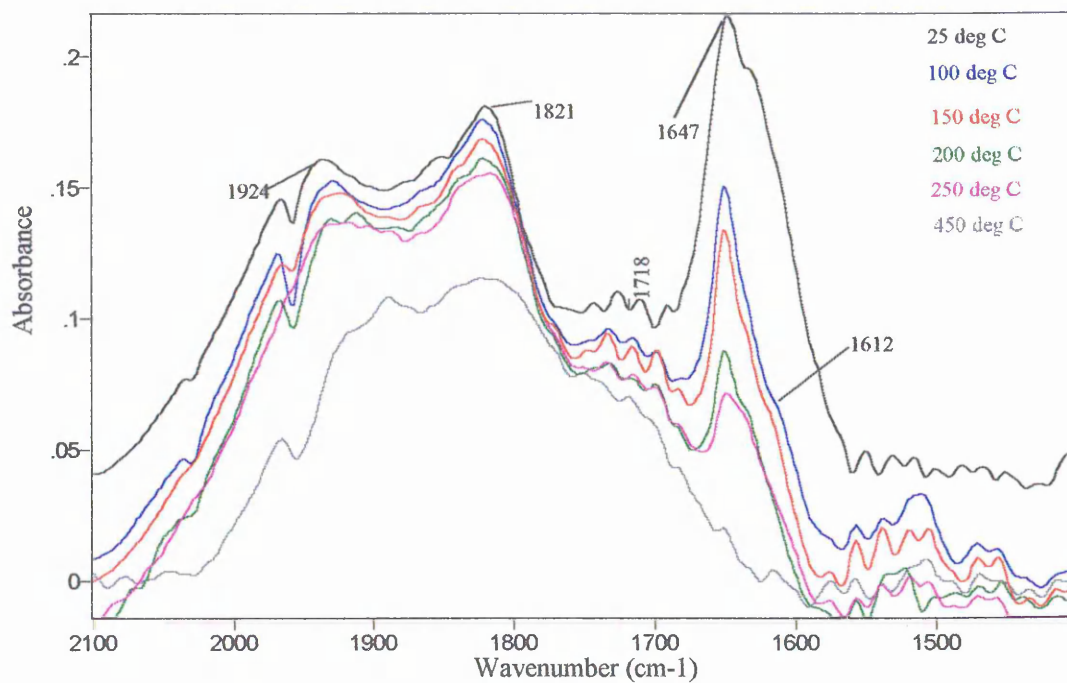


Figure 3.25 Halloysite. The effect of temperature. The 2100-1400 cm^{-1} region*

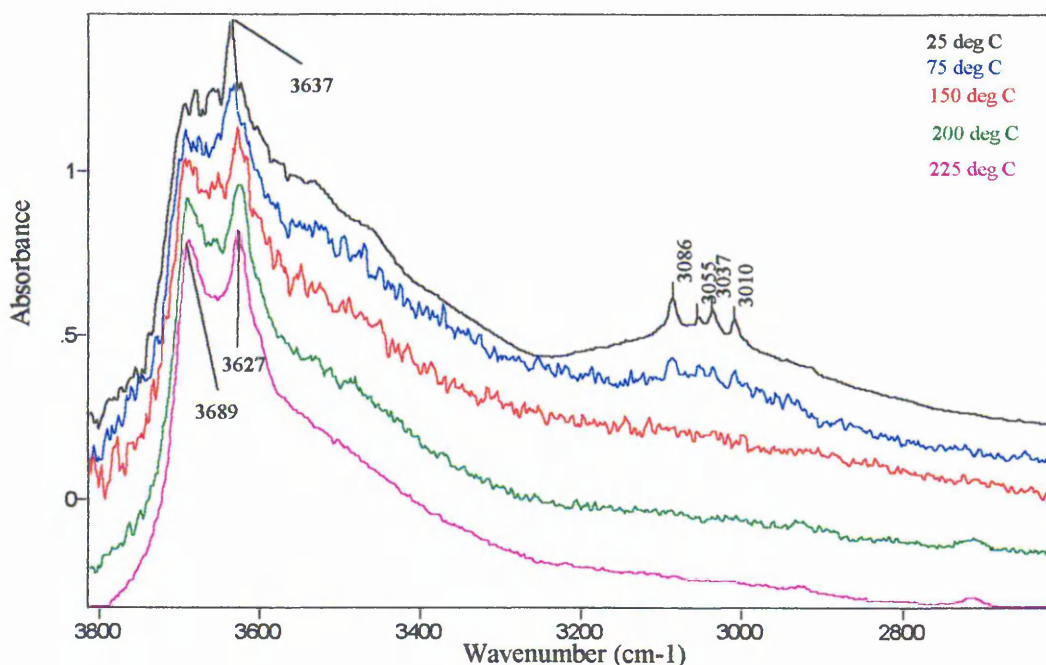


* Data collected by Marian Centeno at MRI, Sheffield Hallam University.

There was a very high contribution from water vapour in the halloysite VT DRIFT spectra, and smoothing of the stretching and bending regions has been used to highlight the changes in the band shapes compared with pyridine. The smoothing method was binomial, and no bending region spectrum was smoothed by more than 9 points, and no stretching region spectrum was smoothed more than 5 points. The water vapour contribution was thus minimised, but band shapes and intensities were not altered.

3.3.5 VT-DRIFTS of pyridine exposed halloysite.

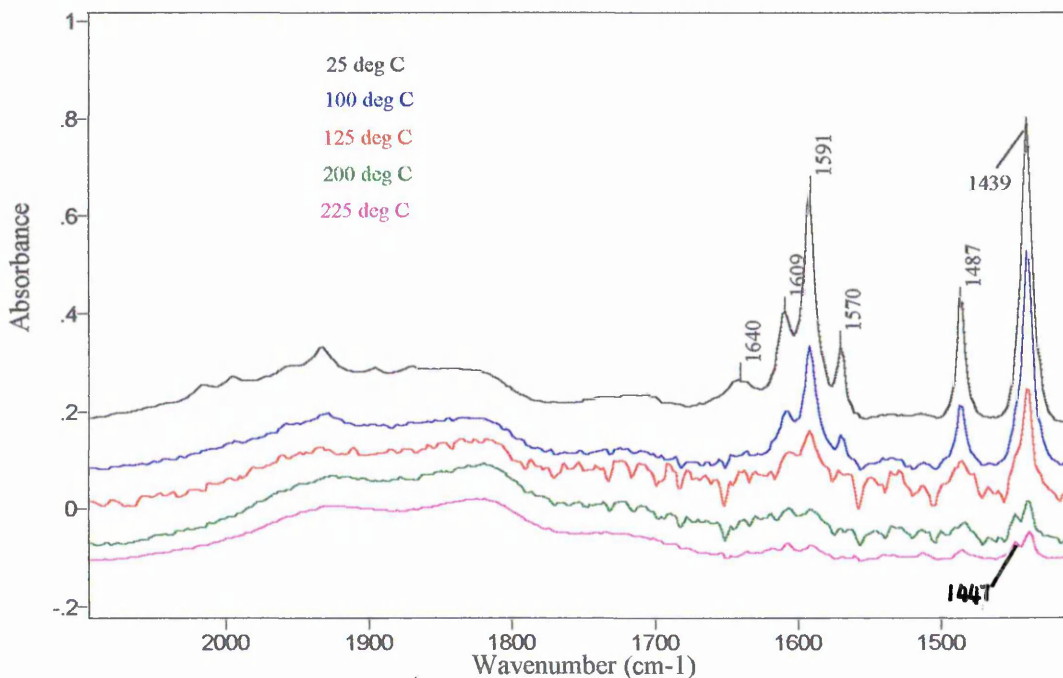
Figure 3.26 Halloysite-pyridine. The effect of temperature. The 3800-2400 cm^{-1} region*.



At room temperature, there were three distinct bands at 3087, 3037 and 3010 cm^{-1} , which are assigned to the CH stretching modes of pyridine. At 75 °C, the 3693 band has begun to re-emerge, indicating that some of the intercalated pyridine has been expelled, and there is now some hydrogen bonding between adjacent halloysite sheets. The bands at 3087, 3037 and 3010 cm^{-1} have reduced in intensity, and are now represented by one broad band centring at c 3050 cm^{-1} . Again, this illustrates the loss of intercalated pyridine. At 150 °C the 3695 cm^{-1} is significant in peak height, but is not as intense as

the 3631 cm^{-1} band. At 200 °C, there is little or no evidence of intercalated pyridine in the 3087-3010 cm^{-1} region, and at 225 °C the spectrum in the stretching region resembles that of a poorly order kaolin, e.g. after 30 minutes ball milling (see Chapter 2).

Figure 3.27 Halloysite-pyridine. The effect of temperature. The 2100-1400 cm^{-1} region.*



Three combination bands are present at 1930 and 1823 and 1730 cm^{-1} as in the kaolin spectrum. At room temperature, the pyridine exposed halloysite spectrum shows bands characteristic of hydrogen bonded pyridine, represented by the very intense band at 1592 cm^{-1} . There is no conclusive evidence of a Brønsted band at 1540 cm^{-1} . At 100 °C the relative intensities of the 1440, 1490 and 1592 cm^{-1} bands are very similar to those at room temperature. However, at 150 °C, the pattern is very different (not shown, but very similar to 200 °C spectrum). XRD data shows that halloysite structural collapse occurs before 100 °C, and thus pyridine has been expelled from between the mineral layers. The overall intensity of all the pyridine bands has been greatly reduced with respect to the halloysite structural bands at 1930 and 1823 cm^{-1} . There appears to be a shoulder on the 1439 cm^{-1} at 1449 cm^{-1} . This may indicate either the formation of a new type of Lewis association, the Lewis site may have become visible due to the decrease in

intensity of the 1439 cm^{-1} band (see Figure 3.60). At $200\text{ }^{\circ}\text{C}$, pyridine bands are still present. The intensity of the Lewis band at 1448 cm^{-1} has now become more significant. The band characteristic of hydrogen bonded pyridine at 1590 cm^{-1} is still present. At $225\text{ }^{\circ}\text{C}$, there is still evidence of pyridine adsorption via hydrogen bonding and Lewis type associations. These bands are very resistant to heat, and it is postulated that when the layers of halloysite collapsed at approximately $100\text{ }^{\circ}\text{C}$, pockets were formed towards the middle of the sheets and pyridine became trapped therein. The quantity of expanded material in the sample was below the detection limit of the x-ray diffractometer.

Thus, at lower temperatures, the major type of pyridine-halloysite association was by hydrogen bonding between the layers of the mineral. As temperature increased, Lewis type binding became more significant. Evidence of Brønsted type binding was not distinguishable from the water vapour contribution, and thus was assumed to be negligible.

3.3.6 VT-DRIFTS of ball-milled (FM) kaolin-pyridine.

3.3.6.1 Unmilled kaolin-pyridine. The 3800-2600 cm^{-1} region.

Figure 3.28 Comparison of unexposed and pyridine exposed kaolin (room temp.).

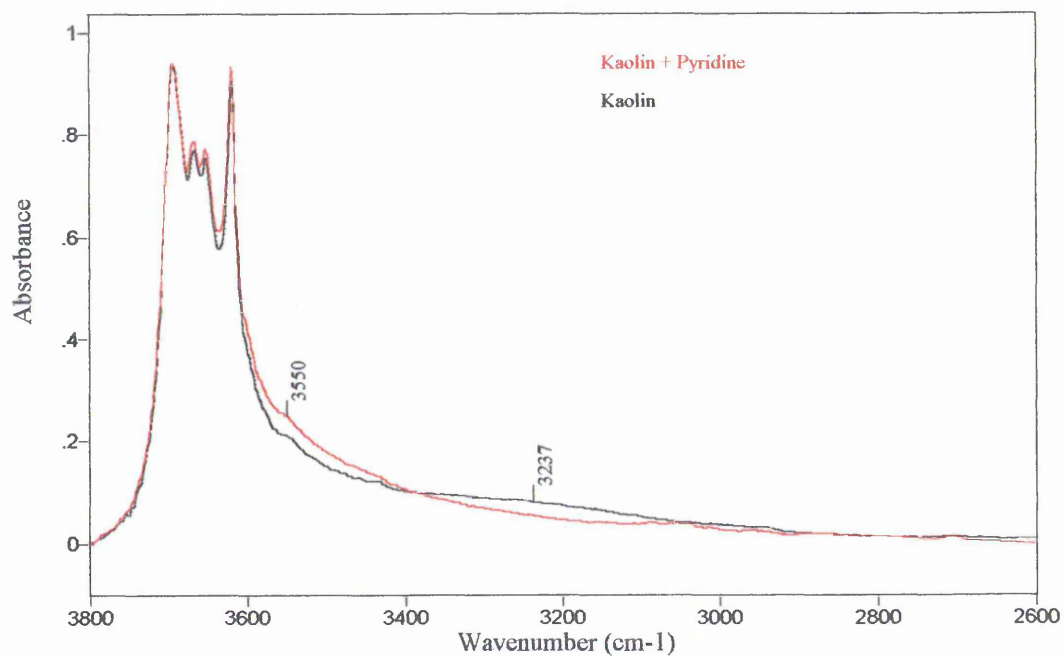
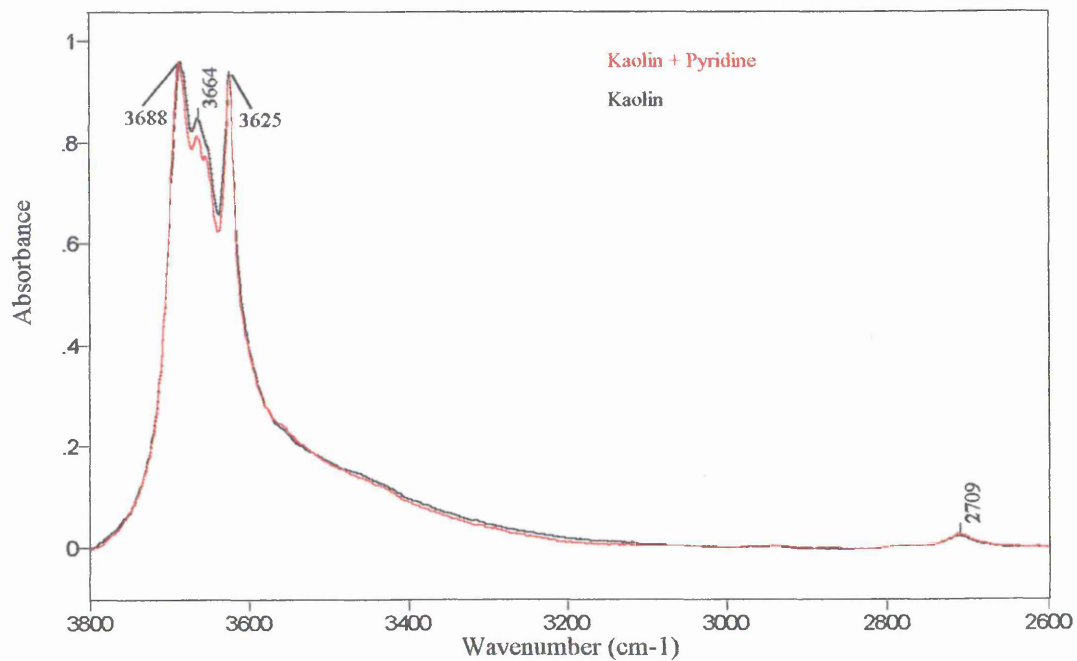


Figure 3.29 Comparison of unexposed and pyridine exposed kaolin (250 $^{\circ}\text{C}$).



3.3.6.2 3 minute milled kaolin-pyridine. The 3800-2600 cm^{-1} region.

Figure 3.30 Comparison of unexposed and pyridine exposed kaolin (Room temp.).

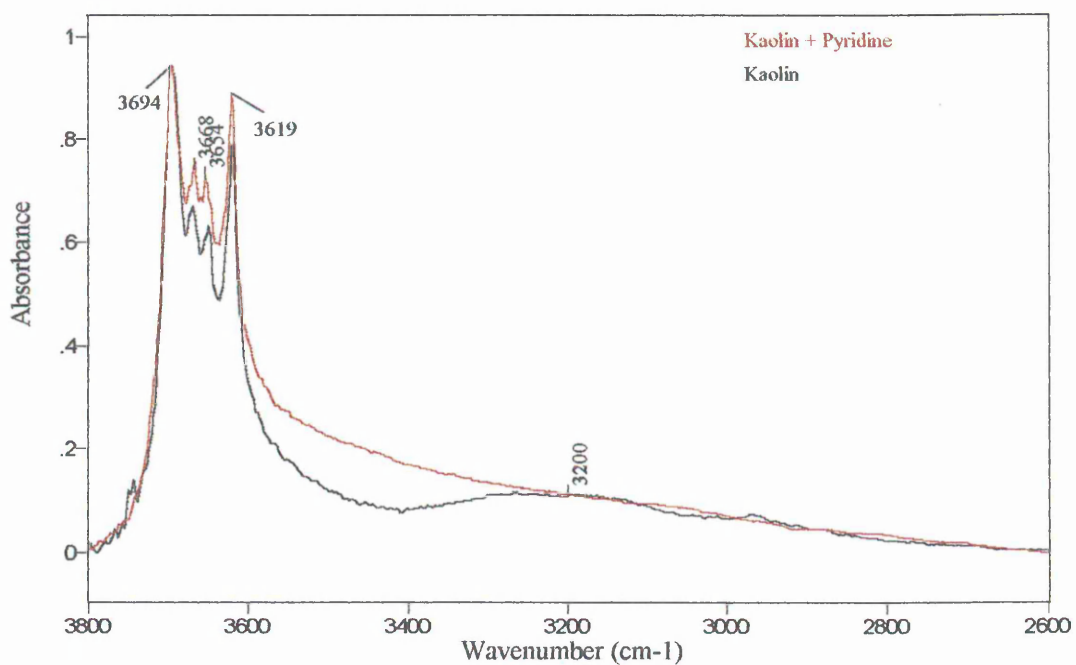
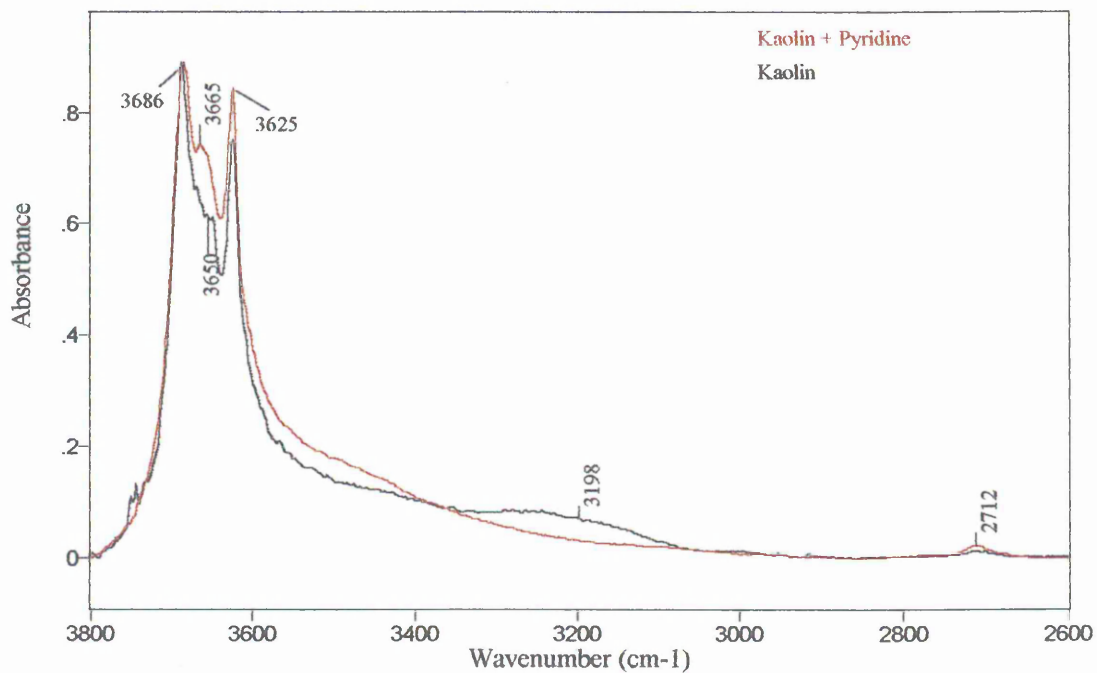


Figure 3.31 Comparison of unexposed and pyridine exposed kaolin (250 $^{\circ}\text{C}$).



3.3.6.3 10 minute milled kaolin-pyridine. The 3800-2600 cm^{-1} region.

Figure 3.32 Comparison of unexposed and pyridine exposed kaolin (Room temp.).

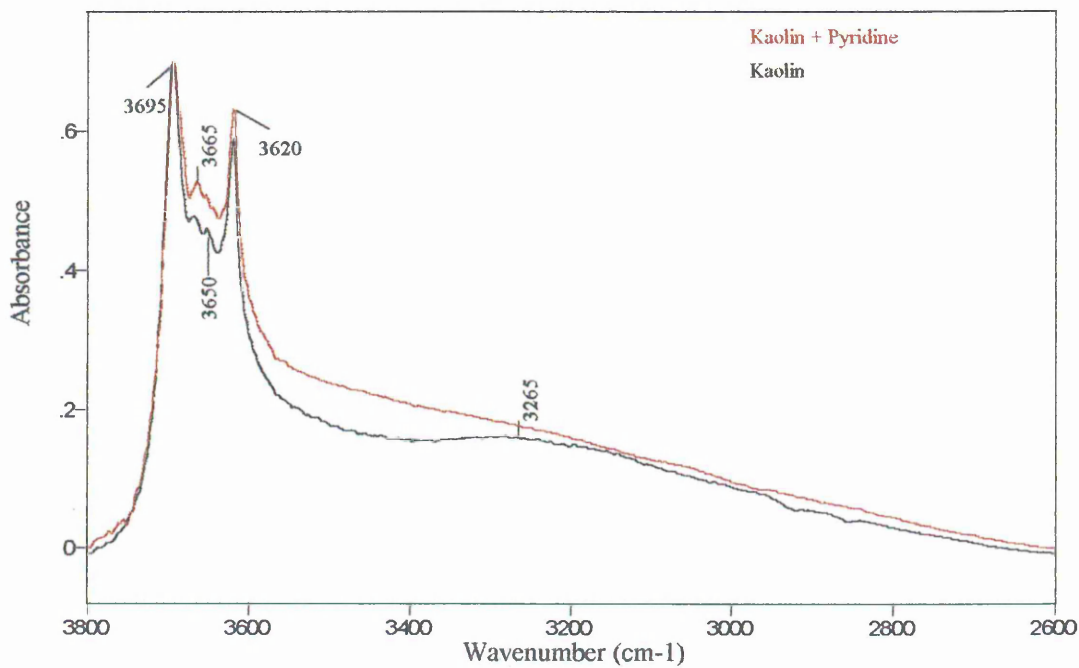
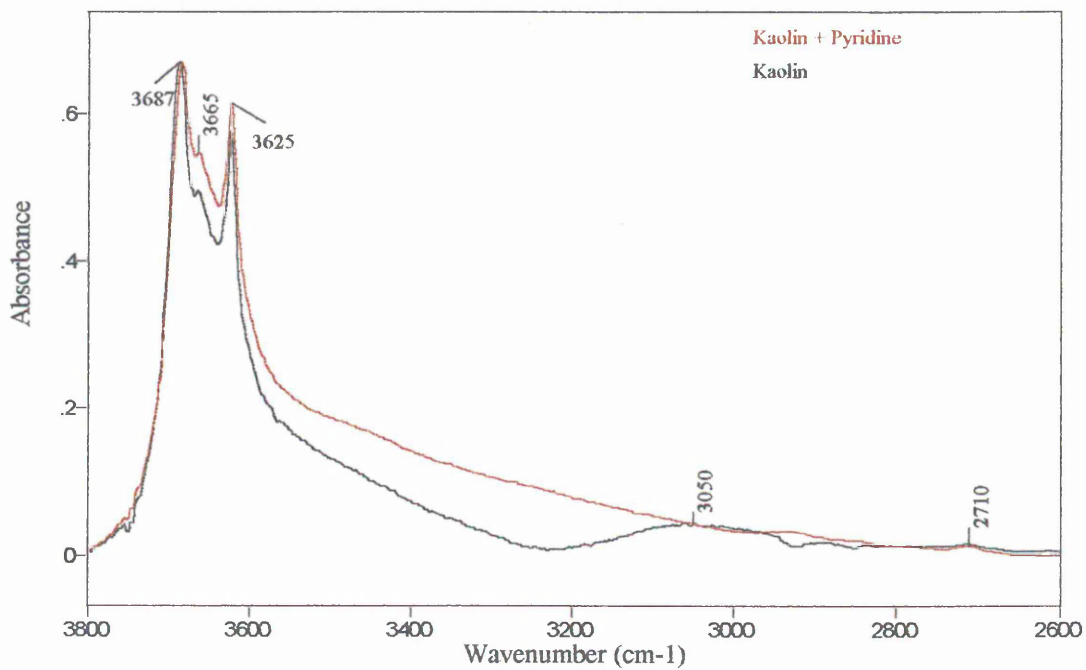


Figure 3.33 Comparison of unexposed and pyridine exposed kaolin (250 °C).



3.3.6.4 30 minute milled kaolin-pyridine. The 3800-2600 cm^{-1} region.

Figure 3.34 Comparison of unexposed and pyridine exposed kaolin (Room temp.).

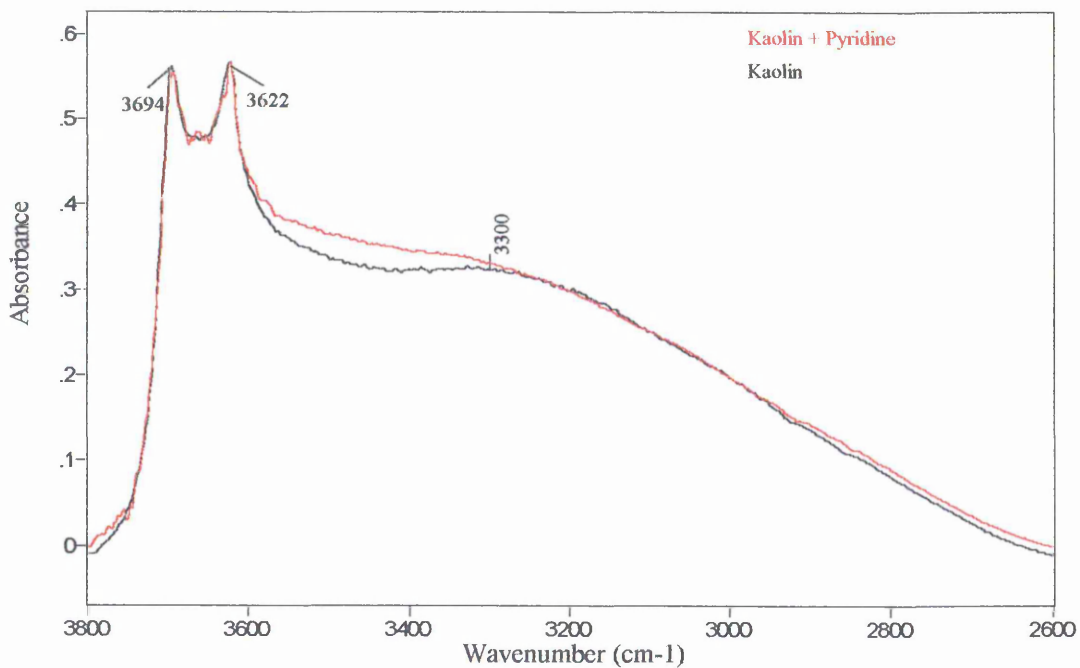


Figure 3.35 Comparison of unexposed and pyridine exposed kaolin (250 °C).

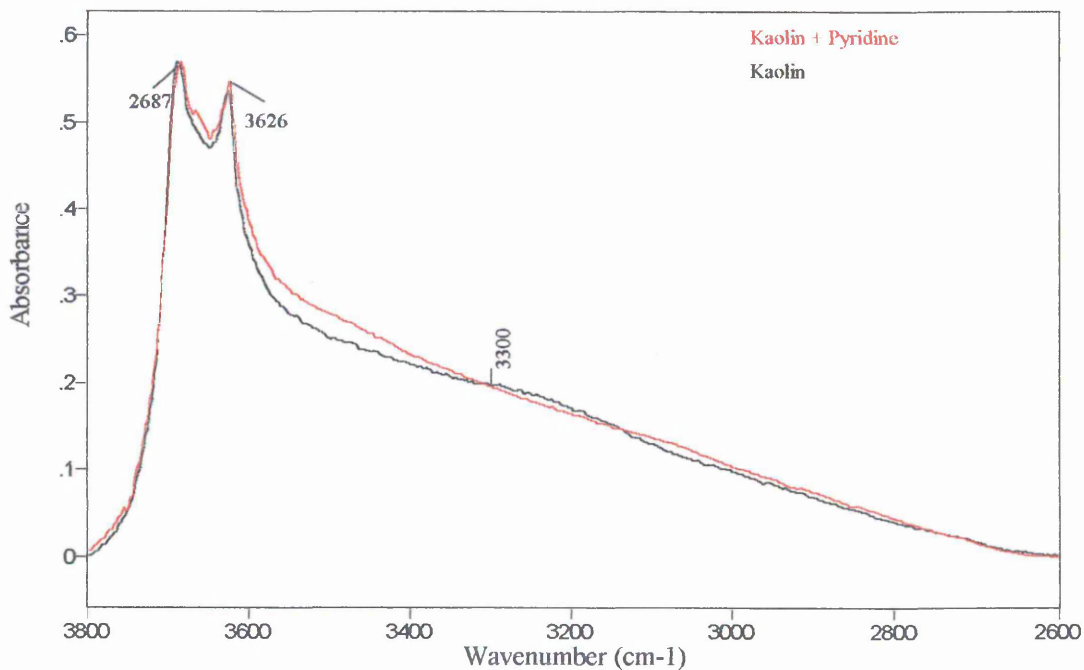


Figure 3.28 to Figure 3.35 above illustrate that gross changes in the water stretching region were difficult to detect after pyridine exposure. However, the relative intensity of the c 3695 cm^{-1} decreased with respect to the 3620 cm^{-1} band. There was also a systematic increase in the intensity of the c 3400 to 3600 cm^{-1} region. These alterations indicate the perturbation of the 3695 cm^{-1} band, due to hydrogen bonding between the inner surface hydroxyls and pyridine, thus a shift of this band to lower frequency was observed¹³. These changes indicated that there was some intercalation of pyridine, either between the slightly expanded edges of kaolin, or into the halloysite. Due to the small amount of intercalation, and to the intensity of the water bands intrinsically present at this frequency (discussed in Chapter 2), the precise frequency of the additional hydroxyl-pyridine band was not discernible. The increase in intensity of the c 3400 to 3600 cm^{-1} region appears to be similar (in principle) to that observed in the work by Sugahara *et al*²

3.3.6.5 Unmilled kaolin-pyridine. The 2100 1400 cm^{-1} region.

Figure 3.36 Comparison of unexposed and pyridine exposed kaolin (room temp.).

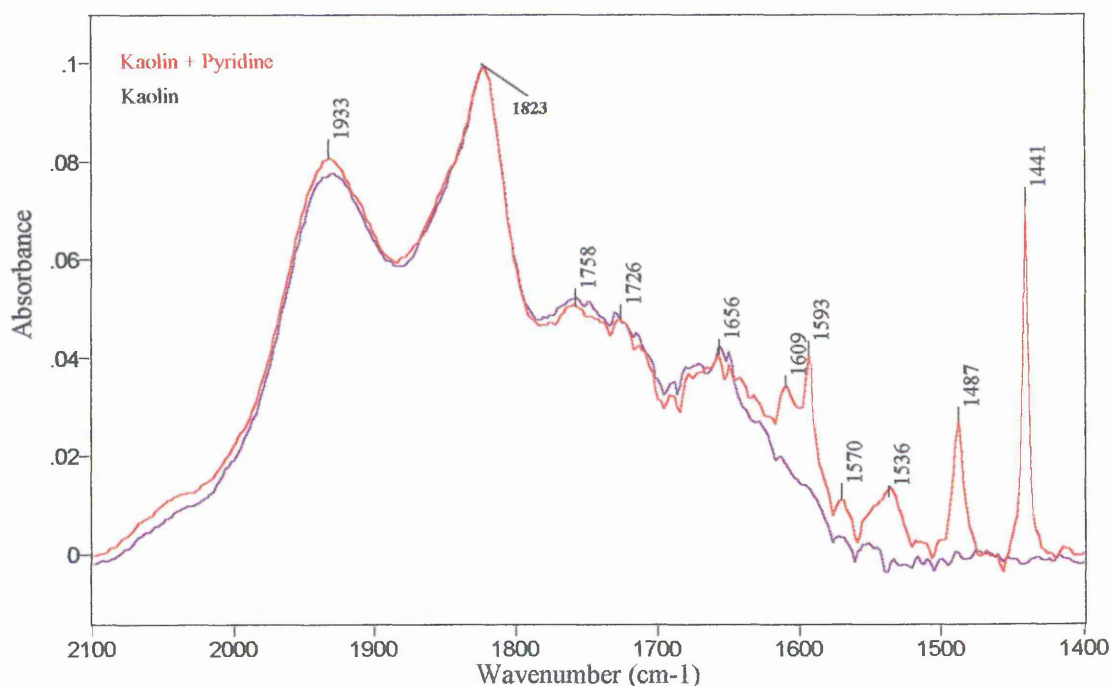
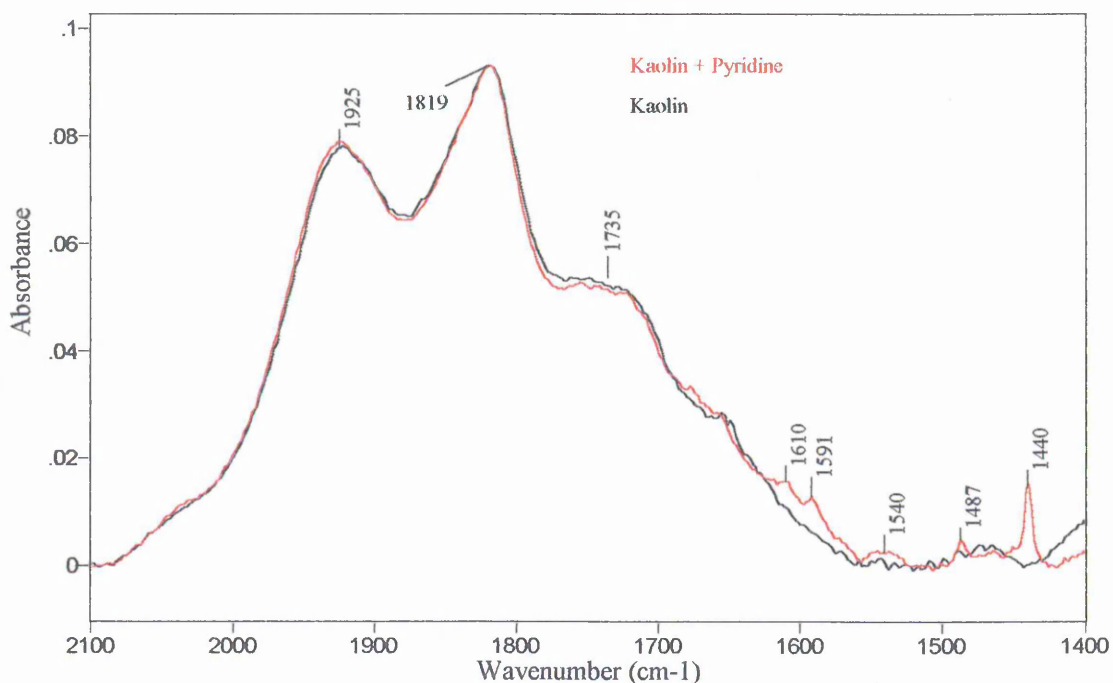
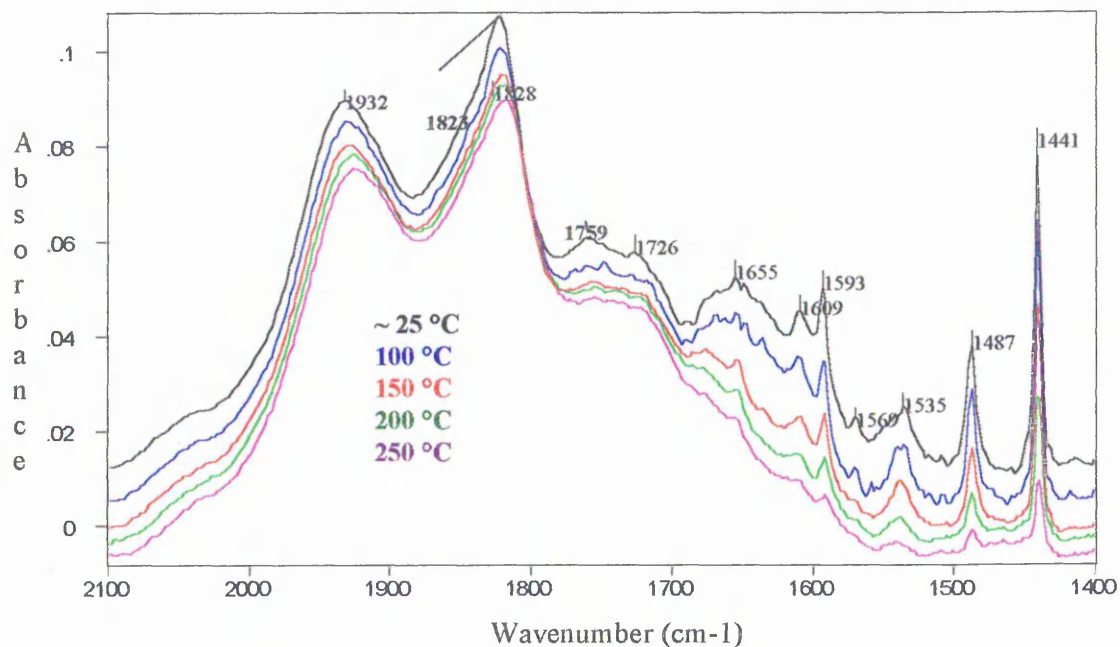


Figure 3.37 Comparison of unexposed and pyridine exposed kaolin (250 °C).



Spectra in the bending region (like those in the stretching region for this sample) show little change in the water modes before and after exposure to pyridine. However, in the bending region, distinct bands characteristic of pyridine adsorption can be observed. The appearance of two overlapping pyridine bands at 1610 and 1593 cm⁻¹ makes the precise quantification of the water mode ν (at 1653 cm⁻¹) difficult. It is also possible that bands corresponding to Brønsted bound pyridine at 1605 and 1630 cm⁻¹ are hidden beneath the water band.

Figure 3.38 Unmilled kaolin-pyridine. The effect of temperature. The 2100-1400 cm^{-1} region.



Hydrogen bonding is undoubtedly present in the unmilled-pyridine exposed kaolin spectra at room temperature, due to the characteristic relative intensities of the 1440 and 1490 and 1590 cm^{-1} bands (i.e. a strong 1440 cm^{-1} band and a relatively weak 1490 cm^{-1} band in combination with a relatively strong 1590 cm^{-1} band). Some of the intensity of the 1440 cm^{-1} could be due to Lewis bound pyridine, but upon heating, the relative intensity of the three bands remain quite constant up to very high temperatures. Thus, it seems that only a small proportion of the 1440 cm^{-1} intensity at room temperature was due to Lewis bonding. Even at 250°C there was still clear evidence of bands at these positions.

A band is present at 1535 cm^{-1} which corresponds to Brønsted bound pyridine. This band is broader than the characteristic hydrogen bonding or Lewis bands, and it also remains until high temperature. It should be noted that Brønsted bound pyridine is not found in the pyridine-exposed halloysite. Representative curve fits of the pyridine exposed kaolin are presented below.

Figure 3.39 Unmilled kaolin-pyridine. The 2100-1400 cm^{-1} region. Room temperature curve fit.

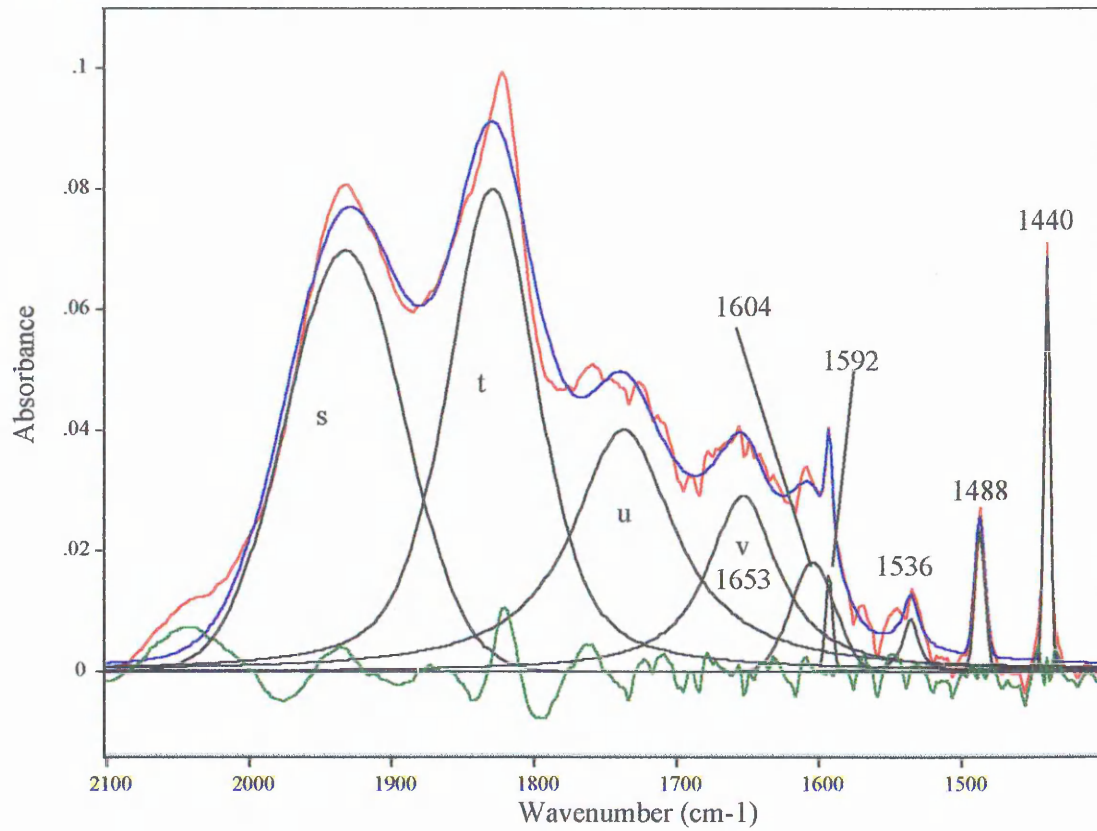


Figure 3.40 Unmilled kaolin-pyridine. The 2100-1400 cm^{-1} region. 150 °C curve fit.

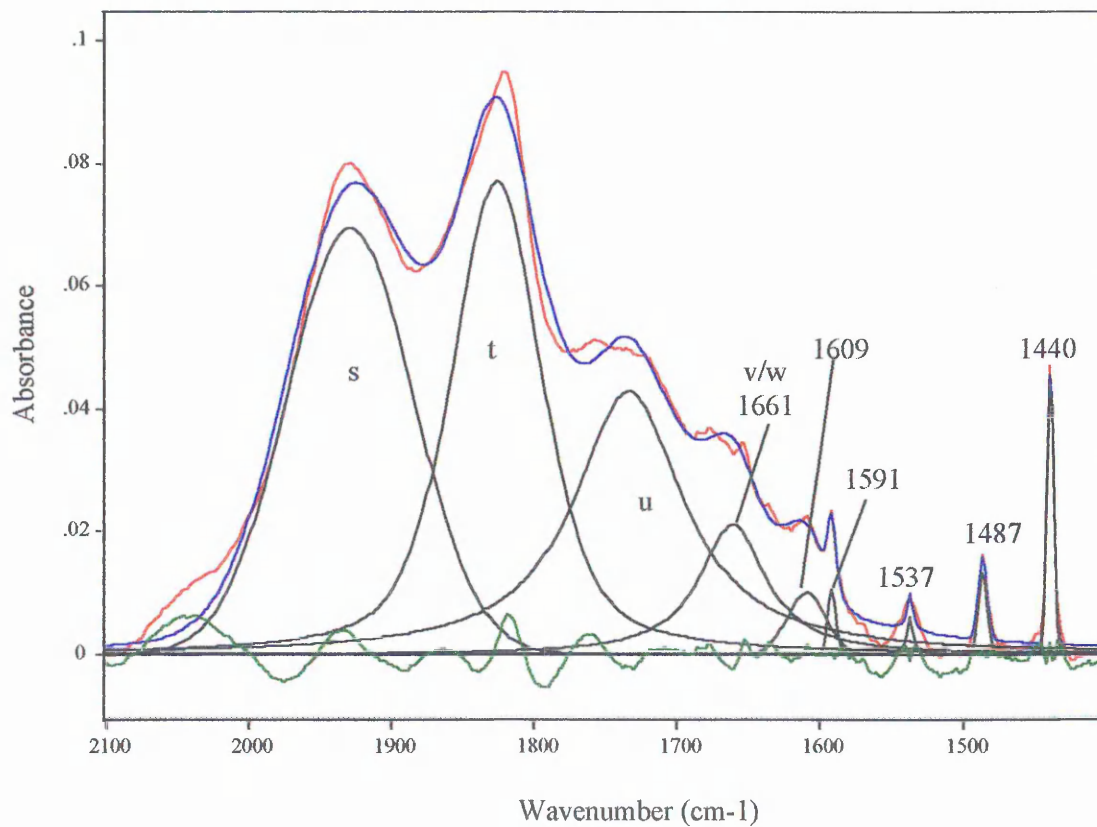
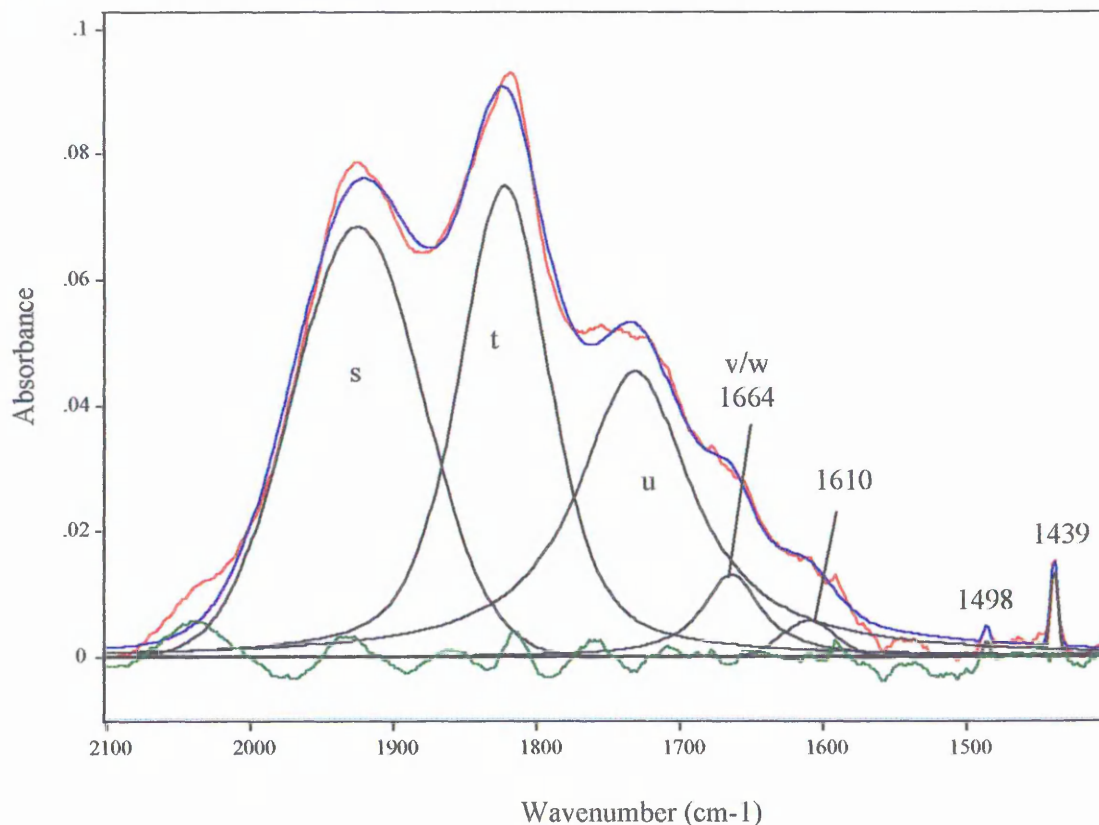


Figure 3.41 Unmilled kaolin-pyridine. The 2100-1400 cm^{-1} region. 250 °C curve fit.



At room temperature, five discrete pyridine bands were present. Their possible assignments are given in Table 3.2 below.

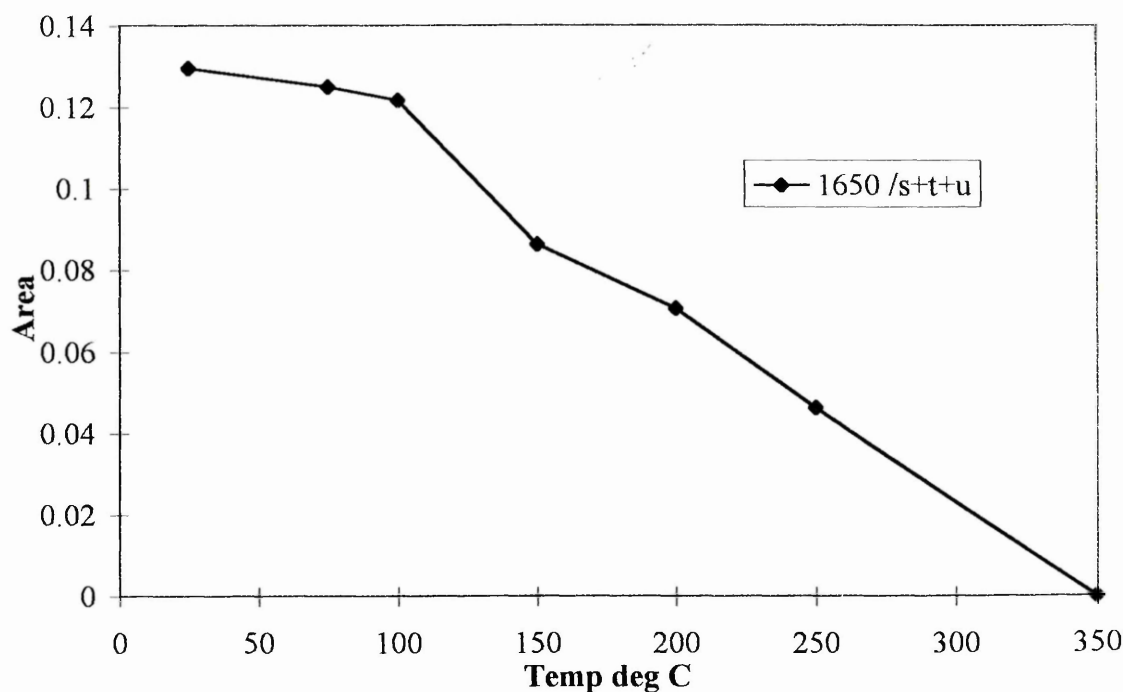
Table 3.2 Possible assignments of pyridine bands at room temperature.

Position (cm^{-1})	Assignment
1670-1620	Brønsted bound pyridine / water
1609	Lewis bound pyridine
1592	H-bonded pyridine
1536	Brønsted bound pyridine
1488	Brønsted or Lewis bound pyridine
1440	H-bonded & Lewis bound pyridine

By examining the thermal stability of the pyridine bands in the 150 °C curve fit), it is possible to deduce the exact nature of the 1592, 1488 and 1440 cm^{-1} bands. The relative intensities of the 1440, 1490 and 1592 °C remain similar up to high temperatures, are thus believed to be due hydrogen bonded pyridine. Due to the presence of hydrogen

bonded organic at such high temperatures, (it was still visible at 250 °C), it is believed that the organic has become trapped between the mineral layers (either kaolin or halloysite). The bonding of pyridine may be to the mineral surface, or to a pyridinium cation. However, the Brønsted band at 1536 is no longer quantifiable at 250 °C, which may indicate that this type of binding is less thermally stable than the Lewis type binding. However, since the band at 1536 cm^{-1} was of low intensity, Brønsted type binding may still be present, but at levels below the detection limits of the curve fitting parameters. It is believed that the pyridine-exposed unmilled kaolin sample is a composite of the spectra of pyridine- intercalated halloysite and adsorbed pyridine on kaolin. Thus, the hydrogen bonded character of pyridine exposed unmilled kaolin is due primarily to the spectral contribution from pyridine-intercalated halloysite. The Brønsted bands observed are due to the interactions of pyridine with the kaolin mineral.

Figure 3.42 Unmilled kaolin-pyridine. The 2100-1400 cm^{-1} region. The change in intensity of the water band (ν) at 1650 cm^{-1} .



The intensity of the water band at 1650 cm^{-1} (Band ν) decreased steadily between 25 and 350 °C. Approximately half the intensity was removed by 200 °C (compared with the equivalent reduction in the unexposed sample at 150 °C (Figure 2.49)). The position of this band in the unexposed sample was also c1650 cm^{-1} . In the pyridine exposed sample, there may also be a contribution from a Brønsted bound pyridine band at 1630 cm^{-1} .

This may explain why the $t_{1/2}^*$ for the pyridine exposed sample was greater than the untreated sample.

Figure 3.43 Unmilled kaolin-pyridine. The 2100-1400 cm^{-1} region. The change in intensity of pyridine bands.

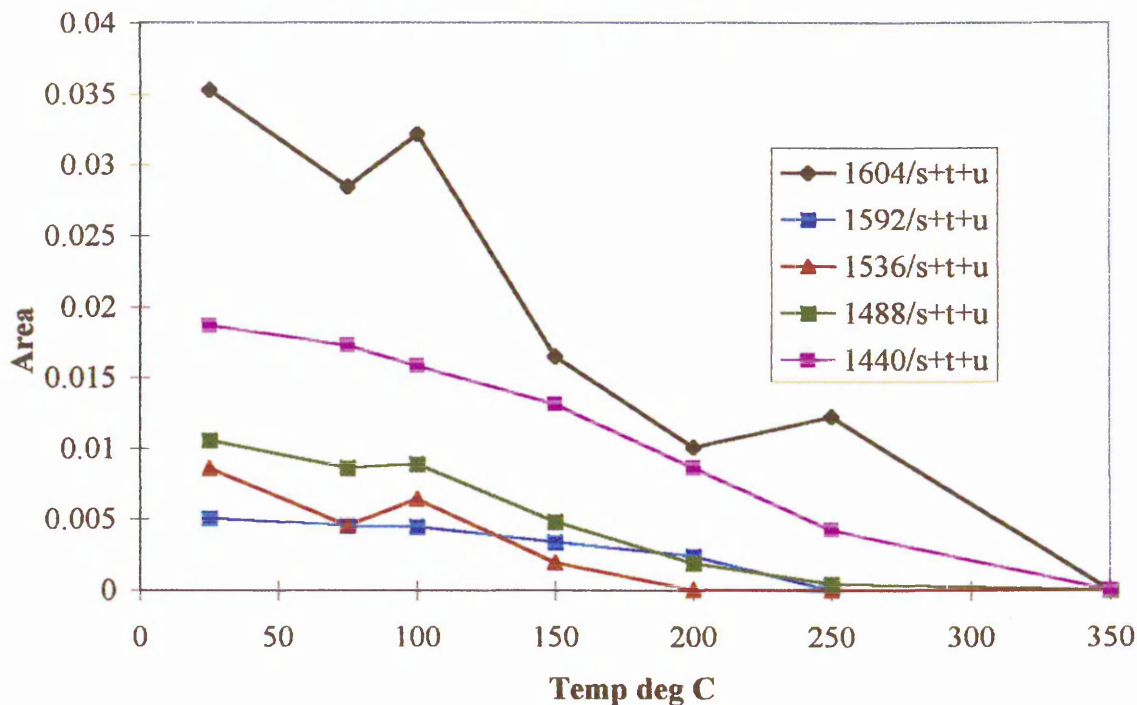
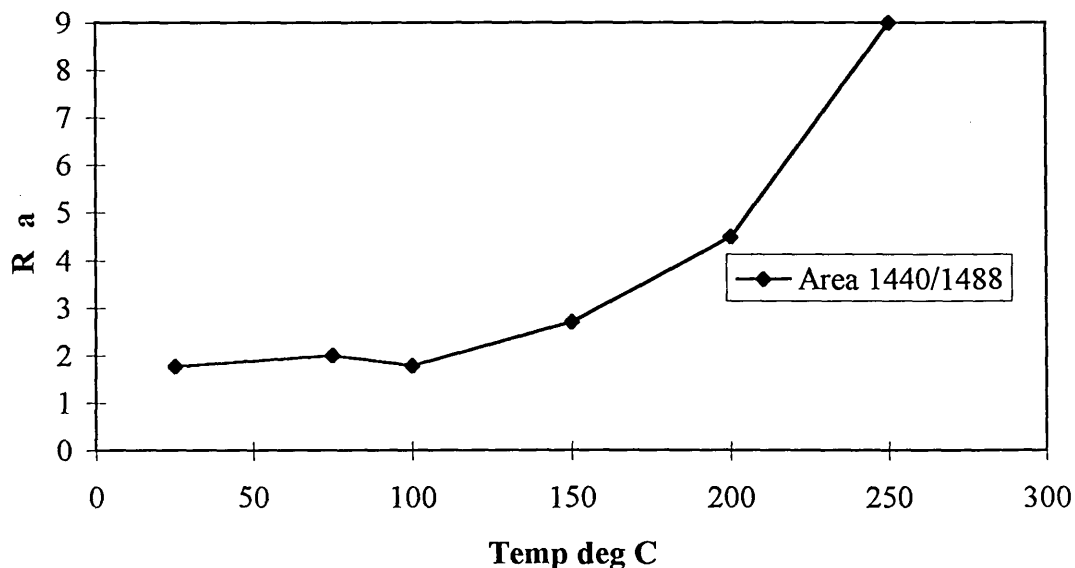


Figure 3.43 shows how the intensities of the pyridine bands vary with increasing temperature. As expected, all bands are seen to decrease as pyridine is being driven from the system. However, it does not show how the bands vary with respect to one another. Of particular interest is how the relative proportions of the Brønsted and Lewis bands alter as temperature increase. A more useful measure of this phenomenon is shown below.

* $t_{1/2}^*$ = the temperature by which approximately 50 % of the initial band intensity has been reduced.

Figure 3.44 Ratio of the area of the 1440 : 1490 cm^{-1} pyridine bands.



The ratio of these bands remained constant up to 100 °C. Thereafter the relative intensity of the 1440 cm^{-1} band became larger with respect to the 1480 cm^{-1} band. The predominant type of binding in the unmilled mineral sample is Lewis type. The extinction coefficient of the Brønsted component of the 1488 cm^{-1} band is higher than that of the Lewis component at the same frequency. Thus, as temperature increases, although the significant contribution from the Brønsted band at 1488 cm^{-1} decreases with respect to the Lewis band at 1488 cm^{-1} , the overall contribution of the Lewis component at 1440 cm^{-1} becomes higher. Thus, the plot above shows that Lewis type binding becomes more significant than Brønsted type binding at temperatures above 100°C.

3.3.6.6 3 minute milled kaolin-pyridine. The 2100-1400 cm^{-1} region.

Figure 3.45 Comparison of unexposed and pyridine exposed kaolin (Room temp.).

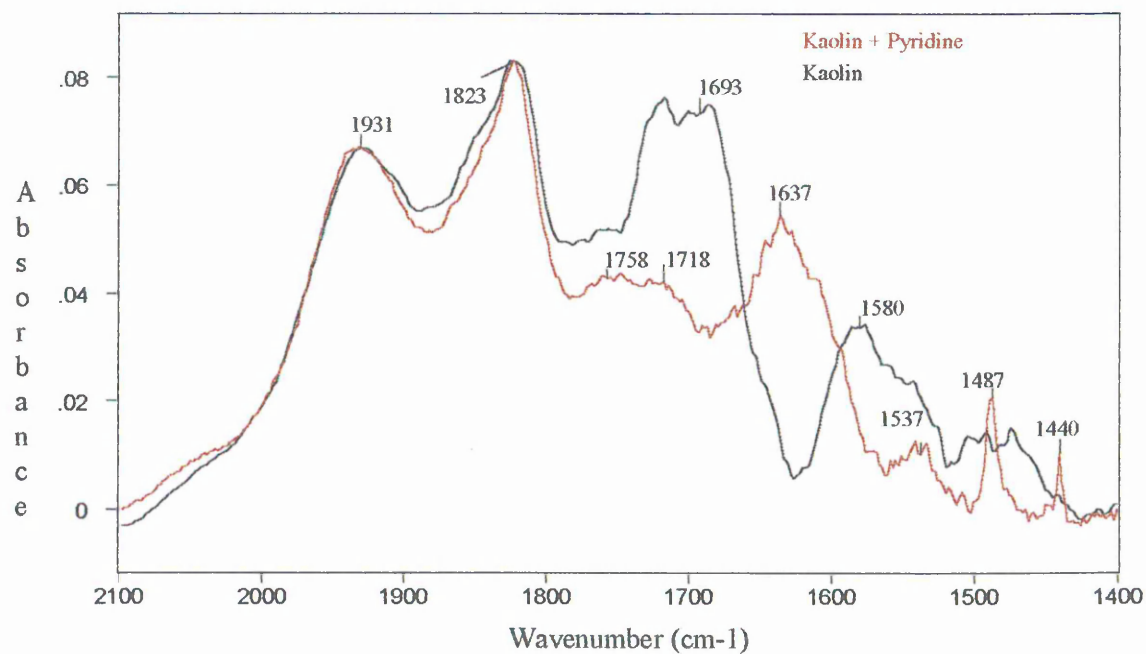
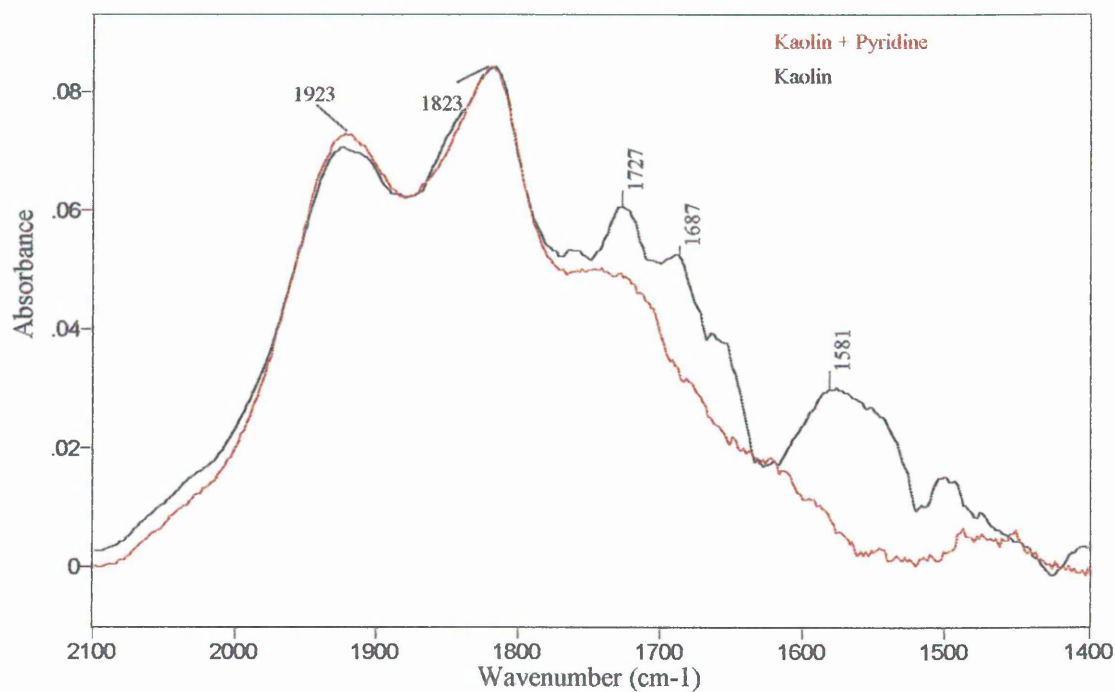


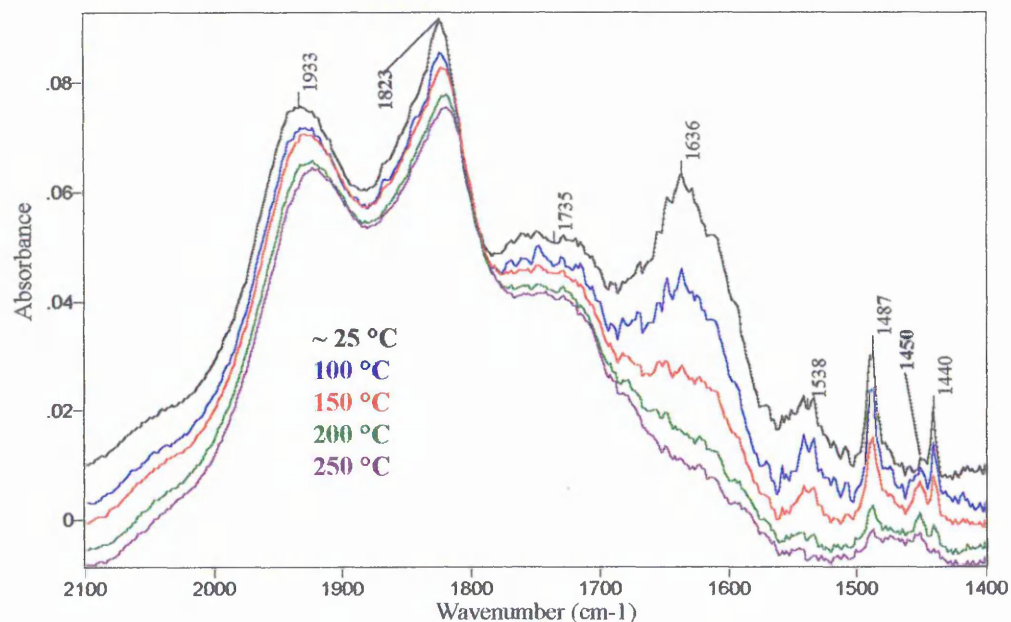
Figure 3.46 Comparison of unexposed and pyridine exposed kaolin (250 $^{\circ}\text{C}$).



The room temperature spectrum of the pyridine exposed 3 minute milled kaolin shows that the intensity in the 1720-1690 cm^{-1} region has decreased, as has the intensity of the broad water bending mode at 1580 cm^{-1} . The intensity of the water band centring at 1637 cm^{-1} has increased, corresponding to an increase in moderately strongly hydrogen bonded surface sorbed water. This effect does not appear to be mimicked in the stretching region, although the broadness of the stretching bands makes precise interpretations in that region difficult. As explained in Chapter 2, the 1580 cm^{-1} band is due to very weakly hydrogen bonded water which becomes “trapped” between, or very loosely bonded to the slightly expanded mineral layers. A possible explanation for the decrease in the 1580 cm^{-1} band, with a concurrent increase in the 1637 cm^{-1} is that water previously trapped is being displaced by pyridine and instead is being more strongly readsorbed to different (edge) sites (also see later). These changes would be difficult to distinguish in the stretching region, since the 1580 cm^{-1} is thought to be associated with the high frequency band (e) at c 3590 cm^{-1} , which is only quantifiable by curve fitting. This band is of relatively low intensity with respect to those surrounding it, and the multiplicity of changes in all the water bands makes isolating the changes of one “hidden” band very difficult. It should be noted at this point that there are two possible mechanisms by which water becomes involved in the mineral-pyridine system. The first is that pyridine displaces some of the more strongly hydrogen bonded water already present on the mineral surface, and that water is then free to readsorb in a more weakly hydrogen bonded manner. Secondly, it is possible that all the surface sorbed water is displaced upon initial pyridine exposure, and the water visible in the spectra has been readsorbed via weak hydrogen bonding during the drying process. It is not possible from these data which mechanism is occurring.

After heating to 250 °C, less water is present in the pyridine exposed kaolin than was the case for the unexposed kaolin, contrary to the behaviour of the unexposed, milled mineral. Evidence (although minimal) of pyridine bands at 1487 or 1440 cm^{-1} was present at this temperature.

Figure 3.47 3 minute kaolin-pyridine (FM). The effect of temperature. The 2100-1400 cm^{-1} region.



The VT DRIFTS spectra of pyridine treated 3 minute ball-milled kaolin showed less total pyridine adsorption than the unmilled sample. This may have been due to a decrease in binding sites available on the kaolin surface due to agglomerate formation during the milling process, or it may be because the halloysite contaminant is no longer swelling in the presence of pyridine (due to structural alterations brought about by the milling process). The associated pyridine was less strongly held after 3 minutes milling, and was all but removed by heating to 250°C, compared with the unmilled pyridine treated sample, which retained the pyridine until heated to 300°C.

The relative intensities of the 1490 and 1440 cm^{-1} bands were different from unmilled kaolin-pyridine spectra, with the 1440 cm^{-1} band being significantly reduced with respect to the 1490 cm^{-1} band. This may be indicative of a reduction in the amount of hydrogen bonded pyridine. It is difficult to assign the bonding mode in the absence of other bands at 1590 cm^{-1} or 1610 cm^{-1} . It is possible that the bands were not visible because they were swamped by the increased intensity of the water band at 1630 cm^{-1} . The apparent absence of these bands is likely to indicate that there is no (or very little) hydrogen

bonded pyridine in this system. Interestingly here, there was another band at 1450 cm^{-1} which was likely to correspond to Lewis type associations.

Although the overall bonding of pyridine to kaolin seemed to reduce after 3 minutes milling, the intensity of the characteristic Brønsted peak appeared to remain relatively constant when compared with the unmilled pyridine exposed sample. It is postulated that after minimal ball-milling there is an increase in the Lewis sites available for pyridine adsorption, with little change in the availability of the relatively small number of Brønsted sites.

Figure 3.48 3 minute kaolin-pyridine (FM). The $2100\text{-}1400\text{ cm}^{-1}$ region. Room temperature curve fit.

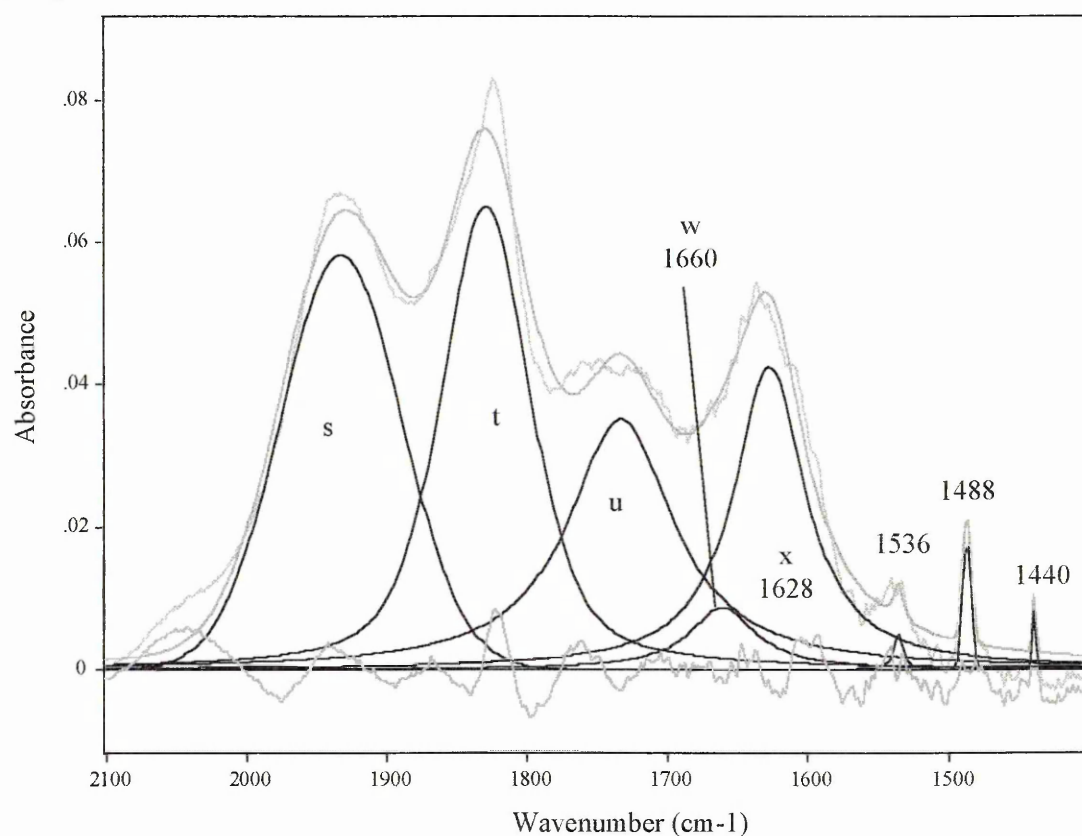


Figure 3.49 3 minute kaolin-pyridine (FM). The 2100-1400 cm^{-1} region. 100 °C curve fit.

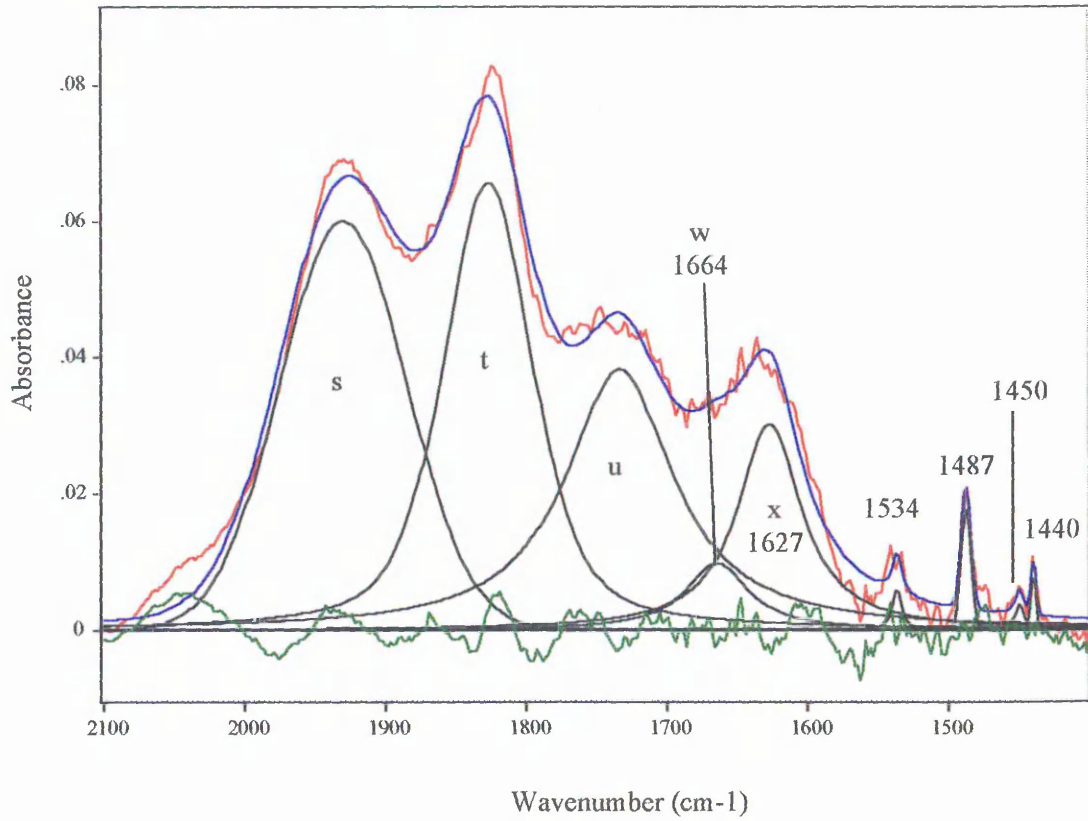
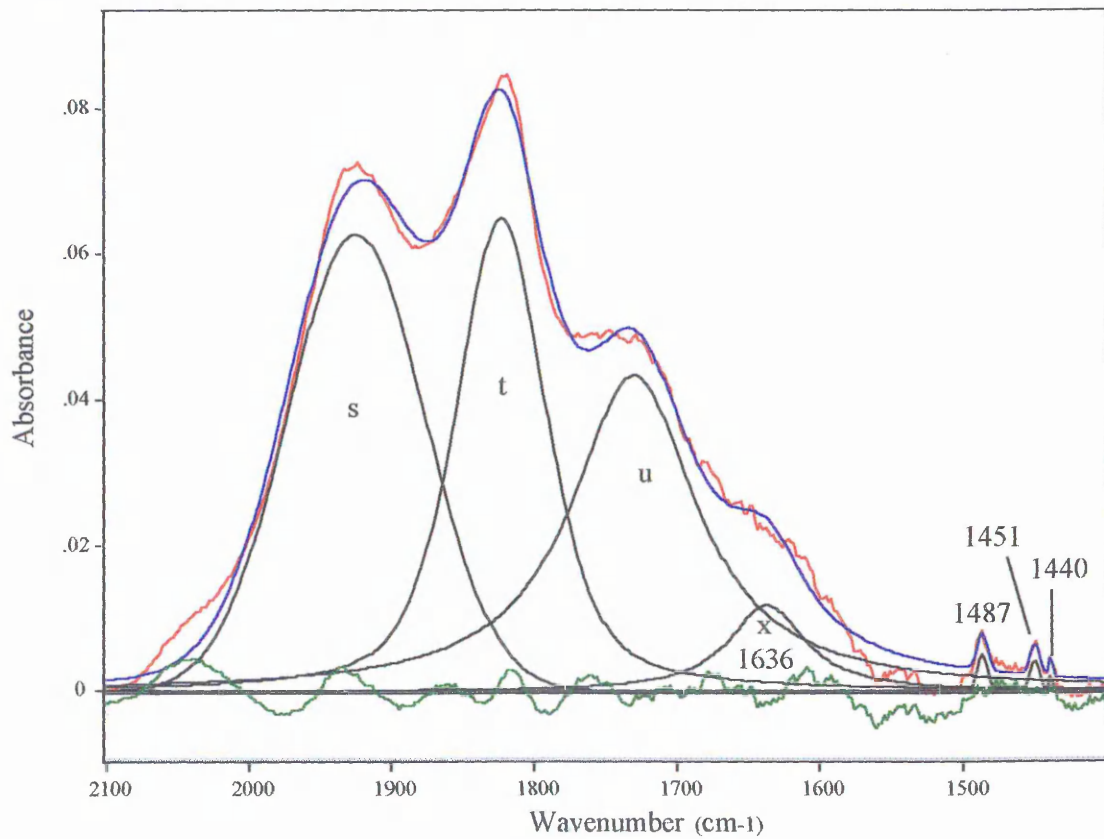
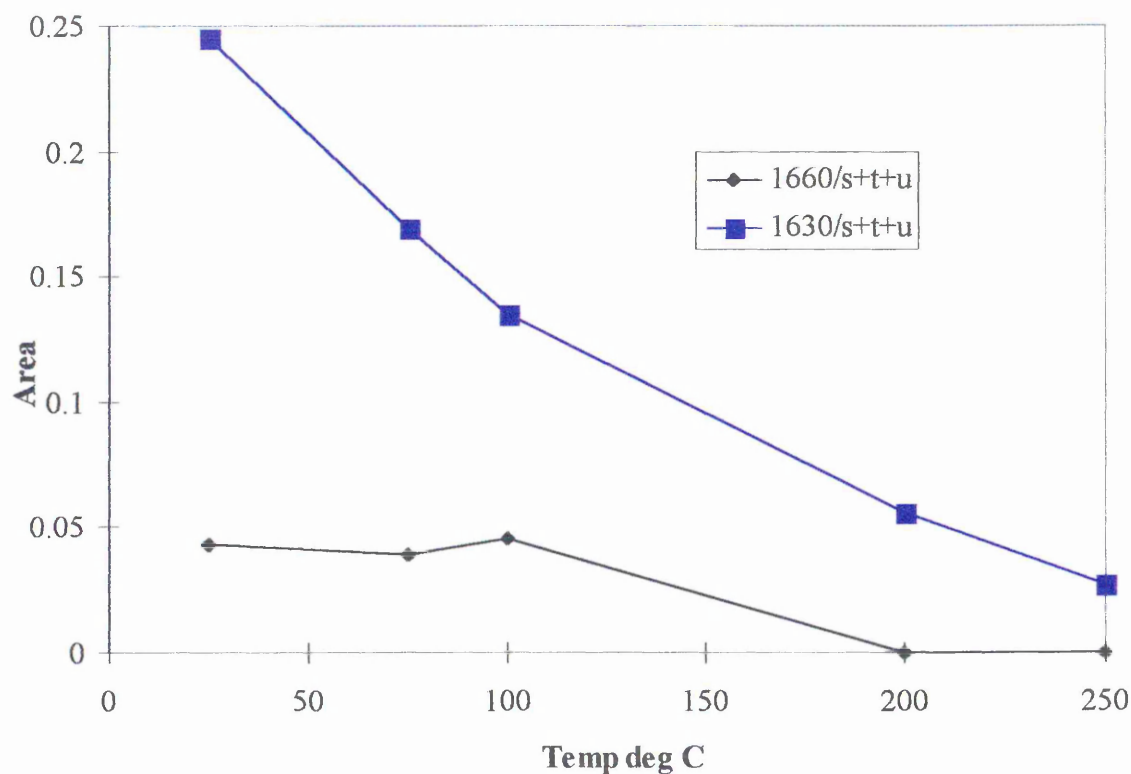


Figure 3.50 3 minute kaolin-pyridine (FM). The 2100-1400 cm^{-1} region. 200 °C curve fit.



At room temperature a Brønsted bound pyridine band at 1536 cm^{-1} was present. Bands at 1488 and 1440 cm^{-1} were also present, but the relative intensities altered dramatically compared with those in the unmilled, unexposed kaolin sample. In the pyridine exposed 3 minute milled sample, the 1488 cm^{-1} band was more intense than the 1440 cm^{-1} band. The thermal stability of the 1440 and 1488 cm^{-1} bands indicate that they represent mostly Lewis bonded, rather than physisorbed pyridine. At $100\text{ }^{\circ}\text{C}$, another band at 1451 cm^{-1} became more obvious. It was present in the room temperature spectrum also, but was partially concealed by the stronger 1440 cm^{-1} band. The band at 1451 cm^{-1} is thought to represent Lewis type binding. Overall, there was a decrease in the total number of hydrogen bonding sites compared with the unmilled sample, but a similar number of Brønsted type sites. The increase in Lewis associations at elevated temperature could be because milling induced the formation of Lewis type sites on the surface of kaolin or on the surface of halloysite (or both). The decrease in hydrogen bonding is likely to be due to the reduced capacity of halloysite to intercalate the organic after milling. At 250°C , the relative intensities of the 1440 and 1450 cm^{-1} bands compared with the 1490 cm^{-1} band resembles the pattern seen in the pyridine exposed halloysite sample at that temperature.

Figure 3.51 3 minute kaolin-pyridine (FM). The 2100-1400 cm^{-1} region. The change in intensity of water bands at 1660 & 1630 cm^{-1} .



The water in this sample has altered dramatically compared with that in the unexposed 3 minute milled sample (Figure 2.55). In that sample, water bands were present at c1670 and 1580 cm^{-1} . After treatment with pyridine, the 1670 cm^{-1} mode shifted to 1660 cm^{-1} , indicating an increased proportion of more weakly hydrogen bonded water. Curiously, the 1580 cm^{-1} band has all but disappeared after pyridine treatment. However, it has been replaced by another band at 1630 cm^{-1} . This may indicate a shift of water which was initially trapped between agglomerate particles, or from between the partially expanded edges of the kaolin sheets to broken edge sites, where the water may bond more securely. Most of the water in the pyridine treated sample was removed by 250 °C, whereas in the unexposed sample, water remained clearly evident beyond 500 °C. An interesting feature of Figure 3.52 below is that it visualises the increase in the contribution from the Lewis band at 1450 cm^{-1} as temperature increases. As predicted, the relative intensities of the other bands reduce as temperature increases. Again, a plot of the ratio of the relative intensity of the 1440 and 1450 cm^{-1} to that of the 1488 cm^{-1} band reveals more about relative proportions of Lewis to Brønsted type sites (see Figure 3.52)

Figure 3.52 3 minute kaolin-pyridine (FM). The 2100-1400 cm^{-1} region. The change in intensity of pyridine bands.

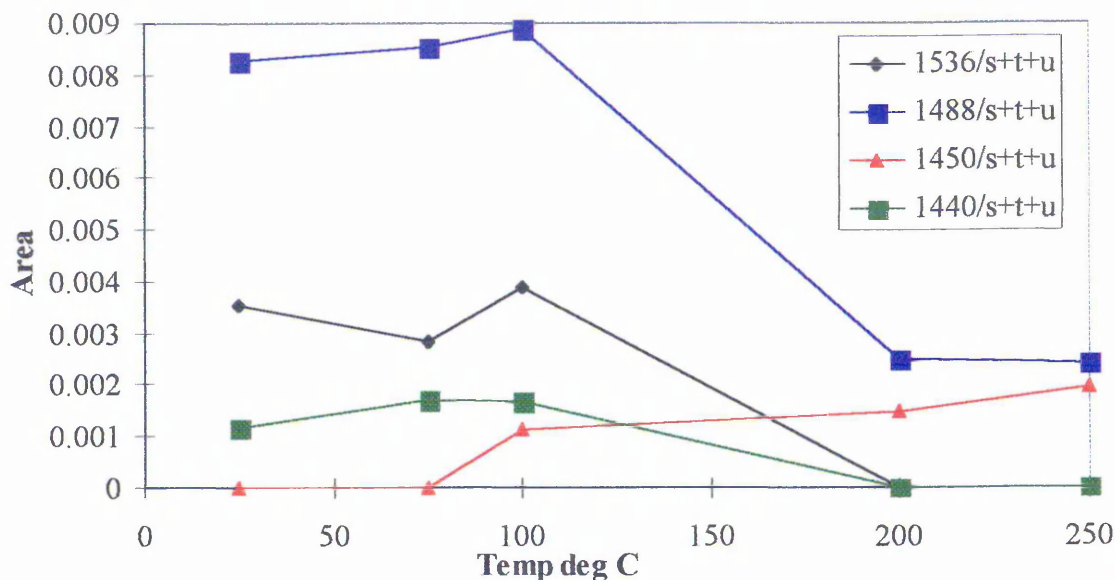
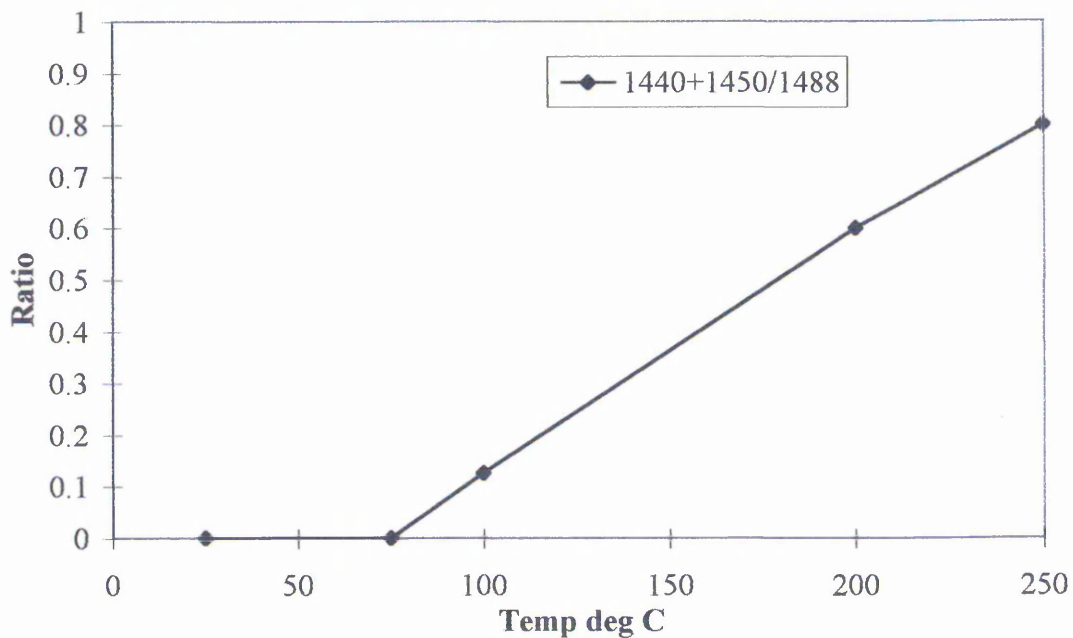


Figure 3.53 Ratio of the area of the 1440 & 1450 : 1488 cm^{-1} pyridine bands.



The relative intensities of the 1440 + 1450 cm^{-1} bands remained virtually constant up to 75 $^{\circ}\text{C}$. Thereafter, the relative intensity of the 1440 and 1450 increased rapidly compared with the 1488 cm^{-1} band. This indicates, that at temperatures above 75 $^{\circ}\text{C}$, the relative contribution from Lewis type binding increases with respect to the contribution from Brønsted type.

3.3.6.7 10 minute milled kaolin-pyridine. The 2100-1400 cm^{-1} region.

Figure 3.54 Comparison of unexposed and pyridine exposed kaolin (Room temp.).

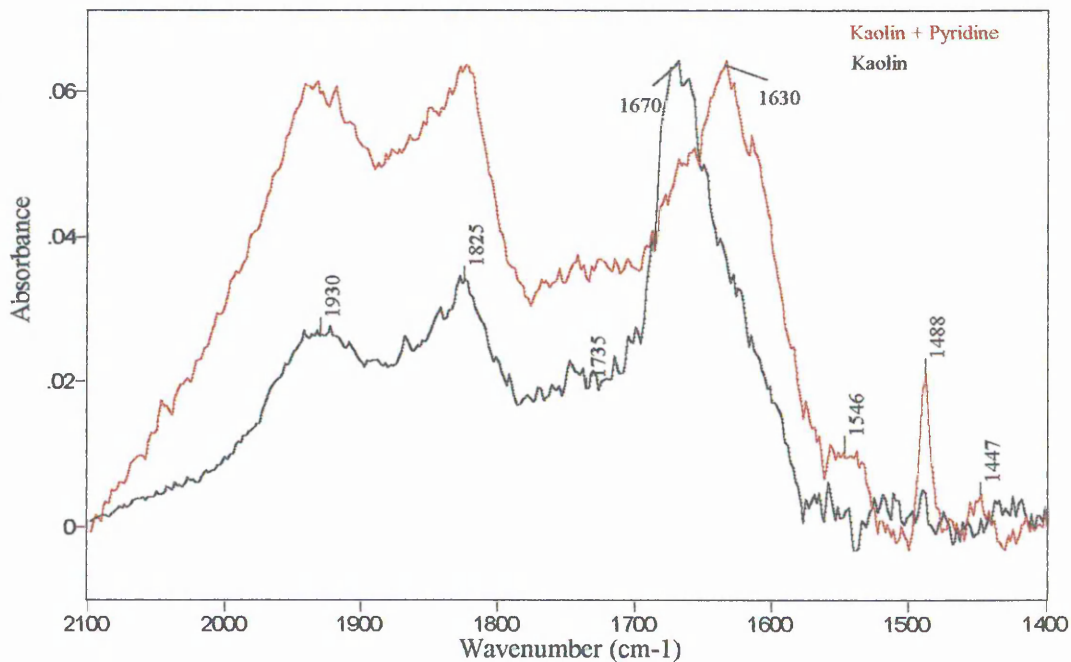
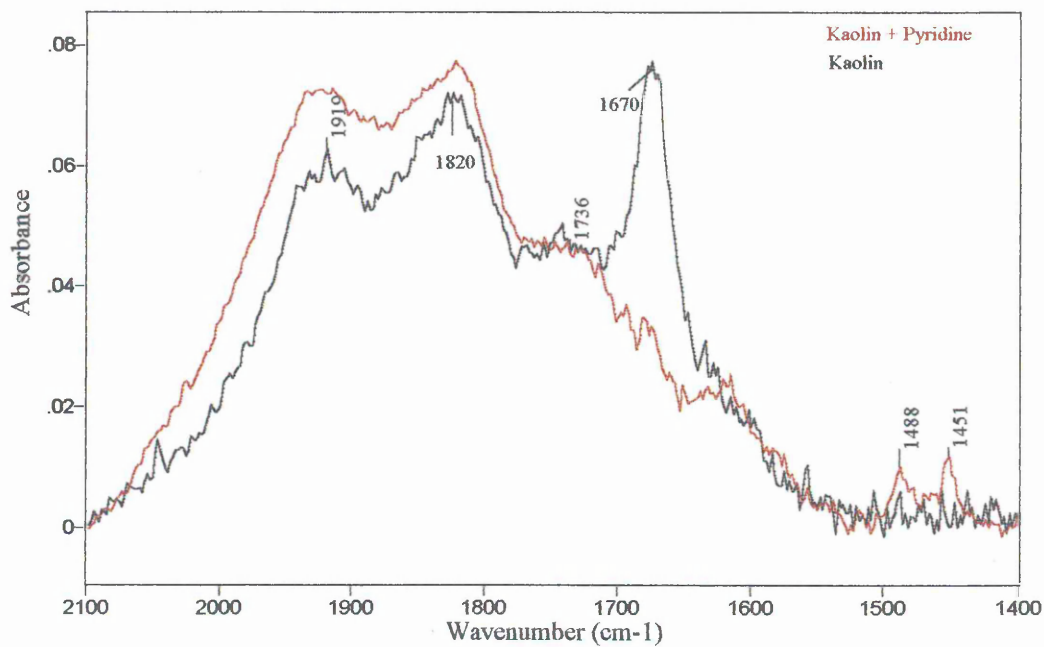
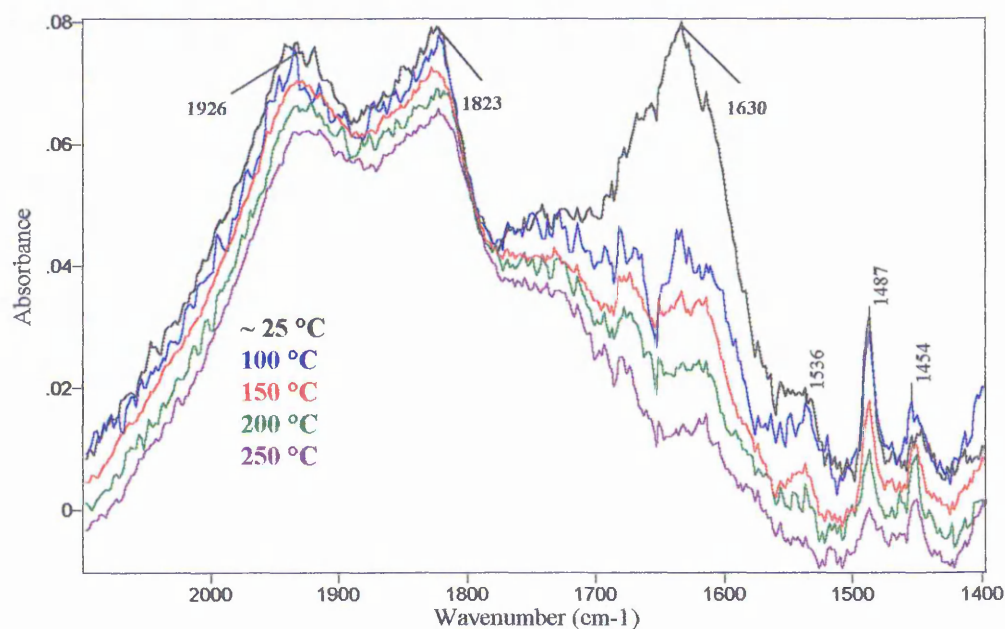


Figure 3.55 Comparison of unexposed and pyridine exposed kaolin (250 °C).



At room temperature (Figure 3.54) there was an overall decrease in the intensity of the water bands. There has been a shift to decreased frequency (i.e. to more weakly hydrogen bonding) in the pyridine exposed sample, compared with the unexposed 10 minute milled kaolin. Distinct pyridine bands are observed. At 250 °C (Figure 3.55), the very intense water mode present in the unexposed sample at 1670 cm^{-1} has been greatly reduced. Some pyridine bands persist at this temperature, but the intensities of the 1540 and 1488 cm^{-1} bands have now been reduced.

Figure 3.56 10 minute kaolin-pyridine (FM). The effect of temperature. The 2100-1400 cm^{-1} region.



The spectrum at room temperature differs from the 3 minute-pyridine (RT) spectrum in that there is now no distinguishable 1440 cm^{-1} band. The 1490 cm^{-1} band was of relatively high intensity compared with the 1454 cm^{-1} band. There was a Brønsted band at 1536 cm^{-1} . Thus, at room temperature, the spectrum indicated the presence of Brønsted and Lewis type associations, with no evidence of hydrogen bonding. After heating the 10 minute kaolin-pyridine sample, the intensity of the 1490 cm^{-1} band decreased progressively until, at 200 °C the relative intensities of the 1450 and 1490 cm^{-1} bands were approximately equal. At 250 °C, the 1450 cm^{-1} was more intense than the 1490 cm^{-1} , with a corresponding reduction in the intensity of the 1536 Brønsted band, indicating that there was a change in the available surface sites from Brønsted type to Lewis type.

Figure 3.57 10 minute kaolin-pyridine (FM). The 2100-1400 cm^{-1} region. Room temperature curve fit.

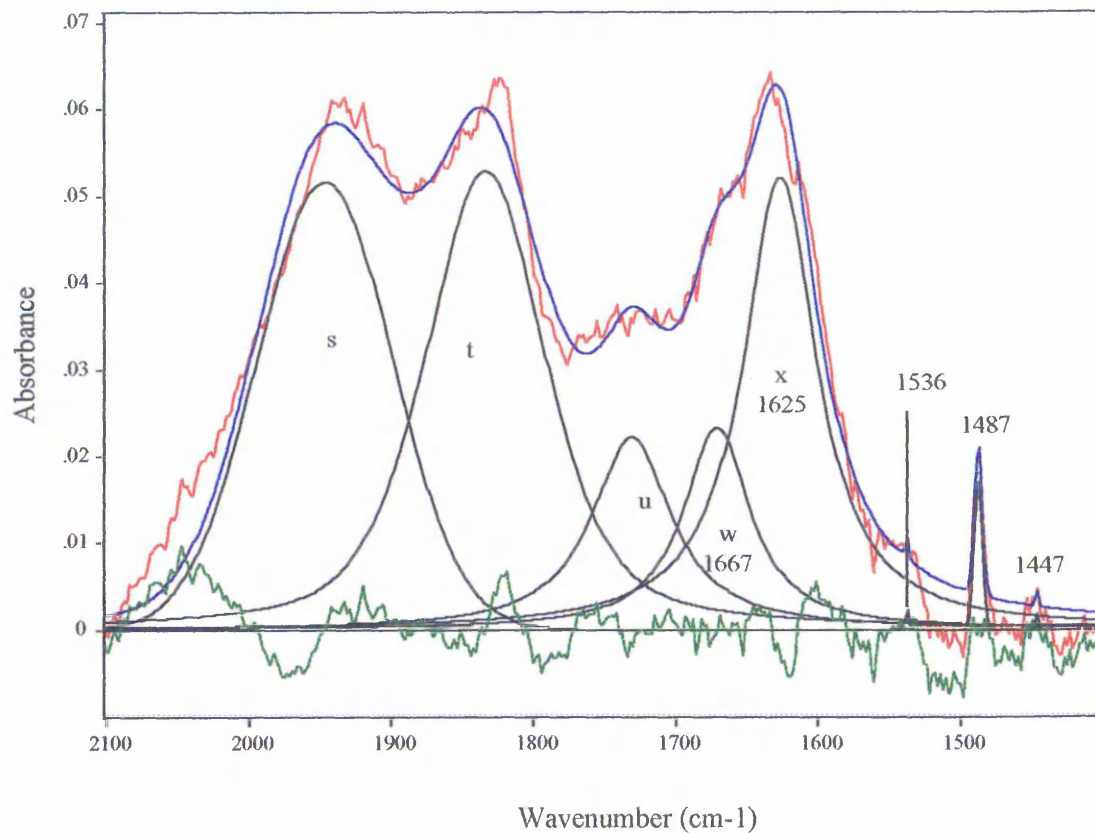


Figure 3.58 10 minute kaolin-pyridine (FM). The 2100-1400 cm^{-1} region. 100 $^{\circ}\text{C}$ curve fit.

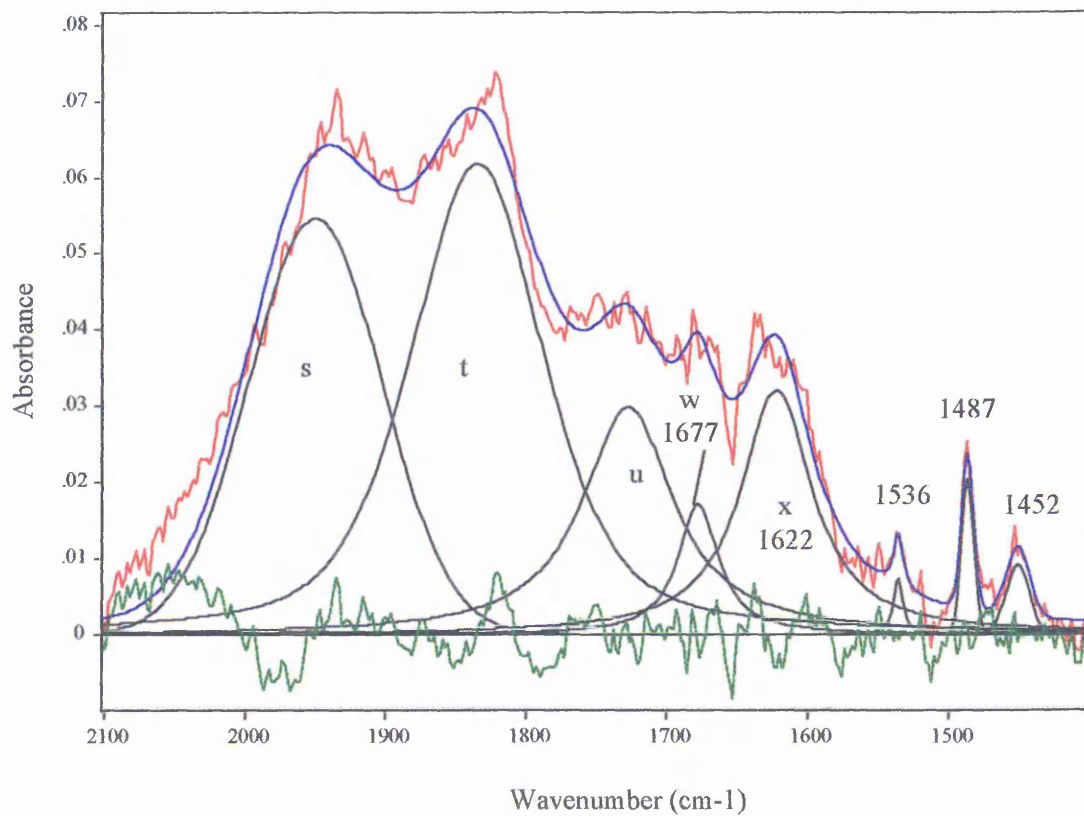
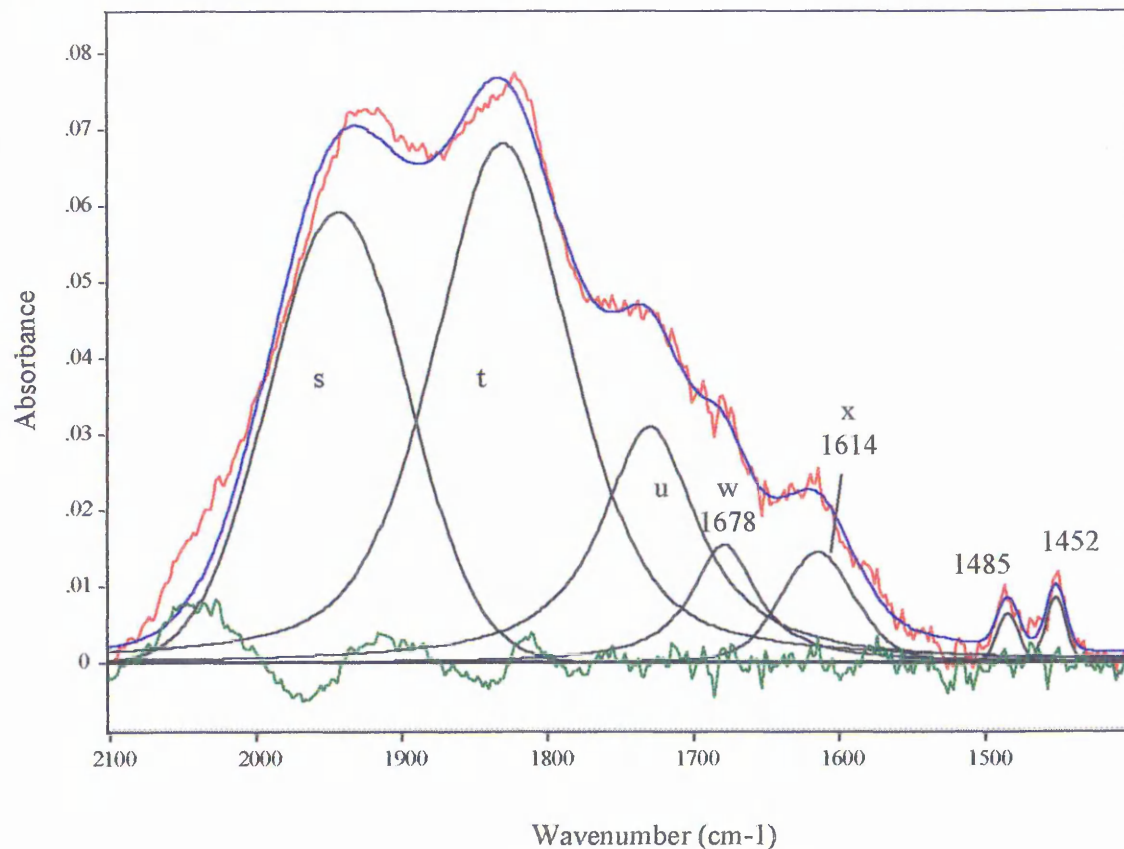
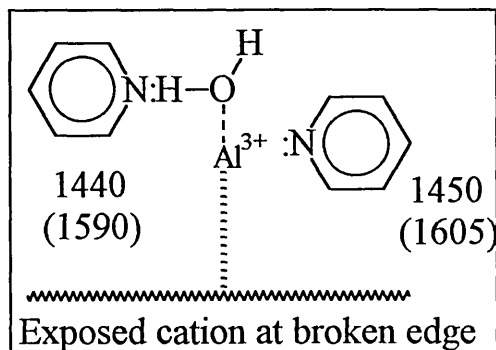


Figure 3.59 10 minute kaolin-pyridine (FM). The 2100-1400 cm^{-1} region. 250 $^{\circ}\text{C}$ curve fit.



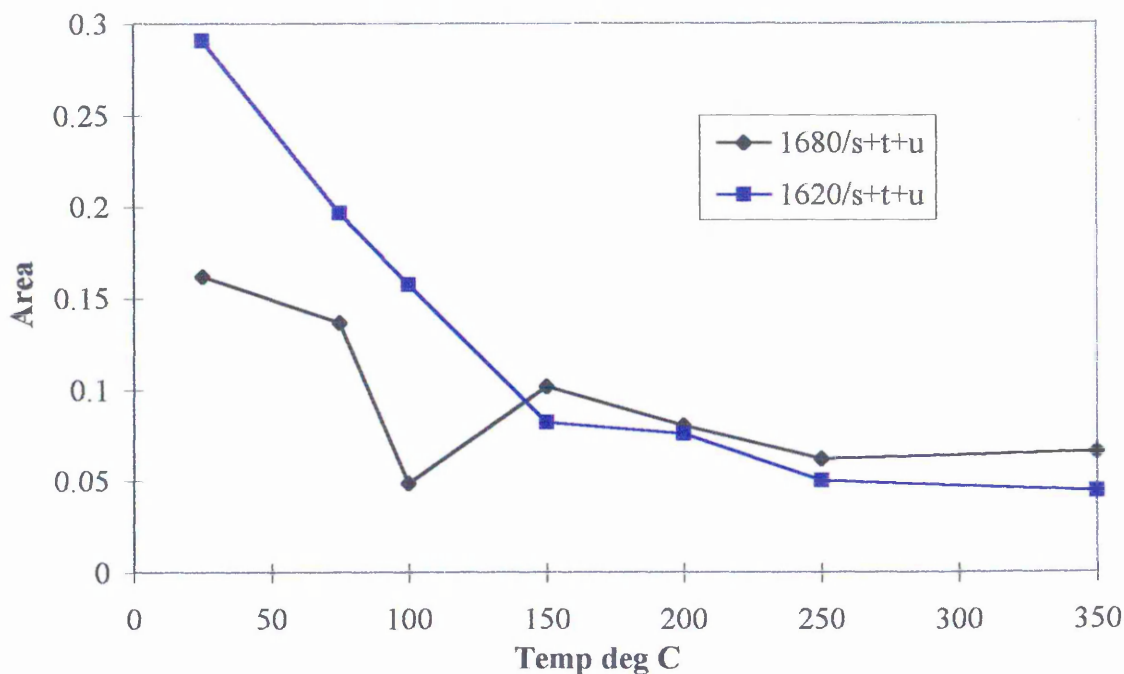
At room temperature, there was an intense band at 1487 cm^{-1} , with a very weak band at 1447 cm^{-1} . A band at 1536 cm^{-1} was present, but was partially masked by the intense water band at 1625 cm^{-1} . Interestingly, the hydrogen bonding band at 1440 cm^{-1} (present in the pyridine exposed unmilled sample and in the pyridine exposed 3 minute milled sample) is no longer present in this sample. There is a band at $\sim 1450 \text{ cm}^{-1}$, corresponding to Lewis type binding. It may be that pyridine is binding as shown below in Figure 3.60, where, after milling the aluminium cations become more exposed and can bond directly to pyridine more easily, thus forming different Lewis type associations. This model is adapted from that proposed by Reis Jr *et al*¹⁶, for the binding of pyridine to the copper cation.

Figure 3.60 Proposed assignment of the 1450 cm^{-1} band.



However, in the light of the pyridine-exposed halloysite results, it is thought that in this system, the band at 1440 cm^{-1} corresponds to hydrogen bonded pyridine, whereas the band at 1450 cm^{-1} corresponds to Lewis bonded pyridine. After heating to $100\text{ }^{\circ}\text{C}$, much of the water was removed and the 1536 cm^{-1} band became more visible. The intensity of the 1452 cm^{-1} band was much increased compared with the room temperature spectrum. The intensity of the 1487 cm^{-1} band did not alter considerably. Upon heating to $250\text{ }^{\circ}\text{C}$, the relative intensity of the 1452 cm^{-1} band became greater with respect to the 1485 cm^{-1} band. The 1536 cm^{-1} band was no longer present. A conversion from Brønsted type to Lewis type binding was thus observed. At $250\text{ }^{\circ}\text{C}$, the intensities of the Lewis bands at 1485 and 1452 cm^{-1} in the pyridine exposed 10 minute milled sample were greater than the intensities of those bands at the lower temperature of $200\text{ }^{\circ}\text{C}$ in the 3 minute milled pyridine exposed sample. This indicates that the 10 minute pyridine exposed milled sample contains a greater number of more thermally resistant Lewis sites than the 3 minute pyridine exposed sample. These sites may be on the surface of pyridine, halloysite or both minerals.

Figure 3.61 10 minute kaolin-pyridine (FM). The 2100-1400 cm^{-1} region. The change in intensity of water bands at 1680 & 1620 cm^{-1} .

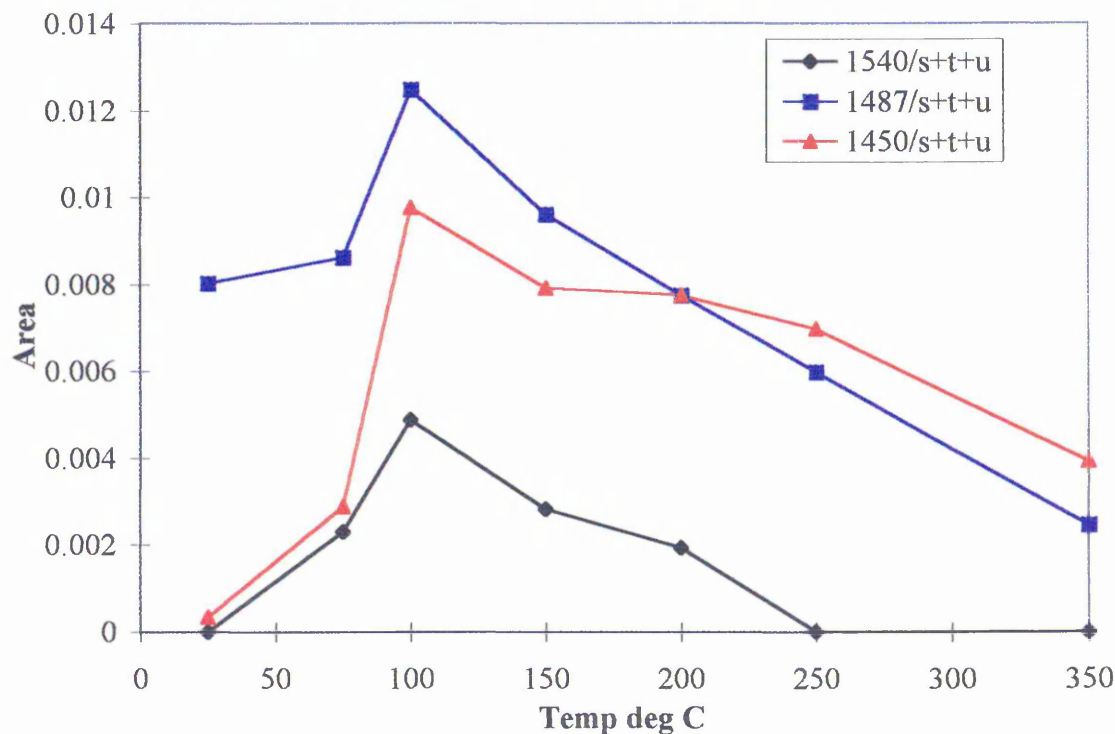


The 1680 cm^{-1} band intensity at 100 $^{\circ}\text{C}$ appears to be unusually low because some of the intensity belonging to this band has been incorrectly allocated to the band at 1620 cm^{-1} (and therefore the latter band should be of lower intensity at 100 $^{\circ}\text{C}$ than is indicated above). In the unexposed sample, water bands were present at c1680 and 1620 cm^{-1} , and at room temperature, the c1680 cm^{-1} was of much greater intensity than the 1620 cm^{-1} band. In the pyridine exposed sample, the lower frequency band at c1620 cm^{-1} (band x) was of greater intensity than the band at 1680 cm^{-1} (band w). This is indicative of a shift from stronger hydrogen bonding in the unexposed sample to weaker hydrogen bonding in the pyridine exposed sample- an effect observed in the 3 minute milled pyridine exposed sample. The pyridine appears to be having a similar effect on the water associated with ball milled kaolin as does the effect of ageing process (see Section 2.3). There too the water becomes less strongly hydrogen bonded.

Another feature of the unexposed 10 minute milled kaolin sample is the frequency shift of band x (at 1620 cm^{-1} at room temperature) to c1600 cm^{-1} . A similar, but less pronounced shift is observed in the pyridine treated sample. Unlike the unexposed sample, there is no evidence of band r at 1580 cm^{-1} in the pyridine exposed sample. As described previously, this band represents water trapped between agglomerates or water between the slightly expanded edges of kaolin. The absence of this band in the pyridine

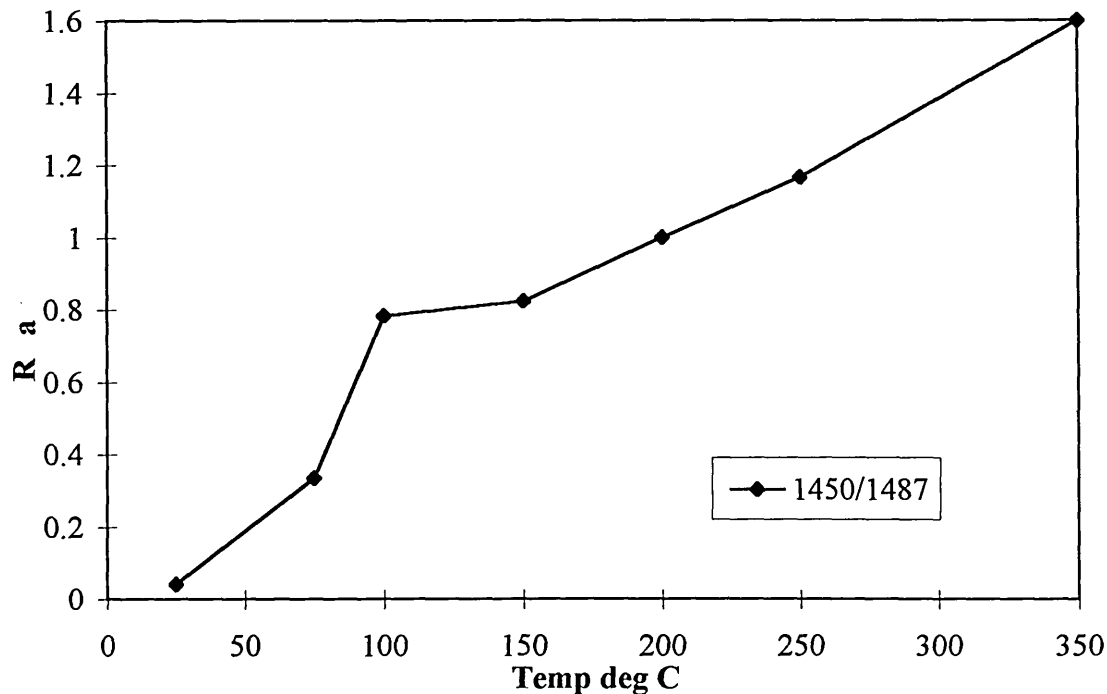
exposed sample supports the hypothesis that pyridine is able to “displace” more weakly bonded sorbed water species. In both cases (unexposed and pyridine exposed), the temperature at which half of the intensity of the water mode at 1620 cm^{-1} was removed was $c125\text{ }^{\circ}\text{C}$. The corresponding temperature for the 1670 cm^{-1} band was $c150\text{ }^{\circ}\text{C}$.

Figure 3.62 10 minute kaolin-pyridine (FM). The $2100\text{-}1400\text{ cm}^{-1}$ region. The change in intensity of pyridine bands.



The 1540 cm^{-1} band appears to be virtually removed by $250\text{ }^{\circ}\text{C}$. It may still be present, but because it is very small it is not discernible by curve fitting. It is not necessarily less thermally stable than the 1450 or 1487 cm^{-1} bands.

Figure 3.63 Ratio of the area of the 1450 : 1490 cm^{-1} pyridine bands.



As temperature increased, the contribution of the 1440 cm^{-1} band increased almost linearly with respect to that of the 1487 cm^{-1} band. This again indicates that although both the Lewis and Brønsted contributions to the 1487 band decrease as temperature increases, the relative contribution of the Brønsted band decreases more significantly than that of the Lewis band. Thus, there is an increase in the relative proportion of Lewis type associations (compared with Brønsted type associations) as temperature increased.

3.3.6.8 30 minute milled kaolin-pyridine. The 2100-1400 cm^{-1} region.

Figure 3.64 Comparison of unexposed and pyridine exposed kaolin (Room temp.).

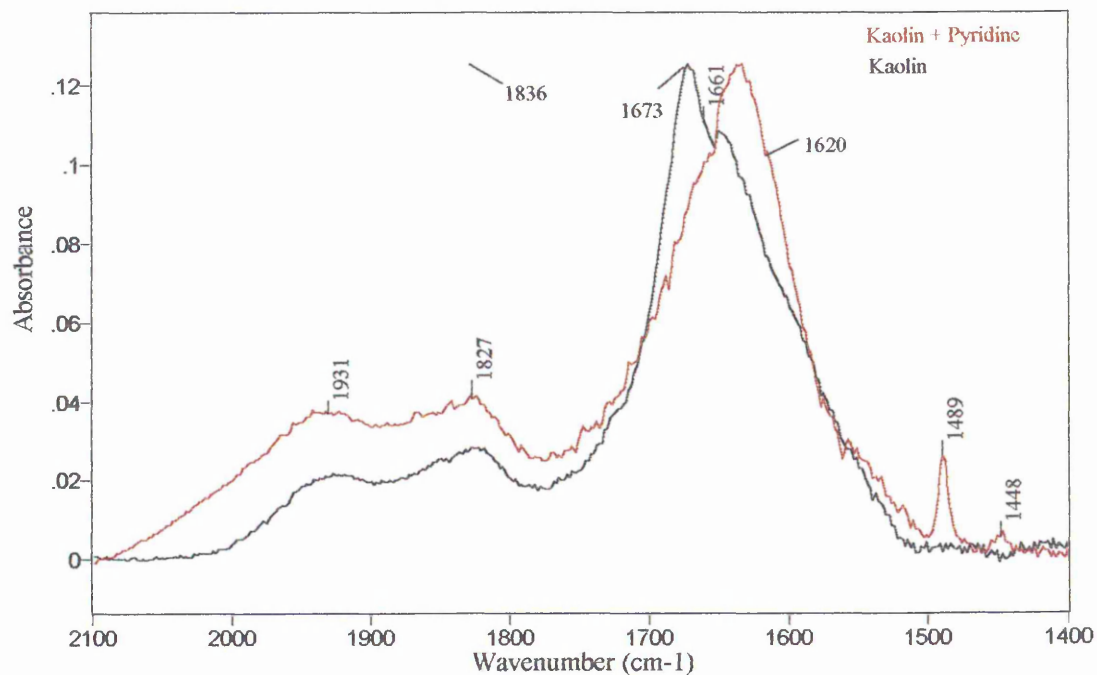
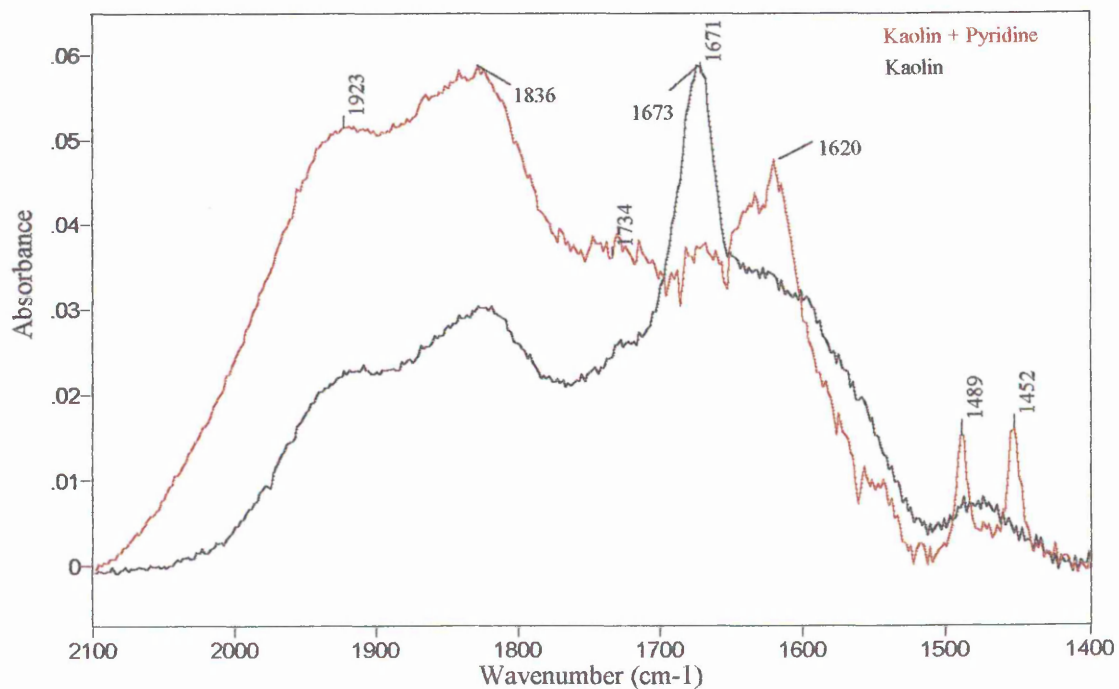
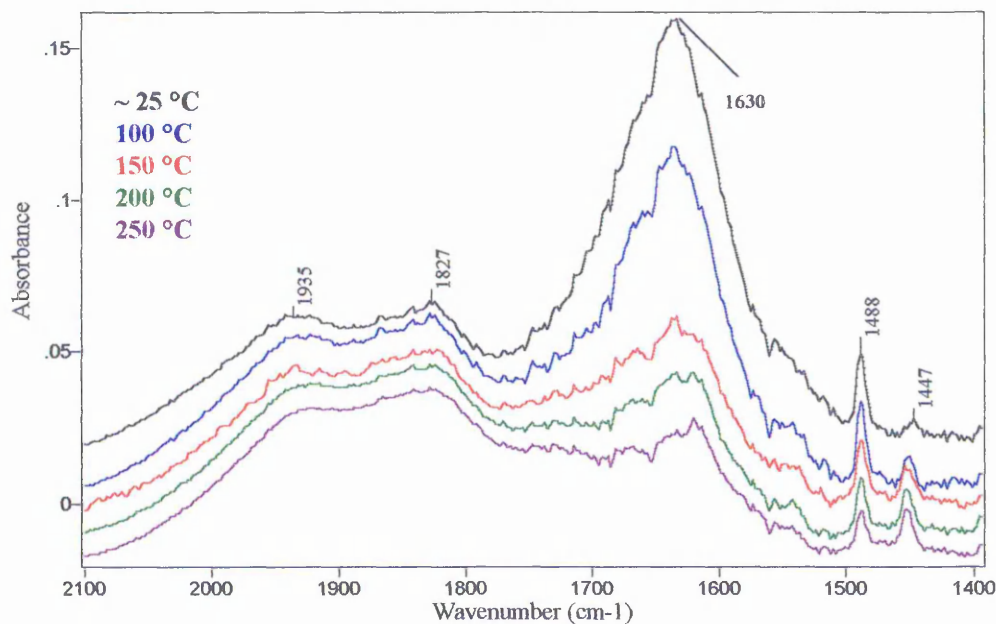


Figure 3.65 Comparison of unexposed and pyridine exposed kaolin (250 $^{\circ}\text{C}$).



At room temperature, the pyridine band at 1488 cm^{-1} was very intense (over half the height of 1827 cm^{-1} kaolin band). This feature is similar to the relative intensities of the same bands in the pyridine exposed unmilled kaolin sample, and more intense than the same pyridine band in the 10 and 3 minute pyridine exposed samples. This seems to indicate that the 30 minute milled kaolin sample was able to adsorb more pyridine than the 3 and 10 minute milled samples. Curve fitting was not carried out on this sample due to the difficulties discussed in Chapter 2. However, general trends can be observed. As well as the pyridine-related changes, the water bands near 3400 cm^{-1} altered markedly during the grinding process, and these findings were discussed in detail in Chapter 2. However, after the exposure to pyridine, the overall amount of sorbed water decreased and there was a marked shift in frequency, representing a relative increase in the proportion of more weakly hydrogen bonded water species compared with the unexposed 30 minute milled kaolin sample. This effect was noted in the pyridine exposed 3 and 10 minute milled samples.

Figure 3.66 30 minute kaolin-pyridine (FM). The effect of temperature. The $2100\text{-}1400\text{ cm}^{-1}$ region.



At room temperature, the relative intensity of the 1490 cm^{-1} band compared with that of the 1450 cm^{-1} was large, indicating the presence of mostly Brønsted type sites. The pyridine adsorbed to this kaolin sample was very thermally stable, but as temperature

increased, the relative intensity of the 1490 cm^{-1} band decreased with respect to the 1450 cm^{-1} band, until at $250\text{ }^{\circ}\text{C}$ the 1450 cm^{-1} appeared to be more intense (due to its broader band width). A band at 1536 cm^{-1} was probably present, but masked beneath the water bands. It became more obvious as the temperature was increased (i.e. as water was removed). Again, as for the 10 minute pyridine exposed kaolin sample, there appeared to be a conversion from Brønsted to Lewis type sites.

Table 3.3 The effects of pyridine exposure on the sorbed water species present on milled and unmilled kaolin. The OH bending region.

	Change in intensity compared with unexposed mineral					Change in intensity compared with unexposed mineral				
	Room Temperature					250 °C				
	V Weakly bonded c 1590 cm ⁻¹	H-Weakly bonded c 1620 cm ⁻¹	Strongly bonded c 1650 cm ⁻¹	H-Strongly bonded c 1670 cm ⁻¹	V Strongly bonded c 1670 cm ⁻¹	V Weakly bonded c 1590 cm ⁻¹	H-Weakly bonded c 1620 cm ⁻¹	Strongly bonded c 1650 cm ⁻¹	H-Strongly bonded c 1670 cm ⁻¹	V. Strongly H-bonded c 1670 cm ⁻¹
0 minute	X	X	≈	X	X	X	≈	≈	X	X
3 minute	↓	↑*	X	↓	↓	↓	X	X	↓†	↓†
10 minute	≈	↑	X	↓	↓	≈	≈	X	↓	↓
30 minute	≈	↑	X	↓	↓	≈	↑	X	↓	↓

X = absence of quantifiable band

≈ = little change in intensity

↓ = decrease in intensity

↑ = increase in intensity

* Not present in unexposed sample.

† Was present in unexposed sample, but not in pyridine-exposed sample.

3.4 Conclusions.

XRD studies of pyridine exposed kaolin highlighted a small amount of swelling mineral present as an impurity in the kaolin sample. Intercalation experiments revealed that this component was likely to be dehydrated halloysite. This mineral is known to swell after pyridine exposure to form a 12 Å intercalate. VT XRD studies showed that there was deintercalation of pyridine by 100 °C (and thus a 7 Å dehydrated halloysite was formed). VT DRIFTS studies indicated that pyridine exposed halloysite showed evidence of pyridine adsorption up to much higher temperatures (i.e. 200 °C). VT DRIFTS studies on pyridine exposed unmilled and milled Cornish kaolin showed that adsorbed pyridine was detected in the spectra up to c 250 °C. Therefore, at lower temperatures, (i.e. room temperature to 100 °C) the spectra collected were composites of pyridine-intercalated halloysite and a kaolin-pyridine adsorption complex. At temperatures above this, the pyridine bands produced were due to kaolin-halloysite and kaolin-pyridine adsorption interactions only.

Pyridine is able to create strong hydrogen bond associations with hydroxyls. Due to the small amount of halloysite impurity, there was a small alteration in the relative intensity of the 3695 and 3620 cm^{-1} bands at lower temperatures, due to the intercalation reaction of pyridine with halloysite. The infrared data presented do not suggest that a significant proportion of this probe molecule binds to the external or internal basal surfaces of kaolin, either before or after ball-milling. Rather, it is likely that pyridine binds to exposed (broken) edge sites, or it may be sorbed between the slightly expanded layers of kaolin at the edges of the stacks. Pyridine was able to displace the more strongly hydrogen bonded water which is trapped between the individual kaolin particles which comprise the large aggregates after ball milling. This water then readsorbs in a more weakly hydrogen bonded manner at exposed edge sites. Thus, the intensity of the more weakly hydrogen bonded water species increases relative to the intensity of the more strongly hydrogen bonded water. Water very loosely attached or physisorbed between the slightly expanded edges of the mineral is also displaced by pyridine (see pyridine exposed 3 minute milled sample). In this case, the water was displaced, but atmospheric water was able to readsorb in a position which was relatively more strongly bound than

before exposure. After pyridine exposure, the total amount of sorbed water decreases relative to the amount in the unexposed samples. Figure 3.67 below shows the proposed mechanism for pyridine binding through surface sorbed water species. As milling time increases there is more surface water, thus Brønsted associations are more likely.

Figure 3.67 Proposed mechanism of pyridine displacement of water in Brønsted type binding.

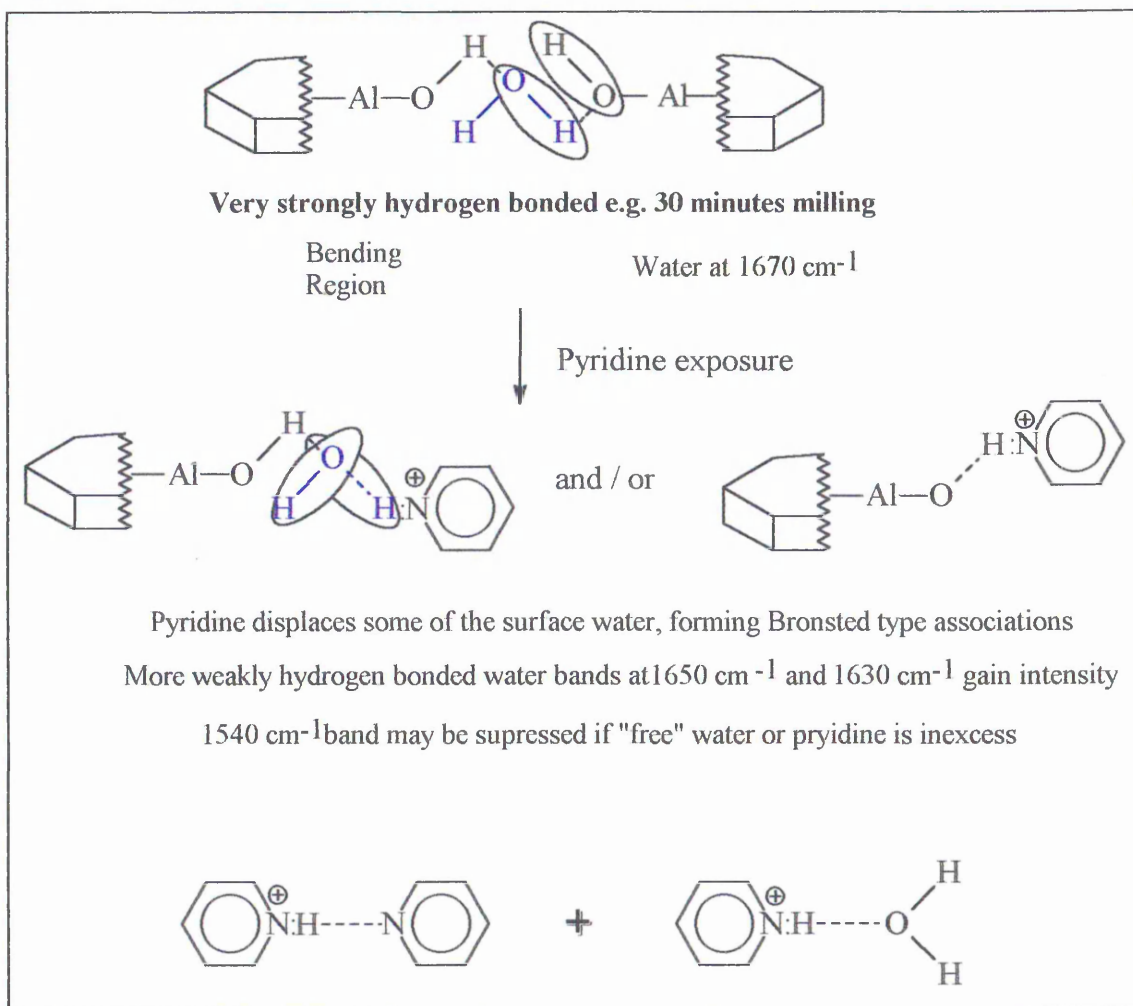
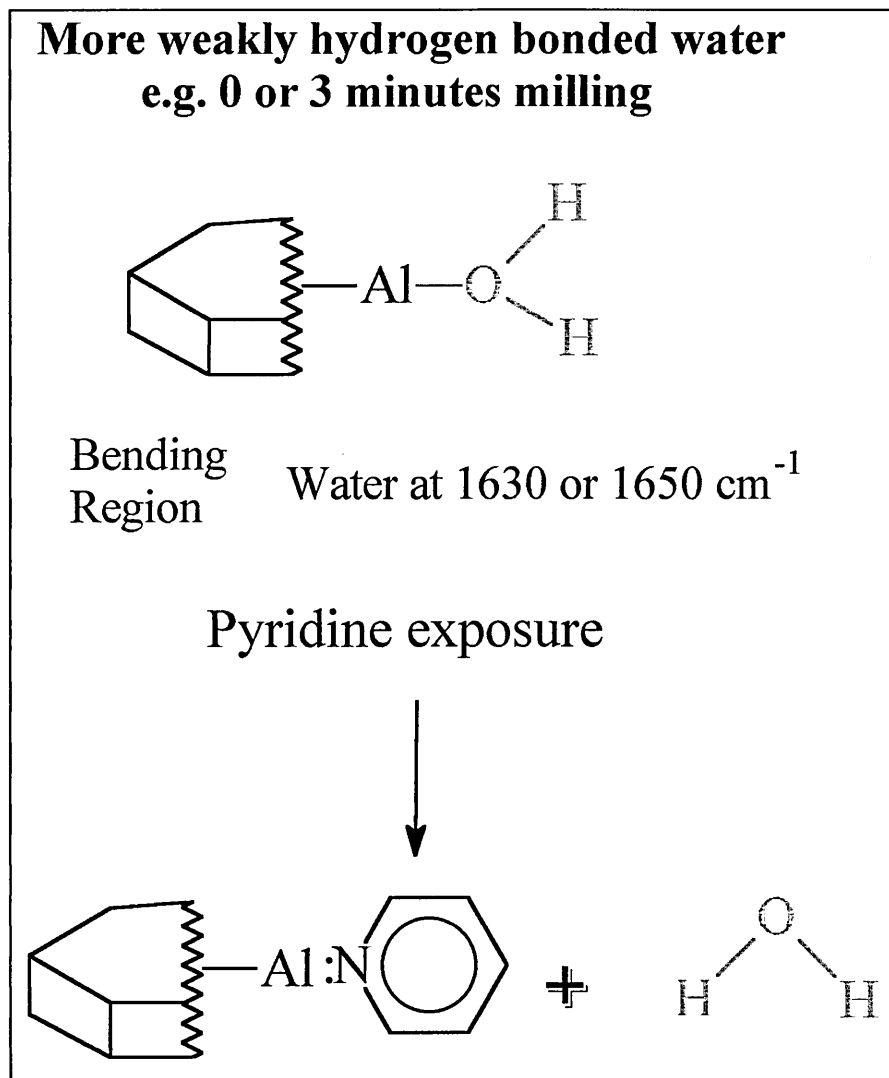
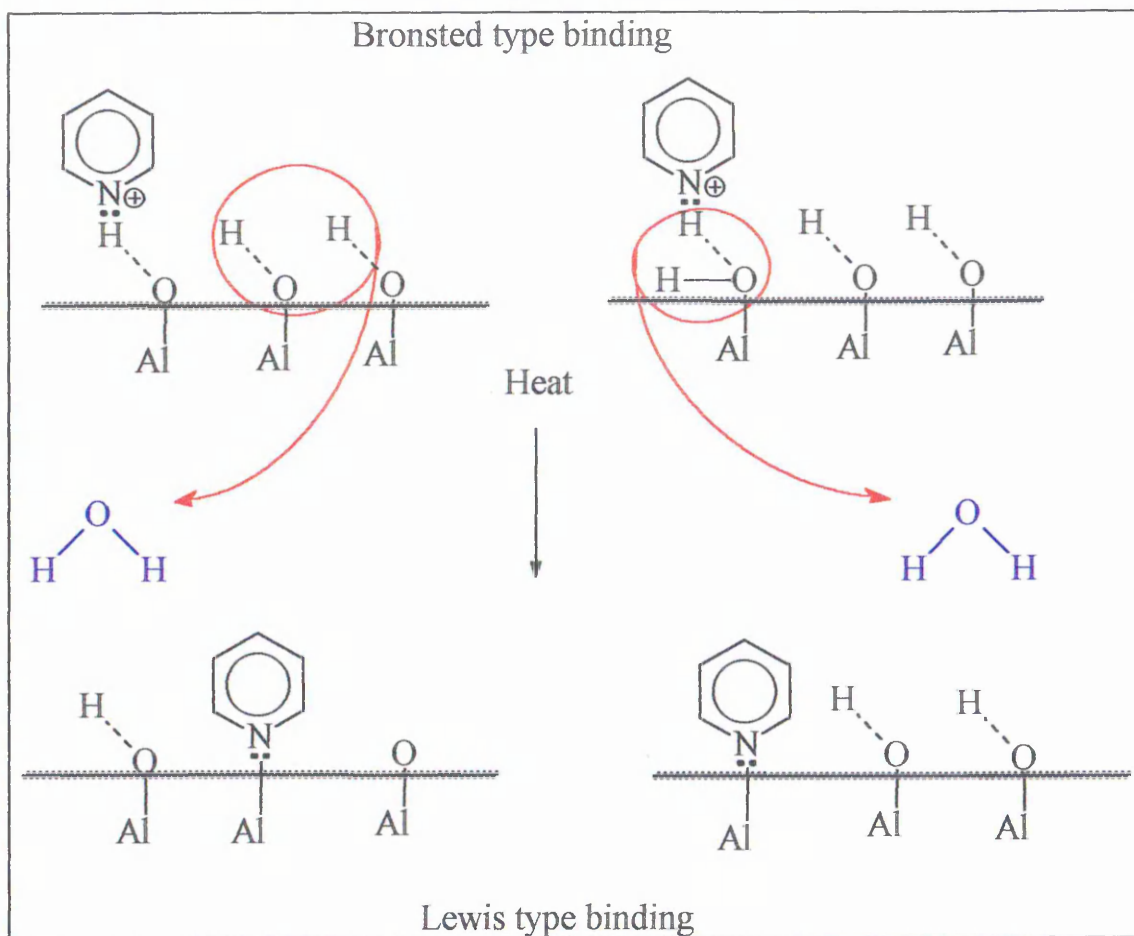


Figure 3.68 Proposed mechanism of pyridine displacement of water in Lewis type binding.



When pyridine acts as a Lewis base, water is displaced as shown in Figure 3.68 above. The organic binds directly to an exposed cation (e.g. Al^{3+}). Figure 3.69 illustrates schematically the conversion from Brønsted type binding to Lewis type binding observed after heating, and thus with the removal of surface water. The reaction may occur in a number of ways. Firstly, the structural dehydroxylation of the mineral could occur, thus exposing an Al cation which is available for direct bonding to a pyridine molecule. Alternatively, Lewis binding could be facilitated by the removal of surface sorbed water (or hydroxyls). This also results in the exposure of an Al^{3+} cation although it is not as a result of structural dehydroxylation.

Figure 3.69 Conversion from Lewis type binding to Brønsted type binding.



Lewis type binding was more prominent compared with Brønsted binding at room temperature in the unmilled and 3 minute milled kaolin samples. It also becomes the more likely type of attachment as water is removed by heating. Pyridine and /or heat are able to remove the small amount of surface-sorbed water (or hydroxyls). This allows the pyridine to bind directly to the exposed cation. The water “released” from the kaolin surface is able to bind with excess pyridine (probably the case at room temperature if no diagnostic 1540 cm^{-1} band is present), or is removed from the DRIFTS cell by the constant nitrogen flow.

When pyridine displaces the more strongly hydrogen bonded water (“adhesive water at 1670 cm^{-1}) it is likely that the agglomerates become dispersed. When the larger particles split, a variety of other water environments remain. There is always a mixture of water in different environments (characterised by the bands at 1650 and 1630 cm^{-1}) This explains why in all the samples (milled and unmilled) at room temperature , there is

always a mixture of Lewis and Brønsted type binding. Pyridine is also able to adsorb to the edge sites of halloysite in the manner described above.

3.5 References.

- ¹ Johnston CT (1996). Sorption of organic compounds on clay minerals: a surface functional group approach. In CMS Workshop Lectures, Vol 8, Organic Pollutants in the Environment, Sahwney B, ed. (1996), The Clay Minerals Society, Boulder, CO, 1-45.
- ² Sugahara Y, Satokawa S, Yoshioka K, Kuroda K & Kato C (1989). Kaolinite-pyridine intercalation compound derived from hydrated kaolinite. *Clays and Clay Minerals* **37**, 2, 143-150.
- ³ Ukrainczyk L & Smith KA (1996). Solid state ¹⁵N NMR study of pyridine adsorption on clay minerals. *Environmental Science Technology* **30**, 3167-3176.
- ⁴ Breen C, Deane AT & Flynn JJ (1987). The acidity of trivalent cation-exchanged montmorillonite, temperature programmed desorption and infrared studies of the desorption of pyridine and n-butylamine. *Clay Minerals* **22** 169-178.
- ⁵ Bodoardo S, Figueras F & Garrone E (1994). IR study of Brønsted acidity of Al-pillared montmorillonite. *Journal of Catalysis* **147**, 223-230.
- ⁶ Ukrainczyk Lewis & Smith KA (1996). Solid state ¹⁵NMR study of pyridine adsorption on clay minerals. *Environmental Science Technology* **30**, 3167-3176.
- ⁷ Bagshaw SA & Cooney RP (1993). FTIR surface site analysis of pillared clays using pyridine probe species. *Chemical Materials* **5**, 1101-1109.
- ⁸ Chevallier S, Franck R, Suquet H, Lambert JF & Barthomeuf D (1994). Al-pillared saponites. Part 1-IR studies. *Journal of the Chemical Society. Faraday Trans.* **90** (4), 667-674.
- ⁹ Connerton J, Joyner RW & Padley MB (1995). Characterisation of the acidity of well defined Cu-ZSM-5 catalysts using pyridine as a probe molecule. *Journal of the Chemical Society. Faraday Trans.* **91** (12), 1841-1844.
- ¹⁰ Kooli F, Martin C & Rives V (1997). FT-IR spectroscopic study of surface acidity and 2-propanol decomposition on mixed oxides obtained upon calcination of layered double hydroxides. *Langmuir* **13**, 2303-2306.
- ¹¹ Kiviat FE & Petrakis L (1973). Surface acidity of transition metal modified aluminas, infrared and nuclear magnetic resonance investigation of adsorbed pyridine. *The Journal of Physical Chemistry* **77**, 10 1232-1239.
- ¹² Breen C (1991). Thermogravimetric study of the desorption of cyclohexylamine and pyridine from an acid-treated Wyoming bentonite. *Clay Minerals* **26**, 473-486.
- ¹³ Yariv S (1992) The effect of tetrahedral substitution of Si by Al on the surface acidity of the oxygen plane of clay minerals. *International Reviews in Physical Chemistry* **11**, 2, 345-375 (and references therein).

- ¹⁴ Yariv S (1996). Thermo-IR-spectroscopy analysis of the interactions between organic pollutants and clay minerals. *Thermochimica Acta* **274** 1-35.
- ¹⁵ Breen C (1980). Thesis: Neutron scattering and cognate studies of sheet silicates. University College of Wales, Aberystwyth, Dyfed, Wales.
- ¹⁶ Reis Jr AS, De Alencar Simono J & Chagas AP (1996). A thermodynamic study of the interactions of monoinic kaolinite with N,N-Dimethylacetamide (DMA) and Pyridine (PY). *Journal of Colloid and Interface Science* **177** 188.
- ¹⁷ Billingham J, Breen C & Yarwood J (1996). *In situ* determination of Brønsted/Lewis acidity on cation-exchanged clay mineral surfaces by ATR-IR. *Clay Minerals* **31**, 513-522.
- ¹⁸ Breen C (1991). Thermogravimetric and infrared study of the desorption of butylamine, cyclohexylamine and pyridine from Ni- and Co- exchanged montmorillonite. *Clay Minerals* **26** 487-496.
- ¹⁹ Ledoux RL & White J (1966) Infrared studies of hydrogen bonding of organic compounds on oxygen and hydroxyl surfaces of layer lattice silicates. *Proceedings of the International Clay Conference*. Jerusalem, Israel. Vol 1 (Theng ed.). 361-374.
- ²⁰ Lipsicas M, Raythatha R, Giese Jr RF, Constanzo PM (1986). Molecular motions, surface interactions and stacking disorder in kaolinite intercalates. *Clay and Clay Minerals* **34**, 6 635-644.
- ²¹ Breen C & Lynch S (1988). Reexamination of the kinetics of the thermal desorption of dimethyl sulphoxide and N-methyl-formamide from a Greensplatt kaolinite. *Clays and Clay Minerals* **36** 19-24.
- ²² Johnston CT & Stone DA (1990). Influence of hydrazine on the vibrational modes of kaolinite. *Clays and Clay Minerals* **38**, 2 121-128.
- ²³ Kirsch H, (1968) "Applied mineralogy", Chapman and Hall (London).
- ²⁴ Bailey SW (1990) Halloysite-a critical assessment. *Proceedings of the 9th International Clay Conference*. Strasbourg. Vol 86 (Farmer VC & Tardy eds.)
- ²⁵ Singh B (1996). Why does halloysite roll?-a new model. *Clays and Clay Minerals* **44**, 2, 191-196.
- ²⁶ Churchman GJ & Carr RM (1975). The definition and nomenclature of halloysites. *Clays and Clay Minerals* **23**, 382-388.
- ²⁷ Constanzo PM & Gieste RF Jr (1990). Ordered and disordered organic intercalates of 8.4Å synthetically hydrated kaolin. *Clays and Clay Minerals* **2**, 160-170.
- ²⁸ Wada Kaolin (1961). Lattice expansion of kaolin minerals by treatment with potassium acetate. *American Mineralogy* **46**, 78-91.
- ²⁹ Range KJ, Range A & Weiss A (1969) Fire clay type kaolinite or fire clay mineral? *Experimental classification of kaolin-halloysite minerals*. *Proceedings of the International Clay Conference*. Tokyo. Vol 1 (Lewis Heller ed.). Israel University Press. Jerusalem. 3-13.
- ³⁰ Theng BKG, Churchman GJ, Whitton JS & Claridge (1984). Comparison of intercalation methods for differentiating halloysite from kaolinite. *Clays and Clay Minerals* **32**, 4, 249-258.
- ³¹ Frost RL, Tran TH, Rintoul Lewis & Kristof J (1998). Raman microscopy of dickite, kaolinite and their intercalates. *Analyst* **123**, 611-616.

-
- ³² Gábor M, Tóth M, Kristof J & Komáromi-Hiller G (1995). Thermal behavior and decomposition of intercalated kaolinite. *Clays and Clay Minerals* **43**, 2 223-228.
- ³³ Tunney J & Detellier C (1994). Preparation and characterisation of an 8.4Å hydrate of kaolinite. *Clays and Clay Minerals* **42**, 4, 473-476.
- ³⁴ Carr RM & Chih HWA (1971). Complexes of halloysite with organic compounds. *Clay Minerals* **9**, 153-166.
- ³⁵ Churchman GJ, Whitton JS, Claridge GGC & Theng BKG (1984). Intercalation method using formamide for differentiating halloysite from kaolinite. *Clays and Clay Minerals* **32**, 4, 214-248.
- ³⁶ Hillier S, (Personal Conveyance). Soil Science Group, Macaulay Land Use Research Institute, Craigiebuckler, Aberdeen.

4. Kaolin-organic acid interactions.

4.1 INTRODUCTION.....	251
4.1.1 <i>The effects of pH on acids.</i>	252
4.1.2 <i>The effects of pH on mineral surfaces.</i>	254
4.1.2.1 <i>The amphoteric nature of the Al-OH surface layer of kaolin</i>	254
4.1.3 <i>The adsorption of oleate/oleic acid to minerals.</i>	258
4.1.4 <i>The adsorption of other industrially significant organics onto kaolin.</i>	266
4.2 EXPERIMENTAL.	267
4.2.1 <i>Method development.</i>	267
4.2.2 <i>Materials.</i>	269
4.2.3 <i>Sample preparation.</i>	269
4.2.4 <i>Concentration of oleic acid theoretically available for adsorption.</i>	270
4.3 RESULTS OF INFRARED STUDIES.	272
4.3.1 <i>pH 3.</i>	272
4.3.1.1 <i>Water washed kaolin (pH3).</i>	272
4.3.1.2 <i>Oleic acid treated kaolin (pH 3).</i>	273
4.3.2 <i>pH 9.</i>	280
4.3.2.1 <i>Water washed kaolin (pH 9).</i>	281
4.3.2.2 <i>Oleic acid treated kaolin (pH 9).</i>	282
4.3.3 <i>pH 12.</i>	286
4.3.3.1 <i>Water washed kaolin (pH 12).</i>	286
4.3.3.2 <i>Oleic acid treated kaolin (pH 12).</i>	287
4.4 CONCLUSIONS.	289
4.5 REFERENCES.....	295

FIGURE 4.1 C/S OLEIC ACID.	252
FIGURE 4.2 THE EFFECT OF pH ON OLEIC ACID.	253
FIGURE 4.3 PROPOSED MECHANISMS OF BINDING OF A NEUTRAL ORGANIC ACID TO KAOLIN SURFACE.	254
FIGURE 4.4 THE EFFECT OF pH ON THE SURFACE OF KAOLIN.	254
FIGURE 4.5 STACKING CONFIGURATIONS OF KAOLIN PARTICLES.	256
FIGURE 4.6 PROPOSED MECHANISMS FOR THE ADSORPTION OF OLEATE TO APATITE.	260
FIGURE 4.7 SCHEMATIC OF THE ADSORPTION OF BRIDGED AND CHELATING BIDENTATE ADSORBED TO HAEMATITE SURFACE ⁷	262
FIGURE 4.8 WATER WASHED KAOLIN (pH 3).	272
FIGURE 4.9 OLEIC ACID TREATED KAOLIN (pH 3).	274
FIGURE 4.10 SUBTRACTED SPECTRA OF OLEIC ACID TREATED KAOLIN (pH 3).	276
FIGURE 4.11 SUBTRACTED SPECTRA OF OLEIC ACID TREATED KAOLIN (pH 3). NORMALISED TO THE 1468 CM ⁻¹ BAND.	277
FIGURE 4.12 OLEIC ACID TREATED, RINSED KAOLIN (pH 3).	278
FIGURE 4.13 SUBTRACTED SPECTRA OF OLEIC ACID TREATED, RINSED KAOLIN (pH 3). NORMALISED TO THE 1468 CM ⁻¹ BAND.	279
FIGURE 4.14 COMPARISON OF 50 MG OLEATE TREATED SAMPLES (RINSED AND UNRINSED) NORMALISED TO THE 1468 CM ⁻¹ BAND.	280
FIGURE 4.15 WATER WASHED KAOLIN (pH 9).	281
FIGURE 4.16 OLEIC ACID TREATED KAOLIN (pH 9).	282
FIGURE 4.17 SUBTRACTED SPECTRA OF OLEIC ACID TREATED KAOLIN (pH 9).	283
FIGURE 4.18 RINSED KAOLIN-OLEIC ACID pH 9.	284
FIGURE 4.19 SUBTRACTED SPECTRA OLEIC ACID TREATED, RINSED KAOLIN (pH 9).	285
FIGURE 4.20 WATER WASHED KAOLIN (pH 12).	286
FIGURE 4.21 OLEIC ACID TREATED KAOLIN (pH 12).	287
FIGURE 4.22 SUBTRACTED SPECTRA OLEIC ACID TREATED KAOLIN (pH 12).	288
FIGURE 4.23 SCHEMATIC OF THE PROPOSED PARTIAL INTERCALATION MECHANISM OF OLEIC ACID INTO HALLOYSITE.	289
FIGURE 4.24 MICELLE FORMATION AND THE ASSOCIATION WITH A MINERAL SURFACE.	291
FIGURE 4.25 PROPOSED MECHANISM OF MICELLAR ADSORPTION AT pH 12.	292
TABLE 4.1 OBSERVATIONS OF THISTLETHWAITE <i>ET AL</i> ¹⁷	259
TABLE 4.2 OBSERVATIONS OF GONG <i>ET AL</i> ³⁴	261
TABLE 4.3 PROPOSED ASSIGNMENTS AND SOME ADSORPTION MECHANISMS OF CARBOXYLIC ACID ON MINERAL SURFACES.	264

4.1 Introduction.

During the industrial processing procedure involved in the extraction and purification of kaolin, many organic molecules, such as carboxylic acids, polymers and surfactants, are utilised. Generally, these chemicals are added to the mineral in aqueous solution at ambient temperature. The pH of the mixture may be adjusted using acid (e.g. HCl) or alkali (e.g. NaOH). Changes in pH and/or the interactions of the organic species with the mineral surface can dramatically alter the physical properties of the mineral. This chapter describes how, on a molecular level a representative organic acid, interacts with the surface of kaolin in an aqueous, pH adjusted environment. The chosen representative adsorbate molecule was oleic acid. The spectrum of the chemically treated mineral may not be simply a composite of the mineral and probe molecule, since shifts are likely to occur in one or more of the bands associated with each. This is due to the altered environment which is created by the interaction of the mineral with the probe.

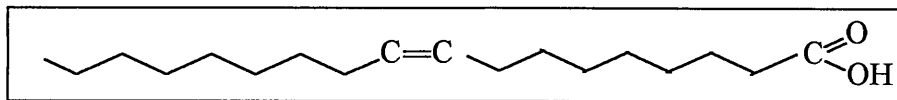
Unlike swelling clays such as montmorillonite and hectorite, kaolin, with its comparatively small surface area, does not adsorb a large quantity of organic molecules, so a very sensitive monitoring technique such as DRIFTS is required to assess the nature of the adsorbed species at a molecular level. Since kaolin has relatively few sites available for interactions with organics, representative probe molecules must be chosen with care, to ensure that they interact with the available sites and provide an observable, diagnostic signal. Oleic acid was chosen as the probe molecule since it contains both the carboxylate group and the hydrocarbon chain which are of interest industrially, (since carboxylic acids and HC polymers are used in the processing procedure), yet it has a short enough HC chain to facilitate academic study. Adsorption of oleic acid / oleate onto other minerals has been well studied and this has led to a well documented (if at times muddled) faction of assignments of adsorption bands. Adsorption of organics to mineral surfaces from dilute solution can depend upon many factors, including solution pH, the surface properties of the mineral and the availability of reactive sites thereon, the functionality of the adsorbate, and the reaction temperature. The more important of these issues will be discussed in the literature review that follows.

In this chapter, oleic acid (*cis*-9-octadecanoic acid, C₁₈H₃₄O₂) (see Figure 4.1) was chosen as a model probe molecule as a precursor to the study of the interactions of kaolin with polymers widely used in the mineral processing industry, such as polyacrylate and polyacrylamide. Although the interactions of such molecules with kaolin have been studied (¹ and references therein), there is little information regarding the interactions at a molecular levels. Oleic acid is also added to mineral suspensions in the paper making industry, where kaolin is often used as a coating pigment⁶. It may also be added to suspensions of hydrophobic particles to increase aggregate formation. The adsorption of these and other polymers to kaolin have been discussed in the literature^{2, 3,4,5}, although literature using infrared spectroscopy as the method of investigating the interaction of polymers with kaolin is very rare. Rogan⁶ used adsorption isotherms to studied the adsorption at the macroscopic level of oleic acid to various minerals including kaolin. Oleic acid adsorption was found to be low and that the adsorption process followed the Langmuir model.

The only IR study found discussing the adsorption of oleic acid onto kaolin contained spectra of poor quality and it was concluded that under the experimental conditions in use, neither oleate nor oleic acid adsorbed to kaolin⁷. However, this work also explained the adsorption characteristics of oleate/oleic acid on haematite. The study was carried out at pH 7.5, and the organic was found to adsorb, giving bands at 1580 cm⁻¹, assigned to bridged bidentate and 1710 cm⁻¹, corresponding to dimers of oleic acid adsorbed via hydrocarbon chain associations with chemisorbed oleate. Oleate / oleic acid was found to adsorb more readily to haematite than to kaolin.

4.1.1 The effects of pH on acids.

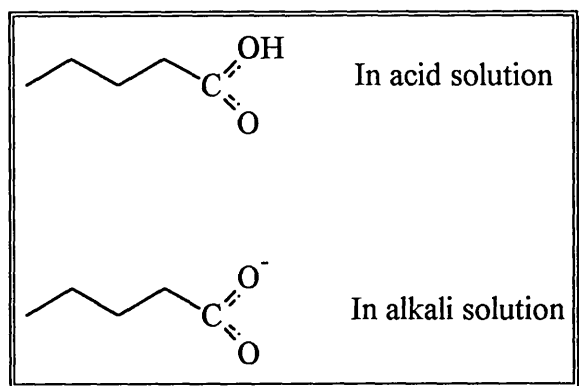
Figure 4.1 *Cis* Oleic acid.



Oleic acid is known to intercalate into kaolin using the entraining agent hydrazine-hydrate, and IR data were discussed by Sidheswaran et al⁸. It is also possible, by the use of entraining agents, for potassium salts of carboxylic acids to become intercalated into kaolin⁹. It is strongly believed that in the industrial situation, conditions of treatment do

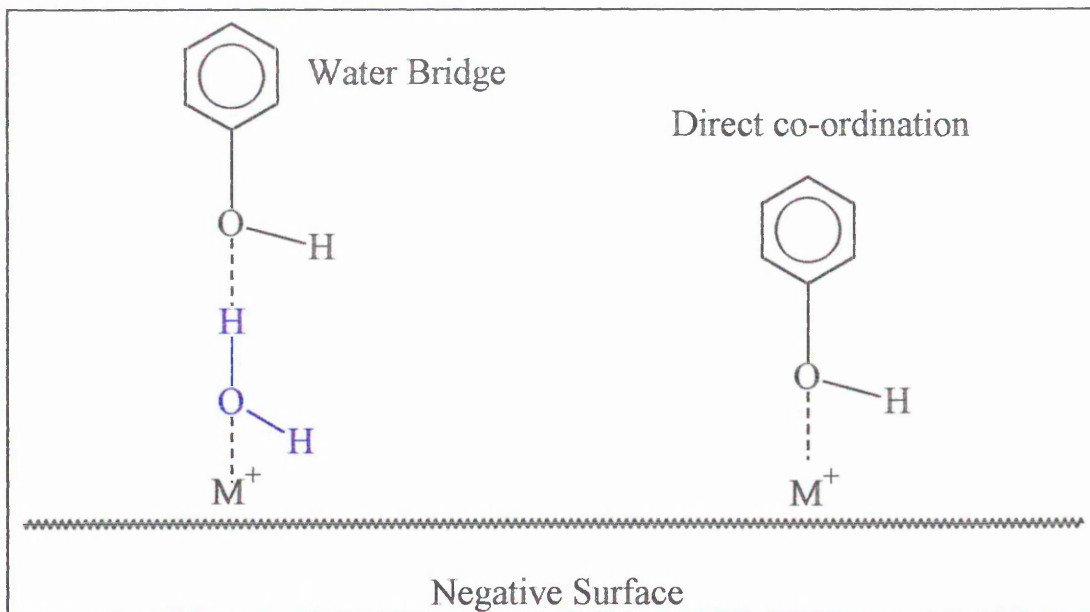
not facilitate the intercalation of the chemical reagents, and therefore, in the present work the intention was not to affect intercalation but to monitor the surface adsorption at a range of pHs.

Figure 4.2 The effect of pH on oleic acid.



It was calculated that at pH above 8.6, oleate ions predominate¹⁰ (pH 8.5 quoted in Gong *et al*³⁴.) below pH 7 the acid form predominates, and between pH 7 and 8.5, both species exist in significant amounts³⁴. Obviously, at all pHs an equilibrium always exists between the two species. In the anionic form (RCOO⁻), it is thought that organic acids will have little, if any interaction with the clay surface and that neutral organic acids react weakly, principally via a water bridge or via direct co-ordination to an exposed (or exchangeable) cation¹¹ as shown in Figure 4.3 below.

Figure 4.3 Proposed mechanisms of binding of a neutral organic acid to kaolin surface.

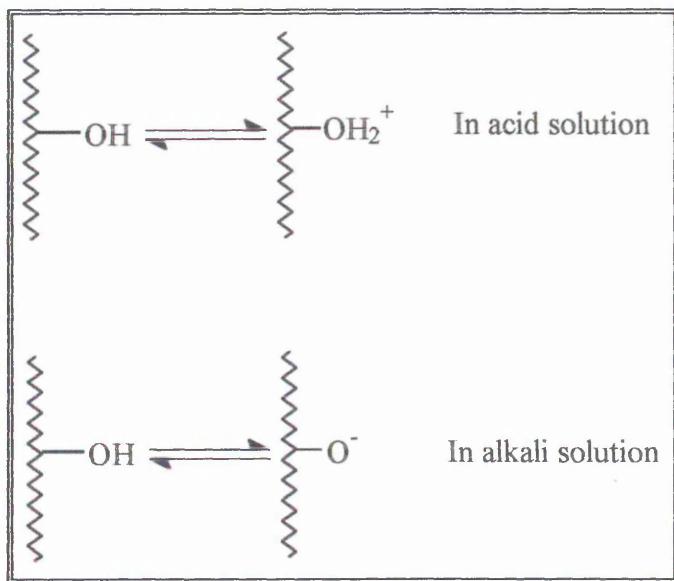


(Adapted from publication by Johnston⁴)

4.1.2 The effects of pH on mineral surfaces.

4.1.2.1 The amphoteric nature of the Al-OH surface layer of kaolin

Figure 4.4 The effect of pH on the surface of kaolin.



The reactive surface sites of kaolin are predominantly dominated by oxy-anions coordinated to underlying cations. These oxygens are amphoteric and partially coordinated oxy-anions can interact strongly with protons, therefore neutralising the

surface's inherent negative charge. At high pH, the oxy-anion surfaces are typically negatively charged and many anions will lack protons (i.e. O⁻). At low pH, singly protonated oxy- anions can bind additional protons, thus inferring a positive charge. These oxygen ions may be bonded to either Si or Al. It is commonly believed that the basal faces of kaolin platelets have a permanent negative charge, whereas the exposed edges have a pH dependant charge. Furthermore, the AlOH sites are more amphoteric in nature than the predominantly acidic SiOH sites¹⁵.

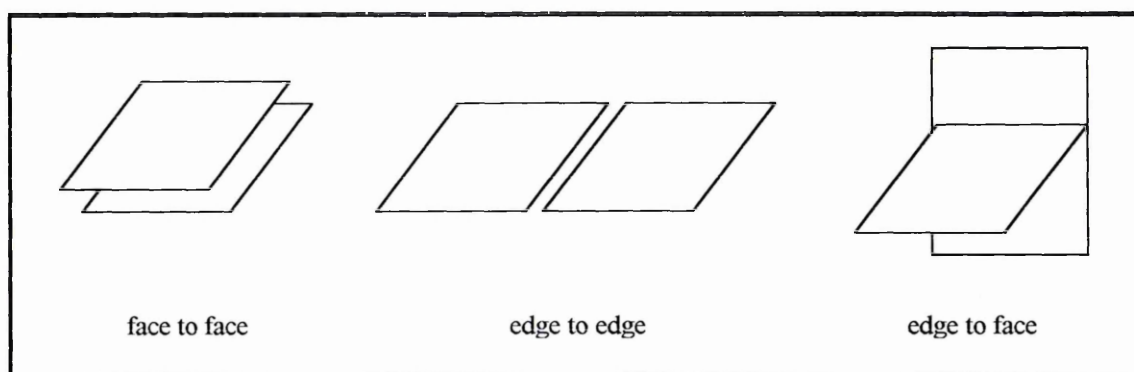
At high pH, it is also possible that Na (from the NaOH used to adjust the pH of the water) can interact with the surface, thus forming AlO-Na. The surface charge can also be altered by the temperature of the kaolin suspension at a given pH¹⁵. Attack by concentrated acid is known to dissolve the Al containing octahedra preferentially compared with the silica tetrahedra. This results in the appearance of free silica, and leads to an increase in pore volume and specific surface area¹². Base attack ultimately leads to the dissolution of weakly bound amorphous silica and the removal of structural SiO groups from the tetrahedral sheet. However, these groups are not readily soluble, and it is believed that significant dissolution by base attack would not occur at the pH levels used in the current work. It is likely that besides the chemistry of the oleate and sodium (from the oleic acid and from the addition of NaOH used for pH adjustment) in solution, other ions could influence the formation and structure of the adsorbed layer (for example, free Al³⁺ ions).

Kaolin can become dispersed, aggregated or flocculated depending on the nature of the medium in which it is suspended. A common tool employed to alter the state is the alteration of pH. The effect of the treatment is dependant upon the PZC of the mineral, which varies greatly between samples. However, the precise determination of the interactions between clay particles at varied pH remains the subject of much controversy. Three of the more detailed papers in this area are reviewed below.

Kretzschmar *et al*¹³, conducted a study to examine the effects of humic acid and pH upon kaolin particle dispersion. They determined that the average PZC of sodium exchanged kaolin was 4.8 (i.e. the average of the edge and face isoelectric points) and the PZC for the edge sites of the same kaolin was pH 5.8. When the ion exchanged mineral was allowed to sediment under gravity, it was found that the coagulation rate

was reduced at pH above 5.8. It was deduced that at pH less than the PZC of the edge surfaces, the edges carry a positive charge, and edge to face (E-F) coagulation occurred due to electrostatic and van der Waal's forces (see Figure 4.5 for configurations). The rate of coagulation was not affected by the addition of NaClO₄. At pH higher than the PZC of the edges, (i.e. above 5.8), all the kaolin surfaces became negative, and edge to face (E-F) interactions were no longer favourable and the coagulation rate decreased. It could be increased again by the addition of the electrolyte, NaClO₄. The rate increased further with increasing electrolyte concentration. Furthermore, it was suggested that ionic strength influenced the type of interaction (i.e., E-E, E-F etc.) At pH less than the edge PZC, and at low ionic strength, E-F associations predominated. Complete deflocculation occurred at high pH. At all pHs, F-F interactions predominated if the ionic strength was high.

Figure 4.5 Stacking configurations of kaolin particles.



Ma and Pierre¹⁴ investigated the surface and edge charges of kaolin. It was determined that at pH 6.9, (in suspension with deionised water) kaolin has stable negative charges on the faces, and positive charges on the edges (corroborated by Kretaschmar *et al*¹³.) Using NaOH and HCl to alter the pH of the suspension, they determined that the isoelectric point of kaolin (i.e. the average of the edge and face isoelectric points) was at pH 3.7 (lower than that determined by Kretaschmar *et al*¹³). At both high and low pH, they determined that F-F associations were predominant, although theory predicted that at low pH E-F interactions were predicted, and at high pH E-E interactions were predicted. It was postulated that the difference between theoretical and experimental data was due to the increased frequency of collisions F-F, compared with those of E-E or E-F (given that the surface area of the faces is larger than that of the edges). The nature

of the F-F associations led to randomly connected particles in suspension at pH 2, and the formation of a “bookhouse” structure at pH 6. At pH 2, the kaolin adsorbed protons, and therefore become positively charged. Coalescence did not immediately occur because of the repulsive forces between the particles. However, settling occurred quickly due to gravity, and collisions between the more concentrated particles increased in frequency. This led to flocculation, and because the sedimentation was so rapid, the particles packed randomly rather than in a uniform manner. At pH 6, the electrical field surrounding the particles was reduced, and F-F interactions could occur more easily, thus forming aggregates. The bookhouse structure formed. This is similar to the well known cardhouse structure, but in the former, the interactions are F-F, whereas in the latter, interactions are E-E. The bookhouse structures coalesced quickly and formed a completely flocculated, fractal like suspension. It was very porous, and the particles were all joined together via a network throughout the suspension. At high pH (pH 9.5), the zeta potential of the clay became negative, and clay sediments became compacted. The mechanism for this sedimentation was similar to that observed at low pH.

Ward and Brady¹⁵ conducted adsorption experiments using kaolin, quartz (SiO_2) as a model for the tetrahedral layer of kaolin, and corundum (Al_2O_3) as a model of the kaolin octahedral layer, as the substrates for oxalate, acetate and formate adsorption. According to their work, adsorption of organics onto kaolinite occurs primarily at Al^{3+} sites at broken edges, and not at the upper and lower O and OH surfaces of the mineral. Data presented in Chapter 2 regarding the adsorption of pyridine also suggests this phenomenon occurs in kaolin-organic adsorption mechanism. It was found (by Ward and Brady¹⁵) that the tetrahedral layer remained neutral until above pH 7, after which point, deprotonation began, i.e. $\text{SiOH} \rightarrow \text{SiO}^- + \text{H}^+$. The octahedral layer was found to have a PZC of approximately 4. Even at near neutral pH, the Al sites were easily deprotonated to give AlO^- , and were readily soluble. At low pH, unfavourable electrostatic interactions did not favour the adsorption of dissolved Al^{3+} to the neutral or positive surface. At high pH, $\text{Al}(\text{OH})_4^-$ was dissolved from the octahedral layer, but the adsorption of this hydroxy complex was not favoured because of the surface negativity of the mineral.

4.1.3 The adsorption of oleate/oleic acid to minerals.

There have been numerous adsorption studies using this organic molecule, and some are outlined below. The more relevant papers have been reviewed in some detail.

The adsorption of oleic and stearic acids onto a filler, magnesium hydroxide was studied using DRIFTS and other techniques¹⁶. XRD was used to measure the level of structural order in the adsorbed fatty acid metal salt layer (which crystallised on the surface of the mineral). Although the DRIFTS data were analysed, no spectra were included in the paper. Oleate was found to adsorb at 12 mg per gram after 1 week of exposure. It was determined by XRD, FMC (flow micro-calorimetry) and IR data, that at low acid concentration, carboxylate adsorbed perpendicularly to the mineral surface in “1/2 salt form (termed “mono-oleate” in the work presented herein). It should be noted that the IR studies upon which the type of adsorption was based, were carried out on the extracted supernatant, rather than on the mineral sample. The packing of this monolayer was inefficient and disordered due to the steric effects of the kinked C-C chain. Bonding was not thought to be through the double bond. In the presence of excess acid, a “full salt” di-oleate was formed, which was soluble in the solvent used (heptane), but would otherwise have remained on the surface. Thus, initially monolayer coverage was achieved, followed by multilayering of the acid in the salt form. According to these workers, there are two types of substrate: non reactive, where physisorption occurs, and reactive, where salt formation by chemisorption occurs. The magnesium hydroxide studied must be classed as a reactive substrate. Titania pigments were said to exhibit both types of behaviour.

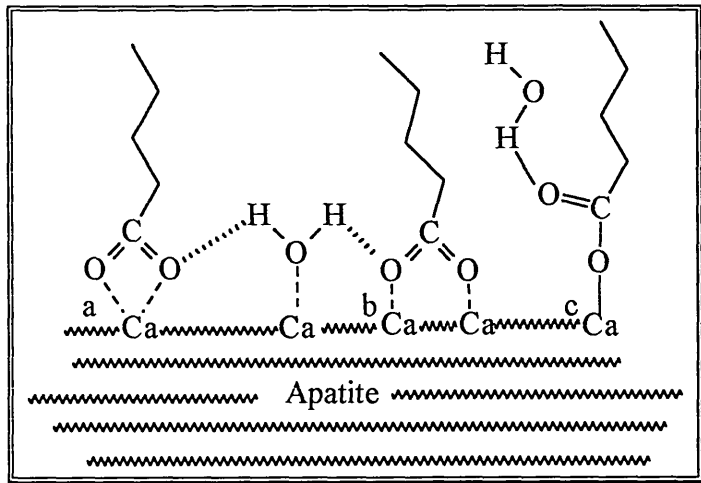
Thistlethwaite *et al*¹⁷, selected oleate as a probe molecule in their surface characterisation of zirconia (ZrO₂). The findings of this work may be useful in the interpretation of the work presented herein, since zirconia also has an exposed surface hydroxyl layer. However, their results suggested that electrostatic interactions alone could not account for the observed spectra, and it was concluded that another driving force, such as the co-ordination of oxygen lone pair electrons into vacant zirconium 3d orbitals, was involved in the adsorption process. The findings of the referenced study are summarised below.

Table 4.1 Observations of Thistlethwaite *et al*¹⁷.

pH	Observations of Thistlethwaite <i>et al</i> ¹⁷ .
12	There was no evidence of chemical adsorption. 1573 and 1538 cm ⁻¹ bands were attributed to precipitated oleate in 2 different orientations. (Were found not to correspond to adsorbed oleate as previous assignments have suggested.)
9	Species adsorbed were oleate ion and oleic acid dimer. No 1573 / 1538 cm ⁻¹ bands, therefore precipitation did not occur at this pH. 1713 corresponded to ν_s (C=O) of adsorbed oleic acid dimer. This band (marginally shifted) also appears in the spectrum of bulk liquid oleic acid, which is present mostly in the dimer form. 1548 cm ⁻¹ band corresponded to the ν_{as} (-COO ⁻) of adsorbed oleate anions. This feature would not be expected at this pH, since the surface would be dominated by negative charge. The phenomenon was explained if the COO ⁻ interacted with lone electron pairs on zirconia.
6	Species adsorbed were oleate anions and oleic acid monomer. The latter via hydrogen bonding of C=O to ZrOH ₂ ⁺ .
3	Stronger adsorption compared with pH 6, due to more favourable electrostatic interactions. Adsorbed species were oleic acid monomer and oleate anions. 1681 cm ⁻¹ band represented C=O stretch of oleic acid monomer, hydrogen bonded to the ZrOH ₂ ⁺ (as pH 6). 1556 band represented ν_{as} (-COO ⁻) of adsorbed oleate anions (as pH 9). 1379 band corresponded to C-OH stretching of oleic acid. However, it does not appear at pH 9 or 6, where acid adsorption is also present. This phenomenon was not fully understood, but may be due to some kind of HC tail interaction.

The study of the interaction of oleate/oleic acid with apatite (Ca₅[(F,Cl,OH)(PO₄)₃]) have attracted considerable interest^{18,19,22,34}. Meilczarski & Cases¹⁹ carried out adsorption of oleate to apatite and proposed an adsorption scheme as shown in Figure 4.6 below, where attachment may occur by one or all of these processes.

Figure 4.6 Proposed mechanisms for the adsorption of oleate to apatite.



Type a binding shows chelating monodentate, type b, bridged bidentate and type c the hydrogen bonded anionic monomer. It was found that water was an important stabiliser for the chemisorption of oleate and that the higher coverages of oleate were formed by a three dimensional condensation (surface precipitation) mechanism, where precipitation could be directly on the surface of apatite, thus forming up to monolayer coverage, then the chemisorbed oleate/oleic acid molecules are able to function as adsorption nuclei for the formation of additional layers (a phenomenon also observed by Gong *et al.*, in the study of oleate / oleic acid adsorption onto haematite²⁰ and apatite³⁴). Apatite interactions with oleic acid / oleate were also studied by Ince *et al*²¹, who determined that at pH 10, adsorbed organic was predominantly in the oleate form (represented by an intense IR band at 1560 cm^{-1}), and at pH 4, acid adsorption predominated (represented by an IR band at 1735 cm^{-1}). Adsorption at pH 4 was decreased by approximately 35 % compared with that at pH 10 according to floatation and IR data.

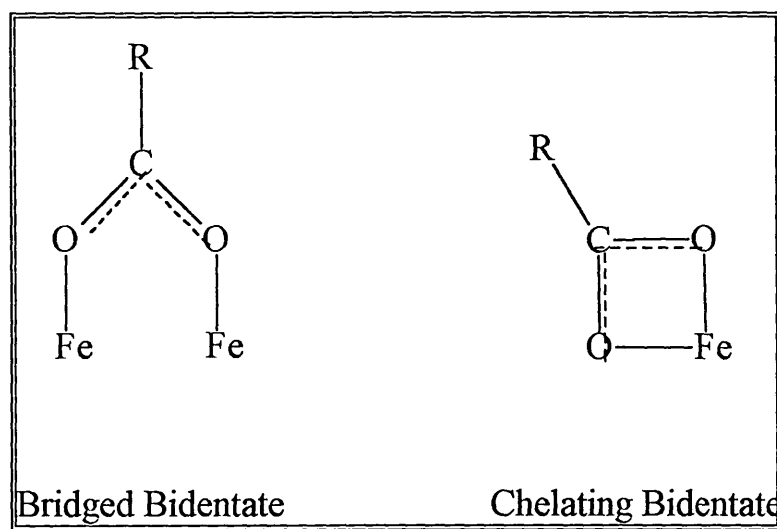
Another comprehensive study was carried out by Gong *et al*³⁴, who examined oleate / oleic acid adsorption on apatite. Although in most assignments, the work was in agreement with Thistlethwaite *et al*¹⁷, some discrepancies arose in the mode of adsorption. The findings of the study by Gong are summarised below.

Table 4.2 Observations of Gong *et al*³⁴

pH	Observations of Gong <i>et al</i> ³⁴
9.8	1574 / 1540 cm ⁻¹ doublet at high, low and mid concentration of oleate / oleic acid, representing (-COO ⁻) of chemisorbed “bulk” organic. Probably attached to surface by HC tail interactions. The intensity of the doublet increased as concentration of organic increased. When the calcium is dissolved from the structure of the mineral, 2 oleate ions may bind to it, thus forming Ca-oleate. If this adsorbs to the surface a precipitate is formed, and a doublet at 1574 / 1540 is produced. The carboxylate end of the molecule may bind to the phosphate anion on the mineral surface by ion-dipole interaction and / or the non polar HC tails be attached to the surface via interactions with the HC tail of molecules already attached.
8	1574 / 1540 cm ⁻¹ doublet at high concentration, removed after washing and replaced with 1550 cm ⁻¹ singlet. This represented bulk precipitated oleate being removed after washing, thus exposing the chemisorbed oleate (always present, but masked by intense doublet). At low concentration, only 1550 cm ⁻¹ present (no doublet). The 1550 cm ⁻¹ was persistent after washing in all cases.
6	Singlet at 1550 cm ⁻¹ present at all concentrations which persisted after washing. Assigned to strongly adsorbed ν_{as} (COO ⁻) chemisorbed oleate. Additional band at 1713 cm ⁻¹ at high concentrations. Representing adsorbed oleic acid dimer. This band reduced with decreasing concentration and after washing.

The bands at 1580 and 1518 cm⁻¹ were assigned to bridged and chelating bidentate molecules respectively.

Figure 4.7 Schematic of the adsorption of bridged and chelating bidentate adsorbed to haematite surface⁷.



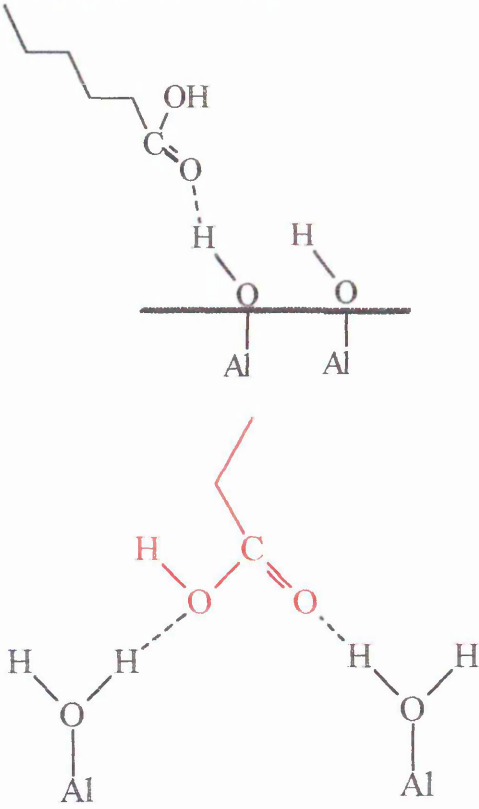
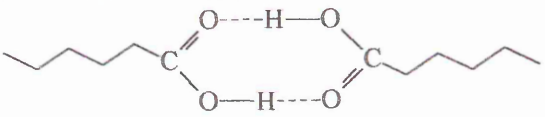
Gong⁷, Gong *et al*²⁰, and Morgan *et al*¹⁰, studied oleate adsorption to haematite. This mineral may be a more suitable model for kaolin, since its formula (Fe_2O_3) leads to the formation of surface OH groups (not dissimilar to those available on the surfaces of kaolin), whereas apatite has mainly exposed oxygens (from phosphate ions) available on its surface. Gong⁷, chose IR spectroscopy as the mode of study, and the results are shown below. It should be noted that the referenced work was a study of differential adsorption characteristics of kaolin and haematite, and in that work oleate / oleic acid was found not to adsorb to kaolin under the conditions used (possibly due to the preferential adsorption of oleate / oleic acid to haematite). However, the organic was found to adsorb to haematite, and there were observed discrepancies between the modes of adsorption of oleate to haematite compared with adsorption to apatite³⁴. On haematite in suspension at pH 7.5, oleate / oleic acid was found to adsorb directly to the surface of the mineral in the bridged bidentate form (with an IR band at 1580 cm^{-1}) and the acid dimer form (with a band at 1710 cm^{-1}) which adsorbed via HC chain interactions with the chemisorbed oleate species. Another band at 1440 cm^{-1} was observed, assigned to the antisymmetric stretch of (COO^-). Bands at 1518 and 1550 cm^{-1} were not observed in this system. In Gong *et al*²⁰, the adsorption characteristics varied from those observed in the other work (Gong⁷). However, several of the experimental parameters were altered, for example, different concentrations, different organic and different mineral sample. Therefore, the results are not directly comparable. In this study⁽²⁰⁾ it

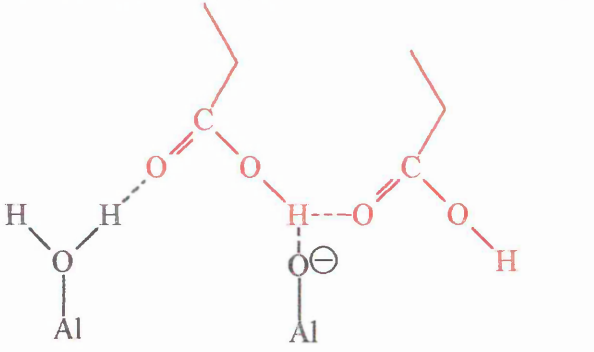
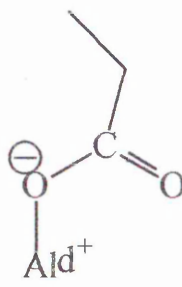
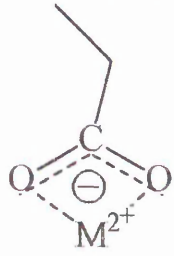
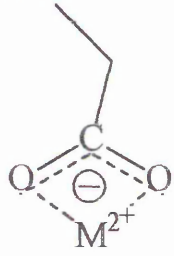
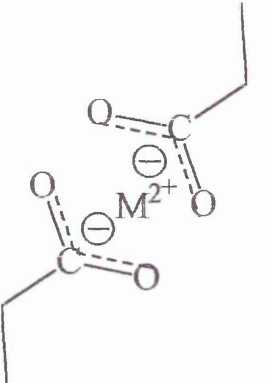
was concluded that chemisorption of oleate took place under all conditions (pH 6, 8 and 9.8). Acid dimer (1713 cm^{-1}), adsorbed via HC chain associations was found at pH 6, and pH 8, but not pH 9. Chemisorbed species existed at all pHs as chelating bidentate (1518 cm^{-1}) or bridged bidentate (at 1580 cm^{-1}) (assignments given by the author of the referenced work). At pH 8 and pH 6, hydrogen bonded oleic acid monomer was observed in low concentration on the mineral surface (at 1738 cm^{-1}).

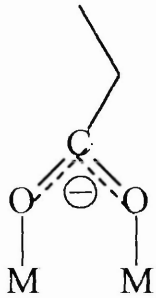
There is obviously a significant discrepancy between the assignments for the doublet at 1537 and 1570 cm^{-1} (e.g. attributing the bands to bidentate and unidentate calcium oleate species respectively²² and weakly attached calcium dioleate precipitates²³ or chelating bidentate and bridged bidentate²⁰). However, the general opinion in much of the literature agrees with the general assignment given by Gong *et al*³⁴, in that the bands represent “oleate in 2 different forms”. In the discussion of the work presented herein, it is assumed that metal -oleate does exist as precipitated layers, and gives a doublet at $c\ 1580$ and 1518 cm^{-1} - the bands may represent the “mono-oleate” and “di-oleate” conformations (see Table 4.3). It is not possible at this time to distinguish the assignments of the individual precipitated salt forms. The precipitate is associated via the HC tails of organic species directly bonded to the mineral surface. Singlet bands at 1580 and 1518 cm^{-1} can be formed if monodentate or chelating bidentate binds directly with the surface of the mineral. Furthermore, it is assumed that the band at $c\ 1550\text{ cm}^{-1}$ represents adsorbed oleate at close to monolayer coverage²³.

Table 4.3 below shows the interpretations of the mineral-sorbed oleate / oleic acid bands determined from a review of the current literature. These assignments have been used to explain the work presented herein.

Table 4.3 Proposed assignments and some adsorption mechanisms of carboxylic acid on mineral surfaces.

Frequency (cm ⁻¹) / Comments	Assignment / Comments
3007	-CH= antisymmetric stretch
3959	vas (-CH ₃)
3922	vas (-CH ₂ -)
2880	vs (-CH ₃)
2852	vs (-CH ₂ -)
1738 ν(C=O) Carbonyl stretch of oleic acid monomer hydrogen bonded surface	
1700-1715 ν(C=O) Carbonyl stretch of carboxylic (oleic) cyclic acid dimer in precipitate or sideways dimer bonded directly to	

partially deprotonated surface		
1580 singlet monodentate bound directly to the surface or		
1536 singlet chelating bidentate bound directly to the surface		
c1580/1536 doublet precipitated oleate interacting with the surface via HC tail associations.	 <p data-bbox="693 1372 883 1415">"mono-oleate"</p>	 <p data-bbox="1015 1500 1156 1542">"di-oleate"</p>
1655	Water band associated with kaolin surface. Also $\nu(\text{C}=\text{C})$ (low intensity).	
1670-1620	Water associated with kaolin surface (broad bands).	

1550-1560 surface sorbed $\nu_{as}(\text{COO}^-)$ carboxylate anion (adsorbed up to monolayer coverage) in bridged bidentate conformation.	
1468-47	$\delta(\text{CH}_2)$ scissoring.
1440	vs $(-\text{COO}^-)$

4.1.4 The adsorption of other industrially significant organics onto kaolin.

The adsorption of many other significant compounds onto kaolin have been studied, for example, small carboxylic acids²⁴ (on silica), short chain alcohols²⁵, surfactants^{26,27}, polyacrylamides⁴, polyacrylic acid and SDS^{28,29,30}. Kretzschmar *et al*¹³, investigated the effect of the addition of humic acid to a pH adjusted sodium exchanged suspension. The addition was found to decrease the coagulation rate at pH 6 and 4. Under acidic conditions (i.e. pH below the PZC of the edges of the mineral), adsorption occurred by a number of mechanisms to the edges of kaolin, and caused a reversal in edge charge from positive to negative. Therefore, E-F coagulation was prevented (as is the case at pH above the edge PZC). Therefore, humic acid adsorption was said to increase the colloidal stability because of the edge charge reversal. It was thought that interactions between polymer chains did not influence the adsorption of this acid at pH 4 or pH 6, and coagulation was found to be due to electrostatic forces only. However, at higher ionic strength, polymer chains may have been influential in colloidal stability. Humic acid was found to adsorb more strongly under acidic conditions. Oxalate / oxalic acid was found by Ward & Brady to adsorb primarily at Al-exposed edge sites at near or less than neutral pH¹⁵. The increase in adsorption oxalate / oxalic acid at lower pH are contrary to the decrease in adsorption of oleate / oleic acid at low pH in the work by Ince *et al*²¹.

4.2 Experimental.

4.2.1 Method development.

Previous work by the author involving *cis* oleic acid adsorption from pH adjusted solution at a concentration of 5×10^{-4} M was carried out. Although simple in concept, the study was fraught with stumbling blocks which had to be overcome before reliable data were obtained. In this work there were many variables-some easily controlled by the experimentalist, such as contact time and others less easily controlled (and monitored) such as particle agglomeration. During the evolution of the experimental procedures, these difficulties were largely overcome and some of the problems and their solutions follow:

The relatively high concentration of oleic acid was initially selected since kaolin has a limited surface area available for organic interactions (when compared with other minerals). However, oleic acid is not readily soluble at all pHs and it was suggested that 5×10^{-4} M is the maximum concentration of the acid which can be dissolved before micelle formation begins¹⁷ (i.e. just below the critical micelle formation (CMC) value of 7×10^{-4}). Despite the reported solubility of oleic acid in water, dissolution at pH 3 and 9 was difficult, and often incomplete. A number of methods were attempted to completely dissolve the acid, including heating to 60 °C for 2 hours, shaking, sonication and the addition of iso propanol as a solvent. However, the dissolution remained incomplete. Adsorption of oleate species to the kaolin surface was apparent after inspection by DRIFTS, but repeat experiments showed some discrepancies regarding relative peak intensities (although peak position, and thus spectral interpretation, remained constant throughout).

It was postulated that the conformation of the carbon chain in the *cis* form may be causing a steric hindrance effect and thus either preventing the oleate from dissolving fully and/or causing uncontrollable alterations in the mechanism and sequence of attachment to the kaolin. For these reasons, the experiment was repeated using the straight chain *trans* form (98% pure elaidic acid from Lancaster Synthesis). However, this exacerbated the dissolution problem. Not only was the *trans* form solid at room

temperature, (unlike the liquid *cis* form) but it was practically insoluble at all pHs (including pH 12).

The difficulties associated with the initial oleic acid work led to a modified experimental method, the results of which are presented herein. The oleic acid concentration was lowered to 1×10^{-4} M in order to further minimise the solubility problem.

It was also postulated that the treatment of the kaolin at low or high pH could dissolve some of the kaolin lattice, thus releasing extraneous ions into solution which may interfere with the adsorption process. In particular, aluminium is likely to be released into solution, and according to Kretzschmar *et al*¹³, this can then reprecipitate onto the edge surface and increase the Al : Si ratio. This leads to an increase in the PZC and can alter the adsorption characteristics of the clay. However, it is thought that a dramatic change in PZC is only affected at concentrations of 1M or more. For this reason, acid and base washing used in the work presented herein was carried out at low concentration.

To minimise this effect, the kaolin samples were initially washed in water at the reaction pH, thus removing many of the superfluous ionic contaminants (ions which could potentially be dissolved from the kaolin structure). The possible dissolution of the kaolin mineral lattice is an effect which has historically not been well documented. However, it was discussed by Siracusa & Somasundaran³¹ in kaolin adsorption studies, and has often been discussed in studies of other minerals such as fluorite and apatite. It was determined that above pH 4.7, dissolution of kaolin can occur and lead to the formation of a new gibbsite phase. This strongly influenced the surface properties of kaolin, and it was postulated that the high concentrations of Al^{3+} above pH 4.7 could be important in a kaolinite system contacted with anionic surfactants due to the possibilities for complexation, precipitation or adsorption activation. The electrolyte concentration used for dissolution was much higher than the concentrations of acid/base used in the work herein. However, the possibility of dissolution (and the related effects) is worthy of note. It is likely that in a number of studies, this effect was not considered at all in the data analysis. This may be one reason for the huge divergence in the spectral interpretations between workers.

In order to obtain a less ambiguous representation of the IR spectra, spectral subtraction was carried out. This involved subtracting a blank spectrum (i.e. the spectrum of the pH adjusted water washed kaolin) from that of the oleate exposed sample spectrum. Subtraction was carried out using the Grams software described in Chapter 1, and was deemed to be complete when the intensity from the kaolin combination bands at 1935, 1835 and 1735 cm^{-1} was as close to baseline as possible.

4.2.2 Materials.

In all cases, the kaolin used was the unmilled, chemical free, Cornish kaolin. The *cis* oleic acid was 99 % pure, obtained from Sigma Aldrich. The deionised water used throughout had an initial conductivity $< 10 \mu\text{S}$. Analytical grade NaOH or HCl were used to adjust the pH of the water/solutions. KBr used for sample dilution to 5% (99 % pure and purchased from Sigma Aldrich) was heated to 500 °C for at least 2 hours to burn off any organic contaminants. It was cooled and stored prior to use in a dry environment to minimise the uptake of atmospheric water or contaminants.

4.2.3 Sample preparation.

Oleic acid solutions were made up using deionised water adjusted to pH 3, 9 or 12. Oleic acid at pH 12 dissolved immediately and required no further treatment. At pH 9 and 3 difficulties in dissolution were encountered. To obtain maximum dissolution, the solutions were shaken vigorously for 5 minutes, followed by 1 hour of sonication, 2 hours at approximately 60 °C, and finally vigorous shaking for a further 10 minutes. This procedure resulted in almost complete solubilisation of the oleic acid at pH 9, but still limited solubility at pH 3. Solutions were again shaken vigorously before adding to the kaolin suspensions.

50, 100 and 150 mg of kaolin were weighed and mixed very lightly for 40 seconds by hand to ensure a powdered appearance. The kaolins were mixed with 500 ml of pH adjusted (3, 9 or 12) deionised water and sonicated for 1 hour to ensure adequate dispersion and washing. Samples were centrifuged for 1 hour at 17,000 rpm and the

sample pellet recovered and allowed to dry under ambient conditions overnight. These samples are referred to as “water washed”.

The washing process was repeated using fresh samples, but the recovered sample was then contacted with 1×10^{-4} M pH adjusted oleic acid solution.

After shaking at room temperature for 2 hours, the oleic acid treated kaolins were recovered by centrifuging under the conditions described above. The samples were halved, with one half being dried at room temperature over night. The samples dried at this point are referred to as “oleic acid treated” kaolins.

The other half of the samples were rinsed by shaking in pH adjusted water for 1½ hours at room temperature. The rinsed samples were then centrifuged (again under the same conditions), the pellets recovered and the sample allowed to dry over night at room temperature and are referred to hereafter as “acid treated, rinsed” samples.

It should be noted that in order to ensure that the species in solution at a given pH were not altered, the mass of kaolin sample added to the solution was varied, rather than the oleic acid concentrations, which were kept constant at 5×10^{-4} M. A range of “available” oleic acid concentrations was achieved by adding kaolin samples of mass 50, 100 or 150 mg to the solution. This method of sample preparation was based on an idea by Cenens & Schoonheydt³² which was used successfully by Breen & Rock³³ in a study of competitive adsorption of dyes onto montmorillonite. DRIFTS spectra were obtained using the parameters given in Chapter 1. All samples were mixed lightly with KBr for 40 seconds to ensure adequate dispersion just prior to scanning. Data manipulations were carried out using the Grams software package (see Chapter 1).

4.2.4 Concentration of oleic acid theoretically available for adsorption.

Assuming that all the oleic acid has dissolved,

Total concentration of oleic acid (mol wt = 280) available in 100 ml of water

$$= \quad 100 \text{ ml} / 1000 \text{ ml} \times 1 \times 10^{-4} \text{ M} \times 280 = \quad 2.8 \text{ mg}$$

Therefore, for 50 mg kaolin samples, oleic acid available per gram of kaolin

$$= \quad 2.8 \text{ mg} / 50 \text{ mg} = \quad 56 \text{ mg g}^{-1} \text{ or}$$

$$= 56 \text{ mg} / 280 = 0.20 \text{ mmol g}^{-1}$$

for 100 mg kaolin samples, oleic acid available per gram of kaolin

$$= 2.8 \text{ mg} / 100 \text{ mg} = 28 \text{ mg g}^{-1} \text{ or}$$

$$= 28 \text{ mg} / 280 = 0.10 \text{ mmol g}^{-1}$$

for 150 mg kaolin samples, oleic acid available per gram of kaolin

$$= 2.8 \text{ mg} / 150 \text{ mg} = 18 \text{ mg g}^{-1} \text{ or}$$

$$= 18 \text{ mg} / 280 = 0.06 \text{ mmol g}^{-1}$$

Assuming that the surface area of kaolin is uniform at c $30 \text{ m}^2 \text{ g}^{-1}$, the total oleic acid available per m^2 of kaolin is:

for 50 mg kaolin samples

$$= 0.20 \text{ mmol g}^{-1} / 30 \text{ m}^2 \text{ g}^{-1} = 0.0067 \text{ mmol m}^{-2}$$

$$= 6.7 \mu\text{mol m}^{-2}$$

for 100 mg kaolin samples

$$= 0.10 \text{ mmol g}^{-1} / 30 \text{ m}^2 \text{ g}^{-1} = 0.003 \text{ mmol m}^{-2}$$

$$= 3.3 \mu\text{mol m}^{-2}$$

for 150 mg kaolin samples

$$= 0.06 \text{ mmol g}^{-1} / 30 \text{ m}^2 \text{ g}^{-1} = 0.002 \text{ mmol m}^{-2}$$

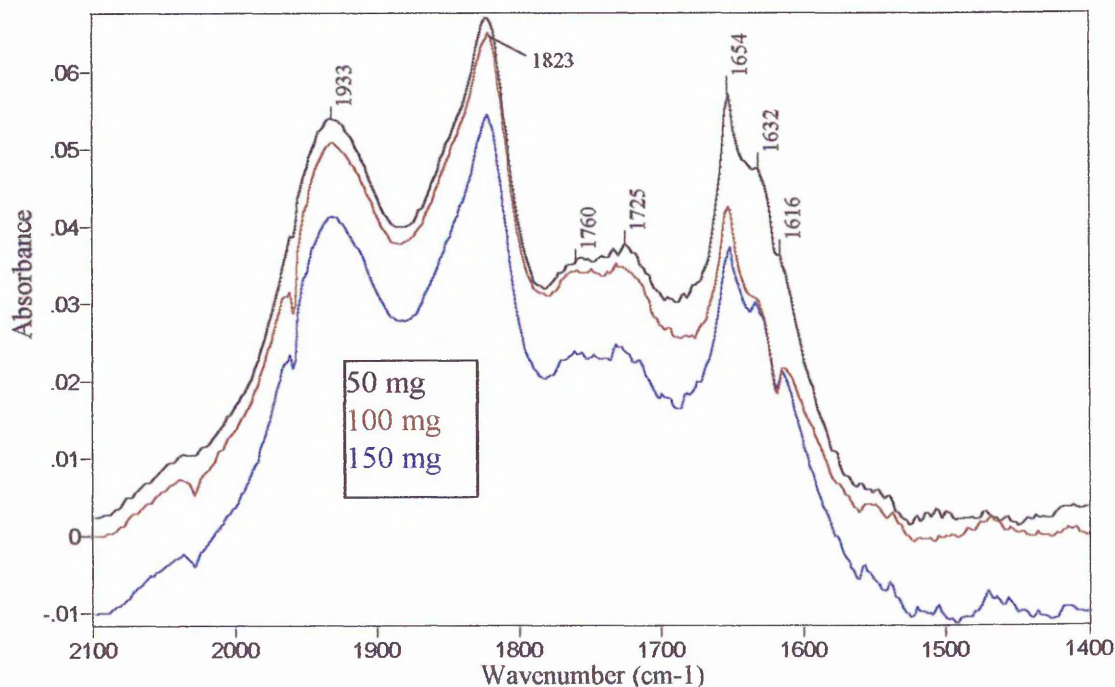
$$= 2.0 \mu\text{mol m}^{-2}$$

4.3 Results of infrared studies.

4.3.1 pH 3.

4.3.1.1 Water washed kaolin (pH 3).

Figure 4.8 Water washed kaolin (pH 3).



A band, representing the bending mode, $\delta(\text{OH})$, of water, at 1650 cm^{-1} with a shoulder at around 1633 cm^{-1} was present in all samples. There may also be a shoulder at $c 1620 \text{ cm}^{-1}$. The water bending mode was shaped differently in kaolin which has not been exposed to additional water (after the initial extraction process). The increase in intensity at lower frequency is likely to be due to the adsorption of additional surface water after water washing. The assignment of the water bending modes have been discussed in some detail in Chapters 2 and 3. In the work presented herein, the 1650 cm^{-1} band was only seen as a sharp peak in untreated kaolin after long term exposure to atmospheric water (under ambient laboratory conditions) for a number of months. The increase in the intensity in the $c 1650 - 1610 \text{ cm}^{-1}$ region indicates that additional adsorbed water is moderately or weakly hydrogen bonded. There does not appear to be an increase in the 1670 cm^{-1} region, which corresponds to strongly hydrogen bonded water.

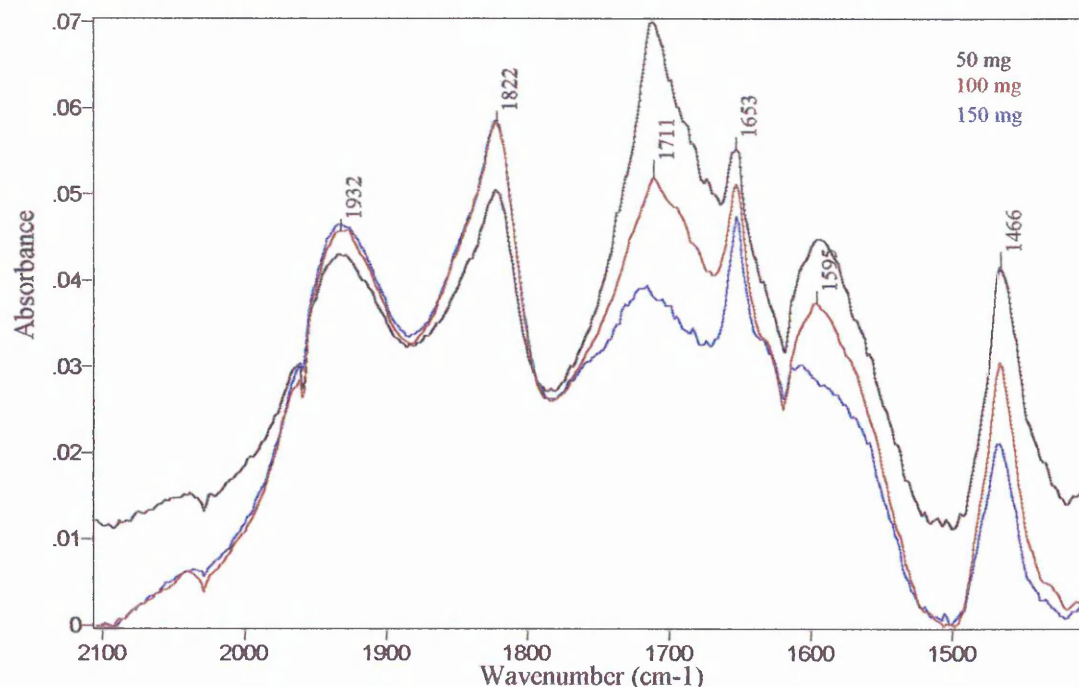
In the present oleate study, drying conditions were very mild (overnight under ambient conditions). The additional water present on the surface may be due to an incomplete drying of the sample, or due to the dry sample reabsorbing atmospheric water. It may also be a result of the expansion of the halloysite impurity. It is not possible to determine which hypothesis is correct.

Interestingly, the intensities of these bands seemed to alter after the oleic acid and subsequent washing treatments. There appeared to be a shift in the unresolved 1630-1650 cm^{-1} band, with the water tending towards the 1650 cm^{-1} position after both treatment stages. This may represent the replacement of more weakly hydrogen bonded water by oleic acid / oleate and / or the adsorption of the organic increasing the hydrophobicity of the sample.

4.3.1.2 Oleic acid treated kaolin (pH 3).

There were problems in the initial dissolution of the 1×10^{-4} M oleic acid, and as with the pH 9 data, the precise concentration of oleic acid in the stock solution is not known. However, as all the oleic acid treatments were made using the same stock, it is feasible to assume that all the samples were exposed to equal concentrations of oleate species.

Figure 4.9 Oleic acid treated kaolin (pH 3).



At this pH, it is expected that the organic and the surfaces (and edges) of the mineral will be protonated. It may therefore be predicted that the oleic acid treated kaolin spectrum would show an acid band at c 1711 cm^{-1} , corresponding to $\nu(\text{C}=\text{O})$ carbonyl stretch of adsorbed oleic acid dimer. The band may also represent the hydrogen bonded acid monomer, but the relatively low frequency suggests that it is probably due to dimer. After the initial acid treatment there was indeed a very intense and sharp acid dimer band at 1711 cm^{-1} superimposed upon the kaolin combination band at c 1730 cm^{-1} . The intensity of the acid band increased as the available concentration (per unit mass of kaolin) of oleate / oleic acid increased. The water band at 1650 cm^{-1} may have increased slightly, but this could be due to atmospheric differences during drying. There is also a band at 1650 cm^{-1} representing the C=C stretching vibration, and it is possible that after acid treatment, a small proportion of the intensity here is due to this vibration.

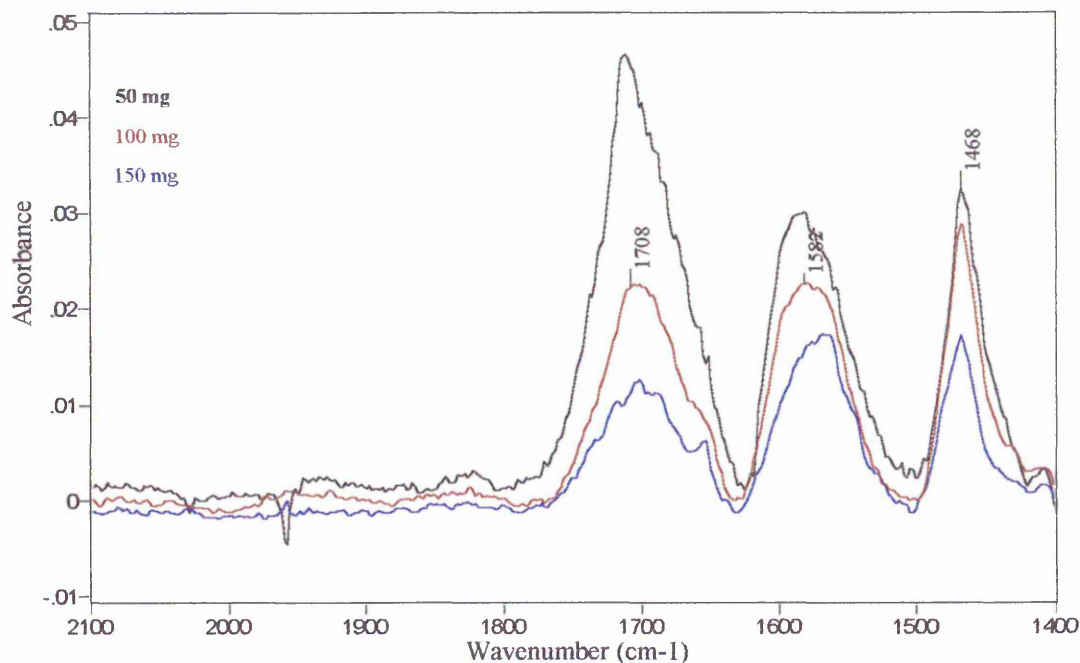
The 1466 cm^{-1} band, corresponding to (CH_2) scissoring also increased as the available concentration (per unit mass of kaolin) of oleate / oleic acid increased. Surprisingly, a broad band was observed which could correspond to the $\nu(\text{COO}^-)$ carboxylate anion antisymmetric stretching mode at c $1550\text{--}1600\text{ cm}^{-1}$. The intensity of this band decreased

in the order of 50>100>150 mg kaolin. It had poorly defined shape, and was not a doublet. Doublet characteristics are thought to be observed when anionic oleate is precipitated onto the mineral surface. Since the anionic form must be at low concentration at this pH, it follows that doublet character is extremely unlikely to be observed. It is also possible that this band corresponds to H_3O^+ , however, this seems an unlikely assignment since it was not present in the water washed sample. According to Gong *et al*³⁴, who studied the adsorption of oleate to apatite, around 1% of oleate (emulsified) in water will exist as the singly charged monomeric carboxylate ion at pH<7, with most of the remaining 99% being liquid oleic acid. If the singly charged monomeric carboxylate ion is strongly bound to the surface, it could account for a significant proportion of the adsorbed species.

Thistlethwaite *et al*¹⁷, also saw similar results in their study of oleate adsorption to zirconia. It was concluded that the persistence of the oleate anion band (in their work at 1556 cm^{-1}) at pH 3 was due to the stabilisation of the anion via electrostatic interaction by the positively charged zirconia surface. The kaolin surface may effectively be stripping a proton from the carboxylic acid.

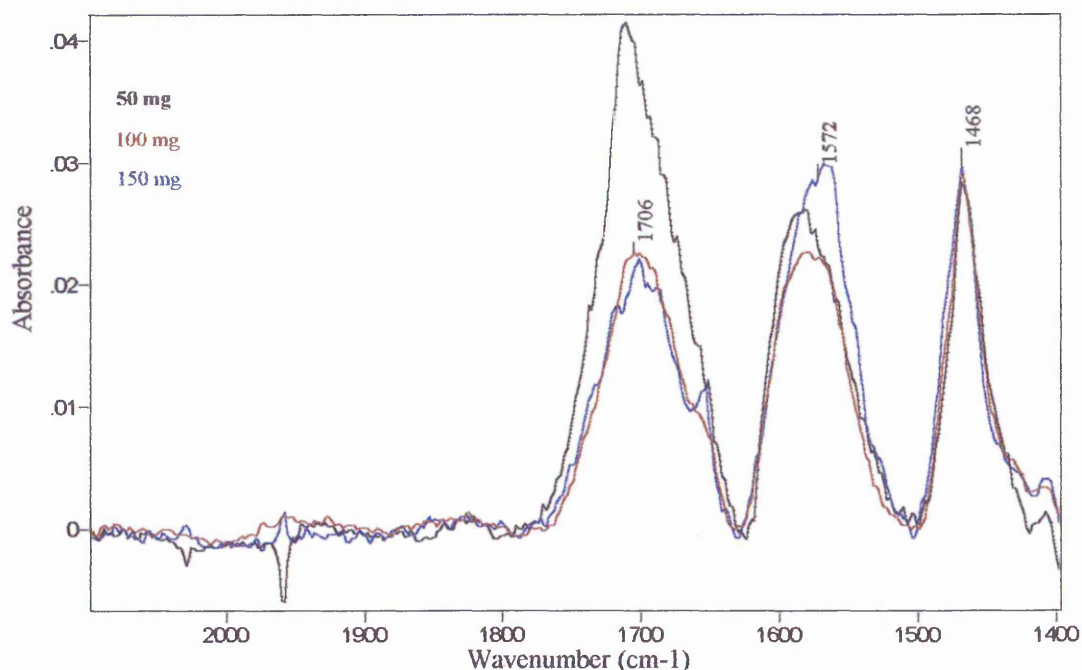
In the pH 3 water washed and oleic acid treated kaolin samples, there was a sharp decrease in intensity at c 1620 cm^{-1} . The cause of this feature is not known at this time. It was postulated that the decrease in intensity may be altering the shape and/or position of the band observed. Since the assignment of the broad feature centring at 1595 cm^{-1} was so ambiguous, spectral subtraction was used to endeavour to eliminate the spectral aberration, thus elucidating the true shape and frequency of the band. The results of the spectral subtraction are shown below.

Figure 4.10 Subtracted spectra of oleic acid treated kaolin (pH 3).



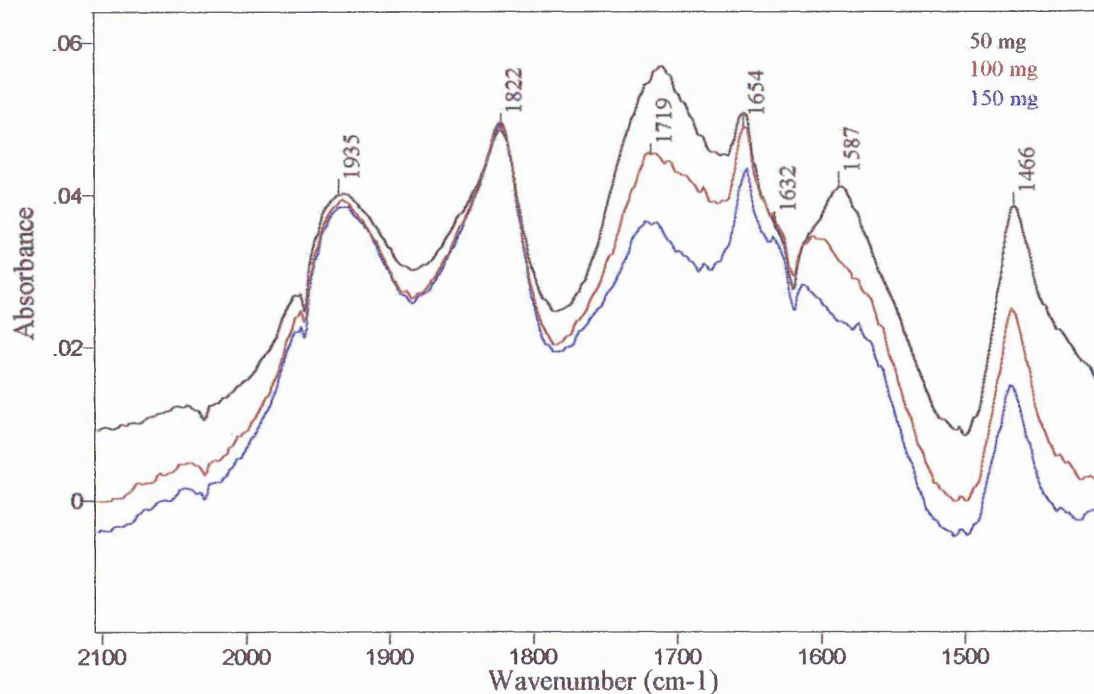
The subtraction results give clear evidence of strong bands at 1708, 1585 and 1468 cm^{-1} . It appears therefore, that the spectral aberration resulted in an apparent shift of the organic band formerly at 1595 cm^{-1} , and now observed at 1582 cm^{-1} . This observation suggests that oleate is binding directly to the surface via monodentate binding. The band centring at 1708 cm^{-1} suggests acid dimer interactions. It is not possible to distinguish which type of dimer is present. If the sideways dimer is present, it may bind directly to the surface. If the cyclic dimer is present, it may bind only via HC chain interactions with chemisorbed species. In the 100 and 150 mg samples, the 1708 cm^{-1} band is smaller than the other spectral features. However, in the 50 mg sample, the 1708 cm^{-1} band is very intense compared with the other spectral features. This may indicate that initially at lower available oleate/oleic acid concentration, the binding is via monodentate adsorption, and thereafter the acid is becoming associated with the mineral surface via HC chain interactions. Subtracted spectra were normalised to the 1468 cm^{-1} , (which is assumed to represent total organic present), and are shown in Figure 4.11 below.

Figure 4.11 Subtracted spectra of oleic acid treated kaolin (pH 3). Normalised to the 1468 cm^{-1} band.



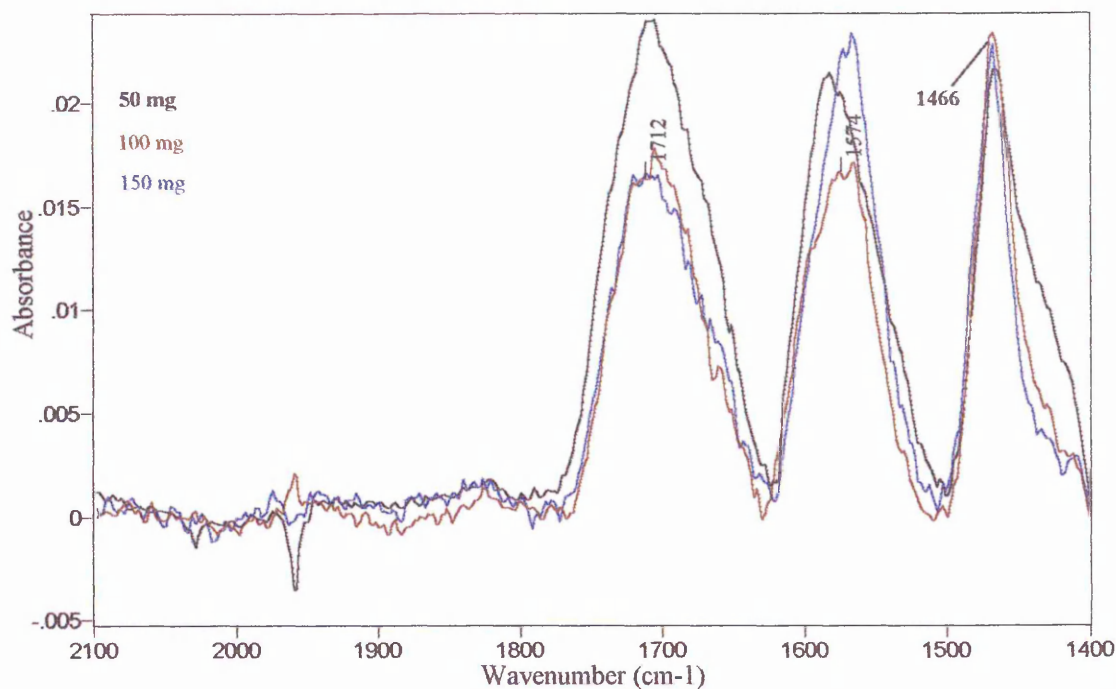
It can be observed that the 50 mg sample has a higher concentration of acid than either of the other two samples. The intensity of the 1572 and 1706 cm^{-1} bands are approximately equal in the 100 mg sample, whereas in the 150 mg sample the intensity of the 1572 cm^{-1} monodentate band is of greater intensity than the 1706 cm^{-1} acid band. This seems to suggest that as the concentration of available organic increases per unit mass of kaolin, so do acid interactions. Initially (i.e. at low available organic concentration), it seems that oleate is sorbed preferentially on to the surface in the monodentate form. As available amount of oleic acid increases, there becomes a greater proportion of acid, until at high concentration of available organic, acid interactions predominate. From these data whether the acid is precipitated or sorbed cannot be determined. However, rinsing the oleate-exposed samples proved to yield interesting results discussed below.

Figure 4.12 Oleic acid treated, rinsed kaolin (pH 3).



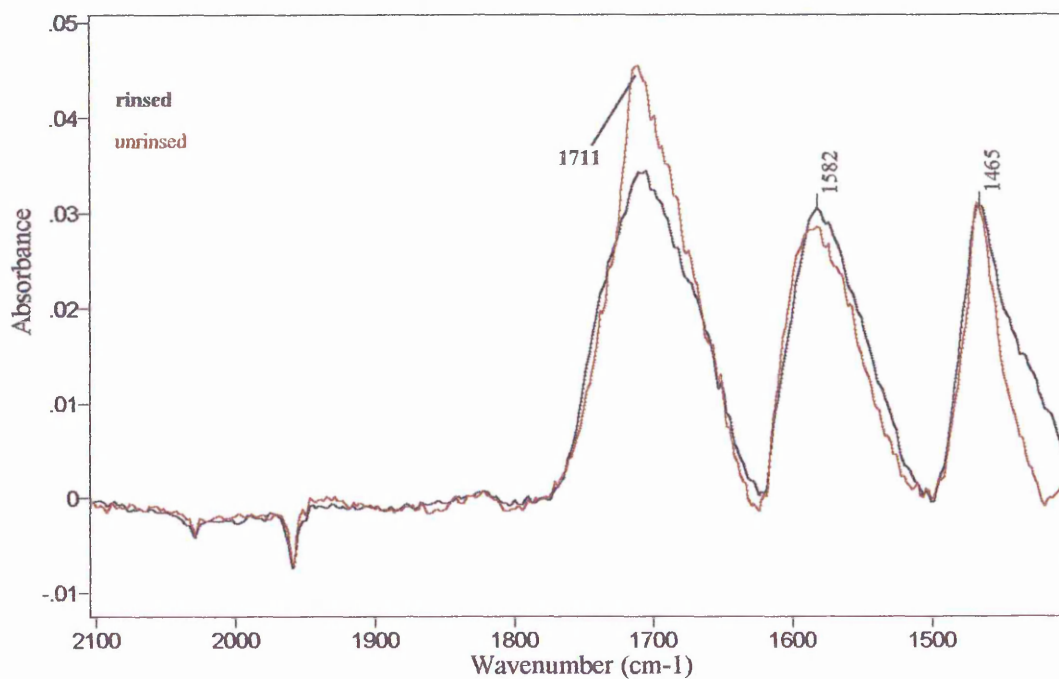
After rinsing, the intensities of all the oleate / oleic acid bands decreased (particularly the oleic acid band at 1711 cm^{-1}). The reduction in the intensity of the bands after such mild rinsing suggests that the species were not strongly bound to the surface. However, the presence of a singlet at 1587 cm^{-1} confirms that the adsorption of the monodentate species persists after washing. There remained increased acid dimer intensity at 1711 cm^{-1} , which also provides evidence for strongly adsorbed acid.

Figure 4.13 Subtracted spectra of oleic acid treated, rinsed kaolin (pH 3). Normalised to the 1468 cm^{-1} band.



The 50 mg and 100 mg samples showed decreases in the total amount of sorbed species, although the relative intensities of the bands remained fairly similar before and after rinsing. However, the 50 mg sample lost a considerable amount of intensity from the 1712 cm^{-1} acid band after rinsing (see Figure 4.14). This indicates that some of the acid species are more weakly bound than the monodentate species. It is believed that the observed decrease in acid intensity corresponds to the removal of loosely bound precipitated acid which was formerly interacting via HC chain associations. The acid remaining after the rinsing process is likely to be due to hydrogen bonded monomer or the sideways dimer bonded directly to the mineral surface. The increase in the width of the 1466 cm^{-1} band after rinsing is not understood at this time (although it may represent the appearance of the $\nu_{\text{as}}(\text{COO}^-)$ band at 1440 cm^{-1} , with a concurrent decrease in the amount of sorbed acid species).

Figure 4.14 Comparison of 50 mg oleate treated samples (rinsed and unrinsed) normalised to the 1468 cm^{-1} band.

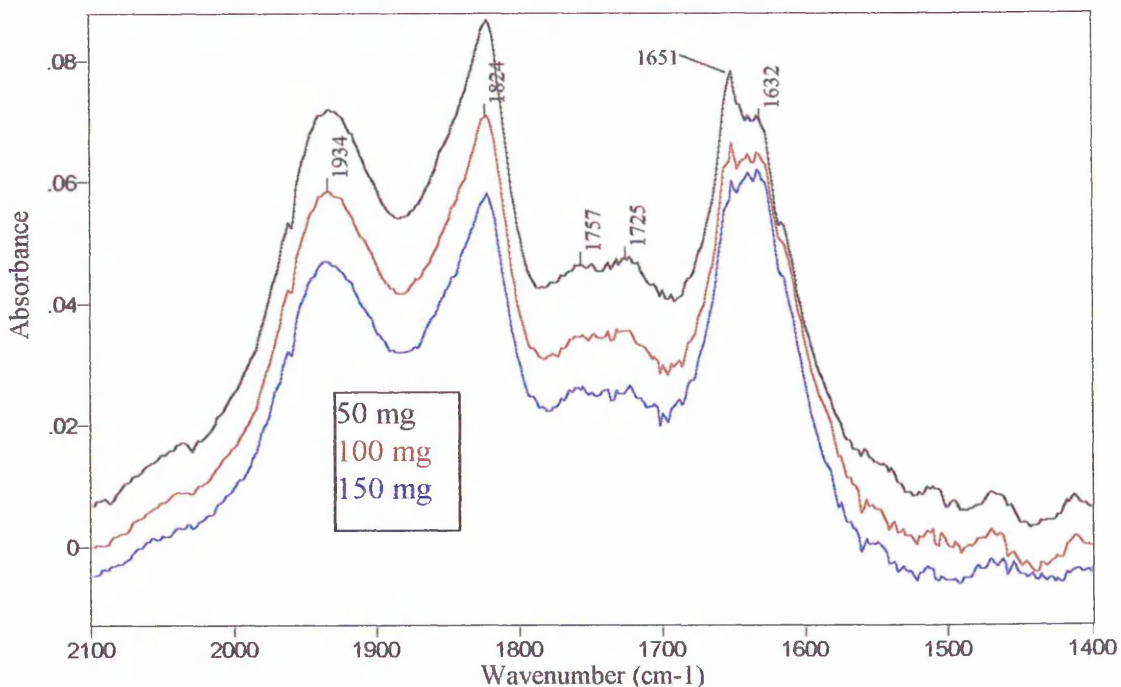


4.3.2 pH 9.

There were problems associated with the dissolution of oleate at lower pHs- pH 9 being no exception, and the level of available oleate in solution was almost certainly reduced when compared with the concentration available in the pH 12 work. However, all the pH 9 results presented here used the same initial concentration of oleate, and so are directly comparable with each other, if not with the pH 12 or 3 data.

4.3.2.1 Water washed kaolin (pH 9).

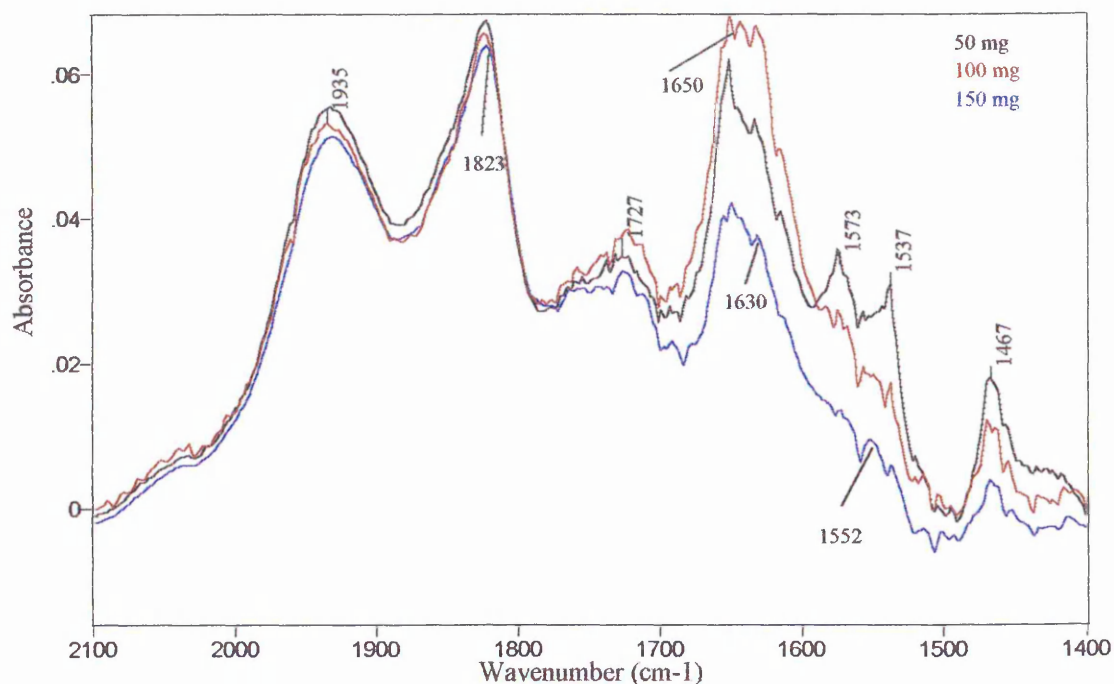
Figure 4.15 Water washed kaolin (pH 9).



pH adjusted water washing resulted in the formation of sharper bands at c1650 and 1630 cm^{-1} with the evidence of another shoulder at c1620 cm^{-1} (compared with unmilled, unexposed kaolin). Otherwise, the spectra were very similar to those of the unmilled, unexposed kaolin.

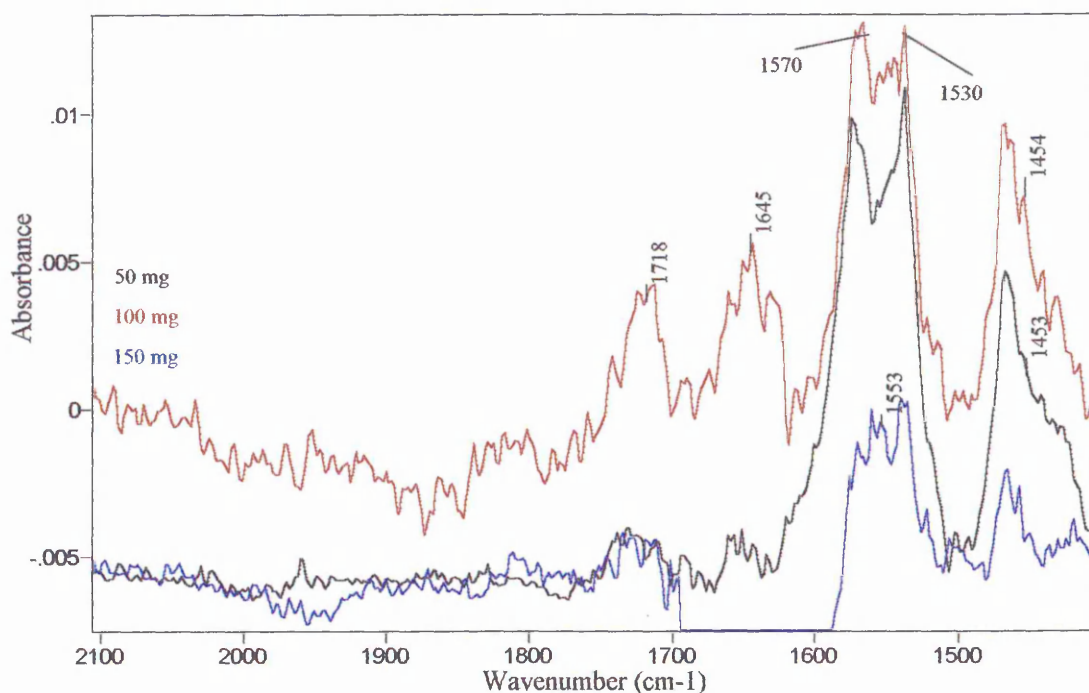
4.3.2.2 Oleic acid treated kaolin (pH 9).

Figure 4.16 Oleic acid treated kaolin (pH 9).



At low kaolin concentration (i.e. high available oleate / oleic acid concentration) there is an obvious doublet at 1573 and 1537 cm^{-1} which corresponds to surface precipitated anionic oleate. The intensity of this doublet was less than that in the pH 12 acid treated sample (see Figure 4.21) (as expected since a reduced amount of oleate was dissolved at pH 9). The doublet intensity decreased as the oleate / oleic acid concentration per unit mass of kaolin decreased. In the 150 mg sample, there was no evidence of the doublet, but there may have been a small contribution from a singlet at 1550 cm^{-1} , corresponding to surface sorbed oleate anion. There was a very slight increase in the broad band centring at c 1720-30 cm^{-1} , which may be indicative of adsorption of the acid monomer present at lower pH. However, since acid at this pH is expected to be at low concentration, it is postulated that the increase in this region was more likely to be due to the interactions of the acid monomer adsorbed via hydrocarbon chain interactions³⁴ with already adsorbed species, or that the monomer was formed in solution and precipitated directly onto the surface during the drying procedure. The 1460 cm^{-1} band was much reduced in intensity compared with pH 3 spectra. A clearer picture is gained from the subtracted spectra.

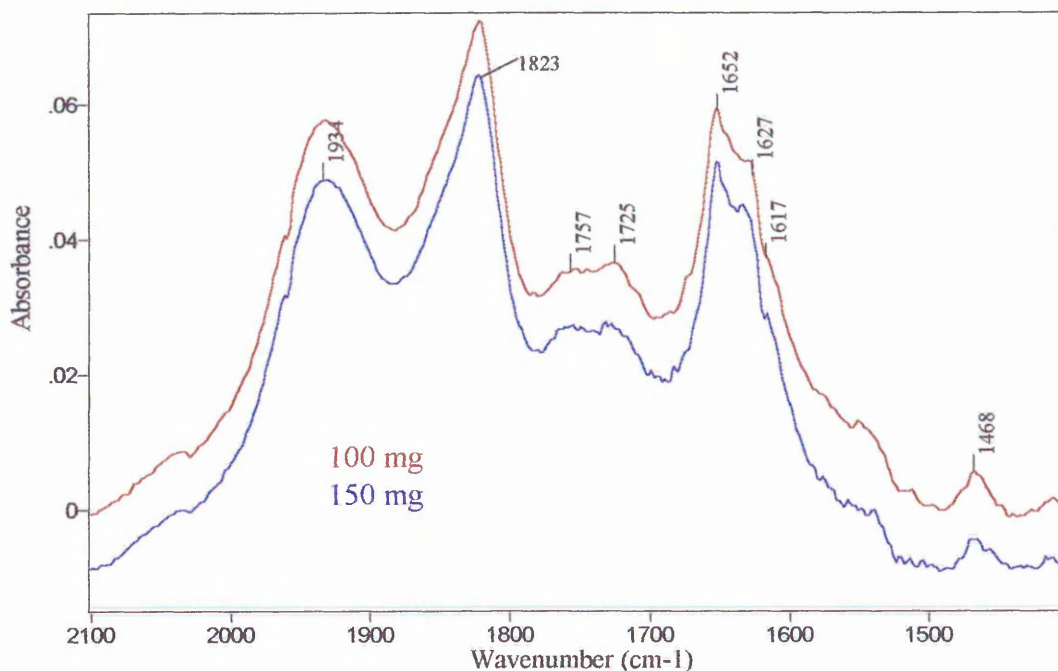
Figure 4.17 Subtracted spectra of oleic acid treated kaolin (pH 9).



The positive band at 1645 cm^{-1} in the 100 mg sample and the negative band in the 150 mg sample at the same frequency represents differences in surface sorbed water. Clearly in the 50 and 100 mg samples, there is a significant contribution from the $1570/1530\text{ cm}^{-1}$ doublet, corresponding to precipitated oleate salts. The 150 mg sample shows evidence of a band centring at 1553 cm^{-1} , corresponding to surface sorbed carboxylate in the bridged bidentate conformation. All samples show some evidence of a band at 1718 cm^{-1} , corresponding to the acid monomer. This band in the 100 mg sample is of the greatest intensity. At this time, it is not known why it should be highest intensity in this sample, rather than in the 50 mg sample.

It is believed that at pH 9, all samples have the carboxylate anion adsorbed to the surface in the bridged bidentate conformation. At low loading (high kaolin concentration) the corresponding band at 1553 cm^{-1} is observed. In both the 100 and 150 mg samples, however, this band is overlaid with the doublet bands at 1570 and 1530 cm^{-1} corresponding to oleate salt precipitation. A small amount of acid is associated with the surface, with a band at 1718 cm^{-1} , corresponding to weakly hydrogen bonded monomer (most likely) or dimer. The precipitate is very loosely attached via HC chain interactions with the surface sorbed salt and/or acid.

Figure 4.18 Rinsed kaolin-oleic acid pH 9



The 50 mg sample became contaminated and is not included here.

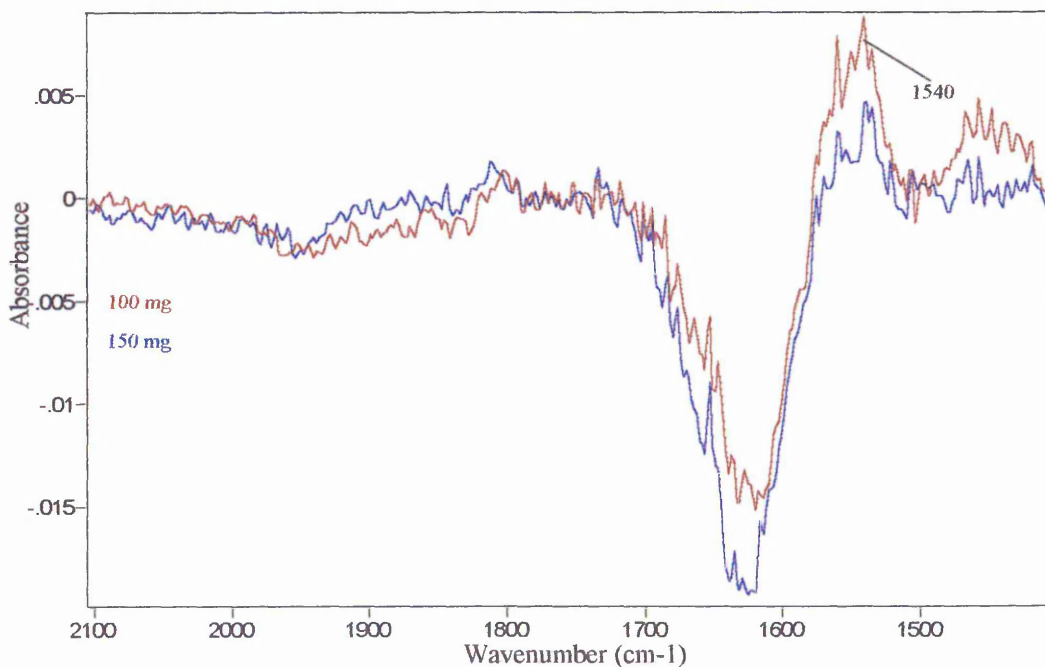
At pH 9, the oleic acid treated kaolin spectra showed marked differences before and after rinsing. It appears that at this pH, the oleic acid / oleate species were initially either very loosely bound, or more likely that they were merely precipitated on the surface of the mineral (supported by the presence of the doublet at 1573 and 1537 cm^{-1} in the sample prior to rinsing). Virtually all of the organic is removed after rinsing. A very small amount is still present, as can be seen by the CH_2 scissoring mode at 1468 cm^{-1} .

The pH 9 oleate exposed and rinsed kaolin samples had slight evidence of a band at 1560 cm^{-1} , since it was not being swamped by very intense doublet bands. The presence of this band supports the belief that it represents surface sorbed carboxylate anion bound in the bridged bidentate conformation.

After rinsing, the doublet disappeared in all cases, supporting the belief that the doublet is formed by salt precipitation. The intensity of the 1467 cm^{-1} $\delta(\text{CH}_2)$ band reduced considerably, indicating that most of the organic was desorbed. The subtracted spectra illustrate the removal of precipitated species after rinsing. Both the 100 and 150 mg

samples now show no evidence of the 1570/1450 cm^{-1} doublet. The more strongly bonded 1550 cm^{-1} bridged bidentate band remains along with a small C-H scissoring band.

Figure 4.19 Subtracted spectra oleic acid treated, rinsed kaolin (pH 9).



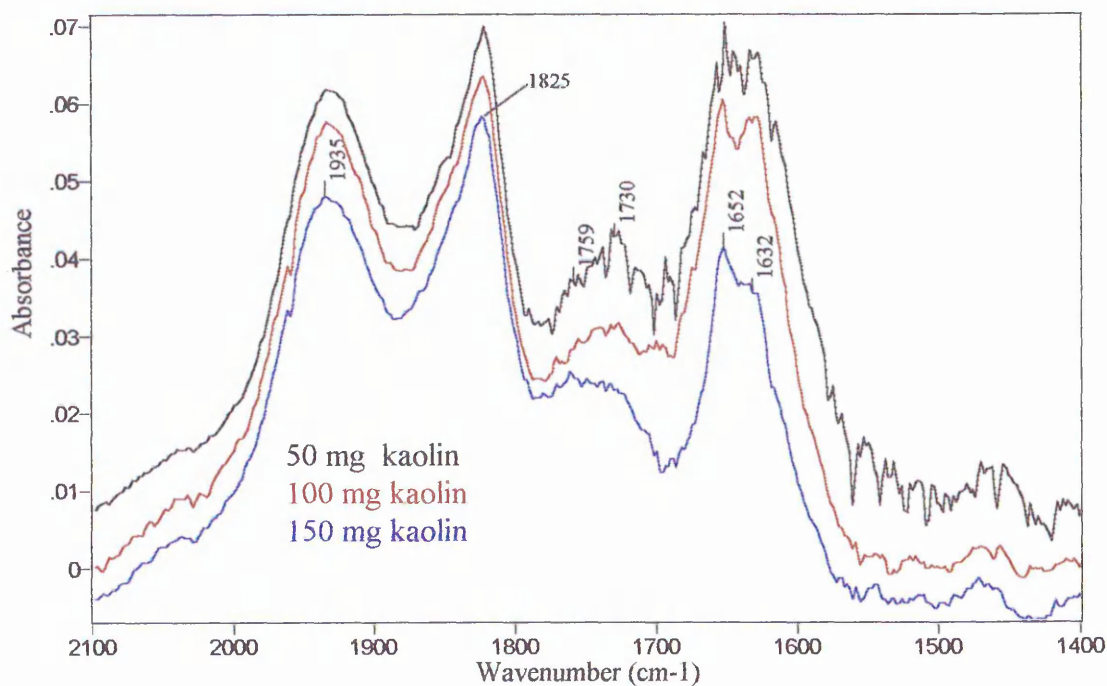
Again, the negative bands at 1645 cm^{-1} represent differences in surface sorbed water.

It is proposed that the reason for reduced and weaker adsorption at pH 9 is due to a combination of the limited solubility of oleic acid in solution, the repulsive forces between the negatively charged surface and organic, and the relatively low concentration (compared with pH 12) of sodium ions in solution, which may form a bridge between the adsorbate and adsorbent.

4.3.3 pH 12.

4.3.3.1 Water washed kaolin (pH 12).

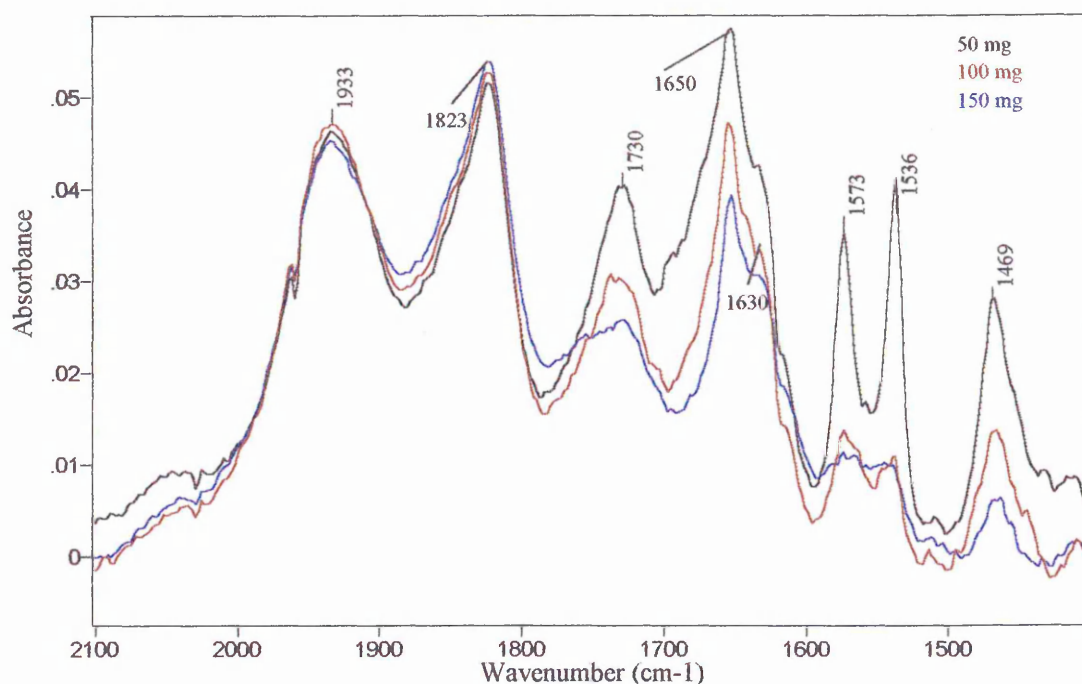
Figure 4.20 Water washed kaolin (pH 12)



Washing at pH 12 greatly increased the intensity of the water bending modes at c 1650 and 1630 cm^{-1} . There does not seem to be a common pattern to the intensity change of these bands at any pH, and probably, the intensity depends primarily upon drying conditions. In this set of experiments, drying conditions (other than time) were not controlled. The relative humidity and ambient temperature can affect the drying of the sample, and thus the intensity of the sorbed water bands considerably.

4.3.3.2 Oleic acid treated kaolin (pH 12).

Figure 4.21 Oleic acid treated kaolin (pH 12)

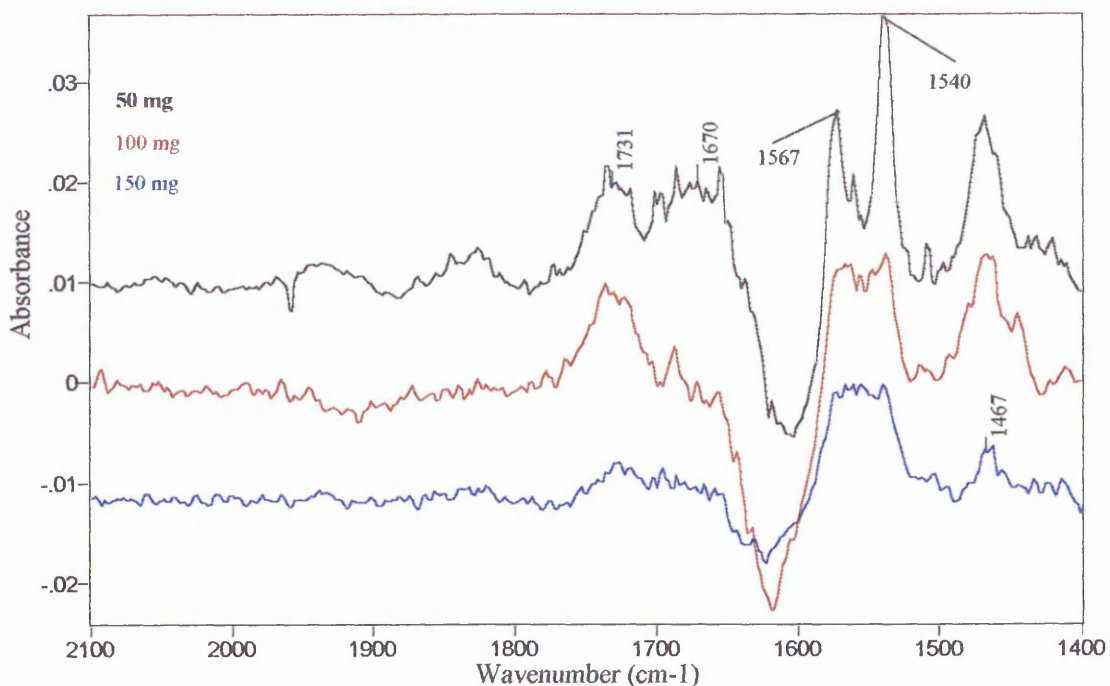


After washing there was very little change in the spectra and therefore, they are not shown here.

As the mass of kaolin increased (i.e. oleate / oleate acid concentration per unit mass of kaolin decreased), the intensities of all the organic bands decreased. Of particular interest is the doublet at 1573 and 1536 cm^{-1} , which becomes greatly reduced in intensity and less well defined as available concentration of oleate / oleate acid per unit mass of kaolin decreased. This supports the theory that the doublet represents precipitate, whilst a singlet at c 1550 cm^{-1} represents surface sorbed oleate.

At pH 12, most of the species present in the kaolin-organic system are expected to exist in the deprotonated form, and therefore, acid adsorption would not be expected at such a high pH. However, clear evidence of acid adsorption was observed, with an increase in the intensity of the band at c 1730 cm^{-1} , characteristic of monomeric acid. It is likely that this acid has become trapped within a micelle which has become adsorbed to, or precipitated on the surface.

Figure 4.22 Subtracted spectra Oleic acid treated kaolin (pH 12).



The band at 1670 cm^{-1} represents differences in the surface sorbed water of the treated and untreated samples. The spectra have been offset and rescaled for clarity. The intensity of the bands at 1731 , 1567 , 1540 and 1467 cm^{-1} increases in the order $150 < 100 < 50\text{ mg}$. In the 50 mg spectrum there is clear evidence of an acid monomer band at 1731 cm^{-1} . There is a strong doublet at 1567 and 1540 cm^{-1} , and an intense 1466 cm^{-1} band. There may be a contribution from acid dimer at $c\ 1700\text{ cm}^{-1}$, but it is difficult to determine whether the intensity is coming from organic, or from incomplete subtraction of the kaolin spectrum. In the 100 mg sample, the intensity of the 1731 and 1677 cm^{-1} has decreased. The doublet has become less well resolved, probably indicating a reduction in the amount of surface precipitate as available organic per unit mass of kaolin has decreased. The doublet is no longer evident in the 150 mg sample, and there is a small amount of acid remaining. A broad band at $c\ 1550\text{ cm}^{-1}$ has become apparent, corresponding to bridged bidentate. Some precipitate may remain, but it is difficult to assess precisely. The band may have shoulders on either side, thus giving it the “square” shape. However, these features may be due to water vapour. It is the opinion of the author that it is likely that a small amount of precipitate does exist.

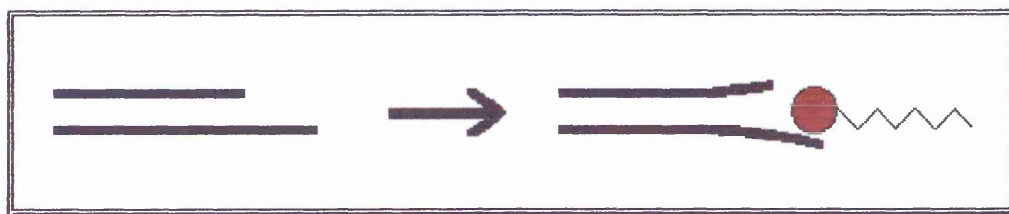
At pH 12, the reason that the doublet (i.e. precipitated oleate) does not decrease after washing is that there is a very strong and complex CH tail interaction system, attaching the precipitate to the surface of the mineral via already surface sorbed oleate / oleic acid species. This is different from the pH 9 system, where, although precipitate was formed before washing, it was easily removed. At pH 12, the kaolin particles are likely to be completely dispersed, but upon the addition of oleic acid, the particles will become flocculated (due to the alteration of surface charge imparted by the sorption of the organic and/or NaOH). Thus, it is likely that the organic has become involved in aggregate formation. A similar mechanism will occur at pH 9, but at this lower pH the oleic acid is less soluble, and therefore micelle formation will be reduced. Thus, the interactions between mineral and organic are weaker at pH 9 than at pH 12.

4.4 Conclusions.

It is believed that most of the adsorption of the organic species at all pHs occurred at exposed Al, AlO⁻, AlOH or AlOH²⁺ sites. It is very unlikely that intercalation of kaolin occurred in this system, but more reasonable is the suggestion that partial intercalation of the halloysite impurity occurred, whereby the oleic acid species became incorporated into the halloysite sheets only at the edges of the stacks as shown in Figure 4.23.

It is likely that the acid treatment dissolved some of the structural aluminium of the octahedral sheet of both halloysite and kaolin. It is possible that the breach induced in the structural integrity of the mineral resulted in the formation of an opening into which the oleic acid was more easily incorporated.

Figure 4.23 Schematic of the proposed partial intercalation mechanism of oleic acid into halloysite.



At pH 3, oleic acid was very insoluble. Most of the oleic acid in solution existed as RCOOH. Most of the surface species of kaolin existed as Al-OH. The characteristics of

the system favoured adsorption, but due to the low solubility of oleic acid, a reduced concentration was available in solution and adsorption was limited by that concentration. Organic bound directly to the mineral surface existed as monodentate and acid monomer or dimer. Acid was also present as a weakly associated precipitate which was removed after washing.

At pH 9, oleic acid was not readily soluble. Much of the oleic acid in solution existed as RCOO^- . Most of the surface species of kaolin existed as Al-O^- . Adsorption between these two species was not favourable. Adsorption was limited equally by reduced solubility and unfavourable electrostatic interactions. Adsorption was very low, and precipitated material was removed by gentle washing. Organic adsorption was limited, but primarily the adsorbed species was monodentate in character. There was evidence of precipitation of two distinct forms of oleate salt (probably Al or Na salt) and a small amount of acid monomer. All precipitate was removed after washing, but a small amount of surface bound material remained.

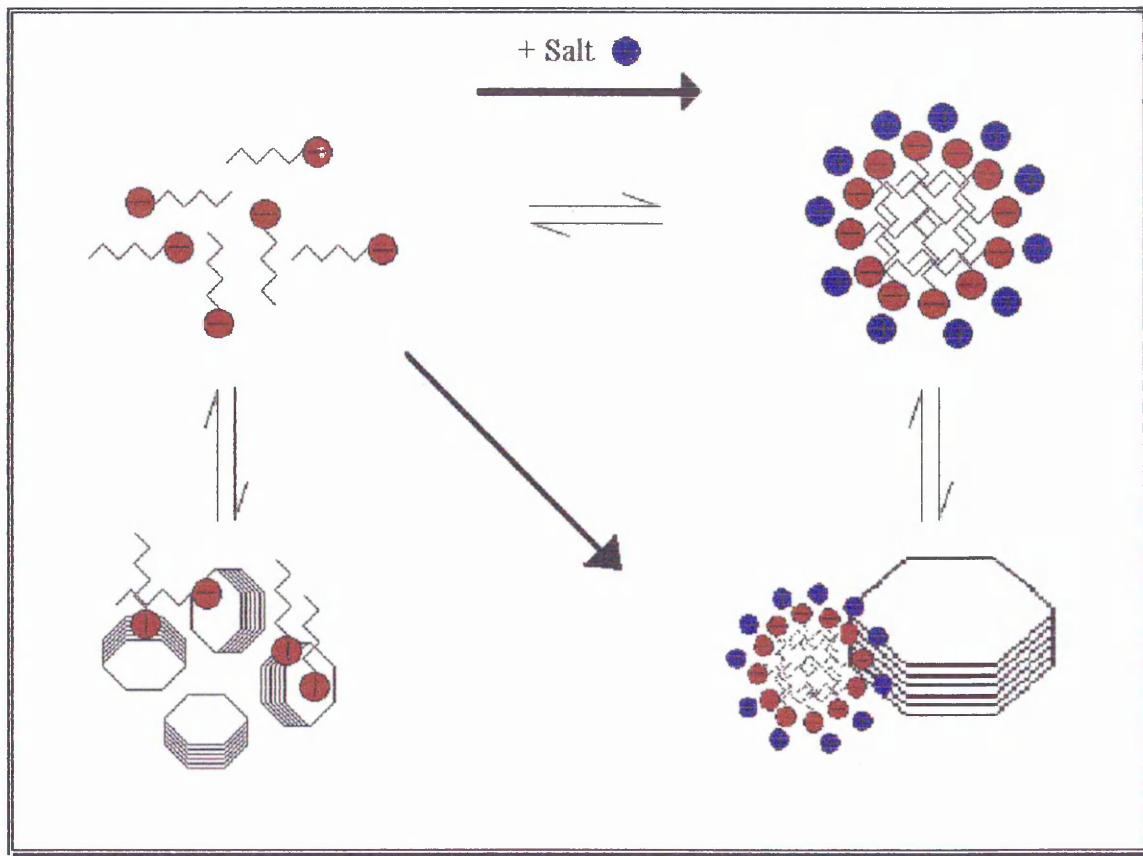
At pH 12, adsorption between the negatively charged organic and mineral surface was not favourable. However, considerable adsorption did occur. Adsorption and strongly attached surface precipitation was considerable due to the high concentration of oleic acid / oleate in solution. Adsorption was limited by the incompatibility of the reactive species. Interactions with the surface were via the carboxylate anion bonded in the bridged bidentate conformation, and by indirect association of acid monomer or dimer with the surface. Significant precipitation of oleate metal salts occurred. The precipitate was not readily removed by washing.

Although the concentration of oleic acid used was below the CMC, the addition of NaCl, or HCl could have altered the salt balance sufficiently for micelle formation to occur. This is particularly true at pH 12 where there is a high concentration of sodium in the water. This could explain why acid is seen at high pH. If the acid form becomes trapped inside the micelle, it can exist at very high pH. Oleate / oleic acid is very soluble at high pH, and the increased concentration would further encourage micelle formation. Figure 4.25 shows a possible schematic mechanism for some of the reactions occurring at pH

Chapter 4
Klein Organic Field Interactions

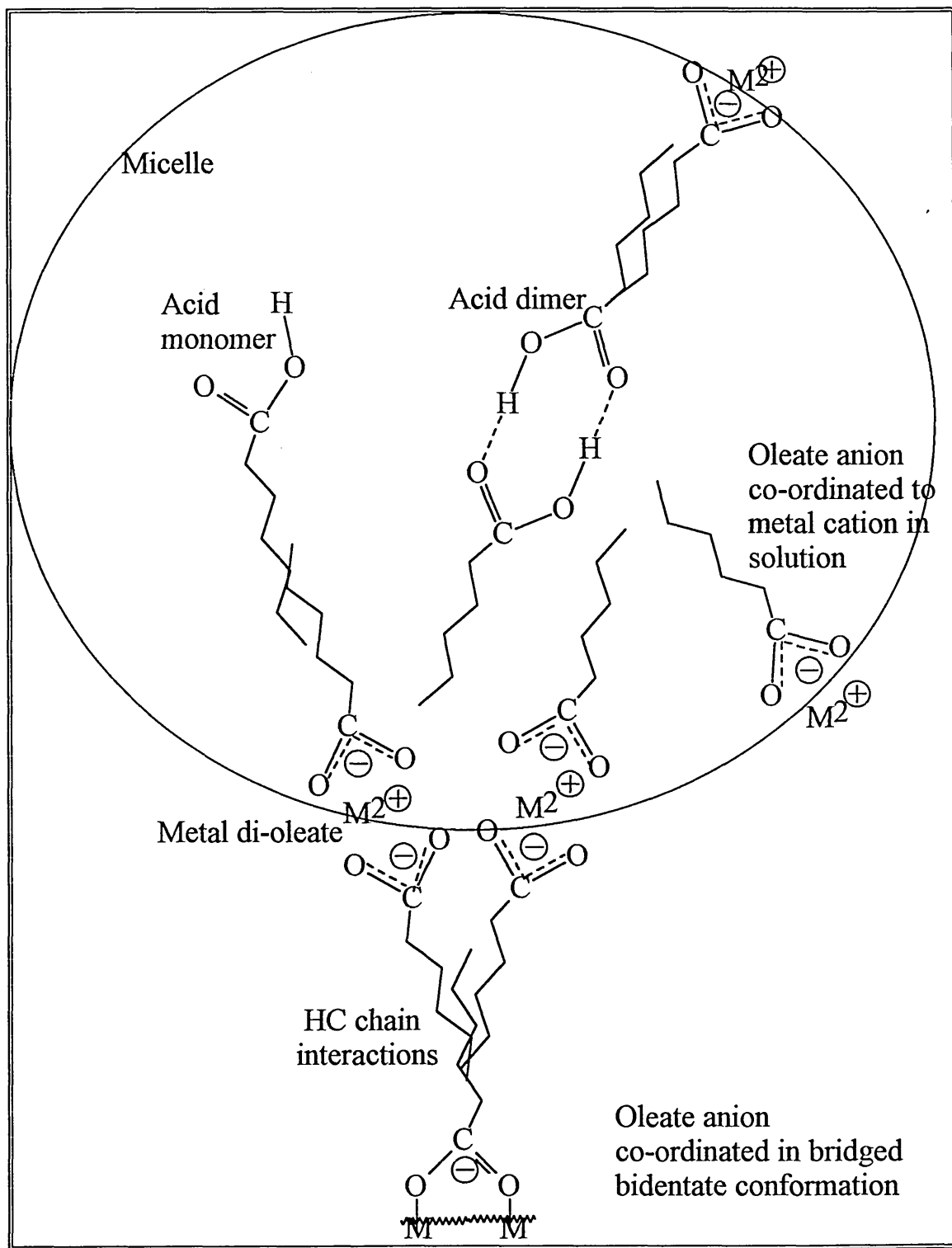
12. It should be noted that HC chain interactions do not depend upon micelle formation, and associations can occur with “free” organic in solution in the same way.

Figure 4.24 Micelle formation and the association with a mineral surface.



Organic association may be due to the interactions with individual oleate molecules at the mineral surface, or via micelle bonded through existing surface sorbed species via HC tail interactions. Micelles may also sediment on the surface of the mineral during the drying process. Micelles may be formed either in solution, or by the compaction of organic at the mineral surface. It is not possible to distinguish using DRIFTS which mechanism is occurring. Horizontal ATR may be able to elucidate information (see Chapter 5)

Figure 4.25 Proposed mechanism of micellar adsorption at pH 12.



It should be noted that the diagram above is a simplified representation only and it does not intend to imply micellar binding occurs via only one surface site interaction. Multiple anions adsorb at the surface of the mineral, and these lead to interactions with micelles via HC chain interactions. The micelles may trap a great number of different species within them. Experimental data suggests that acid dimer or monomer can become encapsulated within the micelle. The formation of dioleate between the micelle and molecules interacting with the surface through HC interactions, results in the formation of strongly held precipitated salt which is resistant to washing.

Adsorption characteristics were found to be similar to those observed by Gong²⁰ et al on the adsorption of oleate/ oleic acid to haematite, in that chemisorption was found to occur at low, mid and high pH. The mechanisms of adsorption were different however. The findings of the present work bore no resemblance to those of Gong⁷ in the shear flocculation of haematite from kaolin study. The findings of the present work were very similar at low and mid pH to the results obtained by Gong³⁴ et al., in the study of the adsorption of oleate/oleic acid on apatite. At low pH, the results differed, but this is not surprising, since the pH of the referenced work was 6, whereas in the work presented herein, the low pH value was 3. pH 6 is likely to be at approximately the PZC of kaolin, whereas pH 3 will be below the PZC. Thus, different results are to be expected.

Thistlethwaite¹⁷ studied adsorption of oleate / oleic acid onto zirconia at pH 9, 6, and 3 and observed similar general trends in adsorption mechanisms (i.e., the presence of acid and salt at high pH, with the presence of a doublet at 1573 / 1538 cm^{-1}) and the increased presence of acid and a salt singlet band at 1556 cm^{-1} at low pH. However, stronger adsorption at pH 3 compared with pH 12 was observed (pH 9 data was not comparable since a different concentration of oleate / oleic acid was used. This was not corroborated by rinsing evidence in the current study, where pH 12 adsorption was very strong, pH 3 was weaker, and adsorption at pH 9 was very weak. The strong associations observed at pH 12 could be an effect of the dissolution -readsorption of Al^{3+} on the kaolin surface³¹, leading to an increase in the number of active sites present at high pH, however, this is not corroborated by evidence at pH 9.

According to the definitions given by Liauw *et al*¹⁶, kaolin is a reactive substrate, where salt formation by chemisorption occurs.

4.5 References.

- 1 Pefferkorn E, Nabzar Lewis & Carroy A (1985). Adsorption of polyacrylamine to Na kaolinite: Correlation between clay structure and surface properties. *Journal of Colloid and Interface Science* 106, 1, 94-103.
- 2 Page M, Lecourtier J, Noik C & Foissy A (1993). Adsorption of polyacrylamides and of polysaccharides on siliceous materials and kaolinite: Influence of temperature. *Journal of Colloid and Interface Science* 161, 450-454.
- 3 Gill RIS & Herrington TM (1987). The effect of surface charge on the flocculation of kaolin suspensions with cationic polyacrylamides of varying molar mass but similar cationic character. *Colloids and Surfaces* 25, 297-310.
- 4 Lee LT, Rahbari R, LeCourtier J & Chauveteau G (1991). Adsorption of polyacrylamides on the different faces of kaolinites. *Journal of Colloid and Interface Science* 147, 2, 351-357.
- 5 Kronberg B, Kuortti J & Stenius (1986). Competitive and cooperative adsorption of polymers and surfactants on kaolinite surfaces. *Colloids and Surfaces* 18, 411-425.
- 6 Rogan KR (1994). Adsorption of the oleic acid and triolein onto various minerals and surface treated mineral. *Colloid and Polymer Science* 272, 82-98.
- 7 Gong W (1997). DRIFT spectroscopic study of the mechanism of selective shear-flocculation of hematite from kaolinite. *Journal of Wuhan University of Technology* 12, 1-2, 83-93.
- 8 Sidheswaran P, Bhat AN & Ganguli P (1990). Intercalation of salts of fatty acids into kaolinite. *Clays and Clay Minerals* 38, 1, 29-32.
- 9 Sidheswaran P, Ram Mohan SV, Ganguli P & Bhat AN (1987). Intercalation of kaolinite with potassium salts of carboxylic acids: x-ray diffraction and infrared studies. *Indian Journal of Chemistry* 26, 994-998.
- 10 Morgan HS, Ananthapadmanabhan KP & Somasundaran P (1986). Oleate adsorption on hematite-problems and methods. *International Journal of Mineral Processing* 18, 139-152.
- 11 Johnston CT (1996). Sorption of organic compounds on clay minerals: a surface functional group approach. In CMS Workshop Lectures, Vol 8, Organic Pollutants in the Environment, Sahwney B, ed. (1996), The Clay Minerals Society, Boulder, CO, 1-45
- 12 Aglietti EF, Lopez JM & Pereira E (1998). Structural alteration in kaolinite by acid treatment. *Applied Clay Science* 3, 155-163.
- 13 Kretzschmar R, Holthoff H & Sticher H (1998). Influence of pH and humic acid on coagulation kinetics of kaolinite: A dynamic light scattering study. *Journal of Colloid and Interface Science*. 202, 95-103.
- 14 Ma K & Pierre AC (1999). Clay sediment-structure formation in aqueous kaolinite suspensions. *Clays and Clay Minerals* 47, 4, 522-526.
- 15 Ward DB & Brady PV (1998). Effect of aluminium and organic acids on the surface chemistry of kaolinite. *Clay and Clay Minerals* 46, 4, 453-465.

-
- 16 Liauw CM, Rathon RN, Hurst SJ & Lees GC (1998). The use of flow micro-calorimetry and FTIR techniques for characterising filler / organic acid interactions. *Composite Interfaces* 5, 6, 503-514.
- 17 Thistlethwaite PJ, Gee ML & Wilson D (1996). Diffuse reflectance infrared Fourier transform spectroscopic studies of the adsorption of oleate / oleic acid onto zirconia. *Langmuir* 12, 6487-6491.
- 18 Lu Y, Drelich J & Miller JD (1998). Oleate adsorption at an apatite surface studied by ex-situ FTIR internal reflection spectroscopy. *Journal of Colloid and Interface Science* 202, 462-476.
- 19 Mielczarski JA & Cases JM (1993). Nature and structure of adsorption layer on apatite contacted with oleate solutions. 2. In situ and ex situ Fourier transform infrared, NMR and x-ray photoelectron spectroscopic studies. *Langmuir* 9, 3357-3370.
- 20 Gong WQ, Parentich A, Little LH & Warren LJ (1991). Diffuse reflectance infrared Fourier transform spectroscopic study of the adsorption mechanism of oleate on haematite. *Colloids and Surfaces* 60, 325-339.
- 21 Ince DE, Johnston CT & Moudgil BM (1991). Fourier transform infrared spectroscopic study of adsorption of oleic acid / oleate on surfaces of apatite and dolomite. *Langmuir* 7, 1453-1457.
- 22 Mielczarski JA, Mielczarski E & Cases JM (1991). Dynamics of fluorite-oleate interactions. *Langmuir* 15, 500-508.
- 23 Miller JD, Jang WH & Kellar (1995). Comments on "Nature and structure of adsorption layer on apatite contacted with oleate solution. 1. Adsorption and Fourier transform infrared reflection studies". *Langmuir* 11, 3272-3274.
- 24 Young RP (1969). Infrared spectroscopic studies of adsorption and catalysis. Part 3. Carboxylic acids and their derivatives adsorbed on silica. *Canadian Journal of Chemistry* 47, 2237-2247.
- 25 Førland GM, Børve KJ, Høiland H & Skauge A (1995). Adsorption of short chain alcohols from decane solutions onto kaolinite. *Journal of Colloid and Interface Science* 171 261-269.
- 26 Xu S & Boyd SA (1995), Cationic surfactant adsorption by swelling and non swelling layer silicates. *Langmuir* 11, 2508-2514.
- 27 Sjöblom J & Söderlund H (1985). Adsorption of surfactants on some minerals surfaces. Applications to enhanced oil recovery processes. *Finnish Chemistry Letters* 179-185.
- 28 Sastry NV, Séquaris J-M & Schwuger MJ (1995). Adsorption of polyacrylic acid and sodium dodecylbenzenesulfonate on kaolinite. *Journal of Colloid and Interface Science* 171 224-233.
- 29 Somasundaran P & Kunjappu JT (1989). In- situ investigation of adsorbed surfactants and polymers on solids in solution. *Colloids and Surfaces* 37, 245-468.
- 30 Blokus AM, Hoiland H, Gjerde MI & Ersland EK (1996). Adsorption of sodium dodecyl sulfate on kaolin from different alcohol-water mixtures. *Journal of Colloid and Interface Science (Note)* 179, 625-627.
- 31 Siracusa PA & Somasundaran P (1987). The role of mineral dissolution in the adsorption of dodecylbenzenesulfonate on kaolinite and alumina *Colloids and Surfaces*, 26, 55-77.
- 32 Cenens J & Schoonheydt RA (1988). Visible spectroscopy of methylene blue on hectoprite, laponite B and barasym in aqueous solution *Clays and Clay Minerals* 36, 214-224.

Chapter 1 Removal of Organic Contaminants

33 Breen C & Rock B (1994). The competitive adsorption of methylene blue on to montmorillonite from binary solution with thioflavin T, proflavin and acridine yellow. Steady state and dynamic studies. *Clay Minerals* 29, 179-189.

34 Gong WQ, Parentich A, Little LH & Warren LJ (1992). Adsorption of oleate on apatite studied by diffuse reflectance infrared Fourier transform spectroscopy. *Langmuir*. 8, 118-124.

5. Summary.

5.1 GENERAL CONCLUSIONS.....	299
5.1.1 <i>Water</i>	299
5.1.2 <i>Surface sites available for organic interactions</i>	299
5.1.3 <i>The interaction of kaolin with oleate / oleic acid</i>	300
5.2 SUGGESTIONS FOR FUTURE STUDY.....	301
5.2.1 <i>The effects of ball milling on the surface sorbed water and the available binding sites of Cornish kaolin, pure kaolin and halloysite</i>	301
5.2.2 <i>Organic adsorption</i>	302

5.1 General conclusions.

5.1.1 Water.

The types of water present on the surface of unrefined and ball milled Cornish kaolin have been characterised. The water has been grouped into four main types - strongly hydrogen bonded, moderately strongly hydrogen bonded, weakly hydrogen bonded and very weakly hydrogen bonded. The different water environments can be observed using DRIFTS in the bending and stretching regions of the spectrum. Changes in the stretching region are generally less distinct, since the bands are broader than in the bending region. However, changes in both regions have been elucidated by curve fitting of the VT DRIFT spectra, and certain bands appear to have similar thermal behaviour.

As ball milling time increases, so does the kaolin agglomerate size and the amount of surface sorbed water. In freshly milled samples, there is always a greater proportion of strongly hydrogen bonded water compared with the other, more weakly bonded types. However, after ageing, the total amount of water present on the surface decreases, and there is less strongly hydrogen bonded water compared with the more weakly bonded species. The more strongly hydrogen bonded water has thus been preferentially desorbed, or has transformed into the more weakly bonded material. It is postulated that the strongly hydrogen bonded species serve as “adhesive” water between the individual particles which make up the large agglomerates. This theory could be investigated by SEM.

5.1.2 Surface sites available for organic interactions.

The reactive surface sites present on unrefined and ball milled Cornish kaolin have been observed at increasing temperature by the use of the probe molecule pyridine. During the course of the study, a dehydrated halloysite impurity was discovered in the unexposed kaolin. Pyridine is known to intercalate into halloysite and form hydrogen bond associations with alumina and gibbsite sheets therein. Pyridine was able to displace the more strongly hydrogen bonded water which is trapped between the individual kaolin particles which comprise the large aggregates after ball milling (an effect similar to ageing). The hydrogen bonding nature of the halloysite-pyridine interactions became less pronounced as milling increased. Pyridine

adsorption to kaolin was via Brønsted sites in the unmilled kaolin. As milling time increased the mineral surface took on Lewis acid character and less hydrogen bonding occurred. Brønsted associations were present in all the milled (and unmilled) samples and became more significant as milling time increased (as more surface water was present). As temperature increased and water was removed from the sample, more pyridine interactions became Lewis in nature (i.e. direct co-ordination rather than bonding to the surface via a hydroxyl or water molecule). At elevated temperatures, (i.e. above 100 °C), VT XRD indicated that pyridine became desorbed from halloysite, and thus at temperature <100 °C, the spectra produced were composites of the halloysite-pyridine intercalation, halloysite-pyridine adsorption and kaolin-pyridine adsorption interactions. At temperatures > 100 °C, the spectra were composites of halloysite-pyridine adsorption and kaolin-pyridine adsorption interactions. In addition to the intercalation reaction between halloysite and pyridine, this probe molecule is likely to bind to exposed (broken) edge sites on kaolin and/or halloysite, or it may be sorbed between the slightly expanded mineral layers at the edges of the mineral stacks.

5.1.3 The interaction of kaolin with oleate / oleic acid.

A method for studying oleic acid adsorption, over a pH range (3, 9 and 12), onto a Cornish kaolin using DRIFT spectroscopy has now been optimised. The interactions occurring are very complex and changes in pH probably led to a change in the edge surface (and possibly the face surface) charge of the mineral. The organic species is also affected by pH. At pH 3, organic is bound to the surface in the monodentate form. Acid precipitate was loosely associated with the surface via hydrocarbon chain interactions with the strongly adsorbed salt species. At pH 9, total surface adsorption was low. Adsorbed species were monodentate in character. Mono- and dioleate were present as very weakly associated surface precipitates. At pH 12 the salt was associated with the surface in the bridged bidentate form. Association of the hydrocarbon chains of attached molecules with micelles led to high adsorption. The micelles contained acid in monomer and / or dimer form which was observed in the IR spectrum of the treated mineral. The precipitate was strongly held, and there was no significant reduction in intensity after washing.

Organic association may be via acid or salt interactions at the surface of the mineral and / or via hydrocarbon chain interactions with the organic monomer, dimer or micellar form.

5.2 Suggestions for future study.

5.2.1 The effects of ball milling on the surface sorbed water and the available binding sites of Cornish kaolin, pure kaolin and halloysite.

With the benefit of hindsight, kaolin interactions of all kinds have proved to be very complex. For this reason it would be very useful to have a larger sample volume of ball milled kaolin for further study. In the current work, the starting mass of the ball milled samples was 2 grams. The limited sample volume meant that certain measurements could not be made, e.g. surface area measurements (which require larger sample mass). Since kaolin is so sensitive to ball milling, any additional sample prepared would almost certainly have different characteristics to the initial sample, and since ball milled samples were found to alter after ageing, it would not be possible to draw direct comparisons between existing data and those collected from any newly milled sample. For this reason it would be wise to prepare a new and large batch of ball milled Cornish kaolin (from the same source). The time intervals should be shorter and more evenly distributed, and cover a range of effects from very minimal to complete destruction of the mineral lattice. Also ball milled under the same conditions should be a sample of pure kaolin and a sample of pure halloysite. These new samples could be used to confirm the effects seen in the current study and to build a more elaborate network of experimental data. A proposed scheme of work follows:

VT DRIFTS, XRD, TGA, DTA, SEM and surface area measurements should be collected from all the samples prior to ball milling and immediately after ball milling. Aliquots of the milled samples should be stored in dark, airtight containers for reference purposes. Further aliquots of the newly milled and unmilled Cornish kaolin, unmilled and milled pure kaolin and unmilled and milled halloysite should be exposed to pyridine or stored under normal laboratory conditions in non airtight containers for a predetermined time, and the experiments should be repeated. After set periods of ageing, for example at monthly intervals, the experiments should be repeated again and any alterations in the sorbed water or structural characteristics (determined by curve fitting of the IR data) should be noted. It would also be interesting to investigate the role of halloysite (if any) on ball milling induced aggregation of kaolin. Standard samples of kaolin-halloysite mixtures, containing known amounts of halloysite “impurity” should be made and ball milled for varying times (as above). The aggregation of

particles could initially be assessed visually by SEM, and surface area measurement could be taken.

5.2.2 Organic adsorption.

The method used in this thesis to examine the interactions of kaolin with oleate / oleic acid was suitable as an initial investigative work. However, there are a number of studies which would elucidate more information about the interactions. Firstly, it would be advantageous to have complimentary TGA, VT XRD and VT DRIFTS data for a set of samples prepared in the way described in Chapter 4. TGA data would provide information about the total mass of organic interacting with the mineral, VT XRD would determine the degree of intercalation (if any) and the effect of temperature, and would compliment VT DRIFTS data.

At this time it is not clear whether adsorption of this organic occurred on the surface of kaolin or halloysite (or both), and without XRD data, it is not possible to determine whether intercalation of halloysite by oleate / oleic acid has occurred. (It is believed that intercalation of kaolin by oleic acid would not occur under these conditions). Initially, RT DRIFTS studies on pure kaolin and halloysite should be conducted in order to distinguish any differences in adsorption characteristics. VT XRD data should be obtained in order to assess the degree (if any) of swelling of the mineral samples. Changes elucidated in the VT XRD data could then be compared with desorption data gained by TGA and VT DRIFTS analysis.

A study of the interactions of ball milled kaolins would also be useful, since certain industrial procedures utilise milling. The interactions of newly milled Cornish kaolin, milled and unmilled pure kaolin, and milled and unmilled halloysite could be examined over a period of time (as described above).

Generally, the industrial processes use wet, rather than dry, milling. The study of wet-ball milled kaolin samples would thus be very useful. However, wet ball milling would further alter the characteristics of the clay, and structural information such as that discussed in the present thesis would be required before adsorption of organic could be studied.

It would be advantageous to examine the interactions of oleic acid/oleate with kaolin using an *in situ* technique, since sample drying may have a number of effects, for example, alter the pH of the surface or lead to the precipitation of organic. Horizontal ATR would be useful, but there is a problem with looking at aqueous system, since water bands are very intense in the IR spectrum. To overcome this problem, Raman microscopy could be used. Raman spectroscopy is not sensitive to water vibrations, and thus it does not influence the spectrum. If kaolin with large platelets (e.g. $10\mu\text{m}$) was mixed with oleic acid / oleate at different pHs, the surface of the platelet could be mapped. This method could be used to study the interactions of more complex molecules with multiple functional groups and / longer hydrocarbon chains. There is a disadvantage to this system, however, since kaolin is highly fluorescent in Raman studies, and the fluorescence increases with increasing particle size. This problem may be overcome by using a very low powered laser. Excitation of Raman spectra can be achieved using a He-Ne laser (at 322 nm) or a diode laser (at 780 nm). The excitation sources are interchangeable, and fluorescence may sometimes be reduced by altering the wavelength of the radiation used for a particular mineral sample.

Ultimately, knowledge of the available binding sites of a variety of minerals before and after milling, and understanding the effects of the interactions of other organics such as amides, amines and imines could lead to the determination of the mechanisms of the complex interaction involved in the industrial processing and purification procedures.